

X-460-74-232
PREPRINT

NASA TM X- 70740

APPLICATIONS TECHNOLOGY SATELLITE ATS-6 IN ORBIT CHECKOUT REPORT

(NASA-TM-X-70740) APPLICATIONS TECHNOLOGY
SATELLITE ATS-6 IN ORBIT CHECKOUT REPORT
(NASA) 389 p HC \$22.50 CSCL 22C

N74-32318

G3/31 47293
Unclas

AUGUST 1974



GSFC

**GODDARD SPACE FLIGHT CENTER
GREENBELT, MARYLAND**

X-460-74-232

APPLICATIONS TECHNOLOGY SATELLITE

ATS-6

IN ORBIT CHECKOUT REPORT

August 1974

GODDARD SPACE FLIGHT CENTER

Greenbelt, Maryland

APPLICATIONS TECHNOLOGY SATELLITE

ATS-6

IN ORBIT CHECKOUT REPORT

Prepared by:

In-Depth Analysis Group

W. Moore (Fairchild)
Publication Coordinator

W. Prenskey (Fairchild)
Technical Editor

Concurrence:

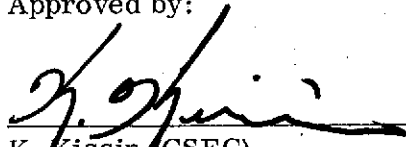


M. Nachman (Fairchild)
Deputy Director, ATS
Systems Engineering

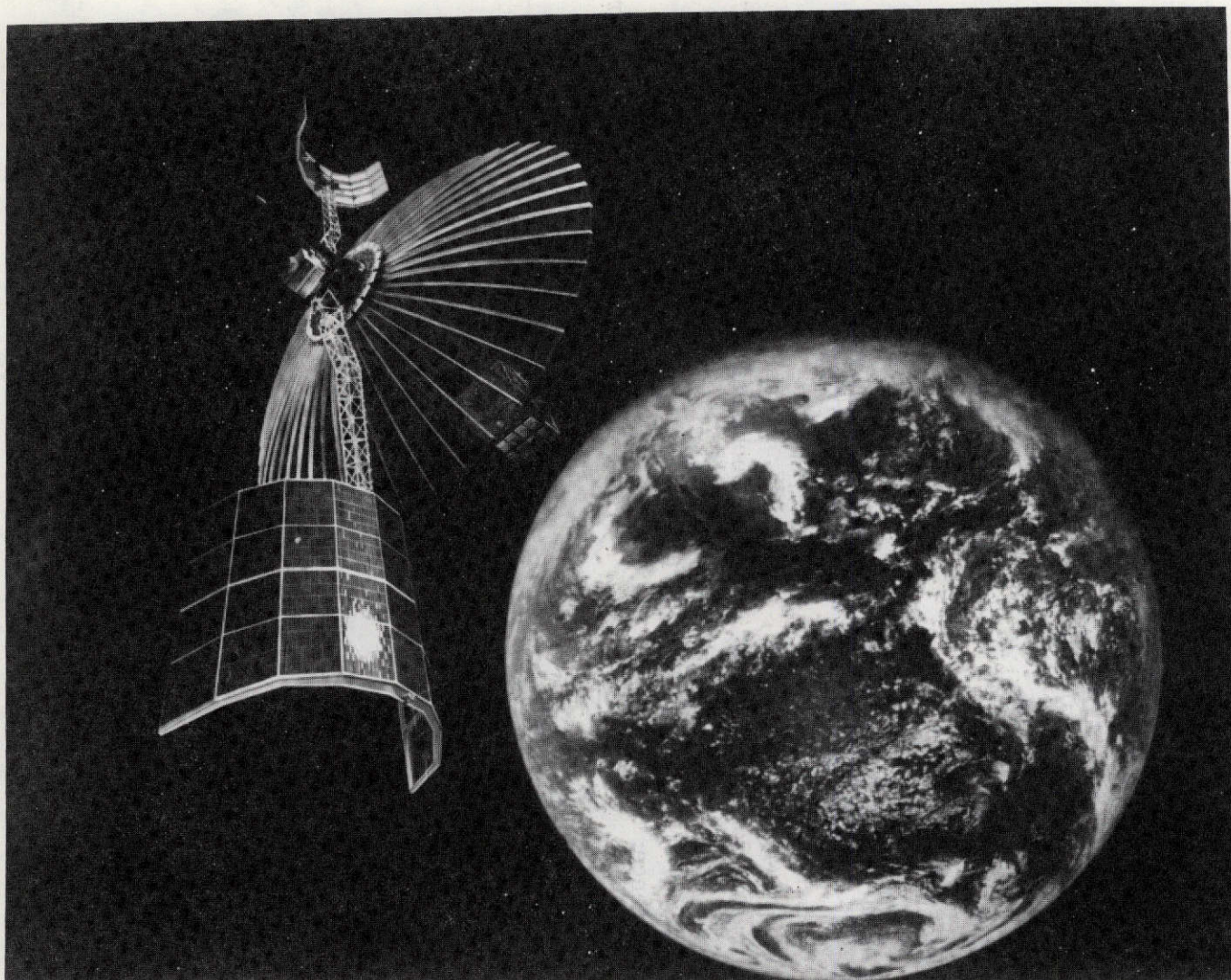


R. Bartlett (GSFC)
In-Depth Analysis Manager

Approved by:



K. Kissin (GSFC)
Mission Operations Director



Frontispiece — ATS-6 In-Orbit Spacecraft

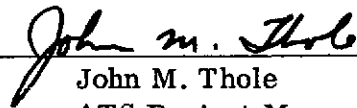
ACKNOWLEDGMENT

Every man knows challenge in life.
ATS-F was a challenge.

Every man knows that in some cases a challenge
requires more effort than was originally
contemplated.
ATS-F was such a case.

Every man knows that once a challenge is
accepted, it cannot be called off without consid-
erable loss of honor.
ATS-F was "a moment with kings!"

The success of ATS-6 (ATS-F) addressed in this report is directly attributable to skill, determination and flexibility of the finest government-industry team with which I have ever had the pleasure of being associated. ATS-6 was truly a team success. To list the individual names of those who made a significant contribution to the success of ATS-6 would require several pages since there are several hundred! However, I would like to take this opportunity to acknowledge and express my personal appreciation to the principal organizations who made the success of ATS-6 possible. These organizations listed in alphabetical order are shown on the following two pages.



John M. Thole
ATS Project Manager

SPACECRAFT AND OPERATIONS

NASA Headquarters

Lewis Research Center

Johnson Space Center

Kennedy Space Center

Goddard Space Flight Center

Goddard Support Contractors:

Boeing Company

Computer Science Corporation

Computer and Software Corporation

Computer Science Technicolor Association

National Scientific Laboratories

OAQ Corporation

Operations Research, Incorporated

Planning Research Corporation

Radio Corporation of America

Raytheon Service Company

Westinghouse Electric Corporation

Wolf Research, Incorporated

Fairchild Industries (Prime Contractor)

Fairchild Subcontractors:

Hercules, Incorporated

Honeywell, Incorporated, Aerospace Division

IBM, Federal Systems Division

Lockheed Missiles and Space Company

Philco-Ford, Western Development Laboratories

Rafuse Association, Incorporated

Rocket Research Corporation

S. J. Industries

Spacecraft, Incorporated

TRW Corporation, Space Systems Division

United States Air Force Support:

Aerospace Corporation

A. F. Eastern Test Range

6555th Aerospace Test Group, USAF

Military Airlift Command, USAF

SAMSO, Air Force Systems Command

SAMSO Contractors:

Martin-Marietta Corporation

Aerojet Corporation

Delco Corporation

McDonnell-Douglas Aircraft Corporation

United Technology Corporation

EXPERIMENTS

Ames Research Center
Appalachian Regional Commission
Department of Commerce
Department of Health Education and Welfare
Department of Transportation
Federal Aviation Agency
Federation of Rocky Mountain States
Maritime Administration
National Oceanic and Atmospheric Administration
Office of the Governor of Alaska
Veterans Administration
U. S. Coast Guard

Canadian Department of Communications
Canadian Ministry of Transport
European Space Research Organization
Indian Space Research Organization

Aerospace Corporation
Comsat Corporation
Hughes Aircraft Company
McDonnell-Douglas Aircraft Corporation

University of California, Los Angeles
University of California, San Diego
University of New Hampshire
University of Minnesota
University of Washington

Goddard Space Flight Center
Goddard Experiment Contractors:
Bell Aerospace Company
Business Technological Systems, Incorporated
Hughes Aircraft Company
General Dynamics Corporation
IBM, Federal Systems Division
ITT Corporation, Aerospace-Optical Division
Martin-Marietta Corporation
Westinghouse Electric Corporation
Xerox Corporation, Electro-Optical Systems Division

**APPLICATIONS TECHNOLOGY SATELLITE
ATS-6
IN ORBIT CHECKOUT REPORT**

FOREWORD

This is the second in a series of reports on the orbital operations of ATS-6 prepared by the In-Depth Analysis (IDA) group. The group organized by Mr. K. Kissin, the ATS-6 Mission Operations Director (MOD), and its functions are described in its initial report, "ATS-6 First Orbit Evaluation", GSFC-X-713-74-177.

From launch, May 30, 1974, through July 2, 1974, the ATS-6 spacecraft and most of the experiments were checked out. On July 2, the scheduling of activities with ATS-6 was turned over to Mr. R. Moore, Chief Project Mission Planner and his staff. At the request of the MOD, the SAPPSAC experiment was run open loop at Rosman on their backup computer from launch through Polaris acquisition. This was done as a backup for real time spacecraft attitude determination. A summary of their work is supplied by Mr. W. Isley and Mr. D. Endres and is included as an appendix to this report. Grateful acknowledgment must be paid to the outstanding contribution made by various individuals belonging to a myriad of organizations which functioned as the operations team resulting in the successful ATS-6 mission to date.

C. Barker - OAO Corporation - Chief Project Operations Controller
R. Burns - Fairchild Industries - Fairchild Operations Manager
G. Demas - GSFC - Control Center Operations Manager
R. DesJardins - GSFC - Spacecraft Simulation Manager
E. Doll - GSFC - Orbit Control Engineer
M. Geller - Westinghouse - Manager, Westinghouse Operations Support
J. Gitelman - GSFC - Project Automatic Data Processing Manager
M. Gunzburg - ORI - Software Consultant
P. McKowan - GSFC - Data Processing Engineer
J. Nieberding - Westinghouse - ATSOCC Software Manager
W. Redisch - GSFC - Systems Engineer
W. Rogers - ORI - Manager, Contingency Operations
D. Stewart - GSFC - Flight Dynamics Manager
P. Zalubus - CSC - Offline Attitude and Orbit Software Manager

Analysis of long term spacecraft performance such as diurnal effects on the parabolic reflector and the attitude control system is continuing. However, an assessment of each spacecraft subsystem is presented here. Based on this evaluation, it is judged that the spacecraft has met all its mission objectives.

The next report on ATS-6 orbital operation will be the first of the quarterly evaluations which will be issued regularly over the duration of the mission. The first quarterly evaluation will present the remainder of the spacecraft antenna patterns not presented here. This phase of the ATS-6 evaluation is under the

direction of Mr. L. Nicholson, ATS-6 Deputy Experiments Manager. This next report will also address a detailed assessment of the performance of each experiment. Other ATS-6 documentary material includes the "Spacecraft Reference Manual", GSFC-460-74-154, developed by Mr. B. Trudell and the "ATS-F Data Book" developed under the direction of Mr. G. Bullock.

Fairchild participation in the preparation of this document discharges their contractual requirement to produce a 30-day report on the orbital operation of ATS-6 under contract NAS 5-21100. The members of the IDA group contributing to this report as reviewed by the subsystem engineers under the editorial direction of Mr. W. Prensky of Fairchild Industries are the following:

FAIRCHILD

W. Altemose
L. Apple
R. Burns
J. Blue
P. De Baylo
S. Folley
M. Frieder
F. Gorsen
H. Greenberg
D. Hawkins
G. Heyman
F. Hornbuckle
R. James
R. Karam
W. King
S. Millikin
W. Moore
J. Mudano
R. Rubock
R. Schrieb
P. Sing
H. Solt
J. Toczylowski
H. Ward
J. Wilson

GODDARD

R. Estes

IBM

J. Davis

NSL

P. Fosher

ORI

M. Gunzburg

WESTINGHOUSE

R. Baldridge
M. Geller
R. Walsh

For additional technical information on the design and/or performance of the ATS-6 subsystems, the following subsystem managers may be contacted:

Structural/Deployment

T. Berry (Fairchild)
D. Miller (Goddard)
T. Swales (Fairchild)
J. Webb (Goddard)

Propulsion

E. Curtis (Goddard)
J. Pylant (Rocket Research)
R. Schreib (Fairchild)
D. Suddeth (Goddard)

Parabolic Reflector

C. Cambell (Lockheed)
C. Courtney (Goddard)
C. Teleki (Fairchild)

Communications

J. Brown (Goddard)
J. Feinstein (Fairchild)
P. Hefferman (Goddard)
R. Tyler (Philco-Ford)

Electrical Power

S. Folley (Fairchild)
F. Hornbuckle (Fairchild)
T. LaVigna (Goddard)

Systems

G. Banks (Goddard)
R. Hall (Fairchild)
B. Keiser (Fairchild)
W. Redisch (Goddard)
J. Thole (ex OFFICIO)
M. Titland (Fairchild)

Thermal Control

M. Coyle (Goddard)
R. Eby (Fairchild)
W. Kelly (Fairchild)

Telemetry and Command

H. Austin (Fairchild)
D. Margolies (Goddard)
A. Toman (IBM)

Attitude Control

R. Freeman (Goddard)
R. Harclerode (Honeywell)
T. Huber (Goddard)
R. Pattishall (Fairchild)
J. Turtill (Fairchild)

Interferometer

A. Kampinsky (Goddard)
J. Mudano (Fairchild)
M. Teichman (IBM)

CONTENTS

	<u>Page</u>
Frontispiece — ATS-6 In-Orbit Spacecraft	ii
ACKNOWLEDGEMENT	iii
SPACECRAFT AND OPERATIONS	iv
EXPERIMENTS	v
FOREWORD	ix

SECTION 1

INTRODUCTION

1.1 GENERAL	1-1
1.2 PURPOSE	1-1
1.3 SCOPE	1-2
1.4 HISTORY OF THE ATS PROGRAM	1-2

SECTION 2

MISSION OBJECTIVES AND SUMMARY OF SPACECRAFT PERFORMANCE

2.1 GENERAL	2-1
2.2 FLIGHT OBJECTIVES	2-1
2.3 SUBSYSTEM REQUIREMENTS/SPECIFICATIONS AND IN-ORBIT PERFORMANCE SUMMARY	2-4
2.3.1 Structural and Deployment Subsystems	2-5
2.3.2 Electrical Power Subsystem	2-5
2.3.3 Thermal Control Subsystem	2-5
2.3.4 Telemetry and Command Subsystem	2-5
2.3.5 Attitude Control Subsystem	2-5
2.3.6 Spacecraft Propulsion Subsystem	2-15
2.3.7 Communication Subsystem	2-15
2.3.8 Experiments	2-19

CONTENTS (Cont'd.)

Page

SECTION 3

FLIGHT CHRONOLOGY

3.0	INTRODUCTION	3-1
3.1	LAUNCH THROUGH SEPARATION	3-1
3.1.1	Launch	3-1
3.1.2	Ascent	3-4
3.1.3	Separation	3-6
3.2	DEPLOYMENT	3-6
3.3	ACQUISITION	3-9
3.3.1	Sun Acquisition	3-9
3.3.2	Spacecraft Activation	3-9
3.3.3	Earth Acquisition	3-13
3.3.4	Yaw Reference Maneuver	3-13
3.4	IN-ORBIT RECONFIGURATION AND SPACECRAFT CHECKOUT	3-13
3.5	CHRONOLOGY OF SPACECRAFT ACTIVITY (DAYS 2-18) . . .	3-14

SECTION 4

SPACECRAFT DESCRIPTION

4.1	INTRODUCTION	4-1
4.2	STRUCTURAL/DEPLOYMENT SUBSYSTEM	4-1
4.3	ELECTRICAL POWER SUBSYSTEM	4-4
4.4	THERMAL CONTROL SUBSYSTEM	4-6
4.5	TELEMETRY AND COMMAND SUBSYSTEM	4-9
4.6	ATTITUDE CONTROL SUBSYSTEM	4-11

CONTENTS (Cont'd.)

	<u>Page</u>
4.7 SPACECRAFT PROPULSION SUBSYSTEM	4-15
4.8 COMMUNICATION SUBSYSTEM	4-17
4.9 EXPERIMENTS	4-20

SECTION 5

STRUCTURAL/DEPLOYMENT SUBSYSTEMS

5.1 STRUCTURAL	5-1
5.1.1 -Y (North) Solar Panel Deployment About Panel/Boom (45°) Hinge	5-1
5.1.2 Conclusions	5-9
5.2 ELECTRICAL	5-10

SECTION 6

ELECTRICAL POWER SUBSYSTEM

6.1 SUBSYSTEM PERFORMANCE	6-1
6.2 PERFORMANCE EVALUATION	6-1
6.2.1 In Orbit Overview	6-1
6.2.2 Launch and Ascent Performance	6-1
6.3 MAJOR COMPONENT PERFORMANCE	6-6
6.3.1 Solar Array	6-6
6.3.2 Battery Performance	6-11
6.3.3 Power Regulation Unit	6-26
6.3.4 Power Control Unit	6-27
6.3.5 Load Interface Circuits	6-27
6.3.6 Shunt Dissipators	6-30
6.4 SOLAR ARRAY SHUNT TAP VOLTAGE FOR SHUNT DISSIPATOR A419	6-30
6.5 CONCLUSIONS AND RECOMMENDATIONS	6-30

CONTENTS (Cont'd.)

Page

SECTION 7

THERMAL CONTROL SUBSYSTEM

7.1	SUBSYSTEM PERFORMANCE	7-1
7.2	THERMAL DESIGN	7-1
7.3	DATA SOURCES	7-3
7.4	SUBSYSTEM EVALUATION	7-3
7.4.1	Launch/Ascent Phase	7-3
7.4.2	Orbital Phase	7-16
7.5	CONCLUSIONS AND RECOMMENDATIONS	7-28

SECTION 8

TELEMETRY AND COMMAND SUBSYSTEM (T&C S/S)

8.1	SUBSYSTEM PERFORMANCE	8-1
8.2	EQUIPMENT PERFORMANCE EVALUATION	8-1
8.2.1	Design Objectives	8-3
8.2.2	Performance Evaluation	8-4

SECTION 9

ATTITUDE CONTROL SUBSYSTEM

9.1	SUBSYSTEM PERFORMANCE	9-1
9.2	LAUNCH AND ACQUISITION	9-4
9.2.1	Sun Acquisition	9-6
9.2.2	Earth Acquisition	9-13
9.2.3	Polaris Acquisition	9-17
9.2.4	Local Vertical Evaluation of ABC	9-23

CONTENTS (Cont'd.)

	<u>Page</u>
9.3 OPERATIONAL MODES	9-23
9.3.1 Reference Orientation	9-23
9.3.2 Offset Pointing	9-26
9.3.3 Station Null Point	9-28
9.3.4 Low Jitter	9-37
9.3.5 Slewing Maneuver	9-44
9.3.6 Antenna Patterns	9-46
9.3.7 Satellite Track	9-46
9.4 INTERFEROMETER	9-46
9.4.1 Earth Acquisition	9-50
9.4.2 Interferometer Performance	9-52
9.5 INERTIA WHEEL UNLOAD	9-55
9.5.1 Wheel Unload Histories	9-62
9.5.2 Three Axis Momentum Storage	9-62
9.5.3 Automatic Unload Performance	9-66
9.5.4 Estimated Unload Fuel Requirements	9-73
9.6 ANOMALIES	9-73
9.6.1 RGA #1 Earth Acquisition Anomaly	9-73
9.6.2 PSA Tracking Anomalies	9-82
9.6.3 YIRU Bias Anomaly	9-91
9.6.4 DOC Command Angle Anomaly	9-91
9.6.5 Interferometer AGC IF #2 Anomaly	9-95

SECTION 10

SPACECRAFT PROPULSION SUBSYSTEM (SPS)

10.1 SUBSYSTEM PERFORMANCE	10-1
10.2 PRELAUNCH/LAUNCH	10-2
10.3 LINE EVACUATION/PROPELLANT BLEED IN	10-4

CONTENTS (Cont'd.)

	<u>Page</u>
10.4 JET USAGE/PERFORMANCE	10-4
10.4.1 Spacecraft Acquisition Maneuvers	10-4
10.4.2 Initial Orbit Correction	10-6
10.4.3 Wheel Unloading	10-6
10.5 TANK BLOWDOWN/PROPELLANT CONSUMPTION	10-8
10.6 COMPONENT TEMPERATURES	10-12
10.7 RECOMMENDATIONS	10-17

SECTION 11

COMMUNICATION SUBSYSTEM

11.1 COMMUNICATION SUBSYSTEM	11-1
11.2 OPERATIONAL MODES	11-3
11.2.1 TDRE	11-4
11.2.2 TRUST	11-4
11.2.3 PLACE	11-4
11.2.4 Monopulse Tracking	11-5
11.2.5 MMW Experiment	11-10
11.2.6 COMSAT Propagation Experiment	11-10
11.2.7 RFI	11-10
11.2.8 VHRP	11-11
11.2.9 VHF High Gain RF Link	11-11
11.2.10 Range and Range Rate	11-11
11.2.11 HET (Health Telecommunication Television) Experiment	11-11
11.2.12 TV Camera	11-12
11.2.13 Radio Beacon Experiment	11-12
11.3 TRANSPONDER SIGNAL CHARACTERISTICS	11-14
11.4 ANTENNA PATTERNS	11-31
11.5 ANOMALOUS PERFORMANCE	11-45

CONTENTS (Cont'd.)

	<u>Page</u>
SECTION 12	
EXPERIMENT SUBSYSTEM (GFE)	
12.1 SUBSYSTEM PERFORMANCE	12-1
12.2 EXPERIMENT DESCRIPTION	12-2
12.2.1 Millimeter Wave Experiment	12-2
12.2.2 Propagation Experiment	12-2
12.2.3 Environmental Measurements Experiment	12-2
12.2.4 Quartz Crystal Microbalance (QCM) Contamination Monitor	12-4
12.2.5 Advanced Thermal Control Flight Experiment	12-5
12.2.6 Ion Engine Experiments	12-5
12.2.7 Very High Resolution Radiometer Experiment (VHRR)	12-5
12.3 OPERATIONAL MILESTONES	12-6
12.4 INTERFACE DESCRIPTION	12-9
12.4.1 Electrical Power Subsystem	12-9
12.4.2 Telemetry and Command Subsystem	12-9
12.4.3 Thermal Control Subsystem	12-10
12.4.4 Special Interfaces	12-10
12.4.5 Interface Performance	12-10
12.5 EXPERIMENT PERFORMANCE EVALUATION	12-13
12.5.1 Propagation Experiment	12-13
12.5.2 QCM Experiment	12-13
12.5.3 ATFE	12-14
12.5.4 VHRR Experiment	12-14
12.5.5 MMW Experiment	12-14
12.5.6 EME	12-14
12.5.7 Ion Engines	12-15
APPENDIX A — SAPPSAC EXPERIMENT	A-1
APPENDIX B — ABBREVIATIONS	B-1

SECTION 1
INTRODUCTION

SECTION 1

INTRODUCTION

1.1 GENERAL

The ATS-6 spacecraft (Figure 1-1), designated as ATS-F prior to launch, was designed and built by the Fairchild Space and Electronics Company, Germantown, Maryland, as prime contractor to the Goddard Space Flight Center, Greenbelt, Maryland, in compliance with NASA Contract NAS5-21100. Other members of the prime team include:

Philco-Ford, Western Development Labs Division, Palo Alto, California (communications module);

IBM, Gaithersburg, Md. (telemetry, interferometer, and command system);

Honeywell Aerospace Division, St. Petersburg, Fla. (attitude control system);

Lockheed Missile Space Center, Sunnyvale, Calif. (nine-meter parabolic reflector); and

Rocket Research Corp., Redmond, Washington (propulsion system).

Following the completion of the ground test program and launch operations at the Kennedy Space Flight Center, the spacecraft was successfully inserted into synchronous orbit on May 30, 1974 and commenced operations in accordance with its mission plan. The primary purpose of the ATS-6 spacecraft is to evaluate a variety of new space communications concepts requiring the use of a geosynchronous spacecraft. This involves deployment of a 30 ft diameter parabolic antenna in space, three-axis stabilization and the ability to utilize the high gain of the antenna through accurate pointing and stability.

1.2 PURPOSE

The purpose of this report is to describe the activities of the ATS-6 spacecraft for the checkout period of approximately four weeks beginning May 30, 1974, and to present the results of performance evaluation of its subsystems and components.

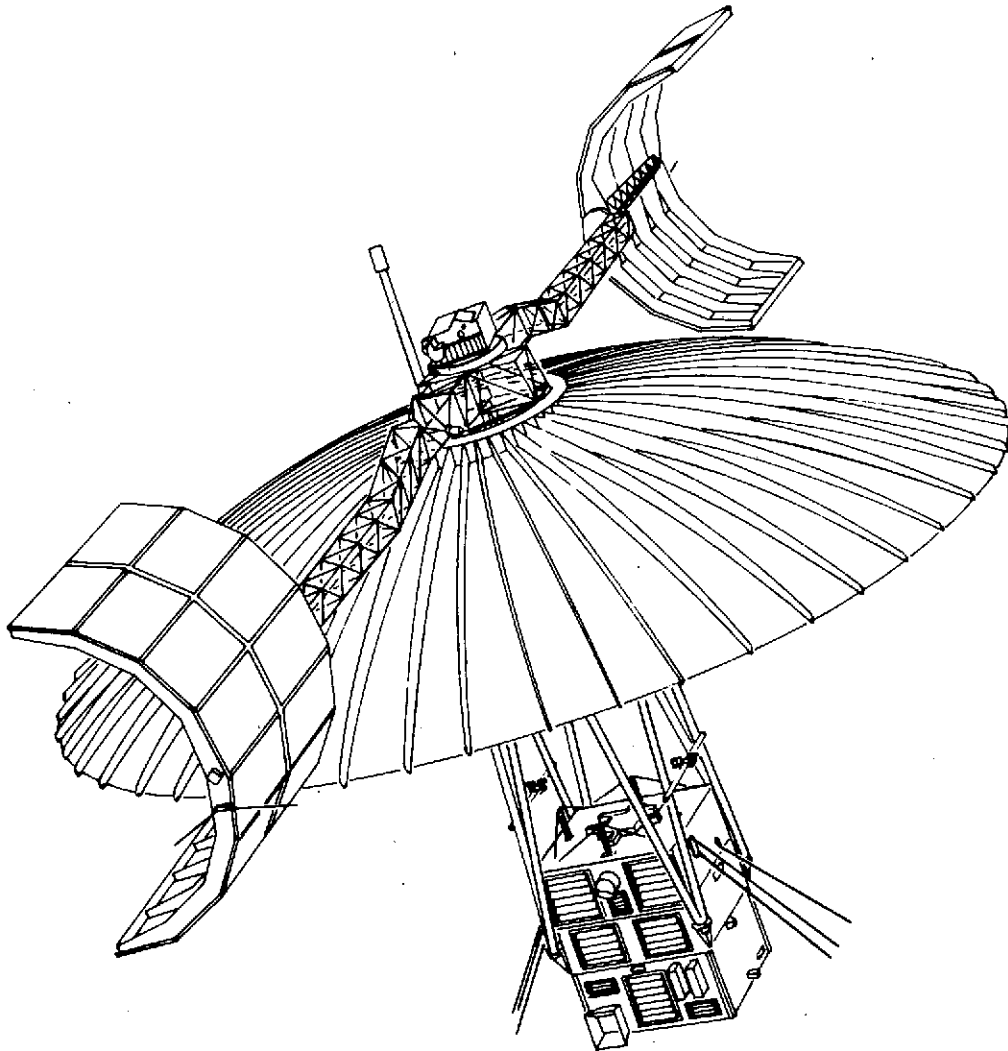


Figure 1-1. ATS-6 Spacecraft

1.3 SCOPE

The scope of this report includes the evaluation of all ATS-6 spacecraft subsystems and components with initial evaluation of GFE experiments.

1.4 HISTORY OF THE ATS PROGRAM

Prior to development of the Applications Technology Satellite (ATS) program, NASA conducted extensive research with communications satellites at low, intermediate, and synchronous orbital altitudes. These spacecraft included passive reflectors such as the 33-meter (100-foot) diameter Echo balloons and active repeaters such as the Relay and Syncom spacecraft.

Upon the completion of these programs, an Advanced Syncom study was conducted to determine the next step to be taken in communications spacecraft. The ATS program was based on the results of this study and incorporated a number of Syncom techniques. These included spin-stabilized configurations with multi-frequency capability.

The first phase of the ATS program included the development, launch, and utilization of five spin-and gravity gradient-stabilized spacecraft, four of which were to be placed in geostationary orbit. Communication satellites operating from this altitude view about 45 percent of the globe as compared to a 320-kilometer (200-mile) orbit spacecraft which views only about three percent of the globe at one time.

ATS-6 is the next logical step in the program and continues and extends the scope of the experiments conducted by ATS-1 through 5.

ATS-1 (ATS-B before launch)

This spin-stabilized, synchronous-altitude satellite was the first ATS to be launched. Soon after its lift-off on December 7, 1966, from Cape Kennedy, Fla., the satellite was maneuvered into its permanent position over the Pacific Ocean and all its systems checked out as fully operational. Since then, all the experiments have been sending a steady stream of data back to the ground stations. A wide variety of services have been performed by ATS-1 in addition to the large number of technological and scientific experiments.

Educational broadcasting to both Alaska and the Pacific Basin is currently being done through ATS-1. Included are college-level seminars and courses at both primary and secondary levels.

ATS-2 (ATS-A before launch)

The second satellite in the ATS series was launched from Cape Kennedy on April 6, 1967. It was intended that this gravity-gradient-stabilized spacecraft be placed in a medium altitude orbit inclined to Earth's equator, so that it would continuously circle the Earth. A failure in the fuel supply system of the Agena rocket prevented the booster from re-igniting at the crucial point in the satellite trajectory, and the satellite went into a highly elliptical orbit. Large forces, caused by the severe decelerations occurring in this very irregular orbit, proved more than the gravity-gradient stabilization system could overcome, and as a result ATS-2 slowly tumbled and rotated. All the systems and experiments onboard functioned as well as possible under these conditions. The spacecraft reentered Earth's atmosphere on September 2, 1969, and was destroyed.

ATS-3 (ATS-C before launch)

The third satellite in the series, a spin-stabilized spacecraft, was put into synchronous orbit on November 6, 1967, from Cape Kennedy. After a perfect launch, it took up its station over the Atlantic Ocean, and all systems have been operating as expected since then.

A significant achievement of this satellite was the first ground-to-spacecraft-to-aircraft communications link over the Atlantic. This historic event took place on November 21, 1967, during a Pan American flight from New York to London.

Probably the most notable achievement of ATS-3 was its sending the first color photograph of Earth in space, obtained from the multicolor spin-scan cloud camera. Another camera on ATS-3, the image dissector camera (IDCS), also obtained many cloud photographs. The spacecraft continues to monitor severe storms.

ATS-4 (ATS-D before launch)

ATS-4 was a gravity-gradient spacecraft launched from Cape Kennedy on August 10, 1968. The Centaur second ignition was never accomplished. As a result, the spacecraft, with Centaur and apogee motor attached, was left in an approximately 100 by 400 nautical mile orbit. Turn-on of all systems and experiments was accomplished; however, little useful data were obtained because of the extreme anomalistic conditions. ATS-4 reentered Earth's atmosphere and was destroyed on October 17, 1968.

ATS-5 (ATS-E before launch)

ATS-5, another gravity-gradient spacecraft, was launched from Cape Kennedy on August 12, 1969. It has contributed much technical and scientific information although it was not de-spun and therefore never stabilized by the Earth's gravity-gradient.

The auroral particles experiments on ATS-5 have now been operating successfully since 1969 and are continuing to provide a large quantity of useful data.

The NASA/GSFC L-band ranging and position location experiments, being conducted from the Mojave ground station to the ATS-5 satellite, have demonstrated the ability to obtain meaningful range measurements using phase modulation/tone modulation at L-band frequencies.

SECTION 2
MISSION OBJECTIVES AND SUMMARY
OF SPACECRAFT PERFORMANCE

SECTION 2

MISSION OBJECTIVES AND SUMMARY OF SPACECRAFT PERFORMANCE

2.1 GENERAL

The principle objective of the ATS-6 program is to demonstrate the feasibility of operating a high-powered communications spacecraft in orbit which would be capable of relaying color TV and other high quality communication signals on multiple frequencies to relatively simple and inexpensive ground receivers located at various points on the earth's surface. To meet this objective, the ATS-6 spacecraft was required to deploy a 30-foot parabolic reflector in space, perform maneuvers in accordance with ground commands to point the reflector to selected points on the earth's surface, and provide the necessary communication links and associated power to receive and rebroadcast communication signals transmitted from the ground.

The ATS-6 spacecraft is considered to be an unqualified success in meeting this primary objective and all defined mission objectives and requirements for the first month in orbit. Spacecraft systems operation has been consistently excellent with relatively few anomalies encountered. Further, due to the built-in flexibility of the spacecraft design, and a sophisticated ground operations and software system, the ATS-6 spacecraft has proven to be dependable and relatively easy to control with a minimum number of operations personnel required. At the completion of the spacecraft evaluation period, all spacecraft systems were fully operational with no loss of redundant or back-up capability. Further, as a result of an excellent initial orbit provided by the Titan III C launch vehicle, only a small portion of the allocated spacecraft jet fuel was used for orbit correction, thereby extending the predicted usable life of the spacecraft beyond the five year design goal.

Specific flight objectives and spacecraft performance summaries are next presented. More comprehensive discussions of spacecraft subsystem performance are presented in sections 5 through 12 of this report.

2.2 FLIGHT OBJECTIVES

The ATS-6 spacecraft flight objectives as defined in the Spacecraft System Specification 862-0001 were all satisfied with specifications being met or exceeded. Results obtained are as follows:

- | | |
|--------------|---|
| Requirement: | Demonstrate the feasibility of deploying a 30-foot Parabolic Reflector with good RF performance up to 6 GHz. |
| Performance: | The 30-foot Parabolic Reflector was successfully deployed 7 hours and 8 minutes after launch. Figure 2-1 is a picture of the reflector taken by a TV Camera aboard the spacecraft |

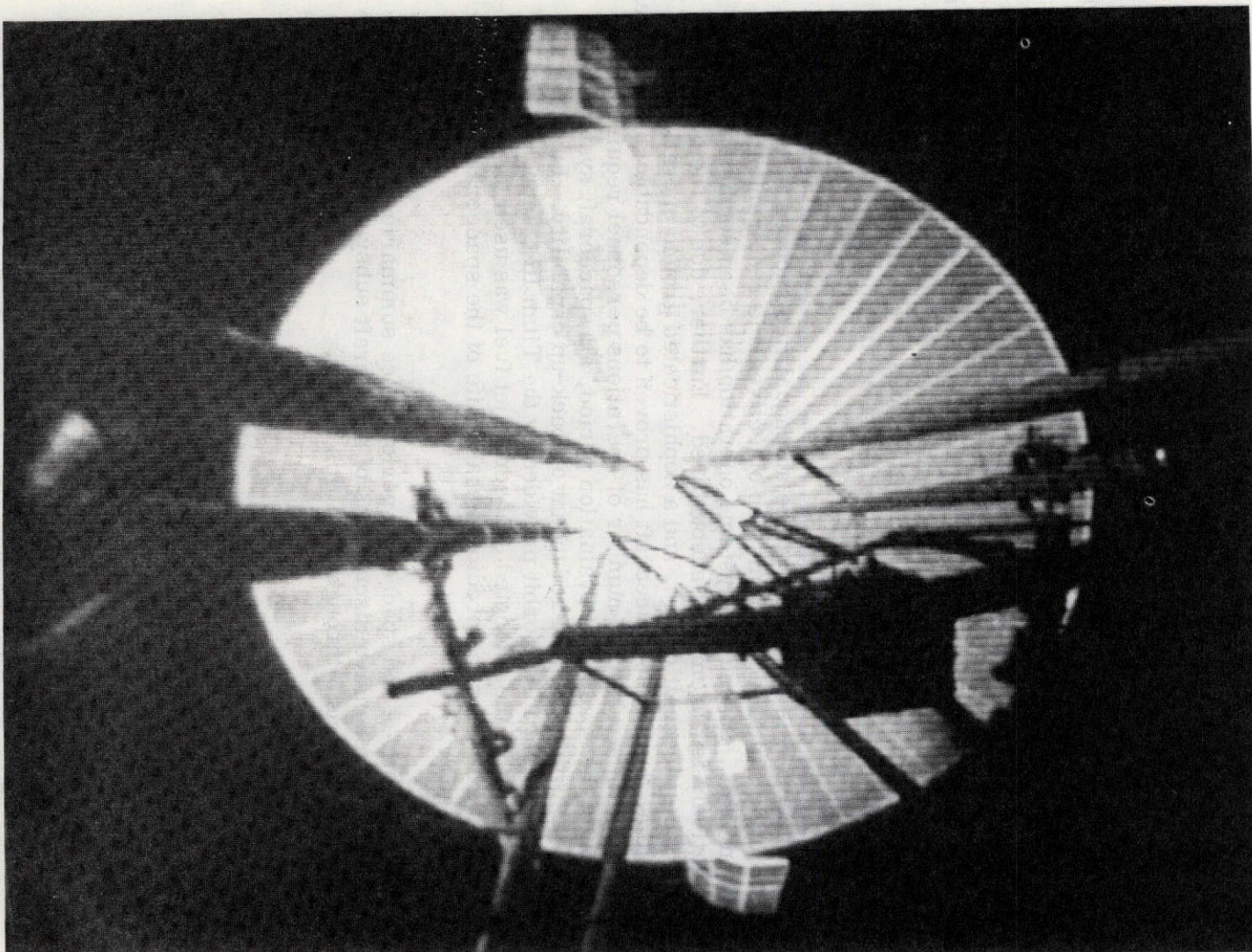


Figure 2-1. TV Camera View of Deployed 30-Foot Reflector

and transmitted over the C-band earth coverage horn three days into the ATS-6 mission. All communications links between 137 and 6350 MHz were successfully supported. A detailed discussion of antenna performance can be found in section 11.

- Requirement:** Provide spacecraft fine pointing of 0.1 degree accuracy over ± 10 degrees off the local vertical, and slewing the spacecraft Z-axis of 17.5 degrees in 30 minutes.
- Performance:** The Attitude Control Subsystem (ACS) achieved a pointing accuracy of 0.04° with a pointing stability of 0.01° in the offset point ground mode using the earth sensor and Polaris Tracker. The ACS achieved controlled slew rates of $1.2^\circ/\text{min}$ which demonstrates a capability of slewing the spacecraft Z-axis 17.5° in less than 15 minutes.
- Requirement:** Demonstrate precision interferometer attitude measuring technology for closed loop servo performance.
- Performance:** When the interferometer was used in the ACS control loop for roll and pitch attitude control, pointing accuracy and pointing stability were within specification and comparable in performance with the earth sensor. The interferometer has a resolution of 0.00142° . When the interferometer was configured for the dual frequency mode, spacecraft roll, pitch, and yaw information was computed in real time at ATS Operations Control Center (ATSOCC).
- Requirement:** Demonstrate capability of forming high-gain steerable antenna beams.
- Performance:** All antenna beams on ATS-6, some of which were offset from boresight, were pointed at ROSMAN and performance data was obtained (see section 11). The antenna beams for the Health Education Telecommunications (HET) experiment (beamwidths of 0.85°) were successfully used to support live TV programs for the Appalachian Regional Commission (ARC), Veterans Administration, the Federation of Rocky Mountain States, and Regionalized Medical School, Health, and Education in Alaska. TV reception has been reported as excellent.
- Requirement:** Demonstrate capability of providing ground-to-ATS-6-to-low-orbiting-spacecraft and return links for the following:
- (1) Z-axis tracking of one low orbit spacecraft.
 - (2) Steerable antenna beams to track two low orbiting spacecraft.

- Performance:** ATS-6 successfully program-tracked a simulated NIMBUS spacecraft to a roll and pitch accuracy of better than 0.2° . During the S-band cross antenna pattern measurement, beam switching was demonstrated by selecting one of the appropriate 21 individual beams as the spacecraft Z-axis was slewed $\pm 6^\circ$ about ROSMAN, first in the E-W direction and then in the N-S direction.
- Requirement:** Provide communication link for the Position Location and Aircraft Communication Experiment (PLACE), the Tracking and Data Relay Experiment (TDRE), the Health Education Telecommunications (HET) Experiment and the Satellite Instructional Television Experiment (SITE).
- Performance:** The communication links for each of the above experiments was successfully demonstrated during the spacecraft checkout period using ground communication equipment located at ROSMAN. As mentioned above, the spacecraft successfully supported the HET TV programs. Beginning July 2, 1974, ATS-6 was declared operational and began weekly program transmission for educational courses at the graduate level from the University of Kentucky (ARC) and medical forum between Veterans Administration hospitals. During the HET operations, the spacecraft, at times, is configured to provide simultaneous broadcasting of two different TV programs to two different geographical locations.
- Requirement:** Provide oriented stable platform at synchronous altitude for experiments to be selected through the Spacecraft and Applications Steering Committee.
- Performance:** The spacecraft was placed in geosynchronous orbit with a planned orbit station above 94° W longitude. In the low jitter mode, the spacecraft +Z axis can point anywhere on the earth's surface with a pointing stability of $\pm 0.005^\circ$.

In summary, all of the major flight objectives imposed on the ATS-6 have been fully satisfied. The detailed performance specifications for the various subsystems, as given in the Spacecraft System Specification 862-0001 and the applicable subsystem specifications, were almost universally satisfied and in most cases exceeded as summarized in the following subsections.

2.3 SUBSYSTEM REQUIREMENTS/SPECIFICATIONS AND IN-ORBIT PERFORMANCE SUMMARY

The performance of each spacecraft subsystem for the first 30 days of in-orbit operation is summarized in the following paragraphs. Detailed information on the performance of these subsystems is provided in subsequent sections of this report.

2.3.1 Structural and Deployment Subsystems

The structural subsystem has met its basic flight requirements, as the spacecraft successfully withstood the launch environment and deployed properly in space with no structural failures evidenced. Alignment of the various sensors (earth sensor, interferometer, and monopulse) has been preserved to within 0.1 degree. The separation system worked very well; the spacecraft angular rates after separation were 0.13, 0.11 and -0.06 deg/sec in roll, pitch and yaw, compared to specified allowable rates of 1 deg/sec about the three axes. Spacecraft deployment was successfully achieved, although a significant delay (≈ 13 minutes) was experienced before the -Y solar array completed its unfold operation and locked up. This anomaly is treated in section 5.0 of this report.

2.3.2 Electrical Power Subsystem

The electrical power subsystem has met or exceeded performance specifications and pre-flight predictions in all areas, as indicated in Table 2-1. Total solar array power capability for spacecraft use is approximately 595 watts, 40 watts higher than the specified value for the summer solstice. Power bus regulation has remained within specification through the entire range of operation including the batteries only (array occulted), array only (batteries being charged), and battery share modes. The highest spacecraft load encountered to date was 650 watts, during a 2-frequency HET mode with C-Band monitor. Bus voltage for all experiments has been 28.0 ± 1 volts (specification value is 28.0 ± 0.45 volts).

2.3.3 Thermal Control Subsystem

The thermal control subsystem has met or exceeded specification requirements, indicating that the louvers and heat pipes are operational and that the external insulation satisfactorily survived the launch environment. A summary of Earth Viewing Module (EVM) component temperature variations is presented in Table 2-2. Table 2-3 presents the external temperature profile during deployment. All components remained within required values ($20^{\circ}\text{C} \pm 15^{\circ}\text{C}$ in the EVM).

2.3.4 Telemetry and Command Subsystem

The telemetry and command subsystem has performed in a highly successful manner providing for normal telemetry, dwell telemetry, and Environmental Measurements Experiment (EME) telemetry in the (FDM) mode over the Prime Focus Feed (PFF) on the 30-foot dish and commanding at VHF and C-Band links. Table 2-4 presents a summary of the performance of this subsystem.

The Ground Attitude Control (GAC) decoder has successfully supported the check-out of the Spacecraft Attitude Precision Pointing and Slewing Adaptive Control (SAPPSAC) experiment.

2.3.5 Attitude Control Subsystem

The attitude control subsystem (ACS) met or exceeded specification requirements in all categories and, with the aid of a sophisticated software system at ATSOCC,

Table 2-1

Electrical Power Subsystem In-Flight Specification Compliance

Component/Parameter	Specification	In-Flight Performance
Solar Array Power @ PRU	555 Watts @ Summer Solstice	595 Watts @ Summer Solstice
Battery Capacity	17.5 Ampere-Hours @ $15^{\circ}\text{C} \leq T \leq 25^{\circ}\text{C}$	Not Measured. However, Battery Charge/Discharge Performance Has Been Excellent. Maximum Discharge 6.5 A-H.
Spacecraft Bus Voltage	$+30.5\text{v} \pm 2\%$	$+30.5\text{v} \begin{smallmatrix} +0.3\% \\ -0.9\% \end{smallmatrix}$
Battery 1 Charge Current Limit	$1.5\text{A} \begin{smallmatrix} +0.15\text{A} \\ -0.08\text{A} \end{smallmatrix}$	$1.5\text{A} \begin{smallmatrix} +0 \\ -0.03\text{A} \end{smallmatrix}$
Battery 2 Charge Current Limit	$1.5\text{A} \begin{smallmatrix} +0.15\text{A} \\ -0.08\text{A} \end{smallmatrix}$	$1.5\text{A} \begin{smallmatrix} +0 \\ -0.03\text{A} \end{smallmatrix}$
Battery 1 Volt/Temp Charge Taper Performance	$26.88\text{v} + 0.2\text{v} @ 17.4^{\circ}\text{C}$ $26.58\text{v} + 0.2\text{v} @ 22.8^{\circ}\text{C}$	$26.9\text{v} @ 17.4^{\circ}\text{C}$ $26.6\text{v} @ 22.8^{\circ}\text{C}$
Battery 2 Volt/Temp Charge Taper Performance	$26.88\text{v} + 0.2\text{v} @ 17.4^{\circ}\text{C}$ $26.58\text{v} + 0.2\text{v} @ 22.8^{\circ}\text{C}$	$26.8\text{v} @ 17.4^{\circ}\text{C}$ $26.5\text{v} @ 22.8^{\circ}\text{C}$
Load Interface CKT (LIC) For QCM	$28.0\text{v} \pm 0.45\text{v}$	27.9v^*
LIC (EME)	$28.0\text{v} \pm 0.45\text{v}$	28.0v^*
LIC (VHRR)	$28.0\text{v} \pm 0.45\text{v}$	28.0v^*
LIC (MMW 1)	$28.0\text{v} \pm 0.45\text{v}$	27.9v^*
LIC (MMW 2)	$28.0\text{v} \pm 0.45\text{v}$	27.9v^*
LIC (PROP)	$28.0\text{v} \pm 0.45\text{v}$	28.0v^*
LIC (ION 1)	$28.0\text{v} \pm 0.45\text{v}$	28.1v^*
LIC (ION 2)	$28.0\text{v} \pm 0.45\text{v}$	28.0v^*
LIC (Signal Conditioning)	$28.0\text{v} \pm 0.45\text{v}$	28.1v^*
Comm Regulator 1	$28.0\text{v} \pm 0.45\text{v}$	28.1v^*
Comm Regulator 2	$28.0\text{v} \pm 0.45\text{v}$	28.2v^*

*No discernable change in telemetered values, hence actual variation has been $< \pm 0.05\text{v}$, based on resolution of processed telemetry data.

Table 2-2

ATS Components Daily Temperature Variation

Day Hour		156 04:00	158 04:00	159 22:50	162 22:50
Component	Specification	°C			
SPS 1					
+ Yaw Valve	5 to 90	43.0	42.0	52.5	54.6
- Yaw Valve	5 to 90	33.0	32.0	45.1	44.3
Pr West Valve	5 to 90	15.8	15.6	21.6	25.0
Bu West Valve	5 to 90	13.6	13.0	24.1	23.7
Line, South	5 to 82	41.0	38.5	48.8	44.3
Line, Middle	5 to 82	35.0	34.5	40.2	40.4
SPS 2					
- Yaw Valve	5 to 90	88.0	76.0	70.8	70.8
+ Yaw Valve	5 to 90	71.0	64.1	59.0	58.7
Pr East Valve	5 to 90	85.0	81.6	71.1	71.3
Bu East Valve	5 to 90	87.0	83.9	73.9	73.9
Line North	5 to 82	66.0	63.7	52.4	52.8
Line Middle	5 to 82	62.0	60.8	48.4	48.7
ESA Pitch Head	-7 to 42	27.4	43.3	2.9	3.5
ESA Roll Head	-7 to 42	28.7	35.5	2.9	3.5
Battery 1	0 to 25	18.5	20.0	17.0	17.0
Battery 2	0 to 25	18.5	20.0	16.9	17.0
S-Band (Heat pipe 4)	5 to 35	28.8	24.0	23.8	23.3
TWTA (Heat pipe 6)	5 to 35	26.6	26.6	26.0	25.5
CM North	5 to 35	28.0	24.8	24.6	24.0
CM South	5 to 35	25.5	22.2	22.0	21.2
SM North	5 to 35	25.0	25.8	25.0	25.2
SM South	5 to 35	24.5	25.4	25.0	25.1
EM North	5 to 35	19.0	22.3	20.0	19.4
EM South	5 to 35	16.5	20.1	18.8	18.8
TLM XMTR 1	5 to 35	36.0	25.2	33.3	33.9
TLM XMTR 2	5 to 35	34.0	33.7	31.7	32.5
TLM XMTR 3	5 to 35	33.2	32.5	30.5	31.3
TLM XMTR 4	5 to 35	29.3	29.1	26.0	27.0
PRU	5 to 35	20.0	21.0	18.7	19.0
HET	5 to 35	28.8	23.8	20.0	23.4
UHF	5 to 35	25.1	22.1	20.8	21.4
EM MMW Dish	5 to 35	26.1	27.0	10.6	10.6
EM MMW Horn	5 to 35	18.4	20.0	9.8	9.7
ION Engine (Heat pipe 4)	5 to 35	19.8	22.3	22.0	21.2

Legend: Pr - primary, Bu - backup

Table 2-3

External Deployment Temperatures

Parameter	Specification	Predicted	Actual
Damper, Panel-End North	-48°C to 46°C	-7°C to 30°C	25°C
Damper, Panel-End South	-48°C to 46°C	-6°C to 30°C	26°C
S/A Boom 2nd Depl Hinge +Y	-140°C to 150°C	-55°C to 116°C	10 to 17°C
S/A Boom 1st Depl Hinge +Y	-140°C to 150°C	-55°C to 116°C	45 to 52°C
S/A Boom 2nd Depl Hinge -Y	-140°C to 150°C	-55°C to 116°C	2 to 7°C
S/A Boom 1st Depl Hinge -Y	-140°C to 150°C	-55°C to 116°C	48 to 55°C
Reflector Rib Sta 173 +Y	-18°C to 34°C	1°C to 18°C	10°C
Reflector Rib Sta 110 +X	-18°C to 34°C	3°C to 20°C	12°C
Reflector Rib Sta 110 -Y	-18°C to 34°C	0°C to 15°C	5°C
Reflector Hub -Y	-160°C to 60°C	-53°C to 35°C	11°C
Solar Array A2	-130°C to 72°C	-10°C to 20°C	-8°C to 15.5°C
Solar Array A5	-130°C to 72°C	-30°C to 45°C	-25°C to 40°C
Solar Array A3	-130°C to 72°C	-28°C to 38°C	-23°C to 32°C
Solar Array A8	-130°C to 72°C	-60°C to 58°C	-58°C to 53°C

Table 2-4

T&C Subsystem Performance Comparison

Parameter	Specification	In Flight Performance
XMTR. Frequency A1	136.23 \pm .003%	136.231469 +.0011%
A2	137.11 \pm .003%	137.109984 -0.000%
A3	136.23 \pm .003%	Has not been powered since launch
A4	137.11 \pm .003%	137.107742 -.0017%
EIRP. Power	-3 dBw min	EIRP not measured; Bit Error Rate (BER) $< 10^{-5}$.
DACU Bit Rate	390.625 \pm .00015%	7-Day check shows accurate to $< 0.00005\%$.
DACU Analog Cal. Voltage	Low 0.265 \pm 0.005 VDC Med 2.565 \pm 0.005 VDC High 5.095 \pm 0.005 VDC	0.265V \pm 0 2.565V \pm 0 5.095V \pm 0
FDM		FDM multiplexing of combined EME data, DACU normal data, and Earth sensor data, has been successfully demultiplexed at both ground stations since first day of flight, via the PFF/30 ft dish.
Receiver/CDD Command Threshold	-107 dBm	Actual margin about threshold is 15 to 27 dB with BER $< 10^{-5}$

proved to be relatively easy to monitor and control from the ground. A summary comparison of ACS performance relative to specification requirements is presented in Table 2-5; more detailed data and discussion may be found in Section 9.

ACS versatility and performance are illustrated in Figures 2-2 through 2-7. These figures were redrawn from graphic displays generated in real time during ACS in-orbit operations.

- (a) Figure 2-2 presents an earth intercept trace of the spacecraft Z-axis about ROSMAN during a programmed pattern maneuver used to generate ATS-6 antenna gain patterns. The 9-segment maneuver displayed was generated by an automatic programmed mode within the on-board digital operational controller (DOC). The mean distance of each slew is approximately 5° about ROSMAN.
- (b) One of the more interesting ACS maneuvers is depicted in Figure 2-3. This figure shows a typical series of events for tracking a NIMBUS low orbiting satellite by: (1) slewing the spacecraft from ROSMAN to the NIMBUS low orbiting satellite intercept point; (2) commanding the DOC into a programmed satellite track mode at the intercept time; (3) terminating the satellite track mode by offset point angle tracking just as NIMBUS goes behind the earth (satellite track can continue even with a low orbiting satellite behind the earth); and, (4) finally returning back to ROSMAN. The attitude errors in roll and pitch during the satellite track mode are shown in Figure 2-4. Attitude errors remained below 0.2 degree (specification value was 0.5 degree). The plot was obtained by comparing the actual real time earth sensor angles against those predicted from the NIMBUS ephemeris predict tables.
- (c) Figure 2-5 represents a time history plot of the interferometer output (in counts) converted to degrees during low jitter mode operation using the Earth Sensor Assembly (ESA). For the 30 minute segment shown, the total change in spacecraft angle as seen from the interferometer was ± 0.005 degree about a moving average. Since the spacecraft was pointing just south of the equator (ROSMAN is 5.8° north of the equator), the interferometer angle changed due to the effects of orbit inclination. The effect of this motion can be seen by the slight changing bias of the interferometer output, approximately 3 vernier counts or 0.0042 degree. The requirement for the mode of operation is an excursion of ± 0.01 degree in 24 minutes. Figure 2-5 indicates an improvement factor of two over the specification value.

When the interferometer was used as an attitude control sensor, pointing stability was better than 0.01 degree in the low jitter mode. When the interferometer is used in its open loop mode, it can be used as an attitude determination sensor. If it is operating in either a coarse only mode or alternating coarse/vernier mode,

Table 2-5

ACS Summary Performance

Mode	Parameter*	Spec	Actual
ABC Sun Acquisition	Time to acquire Pointing accuracy	30 minutes 4.5°	10 minutes 2°
ABCEarth Acquisition	Time to acquire Pointing accuracy	80 minutes 1.0°	50 minutes 0.35°
ABC Local Vertical	Pointing accuracy	1.0°	0.35°
DOC VHF Monopulse	Pointing stability	1.0°	0.5°
DOC S-Band Monopulse	Pointing stability	0.3°	0.01°
DOC C-Band Monopulse	Pointing stability	0.1°	0.002°
DOC Offset Point Ground **	Pointing accuracy	0.1°	0.049°
	Pointing stability	0.1°	0.01°
DOC Low Jitter**	Pointing accuracy	0.5°	<0.1°
	Pointing stability	0.01°	0.005°
	Rate stability (low freq.)	0.001°/sec	0.0003°/sec
DOC Satellite Track	Pointing accuracy	0.5°	<0.2°
DOC Offset Point Slew	Rate	≥0.5°/minutes	1.2°/minutes
	Settling time	≤10 minutes	<3 minutes
DOC Operational Modes	Yaw accuracy using PSA	0.15°	<0.1°

*Indicated parameters pertain to roll and pitch except for the first mode which pertains to pitch and yaw and the last mode which pertains to yaw.

**Either ESA or Interferometer.

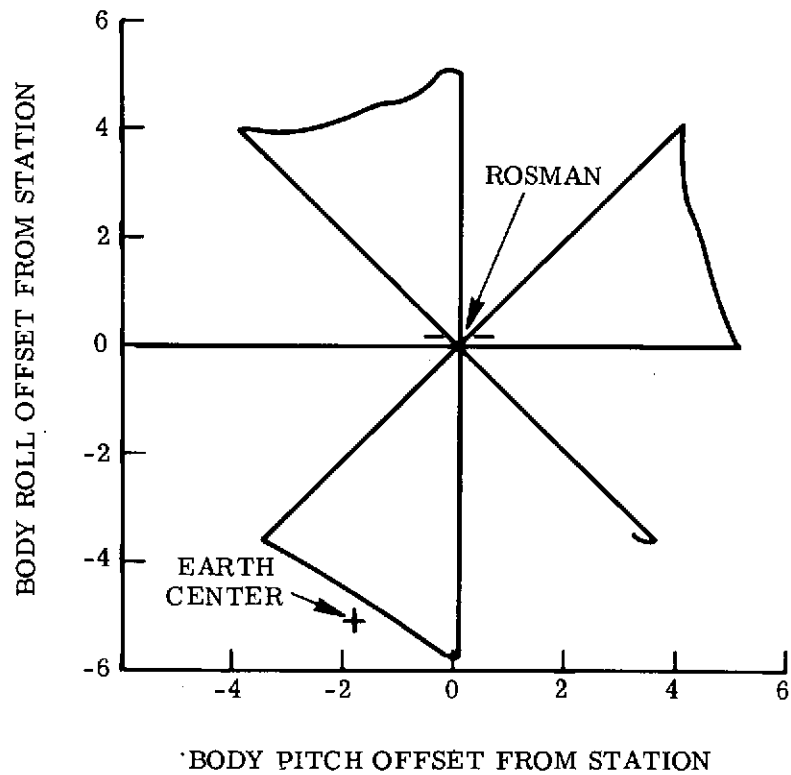


Figure 2-2. 5° Antenna Pattern Maneuver

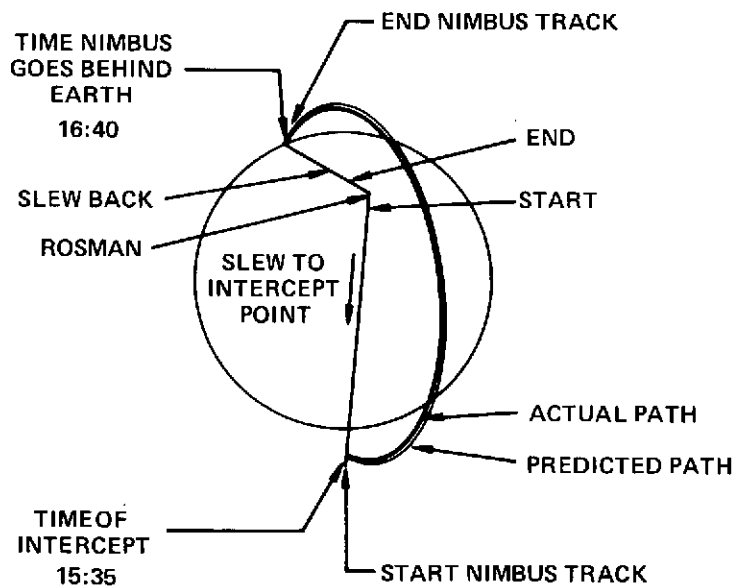


Figure 2-3. ATS-6 Satellite Track of Simulated NIMBUS June 12, 1974

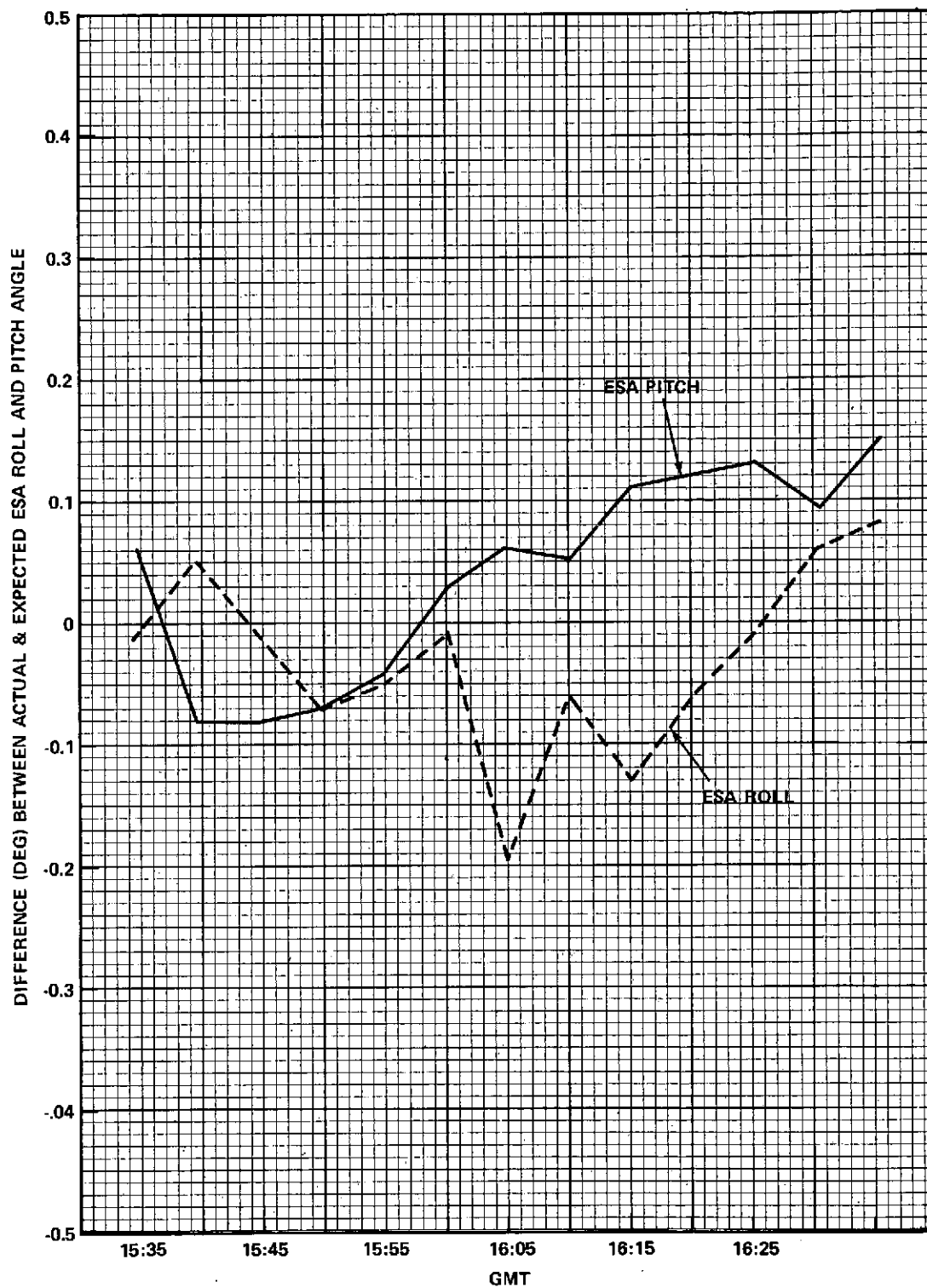
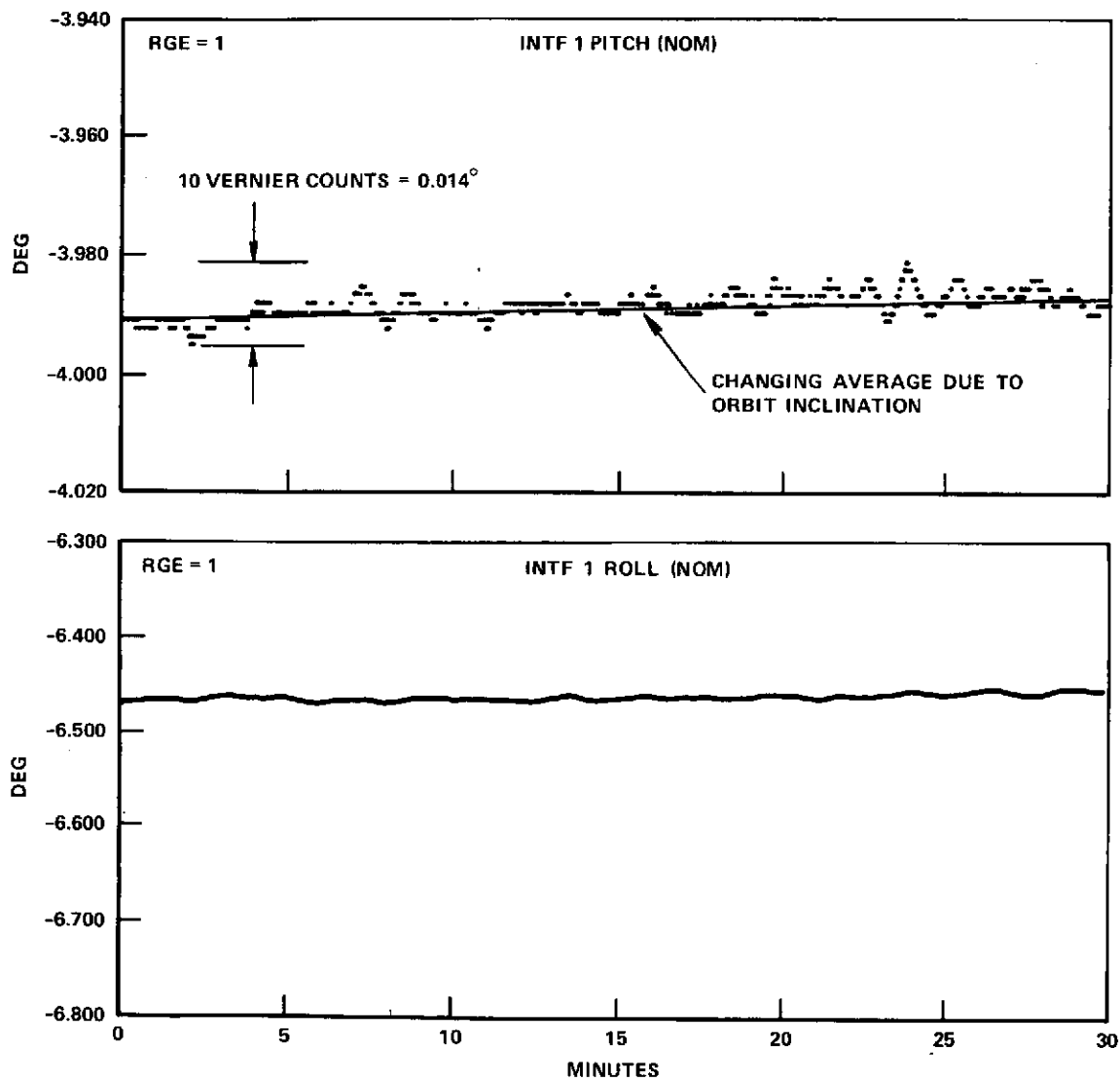


Figure 2-4. Satellite Track June 12, 1974 GMT = 163 DOC Ephemeris
Date GMT 160 Satellite Track NIMBUS Ephemeris GMT 163

INTF 1
DLO STATUS LOCK
INTF POWER ON



START 175:17:34:24.035

STOP 175:18:04:14.152

Figure 2-5. DOC Low Jitter Spacecraft Pointing at Local Vertical

roll and pitch attitude information can be obtained. If, in addition to the above configuration, the interferometer is placed in a dual frequency mode (F1/F2), yaw attitude information can also be obtained. This unique capability has been demonstrated at ATSOCC using the on-line attitude determination program called ONATT.

- (d) Station pointing using the monopulse roll/pitch error signals was successfully accomplished at VHF (153 MHz), S-Band (2253 MHz), and C-Band (6150 MHz). Pull-in range test information for S-Band is presented in Figure 2-6. Just prior to this test, the spacecraft had been in DOC S-Band monopulse for an extended period of time. The ground station signal was then purposely powered down. When the spacecraft had moved approximately 0.36 degree in roll and 0.56 degree in pitch, the rf ground carrier was turned on. The spacecraft then proceeded to pull within 0.01 degree of the S-Band boresight in a little over two minutes.

Figure 2-7 shows the characteristics of the C-Band monopulse in the control loop. The initial conditions for this example consisted of placing the interferometer in the control loop in the DOC Station Null Point mode. When the communication subsystem was configured for C-Band monopulse, the DOC was commanded to select C-Band monopulse in lieu of the interferometer. Pull-in range was approximately 0.1 degree in roll and 0.03 degree in pitch. Variations over the 50 minutes that the C-Band monopulse was in the control loop were about ± 0.002 degree with an offset of 0.03 degree in pitch and roll.

2.3.6 Spacecraft Propulsion Subsystem

Spacecraft Propulsion Subsystem (SPS) performance has been well within specification requirements. Because of the near perfect geosynchronous orbit achieved by the TITAN III C, fuel actually used to place the spacecraft on station (94° W longitude) was below that allocated. The total hydrazine used for the first fifteen days was 3.09 lb as shown in Table 2-6. This compares with a budgeted usage of 21.2 lb; while the total budgeted for the mission is 110.4 lb. At the present time, roll wheel unloading is required approximately every 2 days. Predictions are that 0.75 to 0.90 lb/yr will be required for wheel unload. A figure of 1.4 lb of fuel per year were budgeted for this purpose. Table 2-7 shows that the SPS thruster performance is nominal, however the thrust levels will reduce through the life of the spacecraft at a lesser rate than the reduction in tank pressure.

2.3.7 Communication Subsystem

The communication subsystem has supported the following major experiments:

- Health Education Telecommunications (HET)
- Television Relay Using Small Terminals (TRUST)
- Position Location and Aircraft Communication Experiment (PLACE)

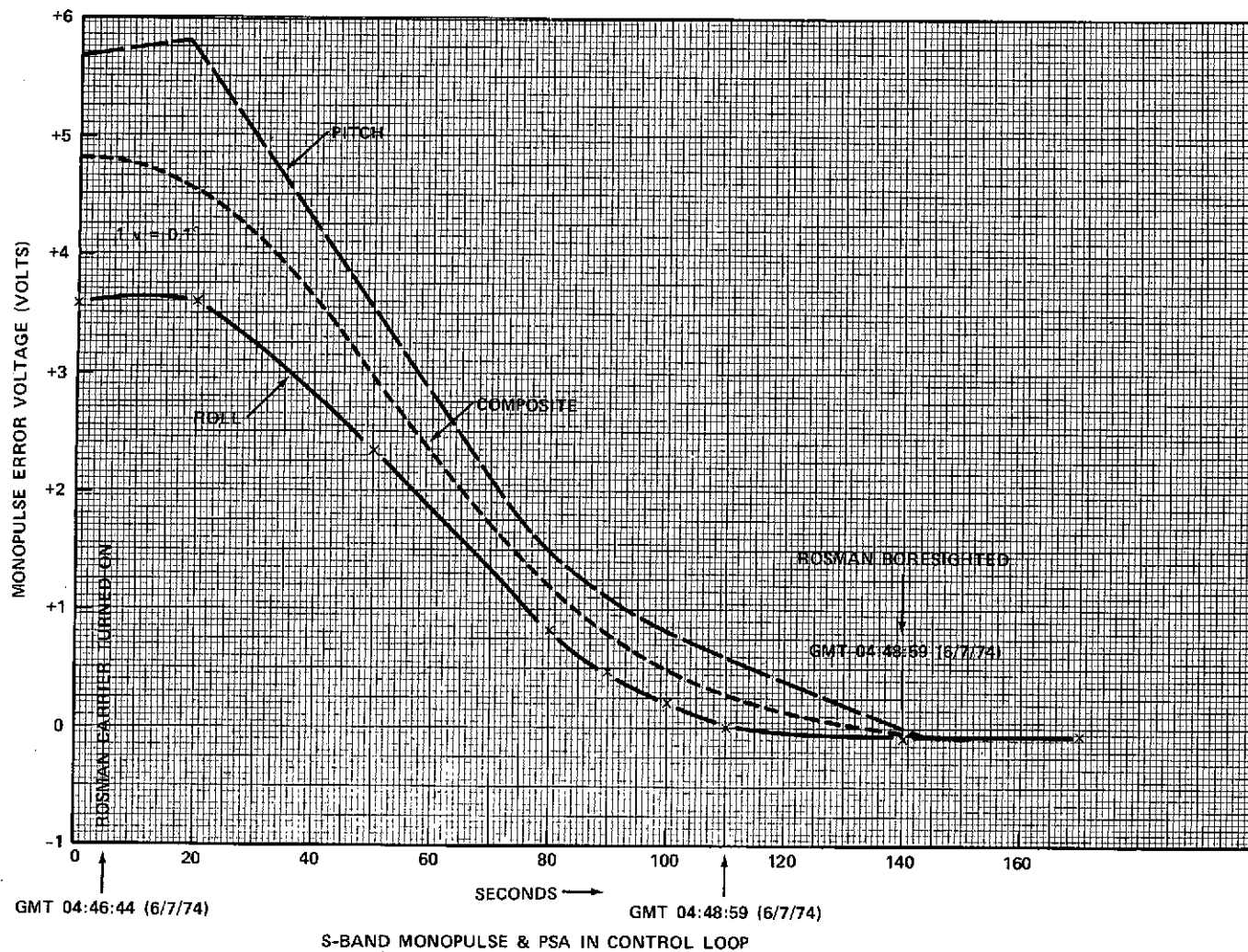


Figure 2-6. S-Band Monopulse Acquisition Test Using Carrier from ROSMAN
(135 seconds required to acquire)

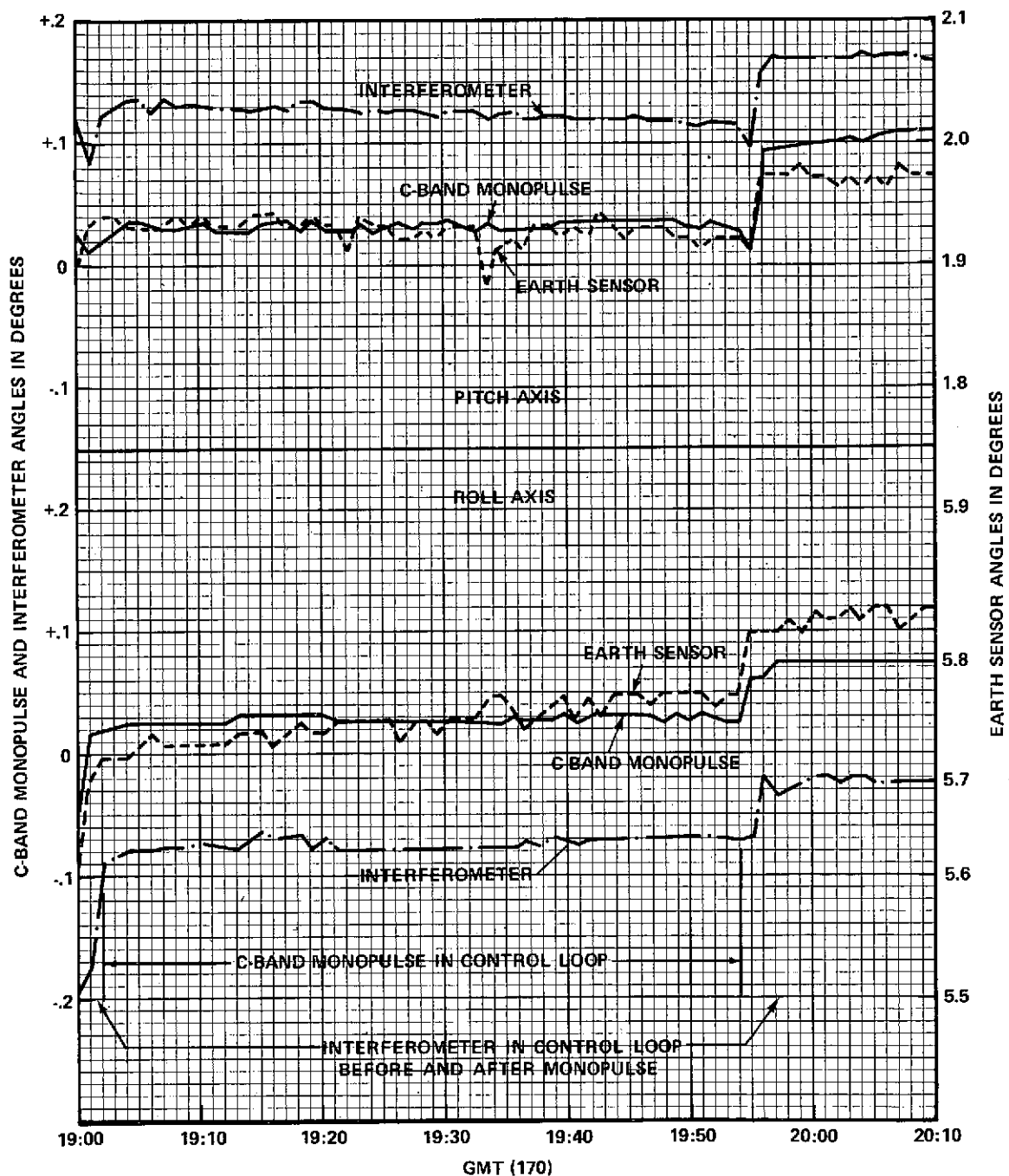


Figure 2-7. C-Band Monopulse Performance Sensor Angles Vs. Time

Table 2-6

SPS Fuel Usage

Purpose	Budgeted Fuel (lbs)	Fuel Used (lbs)
Initial acquisition of Sun, Earth 160° Yaw flip	2.09	1.43
Reacquisition of Sun, Earth, and Polaris	—	0.33
Initial orbit correction	19.11	1.28
11 Wheel Unloads	<u>—</u>	<u>0.05</u>
Total	21.20	3.09

Table 2-7

Thruster Performance

Axis	Change In Wheel Speed RPM	Number of Thruster Pulses	Predicted Impulse-Bit, Lbf-sec	Actual Impulse-Bit, Lbf-sec
Pitch	261	11	0.230	0.276
Roll	286	15	0.318	0.309

Tracking and Data Relay Experiment (TDRE)
Very High Resolution Radiometer (VHRR)
Radio Frequency Interference (RFI)

In addition, monopulse operation at VHF, S-Band and C-Band has been demonstrated.

Most experiments have now been declared operational, which means that activities are now regularly scheduled. In particular, the HET experiment is supporting Educational TV program transmission for the Appalachian Regional Commission and medical TV programs for the Veterans Administration on a weekly basis. VHRR pictures are being taken daily, and the other experiments requiring communication subsystem support are exercised as scheduled.

A preliminary summary of the communication subsystem performance is presented in Table 2-8. Results correlate closely with required values. The initial calculations of G/T and EIRP based on measurements at 2570 MHz and 2670 MHz were below expected values. However, additional tests have indicated that measurement techniques and uncertainties must be refined before definitive statements can be made. Effort is continuing in this direction. A more complete summary of communication subsystem performance will be forthcoming in the first quarterly report.

Figure 2-8 shows the S-Band on-axis receive antenna pattern taken during a N-S programmed antenna pattern maneuver exercise. The solid dots are the measured in-orbit values and the open dots are values taken during the hard dish antenna pattern measurements at Philco-Ford's antenna range. Figure 2-8 indicates very good in-orbit correlation with the test data. The slight bias shown is due to a sensor misalignment between the earth sensor (which was used in the attitude control loop) and the S-Band boresight. This bias is presently being determined and will eventually be programmed into the on-board Digital Operational Controller (DOC).

2.3.8 Experiments

Table 2-9 presents experiment objectives and the projected in-flight performance. Of all the experiments on ATS-6, only two experiments, Millimeter Wave (MMW) and the University of New Hampshire EME experiment have experienced potential failures. One of the two MMW 20 GHz TWTA's has failed to turn on. However, it is expected that 90% of the MMW experiment objectives should be met. The University of New Hampshire EME experiment caused significant electrical transients in the EME during the initial turn-on attempt. No further turn-on commands were issued; evaluation studies are underway.

Table 2-8

Communication Subsystem Performance Comparison

Frequency (MHz)	Antenna	Required G/T (dB/°K)		In-Orbit* G/T (dB/°K) Approx. Peak
		Peak	FOV	
6350	ECH	-17.0	-20.0	-14.0
6350	PFF	13.5	10.5	16.0
2250	On-Axis	9.5	—	10.4
1650	Fan	-2.0	-5.0	-2.6
		EIRP (dBw)		(dBw)
3950	ECH	26.0	24.1	25.7
3950	PFF	48.2	43.5	48.7
2670	S-2	52.3	48.9	TBD**
2570	S-1	52.3	48.7	TBD**
2075	On-Axis	51	—	52.5
1550	Fan	45	42	42.1
860	PFF	51	48	52.6

*Calculated values based on in-orbit measurements and available Rosman ground station parameter values.

**Requires refinement of ground station/spacecraft test set-up.

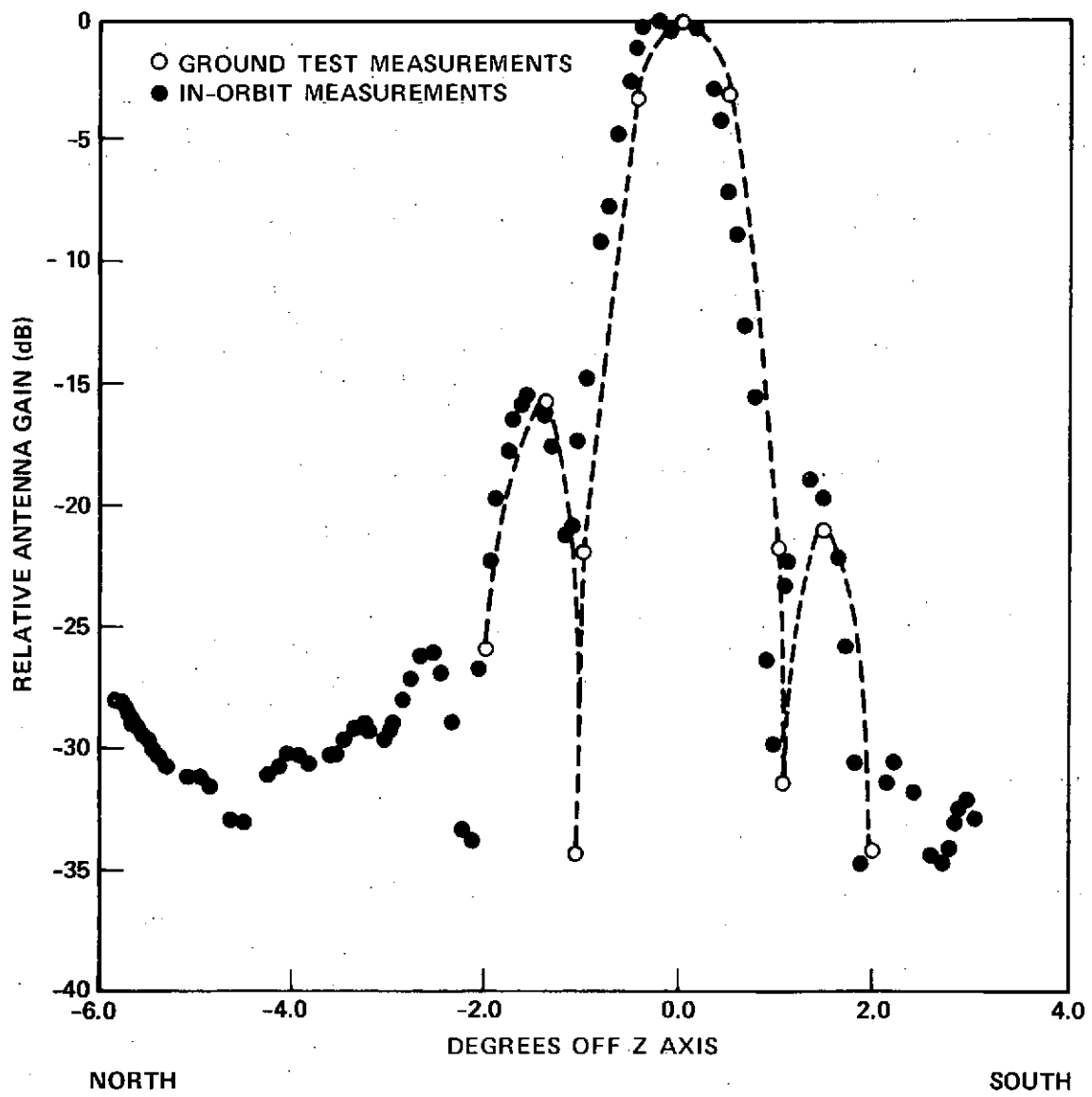


Figure 2-8. S-Band On-Axis Receive at Spacecraft

Table 2-9

Experiment Objective Summary

Experiment	Objective	Projected In-Flight Performance
Propagation	Evaluate site diversity in minimizing the effects of rainfall at millimeter-wave frequencies.	Both 13 GHz and 18 GHz units operated with performance in tolerance. Objective should be met.
MMW	Study the effects of meteorological conditions on propagation at 20 and 30 GHz.	30 GHz units satisfactory, potential 20 GHz transmitter failure. (1 of 2 TWTA's) Minimum 90% of objective should be met.
ATFE	Evaluate the performance of an active feedback Thermal Control System in space.	Experiment operational for 3 weeks. Objective should be met.
VHRR	Test feasibility of observing meteorological phenomena from a 3-axis stabilized satellite.	Experiment is operational. Visible and infrared scans have been successfully made. Data analysis in progress.
Ion Engines	Demonstrate use of an Ion microthruster for North-South station keeping.	Experiment not yet scheduled for operation.
QCM	Provide data on presence of contaminants on spacecraft.	Experiment has been operational since launch. Data analysis in progress. Objective should be met.
EME	Study the spacecraft environment at synchronous altitude.	All experiments have been operated. Anomaly occurred at UNH turn-on, and is being investigated. Objective should be met.
PLACE	To obtain engineering data and practical experience for determining the operational feasibility of an air traffic control satellite system operating in the aeronautical L-band.	Precision bore-sight pointing and operation of all communication links has been successfully demonstrated. Objective should be met.

Table 2-9 (Continued)

Experiment Objective Summary

Experiment	Objective	Projected In-Flight Performance
TDRE	Demonstrate the technology of command and telemetry data transmission between a low altitude satellite and ground station using a geosynchronous satellite as a communications relay.	Successful bore-sight tracking of a NIMBUS ephemeris and operation of all communication links have been demonstrated. Objective should be met.
SITE	Assess the potential value of satellite technology in establishing effective mass communications and instruction in developing countries.	Proper operation of the SITE communication link has been demonstrated. Evaluation of the UHF antenna pattern is underway with initial data being acceptable. Objective should be met.
HET	Evaluate the performance of satellite relay of educational programming and health care delivery to learning centers, hospitals, clinics, and community television distribution systems.	Checkout of the HET communication links has been successfully completed after an initial reversal of ground station polarization was corrected. Evaluation of S-band antenna patterns is underway. Objective should be met after all receiving terminals are properly polarized.

SECTION 3
FLIGHT CHRONOLOGY

SECTION 3

FLIGHT CHRONOLOGY

3.0 INTRODUCTION

ATS-6 was successfully launched into synchronous orbit at 13:00 GMT on Thursday, 30 May 1974. Injection occurred at 19:30:49 GMT into a near perfect orbit. The automatic separation and deployment sequence was successfully completed and the spacecraft was commanded through the sun and earth acquisition, and yaw reference sequences, and with all operations being completed by 02:19 GMT the day after launch. During the next two weeks of flight, the spacecraft was commanded into its normal in-orbit configuration and all systems were evaluated. Following this spacecraft checkout phase, a series of tests was conducted to evaluate the performance of the on-board experiment systems and their respective ground system interfaces. At the end of the first month of flight, all systems had been successfully evaluated with very few anomalies encountered, and the spacecraft was declared operational. An overview time-line for this period is presented in Figure 3-1.

The purpose of this section is to describe, in chronological order, the major orbital operations conducted during this period. Detailed information on the performance of each subsystem is presented in sections 5 through 12.

3.1 LAUNCH THROUGH SEPARATION

3.1.1 Launch

The spacecraft was launched at 13:00:01 GMT aboard the Titan IIIC launch vehicle, number C-27 (Figure 3-2). Spacecraft weight at the time of lift-off was 3078.3 pounds, including the 106.1 pound adapter which remained attached to the Transtage at spacecraft separation.

Prior to launch, the spacecraft was subjected to a series of launch preparation operations and tests at the launch complex culminating in the terminal count-down. During these operations, the spacecraft was commanded and monitored from the System Test Complex Control consoles in the A&E Hangar at Kennedy Space Center. Spacecraft telemetry data was also processed and displayed at ATSOCC via NASCOM during pre-launch and launch operations. This permitted final calibration of ATSOCC's data processing system and verification of ATSOCC launch readiness.

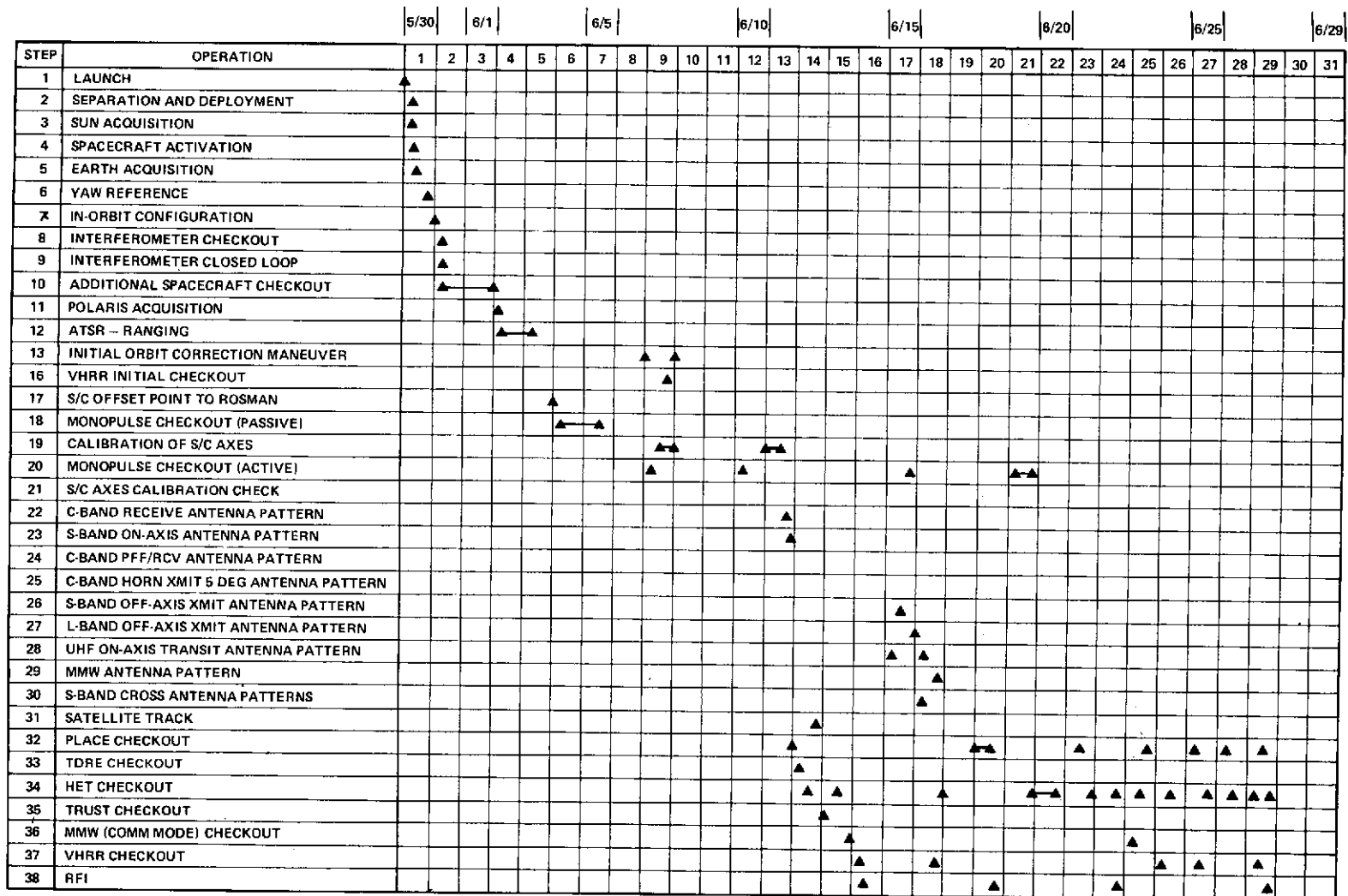


Figure 3-1. Spacecraft Mission Time-Line-First 30 Days

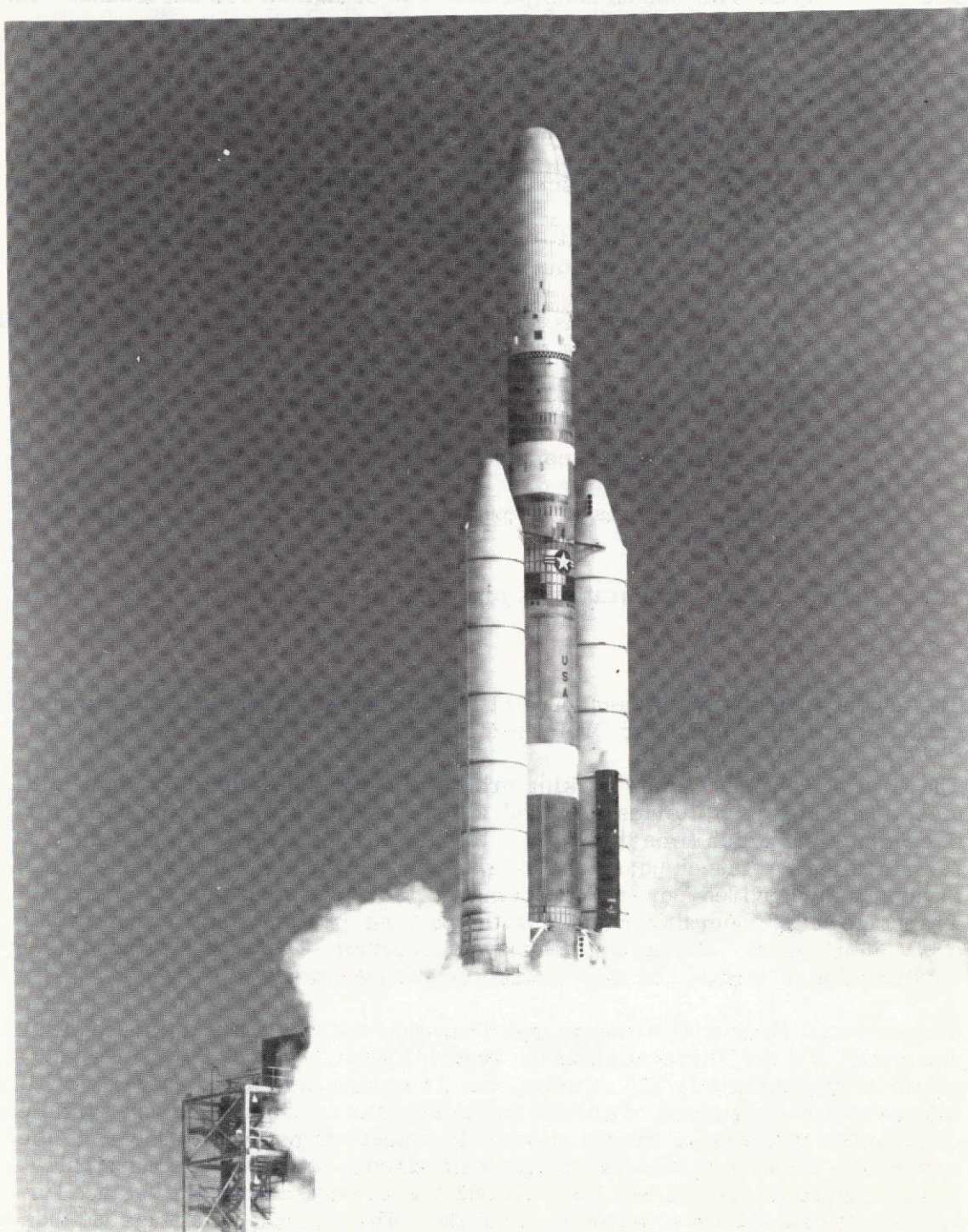


Figure 3-2. Titan III-C Launch Vehicle

The ATS-F Spacecraft launch configuration was established in accordance with the following criteria:

- Launch with spacecraft on internal power (batteries)
- Minimize load to avoid excessive battery discharge
- Provide for telemetry status monitoring
- Avoid requirement to transmit commands to spacecraft prior to separation from Titan Transtage
- Minimize commands required to effect sun acquisition immediately after separation and deployment
- Verify sun sensor performance prior to separation
- Power up selected components for vibration protection
- Minimize commands required to establish in-orbit baseline configuration

The resultant launch configuration is presented in Table 3-1.

3.1.2 Ascent

The ascent trajectory was composed of four orbital phases: Launch into park orbit, Park Orbit, Transfer Orbit, and Injection into Synchronous Orbit.

The first phase, launch into parking orbit, required approximately eight minutes. The internal batteries provided all spacecraft power during the first five minutes at which time the payload fairing was jettisoned. During the remainder of the launch phase and the parking orbit phase, the batteries and arrays both provided power, depending on the sun aspect angle. The Transtage and spacecraft remained in the parking orbit for approximately 1/2 orbit (66 minutes). During that time the spacecraft -Z Axis was pointed along the direction of motion and the -X Axis pointed southward.

At the second equatorial crossing, the Transtage engines fired to inject the spacecraft and the Transtage into the transfer orbit. During this phase, a period of approximately 316 minutes, the Transtage held the spacecraft Z Axis to within 30 degrees of normal to the sun line in order to ensure sufficient illumination of the solar arrays to provide spacecraft power and recharge the batteries. In addition, the Transtage maintained a roll rate (spacecraft yaw rate) of approximately 1 deg./sec. in order to provide a thermal balance for spacecraft components external to the EVM. The nominal Transtage attitude was interrupted three times during the transfer orbit for Transtage telemetry (TLM) readouts. These TLM dipout maneuvers, which lasted approximately 10 minutes each, occurred at approximately 100, 152, and 204 minutes after

Table 3-1

ATS-F Launch Configuration

SUBSYSTEM	COMPONENT CONFIGURATION	RATIONALE
SPS	<ol style="list-style-type: none"> 1) SPS 1 and 2 powered on 2) Tank 1 and 2 valves open; Truss 1 and 2 valves closed; EVM 1 and 2 valves closed; Cross line latch valve closed 3) SPS 1 and 2 prime valve heaters powered on 4) Signal Conditioning Box (SCB) Power On 5) SPS 1 and 2 prime and backup line heaters powered on, automatic, in low heat. 6) SPS 1 and 2 catalyst bed heaters off 	<p>Provide power for SPS instrumentation and valve heaters</p> <p>Permits hydrazine in SPS lines up to thruster latch valves; nitrogen in lines between thruster latch valves and thruster.</p> <p>Prevents freezing of hydrazine in valves.</p> <p>Provides telemetry for line heaters and Thermal Subsystem.</p> <p>Prevents freezing of hydrazine in SPS truss lines; minimizes possibility that a single point failure will result in unacceptably high (explosive) or low (freezing) hydrazine temperature.</p> <p>Not required until acquisition phase; off to reduce power requirements.</p>
ACS	<ol style="list-style-type: none"> 1) Analog, Digital, and Auxiliary Digital Sun Sensors powered on. 2) Polaris 2 sun shutter powered on. 3) RGA 1 and 2 powered on. 4) All other components off. 	<p>Enables verification of sensors during ascent and minimizes commands required for sun acquisition.</p> <p>Protects sensor optics from sun damage.</p> <p>Protects against launch vibration damage, enables verification during ascent, minimizes commands required for attitude acquisition.</p> <p>Minimizes S/C power requirements and battery discharge when solar panels are not illuminated.</p>
T&C	<ol style="list-style-type: none"> 1) DACU 1 in Normal and connected to 136 MHz and 137 MHz transmitters on omni antennas. 2) EME, Earth sensor pitch radiance signal, and DACU 2 are connected to the FDM, but are off. 3) Command receivers and CCD's are connected to the omni antennas. 	<p>Ensures full coverage, regardless of S/C attitude during ascent, separation, and acquisition.</p> <p>Minimizes commands after launch. Conserves power during launch.</p> <p>Ensures full coverage, regardless of S/C attitude during ascent, separation, and acquisition.</p>
COMM	Communication Subsystem is not powered (but is pre-configured for the Standby Mode).	Minimizes power requirements from launch through acquisition as well as minimizing commands required when the Standby Mode is eventually commanded.
POWER	Power Subsystem is in the Normal Mode (main regulating circuits and main chargers will be on with both batteries connected; C/10 charge rate will be on; all fault detecting circuits and non-essential loads will be on).	Power subsystem can be launched in the Normal Mode thereby not requiring any commands under nominal mission operations.
EXP.	<ol style="list-style-type: none"> 1) VHRR chopper motor powered on 2) VHRR sun shutter powered on 3) QCM powered on 4) All other experiments off 	<p>Protects exp. against launch vibrations.</p> <p>Protects exp. optics from sun damage.</p> <p>Obtain exp. data during Titan maneuver.</p> <p>Minimize power requirements.</p>

lift-off. At approximately T + 386 minutes, the Transtage was reoriented for the second burn. At T + 391 minutes, this second burn was accomplished and the Transtage and spacecraft were injected into synchronous (geostationary) orbit. The spacecraft separation command was issued by the Titan Programmer approximately three minutes later.

The predicted and actual times* for the major events during this period are presented in Table 3-2. The orbital parameters for the park; transfer, and synchronous orbits are summarized in Table 3-3 which is based on initial tracking data.

Spacecraft performance during the ascent period was nominal with no problems encountered. Good quality telemetry data was received continuously, except for the periods when the spacecraft was not in the field of view of a tracking station. Battery state-of-charge remained above 75 percent. Booster efficiency was calculated at approximately 89 percent. The ACS rate gyros and sun sensors appeared to be operating properly and readings correlated well with Titan-predicted and telemetered attitudes and rates. During the rotisserie maneuvers, the ACS yaw gyros indicated a rate of 0.98 ± 0.04 deg/sec; the rotation rate was actually 1.00 ± 0.05 deg/sec. The thermal control system operated satisfactorily and temperatures internal and external to the EVM were in the ranges predicted.

3.1.3 Separation

Spacecraft separation was successfully initiated by the Transtage at 19:33:21. The relative separation velocity was approximately 2 ft/sec. Spacecraft tip-off rates, as indicated by the ACS rate gyros, were as follows:

Roll:	0.22 deg/sec
Pitch:	0.11 deg/sec
Yaw:	-0.06 deg/sec

It was subsequently determined that roll rate gyro #1 had an offset error of 0.19 deg/sec. Since its output was being averaged with roll rate gyro #2 during this period, the actual tip-off rate in roll was approximately 0.13 deg/sec rather than 0.22 deg/sec as indicated by telemetry.

3.2 DEPLOYMENT

The automatic deployment sequence was initiated when ATS-6 had separated and cleared the rails attached to the Transtage. The rails were cleared at about 19:33:21 according to ATS rate gyro output changes. At 19:39:18, the 6 minute deployment timer completed its count to start the first deployment motion of releasing both booms from their launch configuration. Based upon rate gyro information, 6 minutes and 2 seconds had elapsed from separation to the start of motion. The first motion was nominally predicted to last 50 seconds, but actually took 74 seconds.

*Actual times derived from spacecraft telemetry are accurate to +3 seconds.

Table 3-2

Times of Major Events During Ascent Phase

Predicted Time	Actual Time	Event	S/C Source
13:00:00	13:00:02	Liftoff	roll, pitch, yaw gyros*
13:00:06	13:00:08	Begin Titan roll	yaw gyro
13:00:10	13:00:13	Begin Titan pitch	roll gyro
13:00:15	13:00:16	Begin Titan yaw	pitch gyro
13:00:30	13:00:31	Begin gravity turn	roll gyro
13:02:01	13:02:03	Jettison SRM's	yaw gyro
13:04:14	13:04:12	Stage two ignition	roll, yaw gyros
13:05:05	13:05:05	Jettison payload fairing	-Z ADSS, roll, pitch, yaw gyros
13:07:42	13:07:45	Stage two tailoff	roll, pitch, yaw gyros
13:47:50	13:26:52	Enter shadow (?)	-Z ADSS
14:21:50	14:22:39	Already left shadow	-X DSS
14:16:54	14:22:39	Already started thermal yaw	yaw gyro
14:40:10	14:40:03	Start reor for TM#5 dipout	pitch, yaw gyros
14:41:24	14:41:40	Reached TM#5 dipout	roll, pitch, yaw gyros
14:45:02	14:15:04	Start reor for thermal yaw	roll, pitch, yaw gyros
14:46:06	14:46:03	Start thermal yaw	roll, pitch, yaw gyros
16:24:20	16:24:21	Start rear for TM#7 dipout	pitch, yaw gyros
16:25:48	16:26:10	Reached TM#7 dipout	roll, pitch, yaw gyros
16:29:20	16:29:22	Start reor for thermal yaw	roll, yaw gyros
16:30:06	16:29:57	Start thermal maneuver	yaw gyros
18:08:38	18:08:42	Start reor for TM#9 dipout	pitch, yaw gyros
18:10:06	18:10:17	Reached TM#9 dipout	pitch, yaw gyros
18:13:38	18:13:40	Start reor for thermal yaw	yaw gyro
18:14:12	18:14:04	Start thermal yaw	yaw gyro
19:26:19	19:26:01	Start reor for T/S burn	roll, yaw gyro
19:27:21	19:27:06	Reached T/S burn attitude	roll, pitch, yaw gyro
19:28:49	19:28:30	T/S small limit cycle	roll, pitch, yaw gyros
19:28:55	19:28:35	Start T/S engines	yaw gyro
19:30:48	19:30:37	End T/S burn and reor for separation	roll, pitch, yaw gyros
19:31:09	19:30:59	Reached separation attitude	roll, pitch, yaw gyros
19:33:15	19:32:54	T/S large limit cycle	yaw gyro
19:33:41	19:33:21	Separation movement	roll, pitch, gyros

Note: Times are accurate within +3 seconds.

*Gyros are the Spacecraft rate gyros.

Table 3-3

ATS-6 Park, Transfer, and Synchronous Orbit Parameters

PARK ORBIT				
	<u>6D Predict</u>	<u>Titan</u>	<u>ETR</u>	<u>Goddard</u>
period (minutes)	92.31		92.2	92.2
apogee height (km)	622.59	(not	611.0	616.28
perigee height (km)	160.8	available)	161.1	148.02
inclination (degrees)	28.612		28.621	28.587
TRANSFER ORBIT				
	<u>6D Predict</u>	<u>Titan</u>	<u>ETR</u>	<u>Goddard</u>
period (minutes)	636.95	636.8	636.9	629.9
apogee height (km)	35,788.1	35,601.7	35,789.9	35,952.3
perigee height (km)	500.74	495.6	488.2	486.9
inclination (degrees)	26.427	26.405	26.449	26.349
SYNCHRONOUS ORBIT				
	<u>6D Predict</u>	<u>Titan</u>	<u>ETR</u>	<u>Goddard</u>
period (minutes)	1,436.69		1,435.6	1,436.312
apogee height (km)	35,821.20		35,806.6	35,818.38
perigee height (km)	35,775.27		35,747.3	35,763.23
inclination (degrees)	1.811	(not	.1794	1.785
sub-sat longitude		available)		
(degrees)	-94.487		-94.420	-94.691
drift rate	0.16°/ day W.		0.11°/ day E.	0.05°/ day W.

The deployment timer again counted to about 6 minutes and enabled the start of the second motion, the skewed hinge release, at 19:46:34. The +Y boom locked into position at 19:50:03. However, the -Y boom did not lock until about 20:02:00. The predicted duration for both events was 200 seconds. The actual deployment time for the +Y boom array was 203 seconds, but the deployment time for the -Y boom array was 802 seconds. The cause of this delay is under investigation. The deployment timer again counted to about 6 minutes and the reflector deployment began 20:08:03. The reflector deployment duration was less than 3 seconds, according to the rate gyros and the timer.

The deployment timer counted for the fourth and last time and enabled final boom motion at 20:14:14, 6 minutes and 11 seconds after reflector deployment. The deployment motion was complete at 20:14:32. Fourth motion duration was actually 18 seconds versus the predicted 10 seconds.

The body rates during the entire deployment sequence, starting at separation, never exceeded 0.23 degrees per second in roll, 0.10 in pitch, and 0.49 in yaw. Table 3-4 summarizes the separation and deployment timelines. Table 3-5 presents the external temperature profile of the spacecraft during deployment.

3.3 ACQUISITION

3.3.1 Sun Acquisition

Following deployment, the ACS was activated, SPS 1 lines were purged of nitrogen, and the sun was successfully acquired as planned using the Analog Backup Controller (ABC), the Rate Gyro Assembly (RGA), the Course/Fine Sun Sensors (CFSS), and jets. Figure 3-3 presents a plot of the spacecraft + roll (+X) axis angle to the sun line during the acquisition maneuver. At the start of sun acquisition, the spacecraft attitude relative to the sun was a Sun azimuth = -50 degrees and a Sun coelevation = -42 degrees (as defined in Figure 3-4). The +X Fine Sun Sensor (FSS) Presence occurred within 6 minutes and 50 seconds and sun acquisition was completed in 10 minutes. No significant overshoot of the +X axis occurred. Conditions at the end of sun acquisition were 0.0 degrees in pitch and 2.2 in yaw. The rates were 0.05, 0.08, and 0.08 degrees per second in roll, pitch, and yaw respectively. Pseudo rate with wheels as torquers was commanded prior to start of earth acquisition. The maximum wheel speeds observed were approximately 250 and 150 RPM in pitch and yaw; roll control is not active in this mode.

3.3.2 Spacecraft Activation

After sun acquisition was completed, the Digital Operational Controller #1 (DOC 1) was powered on (in the monitor mode) and its status was confirmed. EME was powered on, including heaters and the Magnetometer experiment. The quality of the EME data could not be ascertained since the spacecraft had not been configured to transmit EME telemetry. The ATFE experiment was also activated at this time. The communication subsystem was commanded into the "Standby Mode" in preparation for activating the Interferometer. The VHRR cone and patch heaters were also powered on during this sequence.

Table 3-4

Separation and Deployment Time
(Derived from ATS-6 Discrete Event Telemetry)

Event	Time
SEPARATION ENABLE	150:19:33:18
CLEAR SEPARATION RAIL	19:33:21
BOOM RELEASE ENABLE	19:39:18
BOOM RELEASE	19:39:23
+Y BOOM AT 121°	19:40:25
-Y BOOM AT 121°	19:40:34
ARRAY UNFOLD ENABLE	19:46:34
+Y BOOM UNFOLDED	19:50:03
-Y BOOM UNFOLDED	20:02:00
REFLECTOR RELEASE ENABLE	20:08:03
REFLECTOR DEPLOYED	20:08:12
BOOM DROP TO 90° ENABLE	20:14:14
+Y BOOM DROP TO 90°	20:14:29
-Y BOOM DROP TO 90°	20:14:32

Table 3-5

External System Temperatures During Deployment

Day: 150 GMT 19:32:28 Through 20:19:09				
<u>Component</u>	<u>Deploy. Temp. Range</u>	<u>Expected Temp.</u>		
		<u>Max.</u>	<u>Min.</u>	
Boom Hinge 1 - Y	48 ^o to 55 ^o C	100 ^o C	-15 ^o C	
Boom Hinge 2 - Y	2 ^o C to 7 ^o C	100 ^o C	-15 ^o C	
Boom Hinge 1 + Y	45 ^o C to 52 ^o C	100 ^o C	-15 ^o C	
Boom Hinge 2 + Y	10 ^o C to 17 ^o C	100 ^o C	-15 ^o C	
North Damper	25 ^o C	2 ^o C	- 5 ^o C	
South Damper	26 ^o C	-5 ^o C	-10 ^o C	
Refl. Hub (N)	11 ^o C	15 ^o C	10 ^o C	Stowed
Rib St. 110 (N)	5 ^o C	13 ^o C	0 ^o C	
Rib St. 110 (E)	12 ^o C	15 ^o C	10 ^o C	
Rib St. 173 (S)	10 ^o C	30 ^o C	10 ^o C	
Exp. Average T				
Sol Array A2	- 8 ^o C to 15.5 ^o C	5 ^o C		
Sol Array A5	-25 ^o C to 40.0 ^o C	5 ^o C		
Sol Array A3	-23 ^o C to 32.0 ^o C	5 ^o C		
Sol Array A8	-58 ^o C to 53 ^o C	5 ^o C		

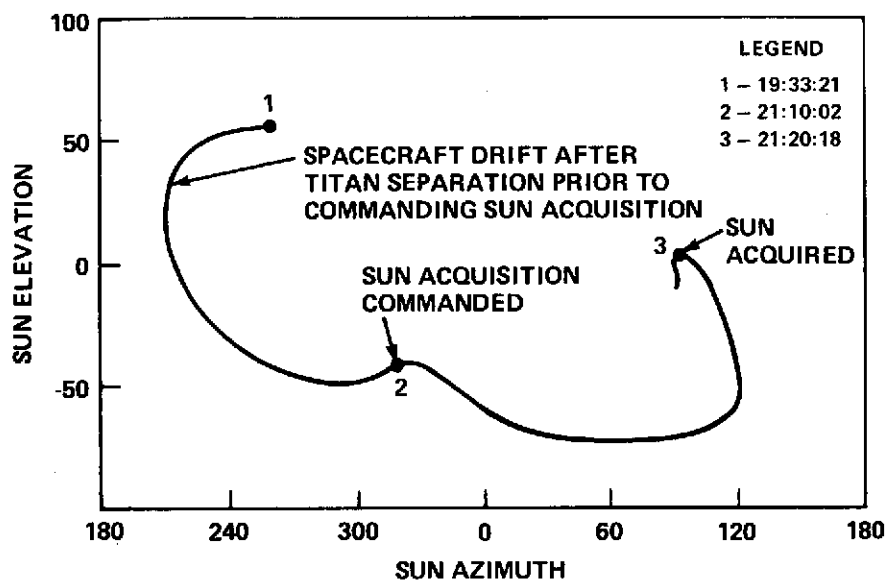


Figure 3-3. Sun Acquisition

\hat{U} = UNIT POINTING VECTOR TO
EXTERNAL OBJECT OF INTEREST

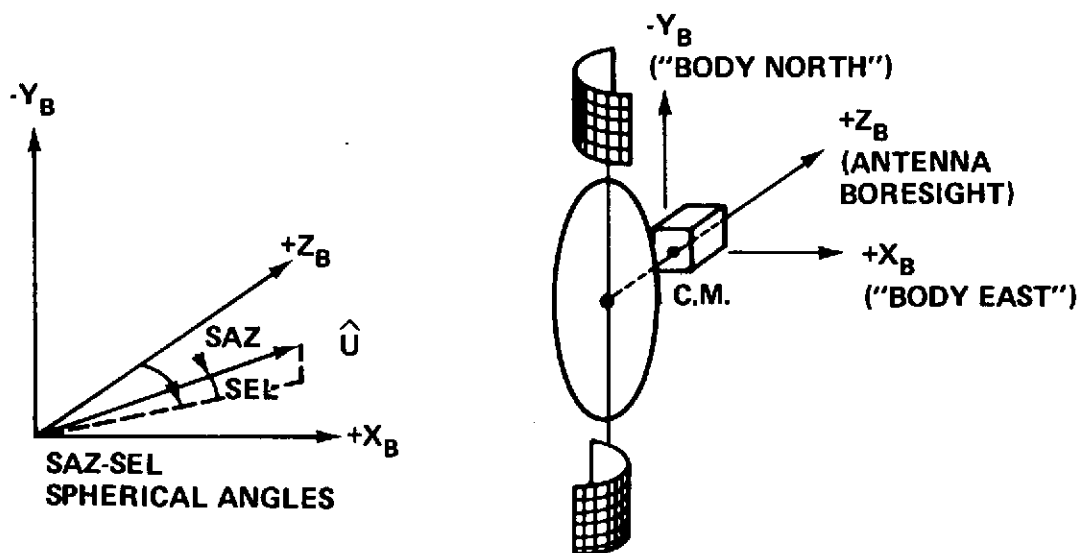


Figure 3-4. ATS-6 Body Coordinate System

3.3.3 Earth Acquisition

The Earth Sensor Assembly (ESA) was turned on 19 minutes prior to the start of earth acquisition. At 21:10, ABC Earth Acquisition was commanded. At the start of earth acquisition, the roll jets fired to develop an apparent spacecraft roll rate of $-0.27^\circ/\text{sec}$. The earth was acquired at approximately 21:20, but with a 2° limit cycle and 7 degree offset in roll. RGA 1 indicated an apparently erroneous roll rate of $-0.19^\circ/\text{sec}$ rate. When rate control was switched from RGA 1 to RGA 2, the ACS successfully completed the earth acquisition maneuver to within 0.35° of local vertical. Spacecraft control for earth acquisition was maintained with the ABC using the Earth Sensor for roll and pitch control and the Coarse/Fine Sun Sensors (C/FSS) for yaw control. Torquer control was switched from jets to wheels after the spacecraft had settled. Because earth acquisition was commanded during the evening terminator as planned, the spacecraft +X axis was pointing westward and the -Y axis was pointed south. Since the nominal flight attitude requires the +X axis to point eastward, and the -Y axis to point north, the flight plan required a near 180-degree yaw maneuver (rotation) to properly orient the spacecraft.

3.3.4 Yaw Reference Maneuver

Following completion of earth acquisition, the Yaw Inertial Reference Unit (YIRU) was checked out prior to its use as the yaw axis sensor. The Telemetry and Command (T&C) subsystem was configured at this time into its normal orbit mode: 1) DACU 2/EME on FDM on the 137 MHz transmitter No. 2 over the Prime Focus Feed (PFF) using the 30 foot dish; and 2) the 154 MHz command receiver switched to the PFF. When the T&C subsystem was switched to the PFF, approximately 11dB increase in carrier to noise ratio was measured both at the ground and the spacecraft.

At approximately 23:45, the spacecraft yaw maneuver was begun by commanding the ABC into a Polaris Winter Acquisition Mode using jets and RGA 2. When the spacecraft X axis was pointed to approximately 20 degrees below the sun (placing the +X axis nearly due east), yaw control was commanded from the RGA to the YIRU. The total time for the completion of the 200 degree yaw maneuver was 33 minutes. Figure 3-5 depicts the trace of this maneuver starting with the -X axis pointing at the sun (0 degree sun elevation) and ending with the spacecraft +X axis pointing east in the orbit plane (20 degree sun elevation).

3.4 IN-ORBIT RECONFIGURATION AND SPACECRAFT CHECKOUT

Following completion of the initial acquisition sequence, the spacecraft was re-configured for orbital operations. The 6-hour timer was checked out and DOC 2 was powered on. Ephemeris data blocks were loaded into both DOC's followed by memory dumps. Analysis of the memory dumps showed both on board digital controller memories unperturbed by the launch. At 13:56 on May 31, 1974, DOC 1 was placed in the ACS control loop using the ESA and YIRU as sensors and the wheels as torquers in the local vertical pointing mode. In the Local Vertical Orbit Plane East mode, the +X axis is aligned in the orbit plane nominally due east and the +Z axis is aligned along the local vertical.

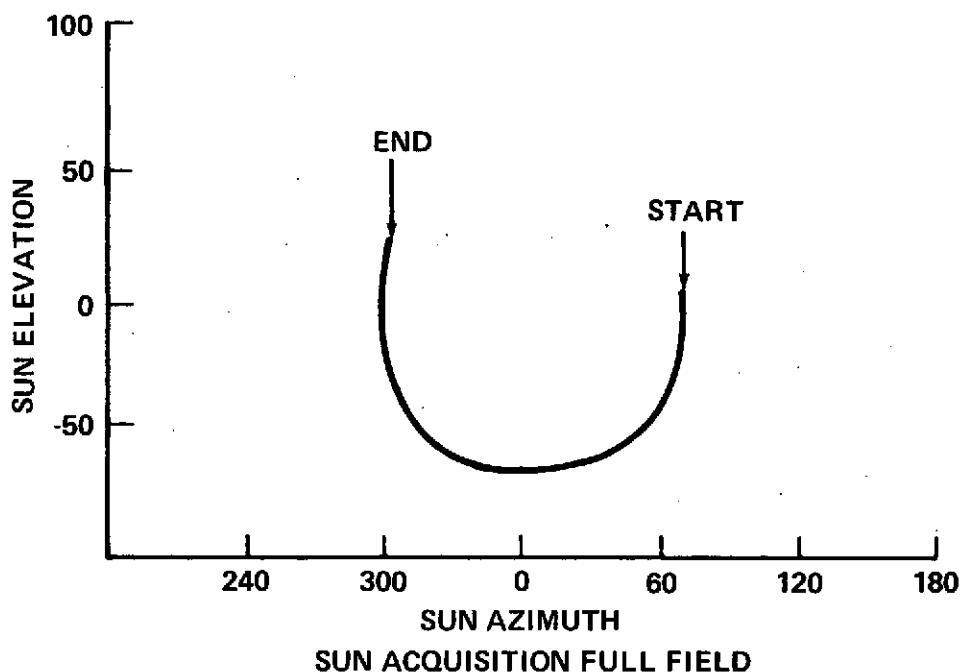


Figure 3-5. 200°-Yaw Maneuver

ATS-6 checkout procedures were conducted from the ATS Operations Control Center (ATSOCC) using an automated computerized test procedure (ref. ATS-6 Initial In-Orbit Operations Procedure, Fairchild Industries document 862-OP-306 dated May 17, 1974). These procedures, previously "debugged" against the spacecraft computer simulator (ATSSIM), were used from launch through the entire spacecraft checkout time period.

3.5 CHRONOLOGY OF SPACECRAFT ACTIVITY (DAYS 2-18)

<u>DAY</u>	<u>ACTIVITY</u>	<u>REMARKS</u>
2	In-orbit Configuration	Configured spacecraft to support planned checkout
		6 hr timer checkout
		DOC 2 turn on and checkout
		DOC ephemeris update and memory dumps
		YIRU calibration
		DOC control using ESA/DSS and ESA/YIRU

<u>DAY</u>	<u>ACTIVITY</u>	<u>REMARKS</u>
	Interferometer Checkout <ul style="list-style-type: none"> ● Passive/Active ● Closed Loop 	<p>Active checkout nominal for 6150 and 6155 MHz frequencies in both modes (coarse and vernier) and both ground stations (ROSMAN and MOJAVE)</p> <p>Closed loop functioned well for both frequencies</p> <p>Interferometer/DOC interface works well for P&R control</p>
3	Additional Spacecraft Checkout	<p>DOC local vertical control mode</p> <p>DOC offset point, ground coordinates (0° lat, 94° W. long)</p> <p>VHF monopulse (monitor only)</p> <p>Radio beacon checkout (no interference problem)</p>
4	Polaris Turn-on	<p>Polaris successfully acquired using gate #3</p> <p>No evidence of arcing or corona</p> <p>Bright object disturbances causing repeated losses of star acquisition</p> <p>Decreased sensitivity forces constant usage of gate #3</p>
	ATS ranging <ul style="list-style-type: none"> ● C-Band Checkout ● TV Camera On ● ATS-R 	<p>C-band checkout showed 0.12 to 2.0 dB glitches* as reported by both Rosman and Mojave ground stations</p> <p>TV camera turn-on was successful. Early pictures showed fully deployed antenna and booms. C-band glitches do not affect the quality of the TV pictures</p> <p>Ranging was conducted for fifteen hours for orbit determination</p>

*Power Dips in Ground Station Receiver AGC's.

<u>DAY</u>	<u>ACTIVITY</u>	<u>REMARKS</u>
5	C-Band TWTA's and Polaris Turn-Off	Hi-voltages were turned off to permit further outgassing and to permit analysis of glitches
6	Offset Point to Rosman	Spacecraft commanded to offset point at equator. Slewed to Rosman and offset point ground coordinates at Rosman.
	Monopulse Checkout (Passive)	Low jitter mode then commanded. Sequence worked excellent.
		Comprehensive checkout of VHF, S-band and C-band monopulse performed while slewing spacecraft to different angles around Rosman. VHF shows significant interference from other earth radiating ground stations.
7	C-Band Turn-On	Glitches still present
	Initial Orbit Correction Maneuver	Fired westward control jet for 480 sec to reduce orbital drift from approx. 0.27° W/day to 0.20° W/day using approx. 0.3 lb of fuel
	ATS-Ranging	Ranged for twenty-four hours to measure accuracy of initial orbit correction maneuver
	C-Band Glitch Investigation	Conducted 16 hrs of cycling all equipment on and off to ascertain cause of C-band glitches. Equipment cycling and usage of redundant equipment did not affect the glitches. Commanding the 10 dB attenuator pad into the I. F. decreases the frequency and amplitude of the glitches in both transmitters. This is the normal mode of operation for C-band usage.
8	Polaris Turn-On and Polaris Yaw Control	Bright object disturbances still present PSA used successfully for yaw control

<u>DAY</u>	<u>ACTIVITY</u>	<u>REMARKS</u>
		Slewed from local vertical to Rosman with ESA and PSA as sensors
	VHRR/IHSDL Checkout	Successfully completed. VHRR pictures were of a good quality. IHSDL works well. Spacecraft in low jitter mode on interferometer during this exercise. VHRR checkout nominal.
9	Final Orbit Correction Maneuver	Fired for 31 mins for final orbit correction. Total fuel consumption was approx. 1.3 lbs of fuel for both maneuvers. Final drift was 0.05° E/day.
10	Calibration of Spacecraft Axes	Calibration of interferometer. Relative sensor misalignments recorded. Data is still being analyzed.
11	Monopulse Checkout (Active)	Checked VHF, S, and C-band monopulse in the control loop.
		S-band worked well; need better pointing at Rosman to fully evaluate C-band (sensor misalignments).
	Propagation Checkout	Nominal
	ATFE Checkout	Nominal
12	L-Band and S-Band Solid State Turn-On	Nominal—no problems
13	C-Band ECH Receive Antenna Pattern	C-band earth coverage horn receive antenna pattern has been completed.
	S-Band On-Axis Antenna Pattern	Antenna patterns completed for <ul style="list-style-type: none"> ● S-band on-axis receive ● S-band on-axis 3 transmit ● S-band on-axis 5 transmit

<u>DAY</u>	<u>ACTIVITY</u>	<u>REMARKS</u>
14	PLACE Checkout	Successfully completed
	TDRE Checkout	Satellite relay link using NIMBUS simulator at Rosman completed.
	Satellite Track	Satellite track mode successfully completed using NIMBUS-5 ephemeris data.
15	UHF Turn-On	Nominal--no problems
	HET Checkout	Ground terminals appear to be RCP as opposed to spacecraft which is LCP. All seven sections of checkout were successfully demonstrated. Glitches have been periodically observed on the HET transmitters.
	MMW (Comm Mode) Checkout	Compatibility of MMW/Comm subsystem interface successfully demonstrated.
16	RFI Checkout	Nominal
	TRUST Checkout	Spacecraft configured to TRUST mode while ground station performed TRUST experiment. Proper spacecraft operation was demonstrated.
17	UHF Antenna Pattern	UHF 5° transmit antenna pattern successfully completed
	EME Checkout	Successfully completed
	Two Station Interferometer	Successfully demonstrated
	S-Band and C-Band Xmit Antenna Patterns	Successfully completed using 3° cloverleafs for S-band off-axis and 5° patterns for C-band horn XMIT
18	S-Band Cross Axis Antenna Pattern	Antenna patterns successfully completed by slewing 6°E, W, N, and South respectively.

<u>DAY</u>	<u>ACTIVITY</u>	<u>REMARKS</u>
	L-Band Pencil Transmit Antenna Pattern	Successfully completed
	L-Band Fan Transmit and Receive Antenna Patterns	Successfully completed
	MMW Antenna Pattern	Antenna patterns successfully completed for 30 GHz horn and 30 GHz parabolic antenna. No pattern for 20 GHz horn was received due to H.V. failure.

SECTION 4
SPACECRAFT DESCRIPTION

SECTION 4

SPACECRAFT DESCRIPTION

4.1 INTRODUCTION

The ATS-6 spacecraft is comprised of the following subsystems:

- a) Structural/Deployment
- b) Electrical Power
- c) Thermal Control
- d) Telemetry and Command
- e) Attitude Control
- f) Spacecraft Propulsion
- g) Communication
- h) Experiments

These subsystems are briefly described in the following paragraphs. Further subsystem details may be found in the ATS-F Spacecraft Reference Manual (Ref. NASA Document X-460-74-154, dated May 1974).

Performance requirements of the ATS-6 spacecraft are defined in Spacecraft System Specification 862-0001D.

4.2 STRUCTURAL/DEPLOYMENT SUBSYSTEM

The Structural/Deployment Subsystem accomplishes the following functions: It provides the packaging required for electronic and electro-mechanical equipment necessary to fulfill the spacecraft mission, the physical means of integrating the Spacecraft and the TITAN III-C launch vehicle, and the means for deploying the solar paddles and parabolic reflector.

The Structural/Deployment Subsystem (Figure 4-1) is comprised of the following elements:

a) Solar Panel and Boom Assembly

Each solar array is made up of sixteen solar panels in semicylindrical form, and has an approximate radius of 54 inches and a length of 94.6 inches. Each array is attached to the end of a support boom that is mounted to the structural hub. Each of the sixteen panels (thirty-two total) is covered with solar cells.

b) Parabolic RF Reflector

The reflector is a 30-foot diameter parabola consisting of flexible aluminum radial ribs supporting mesh that forms a paraboloidal surface. It has a focal length-to-diameter (F/D) ratio of 0.44. During launch the reflector is stowed in a toroidal-shaped container with an outside diameter of about 78 inches.

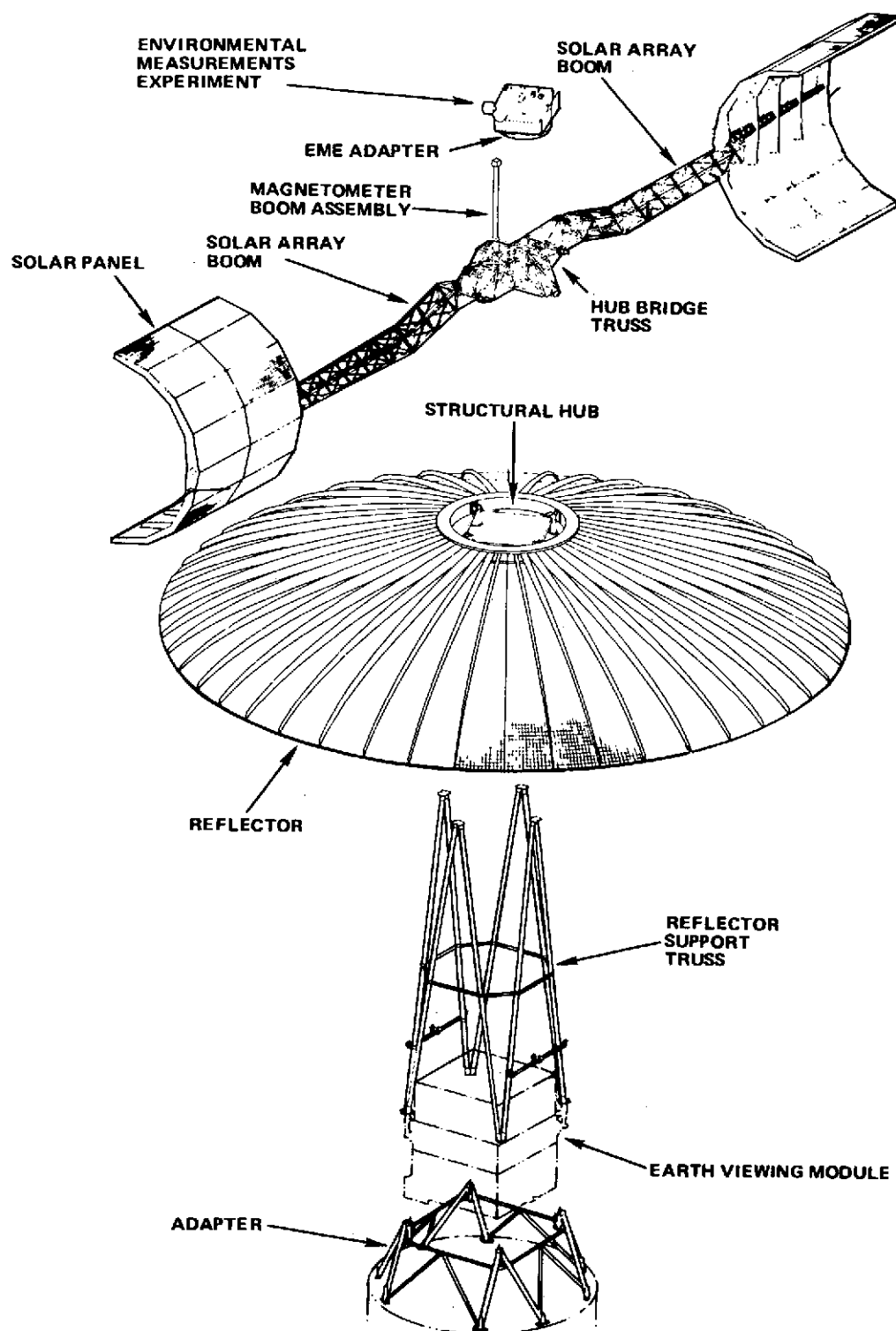


Figure 4-1. Spacecraft Structural/Deployment Subsystem Elements.

When deployed, the ribs unfurl to form the parabolic shape.

c) Reflector Support Assembly

The reflector and solar array trusses are mounted to the structural hub, which is formed like an open square, 41 inches on a side, and 6 inches deep. The Earth Viewing Module (EVM) and the structural hub are interconnected by the reflector support truss, which consists of eight tubular members arranged in a square symmetrical A-frame configuration. The top ends are joined to the four corners of the structural hub. The bottom ends are joined to the adapter and to the EVM at the midpoints of each of the four vertical edges of the EVM.

d) Earth Viewing Module (EVM)

The EVM basic structure is a near cube, 54 inches on a side by 65.45 inches high made up of three subsections. The lower subsection is designated the Experiment Module and contains most of the experiments and all of the earth-viewing sensors. The middle section of the EVM is called the Service Module and contains components of the electrical power subsystem, the telemetry and command subsystem, and the attitude control subsystem. The topmost section is the Communications Module and contains the transponder and three experiments closely associated with the communications subsystem. The prime focus feed for the high gain antenna system is mounted on the top surface of the EVM.

e) Titan Adapter/Separation Assembly

The Adapter Assembly consists of four tubular elements with end fittings which, when bolted to the TITAN III-C form inverted "V's". The adapter provides a surface for the separation system, houses the separation springs and retains the separation pyrotechnic device after separation. The height of the adaptor is approximately 39-1/2 inches.

After separation and stabilization of the spacecraft, the solar panel constraints are released and the solar array support booms deploy about the simple knee joints at the hub bridge truss. Following lock-up of these joints, the solar panels rotate about the skewed hinges, assuming positions above and outboard of the reflector deployment envelope. The reflector is then deployed after which the solar array booms rotate downward about 31.5 degrees and lock in this orbital position. See Figure 4-2 for the various configurations of ATS-6 from separation to full deployment.

The deployed spacecraft spans 51 feet, 8 inches from the ends of the solar arrays, 30 feet across the parabolic reflector, and about 27 feet from the earth-viewing surface of the EVM to the top of the magnetometer. The gross weight is 3078 pounds, including the adapter which remains with the launch vehicle.

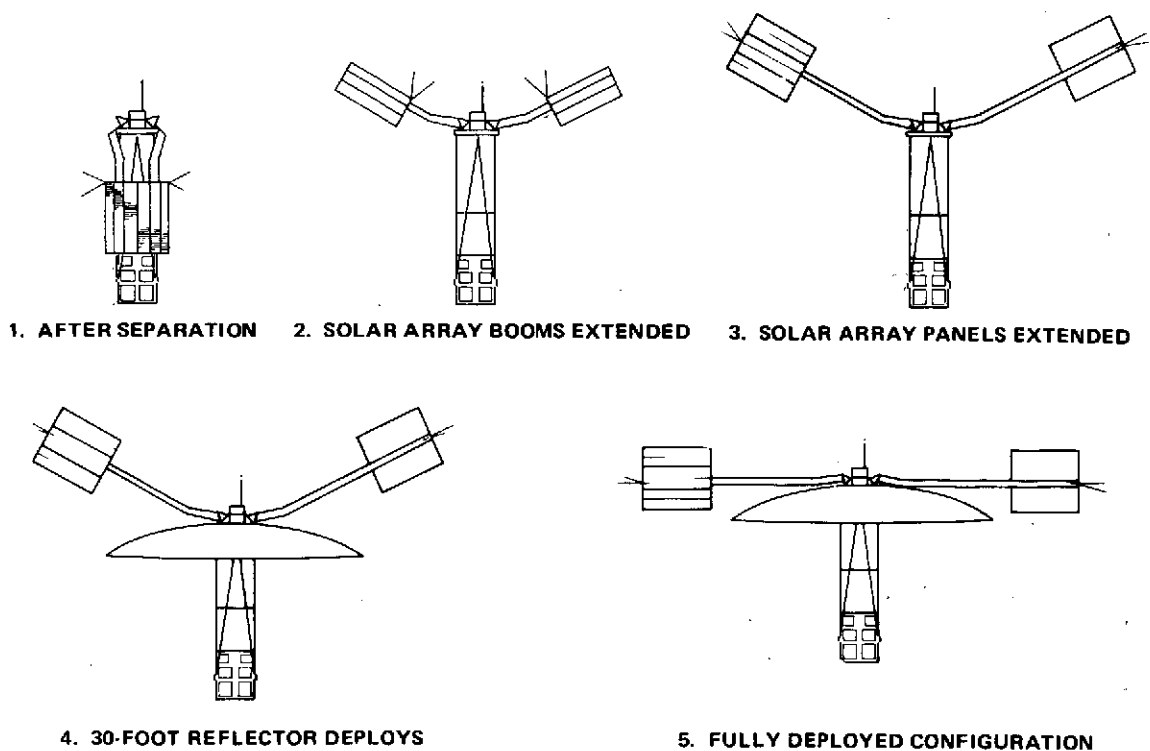


Figure 4-2. ATS-6 Deployment Sequence.

4.3 ELECTRICAL POWER SUBSYSTEM

The Electrical Power Subsystem (EPS) generates, stores, conditions, and distributes electrical energy to the spacecraft subsystems and experiments.

The EPS (Figure 4-3) consists of the following elements:

- a) Solar Cell Arrays
- b) Spacecraft Batteries
- c) Power Regulation Unit
- d) Power Control Unit
- e) Shunt Dissipators
- f) Load Interface Circuits
- g) Squib Interface Unit

The electrical power subsystem derives power from two hemicylindrical solar array panel assemblies aligned parallel to the Y-axis of the spacecraft, extending beyond the 30-foot reflector to avoid shadowing. The solar array output is connected through isolation diodes directly to the spacecraft load bus.

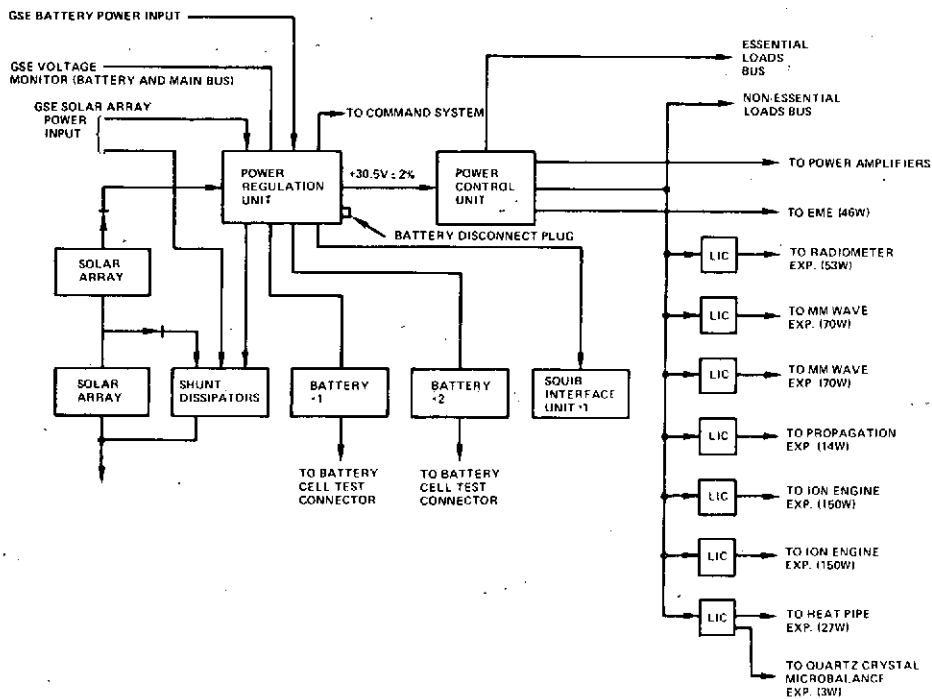


Figure 4-3. Electrical Power Subsystem Configuration .

Energy storage is provided by two 19-cell, 15 A-H, nickel-cadmium batteries which are discharged in parallel. The batteries provide electrical power during occult portions of the ascent phase, eclipse periods and peak loading that exceeds the solar array capability.

The power subsystem is sized to provide continuous peak power of 535 watts for a minimum of 4 hours (using batteries to a maximum of 50% depth of discharge) and a minimum average output of 450 watts for the remaining 20-hour operational day through 2 years in orbit except during occult. A minimum of 290 watt hours to the load is available from both batteries for operation during occult.

The power output from the solar array and batteries is regulated to a voltage level of 30.5 vdc for use by the spacecraft loads. The electrical power system uses partial shunt regulation for regulating the solar array voltage and a boost regulator for regulating the battery voltage.

When excess power is available from the solar array, the battery chargers are enabled to recharge the batteries. Each battery has separate charge control circuits and is normally charged with a current limited (1.5 amp maximum,

C/10) rate with temperature compensated voltage control. When the array power exceeds the load power and battery charge requirements, the excess power is dissipated by shunt circuits.

A common controller provides the necessary error signals for the three major modes of operation: the shunt mode, the charge mode, and the boost mode. These functional modes provide the regulation and charge control for the electrical power subsystem.

Secondary power conditioning at 28 vdc is provided in the electrical power subsystem for the rf solid state power amplifiers and for each GFE experiment through individual load interface circuits. There are seven separately packaged load interface circuits (LIC's) in the EPS. In addition, there are four LIC's contained in the Power Control Unit.

The squib interface unit provides for the safing and arming of electroexplosive devices, for the actuation of these devices, and for monitoring by telemetry. The unit also provides the capability for interrogating pyrotechnic and activator circuits for validation purposes. Current limiting is provided for each squib circuit.

An automatic sequencer, enabled by the separation of the spacecraft from the Titan III C launch vehicle, supplies the signals that start the sequence of deployment events. The automatic sequencer may be overridden by command from the ground at any stage.

4.4 THERMAL CONTROL SUBSYSTEM

Because of the large power capability of the ATS-F satellite and the variety of operating modes, there is a wide fluctuation in the amount of power that must be dissipated from the components within the EVM. The Thermal Control Subsystem maintains the temperature of the mounting surface in the EVM within the range of 5°C to 35°C. It also minimizes temperature variations that would tend to degrade the alignment accuracy of the spacecraft subsystems.

The Thermal Control Subsystem (Figure 4-4) achieves the necessary stabilization of temperature through use of the following elements:

- a) Superinsulation
- b) Thermal Louvers
- c) Heat Pipes
- d) Thermal Coating

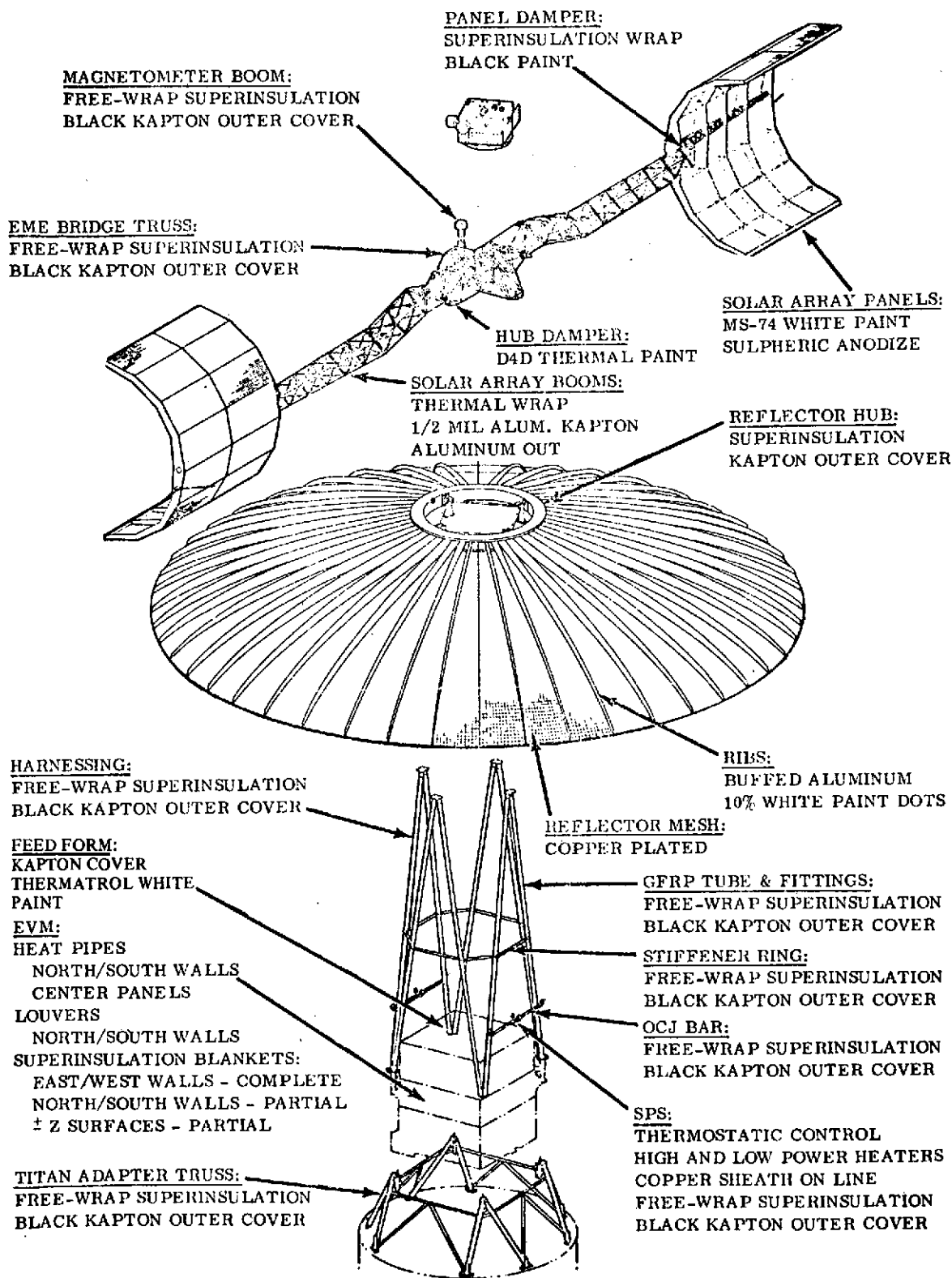


Figure 4-4. Thermal Control Subsystem

The design of the external structure is generally based on the passive approach of using multilayer superinsulation wrap (aluminized mylar interspace with nylon scrim cloth). Superinsulation covers all but the north and south side of the EVM. It consists of 30 layers of 1/4-mil aluminized Mylar with a 2-mil aluminized Kapton coversheet. This combination of a high infrared reflectance material and a low conductance material produces a superinsulation blanket with an effective emittance that does not exceed 0.015. Specially cut blankets and covers are used for the focus feed elements interface and for the earth-viewing face.

Thermal control of the reflector support truss is achieved by covering the truss tubes with multilayer insulation with black as the outer coating ($\alpha = 0.95$ and $\epsilon = 0.85$). The truss material, Graphite Fiber Reinforced Plastic (GFRP), has a coefficient of thermal expansion on the order of 10^{-7} inch/inch/F; therefore, the thermal distortions of the reflector truss are extremely small.

The solar array booms have aluminized Kapton tape in order to insure the uniformity of surface finish which is critical during launch/deployment phase. To minimize the temperature rise of the solar array, the space-viewing side of the substrate is coated with MS74 white paint ($\alpha = 0.40$ and $\epsilon = 0.90$).

The north and south faces of the EVM are honeycomb panels containing 17 square feet of thermal louver arrays. These arrays are rigid, lightweight, polished aluminum frames containing low-friction pivots for the louver blades. The blades are thin, highly polished, specular finish aluminum. They are actuated by bimetallic sensors located in a housing thermally insulated from the exterior environment. When the interior temperature rises, causing the bimetallic sensors to expand, the louver blades open and allow more heat to be radiated into space. A temperature change of 25° F will cause the louvers to rotate from fully open to closed. The surfaces behind the louvers are covered with OSR (Optical Solar Reflector), a vapor deposited silver on 8-mil thick fused silica. This coating provides a low absorptance (α) and a high emissivity (ϵ) and has a low level of degradation in the space environment.

Heat pipes fabricated from 1/2-inch square aluminum tubes are bonded as an integral part of the north and south skin panels and of the transverse bulkhead connecting the north and south panels (Figure 4-4). In all cases the heat pipes run parallel to the top and bottom surface of the EVM. Heat pipes have a high heat transport capability and maintain near isothermal conditions along their length. Ammonia is used as the working fluid because it has a high heat transfer capability and is compatible with aluminum.

The external components of SPS are maintained at the required temperature by utilizing heaters. The heater strips on the propellant line are activated by thermostatic control so as to keep the line at nominal temperatures during all phases of launch and orbit.

4.5 TELEMETRY AND COMMAND SUBSYSTEM

The Telemetry and Command (T&C) Subsystem provides the communication link between the ground operations controllers and the ATS-6 spacecraft. The T&C command capability includes receiving, decoding and distribution of discrete and data word commands to the spacecraft support systems and spacecraft experiments. The T&C Subsystem also provides the command link between the ground station computers and the spacecraft Attitude Control Subsystem during the Ground Attitude Control (GAC) experiment. The T&C telemetry capability includes the multiplexing, formatting, and transmission of analog and digital data from the spacecraft support subsystems and the experiments. A special data link is also provided for voice-bandwidth analog data communication between ATS ground stations.

The T&C Subsystem (Figure 4-5) is comprised of the following active elements:

- a) Two Data Acquisition and Control Units (DACU)
- b) Four VHF Transmitters
- c) Four VHF Receivers
- d) A Data Switching Unit (DSU)
- e) Two Command Decoder/Distributors (CDD)

The T&C Subsystem uses multiple units to provide redundancy to ensure high reliability and protection against a single failure. The antennas used by the T&C Subsystem include two omnidirectional antennas located on the solar panels and the prime focus feed antennas associated with the parabolic reflector. In addition, there is a switchable backup capability of accepting commands through the C-band receiver and telemetering through the C-band transponder.

The Command Subsystem has a capacity of 512 discrete command addresses and 45 data word addresses. Each data word transmission carries nine bits of data. It employs a VHF carrier which is AM-modulated by the FSK "0" and "1" command tones. The "0" and "1" tones are 50 percent AM-modulated by a 128-Hz sine wave clock, which is recovered in the CDD and used for timing within the CDD and for data word transfer to the subsystems. Before command execution, ground personnel verify via telemetry that the command has been received. Then an execute command is transmitted from the ground.

In a special mode, a second pair of FSK "0" and "1" tones, AM-modulated by a 1200-Hz sine wave clock are used to provide the GAC and High Speed Execute (HSE) command capability. The GAC and HSE commands are executed immediately without ground verification. The CDD performs an address check and a parity check on the command prior to issuing the GAC discrete execute pulse.

The telemetry subsystem provides for a maximum capacity of 368 nine-bit words. Five of these words are reserved for telemetry functions including

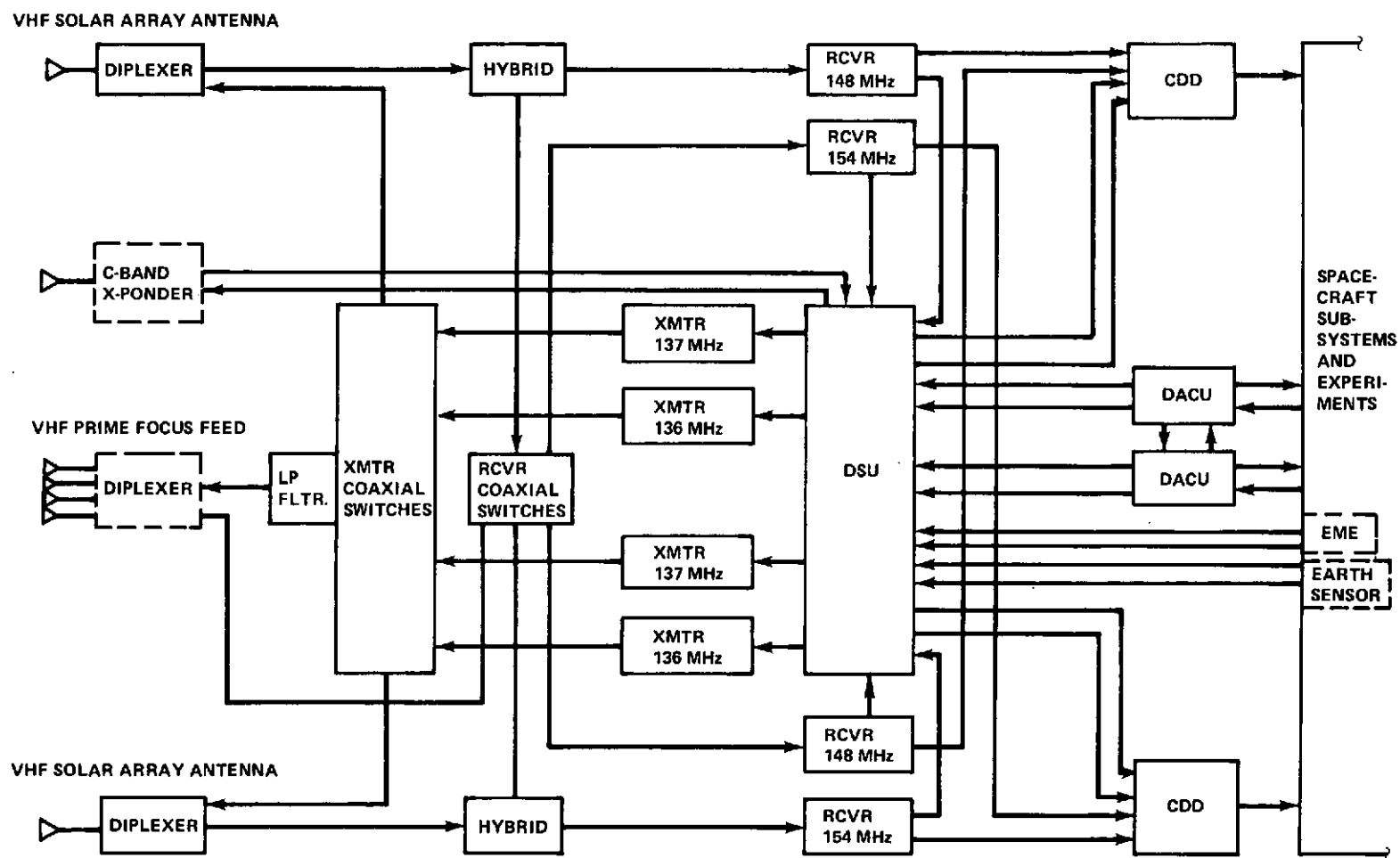


Figure 4-5. ATS-6 Telemetry and Command Subsystem

frame sync. and status. The remaining are used for analog and digital data. In the normal telemetry mode, one of the two DACU's is commanded ON, along with one of the two master oscillators and both time code generators. The DACU samples the input lines from the digital and analog telemetry points in a pre-determined sequence, digitizes the analog levels sampled in a 9-bit analog-to-digital converter, and serializes the digital bits into a nominal 391-bps biphasic bit stream, which is switched by the DSU to the FDM unit or one of the four transmitters under control of ground command.

The prime mode of operation is FM/PM, with normal telemetry (DACU), EME, and voice-bandwidth-analog data frequency-division multiplexed onto the carrier of one of the two transmitters associated with the prime focus feed. This mode takes advantage of the high gain parabolic dish to give both the EME and voice-bandwidth-analog channels adequate margin for high quality link performance. Normal telemetry or EME data can modulate either of the omni-associated transmitters or the prime-focus feed associated transmitters directly in backup modes. Telemetry data can also use the C-band transponder as a back-up downlink.

4.6 ATTITUDE CONTROL SUBSYSTEM

The Attitude Control Subsystem (ACS) serves to stabilize and orient the spacecraft after separation from the launch vehicle. It also provides the necessary attitude stabilization and accurate slewing control for the ATS-6 experiments. The basic functional elements of the ACS (Figure 4-6) needed for 3-axis attitude control are the following:

- a) Sensors (Attitude Control References)
- b) Controllers (Computers)
- c) Torquers (Wheels and Jets)

The ACS uses radiant energy from the Earth and light from Polaris for the prime attitude control references, digital or analog computers as its controlling elements, and three momentum wheels and the attitude control jets of the Spacecraft Propulsion Subsystem (SPS) as its control actuators. Spacecraft reference orientation is defined in Figure 4-7.

Control and reference signals are obtained from the following sensors:

- a) Sun Sensors
- b) Earth Sensor Assembly
- c) Polaris Sensors
- d) Rate Gyros
- e) Yaw Inertial Reference Unit
- f) Interferometer
- g) Monopulse

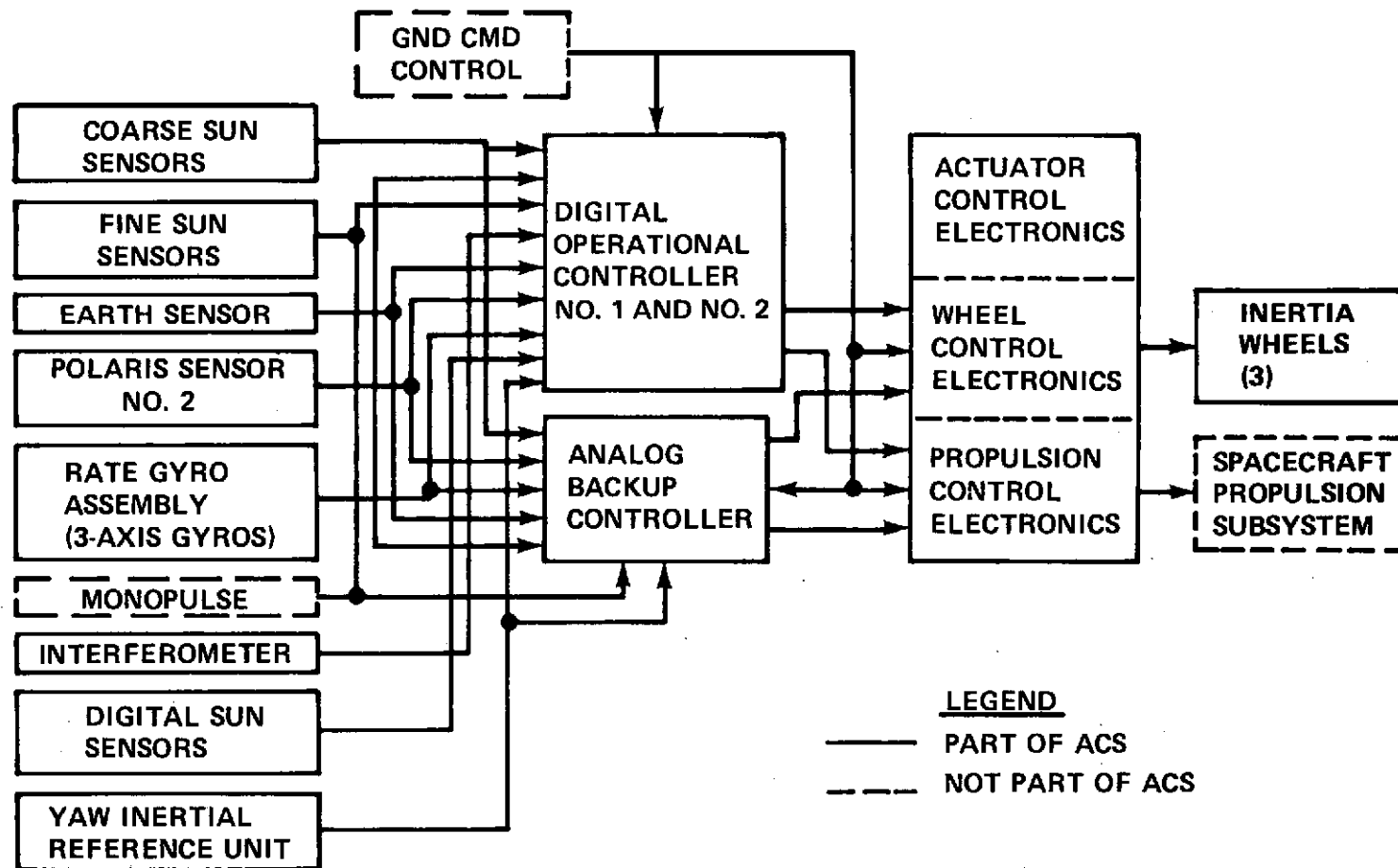


Figure 4-6. Simplified ACS Block Diagram

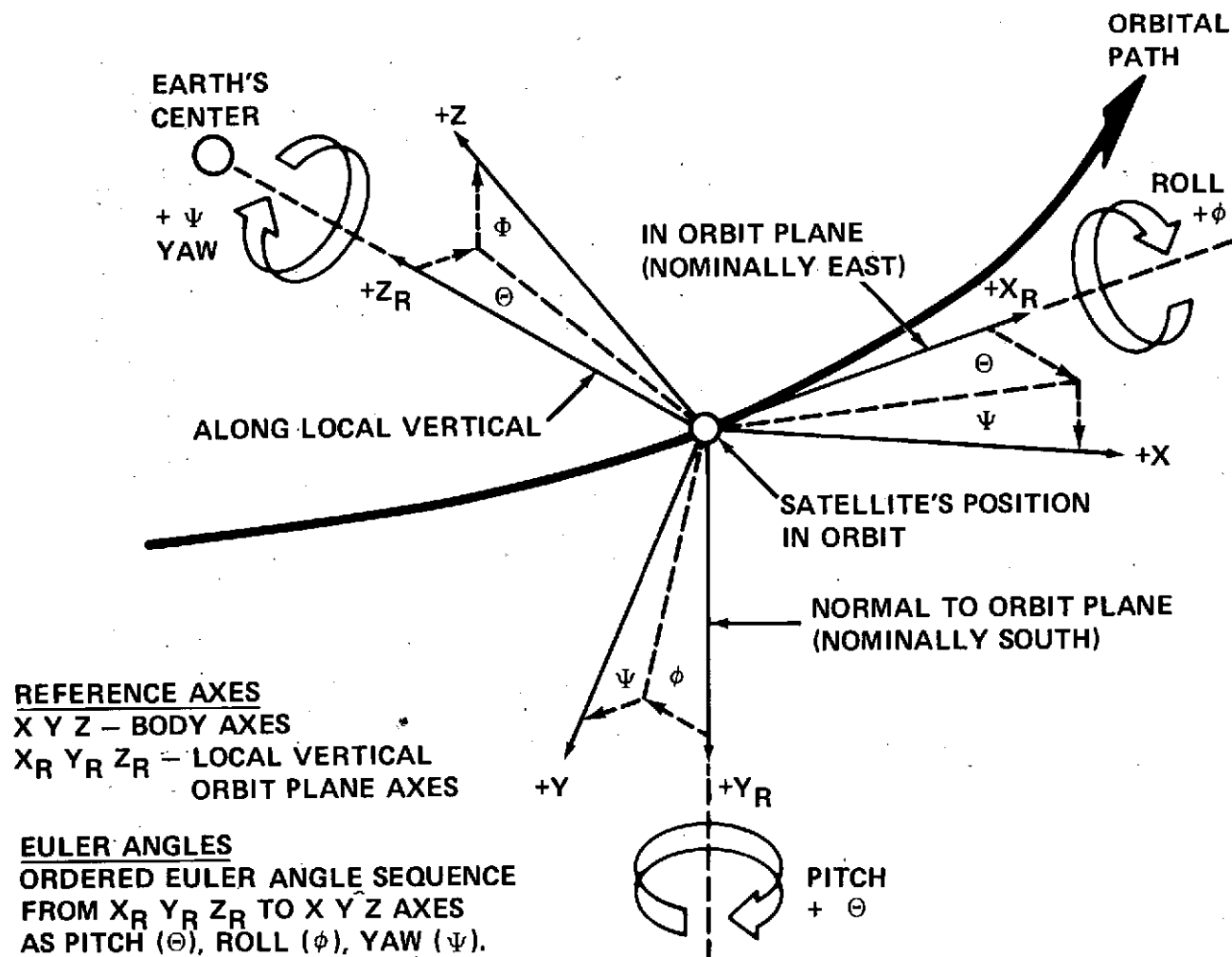


Figure 4-7. Definition of Reference Orientation and Roll/Pitch Yaw Angles

The sun sensors include four coarse-null sun sensor blocks, each providing two-axis sensitivity, two fine-null sun sensors, and two digital sun sensors.

The earth sensor assembly consists of two sensing heads (one roll, one pitch) plus an electronics unit. It is used for earth acquisition during the acquisition modes and serves as the primary roll/pitch sensor for all operational modes.

One Polaris sensor and its conditioning electronics is provided. The Polaris sensor is used during the Polaris acquisition mode and serves as the primary yaw sensor for all operational and most experimental modes.

The three-axis rate gyro assembly (RGA) is used during the acquisition modes for rate damping and for rate compensation. The RGA consists of three, single degree of freedom, spring restrained, rate gyros mounted in an orthogonal frame to sense pitch, roll, and yaw spacecraft rates.

The Yaw Inertial Reference Unit (YIRU) provides a backup to Polaris star tracker No. 2. It consists of a rate-integrating gyro with associated electronics and replaces PSA No. 1. The YIRU can control the yaw axis to an accuracy of ± 1.0 degree for a one-hour period.

The Interferometer, when illuminated by RF energy from a ground transmitter, measures the direction cosines between the spacecraft roll and pitch axes and the line-of-sight vector from the spacecraft to the transmitter. Digital outputs representing these two-direction cosines are provided to the DOC and to telemetry covering the ± 17.5 -degree roll-pitch angle range of the interferometer. When two or more ground transmitters are used, all three (pitch, roll, and yaw) spacecraft attitude angles can be obtained. The latter mode is implemented via telemetry, for pitch and roll, and by ground computation for yaw.

When the spacecraft antenna system operates in a monopulse mode (C-band, S-band or VHF) a pointing error signal is generated for the roll-yaw and pitch-yaw planes with an angular accuracy of $1/50$ beamwidth. This signal interfaces with the attitude control subsystem and the telemetry subsystem. The monopulse can operate at S-band for closed-loop tracking of data relay system satellites as well as for ground pointing at all frequencies.

The Spacecraft has two identical, redundant onboard digital computers for prime attitude control purposes. These components are referred to as Digital Operational Controllers (DOC's). The controlling DOC is selected via ground command. The basic DOC consists of a power supply, central processor, a memory and an input/output section. The DOC provides for block transfer of

data to the telemetry DACU or complete data transfer from memory on command from the ground. It receives its commands from the CDD. The input/output electronics accepts both analog and digital signals and can supply monitoring signals to telemetry, and control signals to sensors and to the Attitude Control Electronics (ACE) for controlling the wheels and jets.

The Analog Backup Controller (ABC) is a simple, low power analog controller that serves as a backup to the DOC's in certain modes at reduced power levels. It consists of a power supply, mode logic, and switching amplifiers.

The actuator control electronics (ACE), which is energized at all times for all modes of operation, includes the wheel drive electronics, the wheel unload logic, the SPS control electronics and associated power supplies, and the signal conditioning circuitry. The wheel drive electronics drives the inertia wheels in response to attitude error signals from the DOC's, ABC, or one of the two CDD's or two GAC decoders. The ACE serves as the power amplifier between the controllers and the inertia wheels or the SPS. The wheels are driven by means of pulse modulation. A pulse modulator, provided in the ACE, accepts signals as generated by the DOC or the ABC and gates the wheel full on or off at a duty cycle which is proportional to spacecraft error.

Three inertia wheels serve as the prime torquers for all modes of operation except acquisition, orbit control, and jet-only control. At the completion of each of the acquisition modes, the wheels can be selected to hold the spacecraft attitude.

The ACE electronics for the SPS consists of the logic to accept the jet firing commands from the two DOC's, the ABC, the two command decode and distribution (CDD) units, and the power drivers to energize the appropriate solenoids in the SPS for attitude control. The ACE provides outputs to 12 attitude control thrusters and 4 orbit control thrusters and power for beaters in these thrusters.

4.7 SPACECRAFT PROPULSION SUBSYSTEM

The Spacecraft Propulsion Subsystem (SPS) provides controlled thrust for orbit control of the ATS-6 Spacecraft, three axis attitude control, and inertia wheel unloading. The SPS accomplishes these functions by providing controlled thrust through the center of gravity of the spacecraft or about the three spacecraft axes. Spacecraft reference orientation is defined in Figure 4-7.

The SPS, shown schematically in Figure 4-8, comprises two parallel, functionally redundant half-subsystems, connected by a latching valve. It is mounted primarily in the earth viewing module (EVM), and consists of a central assembly that includes a mounting plate to which are attached two tanks for hydrazine propellant storage with positive diaphragm expulsion control; fill and drain valves, filters, and latching valves for controlling and/or isolating the propellant feed to the separate attitude and orbit control thruster assemblies.

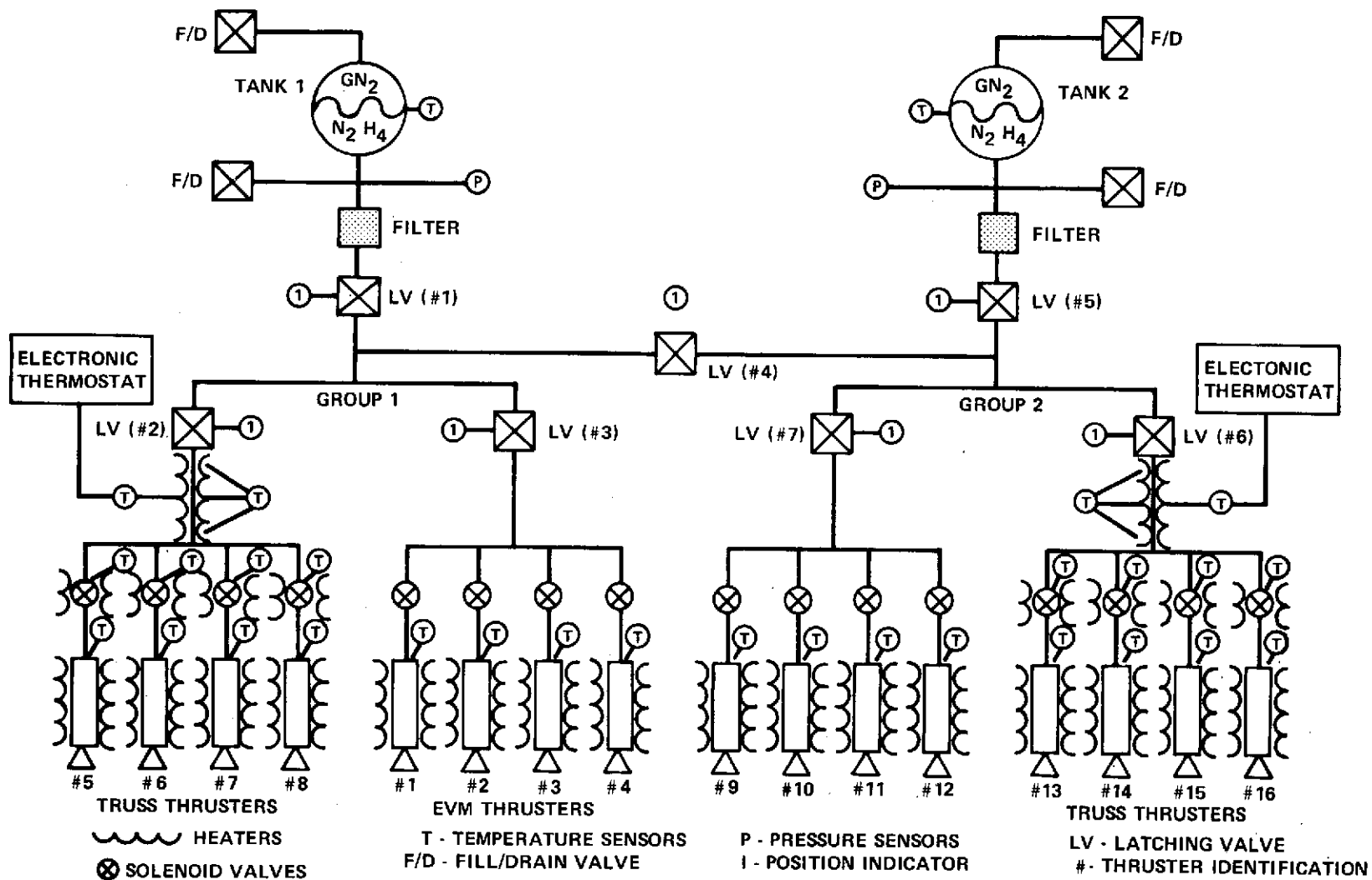


Figure 4-8. Spacecraft Propulsion Subsystem Schematic Diagram

The attitude control (AC) thruster assemblies generate thrust of the required magnitude, duration and response time for jet-only control in roll and pitch, and for inertia wheel momentum unloading. There are four AC thruster assemblies in each parallel half-system located in the EVM.

The truss-mounted orbit control thruster assemblies generate thrust of the required magnitude and duration to impart the desired change in the orbital velocity of the spacecraft, to the east or west, fired singly or in pairs; and to the north or south, fired in pairs. They also provide yaw control. There are four orbit control (OC) thruster assemblies in each half-subsystem.

The SPS weighs 29.5 kg (65 lb) dry and carries 50 kg (110 lb) hydrazine monopropellant fuel and 0.9 kg (2 lb) of nitrogen gas pressurant. The thrusters all have an initial thrust of 0.556 Newton (0.125 lb force) and blow down to 0.222 Newton (0.05 lb force). Their thrust is produced by the spontaneous decomposition of liquid hydrazine into hot ammonia, nitrogen, and hydrogen gases when it comes into contact with the Shell 405 catalyst grains that are held in the thrusters. Solenoid-operated valves control the liquid flow into the thrusters.

The tanks are made of titanium-aluminum-vanadium alloy and each contains a diaphragm to separate the hydrazine and the nitrogen pressurant gas. The tank of each half-system is filled with hydrazine and pressurant gas through separate valves.

A total of seven latching valves can isolate the half-systems from each other and also can isolate each tank, truss mounted thruster group, and EVM-mounted thruster group.

There are two primary modes of thruster operation: pulse mode and steady-state mode. The pulse mode is generally characterized by short ON times, with relatively long OFF times. ON times can be from 0.10 sec to 120 sec. OFF times can be from 10 sec to 86,000 sec. The pulse mode is used almost exclusively for attitude control functions on the spacecraft, and for wheel unloading. The steady-state mode of thruster operation is generally characterized by longer ON times, which can vary from 1.0 sec up to approximately 6 hours. The OFF times are generally from hours to days or months. This mode is used for all orbital control functions on the spacecraft. It is ground-command only.

The total number of pulses expected per mission is approximately 100,000 for attitude control functions, while the total starts for orbital control are approximately 300. Total impulse for attitude control is 4571 lb-sec., and 14,900 lb-sec for orbit control.

4.8 COMMUNICATION SUBSYSTEM

The Communication Subsystem aboard the ATS-6 spacecraft is an integrated multi-frequency RF repeater capable of receiving up to three signals in any of four frequency bands (C, S, L, and VHF), and amplifying, processing, and retransmitting them on any assigned frequency in four frequency bands (C, S, L, and UHF bands).

The Communication Subsystem (Figure 4-9) consists of the transponder and antenna feeds. The transponder provides the basic interface between the experiments in the satellite and ground terminals, and performs frequency generation, translation, and power amplification functions. In some instances the transponder is itself a part of the experiment.

The transponder can be functionally divided into four major areas: the receivers, the IF amplifier assembly, the frequency synthesizer, and the transmitters. Supporting these major areas are the RF input-output circuitry, wideband data unit, monopulse detector, command distributor, and dc-dc converters.

With certain exceptions, all active components are redundant. This includes synthesizer, transmitters, receivers (except L-band), monopulse, wideband data unit and transponder command decoder. The IF is triply redundant. Up-converters and downconverters, with the exception of the UHF upconverter, are not redundant. Operational redundancy is provided in the case of the Health, Education, Telecommunications (HET) experiment with one transmitter at each HET frequency.

The receiver includes preamplifiers, monopulse modulators, mixers, filter and the required interconnecting circuits. Five converters, three for C-band signals and one each for S- and L-band signals, are provided to translate the received signals to the intermediate frequency. All conversion frequencies are derived from a single frequency. The receivers provide C-band, S-band, and VHF monopulse modulators and signal combining.

The IF amplifier consists of an IF input switch matrix, three identical IF amplifiers ($f_c = 150$ MHz, $\Delta f = 40$ MHz or 12 MHz, commandable) and an IF output switch matrix.

The synthesizer uses a single frequency (100 MHz) oscillator from which it synthesizes all the other desired frequencies. It can operate in the coherent mode, wherein the VCO and all the frequencies derived from it are phase-locked to the received signal. In the noncoherent mode a temperature compensated crystal oscillator acts as the reference.

The transmitter portion of the transponder is comprised of the up-converter, the drivers and the power amplifiers for C-band, S-band, L-band, and UHF. Output amplifiers are solid-state, except for C-band which uses TWTA's.

The communication subsystem operates in various modes to fulfill the requirements of the experiments. In the coherent mode all local oscillator signals are derived from a single oscillator phase-locked to the C-band signal carrier transmitted from the ground to the spacecraft. In the noncoherent mode, the local oscillator frequencies are generated within the spacecraft by a highly stable fixed-frequency oscillator with an initial frequency tolerance of ± 10 PPM and a long term stability of better than ± 3 PPM in three months. The primary mode of transponder operation is frequency translation with hard limiting in the IF. This mode can be used with any combination of receiver and transmitter.

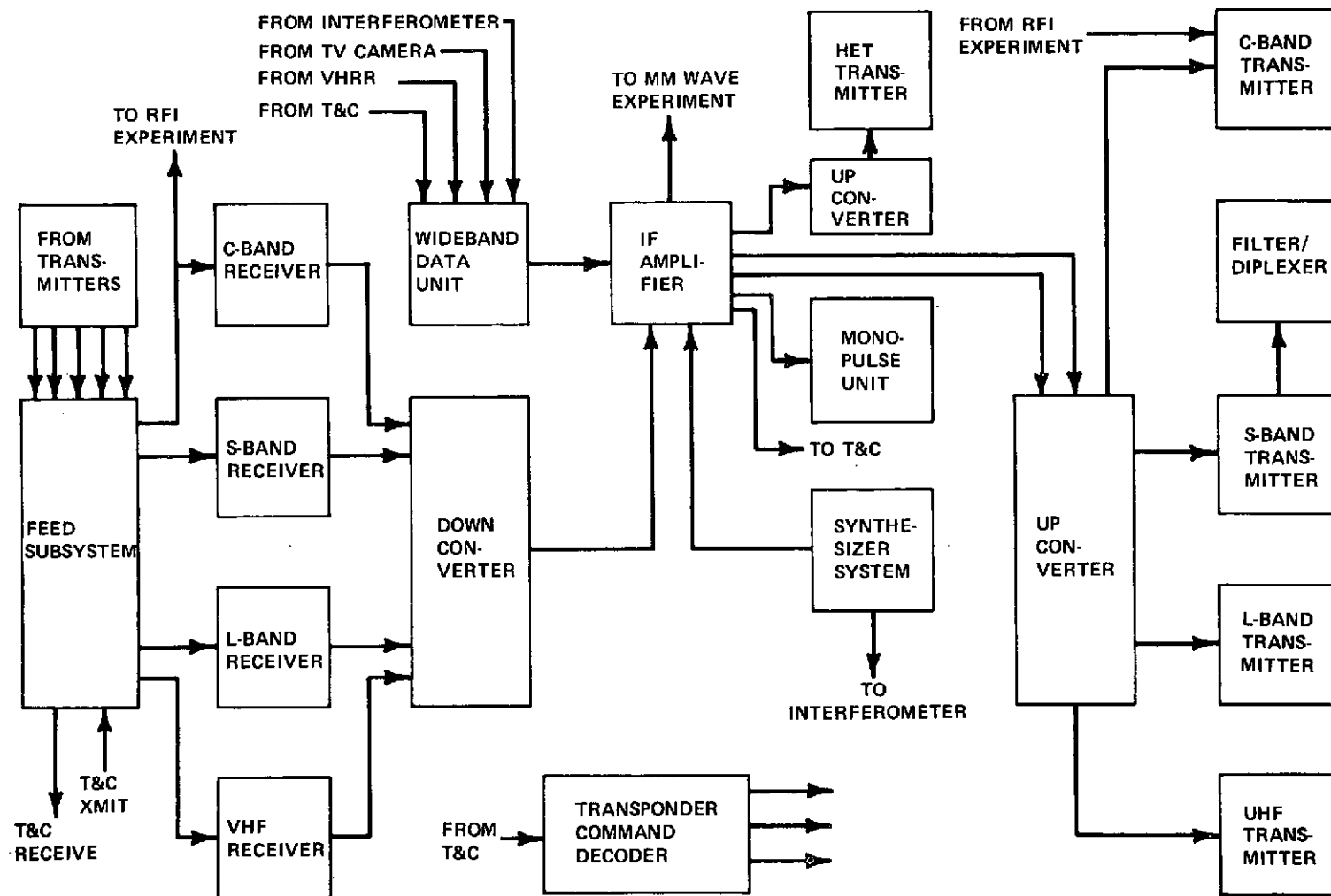


Figure 4-9. Communications Subsystem (Simplified Block Diagram)

A second mode of frequency translation with AGC-controlled linear amplification is available via the 3950 MHz channel of the C-band transmitter only.

The antenna feed assemblies provide radiating and receiving elements for the communication subsystem. The prime focus feed (Figure 4-10) is located on the top surface of the communications module at the focal plane of the high-gain 30-foot parabolic RF reflector to provide antenna illumination. Multiple feeds are used to accommodate the various spacecraft RF frequencies and to permit beam shaping and scanning. In addition to the prime focus feed, Earth viewing horns are located on the bottom surface of the EVM to transmit and receive wide beam C-band signals directly to and from the Earth.

4.9 EXPERIMENTS

The Experiments flown aboard the ATS-6 Spacecraft are located on the structural elements of the spacecraft and in the experiment and communications modules of the Earth Viewing Module (EVM).

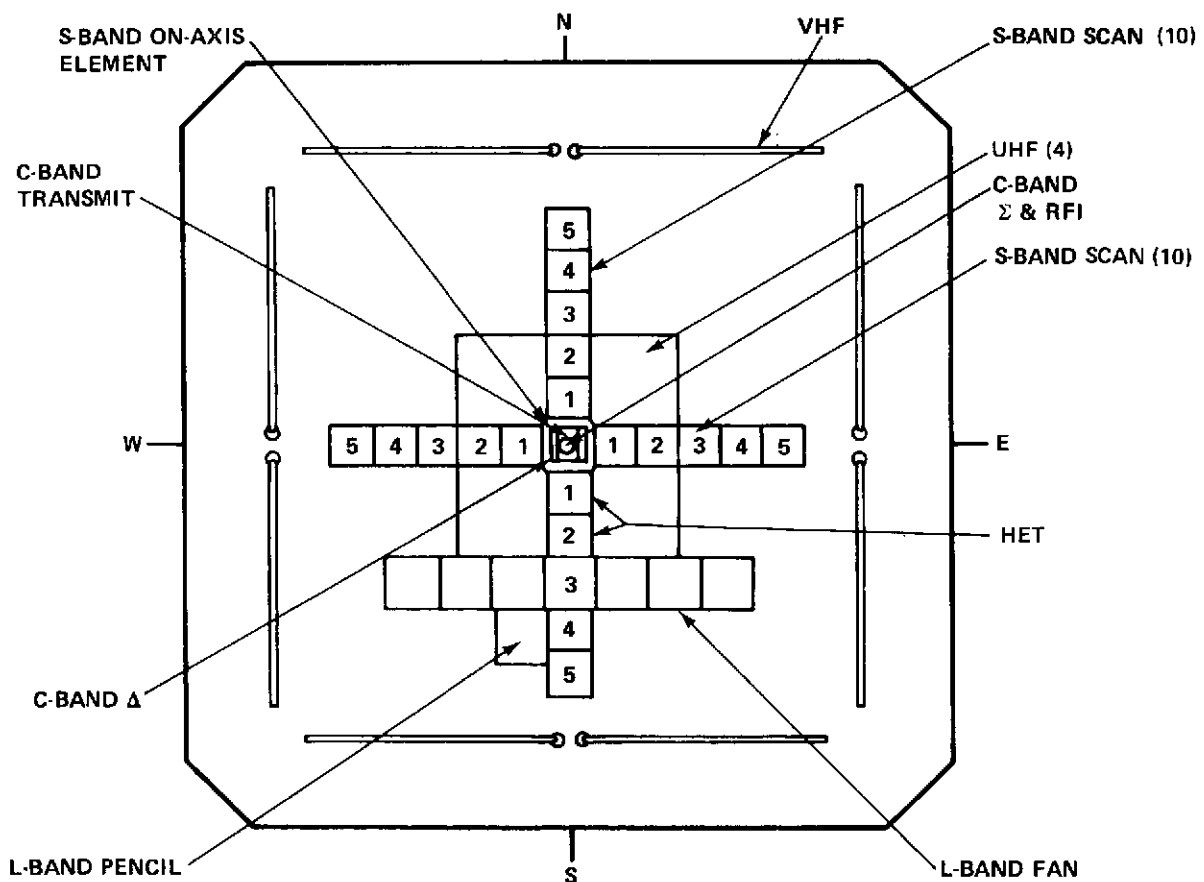


Figure 4-10. Prime Focus Feed.

The primary communications/control experiments are as follows:

a. Position Location and Aircraft Communication Experiment (PLACE)

The PLACE objective is to obtain engineering data and practical experience for determining the operational feasibility of an air traffic control satellite system operating in the aeronautical L-band.

b. Tracking Data Relay Experiment (TDRE)

The TDRE objective is to demonstrate the technology of command and telemetry data transmission at S-band between a low altitude satellite and ground station using a geosynchronous satellite as a communications relay.

c. Satellite Instructional Television Experiment (SITE)

The SITE objective is to assess the potential value of satellite technology in establishing effective mass communications and instruction in developing countries. SITE operates at UHF.

d. Television Relay Using Small Terminals (TRUST)

The TRUST objective is to advance state-of-the-art in space communications at UHF by demonstrating CCIR quality wideband signalling between ATS-6 and inexpensive ground stations.

e. Health Education Telecommunications (HET)

The HET objective is to evaluate the performance of satellite relay at S-band of educational programming and health care delivery to learning centers, hospitals, clinics, and community television distribution systems.

f. Radio Frequency Interference Measurement (RFI)

The RFI objective is to investigate C-band terrestrial noise sources (geographical/noise power distribution).

g. Radio Beacon Experiment (RBE)

The RBE objective is to perform ionospheric/exospheric electron content measurements and study ionospheric propagation effects at 40, 140 and 360 MHz.

h. Spacecraft Attitude Precision Pointing and Slewing Adaptive Control System (SAPPSAC)

The SAPPSAC objective is to investigate computer controlled attitude control performance optimization.

The GFE Experiments are as follows:

a. Millimeter Wave (MMW)

The Millimeter Wave experiment is designed to provide propagation data at 20 GHz and 30 GHz over a 1.44 GHz bandwidth.

The basic objective of the Millimeter Wave (MMW) Experiment is to provide information about propagation characteristics of the earth's atmosphere, and the effect of weather on these characteristics, in order to efficiently use this portion of the electromagnetic spectrum for wideband communications and other scientific purposes. The MMW experiment will measure the propagation characteristics of the atmosphere between the ATS-F spacecraft and the ground by transmitting 20 and 30 GHz test signals from the spacecraft to the experimenter's ground equipment at ROSMAN.

b. Very High Resolution Radiometer (VHRR)

The Very High Resolution Radiometer experiment will utilize a high resolution meteorological camera to refine meteorological research. Pictures will be obtained in the visible and infrared spectrums.

The primary objective of the Very High Resolution Radiometer (VHRR) experiment is to evaluate the feasibility of new techniques in the collection and distribution of meteorological data by means of a synchronous 3-axis stabilized satellite. The radiometer will map both day and night cloud cover of the earth. The data obtained will be used for essential meteorological determinations by the scientific community, as well as for pictorial mapping of cloud motion and storm history.

c. Environmental Measurements Experiments (EME)

The Environmental Measurements Experiment (EME) package is a group of eight experiments carried on board the ATS-6 that are designed to study the spacecraft environment at synchronous altitude and to gain information on electromagnetic-ionospheric interactions. Six of the experiments are designed to obtain data on charged particles

of several different types and over wide energy ranges. A seventh experiment is to provide magnetic field data, to be used in conjunction with the charged particle measurements to determine the dynamic processes which take place in the synchronous orbit environment. The eighth experiment is a continuation of previous ATS engineering studies into solar cell degradation.

d. Propagation

The purpose of the Propagation Experiment is to collect sufficient long-term data on propagation attenuation caused by precipitation for a large number of locations in the U. S. to permit determination of minimum power margins needed in spacecraft communications systems operating at frequencies of 13 and 18 GHz.

e. Ion Engine

The primary objective of the Ion Engine Experiment is to verify and obtain operational data on the utilization of a Cesium ion electric propulsion system. This propulsion system will be used for North-South station keeping orbital maneuvers. A secondary objective is the demonstration of thrust vectoring for attitude control

f. Quartz Crystal Microbalance (QCM)

The primary objective of the QCM Experiment is to provide data regarding the accumulation of contaminants on the spacecraft. Sources of possible contaminants, in addition to general outgassing, include material ejected from the spacecraft propulsion subsystem as well as the propulsion experiment. The QCM uses a crystal whose resonant frequency will change with the amount of material deposited on its active surface. The change, in this case, is linear from 1500 Hz to 50 kHz. If, after 6 to 8 months, the frequency shift should exceed 50 kHz, a special degas heater will be turned on to effectively burn off the accumulated material and return it to approximately its original frequency.

g. Advance Thermal Flight Experiment (ATFE)

The objectives of the Advanced Thermal Control Flight Experiment (ATFE) are:

- 1) To evaluate in space the performance of an active, feedback-controlled, variable conductance heat pipe, a thermal diode

(one-way heat pipe), and a phase-change heat reservoir or thermal accumulator.

- 2) To demonstrate the effectiveness of these recently developed thermal control devices in stabilizing the temperature of space-craft components which undergo marked changes in power dissipation and/or thermal environment.

SECTION 5

STRUCTURAL/DEPLOYMENT SUBSYSTEMS

SECTION 5

STRUCTURAL/DEPLOYMENT SUBSYSTEMS

5.1 STRUCTURAL

The structure of the spacecraft performed nominally from liftoff through orbit injection. Separation from the launch vehicle occurred as planned and spacecraft deployment was nominal except for one event, the slow deployment of the North Solar Panel with respect to the supporting boom.

Table 5-1 presents the ATS-F separation/deployment time lines. Predicted and actual times of events from liftoff are shown. Source of data was the normal telemetry history tape printout. The actual time listed is that at which the event was observed on the S/C telemetry which updated every three seconds. Where more than one event (such as North Boom lockup and South Boom lockup) is covered by a single item, the time of the latest event is indicated. With the exception of the array unfold completion, all times were within a normal anticipated spread. Investigations which were conducted to determine the cause of slow deployment of the North Solar Array are discussed in Section 5.1.1.

Table 5-2 presents the specifications, predicted, and actual temperatures of deployment mechanism components that were monitored during deployment. All temperatures were within predicted values.

Table 5-3 identifies the rotation rates of the spacecraft about the roll, pitch and yaw axes before and/or after various deployment events and was obtained from RGA data. Figure 5-1 presents a time-line plot of the body rates as obtained from the RGA. Significant events are also indicated along the time-line which is presented in GMT. (Lift-off occurred at 1300:00:00 GMT.) Oscillations over an extended period of time (that is, 20+ seconds) are indicated by a wide band. Peak spikes are shown by a line or by figures inserted on the plot.

5.1.1 -Y (North) Solar Panel Deployment About Panel/Boom (45°) Hinge

A number of questions have been raised by the slow deployment of the North panel. Nominal deployment time of the panel about the panel/boom hinge is 3 to 4 minutes with a maximum of approximately 7 minutes; the actual deployment time was approximately 15 minutes and 26 seconds. On-board instrumentation indicates time of release, and hence normal time of start of deployment, and completion of deployment motion. Start of deployment motion is assumed to occur with application of firing current to the array release pyrotechnics. All ground tests of this release mechanism resulted in a nominal release of the

Table 5-1

ATS-F Separation/Deployment Time Lines were as follows:

Event	Expected Time from Lift-off (Hours/min/sec)	Actual Time from Lift-off (Hours/min/sec)	Delta Time
Separation Enable	6/ 37/ 56	6/ 33/ 18	-4/38
S/C Separation	6/ 37/ 59	6/ 33/ 21	-4/38
Start S/A -Booms			
Release	6/ 43/ 59	6/ 39/ 23	-4/36
Comp. S/A Booms			
Lock-up	6/ 47/ 59	6/ 40/ 34	-7/25
Array Unfold Release	6/ 53/ 59	6/ 46/ 34	-7/25
Array Unfold Comp.	7/ 00/ 59	7/ 02/ 00	+1/01
Start Reflector	7/ 06/ 59	7/ 08/ 03	+1/04
Deployment			
Comp. Reflector			
Deployment	7/ 07/ 05	7/ 08/ 12	+1/07
Start Boom Drop	7/ 13/ 06	7/ 14/ 14	+1/08
Comp. Boom Drop	7/ 14/ 05	7/ 14/ 32	+0/27

Table 5-2

Deployment Temperatures

Parameter	Specification	Predicted	Actual
Damper, Panel-End North	-48°C to 46°C	-33°C to 30°C	25°C
Damper, Panel-End South	-48°C to 46°C	-33°C to 30°C	26°C
S/A Boom 2nd Depl Huge +Y	-140°C to 150°C	-55°C to 116°C	10 to 17°C
S/A Boom 1st Depl Huge +Y	-140°C to 150°C	-55°C to 116°C	45 to 52°C
S/A Boom 2nd Depl Huge -Y	-140°C to 150°C	-55°C to 116°C	2 to 7°C
S/A Boom 1st Depl Huge -Y	-140°C to 150°C	-55°C to 116°C	48 to 55°C
Reflector Rib Sta 173 -Y	-18°C to 34°C	-10°C to 19°C	10°C
Reflector Rib Sta 110 -X	-18°C to 34°C	-10°C to 34°C	12°C
Reflector Rib Sta 110 -Y	-18°C to 34°C	-10°C to 34°C	5°C
Reflector Hub -Y	-160°C to 60°C	-53°C to 35°C	11°C

Table 5-3

Deployment RGA Rates
Actual Values Are in deg/sec

Event	Roll	Pitch	Yaw
Before Separation	0.0	+.04	+.08
After Separation	-.14	+.10	-.07
After Boom/Array Release	-.03 to -.18	-.05	-.06 to +.06
After Boom Lock	-.18	-.02	+.06
At Array Unfold Release	-.18	-.02	+.07
Array Unfold Comp.	-.09	+.02	+.10
Reflector Release	-.09	+.03	+.10
Reflector Deploy Comp.	-.09	+.04	+.10
Boom Drop Rel.	-.09	+.04	+.10
Boom Drop. Comp.	-.09	+.06	+.08

C-2

5-4

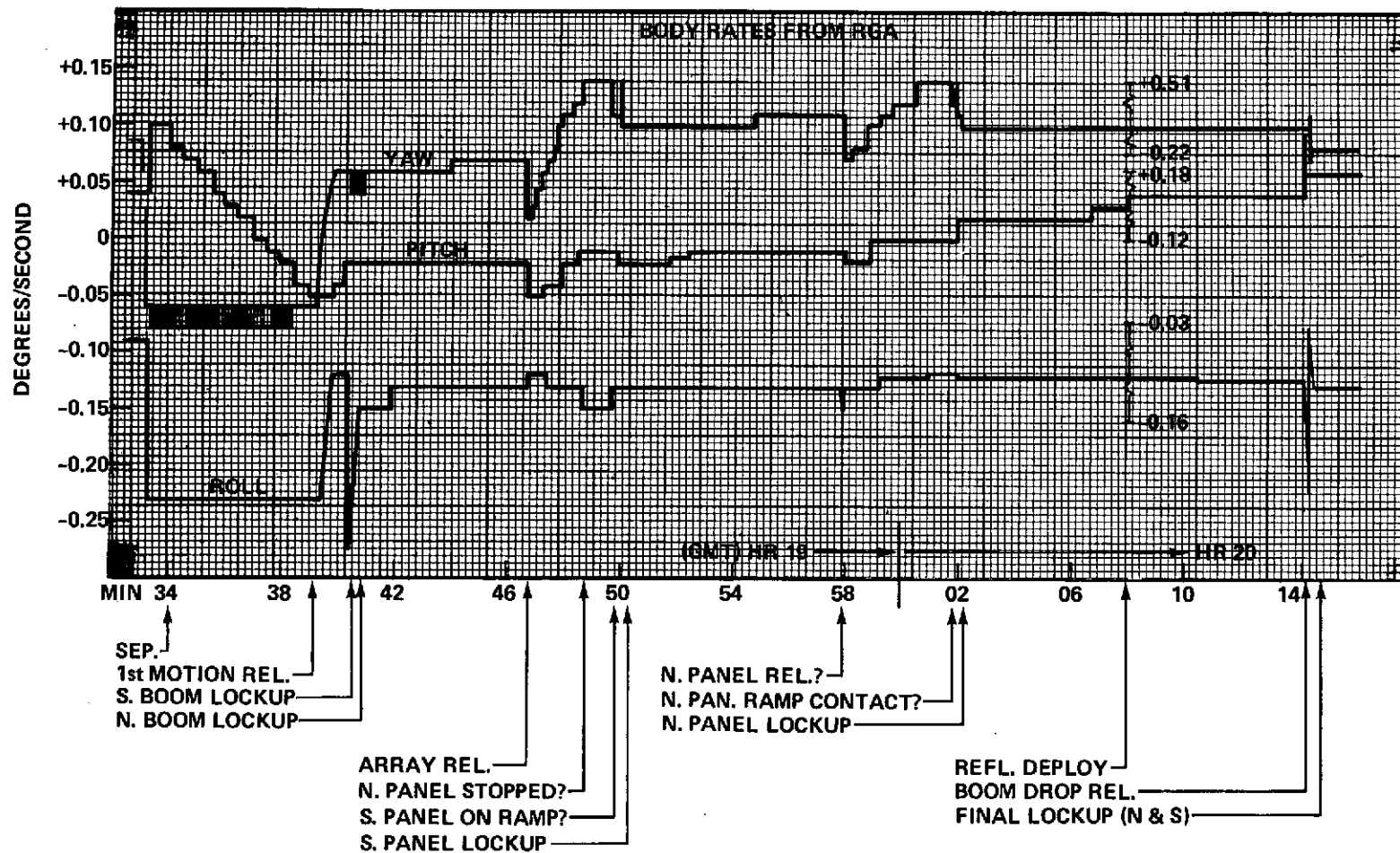


Figure 5-1. Spacecraft Angular Velocities During Deployment

array from the array restraint mechanism. Completion of deployment of the array is indicated by microswitches that are actuated upon correct seating of the deployment hinge lock pins. The position of the array during deployment, therefore, must be determined by indirect means since no direct readout of the array position is included in the spacecraft instrumentation.

Each deployment motion is unique; that is, only one type of motion occurs at any given time during the deployment sequence, although both North and South booms or panels are permitted to accomplish similar motions during the same period of time. The reaction of the spacecraft to the forces produced by deployment motions of the various array and reflector components is indicated by a change in the position of the spacecraft in inertial space. Since the body rates of the quiescent spacecraft were quite low following separation (see Fig. 5-1) motions induced into the body by deployment may be indicated by changes in the sun vector as determined by the on-board solar aspect sensors. Figure 5-2 indicates the Z Co-elevation (Z Co-el) angle (the angle between the spacecraft +Z axis and the solar vector) for that period of time between release of the solar array panels for second motion deployment and completion of the North panel deployment as indicated by North panel lockup. This time frame extends from 19:46:30 thru 20:02:03. DSS data was generally used, but was not available for the period of time immediately preceding release of the array. South panel lockup is indicated on the graph but has little apparent impact on the curve due to the scale used. Point A, however, was quite apparent and prompted further investigation. Careful inspection of the curve also indicated a distinct change in its slope at 20 hours and 2 minutes, the time of North panel lockup and another distinct break at 19 hours and 58 minutes (Point B).

Figure 5-3 is a plot of DSS data (supplemented after reflector deployment with some ADSS data) of the azimuth of the solar vector (ZAZ) with respect to the spacecraft -Y axis for the period 19 hours:46 minutes through 20 hours:15 minutes. The times of array release, South panel lockup, North panel lockup, and Points A and B are indicated. Between Point B and North panel lockup, there are distinct variations from the smooth curve produced outside of these points by the normal body motions. The curve exhibits similar variations during the known time period of South panel motion, i.e., from array release to South panel lockup. The reaction of the motion of the arrays upon the spacecraft is to decrease a negative Z-rate during the first 90 degrees of panel motion and then increase a negative Z-rate during the final 90 degrees of panel motion. This is verified by the curve.

Inspection of Figure 5-3 at Point A indicates a sudden change in slope of the curve; this anomaly, which also appears on Figure 5-2, for the Z co-el, is investigated through an expanded plot as shown in Figure 5-4. Point A is quite apparent. An additional anomaly appears at the point designated as "C". This

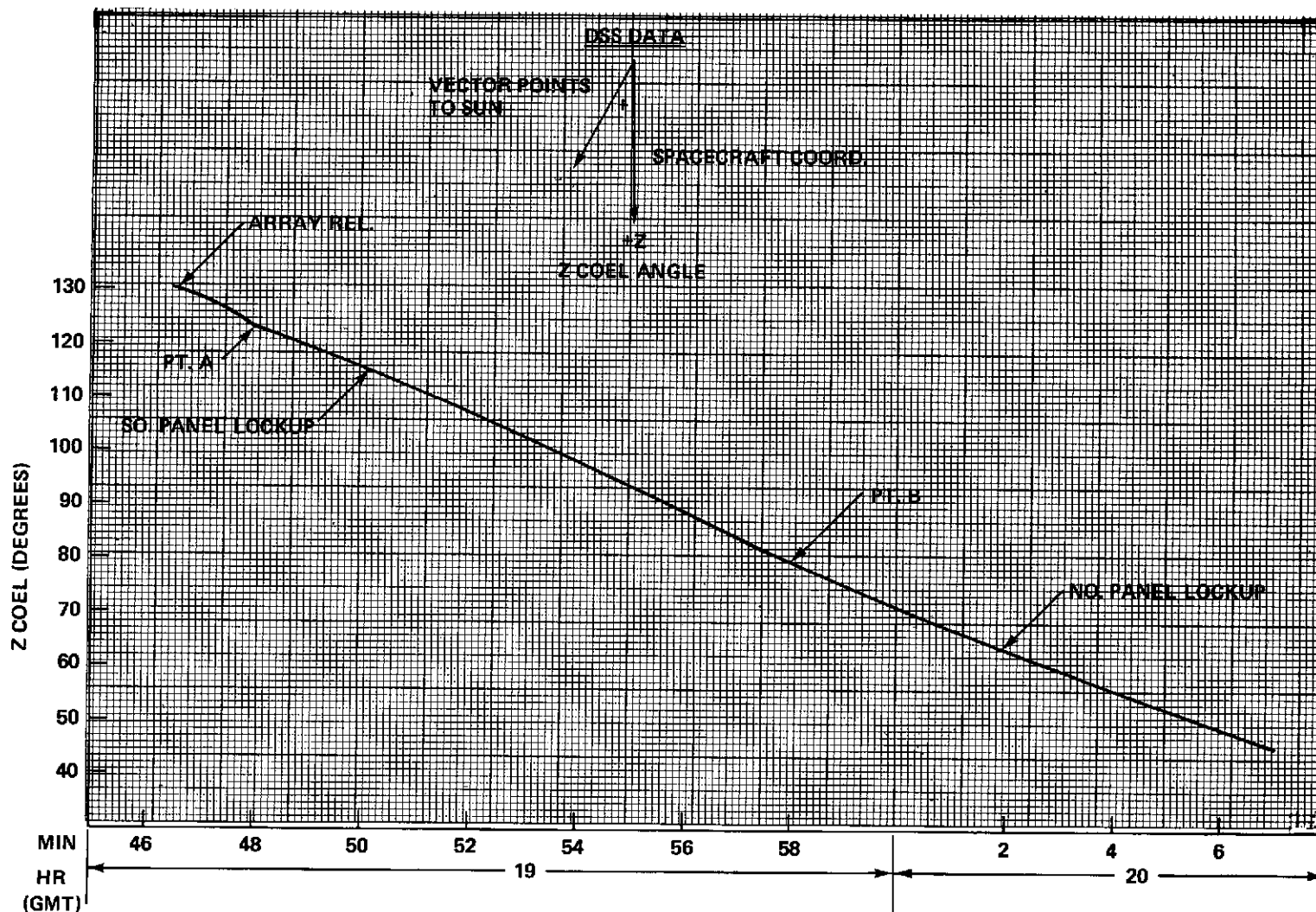


Figure 5-2. Z COEL During Deployment

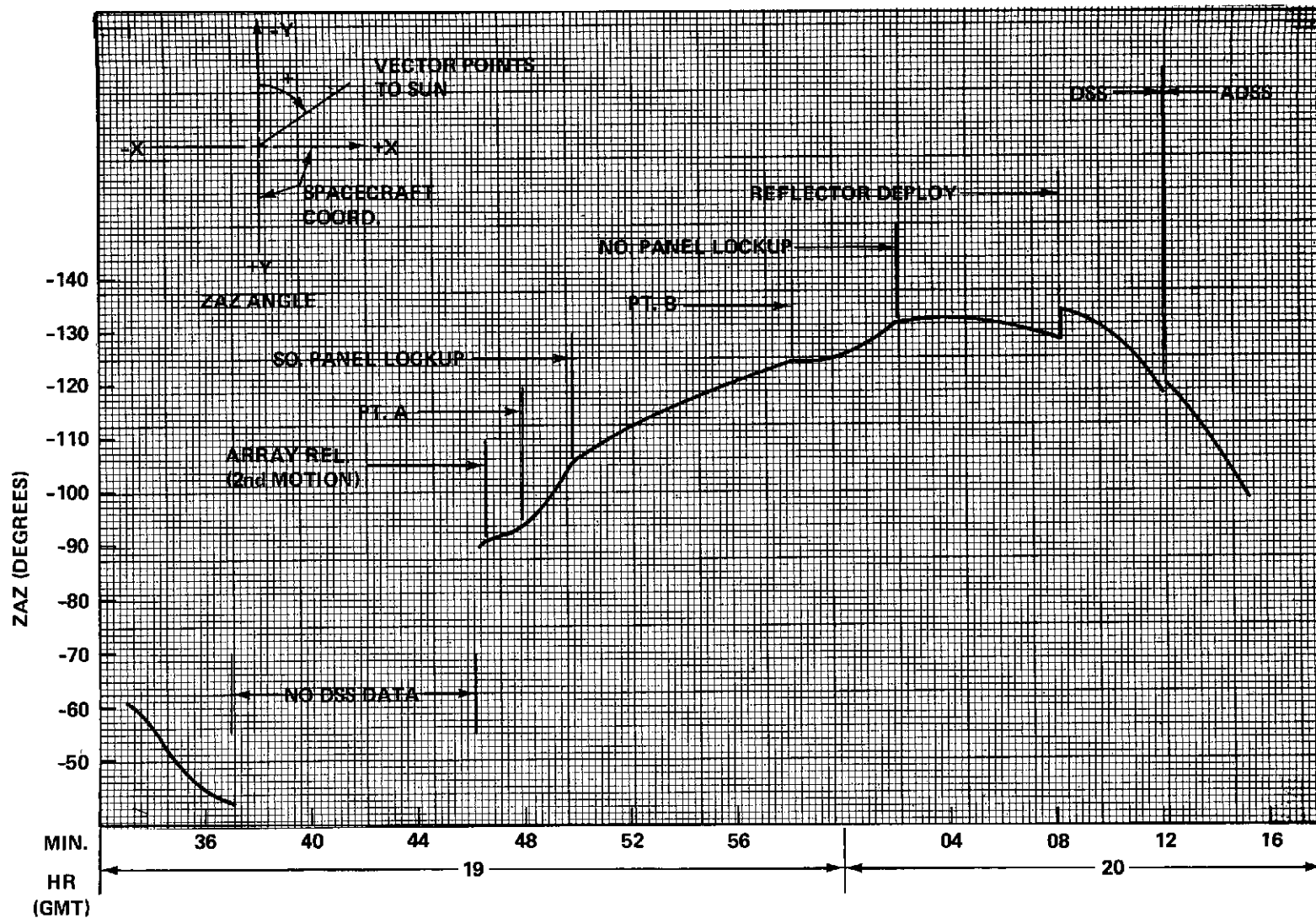


Figure 5-3. ZAZ During Deployment

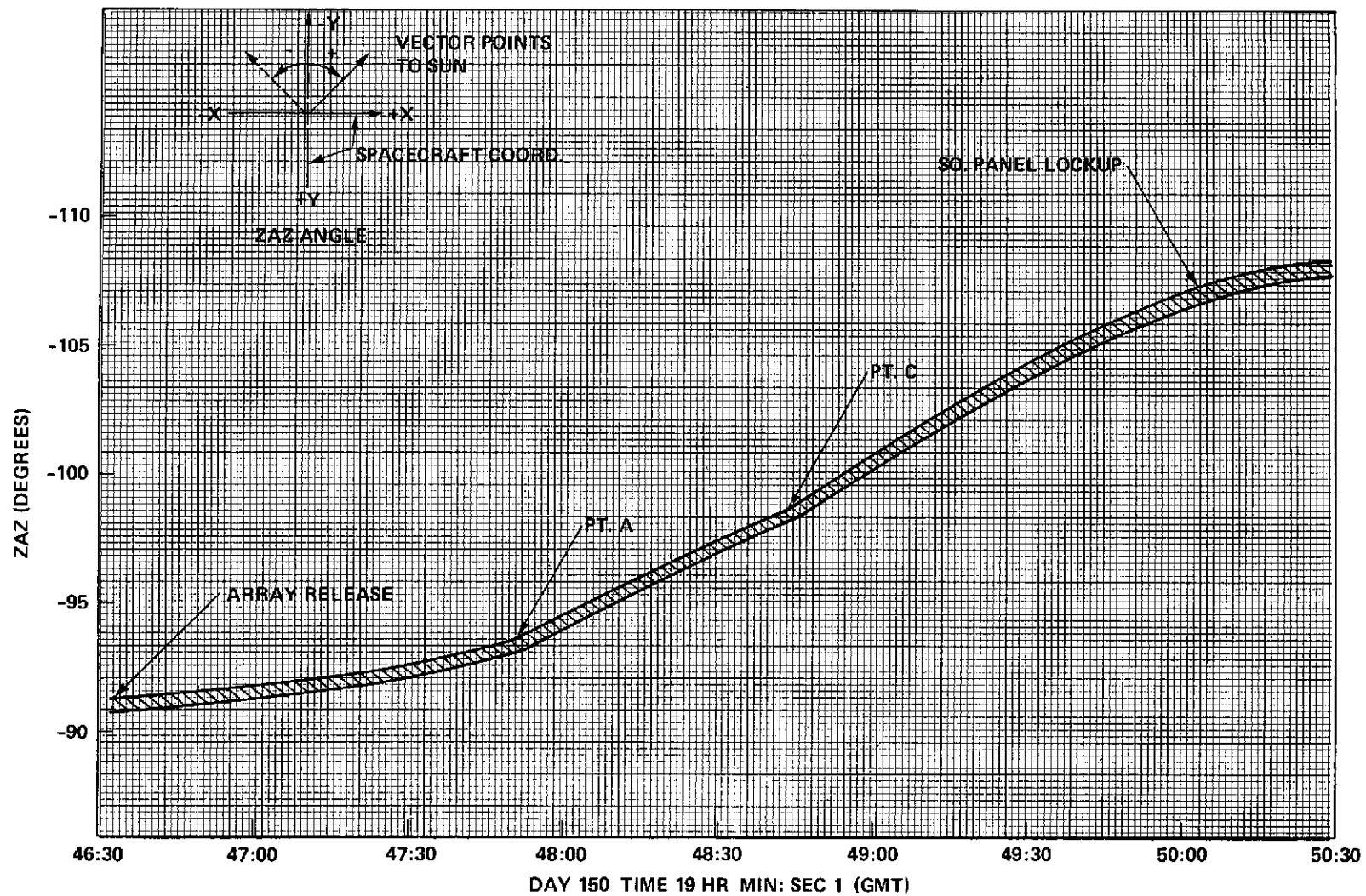


Figure 5-4. ZAZ During Deployment

curve was generated by plotting values of ZAZ, as determined from telemetry and interconnecting adjacent time frame points of ZAZ where such were of the same value. The curve represents a best fit band encompassing all points. The three points of discontinuity in the curve are quite evident. The events which caused the discontinuities at Point A and Point C are not known; however, they may have been caused by a rapid change in the deployment motion of the North array, including a total stop, or intermittent motion.

An inspection of the body rates from the RGA (Figure 5-1) also indicates that substantial variations in yaw velocity occurred during the four-minute period prior to North panel lockup.

Additional confirmation of the position of the North panel is being developed in the following manner:

The angle between the solar vector and each facet of the solar array, both North and South panels, has been developed through a series of equations relating to the solar vector, as determined from Z co-el and ZAZ and geometry about the spacecraft body axes for various positions of the panels about the various hinges. The total shunt current developed in the panels is expected to provide data from which panel position may be determined since spacecraft electrical loads were constant throughout the deployment. The results from preliminary studies appear promising.

There is another line of investigation which may be fruitful. The VHF antennas are located at the outboard end of the solar arrays. The South array antenna operates on a frequency of 136.23 MHz and the North array operates on a frequency of 137.11 MHz. As the solar panels deployed, polarization of the signals received on the ground were altered. These variations effected the AGC levels of ground receivers. Preliminary study of data recorded at Mojave tends to confirm that the North panel accomplished its deployment motion primarily during the four-minute period immediately preceding panel lockup. Additional studies of this data are continuing.

5.1.2 Conclusions

From the above information it is tentatively concluded that the North panel apparently performed the major part (greater than 90 degrees) of its deployment motion during the time period between 19 hours and 58 minutes to 20 hours and 2 minutes.

It is expected that the successful conclusion of the studies described in Section 5.1.1 will establish a position of time history of the North panel motion which can be accepted with confidence. It would be premature to conjecture on the

possible, or probable, cause of the slow deployment of the North panel until the motion history of the panel is known.

5.2 ELECTRICAL

At approximately 6:33:18 hours after launch, the deployment sequence was initiated by the Titan transtage command of Separation Enable. This command powered all spacecraft deployment telemetry lines and the Automatic Deployment Sequencer, a part of the Squib Interface Unit. At that time, all telemetry indications were normal and the automatic sequence was started upon receiving the Separation Fire Command from the Titan transtage.

Table 5-1 includes a time-line for the Automatic Deployment Sequence (Figure 5-5) and graphically presents this time-line. Specific events are numbered on both the time-line and the pictorial and listed as follows:

<u>Event No.</u>	<u>Event Description</u>
1	Separation Enable & Fire
2	Separation Complete
3	Booms Release Enable & Fire
4	South (+Y) and North (-Y) Booms Locked Up
5	Array Unfold Enable & Fire
6	South (+Y) Array Unfolded and Locked
7	North (-Y) Array Unfolded and Locked
8	Reflector Release Enable & Fire
9	Reflector Deployed and Locked
10	Boom Drop Enable & Fire
11	Boom Drop Complete

With the exception of the -Y array unfold event, automatic deployment of the ATS-F was flawless. The Automatic Deployment Sequencer functioned nominally, as did all of the associated microswitches.

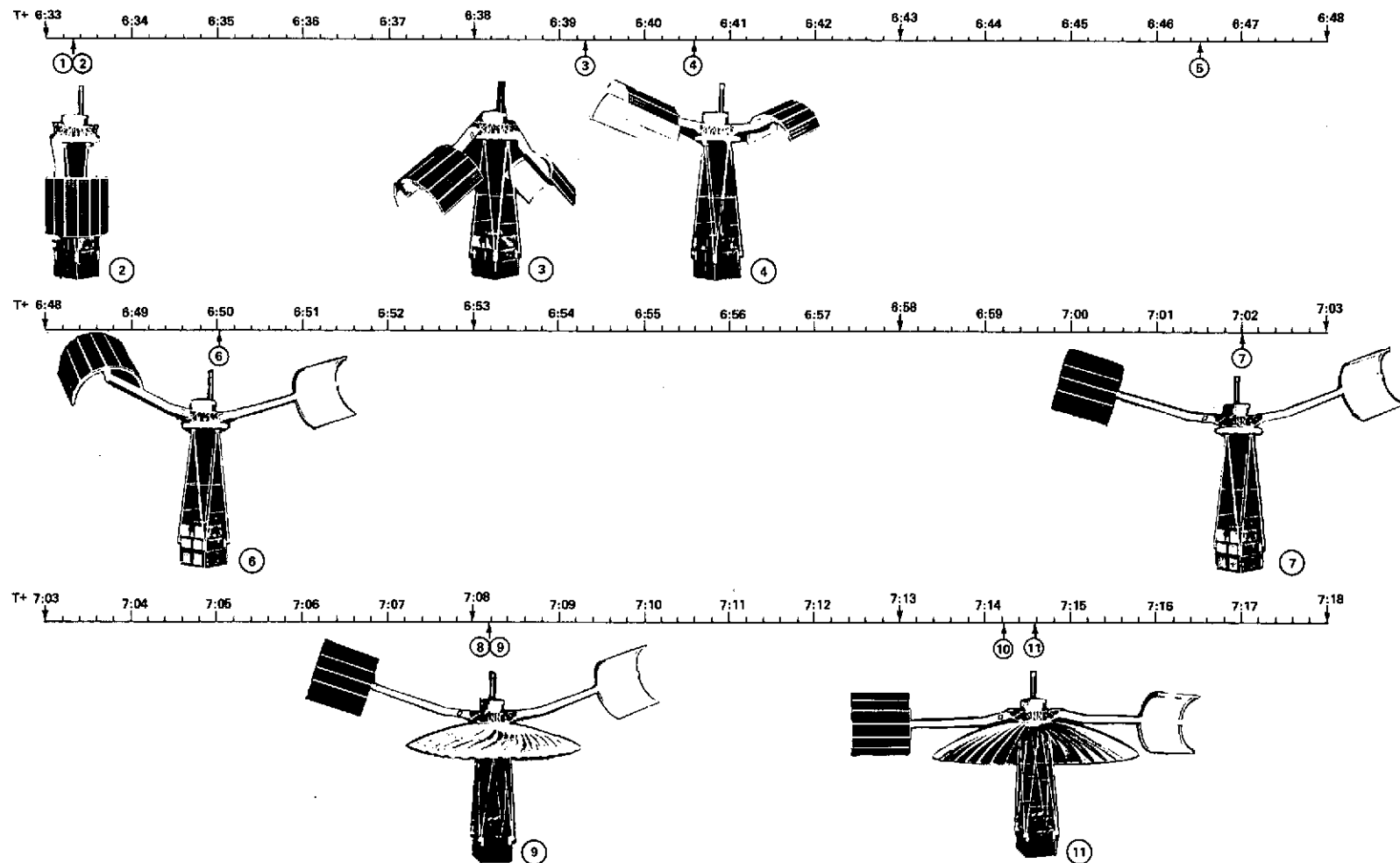


Figure 5-5. Automatic Deployment Sequence

SECTION 6

ELECTRICAL POWER SUBSYSTEM

SECTION 6

ELECTRICAL POWER SUBSYSTEM

6.1 SUBSYSTEM PERFORMANCE

The performance of the ATS-6 Electrical Power Subsystem (EPS) during the first thirty days in orbit has been excellent. All components of the EPS performed not only within specification but within expected beginning of life limits. The solar array performance (available power at the spacecraft bus) was within bounded predictions and higher than nominal prediction. The batteries showed normal characteristics during charge/discharge periods and the power conditioning components performed in complete accordance with predictions.

6.2 PERFORMANCE EVALUATION

6.2.1 In Orbit Overview

Table 6-1 is a specification compliance matrix showing the performance of the major parameters of the EPS. The matrix shows all parameters being well within specifications and within predicted values for beginning of life performance (some of which are detailed in the component section) which is an assurance that no parameter drifts have occurred since pre-launch testing.

6.2.2 Launch and Ascent Performance

The performance and operation of the electrical power subsystem during launch, ascent and deployment was extremely interesting. All major modes of the system were required to operate during this phase, including the solar array "twice power" mode, which occurred after boom first motion of the deployment phase.

Table 6-2 is a sequential history of EPS activity from T-11 (Launch - 11 minutes) when the spacecraft was still on ground power, to T + 7:20 hours when the fourth and final deployment motion was completed. Throughout most of this period, solar array shunt current was a most revealing indicator of spacecraft events, particularly during the deployment sequence.

The following description of the performance of the electrical power subsystem refers to Table 6-2:

T - 11 mins: S/C Powered by Ground Power Supply

The EPS was in the shunt mode with the appropriate spacecraft bus voltage in this mode (+30.6 v). Both batteries were fully charged and their charge

Table 6-1

Electrical Power Subsystem — In-Flight Specification Compliance

Component/Parameter	Specification	In Flight Performance
Solar Array Power @ Power Regulation Unit	555 watts @ Summer Solstice	595 watts @ Summer Solstice
Battery Capacity	17.5 ampere-hours @ $15^{\circ}\text{C} \leq T \leq 25^{\circ}\text{C}$	Not measured. However, battery charge/discharge per- formance has been excellent. Maximum discharge 6 - 5 A-H.
Spacecraft Bus Voltage	$+30.5\text{ v} \pm 2\%$	$+30.5\text{ v} \begin{matrix} +0.3\% \\ -0.9\% \end{matrix}$
Battery 1 Charge Current Limit	$1.5\text{ A} \begin{matrix} +0.15\text{ A} \\ -0.08\text{ A} \end{matrix}$	$1.5\text{ A} \begin{matrix} +0 \\ -0.03\text{ A} \end{matrix}$
Battery 2 Charge Current Limit	$1.5\text{ A} \begin{matrix} +0.15\text{ A} \\ -0.08\text{ A} \end{matrix}$	$1.5\text{ A} \begin{matrix} +0 \\ -0.03\text{ A} \end{matrix}$
Battery 1 Volt/Temp Charge Taper Performance	$26.88\text{ v} \pm 0.2\text{ v} @ 17.4^{\circ}\text{C}$ $26.58\text{ v} \pm 0.2\text{ v} @ 22.8^{\circ}\text{C}$	$26.9\text{ v} @ 17.4^{\circ}\text{C}$ $26.6\text{ v} @ 22.8^{\circ}\text{C}$
Battery 2 Volt/ Temp Charge Taper Performance	$26.88\text{ v} \pm 0.2\text{ v} @ 17.4^{\circ}\text{C}$ $26.58\text{ v} \pm 0.2\text{ v} @ 22.8^{\circ}\text{C}$	$26.8\text{ v} @ 17.4^{\circ}\text{C}$ $26.5\text{ v} @ 22.8^{\circ}\text{C}$
Load Interface CK + (LIC) for QCM	$28.0\text{ v} \pm 0.45\text{ v}$	27.9 v
LIC (EME)	$28.0\text{ v} \pm 0.45\text{ v}$	28.0 v
LIC (VHRR)	$28.0\text{ v} \pm 0.45\text{ v}$	28.0 v
LIC (MMW 1)	$28.0\text{ v} \pm 0.45\text{ v}$	27.9 v
LIC (MMW 2)	$28.0\text{ v} \pm 0.45\text{ v}$	27.9 v
LIC (PROP)	$28.0\text{ v} \pm 0.45\text{ v}$	28.0 v
LIC (ION 1)	$28.0\text{ v} \pm 0.45\text{ v}$	28.1 v
LIC (ION 2)	$28.0\text{ v} \pm 0.45\text{ v}$	28.0 v
LIC (Signal Conditioning)	$28.0\text{ v} \pm 0.45\text{ v}$	28.1 v
Comm Regulator 1	$28.0\text{ v} \pm 0.45\text{ v}$	28.1 v
Comm Regulator 2	$28.0\text{ v} \pm 0.45\text{ v}$	28.2 v

Table 6-2

EPS Launch, Ascent Data

Parameter	T-00:11:00 S/C Powered by GPS	T-00:10:00 S/C on Int. Power	T = 0 Liftoff	T+00:05:08 Fairing Eject	T+00:09:30	T+00:23:11	T+ 39:00 Umbral Transition	T+00:56:01 Eclipse
Solar Array Bus Voltage	30.6	30.4	30.4	30.6	30.6	30.6	30.4	30.4
Solar Array Load Current	6.5	0	0	9.05	9.15	9.5	3.1	0
Solar Array Shunt Current	3.6	0	0	4.59	11.28	18.86	0	0
Battery 1 Voltage	26.7	25.7	24.82	25.2	25.77	26.3	25.77	24.47
Battery 1 Charge Current	0.25	0	0	1.47	1.48	1.48	0	0
Battery 1 Discharge Current	0	3.89	3.9	0	0	0	1.7	3.89
Battery 2 Voltage	26.7	25.6	24.80	25.2	25.75	26.2	25.7	24.44
Battery 2 Charge Current	0.25	0	0	1.48	1.49	1.49	0	0
Battery 2 Discharge Current	0	3.6	3.9	0	0	0	1.67	3.91
Battery 1 SOC	1	1	0.95	0.93	-	-	-	-
Battery 2 SOC	1	1	0.95	0.93	-	-	-	-
VHRR LIC Voltage	28.0	28.0	28.0	28.0	28.0	28.0	28.0	28.0
QCM LIC Voltage	27.9	27.9	27.9	27.9	27.9	27.9	27.9	27.9
S/C Load Current	6.5	5.7	5.7	9.05	9.15	9.5	5.7	5.7

Table 6-2 (Cont'd)

EPS Launch, Ascent Data

Parameter	T+1:24:05 During Sunlight	T+2:35:56 Start of Batt 1 Taper	T+2:38:21 Start of Batt 2 Taper	T+3:08:43	T+3:38:01	T+6:40 Solar Array Twice Power	T+7:20 After Deployment
Solar Array Bus Voltage	30.6	30.6	30.6	30.6	30.6	30.6	30.6
Solar Array Load Current	9.1	9.0	8.7	6.3	6.1	6.5	6.2
Solar Array Shunt Current	11.93	12.0	12.3	14.8	14.9	> 26	15
Battery 1 Voltage	25.06	26.82	26.82	26.82	26.82	26.82	26.82
Battery 1 Charge Current	1.49	1.46	1.23	0.33	0.26	0.28	0.29
Battery 1 Discharge Current	0	0	0	0	0	0	0
Battery 2 Voltage	25.04	26.7	26.76	26.76	26.76	26.76	26.76
Battery 2 Charge Current	1.49	1.49	1.48	0.35	0.25	0.28	0.30
Battery 2 Discharge Current	0	0	0	0	0	0	0
Battery 1 SOC	-	-	-	-	-	-	-
Battery 2 SOC	-	-	-	-	-	-	-
VHRR LIC Voltage	28	28	28	28	28	28	28
QCM LIC Voltage	27.9	27.9	27.9	27.9	27.9	27.9	27.9
S/C Load Current	9.5	7.0	8.7	6.3	6.1	6.1	6.2

currents tapered to 0.25 ampere. Battery state-of-charge (SOC) was 1.0. The spacecraft load current was 6.5 amperes which included charge current, charger drive losses, shunt dissipator drive losses, T&C Subsystem, VHRR, and QCM, experiments.

T - 10 mins: S/C on Internal Battery Power

Here the EPS was in the boost mode with the appropriate S/C bus voltage in this mode of 30.4 volts. An immediate reduction in battery voltage occurred indicating battery discharge with the battery of slightly higher voltage delivering a larger portion of the total discharge current. Spacecraft load current was 5.7 amperes, the reduction from 6.5 amperes being due to the absence of battery charge current, charger drive losses, and shunt dissipator drive losses.

T = 0: S/C Liftoff

All parameters were nominal. Battery voltages had equalized and both batteries were equally sharing the discharge current for the S/C loads. The boost regulator efficiency at this time was a nominal 89.5%. The battery SOC of 0.95 was the value predicted for liftoff.

T + 5:08 mins: Payload Fairing Eject

At this time, an immediate substantial output of array power, sufficient to put the EPS into the shunt mode, was observed. Minimum battery SOC reached 0.93 as predicted, before the fairing ejected. An increase in spacecraft load current from 5.7 A to 9.05 A was caused by battery charge currents (totaling 2.95 A) plus charger and shunt dissipator drive losses. The batteries charged at the maximum limits because sufficient discharge had occurred (as indicated by SOC of 0.93) prior to fairing eject.

T + 23.11 mins: Max. Solar Array Power in Stowed Position

This column indicates the time when solar array output was maximum while the arrays were still stowed. All parameters were nominal. Spacecraft load current increased to 9.5 A due to additional shunt dissipator drive power required to control the large shunt current.

T + 39:00 mins: Umbral Transition

The umbral transition provided an excellent opportunity to observe the EPS in the battery share mode. Here, because the array current (3.1 A) was not sufficient to satisfy the spacecraft load demand (5.7A), the batteries through the boost regulator provided the difference. All parameters were nominal; the spacecraft bus voltage was +30.4 volts in this mode, and because of the absence of charge current, the spacecraft load current was again 5.7 A as it was at liftoff.

T + 56:01 mins: Eclipse

The system again was in the boost mode as it was at liftoff and parameters were nominal.

T + 2:35:56 hours: Start of Battery 1 Taper

At this time, the spacecraft had been back in sunlight enough time for battery charge taper to begin. Battery 1 started taper while battery 2 was still charging at the maximum current limit. All parameters were nominal.

T + 2:38:21 hours: Start of Battery 2 Taper

Approximately three mins after battery 1 started taper, battery 2 entered the taper charge region. All parameters were nominal.

T + 3:38:01 hours: Both Batteries Deep into Taper

Here, both batteries had tapered back to the trickle charge current level.

T + 6:40 hours: Solar Array Twice Power Mode

At boom first motion the arrays extended and both were directed toward the sun. During this period the solar array shunt current exceeded the full scale telemetry calibration limit of 26.0 amperes. In addition, the solar array was also supplying a load current of 6.5 amperes. Because the shunt current calibration limit was exceeded, the exact value of the solar array current is not known. However, the range can be grossly determined on the low end by adding shunt and load current (32.5 A) and on the high end by the array current capability of both array paddles (42 A). The electrical power subsystem had been designed and tested to handle the twice array power mode, which accounts for its satisfactory performance during this period.

T + 7:20 hours: Spacecraft Deployed

The spacecraft successfully completed all deployment motions; the electrical power system was in the shunt mode (15 amps shunt current) and all parameters were nominal.

A complete EPS time line with the actual strip chart recordings for this period is contained in the ATS-6 First Orbit Evaluation report. (X-713-74-177 of June 1974)

6.3 MAJOR COMPONENT PERFORMANCE

6.3.1 Solar Array

All aspects of the solar array performance during the first 30 days in orbit have been good, with only one minor anomaly. This was a higher than normal tap

voltage on one of the shunt dissipators when the shunts were not conducting. This might be indicative of an open or high impedance solar cell string or shadowing effects caused by the omni antenna. (See Section 6.4)

The solar array produced power output of 595 watts which is 7.2% higher than the beginning-of-life predicted value of 555 watts. The thermal performance, additional details of which may be found in Section 7, has been within the pre-flight predictions.

Figure 6-1 is a plot of the still-stowed solar array power from $T = 0$ to $T + 4$ hours. The plot is discontinuous at several places because of numerous ground data losses which occurred during this period. These losses have been attributed to severe electrical disturbances in the Eastern United States. Referring to Figure 6-1, at $T + 5:08$ minutes; the payload fairing was ejected and an immediate substantial power output from the solar array resulted. At $T + 25$ minutes, the array power maximized at 1000 watts which agrees favorably with the predicted maximum of 900 watts during the ascent phase. This high value of power from the still-stowed array was caused by the Earth albedo contribution. As the vehicle climbed to synchronous altitude between $T + 1:30$ hours and $T + 6:27$ hours, the solar array power output was a nominal 670 watts with the predicted power during this period being 660 watts. The predicted solar array power during the ascent phase is shown in Figure 6-2. This extended period of array power allowed the first observation of battery charger performance in the taper charge mode. Spacecraft separation occurred at $T + 6:33$ hours and a steady decrease in shunt current from 15.6 to 7.0 amperes was observed as the spacecraft attitude drifted uncontrolled. The entire spacecraft deployment sequence was observed on the shunt current telemetry, and this has also been detailed in the "ATS-6 First Orbit Evaluation" report.

To date, no discernible solar array degradation has occurred. The solar array power has been monitored frequently since the first day in orbit. However, because of the nonlinearity of the partial shunt/solar array system, the only true indications of solar array power output were obtained when the spacecraft load power exceeded the solar array power ($I_L > I_{SA}$). This makes the solar array power determination a simple multiplication of solar array current by spacecraft bus voltage modified by the sun elevation angle (SEL).

It was necessary to record the sun elevation angle each time array data was taken because SEL was changing continuously due to spacecraft slew maneuvers and offset pointing tests conducted during the checkout period.

Figure 6-3 is a plot of solar array power vs SEL for various days throughout the initial 30-day period. The numbers within the circular data points indicate the number of days after launch day (Day 150) that the data was taken.

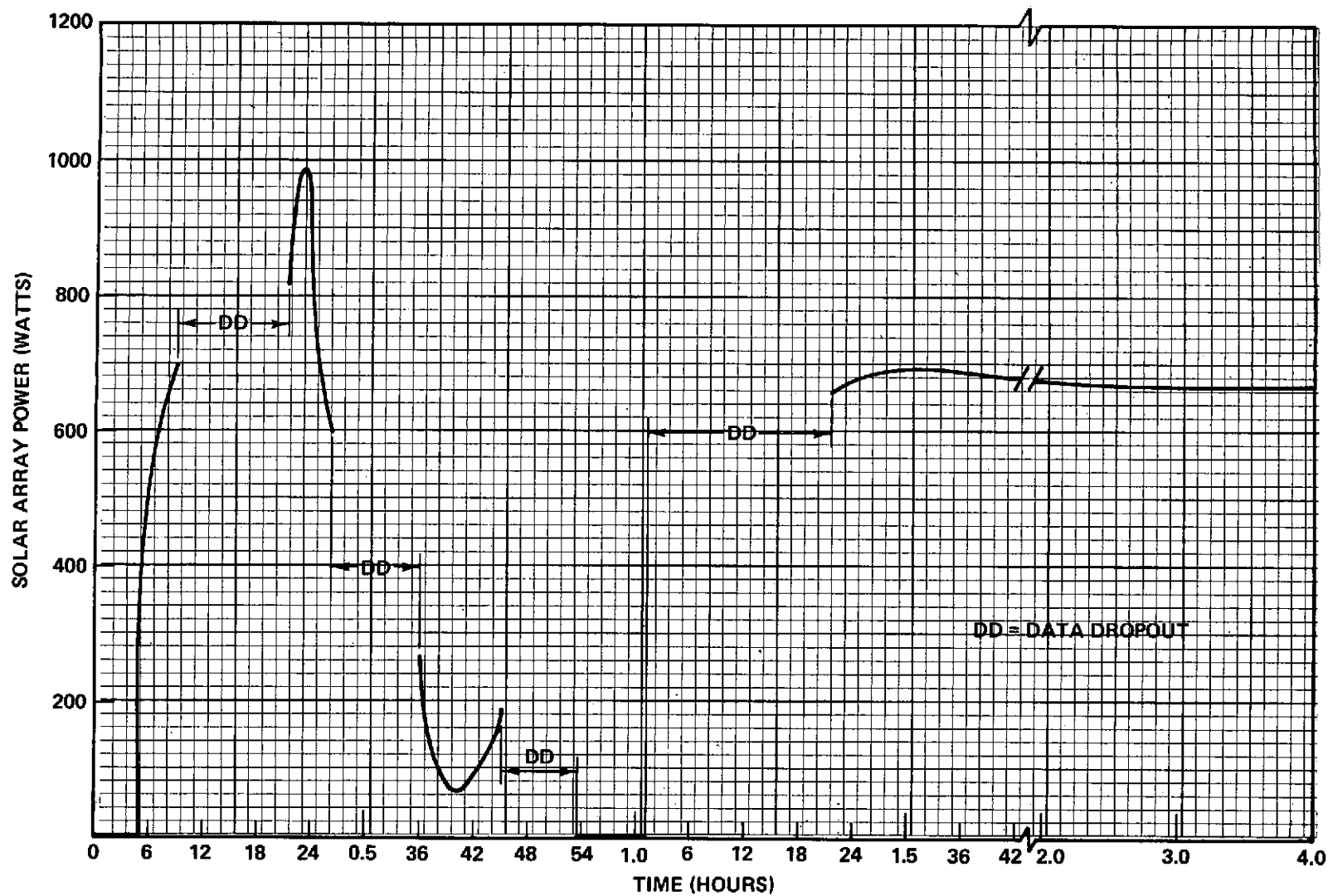


Figure 6-1. Solar Array Power (@ Array) vs Time (T = 0 to T + 4 hrs)

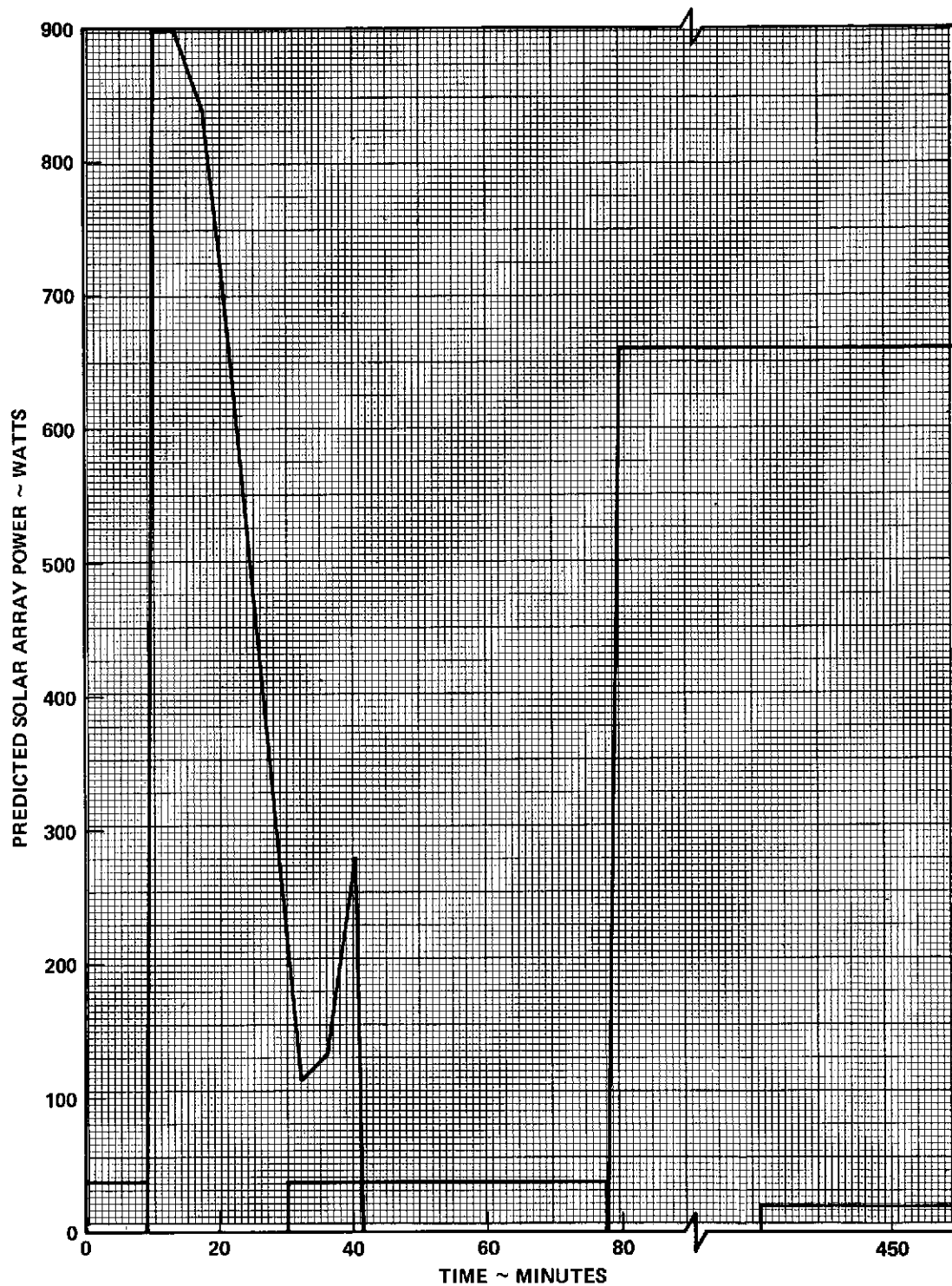


Figure 6-2. Predicted Solar Array Power ~ Watts

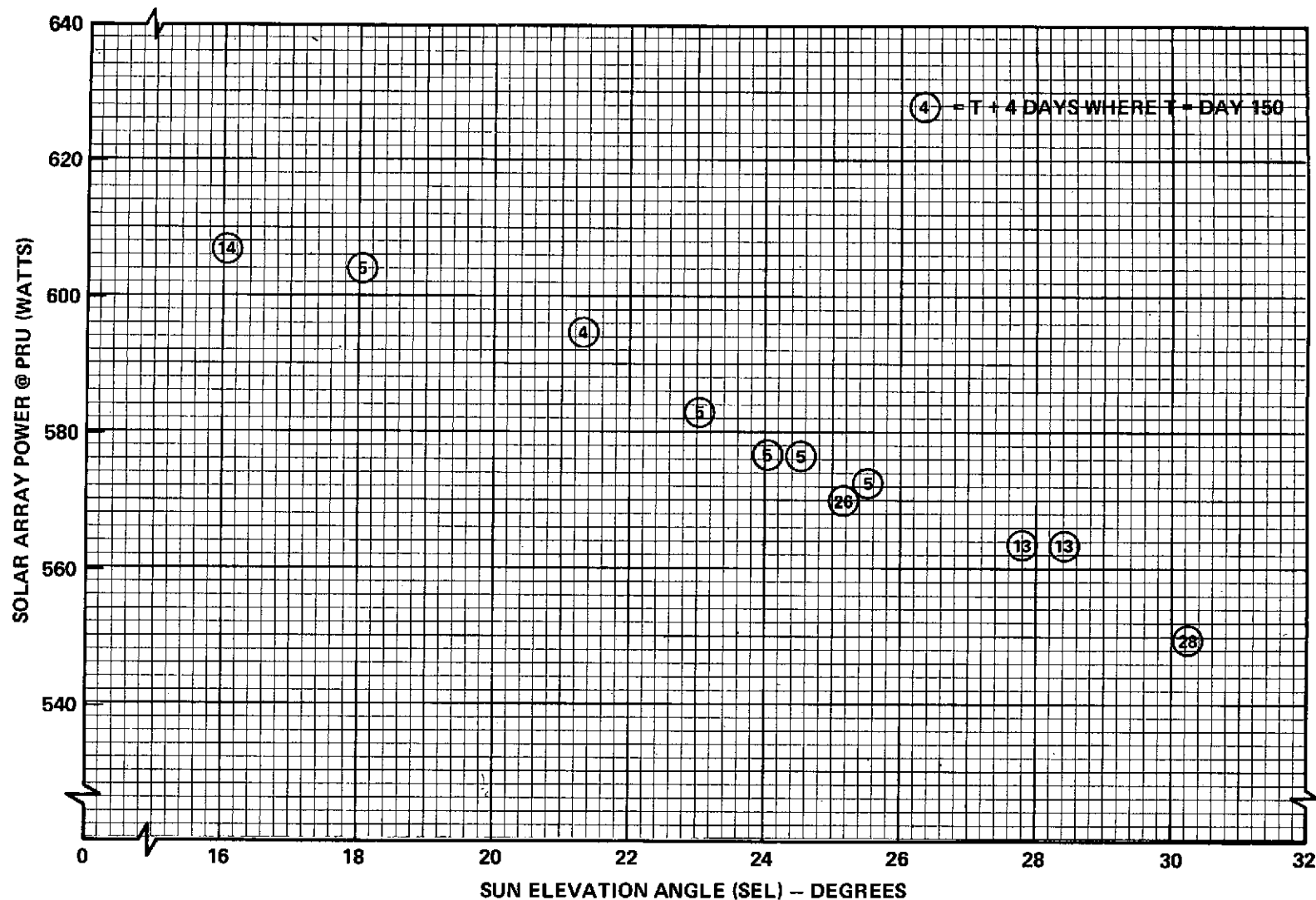


Figure 6-3. Solar Array Power @ PRU vs Sun Elevation Angle for Days 154 thru 164

In order to determine if there had been any array power degradation, it was necessary to normalize this data with respect to a 20° SEL, which is typical for this time of year. A plot of the normalized array power as a function time is shown in Figure 6-4. The normalized plot removes the effects of slewing, off-set pointing, and seasonal variations, leaving only the changes that might be caused by degradation. The fact that this plot has nearly zero slope indicates no discernible reduction in array power due to degradation. The predicted array power degradation for the first month in orbit was 1% which might not be discernible because of resolution limitations.

The data for Figures 6-3 and 6-4 was taken at different times of day through the first 28 days (approximate time of day for each data point can be extracted from the plot). Therefore, it may indicate the uniformity of output power of the ATS semi-cylindrical solar paddle configuration. This proves that both array paddles are well matched and performing well.

6.3.2 Battery Performance

Two 15 ampere-hour batteries in the EPS provide power to the spacecraft during the launch, deployment, occult, and solar array/battery boost share modes. The batteries have successfully supported the launch and deployment phases of the ATS-6 mission and have been used extensively to support all loads in excess of the solar array capability with continuous loads of up to 3.5 amperes each during the operation of the PLACE, HET, and UHF experiments.

6.3.2.1 Battery Charge/Discharge Profile—Launch Day — At the end of the RF silence period (10:30) on launch day, the batteries were discharged 25 watt-hours and recharged. Figure 6-5 illustrates the battery charge/discharge profile on launch day. Taper charge began about 12:00 and both batteries reached 0.25 amperes well before the spacecraft went on internal power at 12:49:39 or 10 minutes, eleven seconds prior to launch. Average launch load for each battery was 3.9 amperes. At payload fairing jettison (T + 00:05:08), discharge was terminated and full (1.48 amperes) charge resumed. Battery state-of-charge as indicated by the state-of-charge program was 93 percent at this point. As the spacecraft went into the earth's shadow, the batteries again discharged, beginning recharge at 14:24. Battery #1 and #2 voltages at the end of discharge were 24.2 and 24.15 volts respectively. These voltages nearly match an estimate of 24.3 volts, which was based on temperature/current extrapolations of the battery acceptance test data. The batteries were recharged and were well into taper at the time of deployment.

6.3.3.2 Battery Temperature—Launch — Pad air-conditioning was removed about three hours prior to launch and the battery #1 and #2 temperatures at this time were 17.6 and 17.8 degrees Centigrade respectively. Figure 6-6 shows

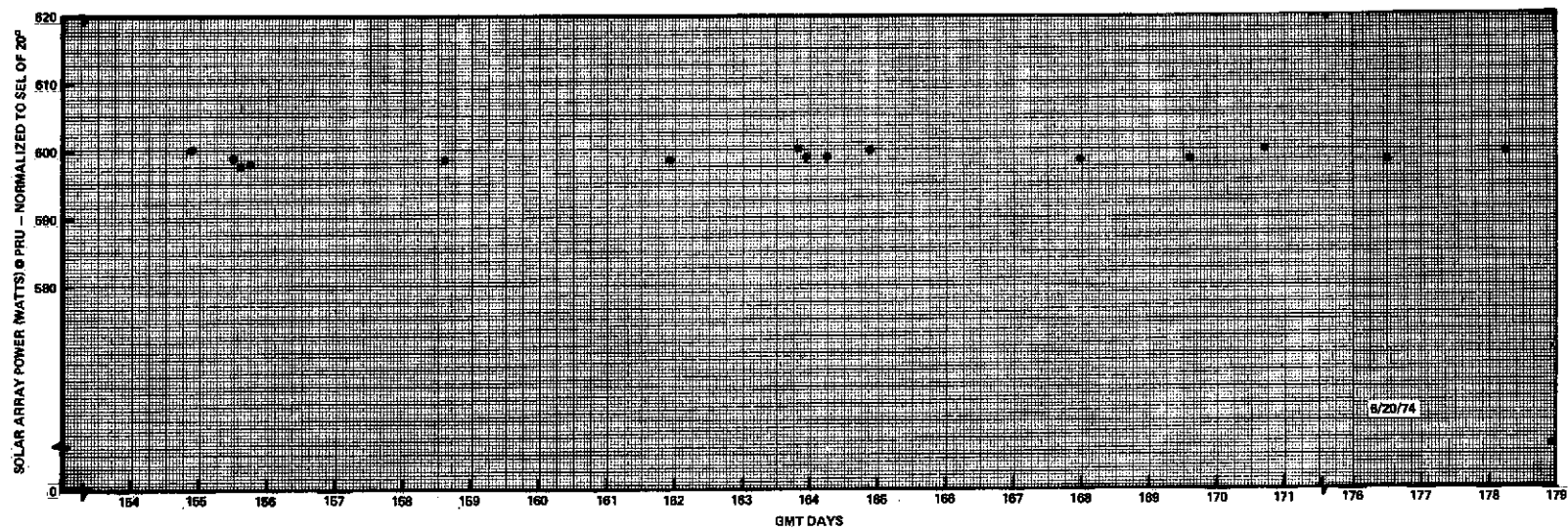


Figure 6-4. Normalized Solar Array Power @ PRU vs Days in Orbit

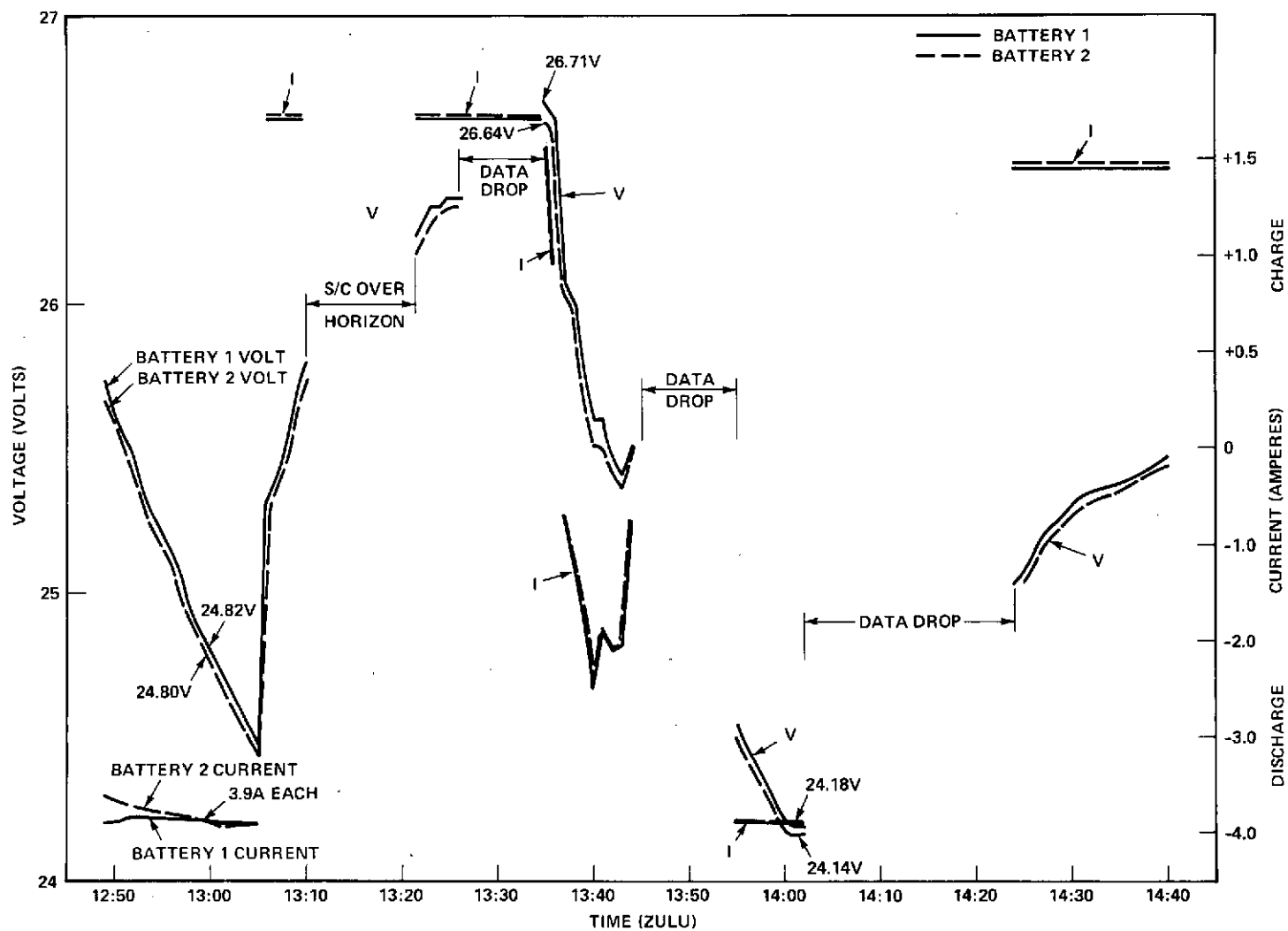


Figure 6-5. Battery Charge/Discharge Profile Launch-Day 150

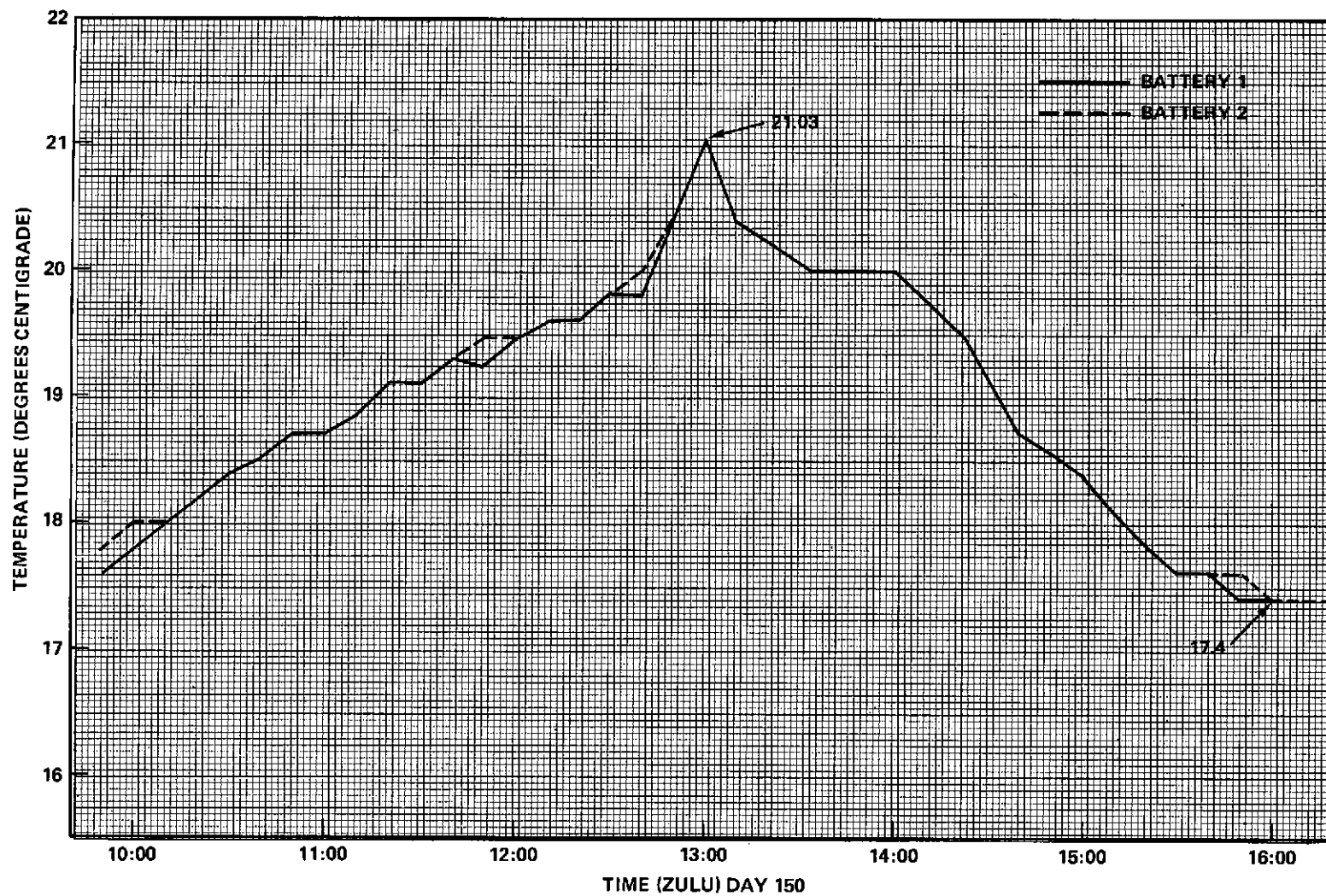


Figure 6-6. Battery Temperatures Launch (13:00)

that both batteries tracked very closely thermally, with battery #2 (the inner battery) warming more quickly and cooling more slowly than battery #1. Maximum temperature difference between the two batteries was 0.21 degrees C. A peak temperature of 21.05 degrees C for each battery was reached at liftoff. Within three hours, both batteries had stabilized at 17.41 degrees C where they remained for about 4.5 hours. After this time, the temperature started to decrease as part of the normal spacecraft thermal cycle. The nearly optimal thermal control during launch, maximized battery performance during this period.

6.3.2.3 Battery Temperature Cycling—Orbit — The extreme battery temperatures experienced during the first two days of orbit were 22.44 degrees C and 15.74 degrees C for battery #1, and 22.79 degrees C and 15.74 degrees C for battery #2. This range is typical of battery thermal performance experienced thus far in orbit and is depicted in Figure 6-7. These temperatures tracked closely with a maximum difference of 0.36 degrees C. Figure 6-8 summarizes battery taper charge and thermal performance for a portion of the third day and all of the fourth day in orbit. Throughout this period, the batteries were on trickle charge. The thermal profile was similar to that shown in Figure 6-7.

6.3.2.4 Capacity vs Temperature — The operational temperature range of 15.5 degrees C to 22.5 degrees C is in the region of maximum effective capacity of each battery. The capacity vs temperature characteristic of the ATS-6 batteries was developed during cell characterization tests and is presented as Figure 6-9. The curve indicates that the battery capacity peaks at about 20 degrees C which is close to the average battery temperature in orbit.

6.3.2.5 Battery Capacity — Between 15 degrees C and 25 degrees C the batteries are capable of delivering well in excess of their rated 15 A-H capacity when discharged at a 7.5 ampere rate. Because the spacecraft has provided an optimal thermal environment for the batteries and the discharge rates have been much lower than 7.5 amperes for each experimental mode, the effective capacity is greater than 15 A-H. Actual capacity under flight conditions may be greater than 20 A-H, providing large operational and life degradation design margins. It is not intended to specifically measure in-orbit capacity, nor is it desirable, but rather battery characteristics may be verified via operational mode testing.

6.3.2.6 Operational Mode Testing — The batteries have successfully supported all in-orbit testing to date including all high power experiment modes and pulse discharges. It is difficult to make a direct comparison of in-flight battery performance data to ground acceptance test data due to the dynamics of the spacecraft and the differences in load currents. However, analysis of charge/discharge data clearly shows that all 38 cells are performing as expected.

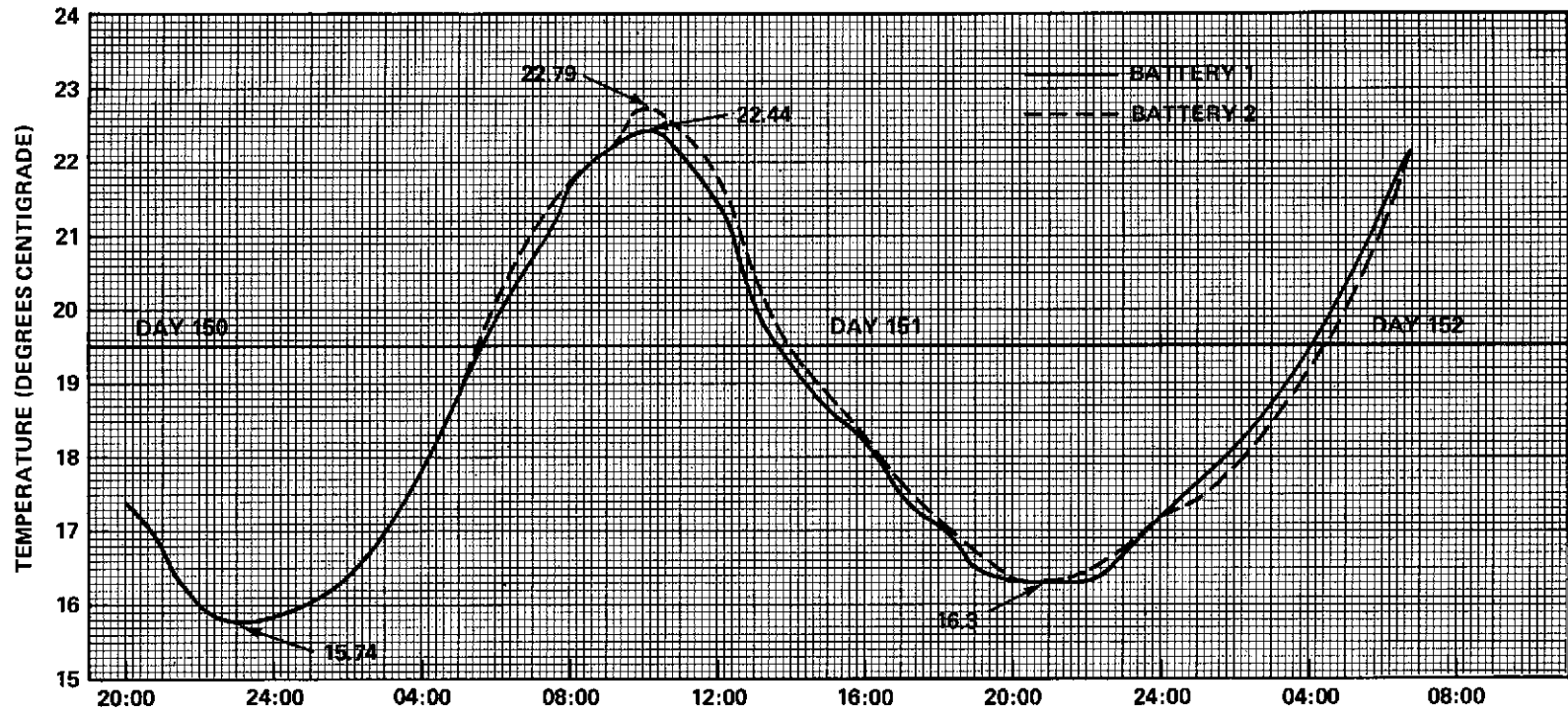


Figure 6-7. Battery Temperature Days 150, 151, 152

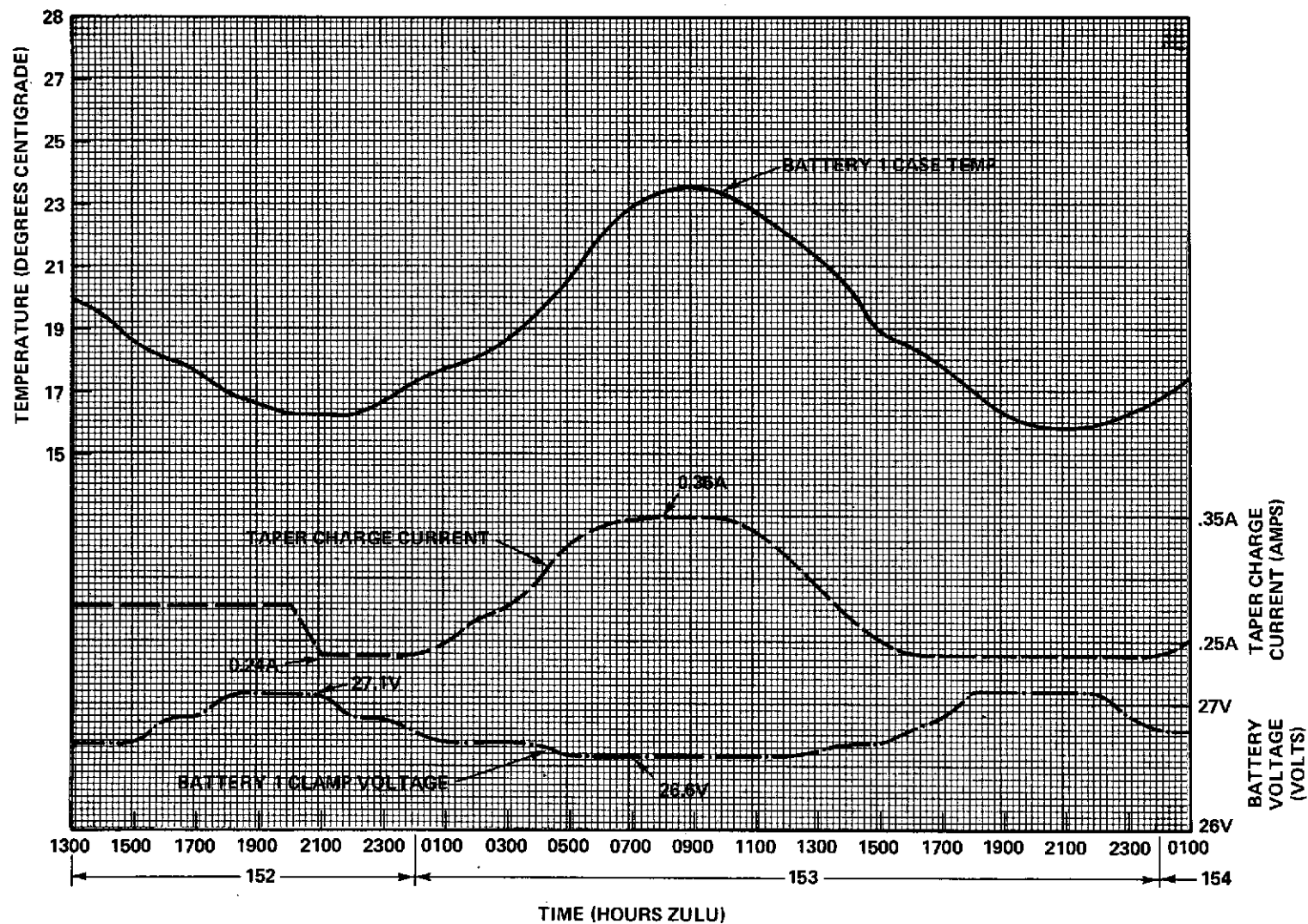


Figure 6-8. Battery Temperature vs Time vs Battery Voltage vs Taper Charge Current

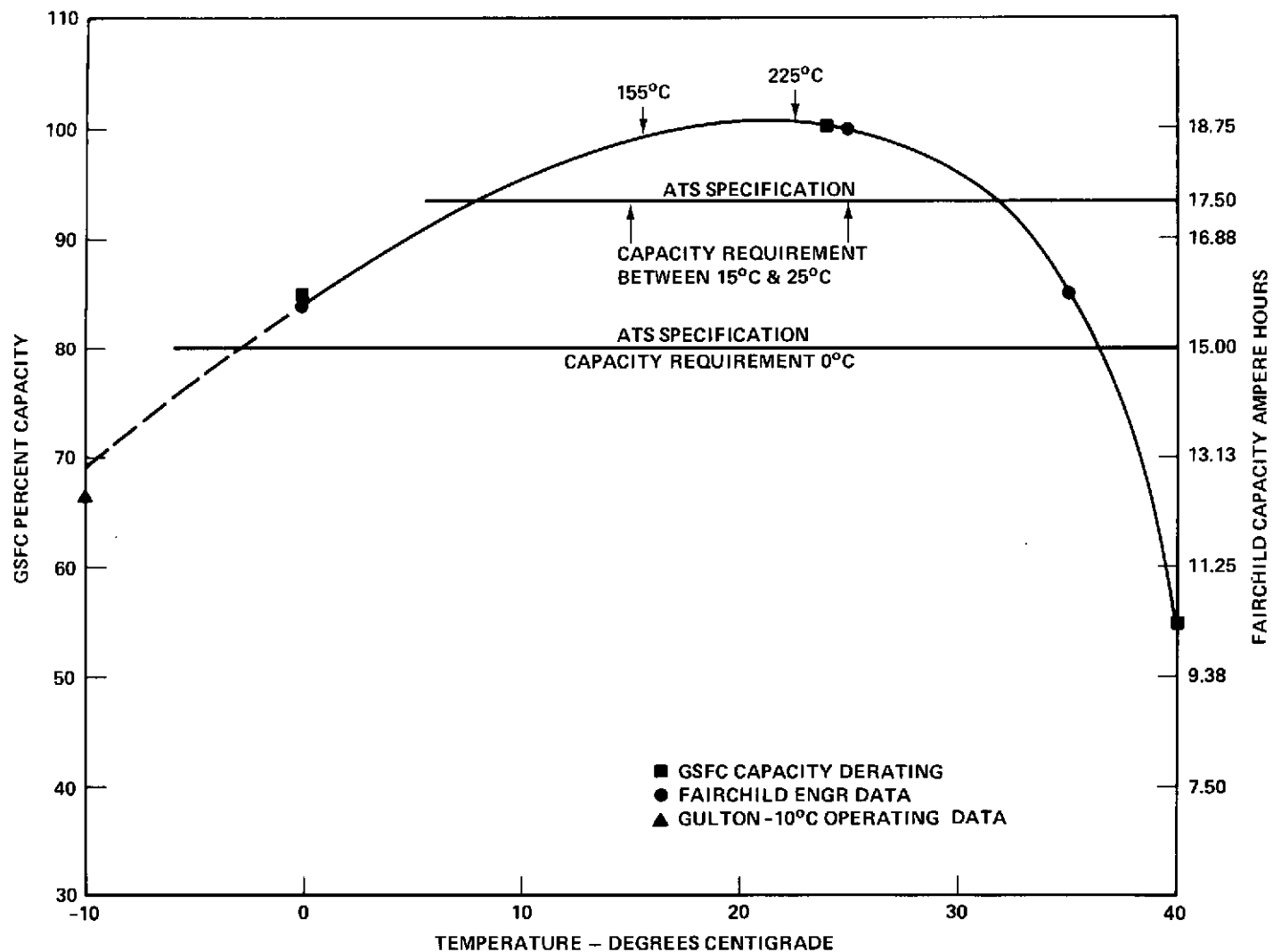


Figure 6-9. Nickel Cadmium Battery Capacity vs Temperature

Figures 6-10 through 6-12 show battery voltages for actual discharges during portions of the in-orbit testing. All three curves show typical discharge characteristics with relatively fast initial decay in battery voltage and a slower, flatter, voltage decrease thereafter. While all three curves are for battery #1, nearly identical plots could be drawn for battery #2. In none of the three discharges did the voltage fall below 23 volts, or 1.21 v/cell. At 29 degrees C, approximately 13.5 A-H would have to be discharged before this voltage would be reached if all cells were operational. This depth of discharge was not reached since all discharges have been limited to 50% (7.5 A-H) maximum. If a cell was shorted, the average cell voltage for the remaining cells would have to be 1.33 volts to maintain a battery voltage of 24 volts. This cell voltage can only be maintained at 29 degrees C if less than 1.25 A-H has been removed. All three plots represent discharges greater than 1.25 A-H and show voltages, well into discharge, of greater than 24 v. Hence all cells are operational.

6.3.2.7 Battery Charge Performance — During the transfer orbit, the batteries were fully charged. Charge rate was 1.49 amperes for both batteries until the state-of-charge was approximately 95 percent (1.2 hours) after which the current tapered to 0.24 amps in 1.6 hours. The average cell voltage during taper was constant at 1.412 and 1.408 volts for battery #1 and #2, respectively. Start-of-taper temperature was 17.6 degrees C which would correspond to a cell voltage clamp of 1.417 volts. Battery #1 and #2 taper clamp voltages at 17.6 degrees C were 26.82 v and 26.75 v respectively, which were within the $26.92 \text{ v} \pm 0.2 \text{ v}$ specification range.

6.3.2.8 Orbital Performance — Figure 6-8 indicates that the charger taper circuitry, including the battery thermistors, have been operating properly, maintaining trickle currents that are temperature compensated and clamping the battery voltages within safe operating limits. A typical voltage/current charge curve is presented as Figure 6-13. This recharge occurred after the 58 percent HET discharge shown in Figure 6-12. Recharge started at 20 degrees C and terminated when the battery temperatures were 21 degrees C. The voltage clamped at 26.6 volts at the time taper charge began. The state-of-charge computer program indicated that taper began at 86 percent (an error of 3% probably due to data drops) since the expected state-of-charge was approximately 89 percent for this temperature. Figures 6-14 and 6-15 are point plots of the actual high and low temperature battery clamp voltages for batteries #1 and #2, respectively during the first fourteen days in orbit. Several low temperature data points appear to be out of the ± 0.2 volt specification limit at the lower temperatures, but actually, the data was taken with taper currents equal to the trickle charge current of 0.24A. At the trickle charge level, the battery voltage tolerance is no longer applicable because the batteries are in a safe low-level constant-current mode. While there may be a slight voltage rise due to the trickle charge, the batteries will safely accept this continuous charge without degradation. The charge taper circuit has been performing as designed.

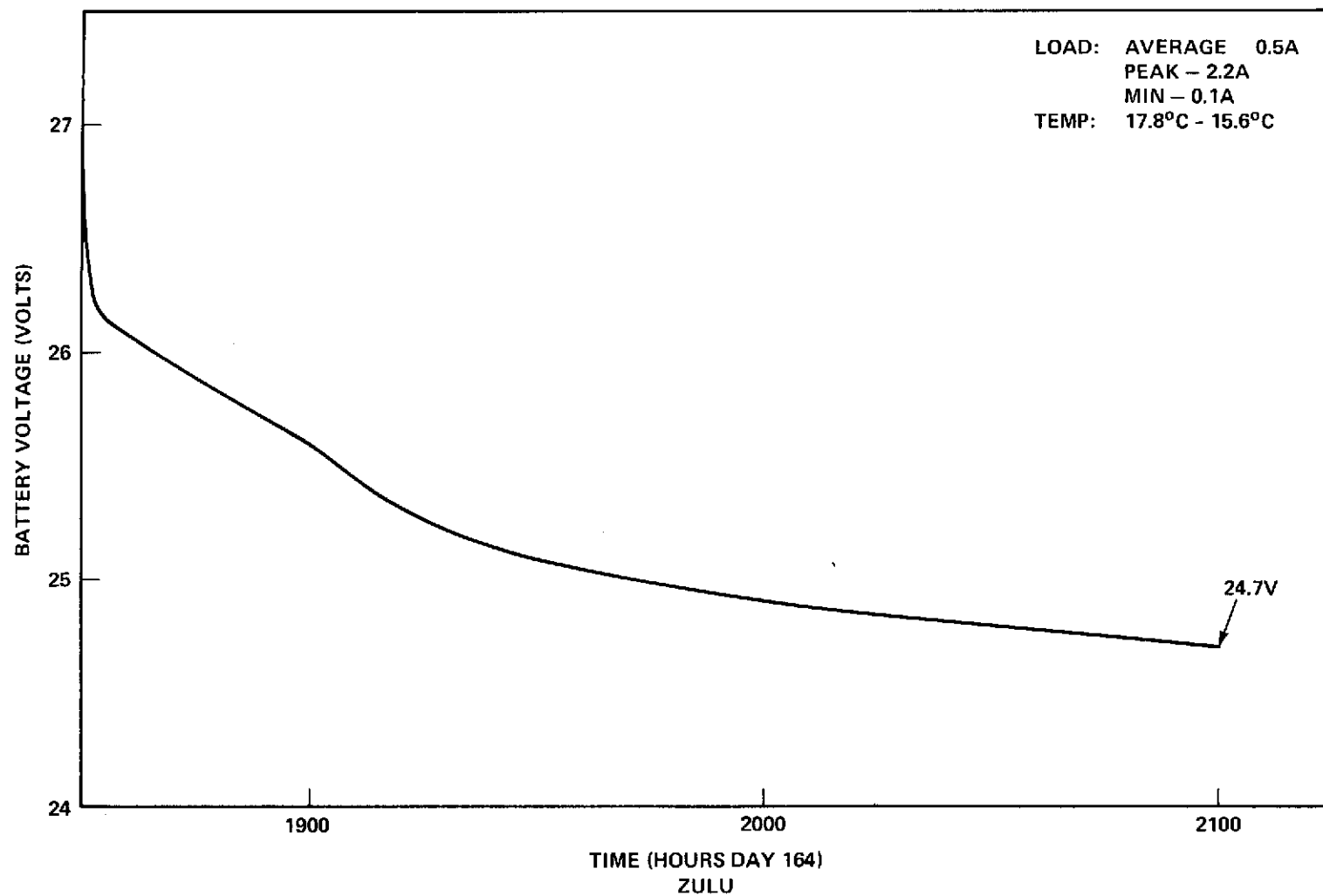


Figure 6-10. Battery 1 Voltage vs Time Place Experiment Discharge Load: Average ~ 0.5 A

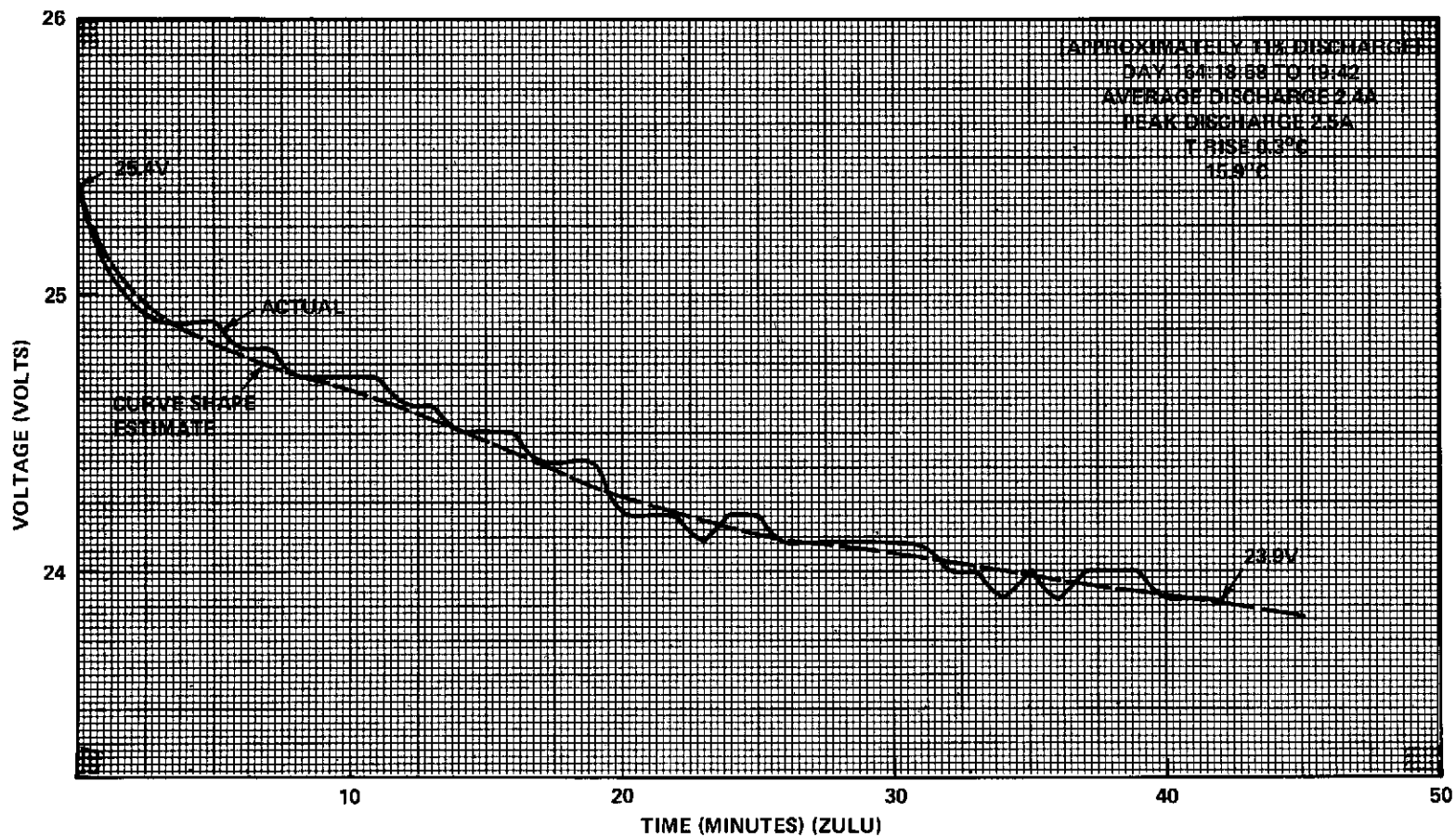


Figure 6-11. Battery 1 Voltage vs Time HET Discharge (Partial)

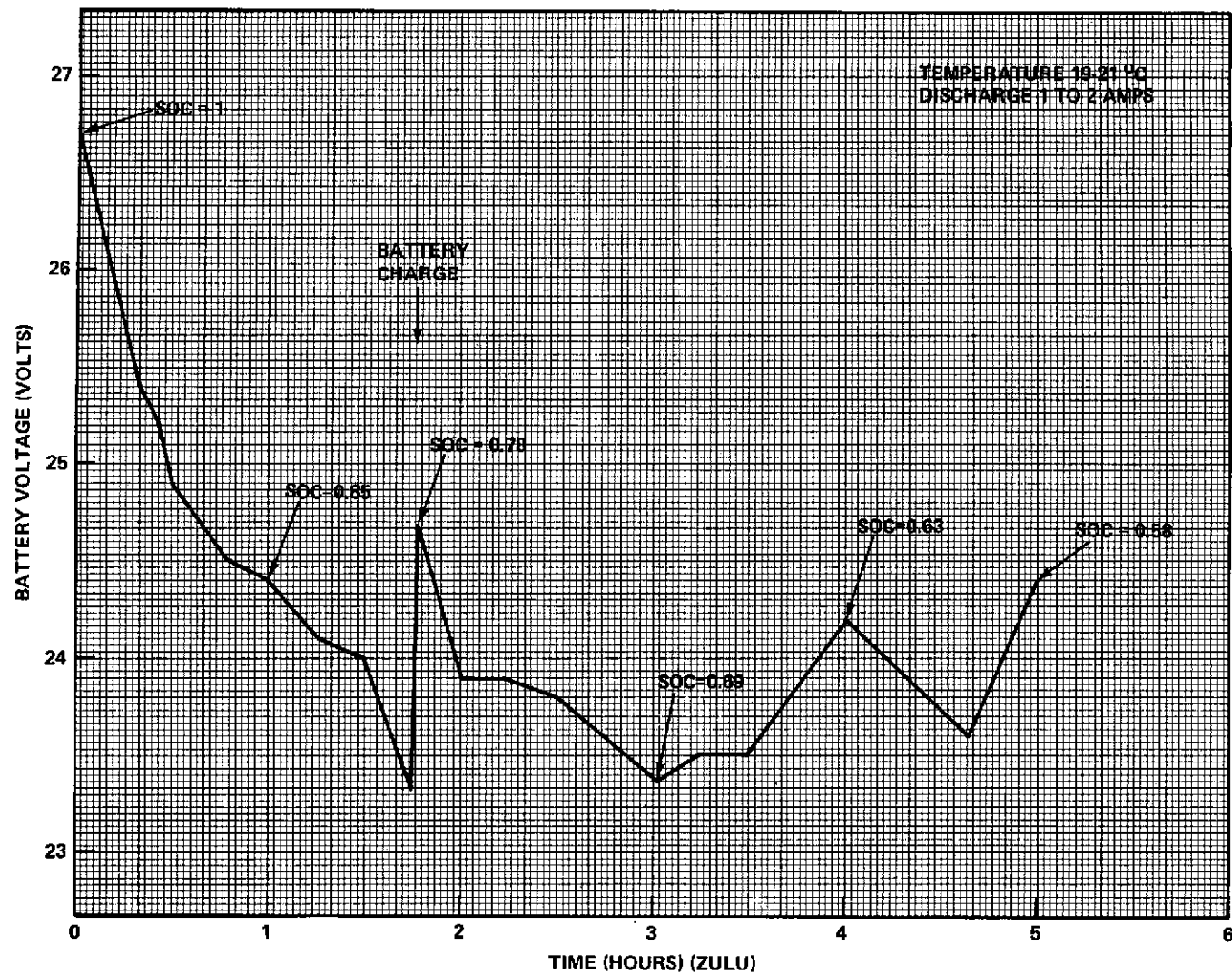


Figure 6-12. Typical Battery Discharge - Voltage vs Time HET Experiment
169: 00: 48 to 169: 05: 29 Battery 1

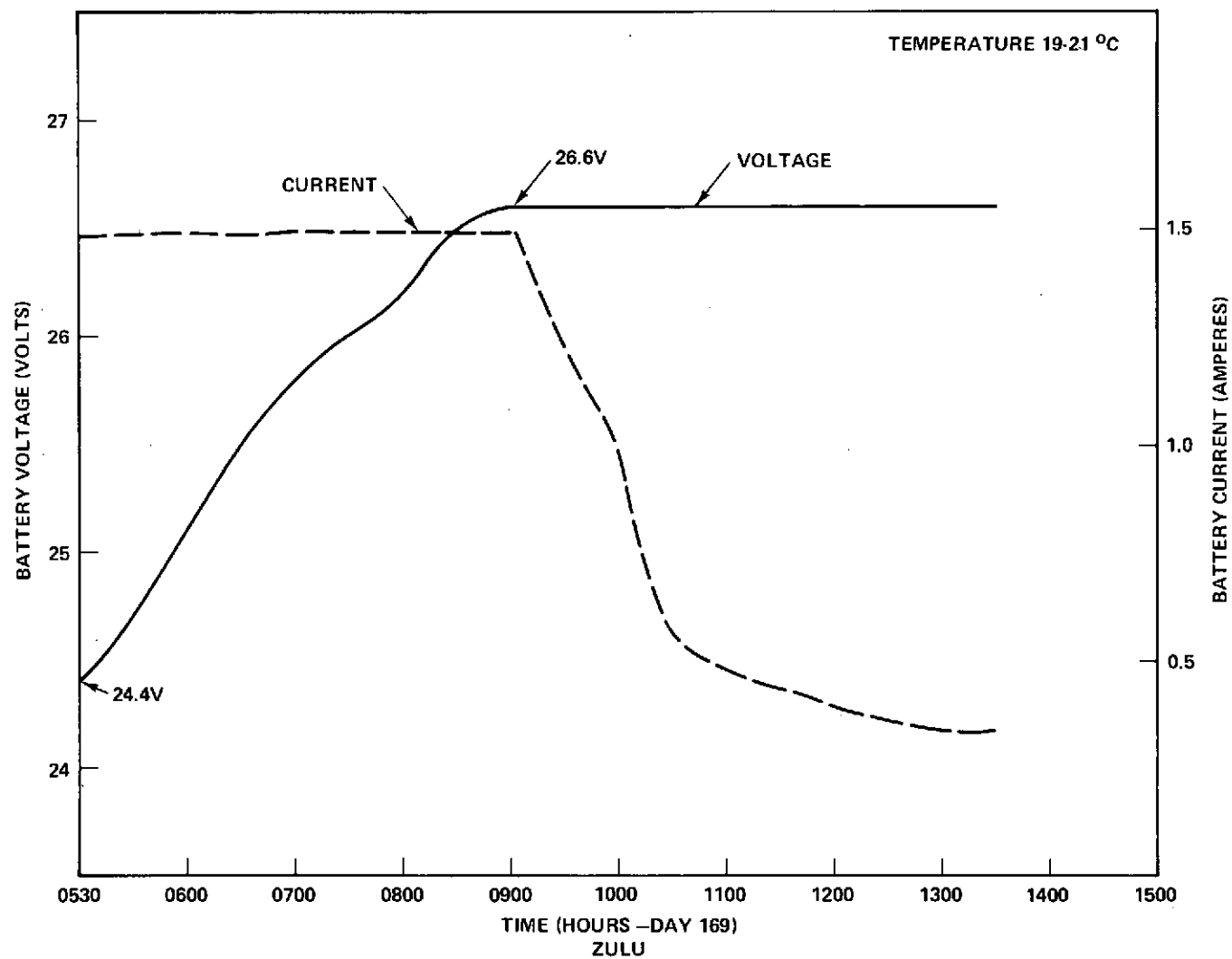


Figure 6-13. Battery Charge Voltage vs Battery Charge Current vs Time Post HET Recharge

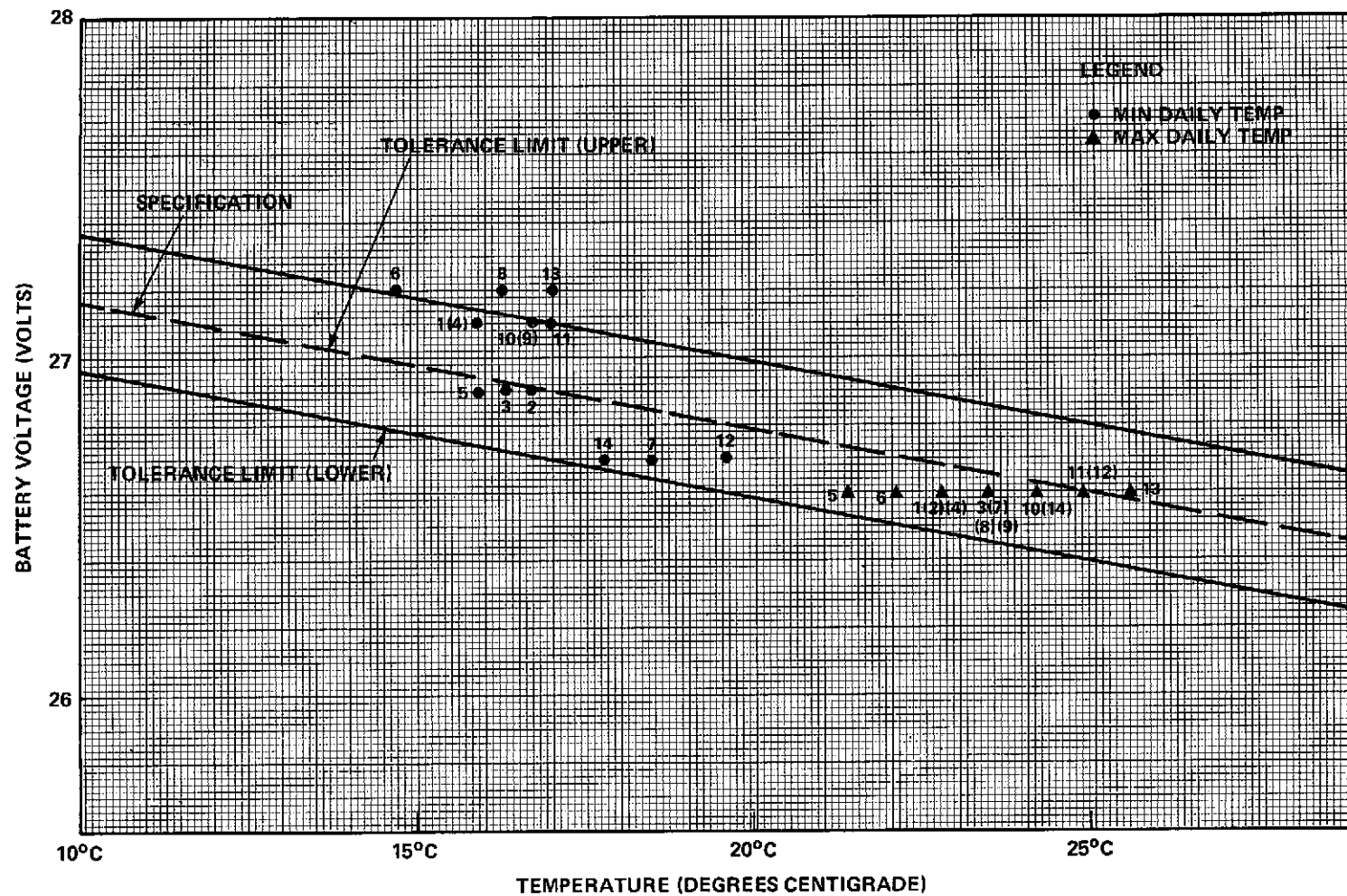


Figure 6-14. Battery 1 Clamp Voltage vs Temperature vs Day in Orbit (Annotated by Day Number)

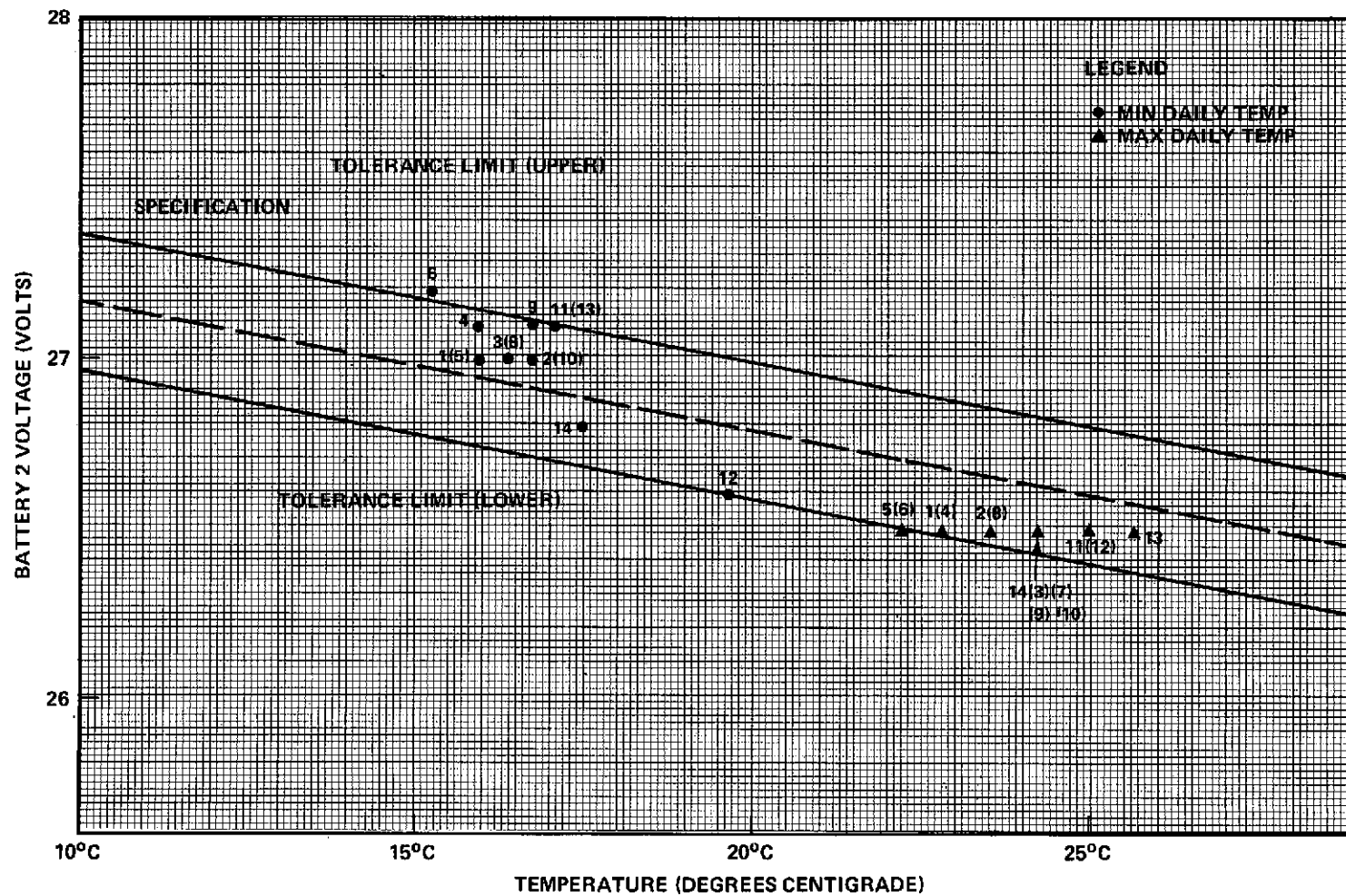


Figure 6-15. Battery 2 Clamp Voltage vs Temperature vs Day in Orbit (Annotated by Day Number)

6.3.3 Power Regulation Unit

The performance of the Power Regulation Unit (PRU) has been normal. Only MAIN PRU functions were used during the first 30 days in orbit, since no requirement has arisen to switch over to any STANDBY function. All of the PRU regulation modes (shunt, charge, boost, and share) were utilized and normal system response was achieved. The heat sink temperature ranged from 16.8°C to 24.5°C, which is well within spacecraft temperature test limits of -5°C to +45°C.

6.3.3.1 Static Performance — Figure 6-16 is typical of the static load performance of the power system bus for the initial 30 days in orbit. The abscissa denotes the beginning-of-life predictions of bus voltage in various modes with the actual in-flight data plotted directly on the I-V curve. Data was taken with the system in the boost mode, boost/charge dead band, charge mode, and shunt mode. The predicted bus voltage in the charge mode was 30.55 volts, but telemetry resolution presents this value as 30.6 volts. All modes have been regulating at the beginning-of-life values which are well within the specification.

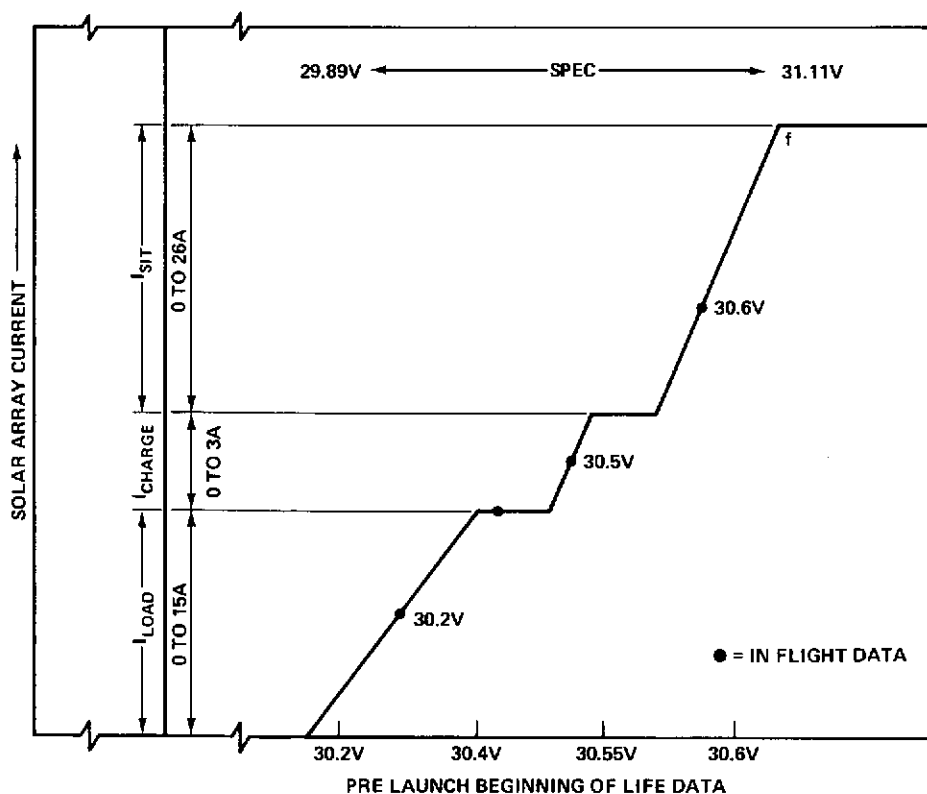


Figure 6-16. Regulated Bus Data

6.3.3.2 Dynamic Performance — Figure 6-17, illustrates the system's reaction in the shunt and charge modes with the variation in spacecraft load current over a four-day period (152:13 to 156:17). The data is straightforward, showing negative differences in shunt current for positive differences in load current and vice versa. The batteries were in taper charge mode, and a comparison of battery temperature with charge current shows that charge current varied directly with temperature. The reason for this is that battery charge efficiency varies inversely with battery temperature.

At 154:19, additional loads were activated to heat the spacecraft and accelerate outgassing. This is shown by an increase in load current to 18 amperes with a concurrent reduction in shunt current. There was still sufficient power from the solar array to maintain the system in the shunt mode and to continue battery charging.

At about 155:11, spacecraft slew maneuvers were commanded resulting in a steady increase in the sun elevation angle to a maximum of 28 degrees. As the angle increased, a decrease in shunt current (corresponding to a reduction in solar array power) occurred. As the sun elevation angle began to decrease at 155:21, shunt current increased. This plot clearly shows interactions among components in the electrical power subsystem and all performance was nominal.

6.3.4 Power Control Unit

The performance of the Power Control Unit (PCU) has been normal. The heat sink temperature ranged between 16.5°C to 30.4°C, well within the spacecraft temperature test limits of -5°C to +45°C.

Table 6-3 shows the performance of the regulated bus voltage of the load interface circuits within the Power Control Unit. All bus voltages were within the +28 volt bus specification.

6.3.5 Load Interface Circuits

All seven of the separately packaged Load Interface Circuits (LIC) have performed normally.

Table 6-4 lists the performance of the Load Interface Circuits. All bus voltages were well within the +28 volt bus specification

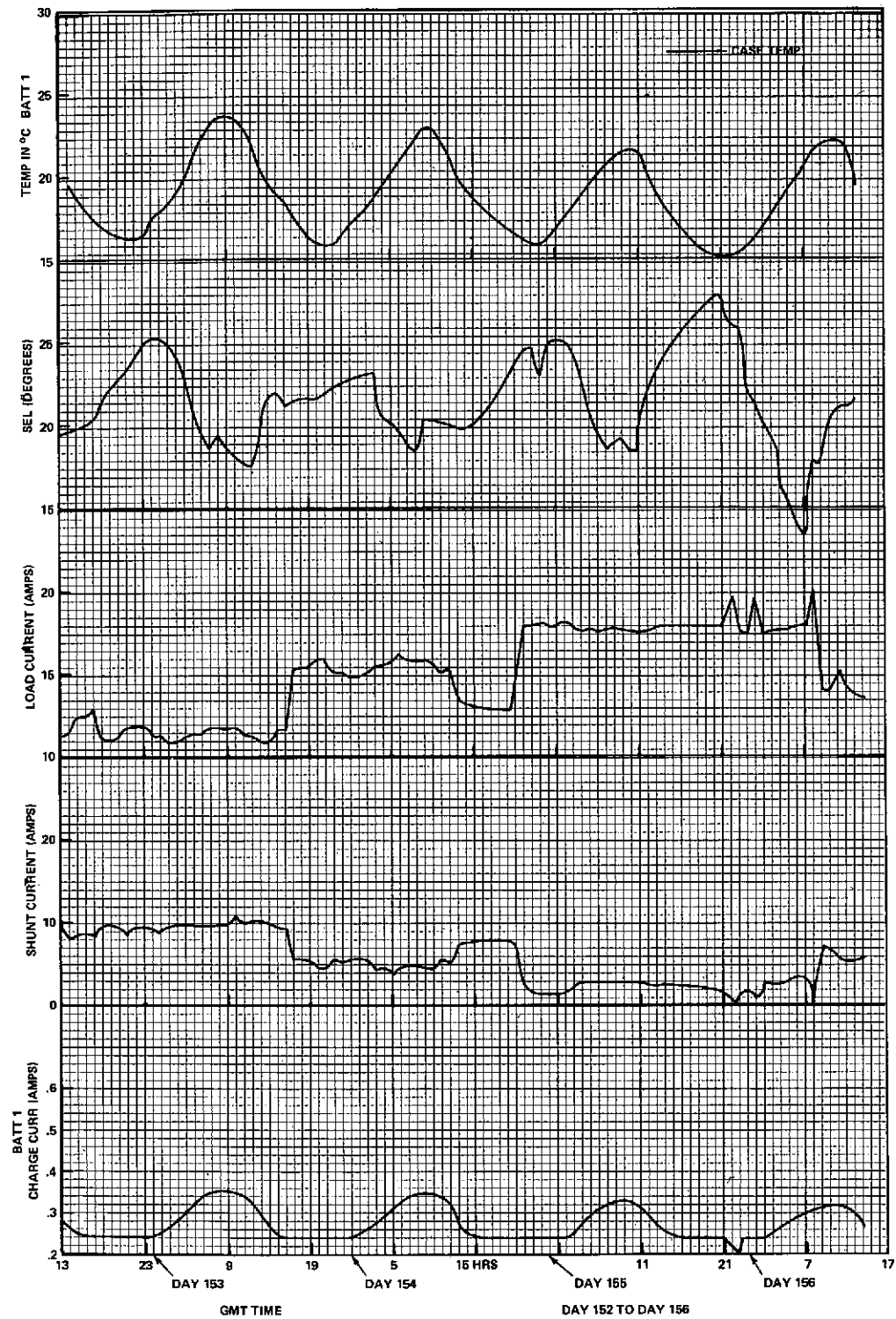


Figure 6-17. Time Line - EPS Parameters

Table 6-3

PCU-LIC Performance

Unit	In Orbit Performance	Beginning of Life Prediction	Specification
Comm Reg. 1	+28.1 v	+28.1 v \pm 0.1 v	+28 v \pm 0.45 v
Comm Reg. 2	+28.2 v	+28.2 v \pm 0.1 v	+28 v \pm 0.45 v
LIC (EME)	+28.0 v	+28.0 v \pm 0.1 v	+28 v \pm 0.45 v
LIC (Signal Conditioning)	+28.1 v	+28.1 v \pm 0.1 v	+28 v \pm 0.45 v

Table 6-4

LIC Performance

Unit	In Orbit Performance	Beginning of Life Prediction	Specification
LIC (QCM)	+27.9 v	+27.9 v \pm 0.1 v	+28 v \pm 0.45 v
LIC (VHRR)	+28.0 v	+28.0 v \pm 0.1 v	+28 v \pm 0.45 v
LIC (MMW 1)	+27.9 v	+27.9 v \pm 0.1 v	+28 v \pm 0.45 v
LIC (MMW 2)	+27.9 v	+27.9 v \pm 0.1 v	+28 v \pm 0.45 v
LIC (PROP)	+28.0 v	+28.0 v \pm 0.1 v	+28 v \pm 0.45 v
LIC (ION 1)	+28.1 v	+28.1 v \pm 0.1 v	+28 v \pm 0.45 v
LIC (ION 2)	+28.0 v	+28.0 v \pm 0.1 v	+28 v \pm 0.45 v

6.3.6 Shunt Dissipators

Figure 6-18 is a plot of solar array shunt current vs. solar array load current which may be useful for future thermal/operational purposes. It provides a measure of the change in shunt current corresponding to a change in solar array load current. The curve was plotted from data taken at various sun elevation (SEL) angles, and normalized to 20°.

Table 6-5 shows how uniformly the twelve shunt dissipators have shared excess power. Two cases are tabulated: (1) low shunt dissipator power ($I_{SH} = 1.7$ A) and (2) medium shunt dissipator power ($I_{SH} = 10.4$ A). Since individual shunt currents are not telemetered, the assumption is made that each shunt current is 1/12 of the total. This is reasonable since ground component testing on all the shunt dissipation showed close current sharing.

6.4 SOLAR ARRAY SHUNT TAP VOLTAGE FOR SHUNT DISSIPATOR A419

During spacecraft operation with the power subsystem in the share mode, the telemetered shunt tap voltage for shunt A419 slowly rose from 22.8 volts to 26.3 volts while the other 11 shunts remained at approximately 21 volts. This increase in voltage could be attributed to a high impedance in one of the strings of solar cells that is controlled by A419. Preliminary study has indicated that one of the strings could be at an increased impedance due to shadowing during the time period of 163:21:35 to 163:22:14. This string is located near the VHF omni antenna on the North array. The same effect might also be the result of high-resistance string connections or open solar cells. At present, the array power output has not changed; however, during later operations when the shunt tap voltage cannot increase to compensate for this impedance (nominally at the two-year design point) there could be a reduction in output power.

Shunt dissipator A419 will be continuously monitored in an attempt to clarify this situation.

6.5 CONCLUSIONS AND RECOMMENDATIONS

All elements of the EPS have performed satisfactorily during the checkout period. Redundant commandable units in the PRU have not been flight-tested as this would have contravened established policy.

It is recommended that the A419 shunt tap voltage be closely monitored through the winter solstice in an attempt to further define the cause and effects of its behavior.

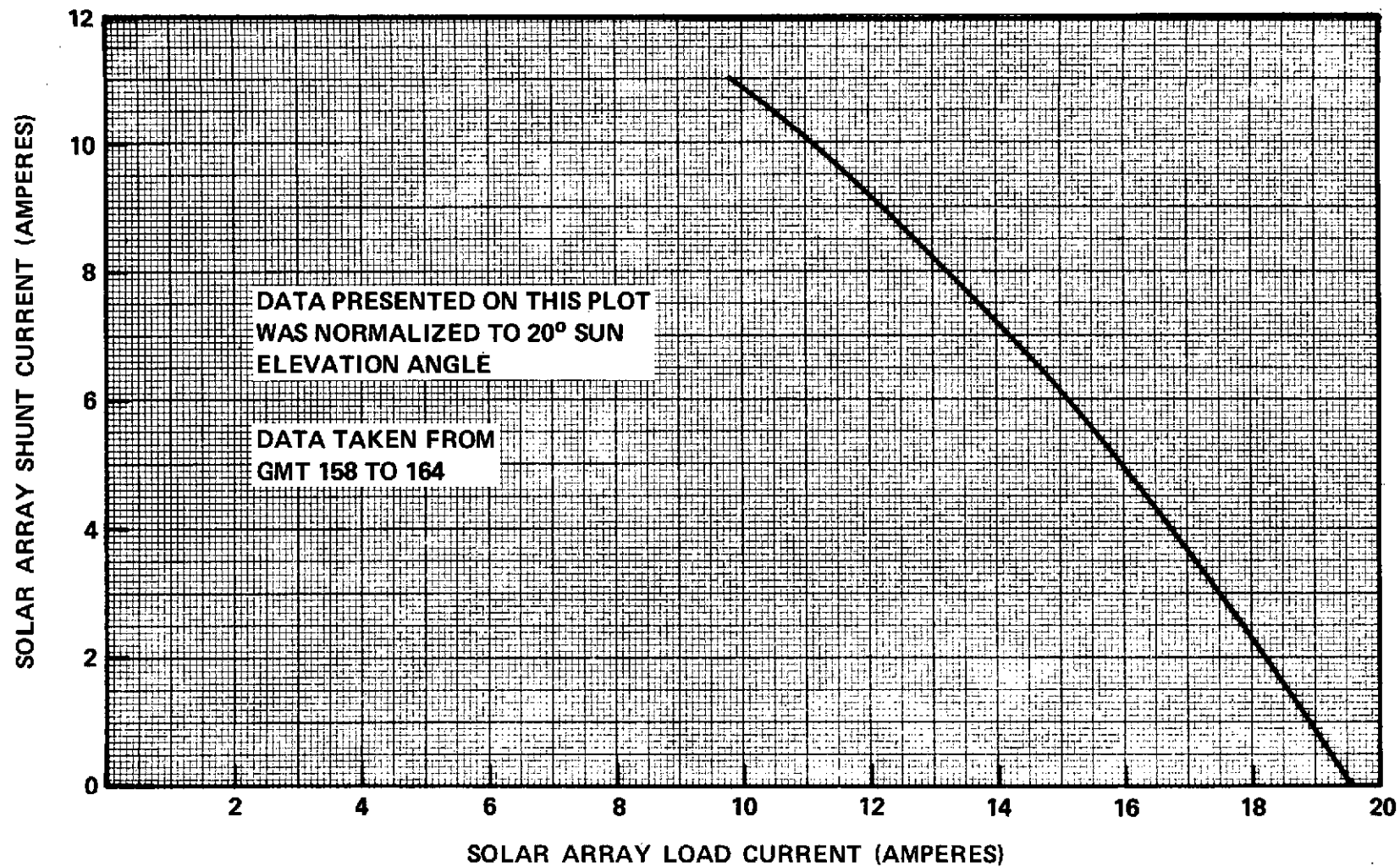


Figure 6-18. Solar Array Shunt Current vs. Solar Array Load Current

Table 6-5

Shunt Dissipator Power Sharing

GMT 190:02:13 $I_{SA} = 17.8 \text{ A}$ $I_{SHUNT} = 1.7 \text{ A}$				GMT 151:22:33 $I_{SA} = 10.2 \text{ A}$ $I_{SHUNT} = 10.4 \text{ A}$		
Shunt Dissipator	Tap Voltage	Dissipator Current	Diss. Power	Tap Voltage	Dissipator Current	Diss. Power
A419	19.2	0.14 A ↓	2.68 w	17.2	0.9 A ↓	15.5 w
A420	19.6		2.74 w	17.6		15.8 w
A421	19.3		2.7 w	16.9		15.2 w
A422	19.1		2.67 w	16.8		15.1 w
A423	19.3		2.7 w	16.9		15.2 w
A424	19.9		2.79 w	16.7		15.0 w
A425	18.8		2.63 w	16.8		15.1 w
A426	19.5		2.73 w	17.5		15.8 w
A427	19.1		2.67 w	16.9		15.2 w
A428	19.7		2.76 w	16.7		15.0 w
A429	19.5		2.73 w	17.5		15.8 w
A430	19.2		2.68 w	16.9		15.2 w

SECTION 7

THERMAL CONTROL SUBSYSTEM

SECTION 7

THERMAL CONTROL SUBSYSTEM

7.1 SUBSYSTEM PERFORMANCE

Evaluation of launch and early in-orbit performance indicates highly satisfactory spacecraft temperature control. The thermal control components consisting of superinsulation blankets, louvers, heat pipes, the optical solar reflectors and coatings appear to be functioning as expected. The SPS valves external to the EVM are experiencing higher temperatures than were predicted by analysis, but the values are within acceptance and qualification ranges. No significant anomalies have been noted during the first thirty days of flight, and analytical projection into the next two to five years indicates acceptable future behaviour.

A brief description is given of the design of the thermal control subsystem and the thermo/structural requirements and specifications.

The discussion is detailed under three major areas:

1. The External Structure, which includes all components exterior to the EVM with the exception of the Spacecraft Propulsion Subsystem.
2. The EVM, with emphasis on the temperature of the batteries, the earth sensors, and the heat pipe walls.
3. The Spacecraft Propulsion Subsystem.

7.2 THERMAL DESIGN

An outline of ATS-6 thermal control hardware is indicated in Figure 7-1 and 7-2. The design of the external structure was generally based on the passive approach of using multilayer superinsulation wrap (aluminized mylar interspace with nylon scrim cloth) with a black coating on the outward surface.

The solar array booms have aluminized Kapton tape to insure the uniformity of the surface finish critical during the launch/deployment phase. Treatment of the solar array panels and of the dampers is shown in Figure 7-1.

The external components of SPS are maintained at the required temperature by heaters. The heater strips on the propellant line are activated by thermostatic control to control line temperatures during all phases of launch and orbit.

The EVM thermal design, shown schematically in Figure 7-2, features louvers on the North/South panels and heat pipes imbedded in the platforms of

components. The transverse beam, also having heat pipes, aids in distributing the dissipated energy along the louvered surfaces. Superinsulation blankets are employed on the East/West sides, and specially cut blankets and covers are used for the focus feed elements interface and for the earth-viewing surface.

Thermal requirements were determined by specifications for equipment internal to the EVM and for the thermo/structural capability of the external structure. A listing of spacecraft temperature levels is shown in Table 7-1 which also includes the background on acceptance and qualification testing.

7.3 DATA SOURCES

Temperature data were obtained from nine telemetry half-pages exhibited on CRT's. The operation consisted of monitoring temperatures associated with the Thermal Control Subsystem, and reporting with recommendations any deviation from prescribed temperature limits. These nine half-pages consist of information pertaining to SPS temperatures external to EVM, the deployment dampers and external structure temperatures, and temperatures at various locations in the EVM. The EVM thermistors are in general located on each component's mounting structure.

Additional thermal data were displayed within half-pages of ACS, RF Interferometer Subsystem, T & C, and SPS.

Additional facilities at the Information Processing Division allowed continuous display of temperature data in graphical as well as digital forms. This offered a "quick-look" at the performance of the spacecraft and was particularly important in evaluating the rise and drop trends in temperature.

7.4 SUBSYSTEM EVALUATION

7.4.1 Launch/Ascent Phase

Continuous monitoring and recording of temperature data was initiated some six hours prior to launch at 150:08:58:33 while final testing and checkout of all systems were being performed. The air-conditioning system was in use until 4 hours before lift-off, and all equipment temperatures remained within acceptance limits. The components that registered maximum temperature rises were the telemetry transmitters. Table 7-2 gives the temperature of the battery case and telemetry transmitter mounting surfaces during the checkout period. The overall thermal performance of the spacecraft during this time was similar to that observed during clean room and RF testing.

The launch phase through fourth motion lock-up was a most critical period since successful deployment was involved. Ascent temperature history profiles had been previously predicted for all components external to the EVM, as represented by thermistor locations, and these were used as guidelines in the thermo/structural performance prior to and during deployment.

Table 7-1
Spacecraft Temperature Levels

Component	Specifications			
	In-Orbit	Launch-Ascent	Acceptance	Qualification
Mounting Surfaces Within EVM (Mean Heat Pipe Temp.)	5°C to 35°C	5°C to 35°C	5°C to 35°C	-10°C to 50°C
Exceptions				
Batteries	0°C to 25°C	0°C to 25°C	0°C to 25°C	-10°C to 35°C
Earth Sensors				
Mounting Surface	3°C to 40°C	3°C to 40°C	3°C to 45°C	-12°C to 45°C
Bolometer	- 7°C to 42°C	- 7°C to 42°C	- 7°C to 50°C	-12°C to 50°C
Polaris Tracker				
Mounting Bracket	5°C to 37°C	5°C to 37°C	- 5°C to 47°C	-10°C to 52°C
Digital Sun Sensors	0°C to 40°C	0°C to 40°C	-40°C to 45°C	-45°C to 50°C
Analog Sun Sensors	0°C to 40°C	0°C to 40°C	-50°C to 50°C	-65°C to 65°C
Feed Farm Elements	-28°C to 56°C	-28°C to 56°C	-28°C to 56°C	-37°C to 71°C
SPS				
EVM Valves & Lines	5°C to 35°C	5°C to 35°C	5°C to 45°C	5°C to 102°C
OCJ Bar Valves	5°C to 90°C	5°C to 90°C	14°C to 96°C	5°C to 102°C
OCJ Bar Lines	5°C to 82°C	5°C to 82°C	16°C to 71°C	10°C to 77°C
Thruster Catheds	-15°C Min.	-15°C Min	-50°C to 800°C	-50°C to 800°C

Table 7-2

Launch Pad Temperatures

Component	Temperature (°C)					
	Batt. 1	Batt. 2	XTLM 1	XTLM 2	XTLM 3	XTLM 4
Time						
150:09:00	17.6	17.6	22.0	17.7	19.3	21.6
150:10:00	17.8	18.0				
150:11:00	18.7	18.7	23.1	23.0	23.1	23.1
150:12:00	19.4	19.4	23.2	23.2	23.2	23.2
150:13:00	21.0	21.0	23.2	23.2	23.2	23.2

Table 7-3 lists predetermined temperature limits and qualification temperature range for launch and deployment. Figures 7-3 through 7-7 are plots of external component temperatures from launch through deployments with some pre-flight predictions noted for comparison purposes.

* * * * *

1. Solar Array Booms: The thermal control treatment of the solar array booms provided the surface properties needed to maintain the average boom temperature at acceptable values. Telemetry data during launch from the two thermistors available for each boom indicated that the local temperatures were well within the limits required, and that the boom deployment occurred at temperatures far less severe than those exercised during ground testing. This is noted in Table 7-3, where a comparison is made between the deployment temperature range and ground testing values. The 1st deployment hinges which are critical at high temperatures, deployed at a maximum temperature of 55°C, whereas the deployment qualification temperature was 139°C. Similarly, the 2nd deployment hinges which are of concern at low temperatures were qualified at -61°C compared to a minimum actual deployment value of 2°C. This comparison shows that a two to three hour delay in initiating deployment under worst solar alignment conditions would still have deployment at qualification temperatures.

It is significant to note that the predicted temperatures for the booms during ascent, as shown in Figure 7-3, corresponded very closely to actual data for parking orbit. This indicates that the analytical methods involving trajectory, solar flux, albedo, and earth flux were accurate.

Table 7-3
Deployment Temperatures

Parameter	Specification	Predicted	Actual
Damper, Panel-End North	- 48°C to 46°C	-7°C to 30°C	25°C
Damper, Panel-End South	- 48°C to 46°C	-7°C to 30°C	26°C
SA Boom 2nd Depl Huge +Y	-140°C to 150°C	-55°C to 116°C	10 to 17°C
SA Boom 1st Depl Huge +Y	-140°C to 150°C	-55°C to 116°C	45 to 52°C
SA Boom 2nd Depl Huge -Y	-140°C to 150°C	-55°C to 116°C	2 to 7°C
SA Boom 1st Depl Huge -Y	-140°C to 150°C	-55°C to 116°C	48 to 55°C
Reflector Rib Sta 173 +Y	- 18°C to 34°C	-10°C to 19°C	10°C
Reflector Rib Sta 110 +X	- 18°C to 34°C	-10°C to 34°C	12°C
Reflector Rib Sta 110 -Y	- 18°C to 34°C	-10°C to 34°C	5°C
Reflector Hub -Y	-160°C to 60°C	153°C to 35°C	11°C

2. Solar Array Panels: A history profile of the solar array panel temperature during flight is shown in Figure 7-4. Although the instantaneous temperatures deviate in absolute value from the predicted averages due to rotisserie and the low thermal mass of the panels, the correlation between predicted and actual averages is excellent and indicates that thermal modeling of the radiation exchange between the various panels during the stowed configuration was accurate.

Array release through full boom deployment appears to have occurred at temperatures ranging from -58°C to 53°C. The location of the array thermistors with respect to solar orientation has a significant effect on the temperature of the individual panels, but judging from the correlation of transfer orbit data with analysis, it appears that all the panels were at temperatures between -60°C and +60°C. Deployment was verified within the qualification range of -130°C to 72°C.

3. Dampers: The most successful damper rate verification testing was conducted at room temperatures. Deployment occurred while the dampers were at 17°C. The qualification temperatures ranged between -20°C to 38°C.

table 7-3 part 2

External System Temps During Deployment

Day: 150 GMT 19:32:28 Through 20:19:09

Component	Actual Deployment Temp. Range	Temperature During Ground Testing Deployment
Boom Hinge 1 -Y	48°C to 55°C	139°C
Boom Hinge 2 -Y	9°C to 7°C	-61°C
Boom Hinge 1 +Y	45°C to 52°C	139°C
Boom Hinge 2 +Y	10°C to 17°C	-61°C
North Damper	25°C	- 20°C to 38°C
South Damper	26°C	- 20°C to 38°C
Refl. Hub (N)	10.7°C	- 18°C to 34°C
Rib St. 110 (N)	5°C	- 40°C to 94°C
Rib St. 110 (E)	12°C	- 40°C to 94°C
Rib St. 173 (S)	10°C	- 40°C to 94°C
Sol Array A2	- 8°C to 15.5°C	-130°C to 72°C
Sol Array A5	-25°C to -40°C	-130°C to 72°C
Sol Array A3	-23°C to 32°C	-130°C to 72°C
Sol Array A8	-58°C to 53°C	-130°C to 72°C

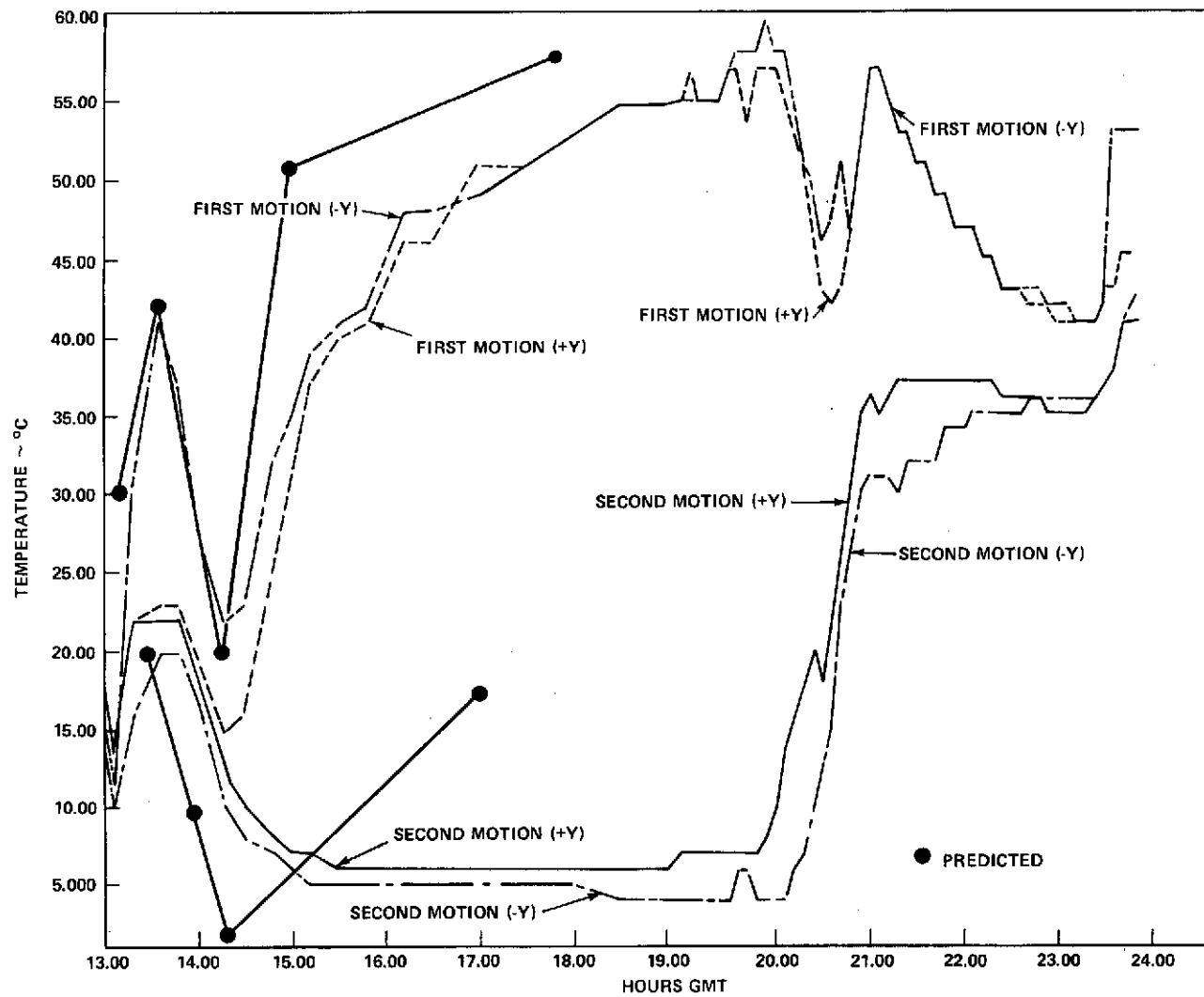


Figure 7-3. Launch Solar Array Boom Temperature

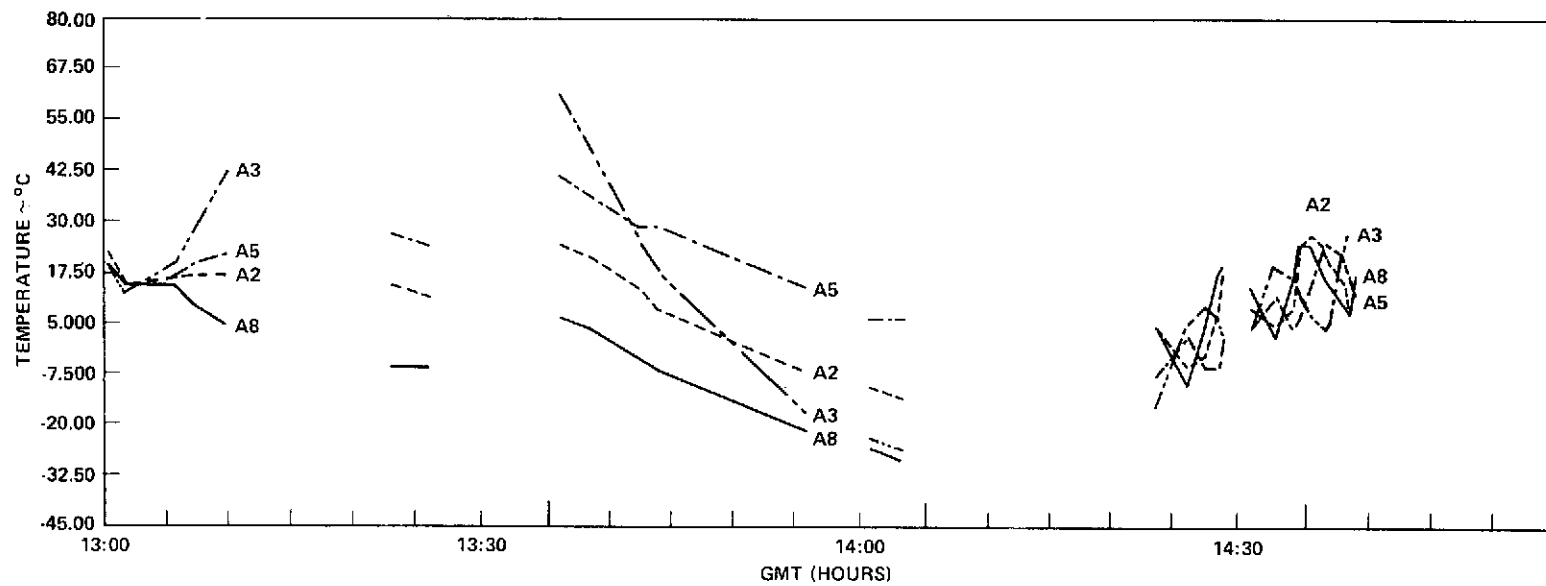


Figure 7-4. Launch Solar Array Temperature

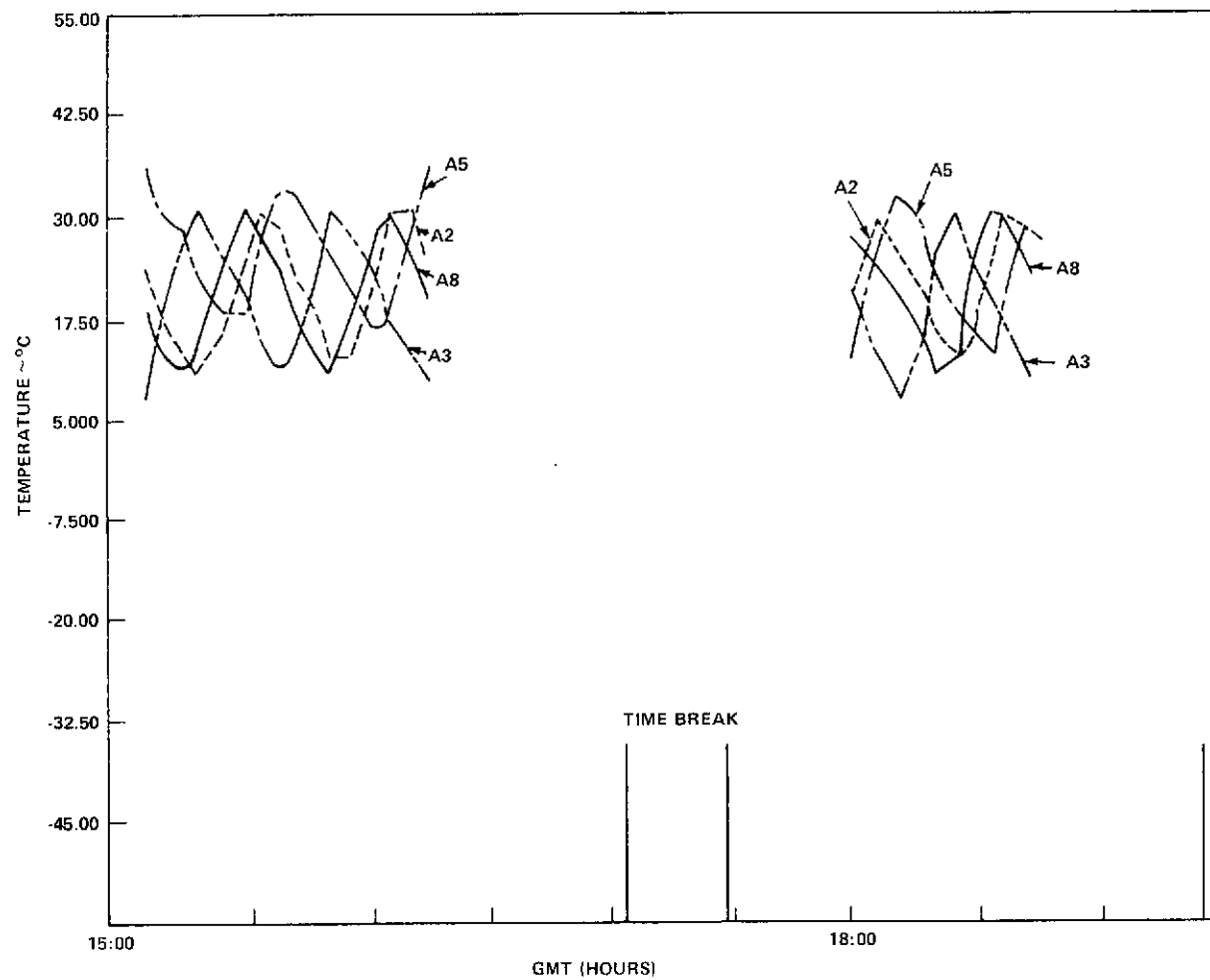


Figure 7-4. Launch Solar Array Temperature (cont'd)

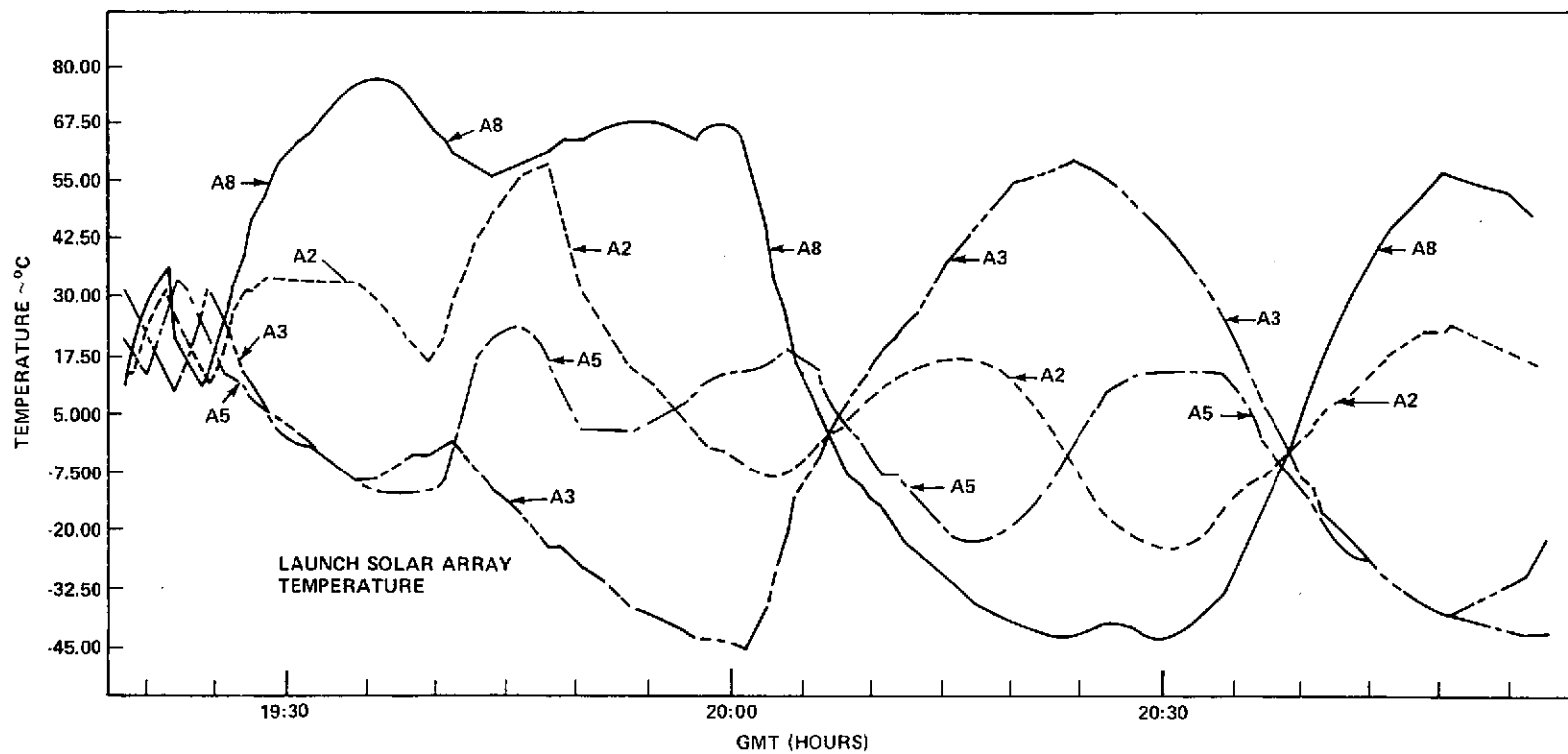


Figure 7-4. Launch Solar Array Temperature (cont'd)

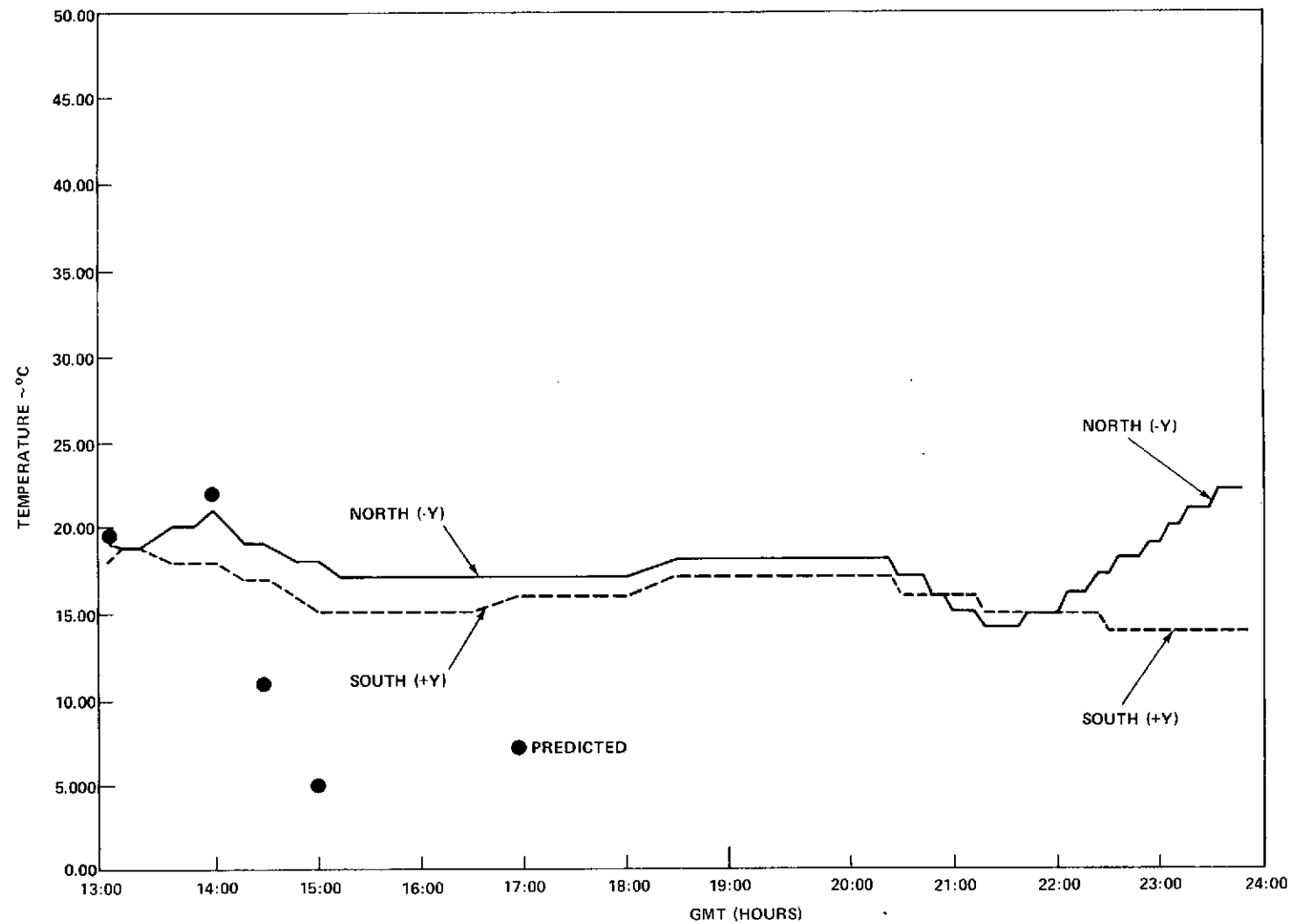


Figure 7-5. Launch Damper Temperature

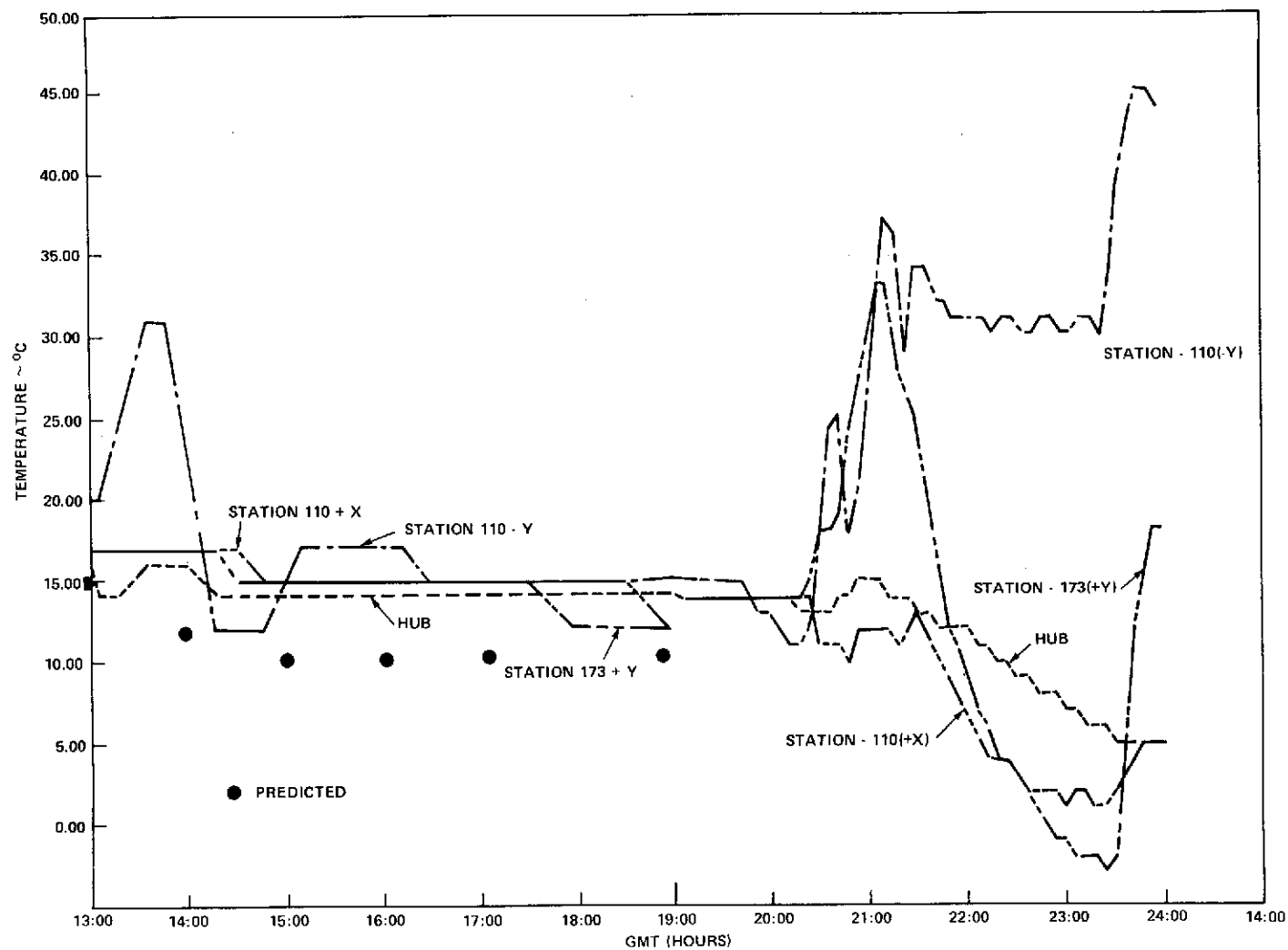


Figure 7-6. Launch Reflector Temperature

7-14

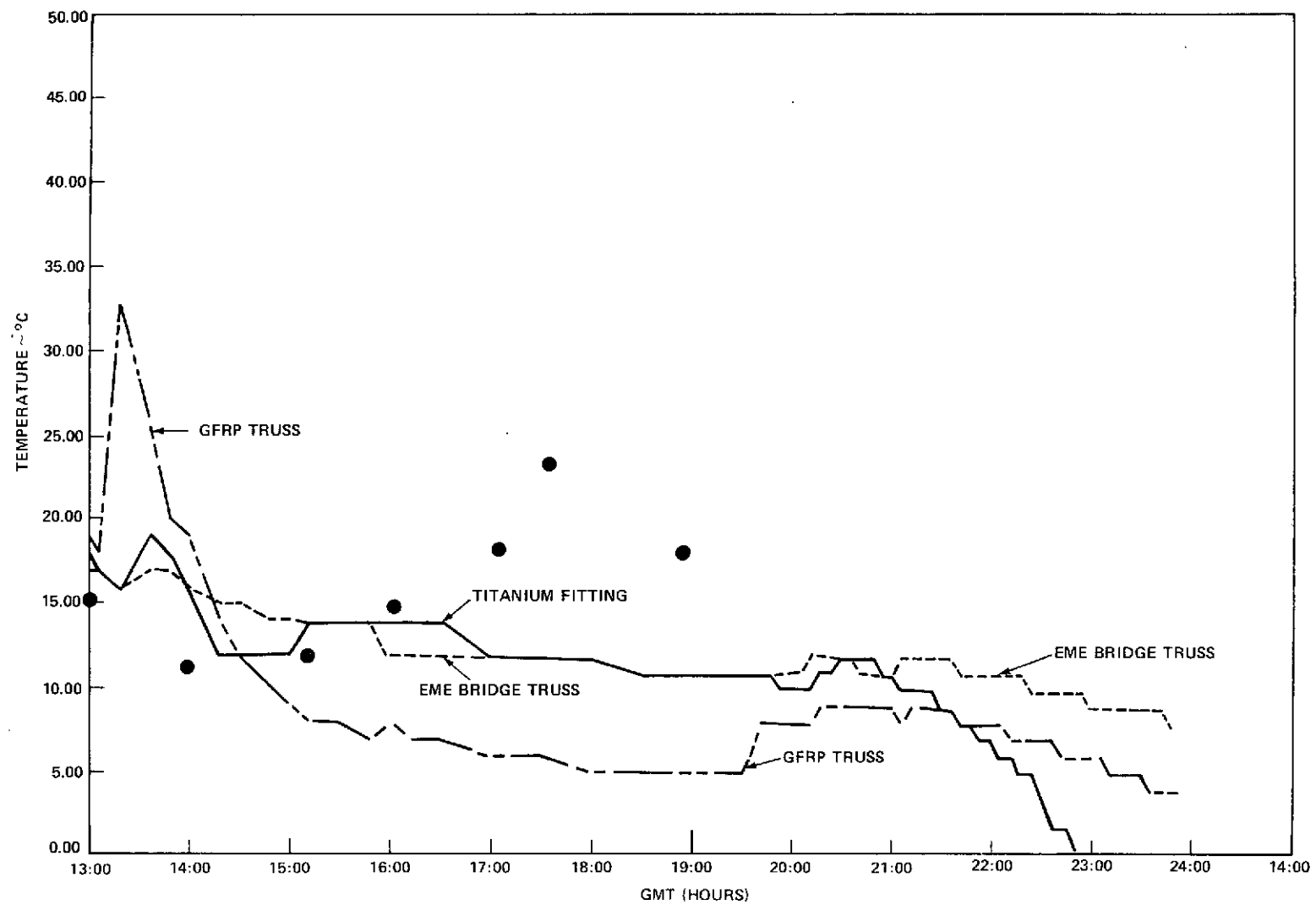


Figure 7-7. Launch GFRP, Fitting and Truss Temperature

Thermal analysis and test of ATS dampers invariably involved assumptions and imposed conditions which magnified the influence of the environment throughout the ascent phase. Since no solar simulation verification was performed for the overall external configuration, worst-case parameters were chosen in evaluating the damper thermal design. Comparison of flight data with predicted temperatures as given in Figure 7-5, shows an extremely effective thermal design. The influence of the space environment and the heat transfer coupling to the boom and torque box all appear to be minor. The slow change of temperature with time of both North and South dampers demonstrates that fabrication of the thermal components (especially the multilayer insulation blanket) was repeatable and that a much higher thermal mass than previously assumed was attained.

4. Reflector: Figure 7-6 shows the reflector temperature history during ascent through fourth motion lockup. It may be seen from Table 7-3 that the values of temperature compare favorably to the levels used in the unfurling tests at Houston facilities. Deployment occurred with the reflector thermistors registering temperatures between 5°C and 12°C. Unfurling tests were conducted with the hub temperature between -18°C and 34°C and the ribs ranging from -40°C to 94°C.

It was concluded from comparison of flight data with predictions that the thermistors on Station 110-Y and on Station 173 +Y were reversed during installation. This had no effect on performance or the evaluation process.

5. Truss/EME Bridge: Figure 7-7 gives the temperature during launch as recorded by thermistors located on the -X GFRP truss and an associated titanium hub fitting. These components were qualified at extreme temperature and mechanical loading conditions and presented no problem during all phases of launch. The data were used to confirm that the spacecraft alignment with the sun was nominal during rotisserie and separation.

The thermistor located on the bridge under the EME package indicated that the insulation wrap in that location is acceptable. Data from this thermistor may be used by EME analysts to evaluate the thermal interface with the structure.

6. EVM: The EVM temperature remained nearly constant during ascent. The batteries and the telemetry transmitters were monitored continuously and the temperature of other components internal to the EVM were observed and recorded. All systems functioned well and average EVM temperatures remained within 2°C of lift-off values.
7. External SPS: Close attention was given to SPS temperatures. The ascent rate-of-rise in temperature of the external SPS was as expected. However, the initial temperature of the valves at the launch pad was higher than assumed in the analysis because the valve heaters had been turned on prior to lift-off. This led to unexpectedly high temperatures at deployment. Comparison between the predicted and the actual launch temperatures for SPS 1

negative yaw valve is given in Figure 7-8. Comparison with Table 7-1 shows that the maximum temperature was still well within acceptance and qualification levels.

* * * * *

7.4.2 Orbital Phase

The thermal performance of the spacecraft in orbit may be judged on the levels of temperature at which the various components function, and on the excursion in temperature due to the changing orientation of the spacecraft with the sun. All data evaluated during the first thirty-day period indicates successful thermal performance. This conclusion is drawn from correlation of flight data with analytical predictions and a comparison with the system's capability in terms of acceptance and qualification test levels.

The EVM achieved a quasi-steady-state condition during the first week in orbit as may be seen in Figures 7-9 through 7-12, which show module temperatures through 120 hours from lift-off. The temperature of the heat pipe panels where the dissipators are mounted remained in the acceptance range of 5°C to 35°C during all spacecraft operational modes. The Communication Module and the Service Module panel temperatures varied by only 2°C to 3°C about a temperature of 25°C. The thermal gradient between the North and South panels was a maximum of 3°C which is an indication of properly operating heat pipes with low resistance across the heat pipe saddles.

Figure 7-10 shows that the mounting panels of the Experiment Module were affected most by time of the day and the location of the sun. The daily change in temperature was about 10°C for the EM. This was 5°C higher than expected, but still within specifications.

As expected, the components in the EVM most sensitive to the external environment were those mounted on the earth-viewing panel in the EM. The variations in temperature of the earth sensor heads and the interferometer horns, and the effect of the earth-viewing panel on the batteries were evaluated in detail and the results are as follows:

1. Interferometer Subsystem: Figure 7-11 shows the variation in the orbital temperature of the interferometer horns. The excursion was 15°C more than expected, but was still within the qualification test levels. A complete analysis of this discrepancy will be possible after acquiring long-term data from which the influence of seasonal orientation can be examined. Preliminary evaluation suggests the possibility of a sizeable conduction path between the ground plane, which experiences severe temperature oscillation, and the mounting brackets of the horn. Another possible cause is that the multilayer Kapton sun shield may not be offering the expected resistance to solar penetration. It should be emphasized, however, that the monitored temperatures have caused no serious concern.

7-17

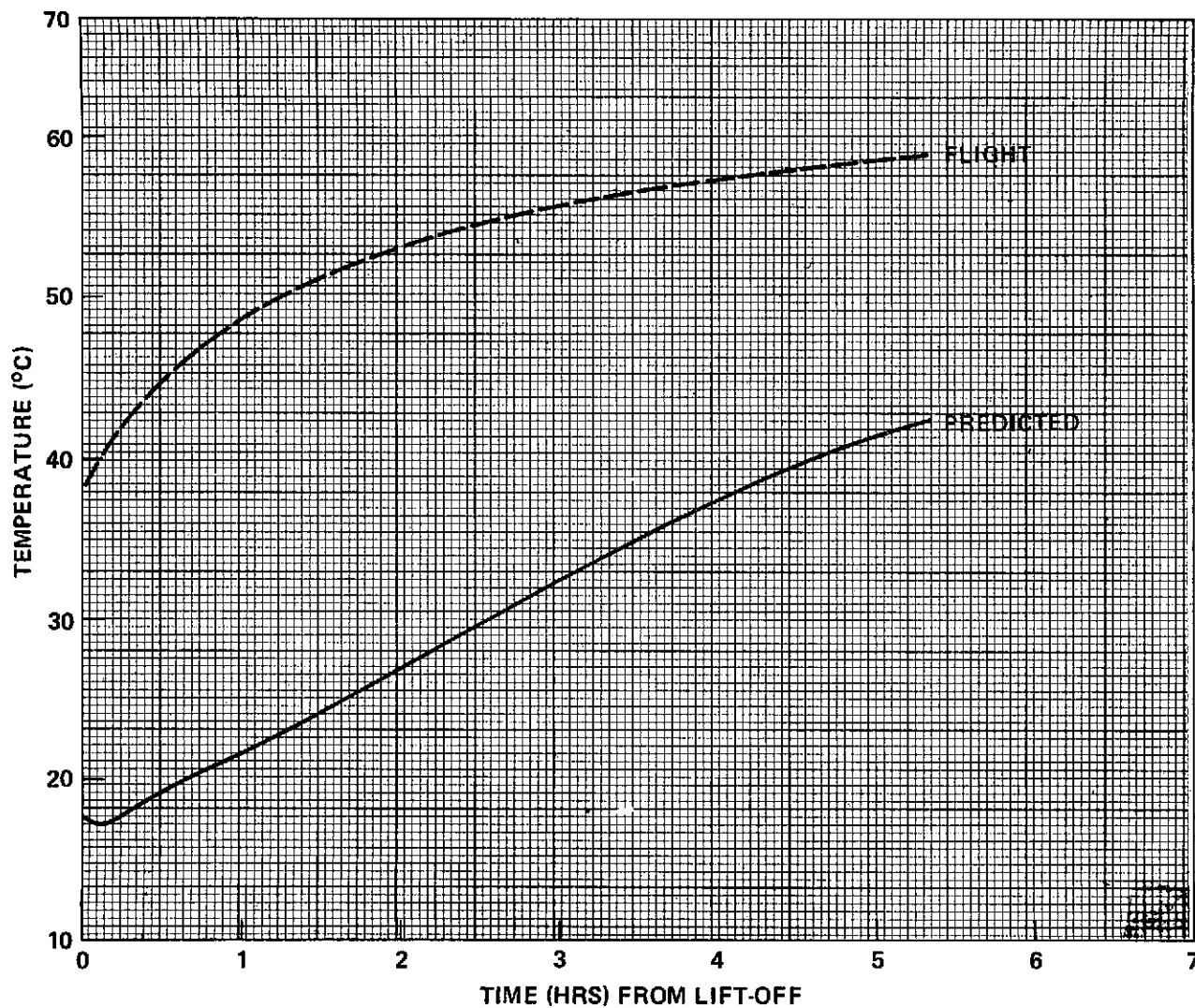


Figure 7-8. SPS 1 Neg. Yaw Valve Temperature

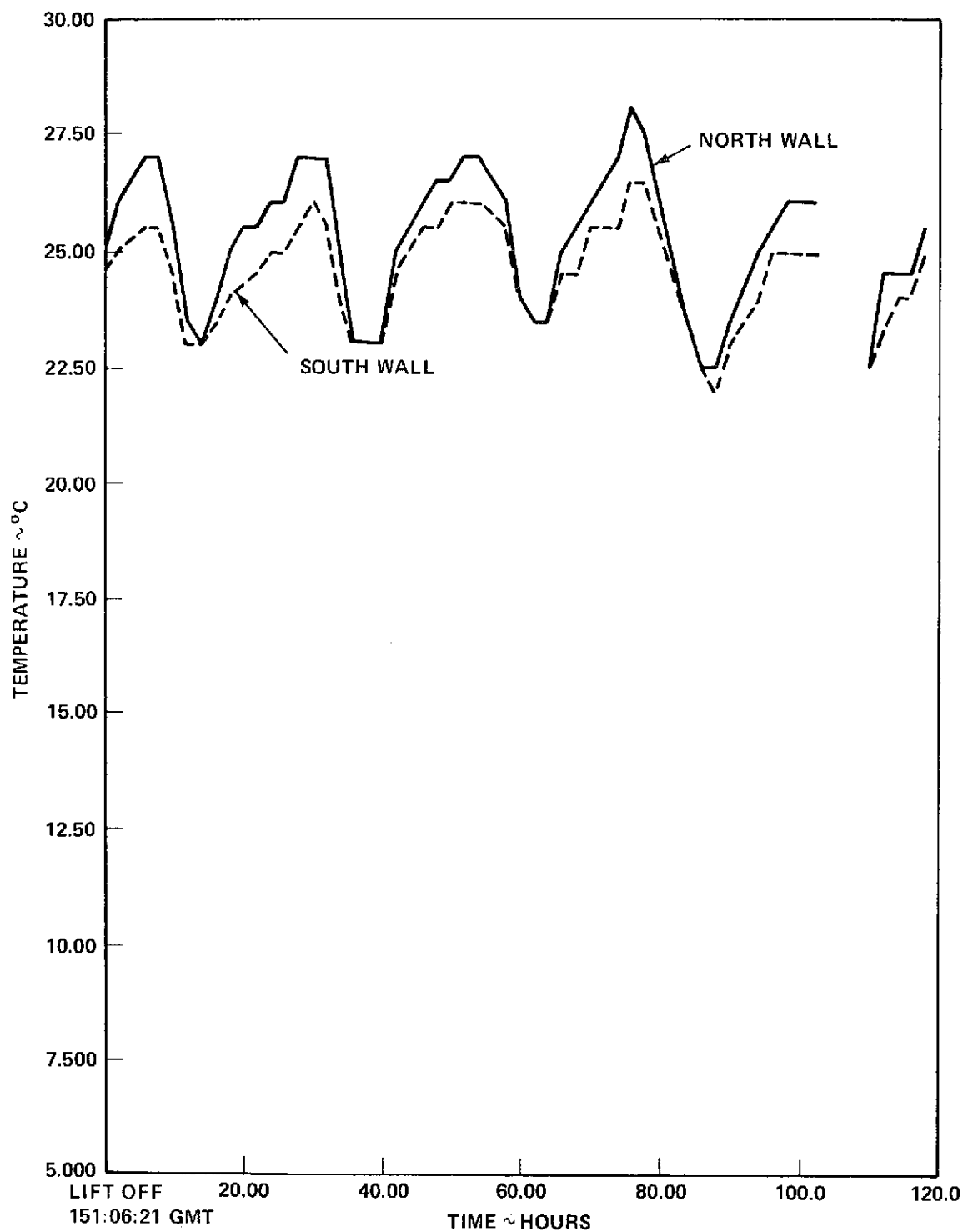


Figure 7-9. Communication Module Temperature

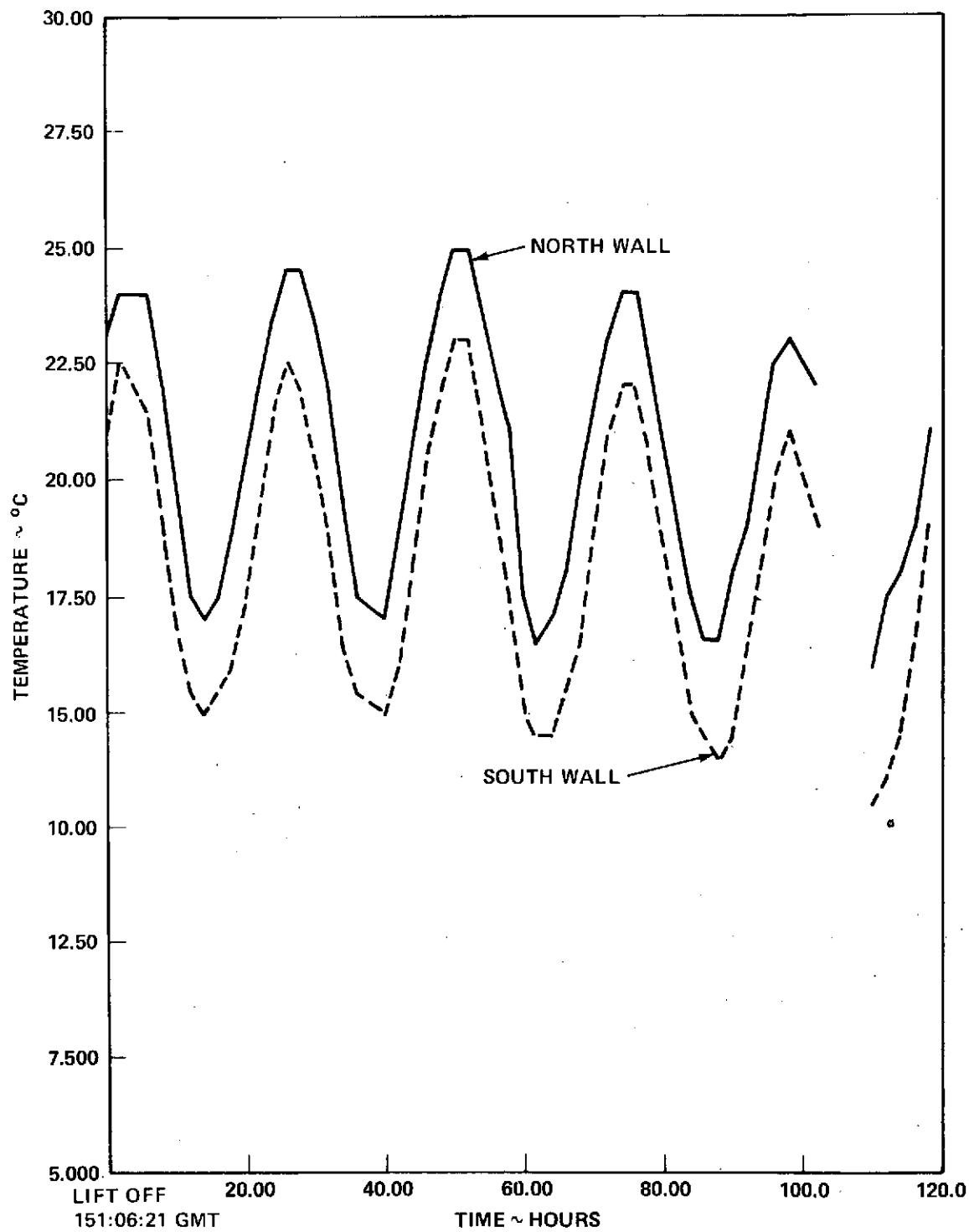


Figure 7-10. Experiment Module Temperature

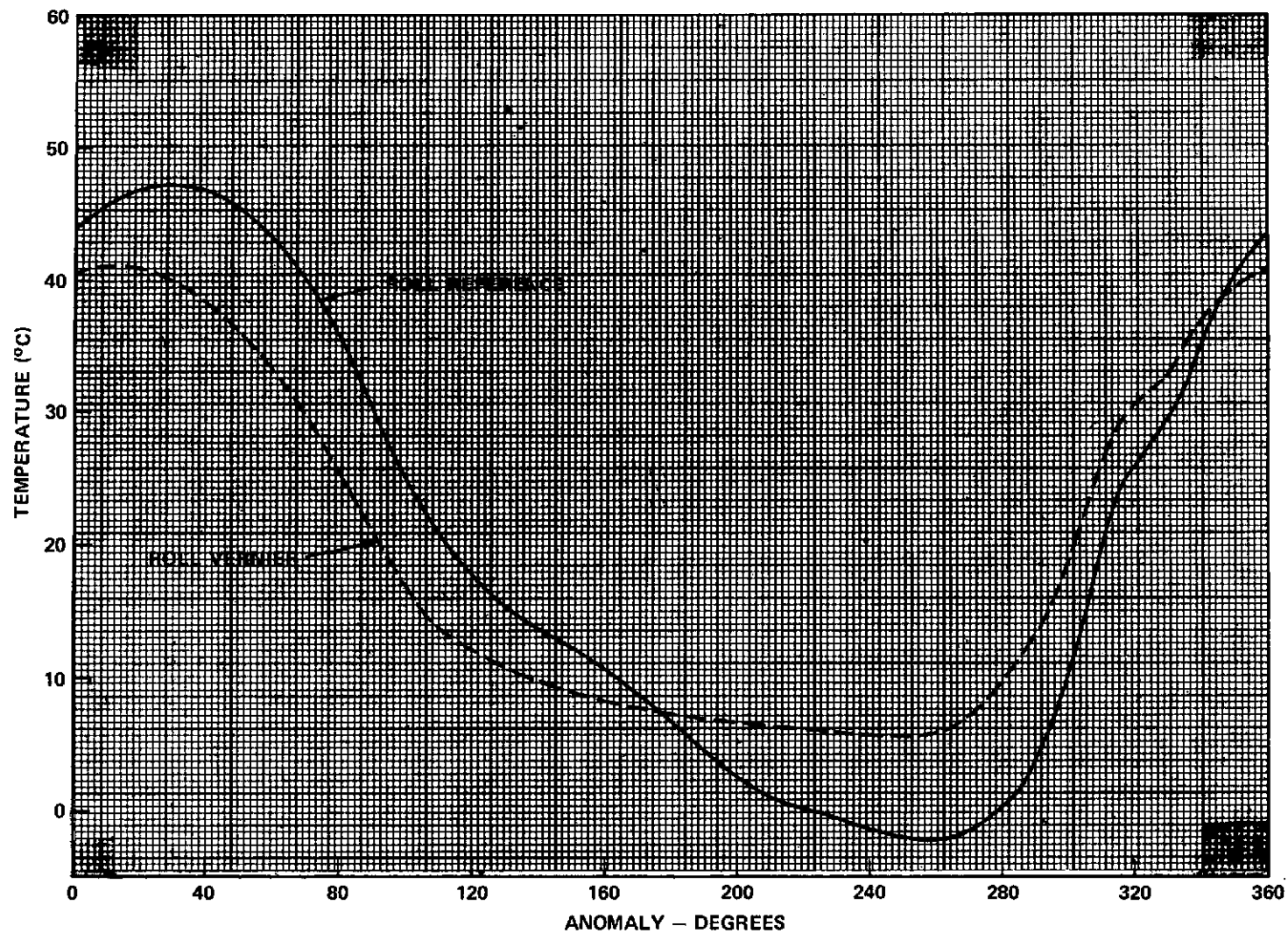


Figure 7-11. Interferometer Horn Temperature

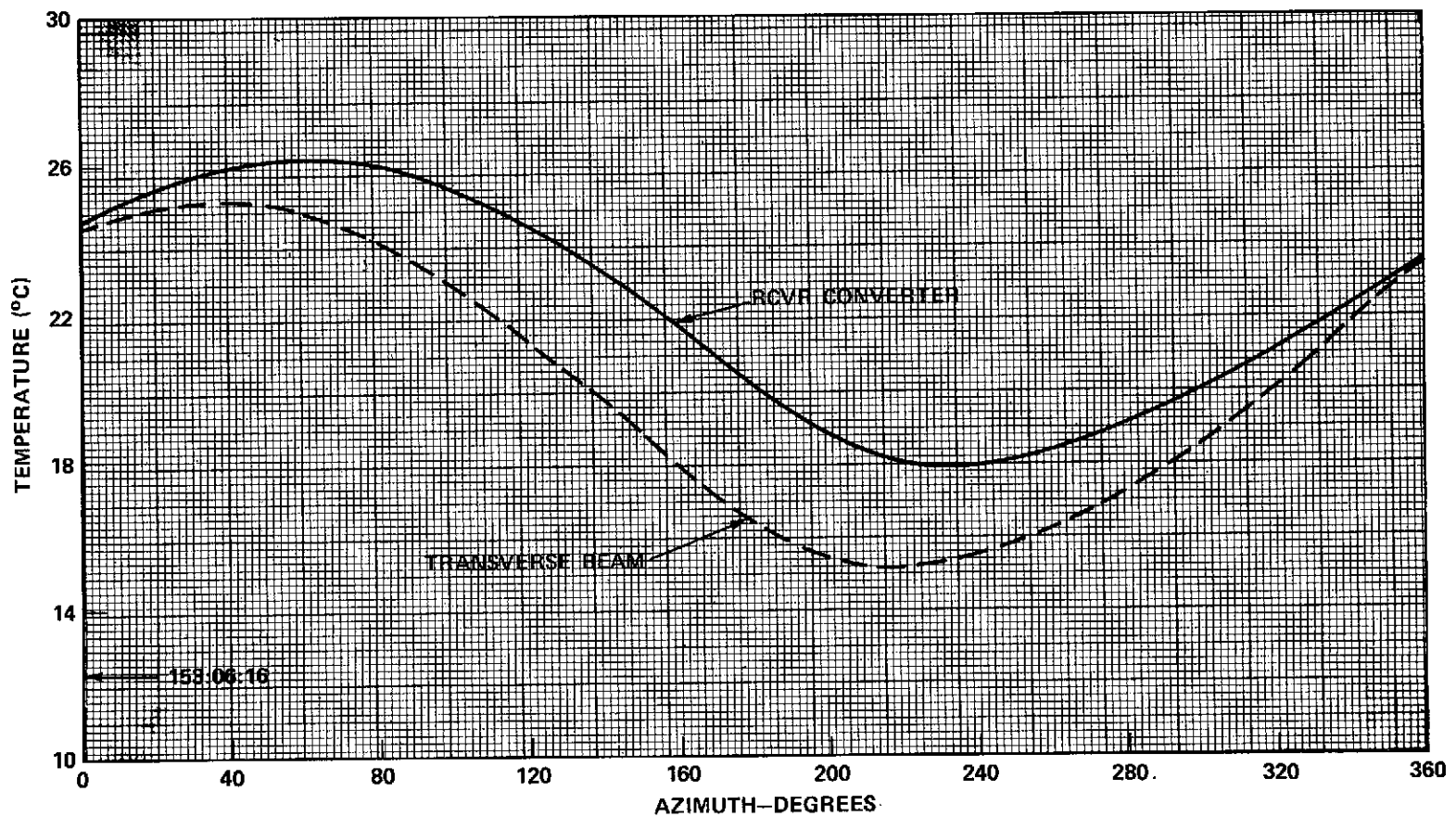


Figure 7-12. Interferometer Temperature

In relationship to the interferometer horns, the RCVR converter temperature was within the nominal band. Figure 7-13 compares the temperature of the RCVR converter with that of the transverse beam on which it is mounted.

2. Earth Sensors: In general, both earth sensor heads were at the same temperatures. The orbital variation is shown in Figure 7-14. The maximum and minimum temperatures were as predicted (Table 7-1).
3. Batteries: The orbital temperatures of the battery cases are shown in Figure 7-15. Only minor effects were realized due to changes in the earth-viewing panel temperatures. This is attributed to the large thermal mass of the batteries and their conductive coupling to the heat pipe South Wall. The difference between the case temperature of the two batteries has been very small.

The thermistors located on the prime focus feed indicated effective design of insulation blankets and solar shield in that area as illustrated by the small excursions in Figure 7-16.

A more complete list of EVM components and associated temperatures is given in Table 7-4.

Of major importance is a tolerable temperature on the SPS. EVM data indicate that the portion of the system inside the EVM is being maintained close to room temperature. The valves mounted on the OCJ bar, however, have a daily temperature excursion of 25°C to 96°C with the cathed heaters off. Although these values compare reasonably well with specification data, previous analyses had yielded results indicating that these temperatures would not exceed 88°C with the cathed heaters on.

A complete evaluation of this discrepancy will be performed when more flight data is available. It is expected that the OCJ bar valves will alternate in registering the higher temperature as the solar vector changes with time of the year, and this information taken over a six-month period should be used to complement the analysis. The results of the 30-day evaluation are as follows:

1. The present daily variation in temperature (12°C to 90°C) is acceptable as compared to acceptance and qualification testing performed on the system.
2. The power dissipation of the valve heaters may have been underestimated. A 10% error could account for discrepancies between analysis flight data.
3. The system is generally biased towards the warm end in order to avoid freezing of the hydrazine. The insulation blankets around the thruster

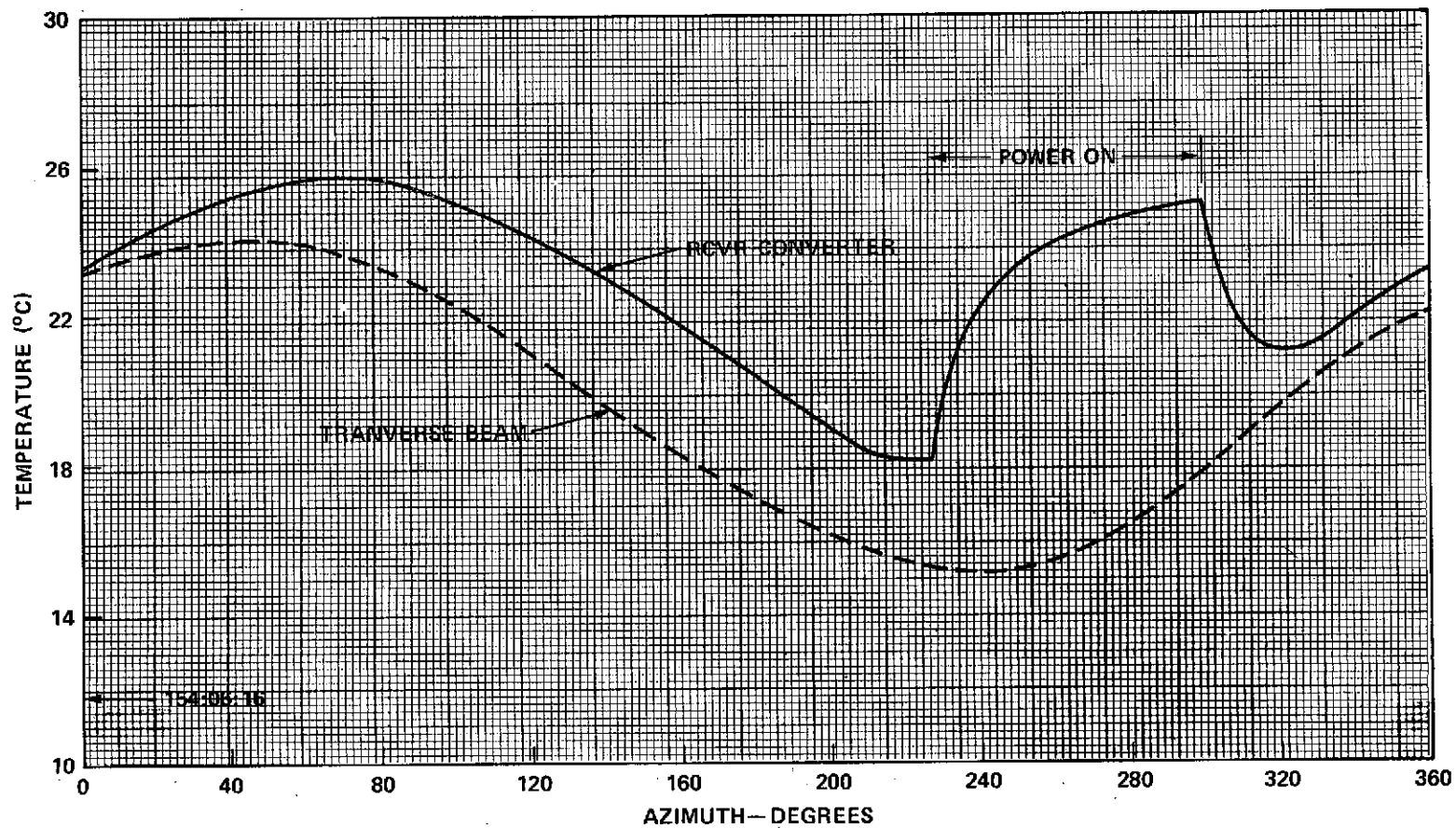


Figure 7-13. Interferometer Temperature

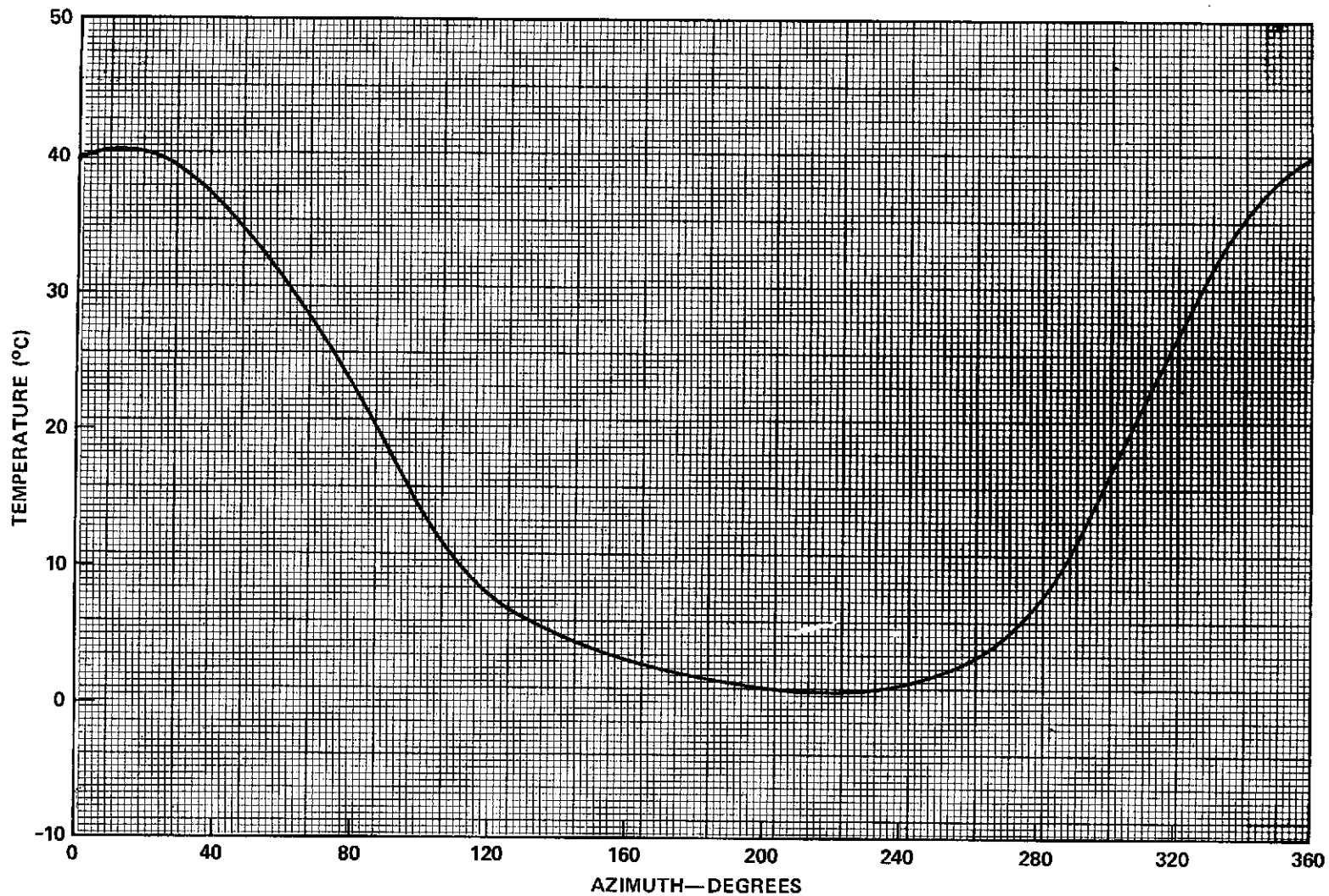


Figure 7-14. Roll Earth Sensor Head Temperature

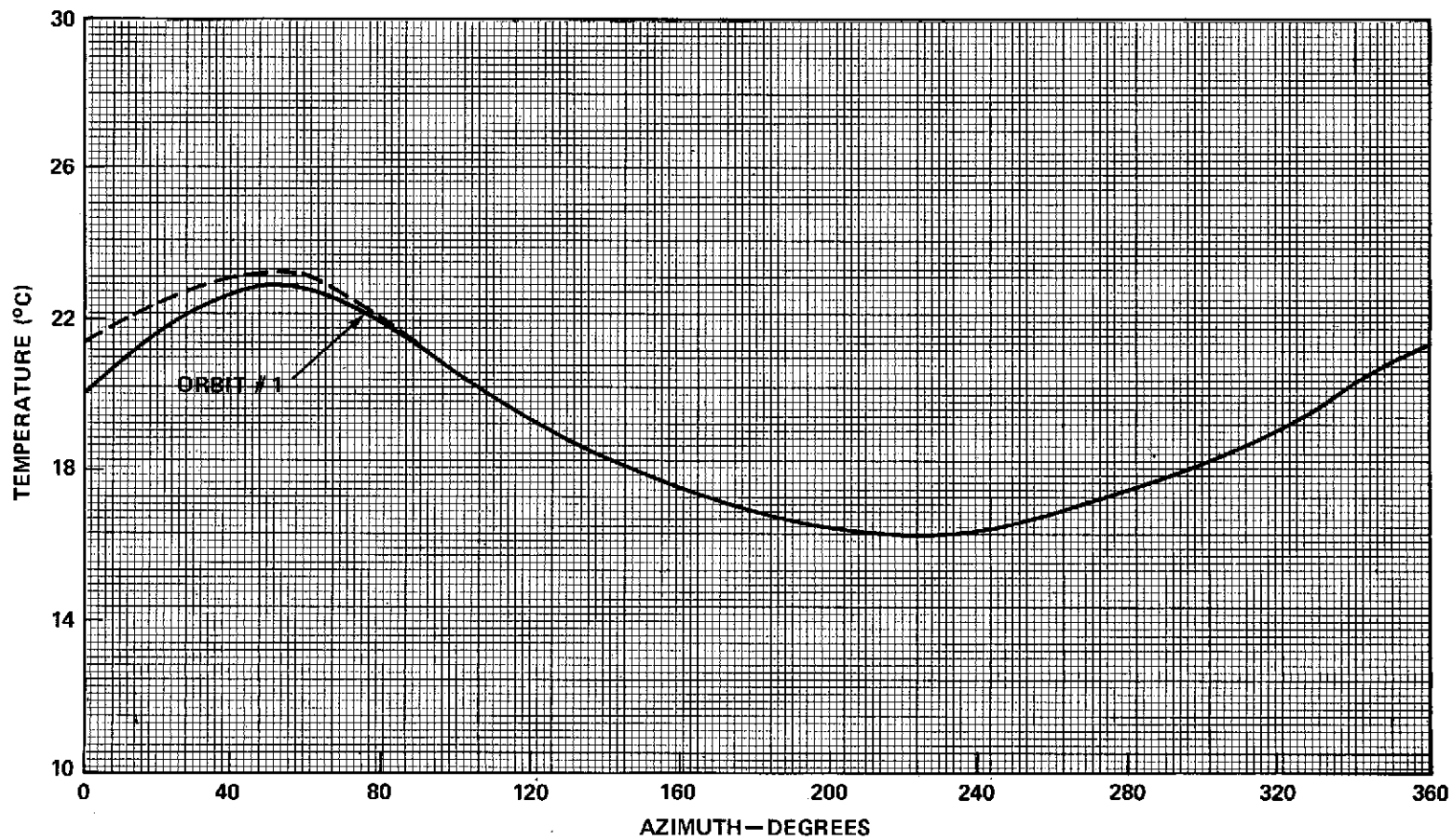


Figure 7-15. Battery Temperature

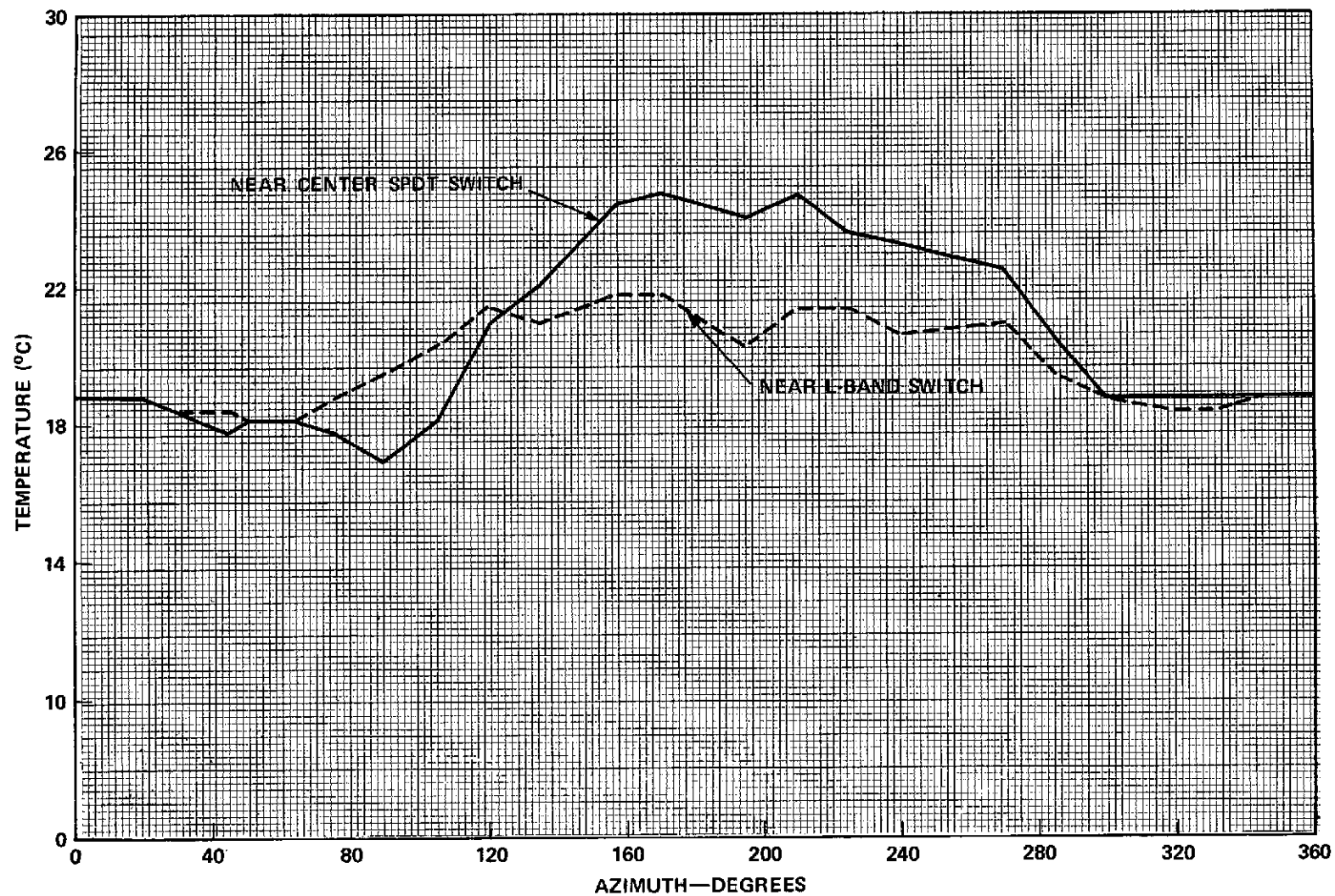


Figure 7-16. Feed Thermistor Temperature

Table 7-4

ATS Components Daily Temperature Variation

Day Hour		156 04:00	158 04:00	159 22:50	162 22:50
Component	Specification	°C			
SPS 1					
+ Yaw Valve	5 to 90	43.0	42.0	52.5	54.6
- Yaw Valve	5 to 90	33.0	32.0	45.1	44.3
Pr West Valve	5 to 90	15.8	15.6	21.6	25.0
Bu West Valve	5 to 90	13.6	13.0	24.1	23.7
Line, South	5 to 82	41.0	38.5	48.8	44.3
Line, Middle	5 to 82	35.0	34.5	40.2	40.4
SPS 2					
- Yaw Valve	5 to 90	88.0	76.0	70.8	70.8
+ Yaw Valve	5 to 90	71.0	64.1	59.0	58.7
Pr East Valve	5 to 90	85.0	81.6	71.1	71.3
Bu East Valve	5 to 90	87.0	83.9	73.9	73.9
Line North	5 to 82	66.0	63.7	52.4	52.8
Line Middle	5 to 82	62.0	60.8	48.4	48.7
ESA Pitch Head	-7 to 42	27.4	43.3	2.9	3.5
ESA Roll Head	-7 to 42	28.7	35.5	2.9	3.5
Battery 1	0 to 25	18.5	20.0	17.0	17.0
Battery 2	0 to 25	18.5	20.0	16.9	17.0
S-Band (Heat pipe 4)	5 to 35	28.8	24.0	23.8	23.3
TWTA (Heat pipe 6)	5 to 35	26.6	26.6	26.0	25.5
CM North	5 to 35	28.0	24.8	24.6	24.0
CM South	5 to 35	25.5	22.2	22.0	21.2
SM North	5 to 35	25.0	25.8	25.0	25.2
SM South	5 to 35	24.5	25.4	25.0	25.1
EM North	5 to 35	19.0	22.3	20.0	19.4
EM South	5 to 35	16.5	20.1	18.8	18.8
TLM XMTR 1	5 to 35	36.0	25.2	33.3	33.9
TLM XMTR 2	5 to 35	34.0	33.7	31.7	32.5
TLM XMTR 3	5 to 35	33.2	32.5	30.5	31.3
TLM XMTR 4	5 to 35	29.3	29.1	26.0	27.0
PRU	5 to 35	20.0	21.0	18.7	19.0
HET	5 to 35	28.8	23.8	20.0	23.4
UHF	5 to 35	25.1	22.1	20.8	21.4
EM MMW Dish	5 to 35	26.1	27.0	10.6	10.6
EM MMW Horn	5 to 35	18.4	20.0	9.8	9.7
ION Engine (Heat pipe 4)	5 to 35	19.8	22.3	22.0	21.2

Legend: Pr - primary, Bu - backup

brackets may have extended slightly beyond their intended border line leading to a reduction in the effective radiating area and hence the higher-than-expected temperatures.

4. The insulation effectiveness of the OCJ bar may have exceeded that experienced during ground thermal vacuum test.

7.5 CONCLUSIONS AND RECOMMENDATIONS

Nominal temperatures at deployment and telemetry data taken during the first 30 days in orbit denote excellent performance of thermal control components. A qualitative projection of the data suggests that the thermal subsystem performance of the EVM will be maintained during the next five years. More detailed analysis will be made possible when data for an extended period in orbit becomes available.

The monitored temperatures in flight correlate very well with the expected values obtained through ground testing and analysis. The discrepancies are in general slight, but in the case of the external SPS and the earth-viewing panel of the Experiment Module, improvements might be recommended for the design of future spacecraft similar to ATS.

It is recommended that continuous thermal data acquisition be maintained for at least the next six months. This will lead to extending the evaluation of the spacecraft in terms of future improvements and analysis as well as early detection of potential problems.

SECTION 8

TELEMETRY AND COMMAND SUBSYSTEM (T&C S/S)

SECTION 8

TELEMETRY AND COMMAND SUBSYSTEM (T&C S/S)

8.1 SUBSYSTEM PERFORMANCE

The Telemetry and Command Subsystem has successfully provided VHF communications for command and telemetry data in support of all spacecraft systems and experiments during launch and mission phases. Flight performance is consistent with prelaunch test results which had shown that the T&C subsystem meets or exceeds all requirements.

Only one anomaly has been observed: an error of approximately 65 seconds in both time code generators occurring at the time of day turnover. This does not adversely affect spacecraft operation.

8.2 EQUIPMENT PERFORMANCE EVALUATION

The Telemetry and Command Subsystem has successfully fulfilled its major design objectives during the first 30 days of operation in orbit. Table 8-1 provides a comparison of spacecraft performance against primary requirements (see para. 8.2.2).

Primary parameters affecting telemetry communications are transmitter frequency, EIRP, modulation index and system noise. Pre-launch tests indicated all transmitters to be operating well within tolerances on carrier frequency and power, modulation indices and spectrum allocations. Flight measurements have quantitatively verified operating frequencies of powered transmitters. RF component and scale model antenna test data support an EIRP estimate of 2 to 3dB above specification. The absence of bit errors in the data received at the ground stations confirm system noise, modulation indices, and EIRP have all met or exceeded requirements.

Analog telemetry data encoding accuracy is monitored by Low, Medium and High calibration voltage channels; permissible tolerance is $1/2$ LSB $\pm 0.25\%$ of the measured parameter. Flight data shows no deviation from design center values, which indicates encoding accuracy is $\leq \pm 1/2$ LSB = ± 5 mV.

Telemetry time base accuracy is important in correlating spacecraft events in time, using the Time Code Generator (TCG) or telemetry bit rate. Flight measurements show absolute rate error to be less than one-third of the allowable error (± 1.5 PPM).

Table 8-1

T&C Subsystem Performance Comparison

Parameter	Specification	In Flight Performance
XMTR. Frequency A1	136.23 \pm .003%	136.231469 +.0011%
A2	137.11 \pm .003%	137.109984 -0.000%
A3	136.23 \pm .003%	Has not been powered since launch
A4	137.11 \pm .003%	137.107742 -.0017%
EIRP. Power	-3 dBw min	Data evaluation to date shows BER < 10^{-5} .
DACU Bit Rate	390.625 \pm .00015%	7-Day check shows accurate to < 0.00005%.
DACU Analog Cal. Voltage	Low 0.265 \pm 0.005 VDC Med 2.565 \pm 0.005 VDC High 5.095 \pm 0.005 VDC	0.265V \pm 0 2.565V \pm 0 5.095V \pm 0
FDM		FDM multiplexing of combined EME data, DACU normal data, and Earth sensor data, has been successfully demultiplexed at both ground stations since first day of flight, via the PFF/30 ft dish.
Receiver/CDD Command Threshold	-107 dBm	Actual margin above threshold is 15 to 27 dB with BER < 10^{-5} .

Command performance is operationally dependent on receiver-decoder thresholds. Flight signal margins above the specified threshold are close to those estimated during pre-launch tests namely 15 to 27 dB. Absence of command failures substantiates existence of a satisfactory service margin.

8.2.1 Design Objectives

The major T&C design objectives were to:

- a. Provide a means of receiving, decoding, and distributing commands transmitted from the ground to the spacecraft subsystem and experiments, through the T&C/VHF Command Receivers or the Transponder C-Band Receiver of the Communication Subsystem.
- b. Provide downlink telemetry transmitters accepting signals from any one of five sources selected by the Data Switching Unit.

Data Acquisition and Control Units (DACU #1, & DACU #2)

The EME (Experiment)

C-Band Discriminator and Filter

Frequency Division Multiplex Unit (FDM) which allows three sources simultaneous use of one transmitter.

Either DACU via 5.4 kHz SCO

EME

Special Data Link (SDL) on a 9.4 kHz SCO, which can select one of five inputs.

CMD RCVR #2

CMD RCVR #3

Earth Sensor Pitch

Earth Sensor Roll

C-Band Discriminator

- c. Provide 3 different uplink RF Coaxial switching configurations between the 4 VHF Command Receivers and the two VHF Omni antennas, (each mounted on an outer edge of a solar panel, and the Prime Focus Feed (PFF) associated with the 30 foot Parabolic Antenna.
- d. Provide 6 different downlink RF coaxial switching combinations between the 4 VHF transmitters and the two VHF Omni antennas, and the PFF. See Figure 8-1.
- e. Provide 4 outputs from the T&C S/S to the Wide Band Data Unit (WBDU) for C-Band downlink data transmission of the following.

DACU #1

DACU #2

EME

FDM

- f. Provide redundant VHF Command Receiver interconnection configurations. See Figure 8-2.
- g. Provide for Command system characteristics as listed in Table 8.2.
- h. Provide telemetry equipment with capabilities listed in Table 8-3.
- i. Provide for VHF voice - bandwidth analog data communication between ATS Ground Stations.

8.2.2 Performance Evaluation

During the first 5 sequences and part of sequence 6 of the orbital procedures the T&C S/S was configured for Launch/Acquisition with no command change after launch.

The configuration was:

DSU-A ON - DSU-B OFF

Uplink configuration #6

RCVR #2 From OMNI -1

RCVR #4 From OMNI - 2

Command frequency 154.20 MHz

NCE address 646 to CDD - 2

No RCVR - CDD crosspatch

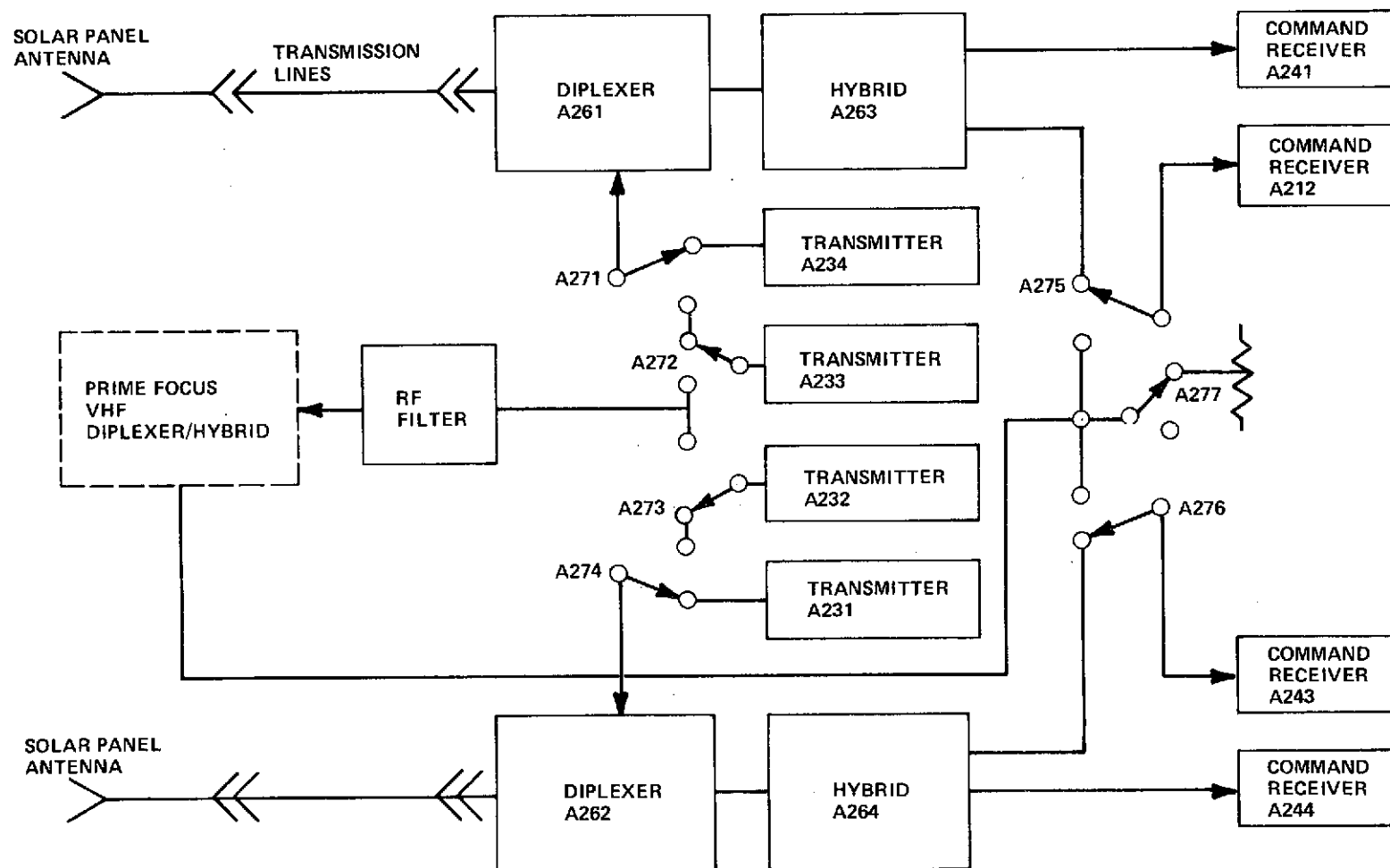


Figure 8-1. T&C RF System

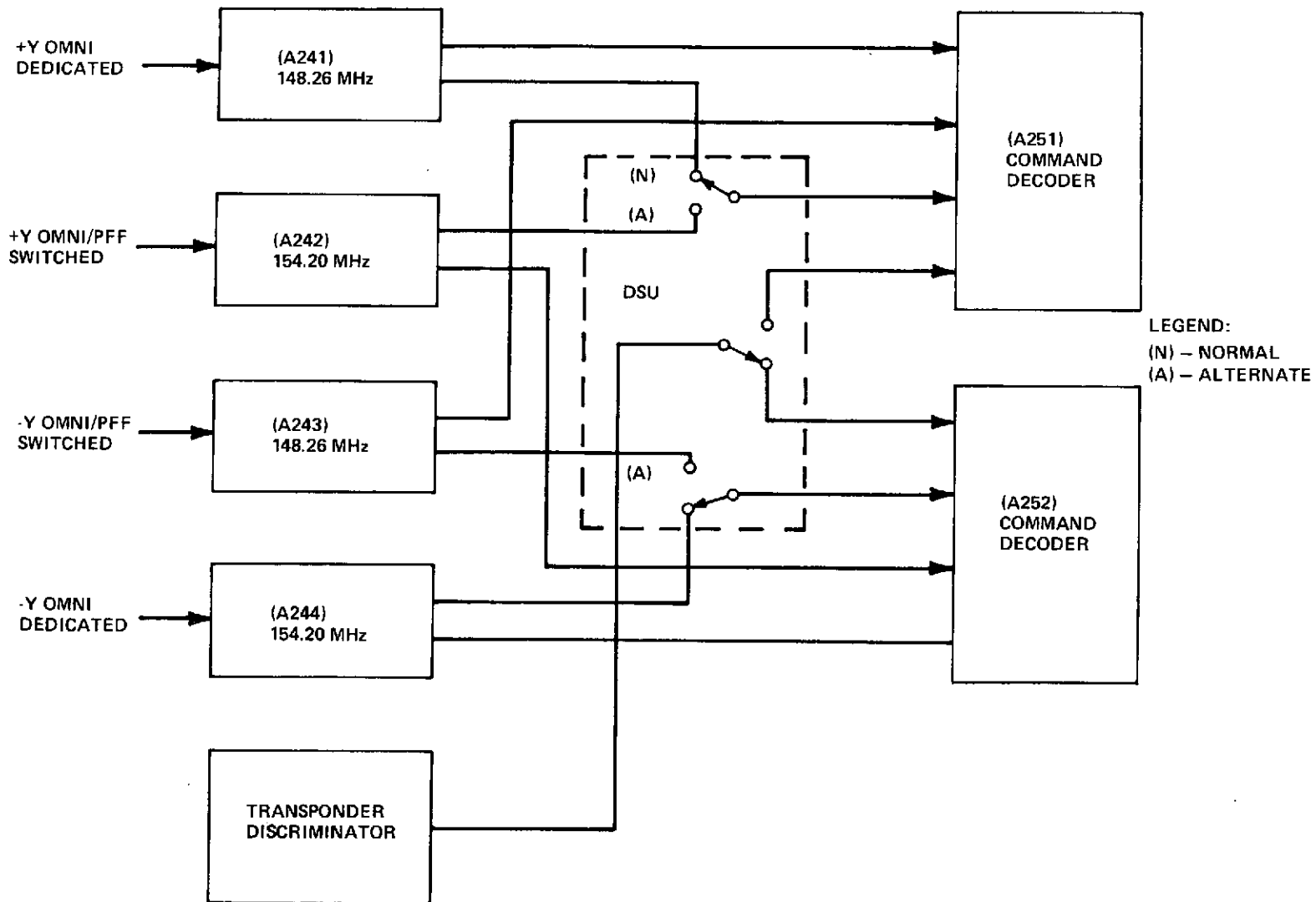


Figure 8-2. Command Receivers/Decoders Interconnections.

Table 8-2

Command System Characteristics

Modulation: PCM/FSK/AM/AM at VHF
PCM/FSK/AM/FM at C-Band
Frequencies: 154.20MHz, Prime
148.26MHz, Standby
C-Band Switch back-up
Antenna: 2 solar panel omnidirectional;
VHF prime focus feed;
C-Band earth coverage horn.

Characteristic	COMMAND MODES	
	Normal Command & Execute	GAC Command
Verification	Ground, via TM	Decoder address
Execute	Digital Command	Execute as received
FSK tones	Logic "0" 7296 Hz Logic "1" 7808 Hz	Logic "0" 8,700 Hz Logic "1" 11,900 Hz
Bit Rate	128 bps	1200 bps
Decoder address	9 bits	7 bits
Frame Length	28 bits	13 bits
Discrete commands	512	—
Data Word addresses	45	—
Data Word length	9	—
ACS Configuration addresses	—	32
Normal Command Execute Options	a) Execute & clear b) Execute & hold	High speed execute of Normal Command
Execute Pulse width	a) 50 ms, nominal b) 250 ms, nominal	11 ms, nom.
Max. Command Rate	2.2/sec*	92.3/sec
Repetitive Execute Rate	4.4/sec	46.1/sec
Time duration command resolution	250 ms	11.25 ms
Command Distribution	a) Array for support subsystems b) Dedicated to experiments c) Remote distributor for transponder	Dedicated to ACS only
Redundancy	Redundant antennas, receivers & decoders	Redundant antennas, receivers & decoders

*Without ground verification before execute.

2.2/sec for 50 ms commands, 1.4/sec for 250 ms Commands. Any rate up to 1.4/sec for either execute pulse width; none between 1.4 and 2.2/sec. Standard format rate required is 1/sec.

Table 8-3
ATS-F Telemetry Parameters

Characteristics	ATS F
Frequencies	136. 23 MHz, 137. 11 MHz
Spacecraft Antennae	Omnidirectional mounted on solar panels. Directional via prime focus feed and parabolic reflector.
Modulation	PCM/PM on omni-associated transmitters, PCM/FM/PM or PM on prime focus feed-associated transmitters
Formatting	Data format Manchester II +180 Fixed format with dwell capability
Bit Rate	390, 625 nominal
Word Length	9-bits
Minor Frame Length	128 words
Minor Frame Period	Approximately 3 seconds
Subcommutation	Last 16 words, 16 deep
Total Format Capacity	368 nine-bit words.
Analog Channels	276
Digital Data	783 bits (87 nine bit words)

Downlink configuration #8

DACU #1 PWR ON

TCG #1 PWR ON - M.O. #1 ON

TCG # 2 PWR ON

DACU #2 PWR OFF

DACU #1 Connected to XMTRS #1 and #4

XMTRS #1 and #4 PWR ON

XMTR #1 Connected to Omni - 2

XMTR #4 Connected to Omni - 1

DACU #2 Connected to FDM 5.4 kHz VCO

FDM PWR OFF

During the balance of the 30-day period the T&C S/S operated in what is considered normal configuration except for limited trial commanding via C-Band to each CDD. The changes to the above are as follows:

Uplink configuration #3

RCVR #2 from PFF

Downlink

DACU #1 PWR ON (usually in dwell)

DACU #2 PWR ON

DACU #1 Connected to XMTR #1 only

XMTR #4 PWR OFF

XMTR #2 PWR ON

XMTR #2 Connected to PFF

FDM Connected to XMTR #2

FDM PWR ON

Earth Sensor to FDM SDL VCO

EME to FDM Baseband

Operating with these two T&C configuration modes the following equipment performance evaluations were made:

Downlink

TRANSMITTERS #1, #4, and #2 Performance.

Frequency and temperature deltas, Output power via Omni-2

DACU #1 and associated TCG-1 performance

DACU #2 and associated TCG-2 performance

FDM performance

Data sources consisted of:

Off-line History Tape processing data.

ATSOCC Sequential Event printouts.

Uplink

CDD #1 Performance (VHF & C-Band)

CDD #2 Performance (VHF & C-Band)

RCVR #2 operation via PFF with AGC as a function of combinations of RBE and C-Band configurations.

Data sources consisted of:

Ground station command time and event tape.

Ground station plots of received signal levels.

IDA Stripchart recordings (real time).

Off-line History Tape data.

ATSOCC Sequential Event printouts.

8. 2. 2. 1 Command Uplink Performance – Figure 8-3 is a plot of the received command receiver input signal levels measured during the yaw flip maneuver between 151:01:48 and 151:02:13. It may be seen that the signal level difference with normal Z-axis local-vertical pointing was approximately 12 to 13 db. With the Z axis pointing at the Rosman groundstation the difference was 14 to 15 db.

Table 8-4 lists the margin above command threshold for each command receiver input during the 30 day operation.

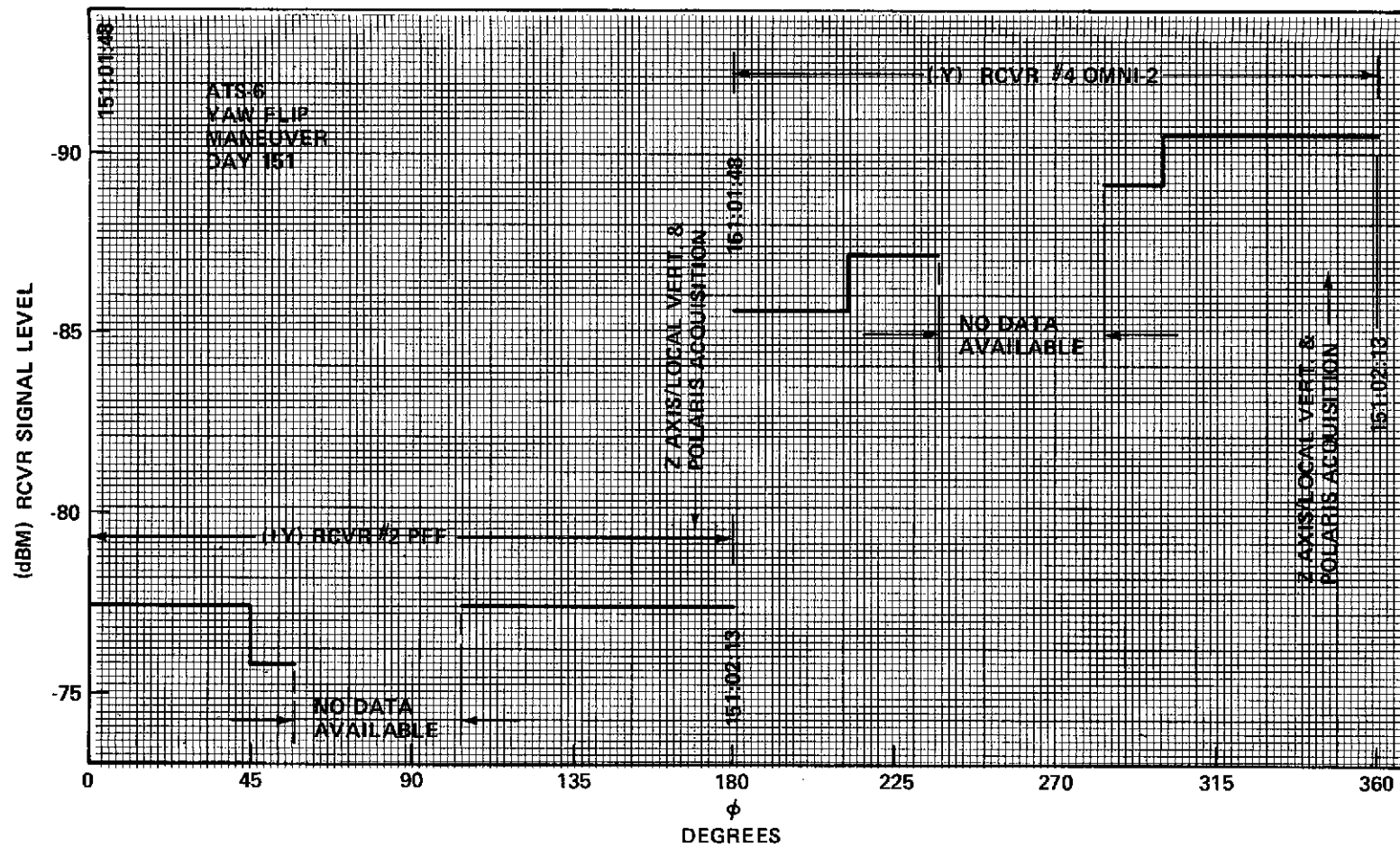


Figure 8-3. Antenna Look Angle from Rosman

Table 8-4

Uplink

Command Receiver Signal Levels

Conditions With S/C in Local Vertical - Reference Orientation	RCVR #1 Omni-1 (+Y)	RCVR #2 Omni-1 (+Y)	RCVR #2 PFF	RCVR #3 Omni-2 (-Y)	RCVR #4 Omni-2 (-Y)
Spacecraft Orbital Data AGC Level	-90 dBm	-92 dBm	-80 dBm	-88 dBm	-90 dBm
Receiver Threshold Measured In Ground Tests	-118.0 dBm	-119.4 dBm	-119.4 dBm	-116.5 dBm	-119.7 dB
Approximate Margin Above Threshold	28 dB	27 dB	39 dB	28 dB	30 dB
Margin Above Spec.	17 dB	15 dB	27 dB	18 dB	17 dB

CDD #1 functioned normally through the C-Band uplink. No command load or execute failures were noted during the limited trials.

CDD #2 was used for all other commanding throughout this period, with no command loads or execute failures noted.

8.2.2.2 Telemetry Downlink Performance - Performance of VHF Transmitters #1, and #2, was normal with data related to ERP output appearing to be in agreement with baseline data from ground tests. Table 8-5 supports these findings.

No anomalies were observed in the operation of the DACU's or the 6 hour timers, which were driven by Master Oscillator #1. However, both Time Code Generators (TCG) were found to be in error by 65.536 seconds following each days turnover. It has been determined, that this condition was present in both units prior to launch. A memorandum explaining in detail, the source of this anomaly will be written by IBM in early July. Ground computer software can be adjusted to correct for this difference.

Temperatures of the VHF transmitters ranged between 38.9°C and 18.4°C during the checkout period.

The transmitter frequencies were checked at both Mojave and Rosman ground-stations and were found to be operating well within the ± 30 parts per million (PPM) specification and very close to pre-launch measurements.

The FDM functioned normally using PFF/30' Dish downlink and exhibited adequate signal to noise margins for good quality data. Demultiplexing of EME

Table 8-5

Downlink

Conditions With S/C in Rosman Pointing - Reference Orientation	136 MHz XMTR #1 Omni 2 (-Y)	137 MHz XMTR #2 PFF
RCVR Input Signal Level at Rosman Ground Station	-116 dbm	-107 dbm
SATAN RCVR Antenna Gain	+ 19 dbm	+ 19 dbm
Space Loss (35,800 Km)	168 db	168 db
ERP at Spacecraft	+33 dbm	42 db
PR-2000 Min. Spec. ERP	+ 27 dbm	N/A
ERP Predicted from Prelaunch Measurement	+ 31 dbm	41 db

data, SDL data, and DACU #2 Normal Data, resulted in satisfactory quality at Rosman and Mojave. A check of the VHF SDL voice link between Rosman and Mojave was also accomplished successfully. DACU #1 data, dedicated mostly to dwell, was satisfactorily received via the Omni antenna.

EME data transmitted direct via XMTR #1 and Omni #2 was received at Rosman with a signal level 12 db above the required PCM threshold. This was accomplished via the 19 db Satan Receive Antenna.

8.2.2.3 Functional Performance Verification — In addition to quantitative performance data given in Tables 8-1 and 8-4, successful spacecraft operations also demonstrate proper T&C subsystem functional performance in the following areas:

RF Equipment

Omni Antennas — coverage, gain and efficiency

Transmission Components — integrity and insertion loss

- Diplexers
- Hybrids
- Coaxial lines & connectors
- Coax switches (A275, A277 have been commanded)

Transmitters — modulation index, modulation noise, thermal control
(A233 has not been powered since launch)

Receivers — sensitivity, output level and SNR, EPS dedicated regulators

Command Decoders

Error rate/data recovery

Interfaces verified

- VHF receivers
- C-Band receiver
- Users

Normal mode commands

- Discrete

- Time duration
- Data Word

GAC mode commands

Data Multiplexers & Clocks

Analog-to-Digital conversion accuracy and stability

Time base accuracy and stability

Enable signal outputs

Master Oscillator cross-strap

Power command control

Output levels

Data Switching

Baseband switching

RF & Baseband relay command matrix operation

Power control for transmitters, FDM and relay matrix

FDM assembly VCO's, filters; modulation indices, SNR, and output level

SECTION 9

ATTITUDE CONTROL SUBSYSTEM

SECTION 9

ATTITUDE CONTROL SUBSYSTEM

9.1 SUBSYSTEM PERFORMANCE

The Attitude Control Subsystem (ACS) serves to stabilize and orient the ATS-6 spacecraft after it separates from the launch vehicle. The three (3) basic functional elements of the ACS are: Sensors (Attitude Control Reference), Controllers (Computers), and Torquers (Wheels and Jets). For its operational modes the ACS uses an Earth Sensor and a Polaris Sensor as prime attitude control references, digital and analog computers as controlling elements, and three momentum wheels and the attitude control jets of the Spacecraft Propulsion Subsystem (SPS) as control actuators.

The performance requirements for the Attitude Control Subsystem are established in Fairchild ATS-F Specification 862-0001D. A simplified block diagram of the ACS is presented in Figure 9-1.

An overall assessment of the ACS performance during the first thirty days of operation is that the ATS-F mission requirements for the Attitude Control Subsystem have been met as summarized in Table 9-1. To date, all non-back-up modes have been exercised with the exception of SAPPAC and Satellite track using S-Band monopulse on the tracked satellite.

Some abnormal system actions were observed. These are summarized below and described in detail in Section 9-6.

Anomalies:

1. Earth Acquisition Anomaly

The ACS did not provide controlled motion to zero attitude error in roll after the earth was acquired by the Earth Sensor (ESA). Instead, the roll angles held at about 8 to 9 degrees with some oscillation. Normal attitude control to zero error was achieved when Rate Gyro Assembly 2 (RGA 2) was substituted for RGA 1 in the control loop. After a review of the data it was concluded that the roll gyro of RGA #1 degraded during launch and/or separation.

2. Polaris Sensor (PSA) Tracking Anomalies

Although operation was usually normal, the PSA has suffered the following problems:

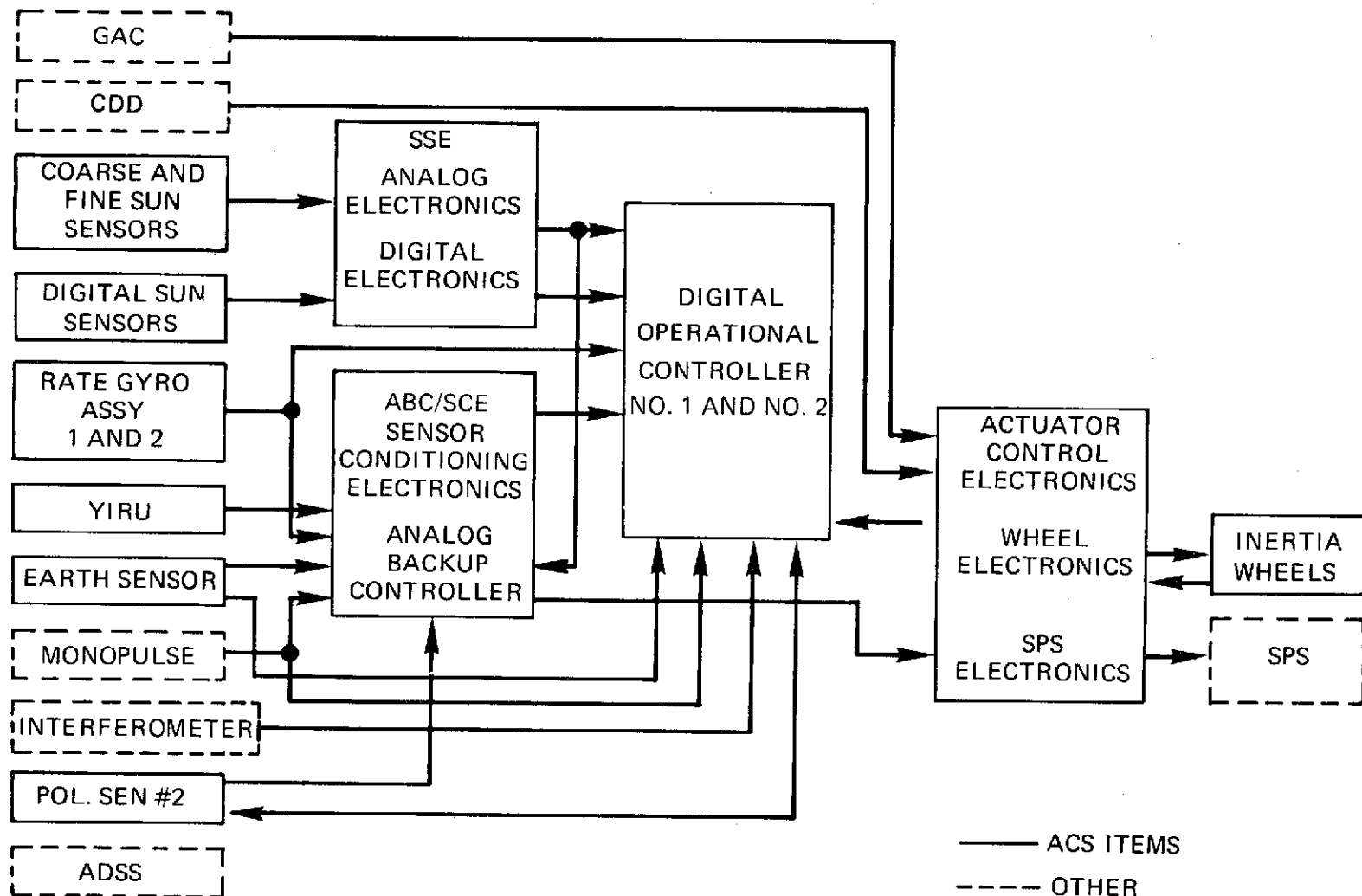


Figure 9-1. Attitude Control Subsystem Block Diagram

Table 9-1

ACS Summary Performance

Mode	Parameter*	Spec	Actual
ABC Sun Acquisition	Time to acquire Pointing accuracy	30 minutes 4.5°	10 minutes 2°
ABCEarth Acquisition	Time to acquire Pointing accuracy	80 minutes 1.0°	50 minutes 0.35°
ABC Local Vertical	Pointing accuracy	1.0°	0.35°
DOC VHF Monopulse	Pointing stability	1.0°	0.5°
DOC S-Band Monopulse	Pointing stability	0.3°	0.01°
DOC C-Band Monopulse	Pointing stability	0.1°	0.002°
DOC Offset Point Ground **	Pointing accuracy	0.1°	0.049°
	Pointing stability	0.1°	0.01°
DOC Low Jitter**	Pointing accuracy	0.5°	<0.1°
	Pointing stability	0.01°	0.005°
	Rate stability (low freq.)	0.001°/sec	0.0003°/sec
DOC Satellite Track	Pointing accuracy	0.5°	<0.2°
DOC Offset Point Slew	Rate	≥0.5°/minutes	1.2°/minutes
	Settling time	≤10 minutes	<3 minutes
DOC Operational Modes	Yaw accuracy using PSA	0.15°	<0.1°

*Indicated parameters pertain to roll and pitch except for the first mode which pertains to pitch and yaw and the last mode which pertains to yaw.

**Either ESA or Interferometer.

1. Tracking a false target in the field of view.
2. Losing lock on Polaris as if not enough light energy was reaching the detector.

The causes of this behavior are presently not understood. Operationally, a Polaris loss-of-acquisition resulted in a yaw axis transient when the ACS logic automatically selected the YIRU for control. A further transient occurred when the PSA was again operating correctly and was automatically re-selected for control in the ACS.

3. Yaw Inertial Reference Unit (YIRU) Bias Anomaly.

Biases are applied to the gyro torquer to negate the effect of inherent gyro drift from its null position. These biases have been disappearing without known cause after about 15 minutes. With the YIRU used as a backup unit, this has little significance; as a prime unit the YIRU would require more frequent updating and ground intervention than originally expected.

4. Digital Operational Controller (DOC) Command Angle Anomaly

Incorrect pitch and yaw command angles were generated by DOC every twelve hours. The incorrect commands existed for about 3 3/4 minutes. The source of the error, a register overflow, has been isolated and the DOC program corrected. No anomalous behavior has been observed since the re-programming.

5. Interferometer AGC IF #2 Anomaly

The Interferometer Subsystem, after being off between days 2 and 5 was commanded on again to perform spacecraft axis calibration. The Interferometer AGC No. 2 failed to respond. After 45 minutes of operation AGC No. 2 responded correctly and continued to perform properly. This anomaly has recurred several times.

9.2 LAUNCH AND ACQUISITION

Table 9-2 summarizes ACS performance during the acquisition modes. With the exception of the initial earth acquisition, the nominal values were met. The exception, which was caused by an RGA anomaly, is discussed in Section 9.6. The only ACS components powered-on during launch were the Rate Gyro Assemblies (RGA), Digital Sun Sensors (DSS), Auxiliary Digital Sun Sensors (ADSS), Coarse/Fine Sun Sensors (C/FSS), and the star tracker (PSA) sun shutter. Spacecraft

Table 9-2

ACS Acquisition Performance

Mode	Parameter	Spec		Actual	
		Nominal	Max		
ABC Sun Acquisition	Time to Acquire	13 min	20 min	5.4	Any Offset to 30° of Sunline
		5 min	10 min	4.6	30° to 4.5° of Sunline
ABC Sun Acquisition	Pointing Accuracy	4.5°		2.2°	P = +0.89° Max. Y = -1.78° Max.
ABC Earth Acquisition	Time to Acquire	30 min	80 min	52 min	Within 4° of Local Vert.
ACC Earth Acquisition	Pointing Accuracy	±1°		R = -.50 P = +.47	Torquer - Jets ΔR = .20°, ΔP = .30°
ABC Local Vertical	Pointing Accuracy	±1°		R = -.33 P = +.35	Torquer - Wheels ΔR = .04°, ΔP = .04°
DOC Local Vertical	Pointing Accuracy	±0.1°		R = -.04 P = +.04	

telemetry data indicated that all the sensors were operational during this period. However, the + X DSS identification bit was not illuminated until after separation because of optical blockage from an adapter leg. The RGA data was compared with the Titan rate data and excellent correlation was observed (see ATS-6 First Orbit Evaluation*). At separation, the tip-off rates were $-.22$, $+.10$ and $-.06$ degrees/second in roll, pitch and yaw. These were well within the specified $0.5^\circ/\text{sec}$, therefore, the "Special Rate Damp" mode was not required and the ACS remained inactive during the deployment phase. Time history plots of RGA data during deployment are presented in Figure 9-2. The spacecraft rates after deployment were $-.13$, $+.06$, and $.08$ degrees/sec in roll, pitch and yaw. Approximately 20 minutes after the Deployment Sequence was completed, RGA #2 was turned off. With both RGA's on the rates were $-.15$, $+.03$ and $+.04$ deg/sec in roll, pitch and yaw. After turning RGA 2 off, the corresponding uncorrected readings were $-.22$, $+.07$ and $+.06$ deg/sec. The difference in roll rate ($-.07$ deg/sec) indicated a fairly large null shift in one or both of the roll Gyros. After completion of deployment and RGA #2 turnoff, evacuation and bleed-in of SPS 1 was performed. Positive roll and positive pitch thruster valves were opened for approximately 7.9 minutes to evacuate the nitrogen gas contained in the lines. The West prime thruster was then commanded open for 5 minutes. Bleed-in was then accomplished, and SPS 1 was ready for operation.

Table 9-3 lists the sequence of events which occurred during the acquisition phases.

9.2.1 Sun Acquisition

After deployment, the spacecraft body rates were low enough to go directly to Sun Acquisition mode without having to use "Rate Damp."

Sun Acquisition was accomplished using the Coarse/Fine Sun Sensor for pitch and yaw attitude control, the RGA for three axis rate information, the ABC as the controller, and SPS 1 as the torquer. This was the planned ACS configuration for acquiring the sun by aligning the +X axis to the sun-line. The ADSS's and DSS's were operational and used by ground control (ATSOCC) to determine spacecraft attitude during the sun acquisition phase. At 150:21:10: (1 hour 37 minutes after separation) ABC Sun Acquisition was commanded. At this time, the + X axis was approximately 122 degrees from the sun-line (Figure 9-3). Figures 9-4 and 9-5 show the pitch and yaw attitude errors, rates, and jet firings versus time, from the start of Sun Acquisition until a steady state attitude was obtained. Two curves are presented for the attitude errors, one being the + X DSS outputs, and the other being the FSS telemetry outputs. As can be seen,

*Goddard Space Flight Center - Report No. X-713-74-177.

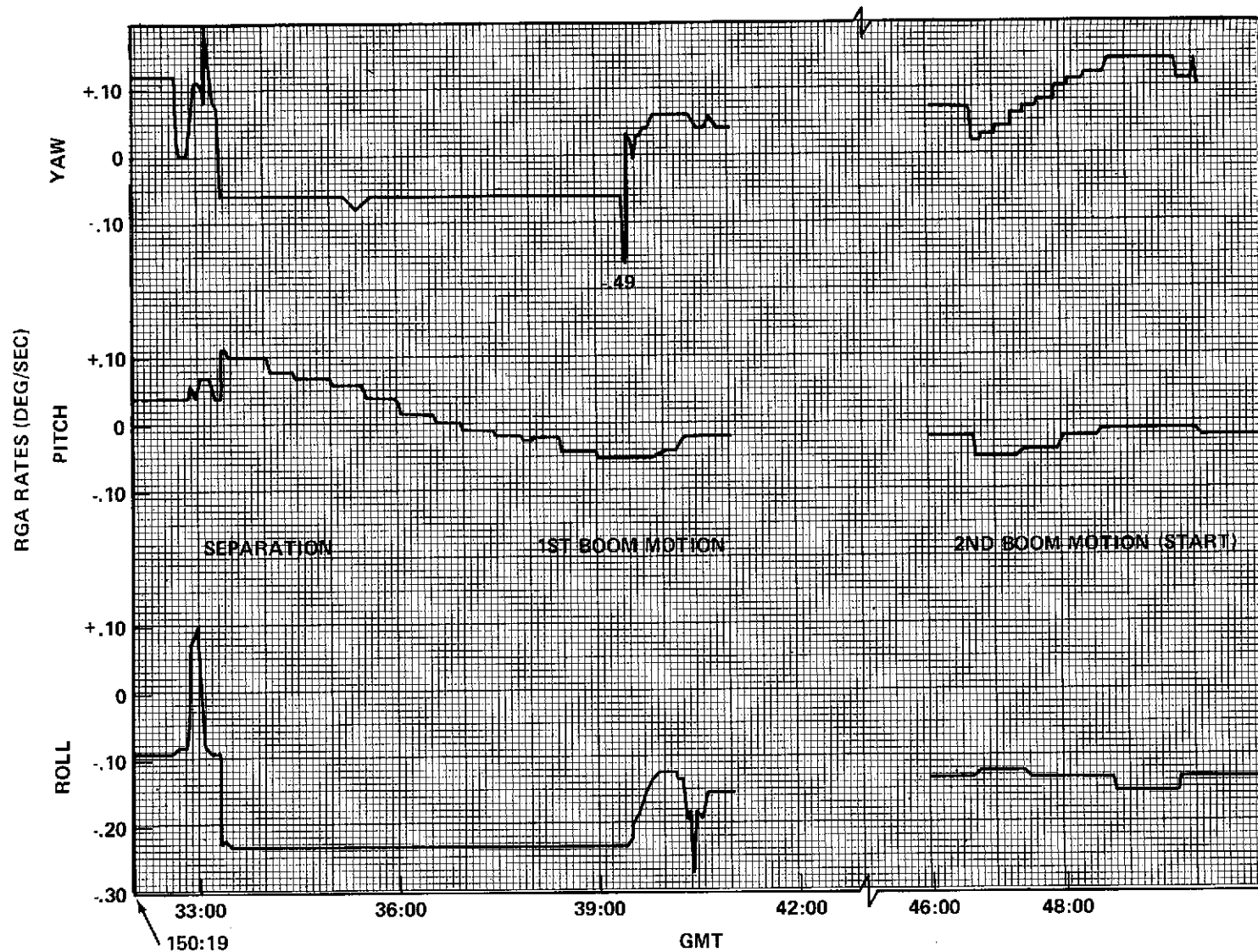


Figure 9-2. Time History of Spacecraft Rates During Deployment

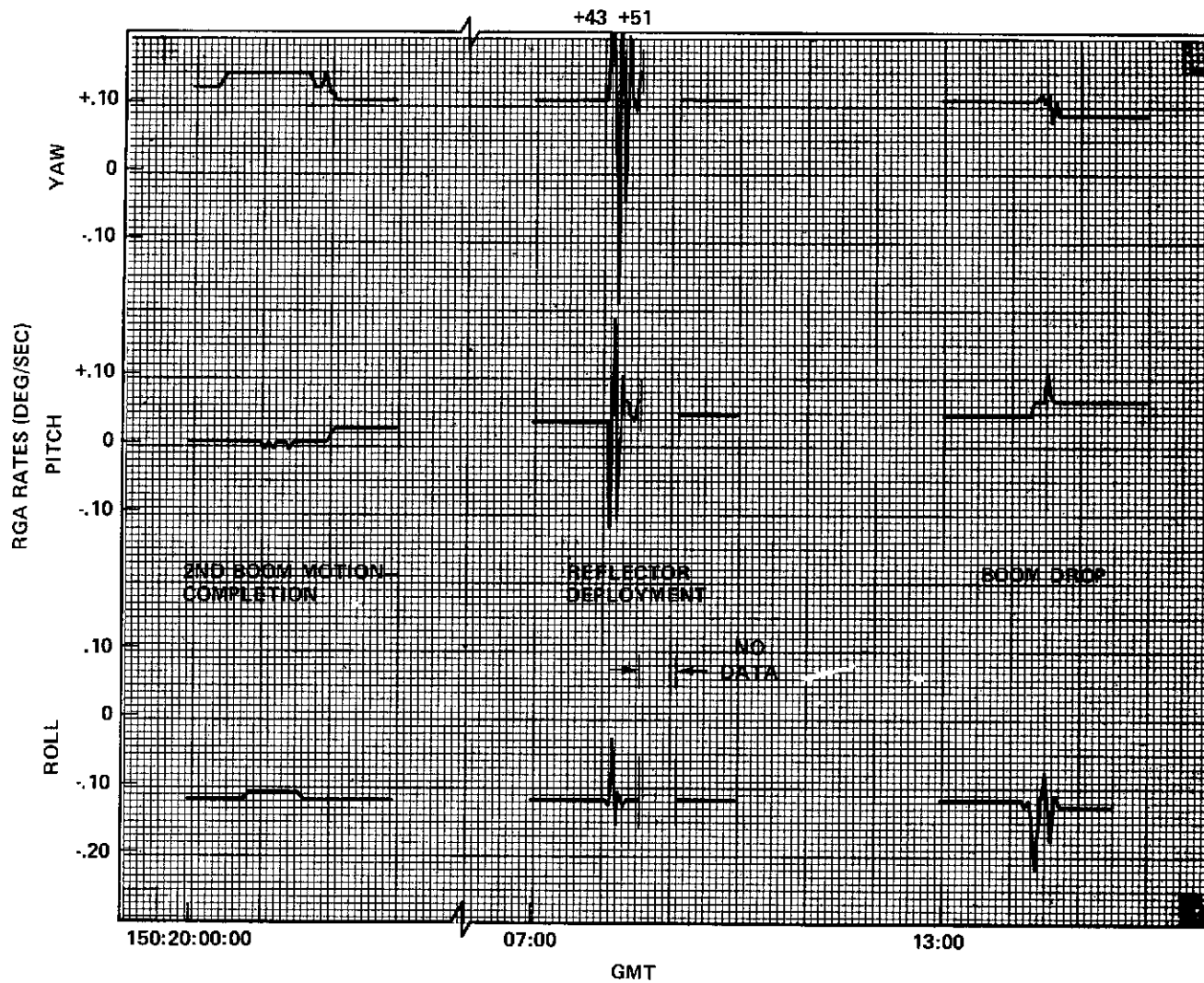


Figure 9-2 (Cont.). Time History of Spacecraft Rates During Deployment

Table 9-3. ACS Acquisition Events

Event	Time	Comment
Liftoff	150:13:00:02	
Separation	19:33:21	Sep. Rates R = -. 22, P = . 10, Y = -. 06
Boom 1st Motion	19:39:23	Init. Rates R = -. 22, P = . 06, Y = -. 06
— Complete	19:40:34	
Solar Array Unfold	19:46:34	$\Delta t(+Y) = 3 \text{ min } 29 \text{ sec}$
— S Complete	19:50:03	
— N Complete	20:02:00	$\Delta t(-Y) = 15 \text{ min } 26 \text{ sec}$
Reflector Deploy.		
— Complete	20:08:12	
Boom Drop		
— Enable	20:14:14	
— Complete	20:14:32	Final Rates R = -. 135, P = . 05, Y = +. 08
Sun Acquisition		
— Command	21:10:02	ZAZ = -140. 5, ZCOEL = 52. 5
— Complete	21:20:18	ZAZ = -91. 27, ZCOEL = 90. 25, Total Angle = 122 Deg.
RGA #2 - Off		$\Delta R = -. 07, \Delta P = +. 04, \Delta Y = +. 02$ °/sec
Pseudo Rate	21:23:09	
Select Wheels	21:35:53	
Cmd. Earth Acq.	23:10:36	
Complete Earth Acq.	151:00:00:00	$\Delta t = 42 \text{ min.}$
Yaw Ref. (ABC Polaris Acq.)	151:01:46	
Yaw Ref. Complete YIRU Control	151:02:15	$\Delta t = 29 \text{ min.}$
DOC Control	151:13:56	DOC Mode — Orbit Plane E (Day 2)
Polaris Acq.	153:14:20	
2nd Sun Acq.	161:11:48	
2nd Earth Acq.	161:12:00	

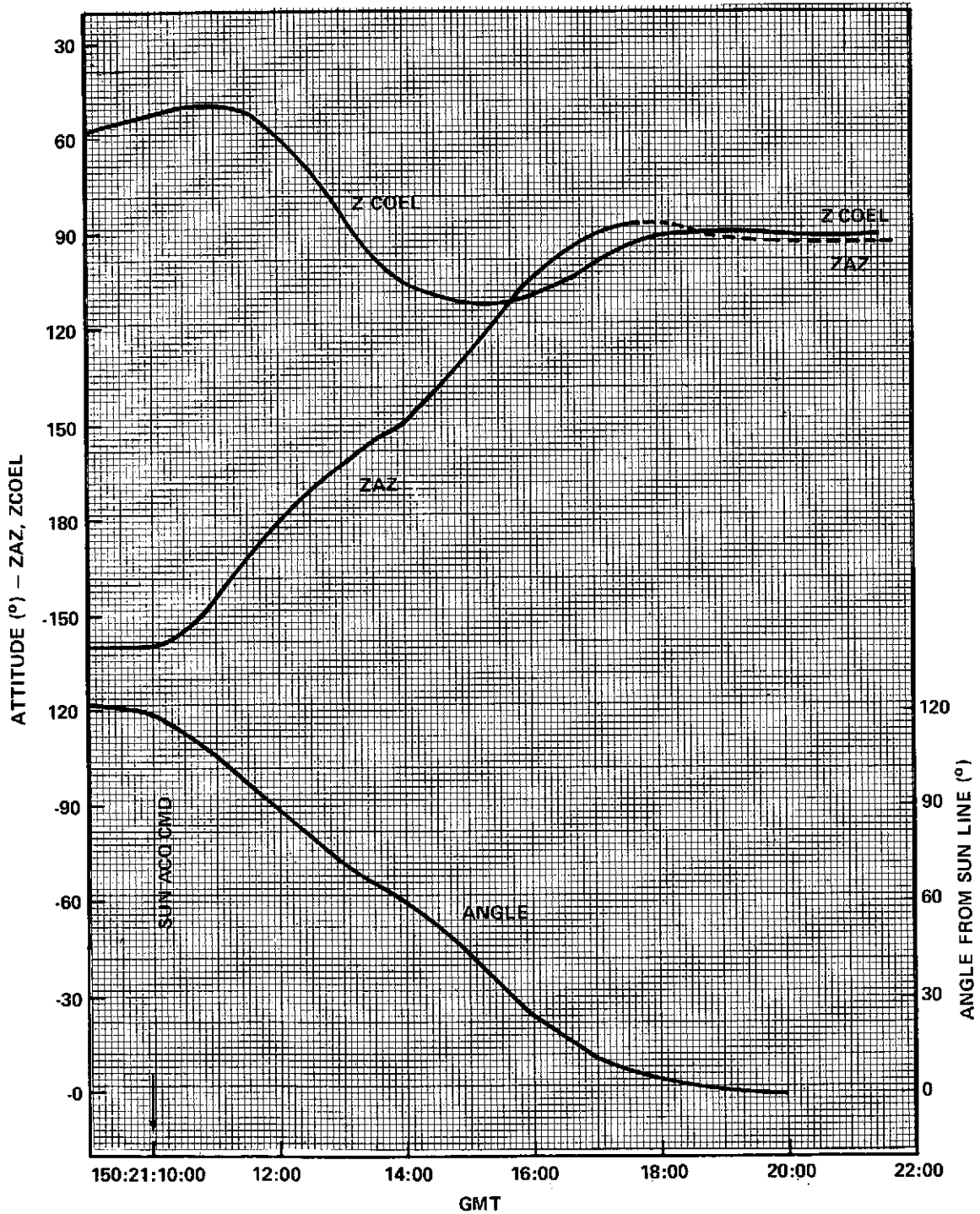


Figure 9-3. Spacecraft Attitude During Sun Acquisition

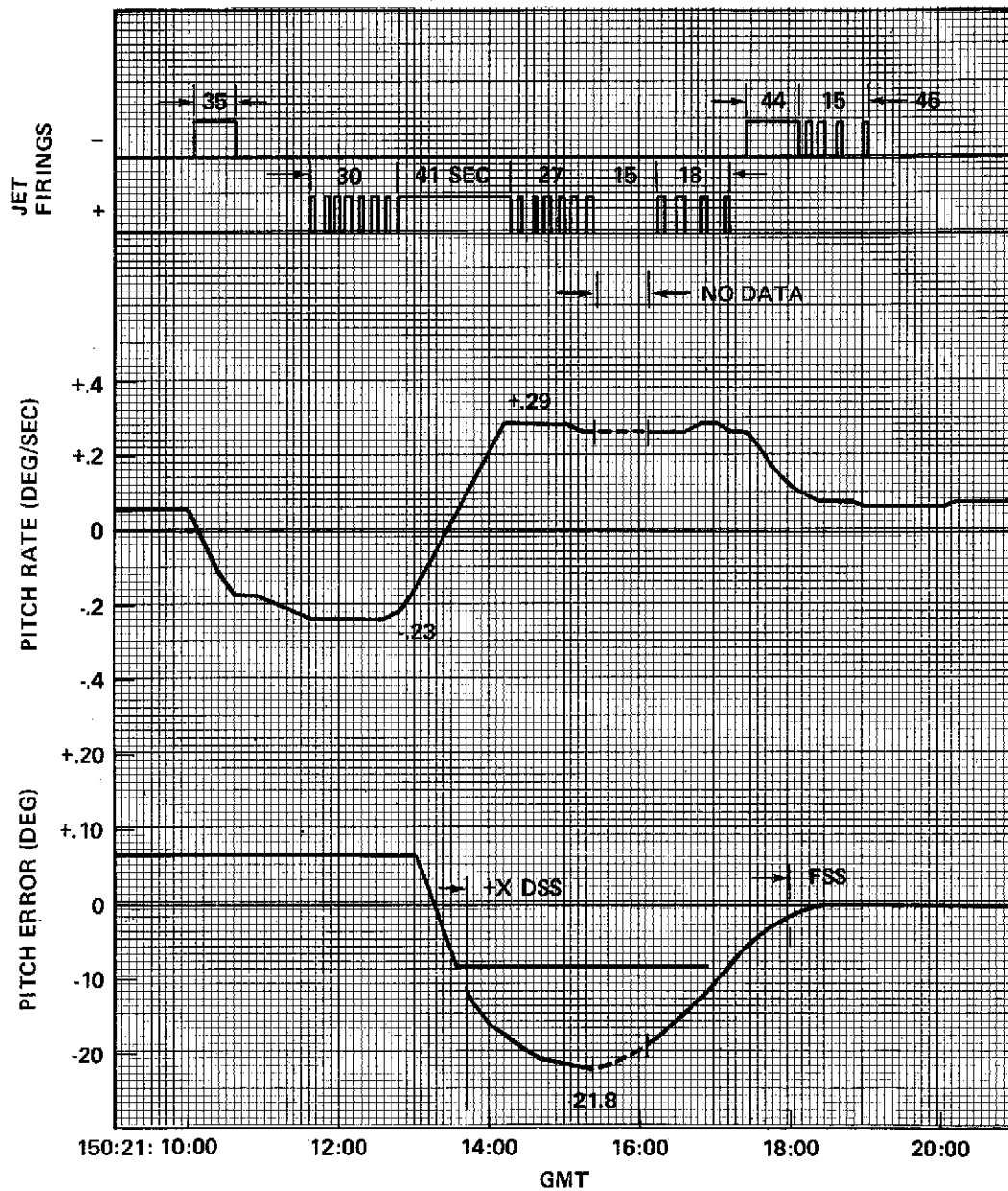


Figure 9-4. Pitch Axis Control During Sun Acquisition

C 1

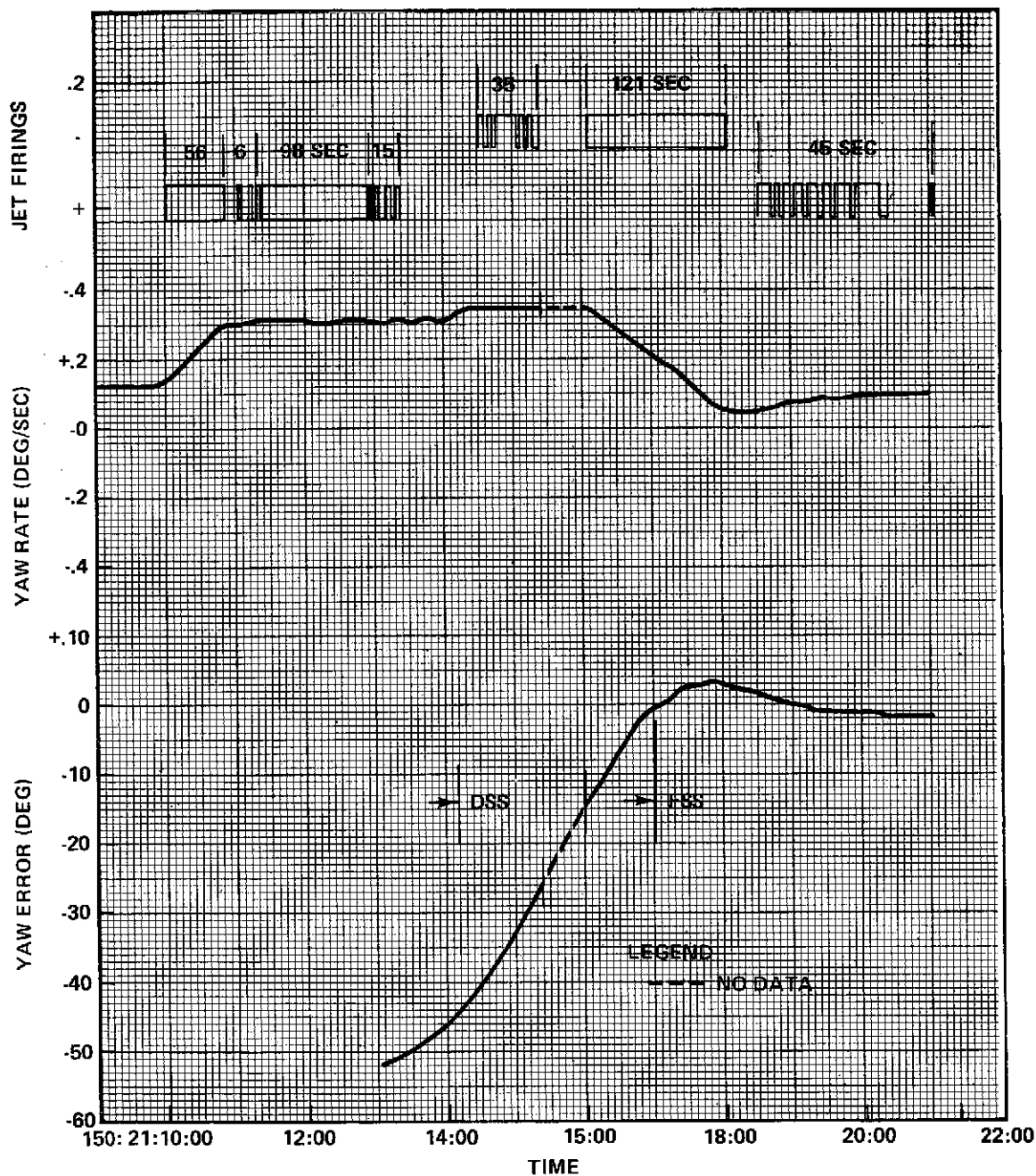


Figure 9-5. Yaw Axis Control During Sun Acquisition

the FSS outputs were saturated until the null plane was within 4.8 degrees of the sun-line. When the C/FSS came out of saturation, it and the + X DSS tracked within .25 degrees. The roll axis was controlled in rate only. Figure 9-6 is a plot of roll rate versus time. Roll rate settled to an indicated value of +.04 deg/sec. As can be seen, the time required for the + X axis to settle out to its steady state value of approximately 2.0 degrees from the sun-line, was 10 minutes. The time to go to and remain within the specification value of 4.5 degrees was 7.5 minutes. The offset from the sun-line was due to RGA biases and the system deadband.

Figure 9-7 shows the pitch and yaw sun acquisition phase-planes, which indicate settling after the initial jet firing and the pitch and yaw rates had built up to approximately $- .23$ and $+ .34^{\circ}$ deg/sec respectively. The phase-planes result from ATS motion involving simultaneous roll, pitch and yaw motions. Therefore, they cannot be used to verify the control system switching lines which are indicated for reference purposes.

The SPS 1 jets were fired during sun acquisition, with pulse widths of 3 sec to 121 sec. (Telemetry resolution is 3 seconds.) Estimated propellant usage was 0.40 pounds of hydrazine.

After steady state attitude was obtained, ABC Pseudo Rate was commanded. The reaction wheels were then powered-on and torquer control was switched from jets to wheels. Figure 9-8 is a plot of pitch and yaw wheel speeds which shows the momentum interchange between axes during the roll. Control on wheels was maintained for 1.4 hours until earth acquisition was commanded. During this time, wheel unloading was not required and DOC 1 and YIRU were powered-on and checked out prior to earth acquisition. No anomalies were found.

9.2.2 Earth Acquisition

The earth was acquired during the first crossing of the terminator plane in the evening of Day 1. The ACS was in its nominal configuration for earth acquisition. The ESA and C/FSS were used for attitude control, RGA 1 for rate, ABC as the controller, and SPS 1 as the torquer. The ESA was powered-on at 151:22:51: so that it could be checked out before the start of the earth acquisition window. The 3 minute warm-up transient occurred as expected. At 22:59 roll and pitch error signals appeared. Interferometer read-out also confirmed earth presence at this time. At 150:23:10 (approximately 5:54 Local Satellite time), ABC Earth Acquisition was commanded and at 23:18 the ESA acquired the earth. At approximately 151:00:02 the ESA roll and pitch errors had been reduced to steady state values of $-.4$ and $-.5$ degrees, respectively. The total time for the ESA roll and pitch errors to reach steady state after ABC Earth Acquisition had been commanded was approximately 52 minutes. The time to maneuver and

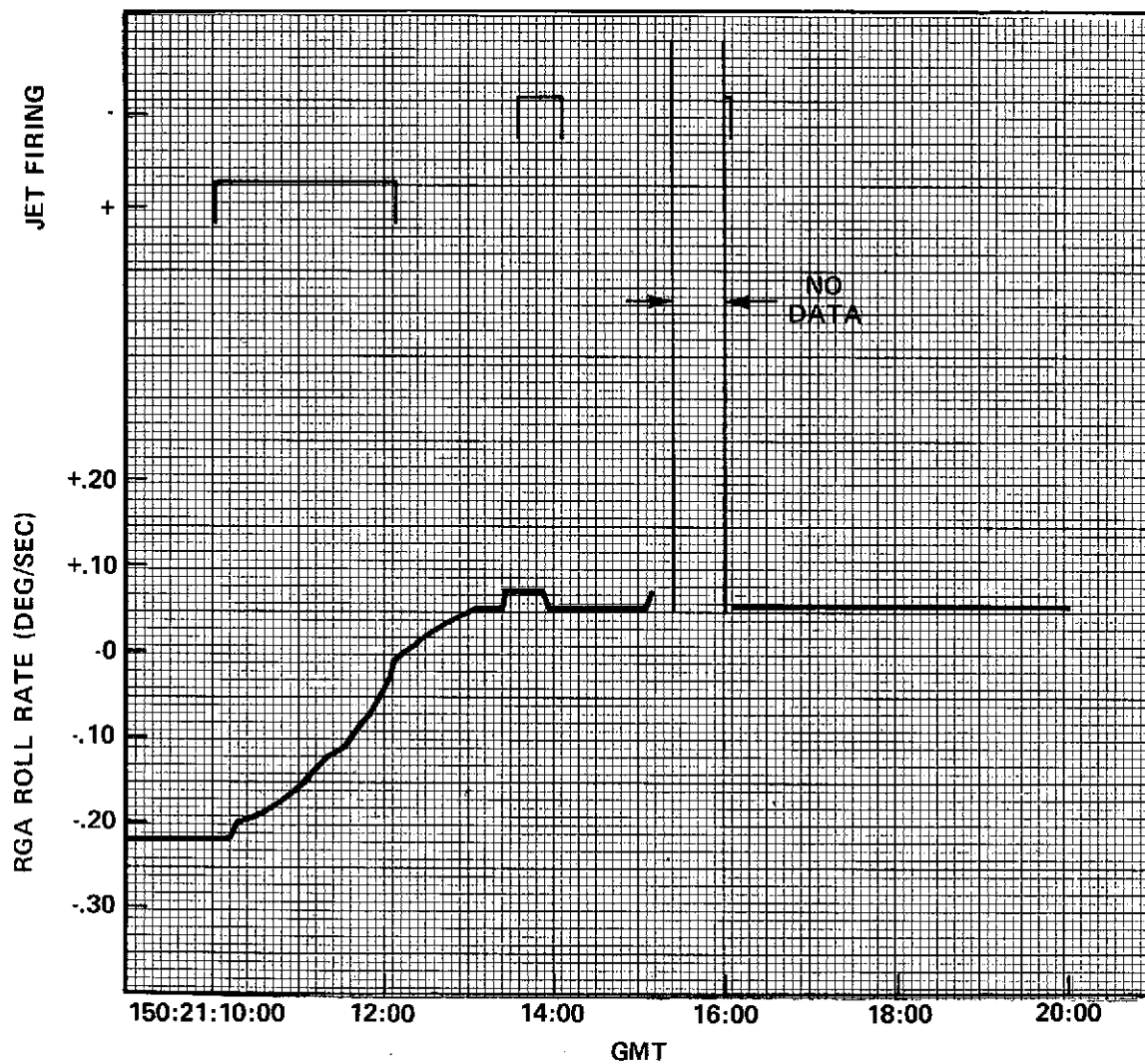


Figure 9-6. Roll Axis Control During Sun Acquisition

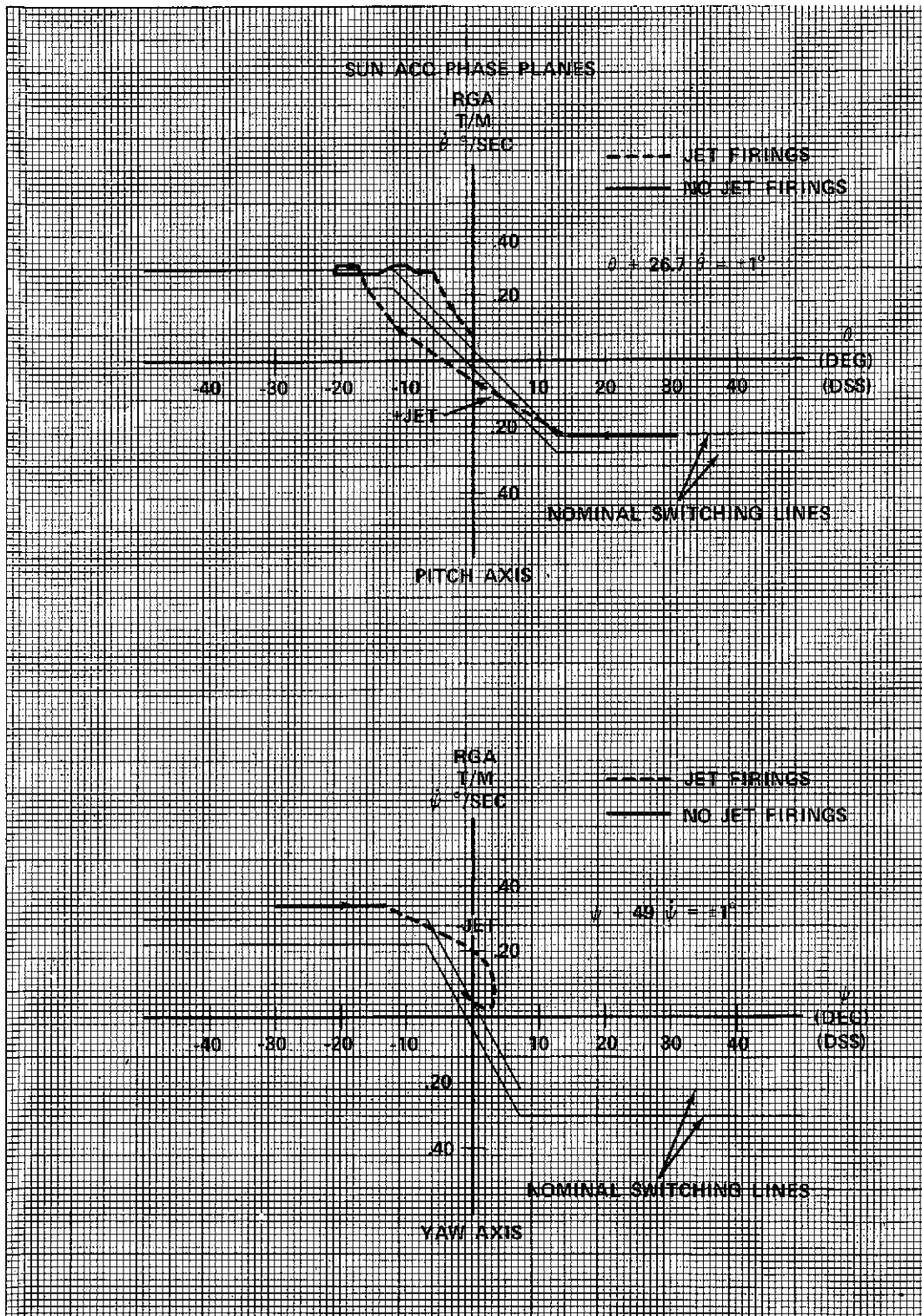


Figure 9-7. Yaw & Pitch Phase Planes During Sun Acquisition

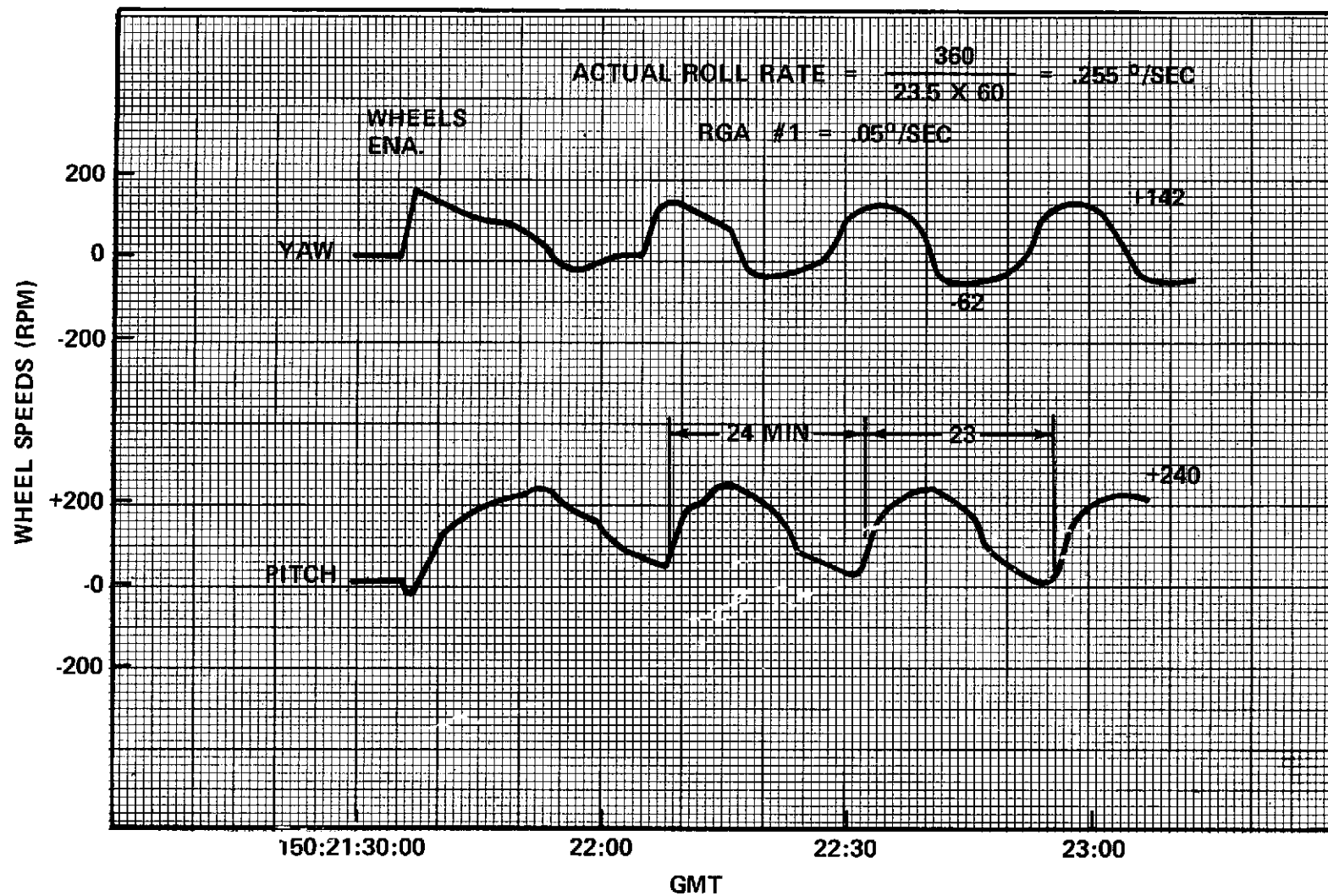


Figure 9-8. Pitch/Yaw Wheel Speed Vs. Time
During Sun Acq. Pseudo-Rate Mode

remain within 4.0 degrees of local vertical was 50 minutes. The specification states that the time to maneuver the +Z axis to within 4.0 degrees of the local vertical shall not be greater than 80 minutes (30 minutes nominal).

The greater than nominal time required to complete earth acquisition was caused by a large (-0.19 degrees/sec) gyro null shift in the RGA #1 roll gyro. Figure 9-9 shows roll axis settling out in a 2° limit cycle with an offset of approximately 7 degrees. Pseudo Rate with wheels was commanded at approximately 150:23:42 resulting in a roll overshoot in excess of 15° (test data showed that earth acquisition is normally lost at a roll angle of approximately 14.6°). ABC earth acquisition was commanded at 23:47 re-enabling jet control. RGA #2 was turned on and RGA #1 off and the spacecraft settled out from an offset of 8.5 degrees in 6 minutes.

Figure 9-10 shows the ESA pitch error, RGA pitch rate, and jet firings as functions of time. The time to settle in pitch from an initial error of 11.5 degrees was 3 minutes during the earth acquisition mode. The yaw axis was controlled by the C/FSS, with yaw attitude error varying between +.89 to -2.67° during this period.

After the roll and pitch errors had reached steady state, ABC Pseudo Rate was commanded taking the RGA out of the control loops. Reaction wheels were then commanded as the torquers. Figure 9-11 is a plot of attitude errors before and after enabling wheels which reduced the limit cycle from .2 - .3 degrees to less than .1 degrees. Estimated propellant usage while in the earth acquisition mode was .96 pounds of hydrazine.

9.2.3 Polaris Acquisition

Polaris acquisition was accomplished in two parts, the first being performed during the first day by rotating the spacecraft about its yaw axis to point the -Y axis toward Polaris. The actual Polaris acquisition was performed several days later.

ABC Polaris Acquisition, Winter, was commanded at 151:01:21 resulting in a negative rotation about the yaw axis (Figure 9-12), while pitch and roll attitude were controlled by the ESA. This was done to avoid slewing the sun across the north face of the EVM. At a (-X) DSS yaw angle of approximately 19 degrees, the yaw rotation was stopped by commanding the yaw into control. This maneuver took 28.4 minutes for a rotation of 200°, thus the yaw rate was -.118 deg/sec. Estimated propellant usage was 0.07 pounds of hydrazine. After the yaw reference maneuver was completed, the ABC was commanded into local vertical using the YIRU as the yaw axis attitude sensor.

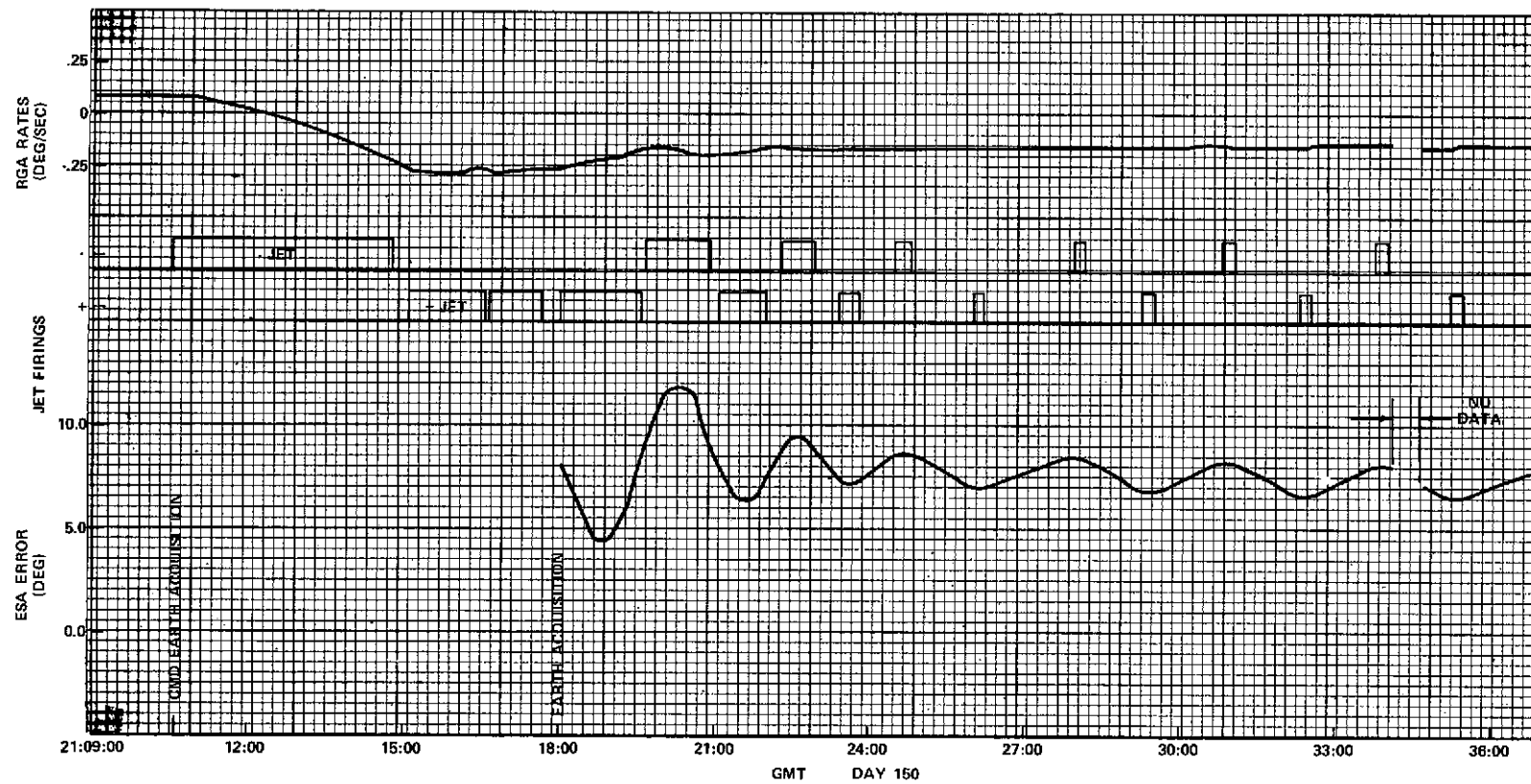


Figure 9-9. Roll Axis Control During Earth Acquisition

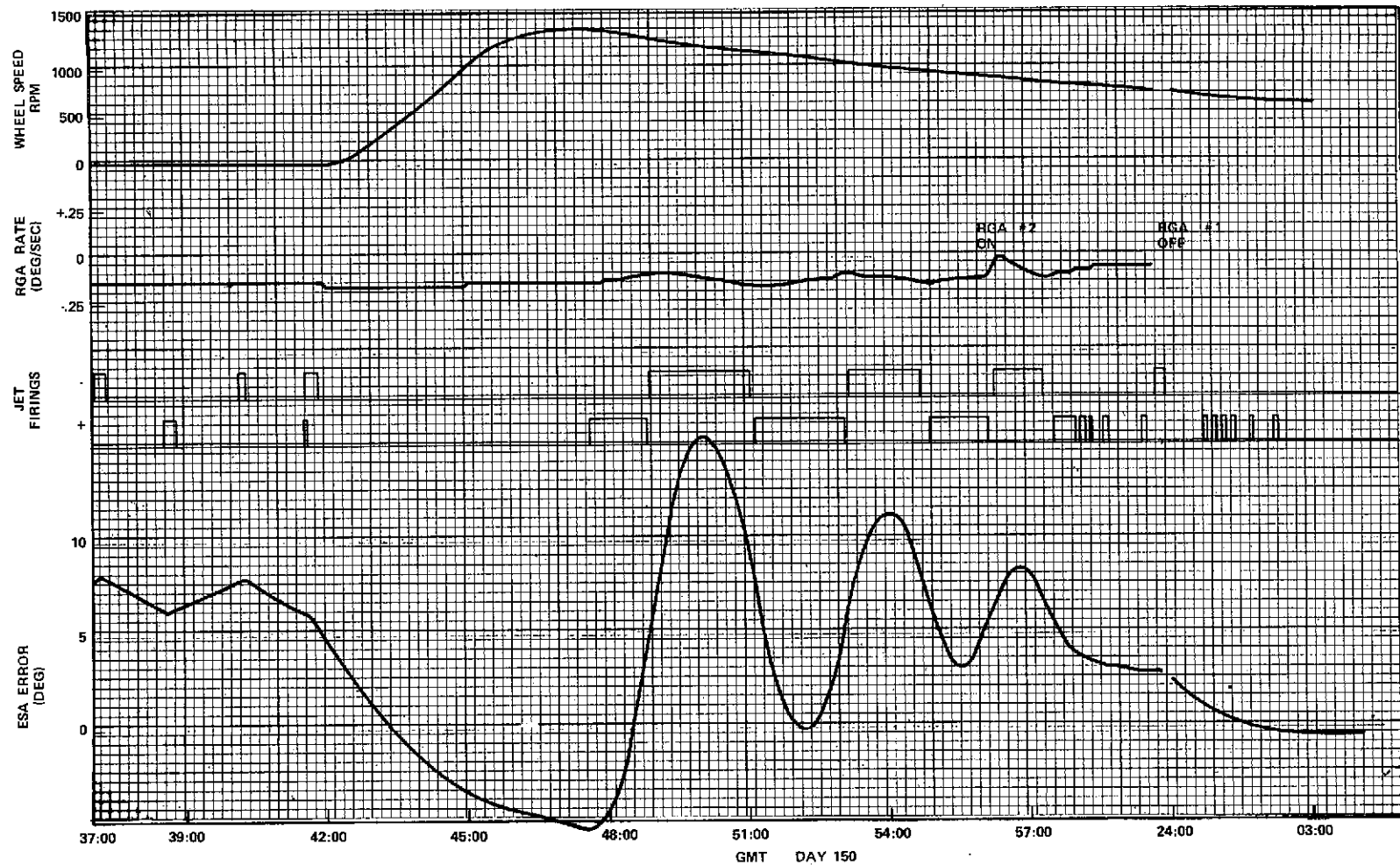


Figure 9-9 (Cont.). Roll Axis Control
During Earth Acquisition

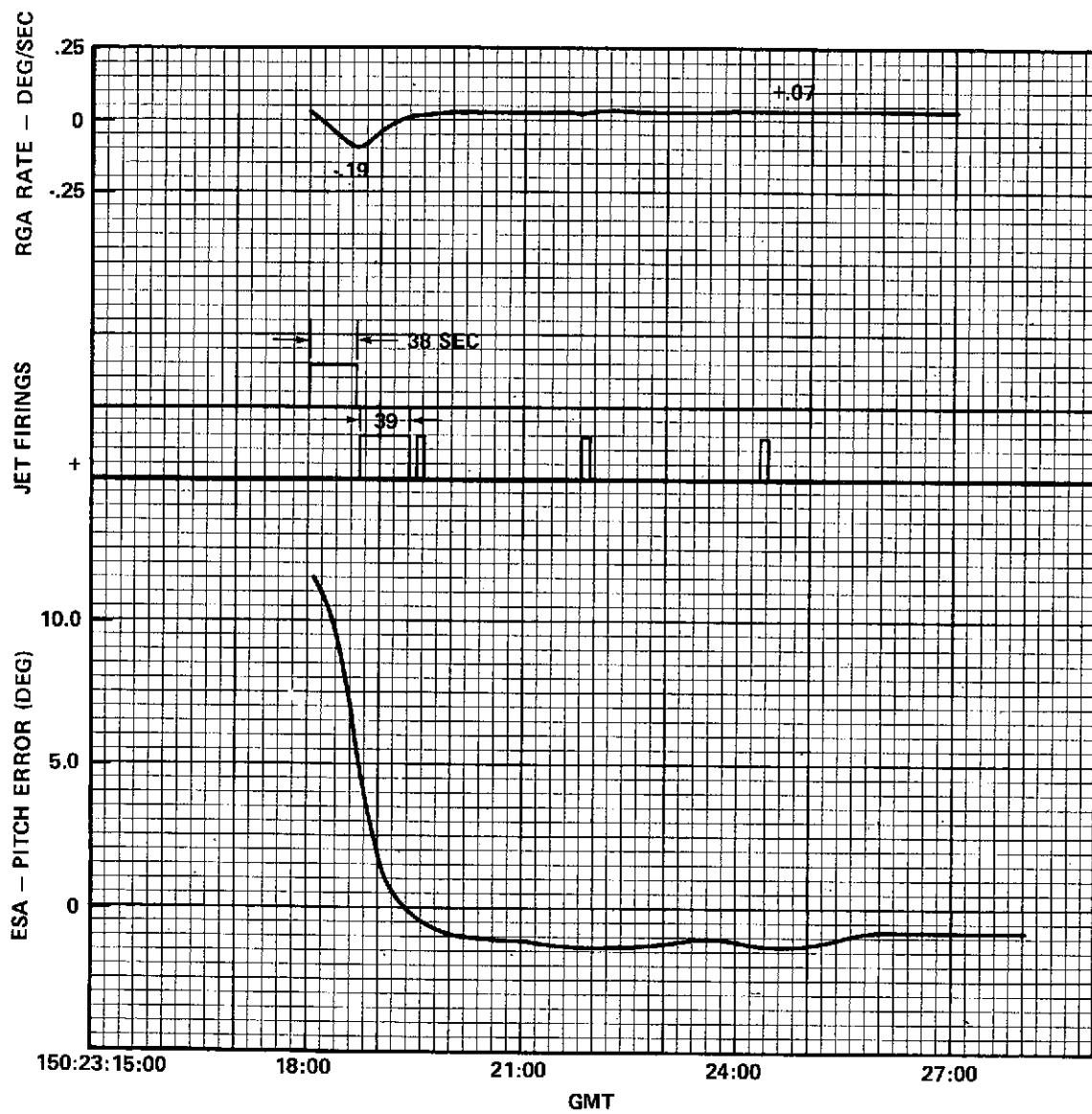


Figure 9-10. Pitch Axis Control During Earth Acquisition

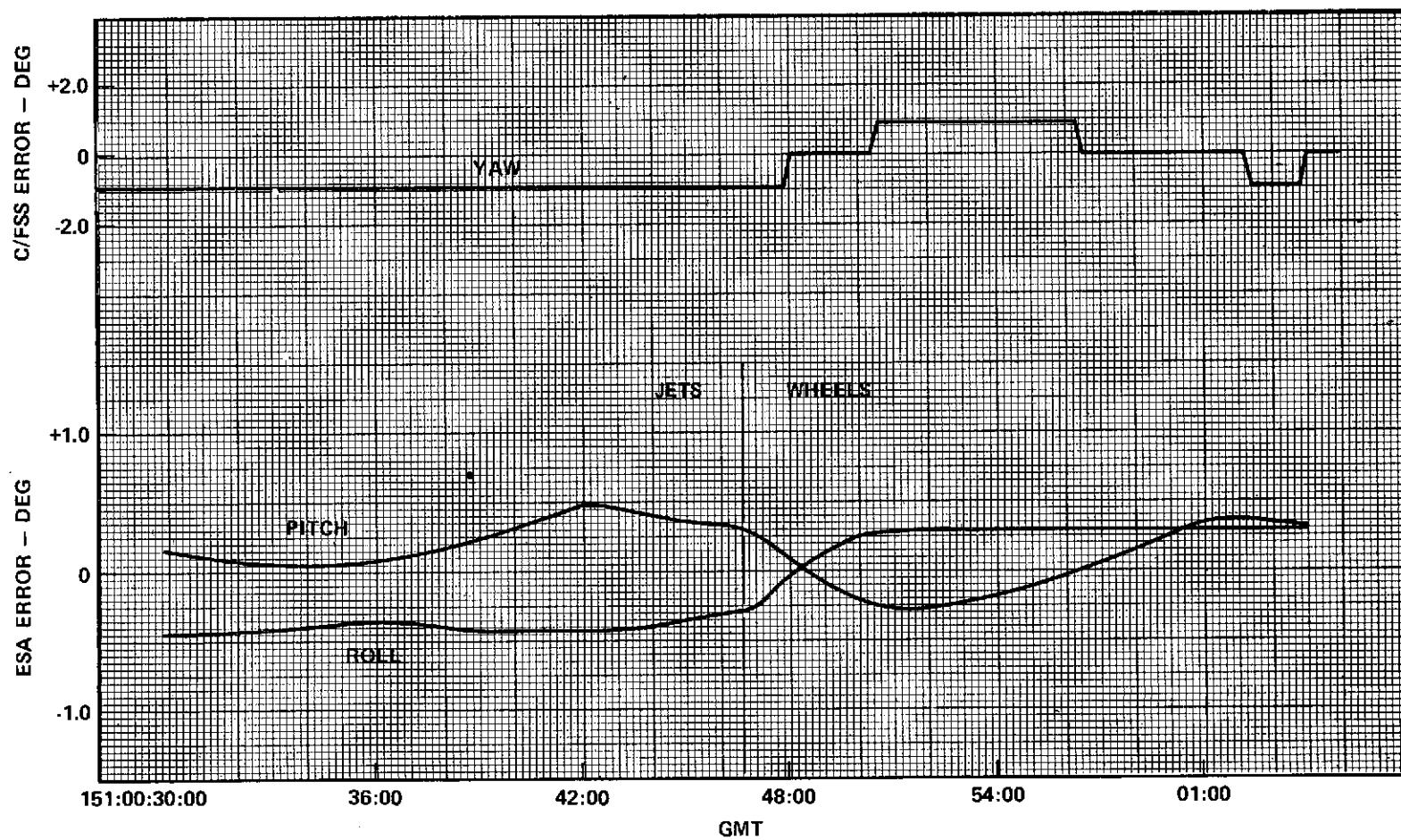


Figure 9-11. Attitude Errors During Earth Acquisition - Pseudo Rate

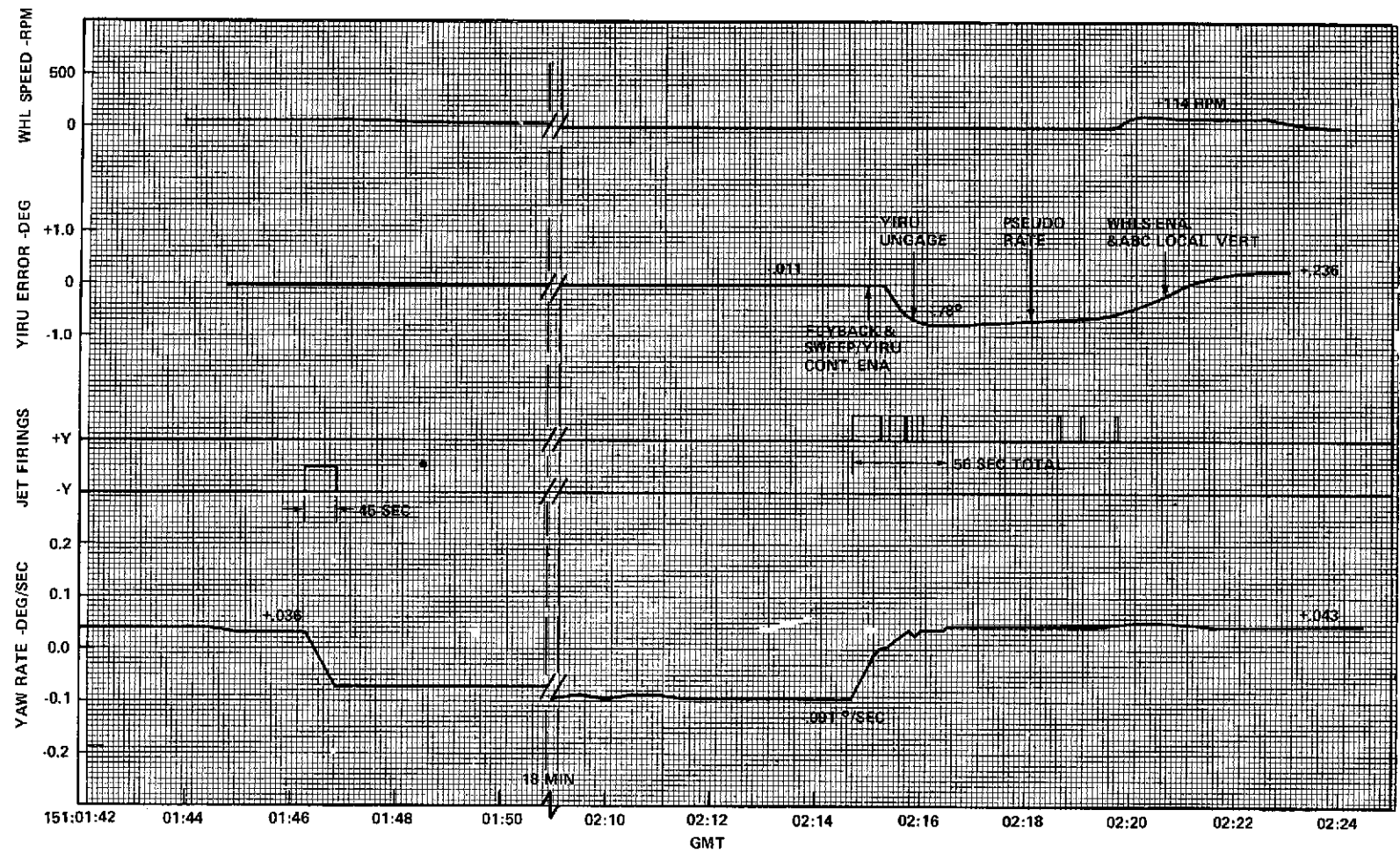


Figure 9-12. ACS Control During Yaw Flip
To Local Vertical Orientation

The PSA was turned on the fourth day and Polaris was acquired. During the Polaris checkout phase, frequent "glitches" were noticed in which a moving particle would appear to be tracked. In most cases, the PSA would reacquire Polaris after a small error build-up; in some cases star acquisition was lost. The PSA was then turned off for three days to allow additional out-gassing. A more complete description of this problem may be found in Section 9.6.

9.2.4 Local Vertical Evaluation of ABC

Local Vertical mode was evaluated at the start of day 2 by commanding DOC 1 to monitor and reference orientation while controlling with the ABC. The DOC attitude error histories for this interval are presented in Figures 9-13 and 9-14, along with ESA error signals. These figures show errors of approximately 0.3 degrees but limit cycles less than ± 0.1 degree, which are within the allowed performance requirements of $\pm 1.0^\circ$. At 152:13:52 the DOC was put in control in the Orbit Plane East mode. The ESA errors were then reduced to less than 0.1 degrees.

9.3 OPERATIONAL MODES

9.3.1 Reference Orientation

The performance requirements for Reference Orientation are that the ATS provide pointing to within ± 0.1 degree in roll/pitch, or ± 0.15 in yaw when using the primary sensing system (ESA and PSA) with either the jets or inertia wheels as actuators with small external torque disturbances. During orbit correction (O. C.) burns, larger errors exist because the external torques are large (2.5 in. - oz. was the actual value seen by the ATS) and these torques must be compensated by the average of the ACS control torques. These in turn can only result from error signals to the ACS. For example, a steady pitch torque of 2.5 in. - oz. will result in a nominal persistent pitch error of 0.23 degree. Actually, a maximum error of 0.5 degrees is specified during O. C. and the maximum observed error of 0.3 degree was adequate to obtain a satisfactory orbit.

The data for reference orientation was obtained during the first orbit correction phase of the mission which was performed from 157:15:47:26 to 157:15:55:27. Prior to this time DOC 1 was configured to maintain the Local Vertical Plane East Orientation (reference orientation) using the ESA and YIRU sensors with the inertia wheels actuators used to control spacecraft attitude. Data acquisition for evaluation of reference orientation was initiated after updating of the ATS ephemeris to the DOC.

DOC 1 was commanded to select jets at 15:23 hours and DACU 1 configured to dwell on the jet fire telemetry (channel 075) for the duration of the orbit

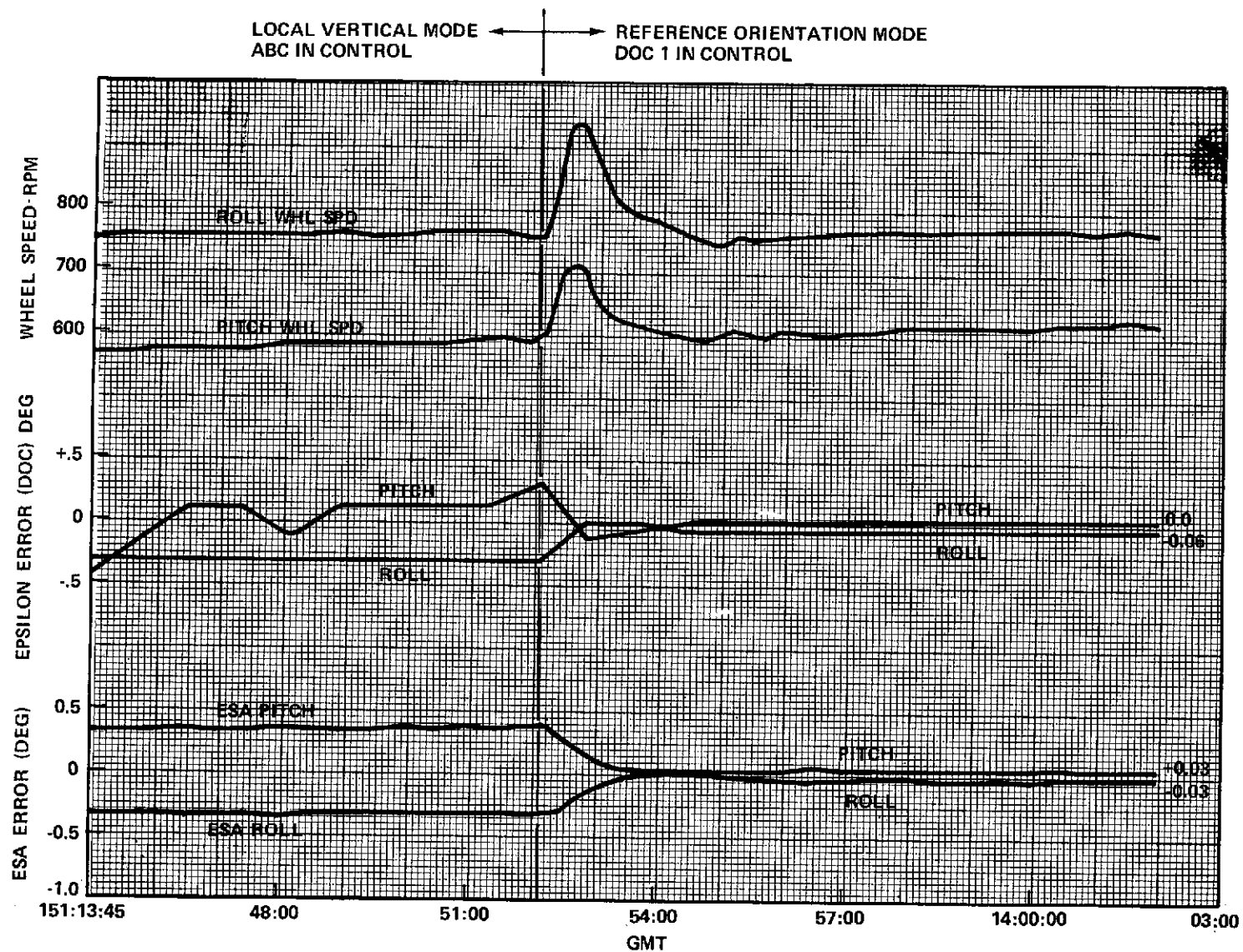


Figure 9-13. ABC/DOC Local Vertical -
Pitch and Roll Axes

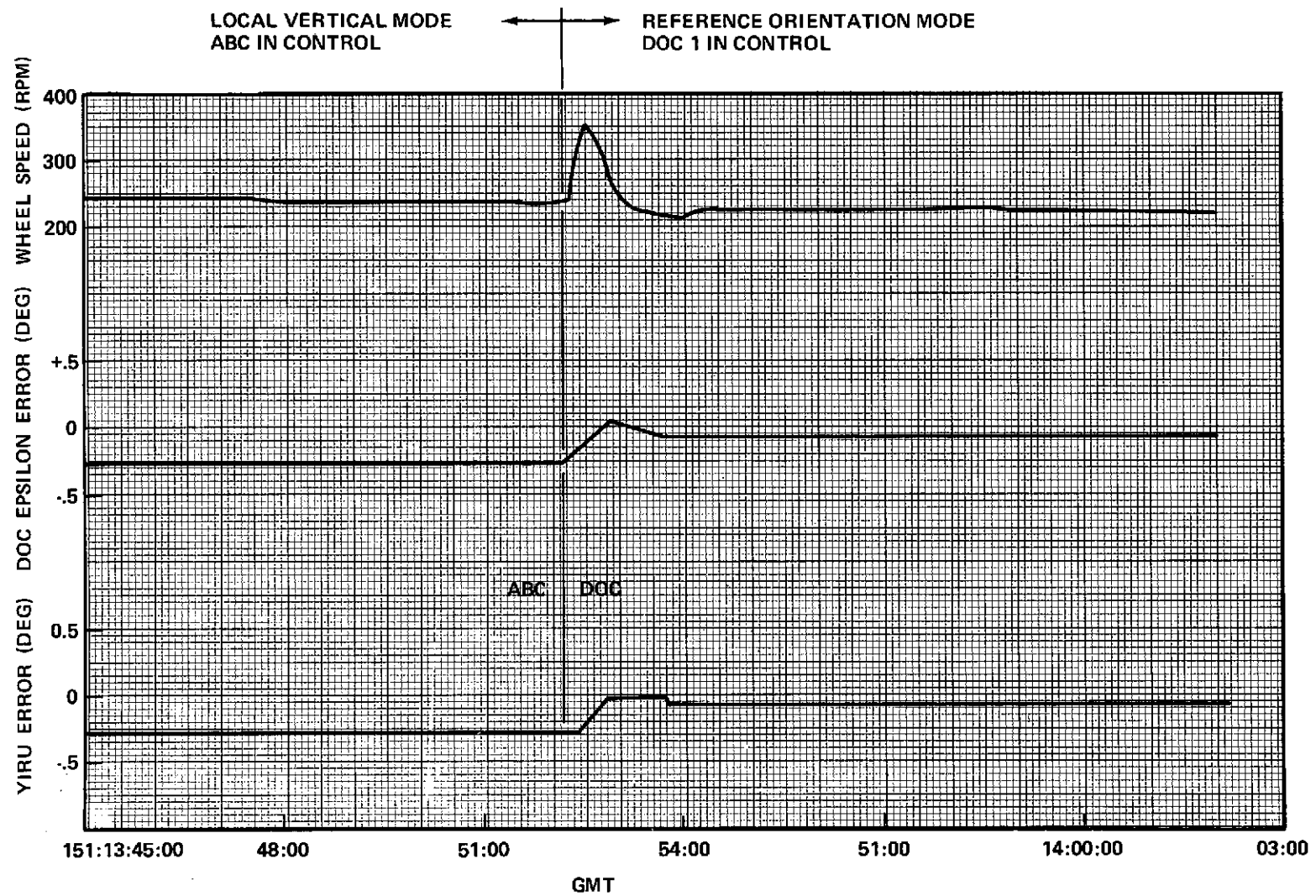


Figure 9-14. ABC/DOC Local Vertical - Yaw Axis

correction burns. Prior to the O. C. maneuver, all three axes were limit cycling within ± 0.055 degrees. During the 481 second SPS 1 westward Jet No. 7 burn, the -pitch jet (No. 3) cycled on and off with a duty cycle of 2.1% indicative of a small westward Jet thrust vector misalignment above the spacecraft center of mass. Thus, the attitude control thrust contributed to the desired ΔV of the maneuver. This duty cycle represents an average disturbance torque due to the center-of-mass offset of about 2.5 oz-in. This indicates that the momentum wheels would have been able to maintain attitude control during the first O. C. maneuver. Roll and yaw attitude control jet duty cycles during the burn were both less than 0.1%. The peak attitude error occurred in the pitch axis ($+0.30$ deg) during the burn.

The second orbit control burn to correct for injection errors was performed during Day 158 (15:49:07 to 16:20:37). A retrograde maneuver was required. The ACS was in the Local Vertical, Orbit Plane East Mode using the ESA and YIRU as attitude sensors, DOC 1 as the controller, and SPS 1 as the torquer. The duration of the O. C. jet firing was 1888 seconds (Jet 7). The orbit was monitored for 24 hours and no further maneuvers were required. Table 9-4 shows the computed orbit parameters before and after the maneuver. The peak attitude errors were 0.055, 0.285, and 0.050 degrees for roll, pitch, and yaw axis, as indicated by the ESA and YIRU outputs. These errors were well within the ± 0.5 degree requirement of the specification. The limit cycle behavior in the pitch axis was similar to that observed during the first orbit correction maneuver and the torques due to the westward jet misalignment were well within the control capability of the attitude control jets.

From orbital change data, the total ΔV was 2.42 ft/sec with a propellant expenditure of 1.01 lbs. which is equivalent to a specific impulse of 221 sec.

9.3.2 Offset Pointing

Offset pointing requires the capability to point the +Z axis to any angle within 10° of the local vertical while using the primary sensors.

The maximum error in pointing the Z axis of the spacecraft and in keeping the X axis parallel to the equatorial plane is specified as ± 0.1 degrees in roll/pitch, and $\pm 0.15^\circ$ in yaw. This requirement is for both ground coordinates and angle track. The control law is the same for both offset pointing modes; the only difference between them is that the DOC command angles vary with time in the ground coordinate mode. This variation with time is necessary to compensate for orbit inclination in controlling the Z axis to a point on the Earth disc. For angle track the DOC pitch and roll command angles are constant with time and the Z axis describes a figure eight on the earth disc about a nominal ground point.

Table 9-4
Initial Orbit Correction

	#1		#2	
	Start	Stop	Start	Stop
EDT	74-06-06 15:47:27		74-06-06 15:49:07	
Orbit Data:				
Semi Maj Axis, km	42186.4	42181.2	42180.9	42160.7
Eccentricity	.0007	.0006	.000624	.000156
Inclination, deg	1.749	1.748	1.748	1.748
RA Node, deg	266.12	266.06	266.06	265.97
Drift Rate, deg/day	.271 W	.203 W	.205 W	.0536 E
Sub Sat Long, deg	96.45	96.44	96.52	96.53
Spacecraft Wt, lb.	2971.0	2970.7	2970.7	2969.7
Jet #7 Duration, sec.		480		1888.4
V, ft/sec		.63		2.42
Wp, lb.		.27		1.01
Thrust, lbf. (ave)		.122		.122
Tank 1 Press, psia	359.4	355.4	357.4	345.4
Tank 1 Temp, °C	26	25	26	25
Remaining Fuel, lb. *	54.2	54.1	54.1	53.1
AC Jet .1 sec Pulses				
-Pitch		103		460
+Yaw	(I, lb sec)	2		43
-Roll		0		15
		(1.22)		(5.42)

*As determined by Maneuver Program

Performance of the Offset Pointing-Ground mode using the ESA was checked by verifying that when using this mode the vehicle in fact pointed to Rosman when it was commanded to do so. The reference attitude to Rosman was established by commanding the vehicle to point towards Rosman in station null point mode using DOC 1 and C-band monopulse. (In this mode the ACS uses either monopulse or interferometer sensors to control the vehicle to "null" on a ground radiation source.) During this referencing maneuver, the interferometer roll and pitch outputs were also monitored. This monitoring continued after Offset Point-Ground to Rosman was initiated using DOC 1 and ESA. As shown in Figure 9-15 the resulting change in vehicle attitude sensed by the interferometer was less than 0.01 degree.

Throughout this period, DOC 2 was in the Offset Point-Ground Monitor Mode using the ESA.

The total error in pointing is the result of (1) errors in DOC's computation of the command angles and (2) errors of the control loop in following the command angles. The 0.01 degree error noted above verifies the small size of the former; the latter errors, measured by DOC, are approximately 0.03-0.04 degrees as shown in Figure 9-16.

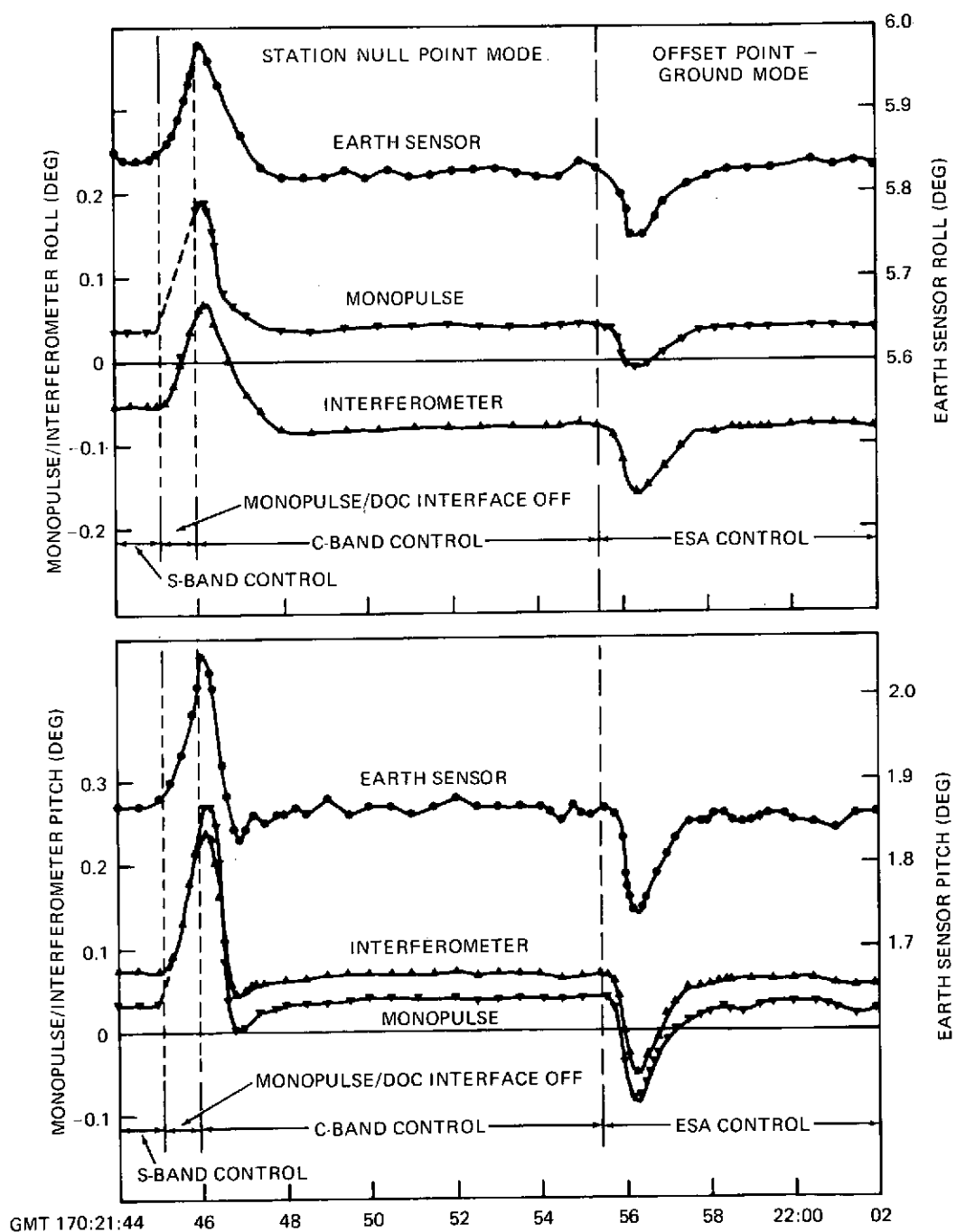
The DOC 1 and DOC 2 yaw attitude error time history is shown in Figure 9-17. No check can be made of yaw axis control to the accuracy required. The excursions seen on the DOC 1 and DOC 2 yaw attitude error are less than 0.05 degree which is within the ± 0.1 degree requirement.

Since the control of the Z axis to a point on the earth disc within 0.1 degree requires a precise yaw Euler angle, it may be said that the accuracy of the yaw Euler angle is sufficient to meet this requirement.

For angle track, the DOC utilizes the same control law as in Ground Coordinate Mode with the simplification of maintaining a constant command angle. Having shown that the Ground Coordinate Offset Pointing mode meets the performance requirements, by inference the performance for the Angle Track Offset Pointing Mode has also been demonstrated.

9.3.3 Station Null Point

All station point null sensors have been utilized for spacecraft control utilizing the DOC. ABC Station Point Null, being a backup to DOC, has not been used. Evaluation of Station Point Null under VHF, S-Band, C-Band, and Interferometer control shows that all specifications were met (see Table 9-5). An evaluation of Station Null Point is presented below.



SENSOR OUTPUTS DURING OFFSET POINT-GROUND AND STATION NULL POINT TO ROSMAN

Figure 9-15. DOC 1 and DOC 2 Roll and Pitch Errors (Time Histories)

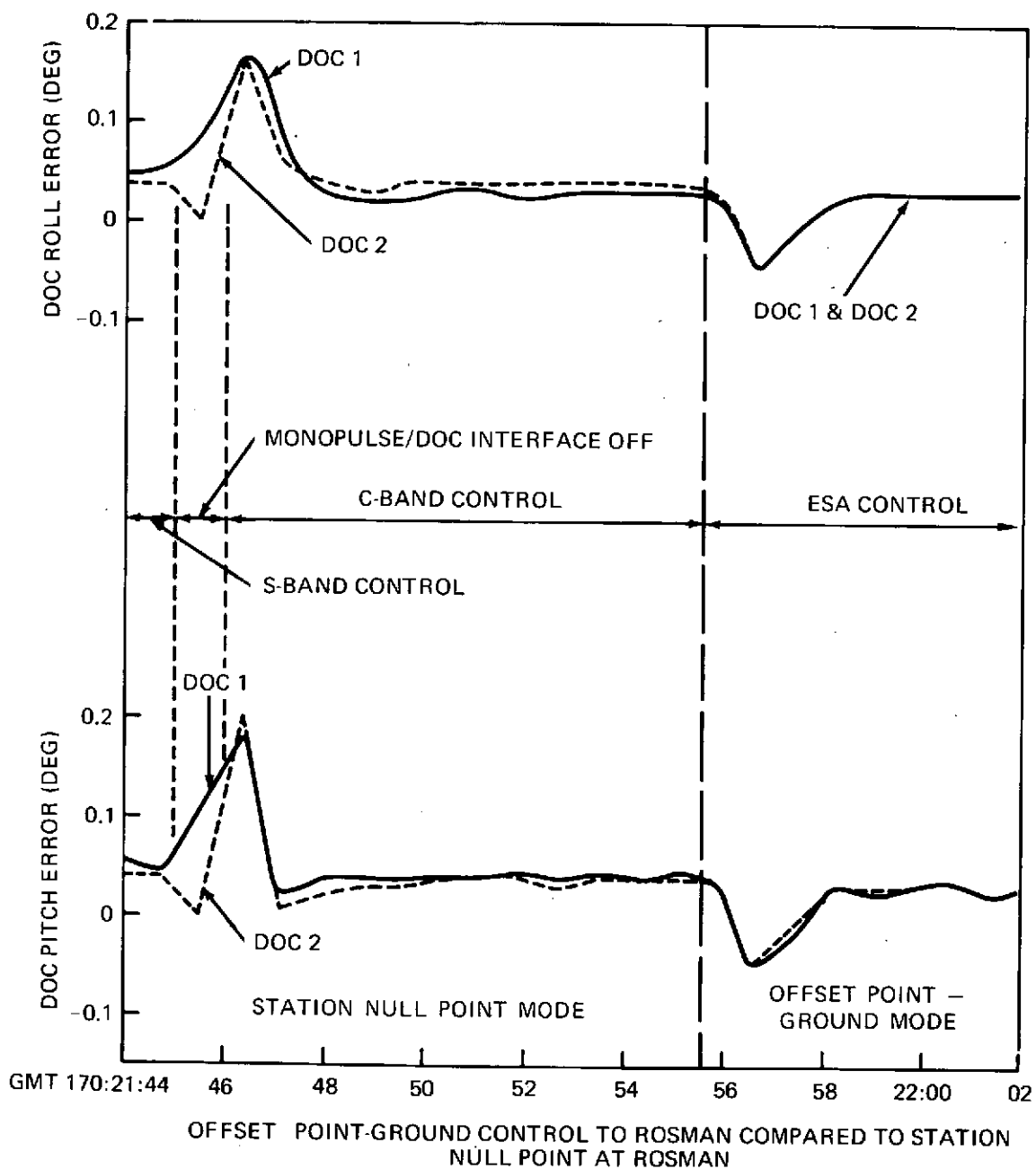


Figure 9-16. DOC 1 and DOC 2 Roll and Pitch Errors (Time Histories)

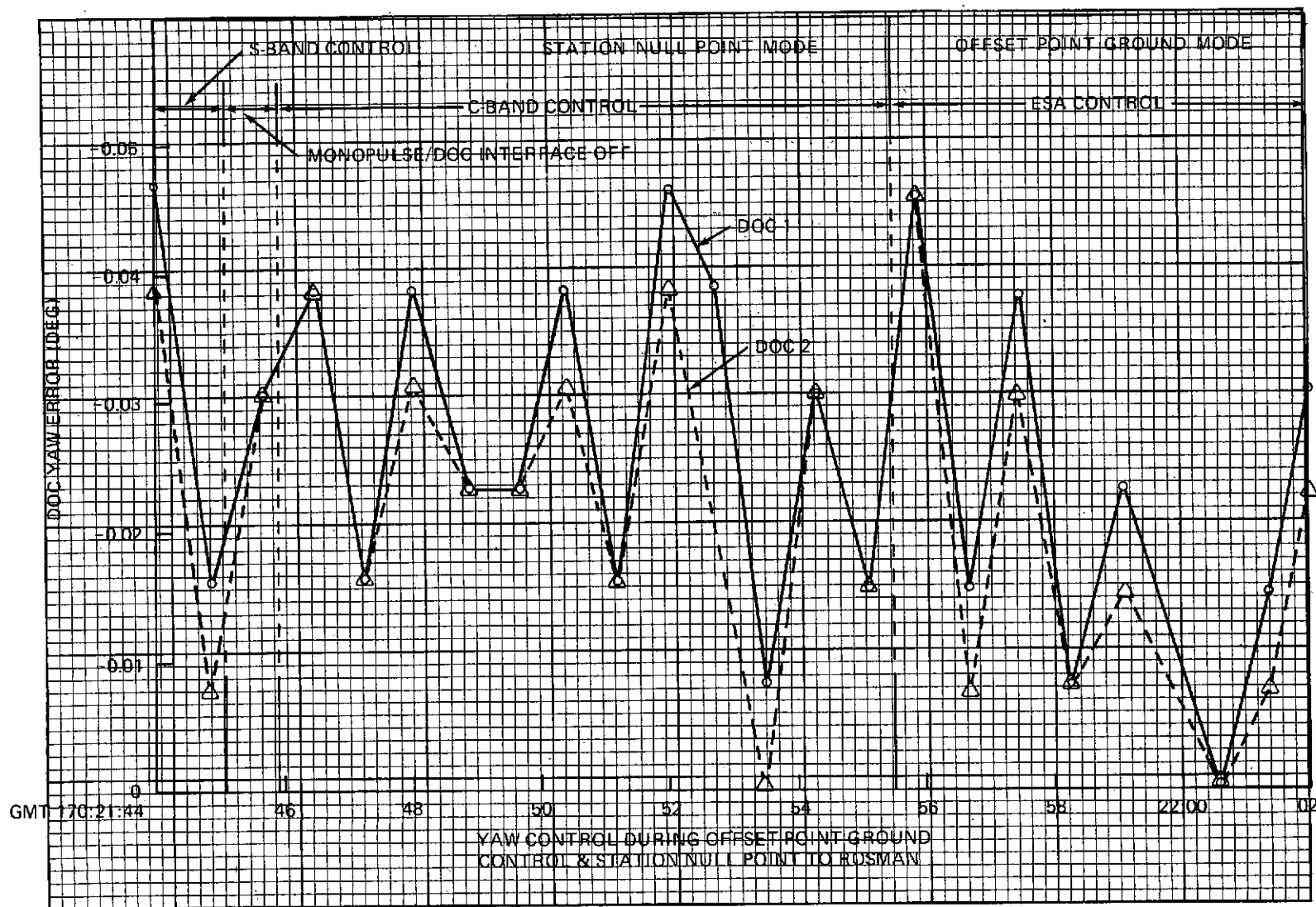


Figure 9-17. DOC 1 and DOC 2 Yaw Errors (Time Histories)

Table 9-5

Station Null Point Performance Summary

	Performance	Specification
VHF	Roll: -0.37 degree offset peak to peak jitter 0.2 deg Pitch: -0.35 degree offset peak to peak jitter 0.4 deg.	± 1 degree about all axes
S-Band	Roll: -.083 degree offset Jitter less than .01 deg RMS Pitch: -.081 degree offset Jitter less than .01 deg RMS	± 0.3 degree about all axes
C-Band	Roll: +.03 degree offset Jitter less than .01 deg RMS Pitch: +.03 degrees offset Jitter less than .01 deg RMS	± 0.1 degree about all axes
Interferometer	Roll: -.04 degrees offset Jitter less than .01 deg RMS Pitch: -.04 degrees offset Jitter less than .01 deg RMS	± 0.1 degree about all axes

9.3.3.1 VHF Monopulse

VHF Monopulse was commanded from 166:35:20 to 166:04:09. Figure 9-18 shows the spacecraft roll and pitch performance under VHF Monopulse control. The Earth Sensor curves show the actual spacecraft motion. The peak-to-peak excursions observed after settling, are within 0.4 degrees in pitch and 0.2 degree in roll. These variations are about VHF indicated null offsets of +0.35 degree in Pitch and -0.37 degree in roll. This is well within the specification requirement of ± 1 degree for roll and pitch axis control. No problems have been encountered while controlling on VHF monopulse although it has been determined that the VHF gain is about three to four times lower than expected. This aspect of the VHF monopulse is discussed in the Section 11 of this report.

9.3.3.2 S-Band Monopulse

S-Band Monopulse control was commanded from 166:04:37 to 166:05:07. Figure 9-19 shows spacecraft roll and pitch performance in this time interval. The average offset errors from null, as indicated by the monopulse errors are -.083 degree in roll and -.081 degree in pitch. RMS jitter about the average value, as determined from ESA data is about 0.01 degrees in both pitch and yaw. This is well within the S-Band pointing requirement of 0.3 degree. No problems have been encountered with S-Band Monopulse control. (See Section 2.3.5)

9.3.3.3 C-Band Monopulse

C-Band Monopulse control was commanded from 170:19:00 to 170:19:50. Figure 9-20 shows spacecraft roll and pitch performance under C-Band monopulse control. The average null offsets in roll and pitch as determined from the monopulse data are +0.03 degree in both roll and pitch. The maximum jitter noted on both roll and pitch based on the interferometer output signals was 0.01 degree.

After C-Band control was verified at 162:01:45, an attempt was made to determine the angular range over which it could establish stable control. After settling on C-Band, the carrier was turned off, the vehicle was allowed to drift 0.1 degree in pitch, and then turned back on again. Figure 9-21 illustrates what occurred. It may be seen that the vehicle never did settle in pitch and roll. Instead, it started to oscillate with a 0.1 degree peak-to-peak amplitude with a two minute period in both axes. In a later test, C-Band was put into control starting with an equal attitude offset but with zero initial rate. This time roll and pitch settled out with minimal oscillations. The acceptable range of initial conditions required to enter C-Band control will require further investigation.

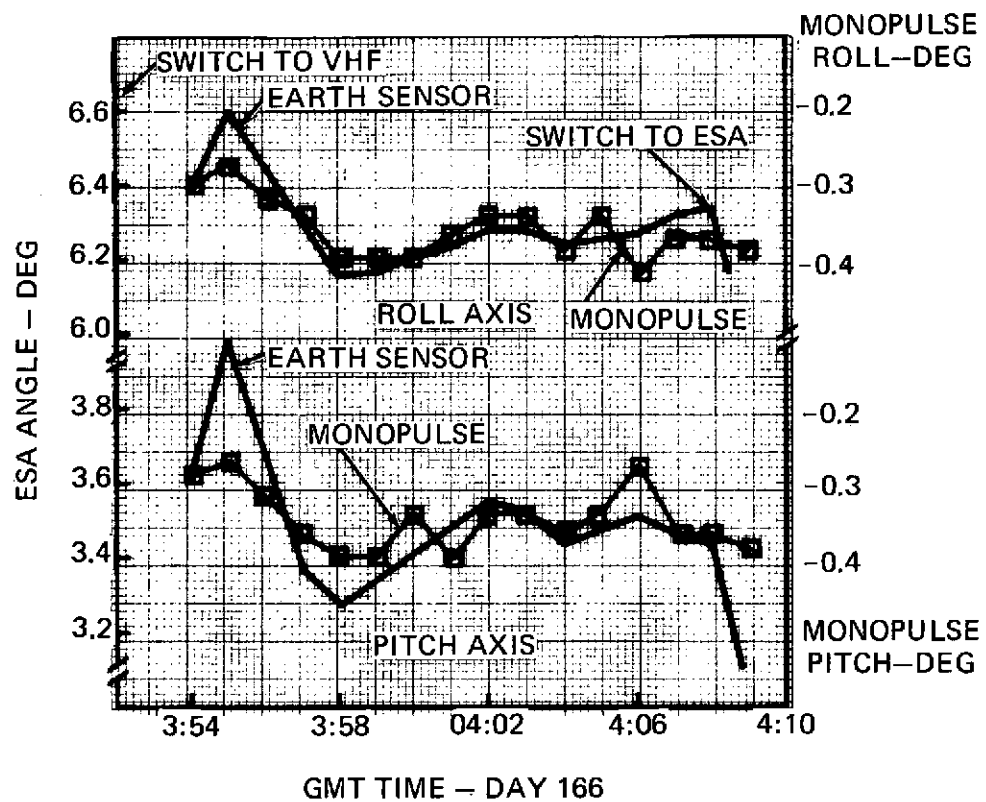


Figure 9-18. Station Null Point Using VHF Monopulse

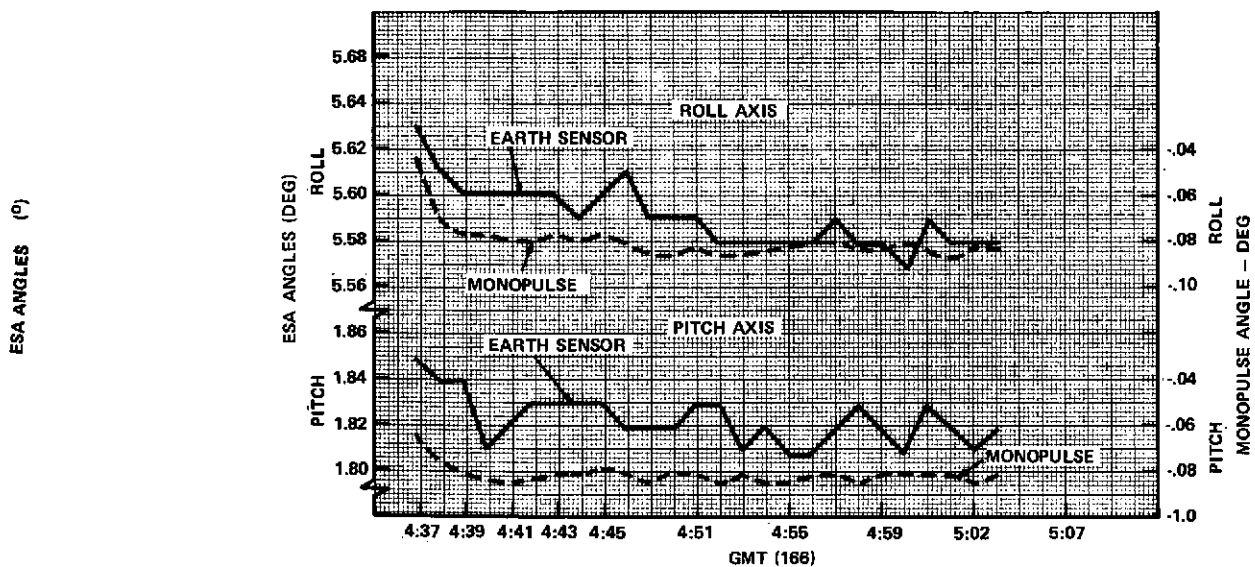


Figure 9-19. Station Null Point Using S-Band Monopulse

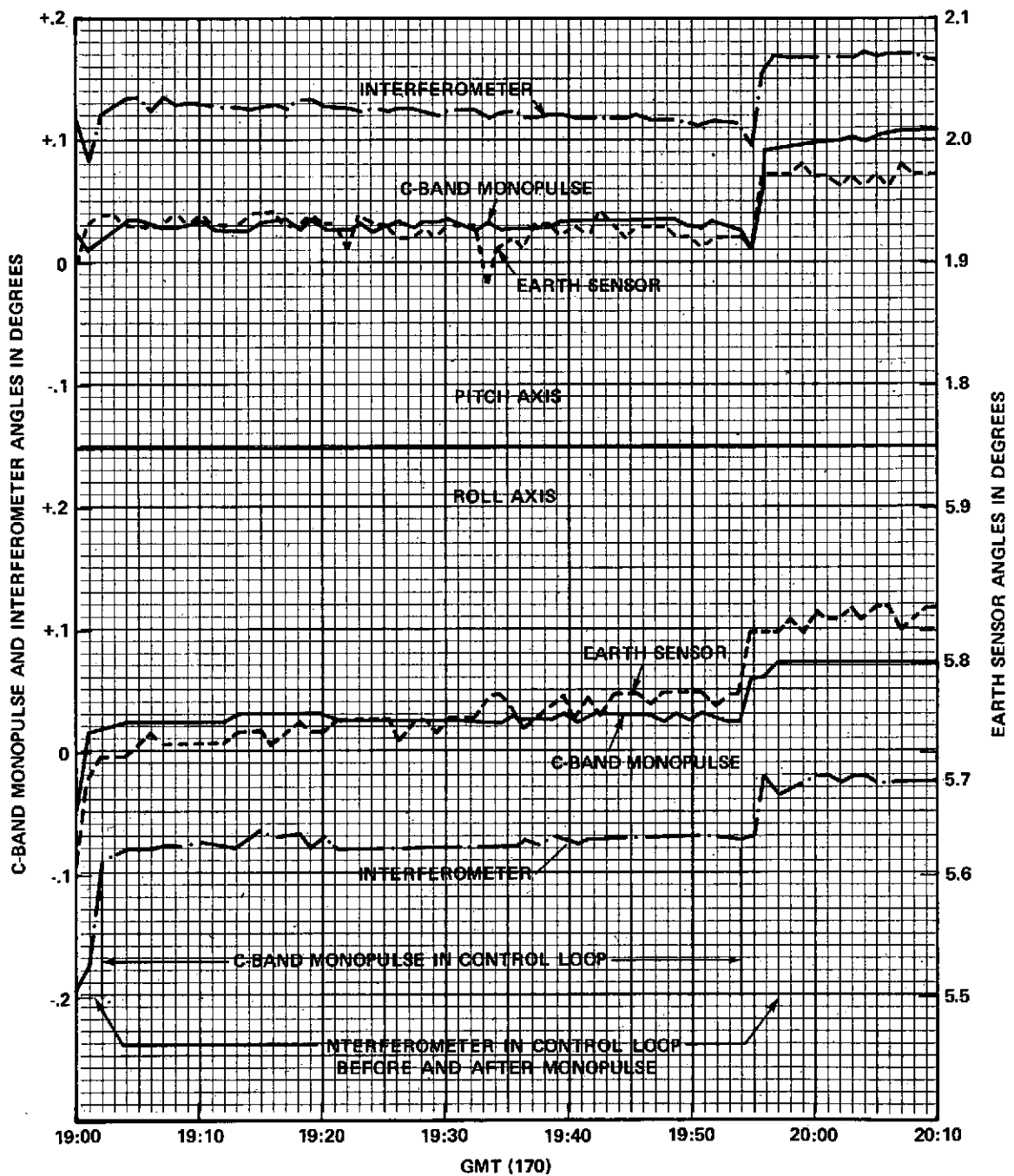


Figure 9-20. Station Null Point Using C-Band Monopulse

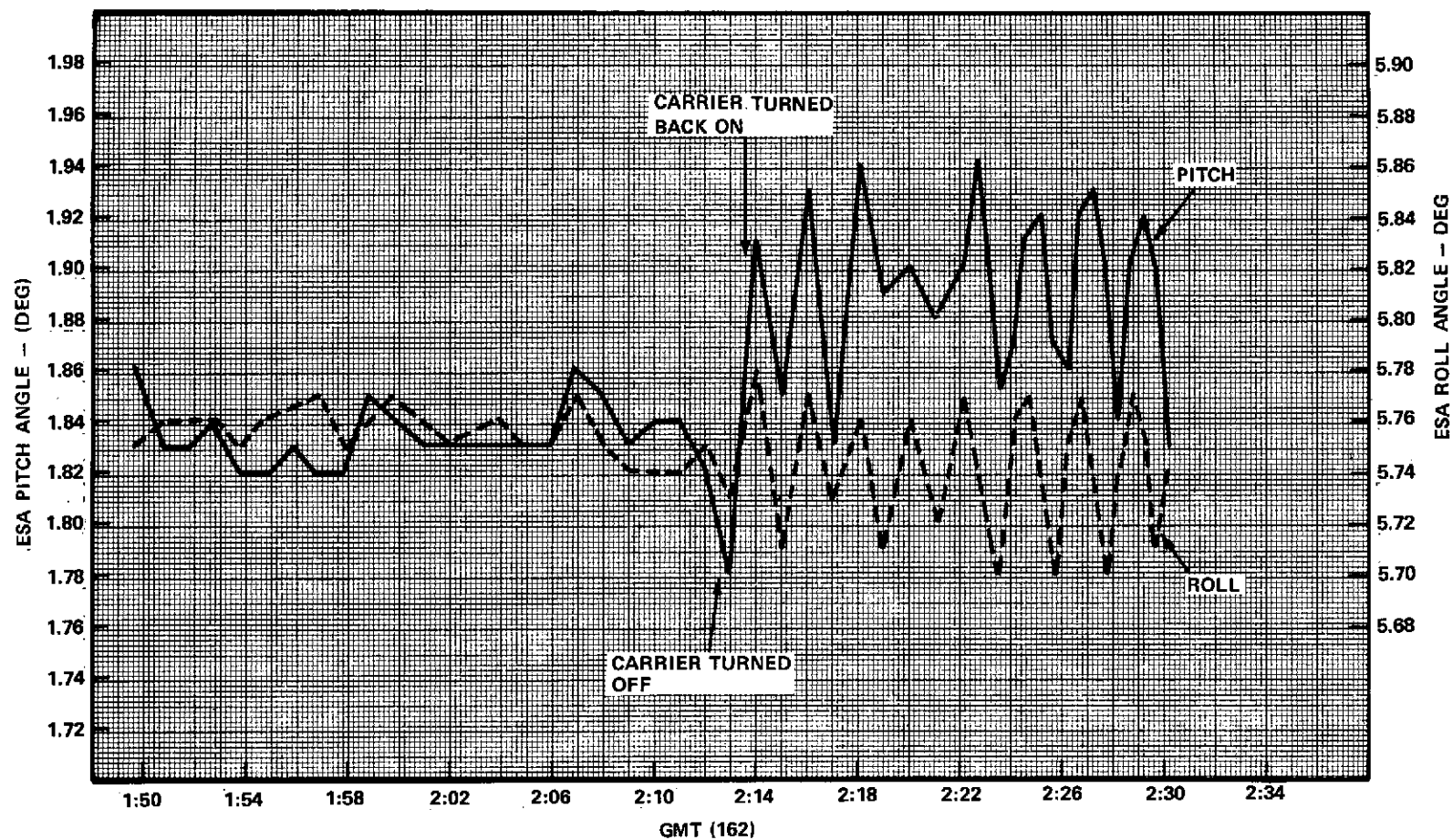


Figure 9-21. Station Null Point Using C-Band Monopulse

9.3.3.4 Interferometer

Interferometer Control was commanded at 162:04:46. Figure 9-22 shows roll and pitch axis performance under Interferometer Control. This data is presented in terms of counts with the conversion to degrees indicated. The average null offsets are $-.042$ degree in roll and $-.040$ degree in pitch. Maximum jitter noted was on the order of $.016$ degree in both roll and pitch, however, the RMS jitter is on the order of 2 to 3 interferometer counts ($.003$ degree to $.005$ degree).

On day 161, with the Interferometer in control, the signal level from Rosman dropped. This resulted in the Interferometer transmitting a constant value to the DOC. The DOC therefore generated a "hard" drive signal to the wheels which forced the spacecraft off the earth, requiring its re-acquisition. Honeywell is developing a software change which will allow the DOC to recognize the counts issued by the interferometer when ground transmission is lost. Upon recognizing this condition a critical fault will be issued and wheel hold will automatically be commanded.

9.3.4 Low Jitter

The primary purpose of the low jitter mode is to support the VHRR experiment. Specification requirements and calculated vehicle performance are given in Table 9-6.

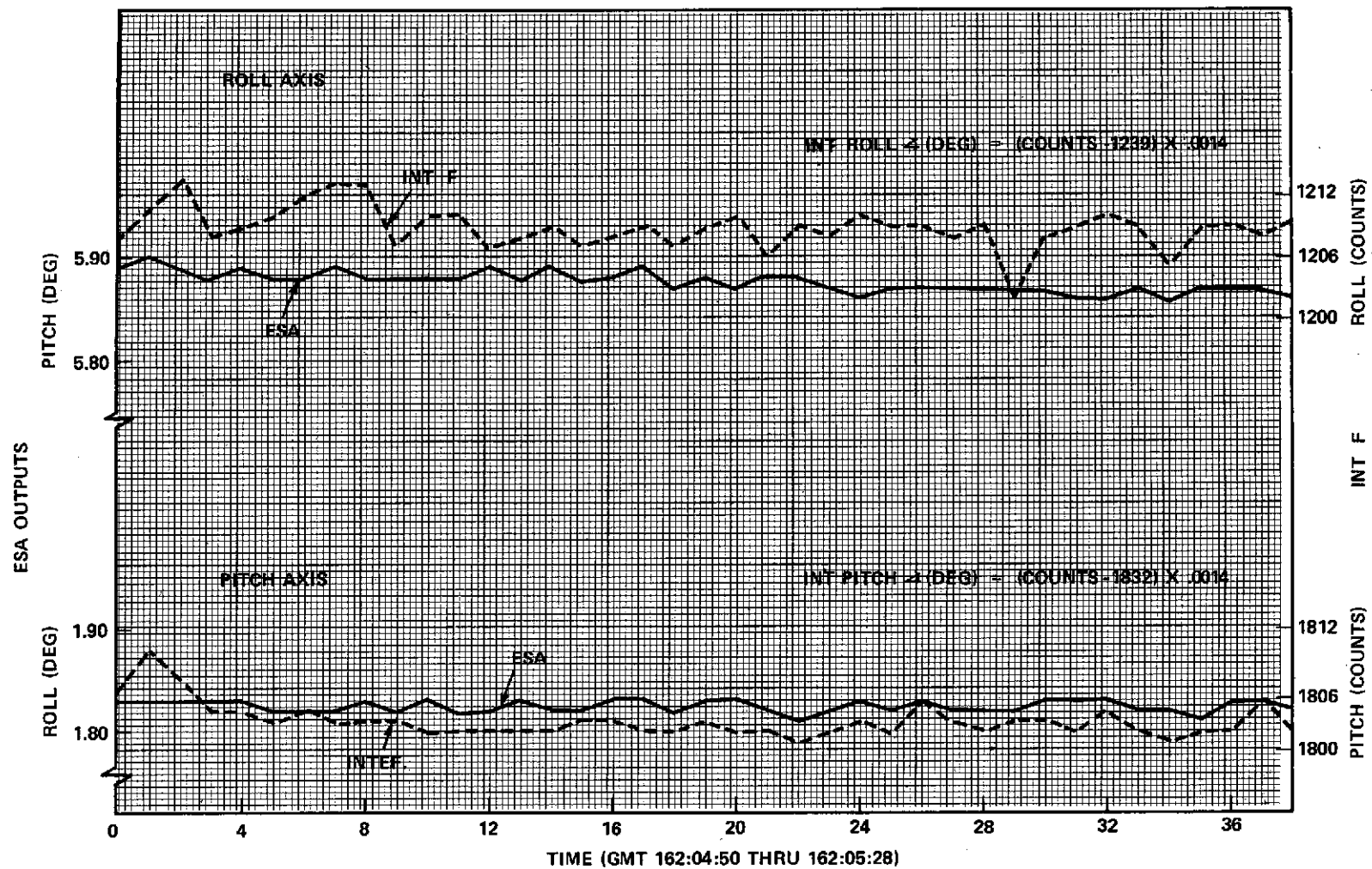
Table 9-6

Low Jitter Performance

	Attitude Changes from Steady State Operating Point (deg)		Attitude Rates (Deg/Sec)		Displacement Between Steady State Operating Point and Nominal Point Command (degrees)	
	Spec. *	Performance	Spec. *	Performance	Spec. *	Performance
Roll	± 0.01	± 0.005	± 0.001	± 0.00015	0.5	0.02
Pitch	± 0.01	± 0.005	± 0.001	± 0.00015	0.5	0.02
Yaw	± 0.01	± 0.02	± 0.001	± 0.0003	—	—

*Over 24 minutes.

Figure 9-22. Station Null Point Using Interferometer



Evaluation of system performance using the on-board sensors (ESA, Interferometer and PSA #2) is difficult due to the noise inherent in the sensors, their readout rates, and their resolution. Resolutions of ESA, Interferometer, and PSA 2 are 0.0055 deg/bit, 0.0014 deg/bit, and .026 deg/bit and maximum update rates are 160 ms, 400 ms, and 22.5 ms, respectively. The effect of the noisy PSA 2 and ESA sensors in improperly indicating vehicle rates is shown in Figure 9-23 where DOC 2 filtered rates are shown as a function of time. A sample of time indicated on this figure was analyzed to determine "true" vehicle rates. This analysis used wheel excitation dwell data to determine the actual torque-time history for the sample period. The alternate torquing due to wheel drive (10 in.-oz.) and wheel rundown (0.74 in.-oz.) results in a change in vehicle rate history as shown in Figure 9-24. These rates are believed to be representative of actual vehicle rates which would be measured by perfect sensors with bandwidth sufficient to include the control actions of the low jitter control loops.

High frequency disturbances outside the control loop bandpass are applied to the system by oscillating components in the VHRR and EME packages. These disturbances are about the pitch and roll axes only. If the satellite were rigid, the effects of those torques on attitude and rate would be negligible. However, the possibility exists of amplification due to structural resonance. Figure 9-25 contains the pitch and roll outputs of the Interferometer with the ACS in low jitter mode using both Interferometer and ESA as pitch/roll sensors. In this data, successive samples are 0.4 seconds apart and the output resolution is 0.0014 deg. per bit. No indication of resonance can be found at any frequency.

Figure 9-25 also indicates the remarkable accuracy in holding roll and pitch errors within one bit (± 0.0014 deg.) of the steady state attitudes. Secular changes in interferometer output are due to the time varying roll and pitch commands while holding on a fixed ground point. Actually, a main source of changing ground pointing error is the 0.004 deg. resolution of the attitude commands generated in DOC. This suggests that a combination of station point and low jitter control loop may provide the ultimate in pointing accuracy. Further, reduced noise in interferometer output when the ESA is used as the pitch-roll sensor suggests that the ESA is a better sensor than the interferometer in the low jitter mode. Apparently, the ESA noise keeps the system in a continual dither about the control point while a definite vehicle displacement is required to change the interferometer output to the control loop. A typical low jitter mode sample of ESA output showing the noise is given in Figure 9-26.

Although a deviation of 0.5 deg. between command Z axis point and actual Z axis point is permitted by specification, actual measured values of 20 low jitter

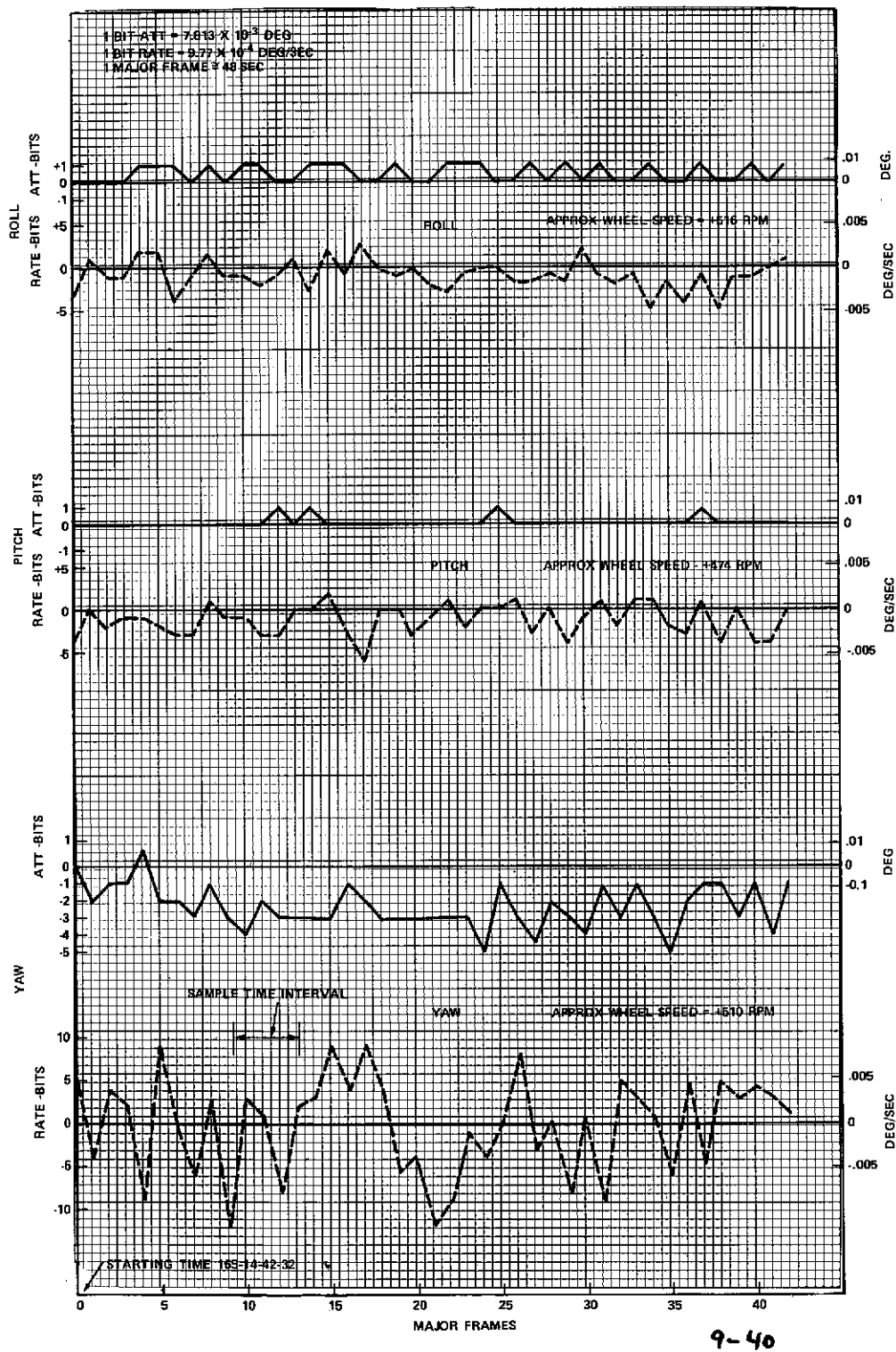


Figure 9-23. DOC 2 Filtered Attitudes & Rates During Low Jitter Mode

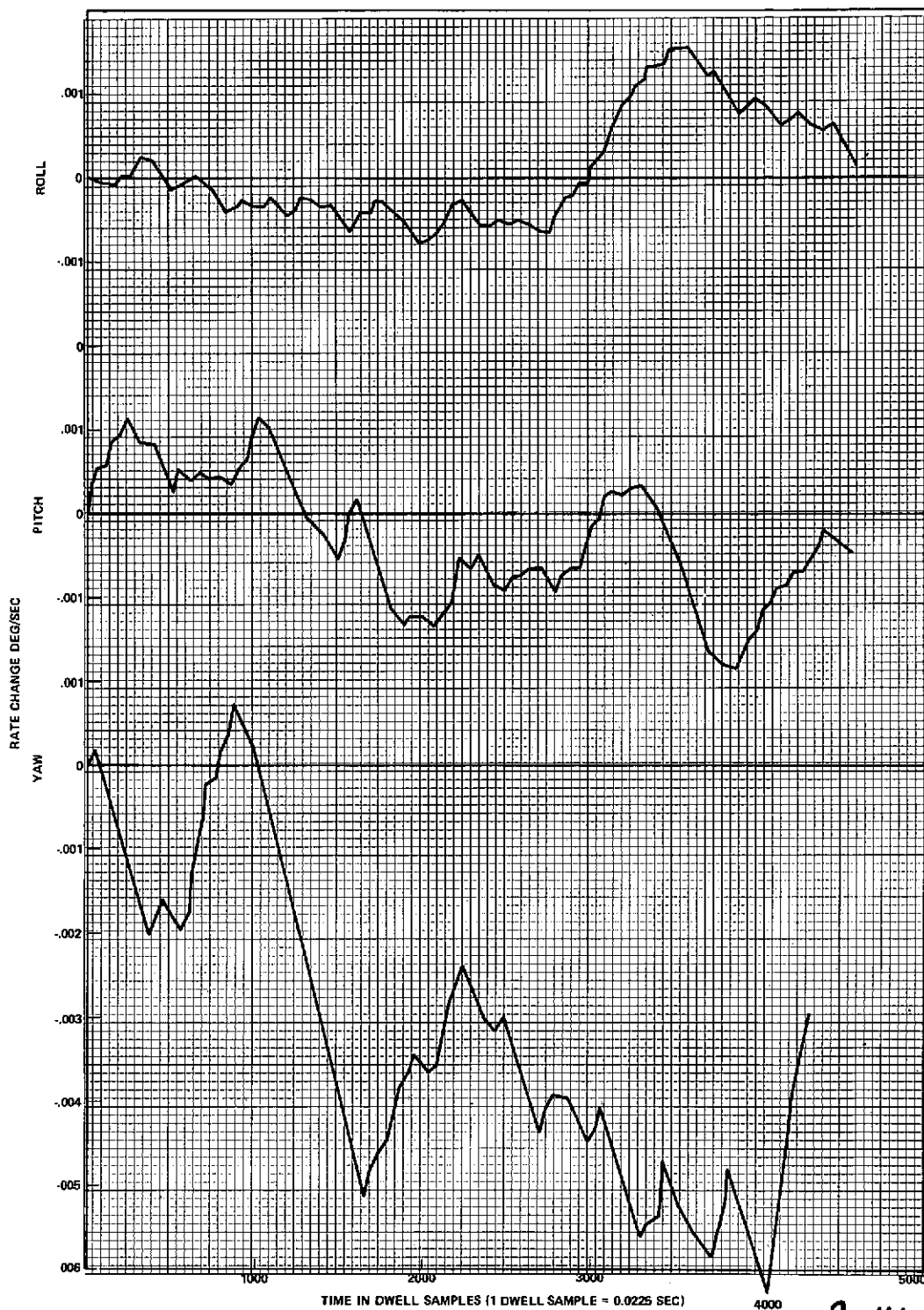


Figure 9-24. Low Frequency Component of Vehicle Rates During Low Jitter Mode

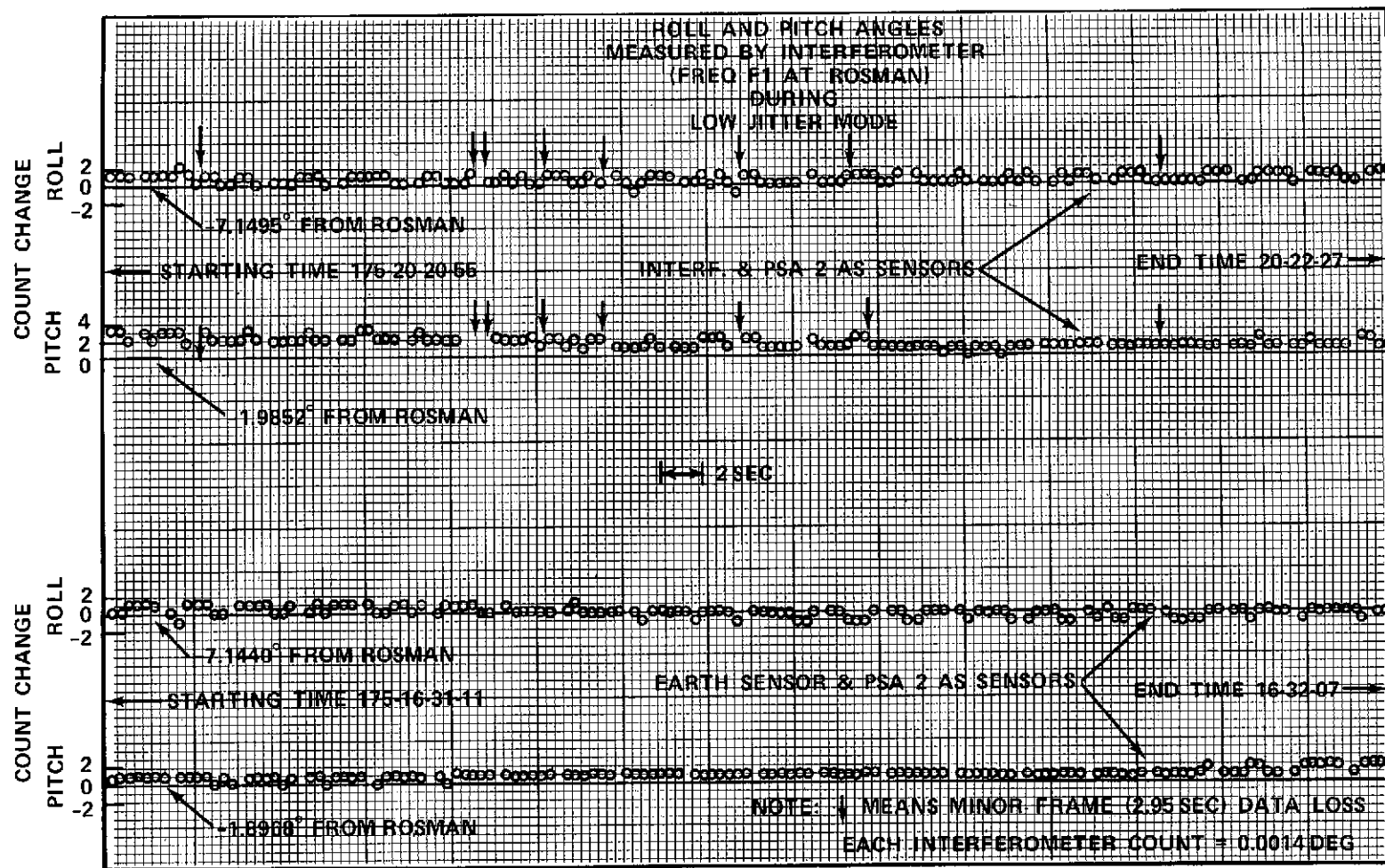


Figure 9-25. Best Resolution Measurements of Pitch and Roll
During Low Jitter Mode

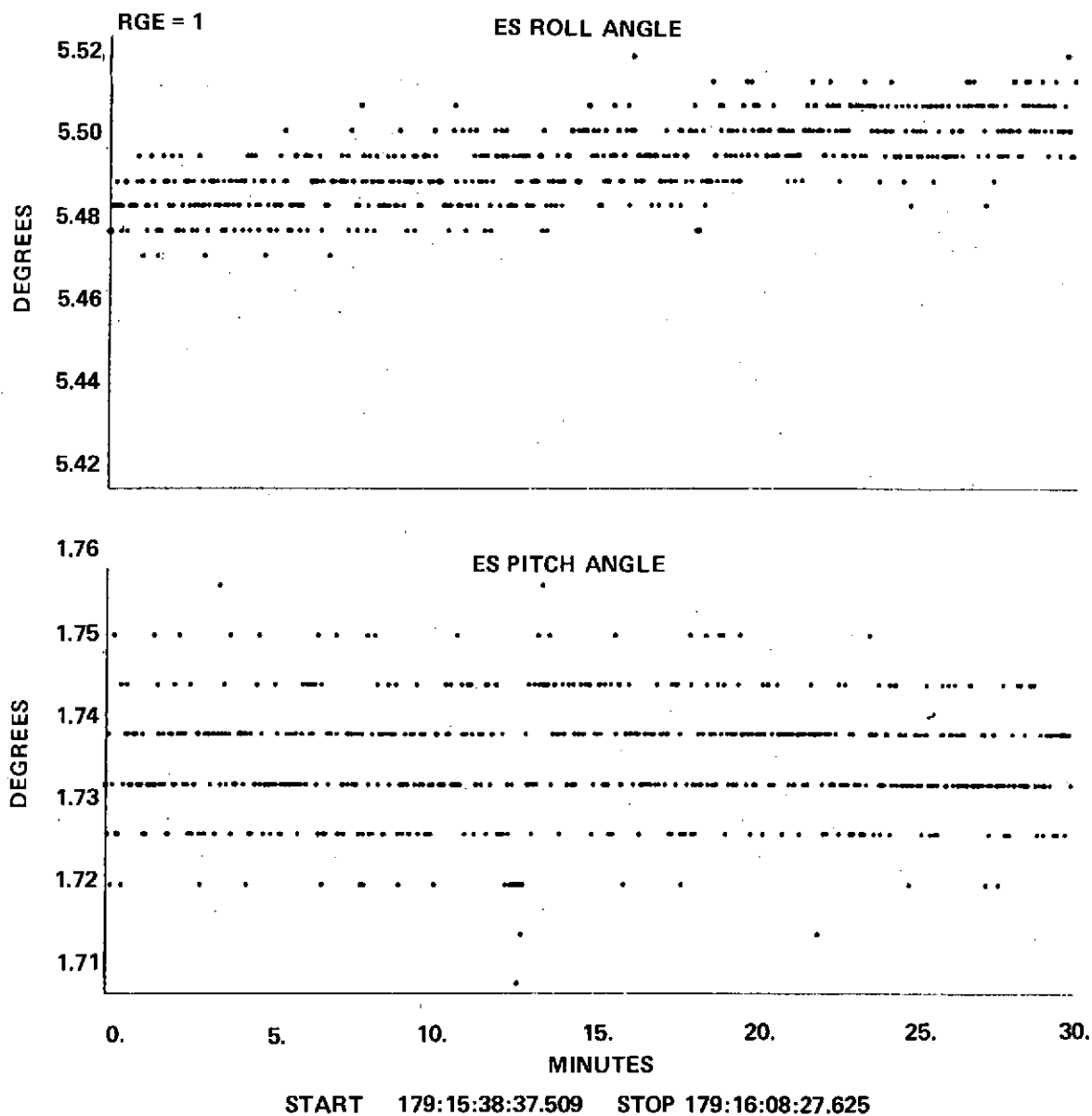


Figure 9-26. Typical ESA Outputs During Low Jitter Mode

mode periods from day 155 to day 180 have never exceeded 0.016 degree in pitch and roll. Figure 9-23 indicates DOC 1 filtered attitude errors (which are sensor errors sampled after a three second lag filter) of .005 degrees in roll and pitch. These offsets (max = 0.02 deg) are due to the attitude error required to accelerate or decelerate the wheels to maintain control in the presence of external torques and the requirement to exchange angular momentum among all wheels during non-reference orientation control modes.

9.3.5 Slewing Maneuver

Controlled slew maneuvers of the spacecraft Z axis were accomplished on several occasions during the checkout period. Most were done to generate antenna patterns. During the maneuvers, the ACS was configured to use the ESA and PSA or YIRU as attitude sensors, DOC 1 or 2 as the controller, and wheels as torquers. The ACS designated mode for slewing is DOC Offset Point, Controlled Slew.

Figure 9-27 is a plot of several slews that were made on day 155 for Monopulse Checkout (Passive). The maneuvers started with the spacecraft pointed at Rosman. The maneuver sequence is also indicated on the plot. The body pitch and roll offset angles are in degrees. For this series of maneuvers, the YIRU was used to control the yaw axis. The maneuver from points 2 to 3 was selected for detailed evaluation. This is a 15 degree maneuver. A cursory look at the data for other slews indicated similar results.

Figure 9-28 contains plots of the roll axis command attitude and attitude error as functions of time for the maneuver. A constant command rate of 1 degree/minute was used. The maximum attitude error at the beginning of the slew was +0.308 degree. The overshoot was 0.402 degree. The specification calls for a maximum attitude error of 1.0 degree, with a design goal of 0.3 degree. The settling time to a static pointing error of 0.1 degree was approximately 2.5 minutes, with the specified requirement being less than 10 minutes.

The specification also states that the time to slew from one edge of the earth's disc to a point on the opposite edge and settle to the specified accuracy (0.1 degree) shall be less than 30 minutes. The angle from a point on the earth's disc to a point on the opposite edge is approximately 17 degrees (maximum). Data taken during the maneuver described above plus the 19 degrees maneuver from points 4 to 5 of Figure 9-27, indicates that a 17 degree slew would take less than 20 minutes, including settling time.

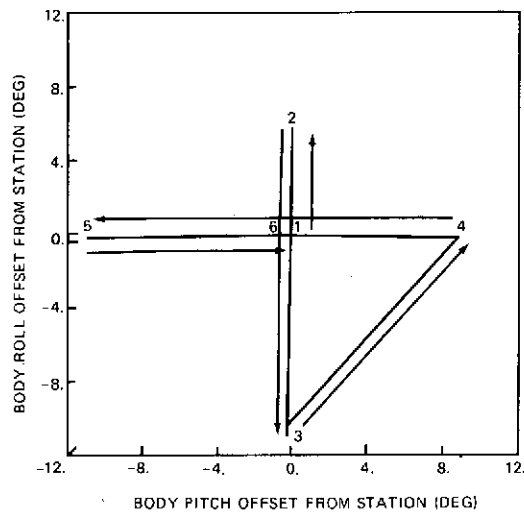


Figure 9-27. Antenna Pattern Maneuver for Monopulse Checkout

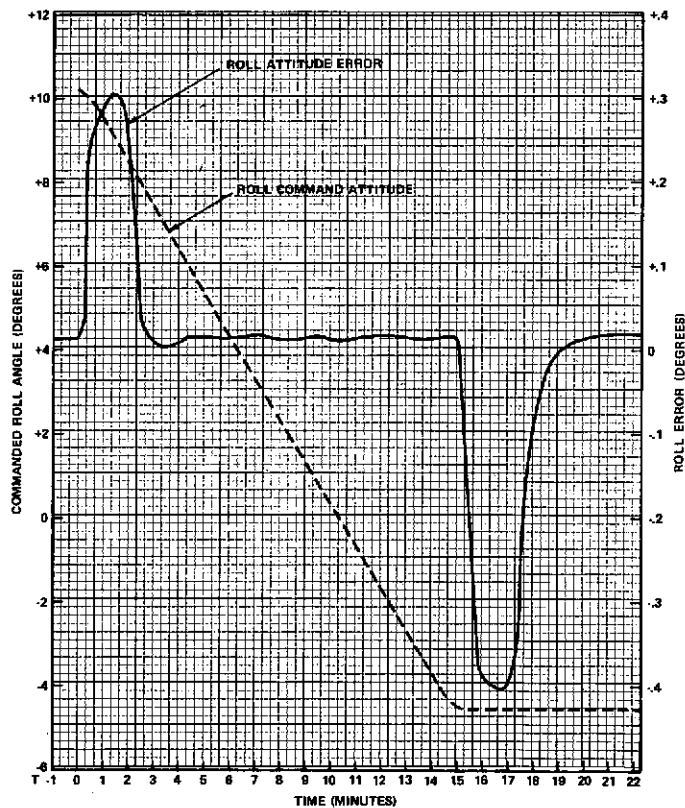


Figure 9-28. Roll Slew Maneuver

9.3.6 Antenna Patterns

The antenna pattern program utilizes a preprogrammed sequence of slews stored in DOC memory. Two patterns are considered for detailed evaluation. Figure 9-29 depicts a 3° pattern and Figure 9-30, a 5° pattern.

The 5 degree maneuver began at 162:16:16 and was completed at 162:18:57. The 3 degree maneuver began at 163:01:46 and was completed at 163:03:15. For both maneuvers, the ACS was configured using the ESA and PSA as attitude sensors, DOC 1 as the controller and wheels as torquers. Both were initiated with the spacecraft axis pointed at Rosman. During the antenna pattern tests, the ACS performed within the attitude error specification of ± 0.2 degrees.

Times for pattern completion (3 and 5 degrees respectively) were 89 minutes and 161 minutes which are within the maximum allowable times of 90 minutes and 180 minutes.

9.3.7 Satellite Track

Satellite Track was performed from 163:14:40 to 163:15:35 using Nimbus as the target satellite. The TDRE experiment was not performed since S-Band data was not transmitted to or from the satellite. The mode was accomplished using the ESA and PSA as attitude sensors, wheels as torquers, and DOC 1 as the controller which generated the attitude command-time profile.

Figure 9-31 is a diagram of the slew from Rosman to the satellite intercept point, the track of the satellite, and the slew back to Rosman at the end of the tracking period. The diagram is an output of an ATSOCC software program.

Figure 9-32 is a plot of the ESA roll and pitch errors as a function of time during the tracking period. The maximum roll error was -0.19 degrees. The maximum pitch error was $+0.15$ degrees. The expected ESA roll and pitch angles were based on orbit predicts using the ATS-6 Ephemeris for day 163.

The peak tracking error was 0.19 degrees. The specification calls for a maximum error of 0.5 degrees, with a design goal of 0.3 degrees.

9.4 INTERFEROMETER

This section describes the evaluation of the ATS-6 Spacecraft Interferometer Subsystem during a passive check-out (no r-f input to subsystem), an active checkout, both single and dual channel (with r-f input to subsystem), and closed loop performance with the ACS.

Max. Attitude Errors
Deg.

Leg #	R	P	Y
1	.048	.055	.039
2	.031	.048	.048
3	.039	.048	.048
4	.039	.039	.039
5	.023	.070	.031
6	.048	.048	.039
7	.048	.039	.031
8	.031	.048	.055
9	.078	.156	.039

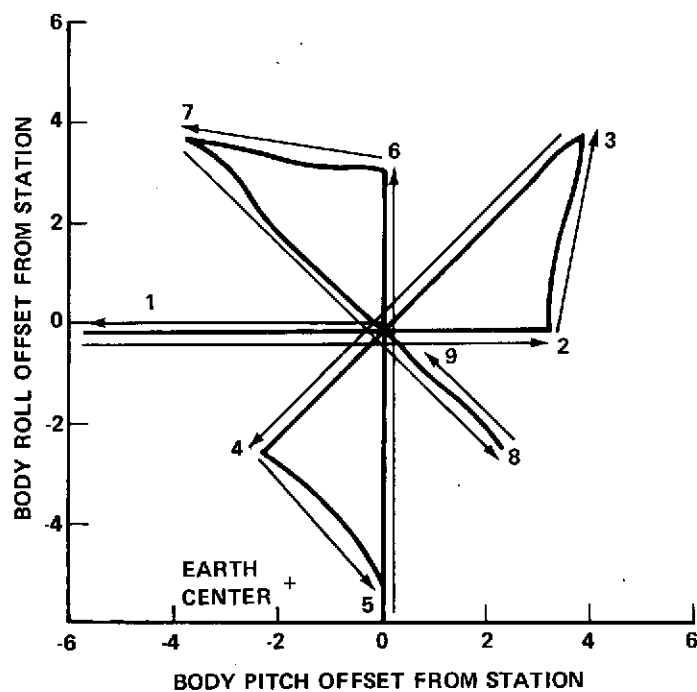


Figure 9-29. Antenna Pattern Maneuver
(3 Degree)

Max. Attitude Errors
Deg.

Leg #	R	P	Y
1	.031	.039	.016
2	.039	.070	.437*
3	.078	.039	.039
4	.039	.070	.070
5	.039	.070	.048
6	.100	.039	.055
7	.039	.039	.039
8	.070	.048	.039
9	.048	.031	.031

*PSA 2 Lost Acquisition

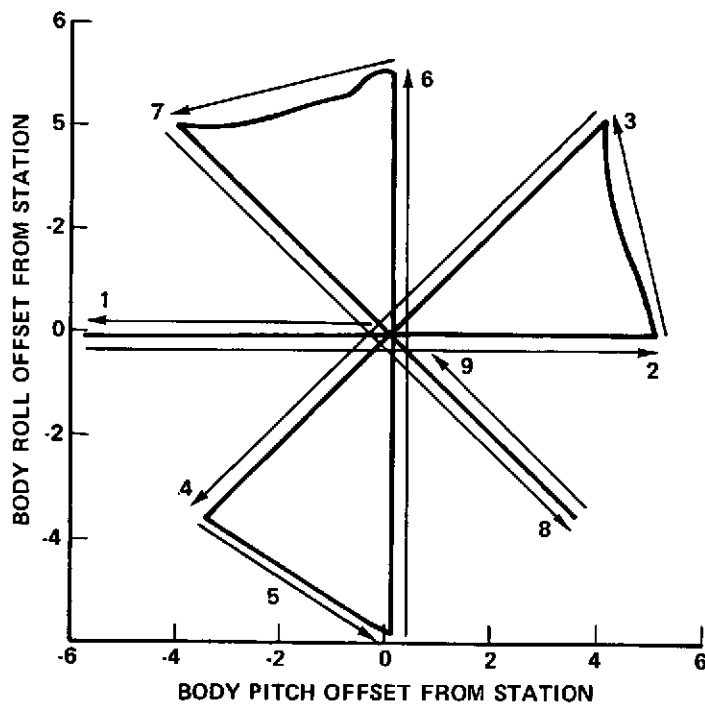


Figure 9-30. Antenna Pattern Maneuver
(5 Degree)

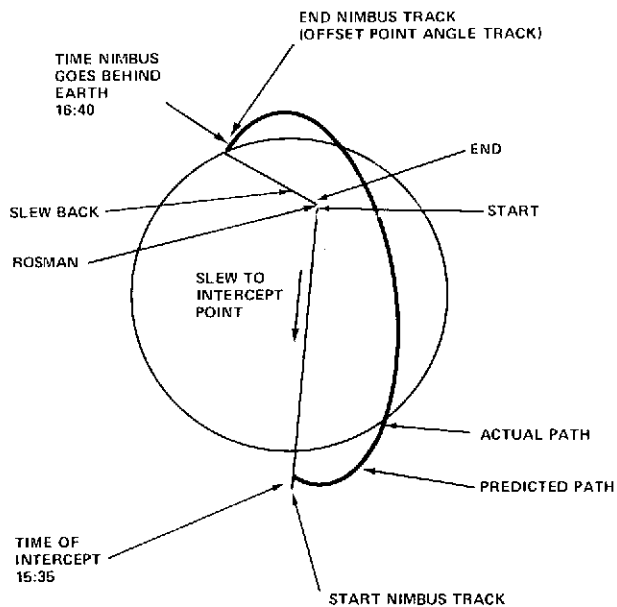


Figure 9-31. Satellite Track of Nimbus

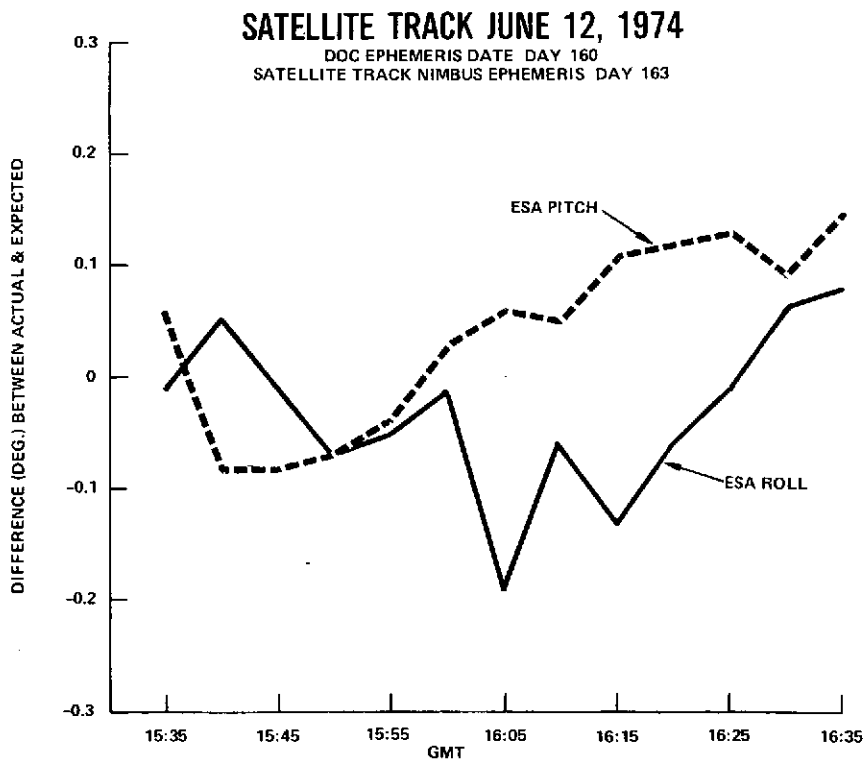


Figure 9-32. Roll and Pitch Errors During Satellite Track Mode

In addition, this report evaluates the in-orbit calibration of the receiver/converter, and confirms the boresight bias which had been loaded into both DOC's prior to launch.

In general, Interferometer performance was satisfactory and within specification for all modes of operation. Table 9-7 compares actual performance with design requirements.

Table 9-7

Interferometer Control Performance

	Actual	Specification
ACS Normal Modes	$\pm 0.049^\circ$	$\pm 0.1^\circ$
ACS Low Jitter Mode	$\pm 0.0056^\circ$	$\pm 0.01^\circ$

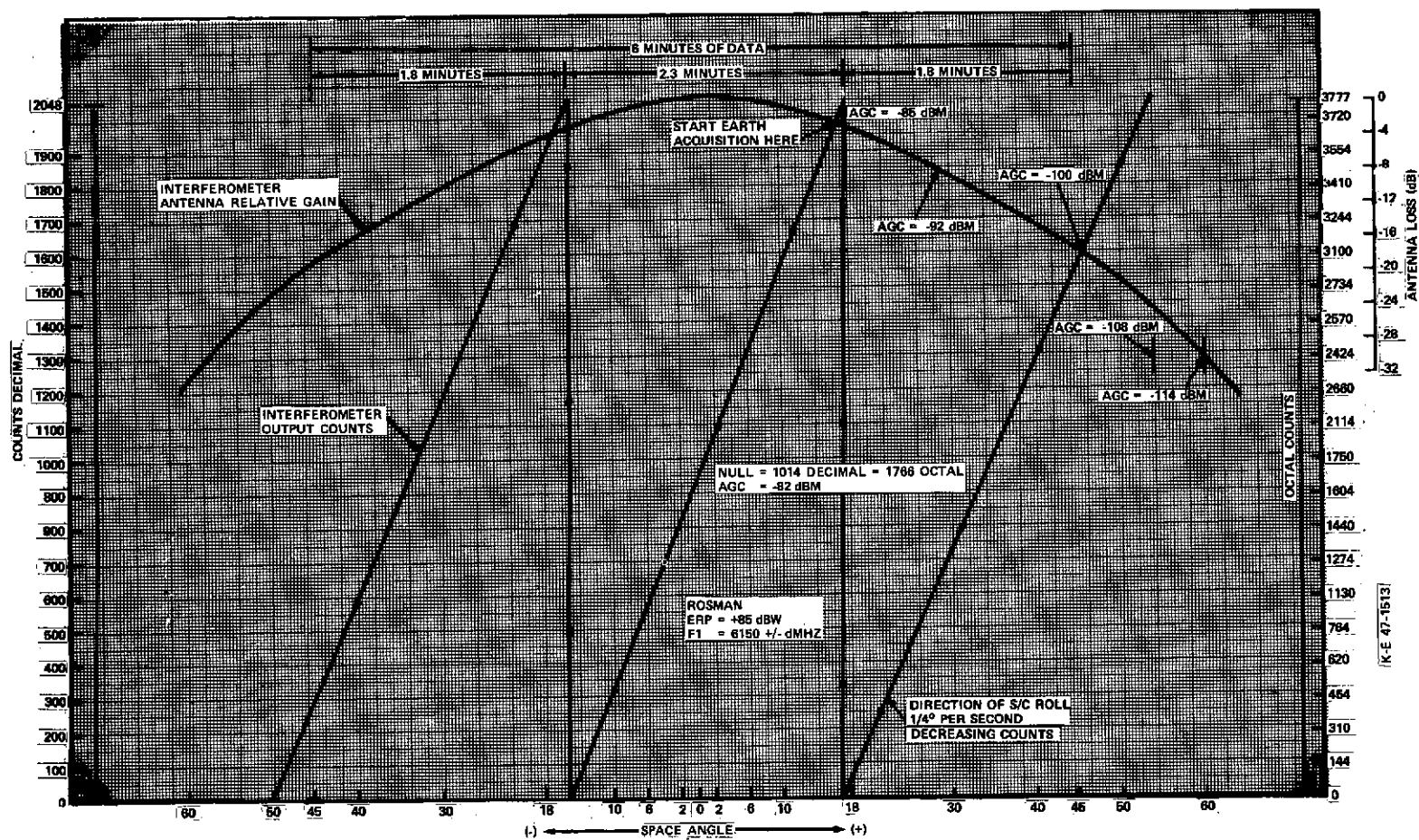
9.4.1 Earth Acquisition

The Interferometer Subsystem was commanded on immediately after Sun Acquisition as a back-up to the Earth Sensor. The Rosman ground station was then radiating at a frequency of 6150 MHz with adequate power to illuminate the Interferometer Subsystem when within its acquisition cone of 90 degrees. By commanding earth acquisition, the spacecraft was required to assume a negative roll rate of 1/4 deg per second, thus requiring a period of 24 minutes to roll 360°. At this rate, the Interferometer received R-F signal from Rosman earth station for 6 minutes out of each 24 minute period.

The Interferometer acquired the Rosman earth signal within the first half of the 90 degree acquisition cone on the first spacecraft roll cycle prior to ESA confirmation. The ESA having an acquisition range of nearly 15 degrees provided data only when the ESA was in view of the Earth's disk, whereas the Interferometer supplied excellent data as much as 35 degrees off of the Earth's disk.

The Interferometer's wide acquisition cone indicated approach of the earth's disk 2 minutes earlier than did the ESA, thereby demonstrating its capability as an earth-acquiring sensor.

Figure 9-33 is a plot of the Interferometer output counts versus space angle relative to the ground transmitter (Rosman) over the acquisition range of ± 45 degrees. An additional parameter plotted on this curve is the antenna gain over the region of interest.

Figure 9-33. Interferometer Counts Vs. Space Angle (Over ± 45 FOV)

9.4.2 Interferometer Performance

9.4.2.1 Passive Checkout

Interferometer passive checkout was accomplished during the second day. For this test, the ground transmitters normally used to uplink 6150 and 6155 MHz from Rosman and Mojave were turned off. The spacecraft synthesizer and the Interferometer subsystem were commanded on.

During this test, all commandable Interferometer modes were verified using strip-chart recorders as well as the Interferometer half-page display.

Temperatures at the Interferometer array, switch module and the Receiver/Converter assembly were monitored, as were the two AGC readings from Channel 1 and 2 of the Receiver/Converter. Additionally, the roll and pitch phase readings for the various modes of operation were monitored for correct output counts. All telemetry responses were as predicted.

9.4.2.2 Active Checkout

During Interferometer active checkout, the ESA and YIRU were in control and the spacecraft was at Local Vertical. The purpose of this test was to calibrate the Interferometer AGC's in both channels over the operating dynamic range and to verify roll and pitch attitude from the output counts.

9.4.2.2.1 AGC Calibration

AGC calibration for channels 1 and 2 was accomplished by transmitting at various power levels from Rosman, first at 6150 MHz and then at 6155 MHz. Data obtained in real time from the Interferometer half-page revealed that tracking between the two AGC's was within 0.8 dB. Figure 9-34, entitled "Receiver Converter Signal Strength Vs. Effective Radiated Power" is a plot of AGC #1. Total dynamic range was not plotted due to ground transmitter limitation. The interferometer specification for 3 sigma performance in pitch and roll is ± 0.018 degrees or ± 12 counts over the dynamic range of 40 dB (-55 dBm to -95 dBm).

A test verification at a power level of -70 dBm (ERP = +97 dBw) into the Receiver/Converter yielded a 3 sigma performance in pitch and roll of ± 0.007 degrees or ± 4.8 counts.

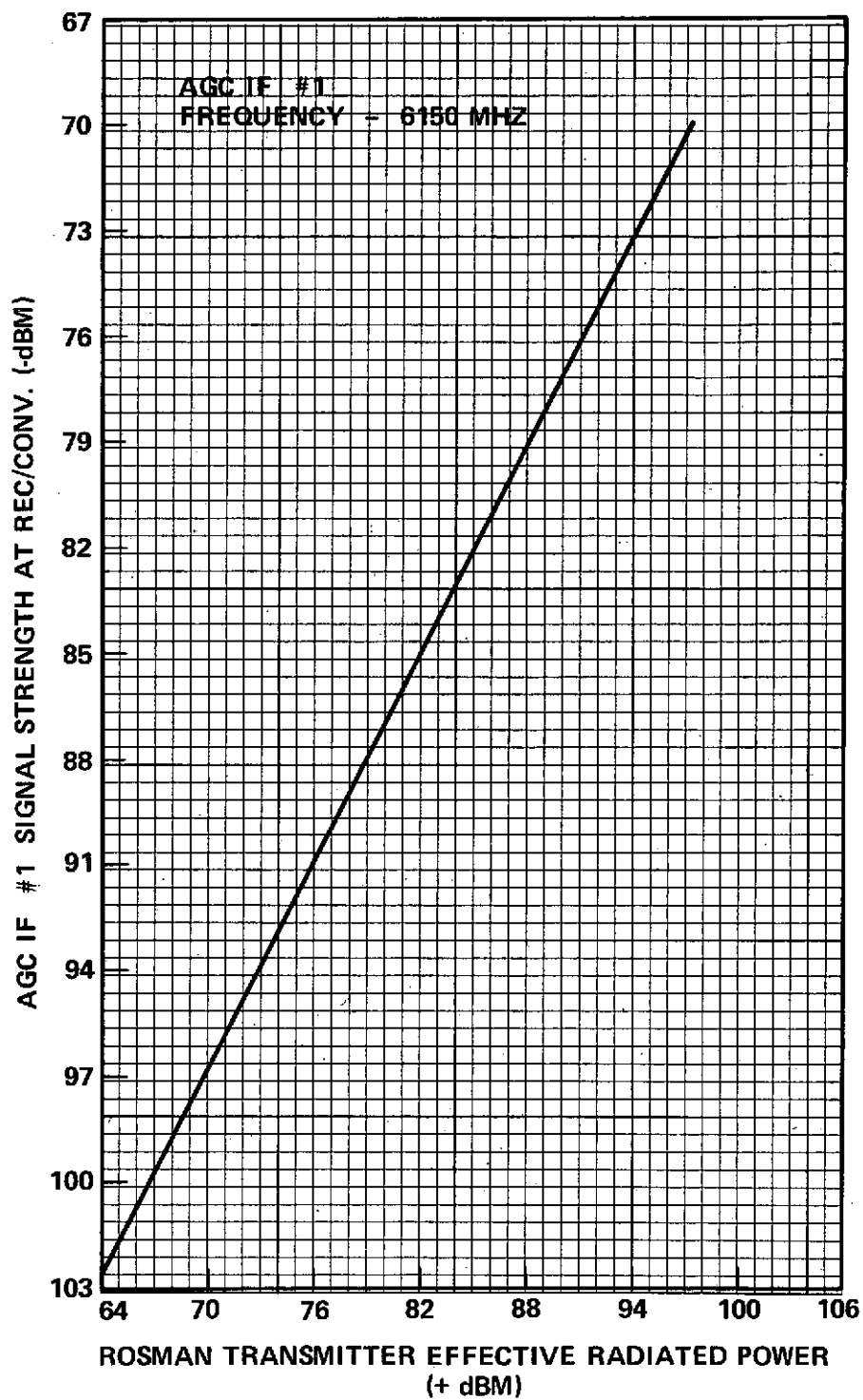


Figure 9-34. Receiver Converter Signal Strength Vs. Effective Radiated Power

9.4.2.2.2 Roll/Pitch Phasing Verification

During this test sequence, the Interferometer phase readings, 5 bit Coarse and 11 bit Vernier outputs to telemetry were converted to equivalent roll/pitch angles. The Interferometer was receiving an RF signal from a Rosman ground transmitter, and the ESA was in control at local vertical. Mojave was not radiating at this time and therefore, the Interferometer was responding only to one frequency, 6150 MHz.

The telemetry recorded for roll and pitch are shown below for the Interferometer normal mode: Counts shown are in decimal.

Rc	Rv	Pc	Pv	151:16:32:45
10	1355	15	0699	

From these counts, the Interferometer roll and pitch angles were calculated. These are the angles between the Rosman earth station and the spacecraft Local Vertical. Tabulated below are the computed Interferometer roll and pitch angles for the above decimal counts and the roll and pitch angles of the earth sensor (relative to local vertical).

<u>AXIS</u>	<u>INTF (Deg)</u>	<u>ESA (Deg)</u>
Roll	-5.5924	0.04
Pitch	-1.5896	0.04

The negative sign indicates that the roll and pitch angles of the Interferometer relative to Rosman (which is boresight for the Interferometer) are correctly phased with the Interferometer Z-Axis at Local Vertical, which is South and West of the Rosman ground station. The magnitude of the roll and pitch angles from Rosman to local vertical are also correct, and are accurate to within ± 0.044 degrees which is the fine deadband of the ACS System in the normal wheel mode.

9.4.2.2.3 Interferometer Closed Loop Performance

Upon completion of open loop testing, the Interferometer was selected as the controlling roll/pitch sensor. The ACS mode selected was an Offset Point to Rosman ground station. Data collected during this period indicated that successful performance was achieved.

Table 9-8 summarizes approximately twenty minutes of data observed during this portion of testing. Recorded in this table are the four Interferometer phase readings: Roll Coarse and Vernier, and Pitch Course and Vernier at 6150 MHz. The computed angle offset from the predicted Interferometer boresight counts for roll and pitch are also shown. For this mode of operation, the Interferometer output excursions and hence the angle offsets from boresight tend to vary as a function of the ACS deadband. For each 0.01 degrees of movement in the deadband region, the output counts will change by seven, i.e., 0.0014 degrees/count. Therefore, in this mode of operation, the full potential of the Interferometer will be limited by the ACS deadband.

9.4.2.2.4 Interferometer Calibration

Utilizing the predicted boresight counts and employing the coarse and vernier equations, transfer curves of counts versus space angle were obtained. These curves, for roll and pitch attitude over the field of view of ± 17.5 degrees are shown in Figures 9-35 through 9-38.

Prior to the ATS-6 launch, the Interferometer predicted boresight bias counts were loaded into the DOC's.

During calibration, the ESA was the controlling roll/pitch sensor. In this spacecraft configuration, the Interferometer phase readings for both Normal Mode and the Calibrate Mode were recorded, for the purpose of computing Receiver/Converter bias. Table 9-9 identifies the counts obtained. The worst case total bias change from those recorded prior to launch was only 5 counts in coarse and 1 count in vernier with a Receiver/Converter flight temperature correction. This is equivalent to an attitude offset of 0.0014 degrees in Vernier. Therefore, the boresight Bias Counts loaded into the DOC's at launch required no change at this time.

9.5 INERTIA WHEEL UNLOAD

During the first two weeks in orbit, the SPS was used an average of once every two days to unload excess wheel momentum. Data for the first four unloads is shown in Table 9-10. Jet impulse values were calculated from wheel-speed time histories during unload operations.

Table 9-8
Interferometer Closed Loop Data
Roll/Pitch Computed Offset
Angle From Rosman

GMT	R_c	R_v	Δ Counts	P_c	P_v	Δ Counts	Computed Angle Offset From Boresight		R/C AGC
							Roll	Pitch	
161:14:21:22	15	1221	-18	16	1845	+13	-0.0252	+0.0182	-96.1 dBm
29:40		1212	-27		1860	+28	-0.0378	+0.0392	
34:43		1222	-17		1863	+31	-0.0236	+0.0434	
38:30		1213	-26		1864	+32	-0.0364	+0.0448	
47:07		1212	-27		1863	+31	-0.0378	+0.0434	

Note: 1 - $R_c/R_v/P_c/P_v$ = Decimal Counts

2 - F_1 Roll Null = 1239 Counts

F_1 Pitch Null = 1832 Counts

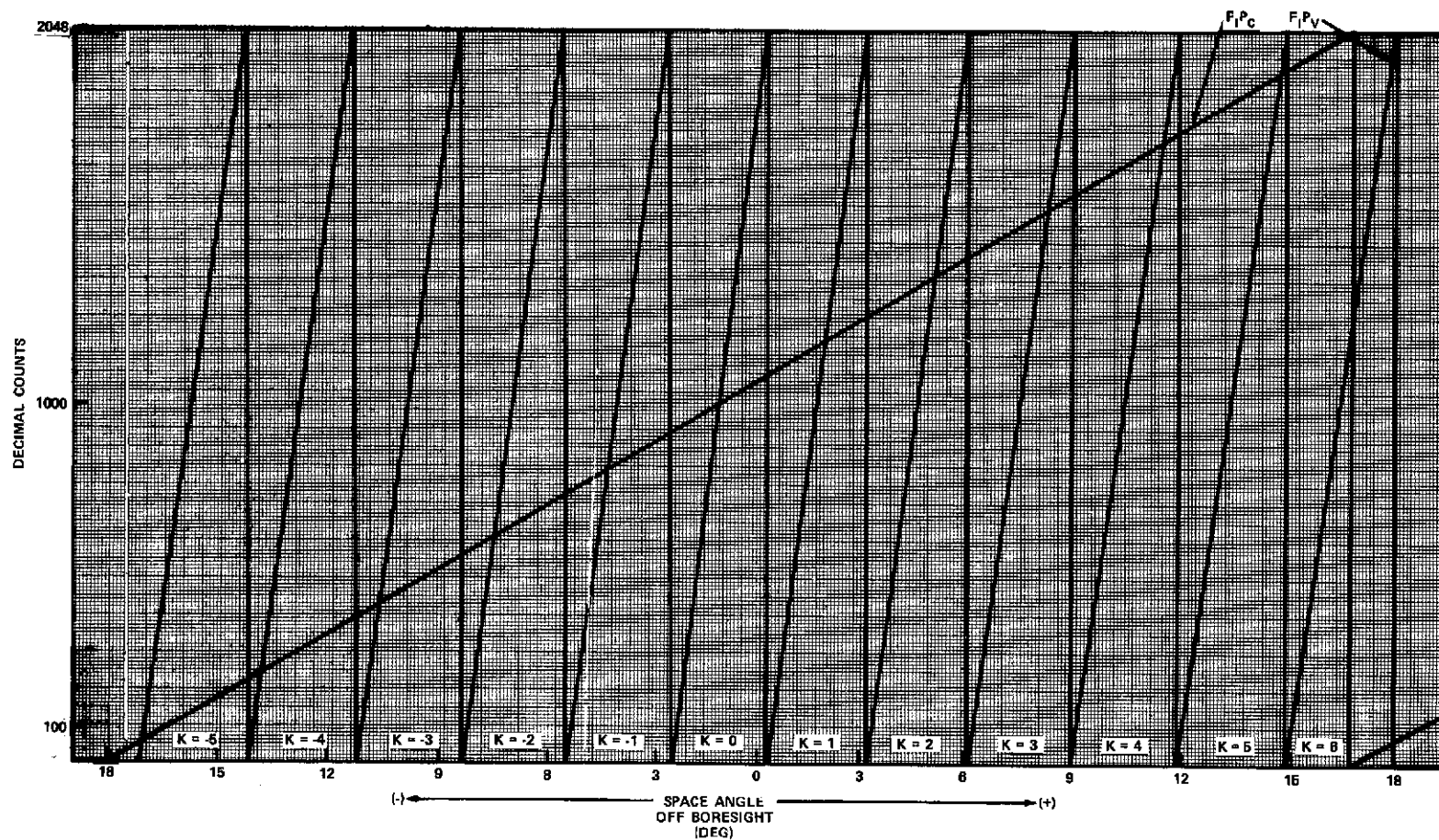


Figure 9-35. Interferometer Predicted Counts Vs. Space Angle
For Freq 1 Pitch Coarse and Vernier

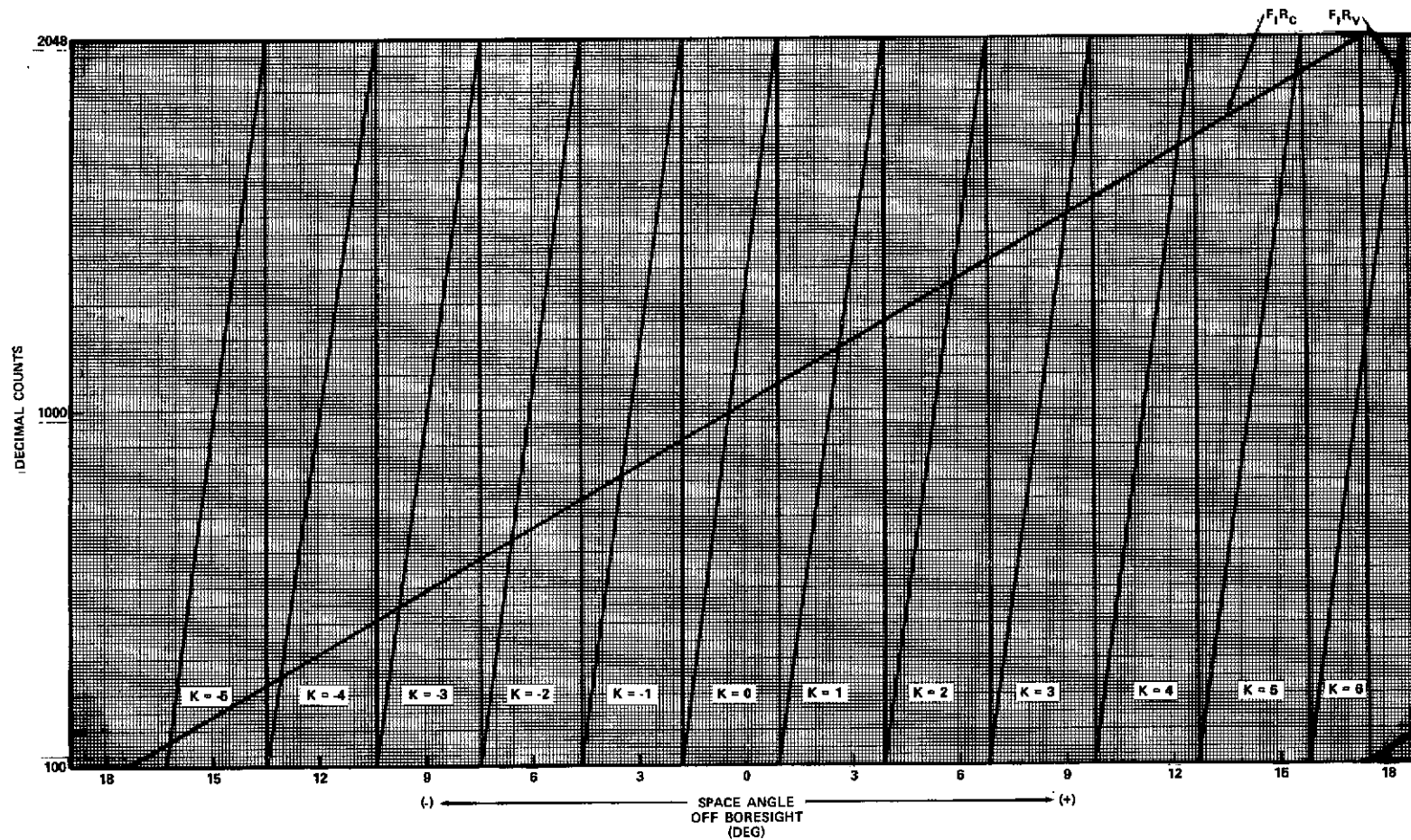


Figure 9-36. Interferometer Predicted Counts Vs. Space Angle
For Freq 1 Roll Coarse and Vernier

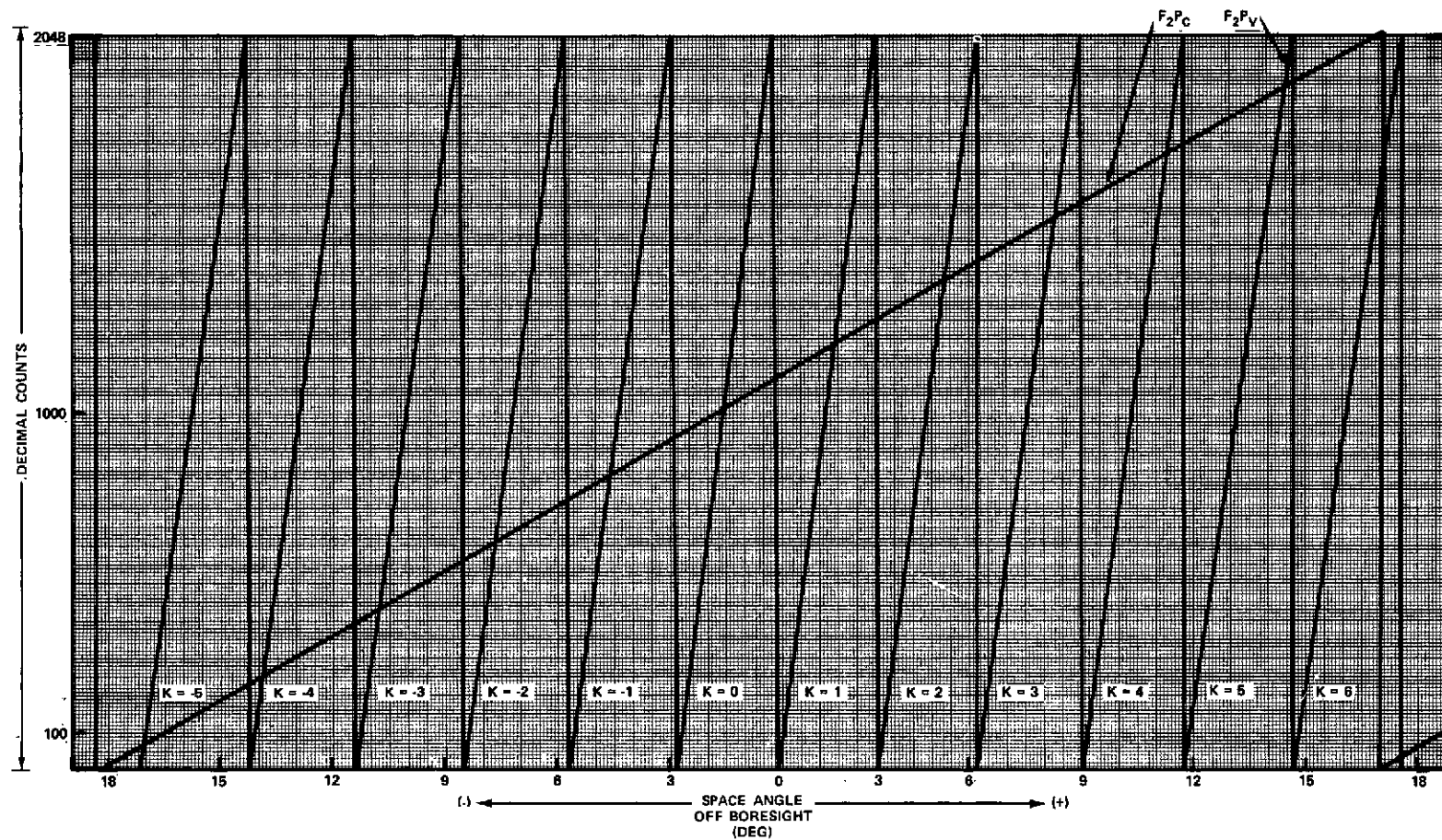


Figure 9-37. Interferometer Predicted Counts Vs. Space Angle
For Freq 2 Pitch Coarse and Vernier

09-6

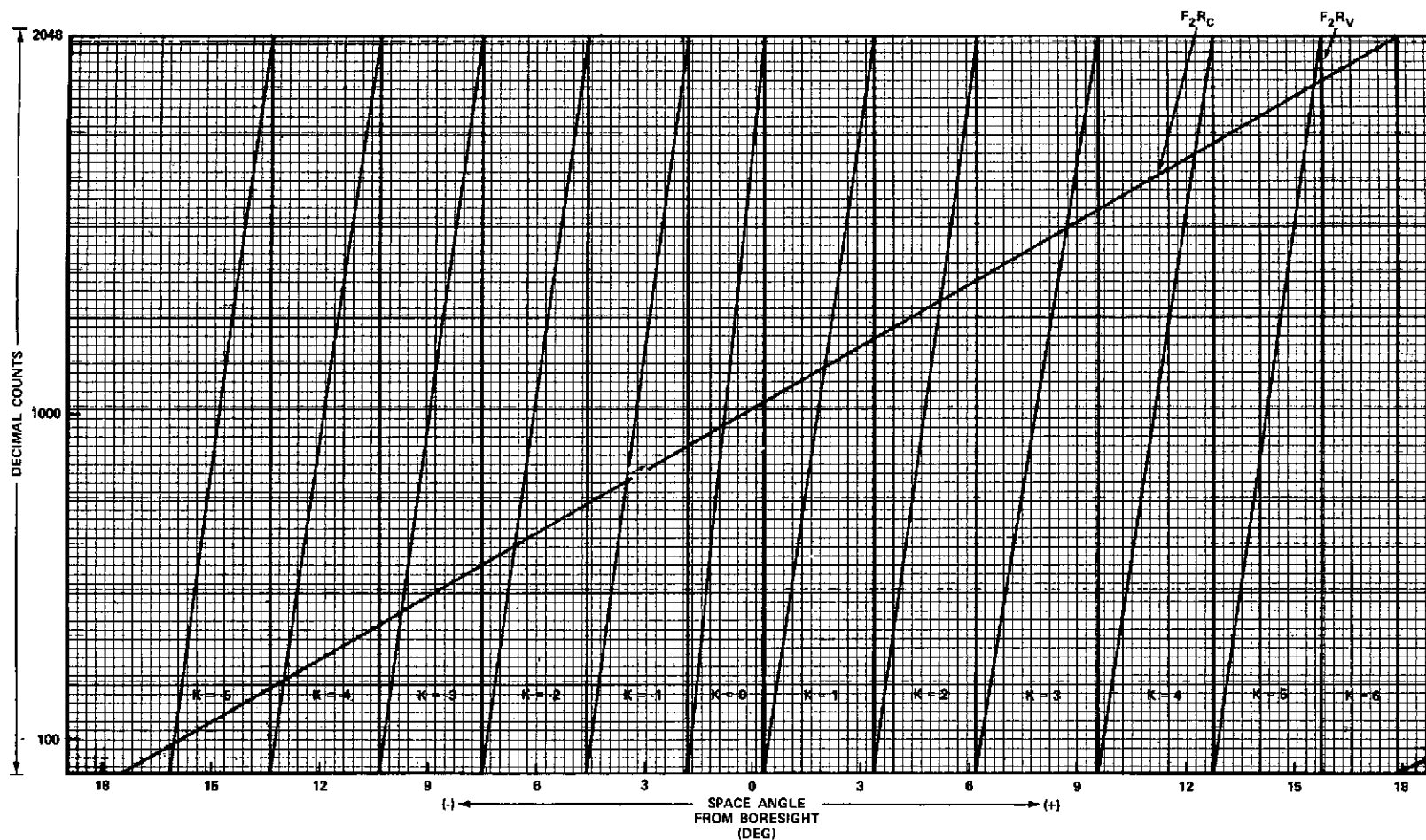


Figure 9-38. Interferometer Predicted Counts Vs. Space Angle
For Freq 2 Roll Coarse and Vernier

Table 9-9
Interferometer Vernier R/C Bias

Mode	Prelaunch		In Orbit	
	Roll	Pitch	Roll	Pitch
Cal-Off	1224	1821	1004	1052
Cal-On	924	308	1117	1070
R/C Bias	1074	1064	1061	1061

Note: No Temperature Correction Applied to These Data

Table 9-10
Wheel Unload

Unload Number	Initial Wheel Speeds RPM			Final Wheel Speed RPM			No. of Pulses			Jet Impulse #Sec/Pulse		
	R	P	Y	R	P	Y	R	P	Y	R	P	Y
1	640	940	—	360	720	—	-15	-11	—	0.020	0.0219	—
2	-1160	-926	-600	-380	-730	-520	+40	+11	+ 8	0.021	0.0192	0.0271
3	820	—	—	360	—	—	-26	—	—	0.0198	—	—
4	835	—	-790	380	—	-930	-25	—	+37	0.0188	—	0.0190
5	840	—	—	380	—	—	-25	—	—	0.0198	—	—
6	1060	—	—	360	—	—	-38	—	—	0.0198	—	—

9.5.1 Wheel Unload Histories

Figures 9-39 through 9-43 present plots of yaw versus roll wheel speeds for the second through the eighth day of flight. Figure 9-39 covers initial wheel turn-on and the first (roll/pitch) wheel unload. Wheel torque saturation occurs at approximately 1400 rpm. The decision to unload was made in order to check the unload system rather than because it was required. The test demonstrated proper action by the automatic unload system. Figures 9-40 and 9-41 present roll/yaw wheel speed plots from 152:19:45 to 155:06:23. During this period the spacecraft was in a local vertical mode of operation. As may be seen from these figures, the stored momentum vector exhibits cyclic components but negligible bias components (the figure traced a closed circle). Figure 9-42 shows a characteristic roll, yaw wheel speed trace for the Z axis pointing at Rosman. In addition to the cyclic components, the momentum trace exhibits a bias of approximately 300 to 350 rpm/day (2 to 2.4 ft-lb-sec/day). The cause of this bias has not been determined as of the writing of this report. Figure 9-43 shows the second unload wheel run down prior to orbit correction and the subsequent wheel momentum build up after reinitiation of wheel control.

9.5.2 Three Axis Momentum Storage

Figure 9-44 presents traces of roll, pitch, and yaw wheel speeds for a 24 hour period beginning at 156:20:00. This time period covers the second wheel unload, orbit control, and re-initiation of wheel control. The pitch axis momentum storage requirements are primarily cyclic in nature with a ± 650 rpm (± 4.4 ft-lb-sec) swing over a 24 hour period. Data to date indicates that pitch axis bias torques are minimal with less than a 20 rpm build-up in wheel speed per day.

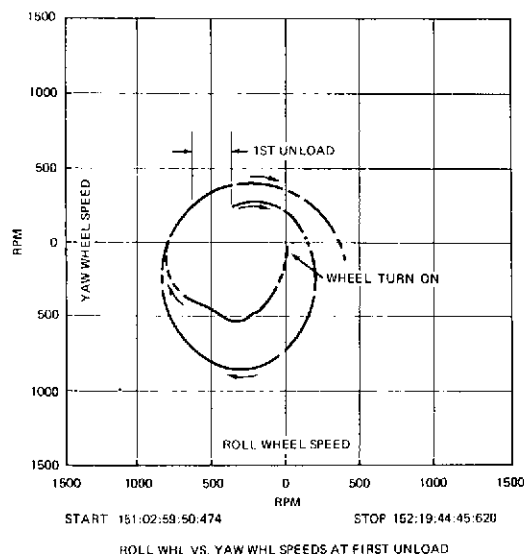


Figure 9-39. Roll WHL vs. Yaw WHL
Speeds at First Unload

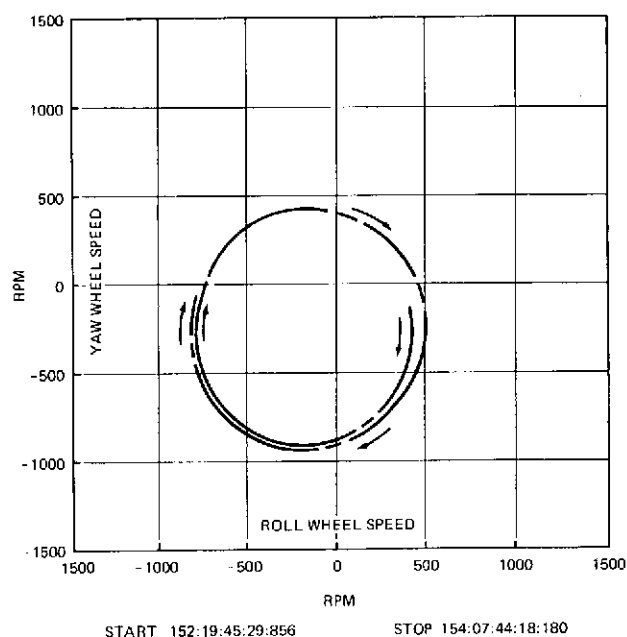


Figure 9-40. Roll WHL vs. Yaw WHL
Speeds (Day 152-154)

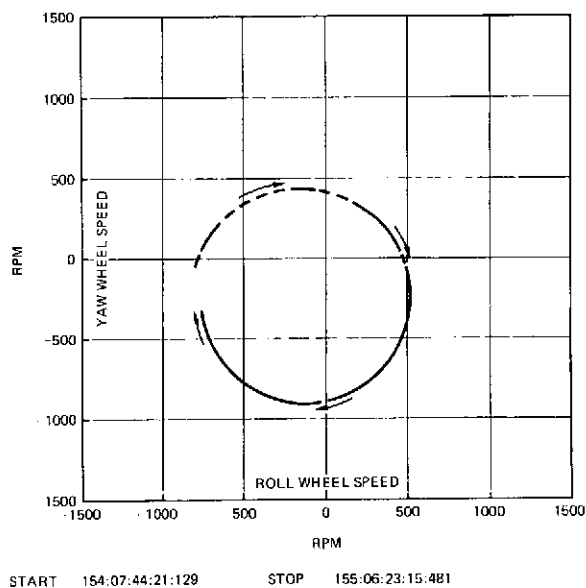


Figure 9-41. Roll WHL vs. Yaw
WHL Speeds (Day 154-155)

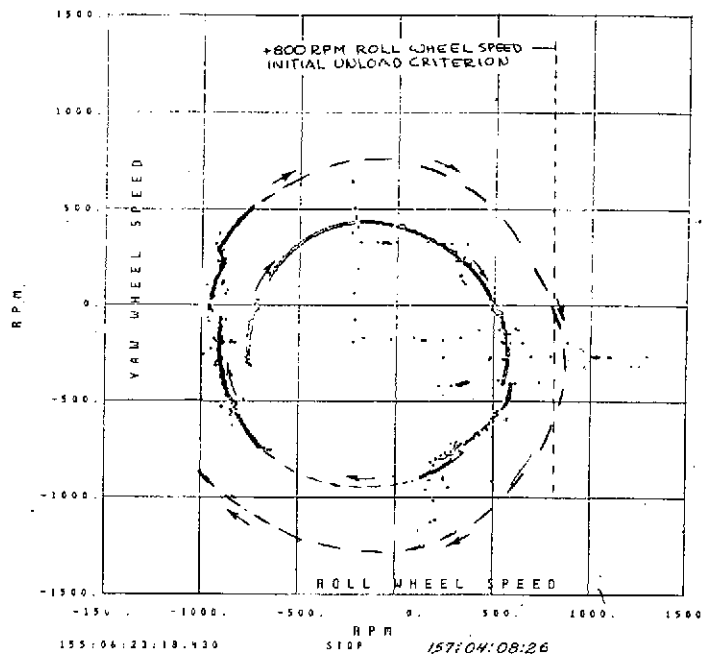


Figure 9-42. Roll Wheel vs. Yaw Wheel Speeds at Rosman

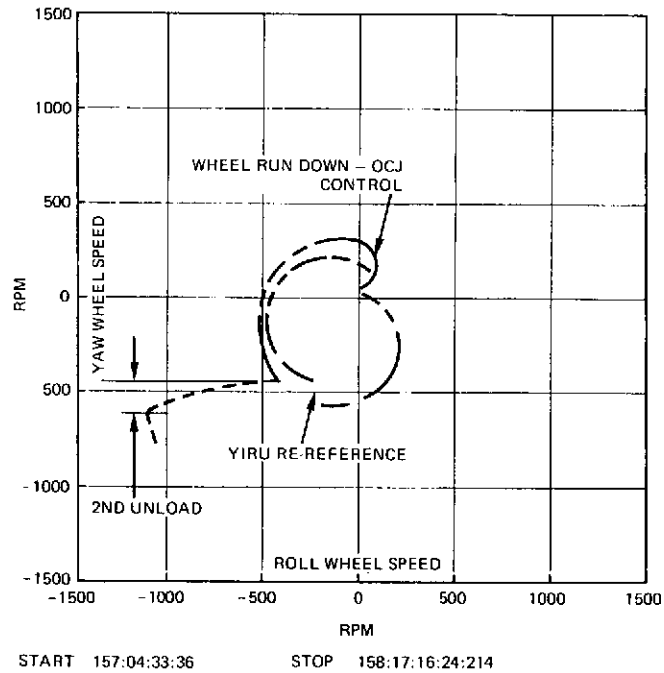


Figure 9-43. Roll WHL vs. Yaw WHL Speeds at Second Unload

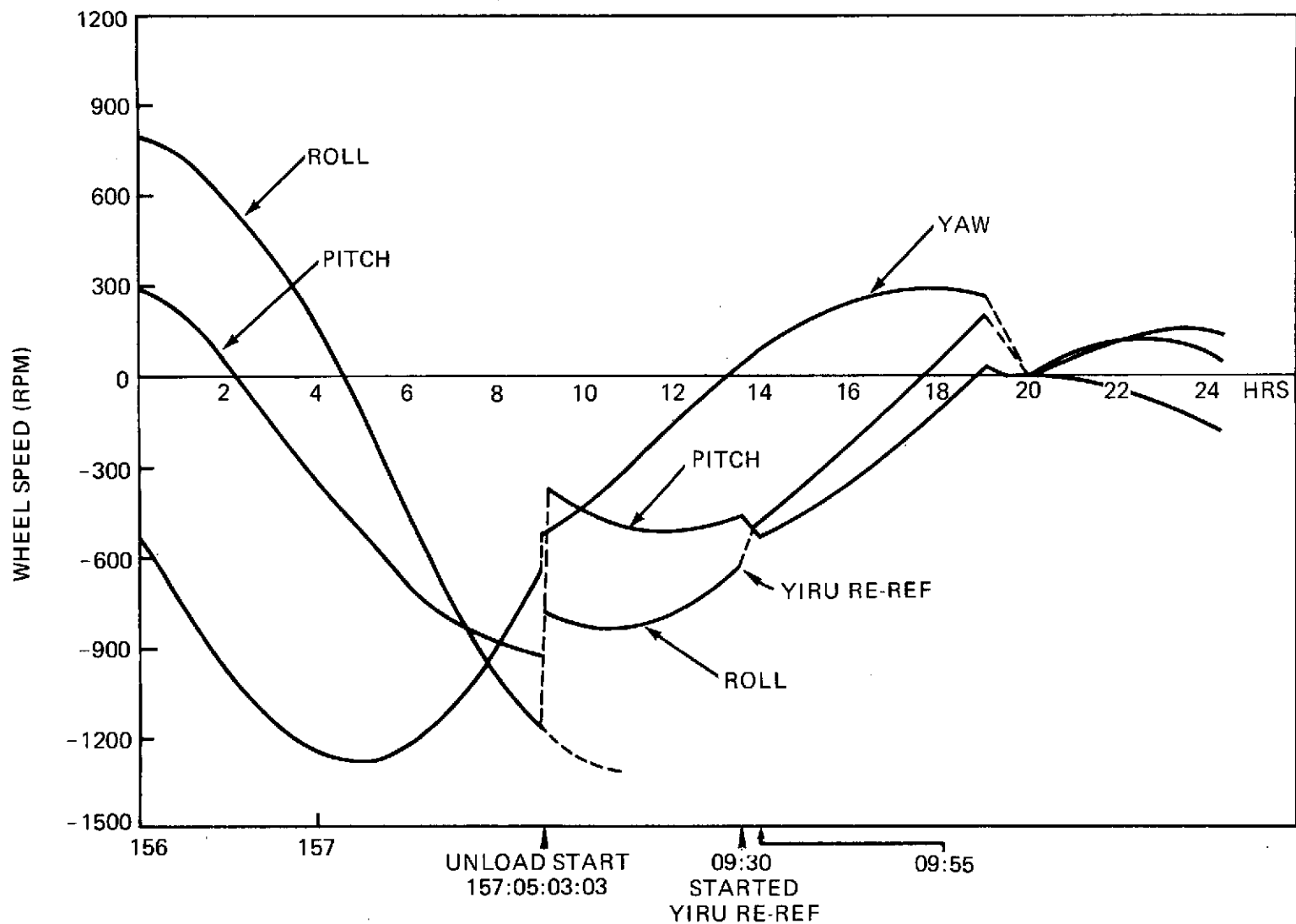


Figure 9-44. Wheel Speeds Over 24 Hours

9.5.3 Automatic Unload Performance

Table 9-11 summarizes the first six ground-initiated automatic unload activities. The table indicates the GMT and wheel speeds existing at the start of unload jet activation. The unload end time indicates the roll, pitch and yaw wheel speeds at the time of the last jet unload pulse for the axis of interest. The jet pulses indicate the total number of jet firing that occurred in the unloading process for each axis.

It can be seen that the average unload cutoff speeds for the roll, pitch, and yaw axes are 390, 735 and 536 rpm respectively. This compares favorably with before launch test values of 376, 736, 533 rpm for these axes.

The unload logic is such that if automatic unload is enabled, and the roll, pitch and for yaw wheel speeds exceed 495, 955, 663 rpm, the jets are fired with a duty cycle of 0.2 seconds on and 10 seconds off (duty cycle = 1/50). The jet commands continue until the previously mentioned unload cutoff speeds are reached. Polarity is such that negative wheel speeds cause positive jet firing which produces positive torques on the vehicle. Thus each positive jet actuation imparts a positive angular momentum impulse on its associated axis. The resultant spacecraft motion is detected by the ACS control sensors and the signals are processed by the DOC. This commands wheel torques which oppose the unload jet disturbance. In controlling against a positive unload jet firing the wheels therefore accumulate positive momentum and the negative speeds tend toward zero. The converse is true for negative jet unload firings.

The nominal jet unload duty cycle of 50:1 has been verified to within 5% via dwell data obtained during momentum unloading.

The "average" unload jet torque is given by,

$$T = \frac{FL}{50}$$

where:

T = Jet Unload Torque

F = Jet Thrust

L = Jet Thrust Lever Arm

Table 9-11
Wheel Unload Occurrences

Unload Start GMT	Unload End GMT	Wheel Speeds			Jet Pulses		
		Roll	Pitch	Yaw	Roll	Pitch	Yaw
151:18:05:39	Start	-636	+948	+228			
	151:18:07:17		+738			-11	
	151:18:07:55	-390			+15		
End Transient	151:18:09:47	-360	+720	+234			
157:05:03:08	Start	-1158	-930	-594			
	157:05:04:16			-540			+8
	157:05:04:46		-732			+11	
	157:05:09:32	-390			+40		
End Transient	157:05:11:47	-384	-780	-504			
163:19:41:10	Start	+822	+618	-366			
	163:19:45:06	+384			-25		
End Transient	163:19:46:59	+369	624	-402			
165:20:24:03	Start	+840	+534	-792			
	165:20:25:11	+390			-26		
	165:20:29:57			-531			+37
End Transient	165:20:31:37	+384	+558	-534			
167:16:39:06	Start	+852	+678	+120			
	167:16:43:01	+402			-25		
End Transient	167:16:44:39	+378	+684	+108			
169:18:03:03	Start	+1062	+738	-42			
	169:18:09:09	+384	+756	-60	-38		
End Transient	169:18:11:45	+378	+756	-72			

The nominal "average" unload torques for both roll and pitch are 2.42 oz-in and 0.97 oz-in for yaw. The difference results from the fact that the roll and pitch jets operate at 6.3 ft. moment arms while yaw jets are at 2.5 ft.

Figures 9-45 through 9-50 depict the wheel speed and unload jet actuation time-histories for the first six automatic unloads. The slope of the wheel speed versus time during unload jet pulsing is indicative of the "average" unload jet torques. Crosscoupling due to unload jet torques interacting with momentum stored in the wheels of orthogonal axes is evident in these plots.

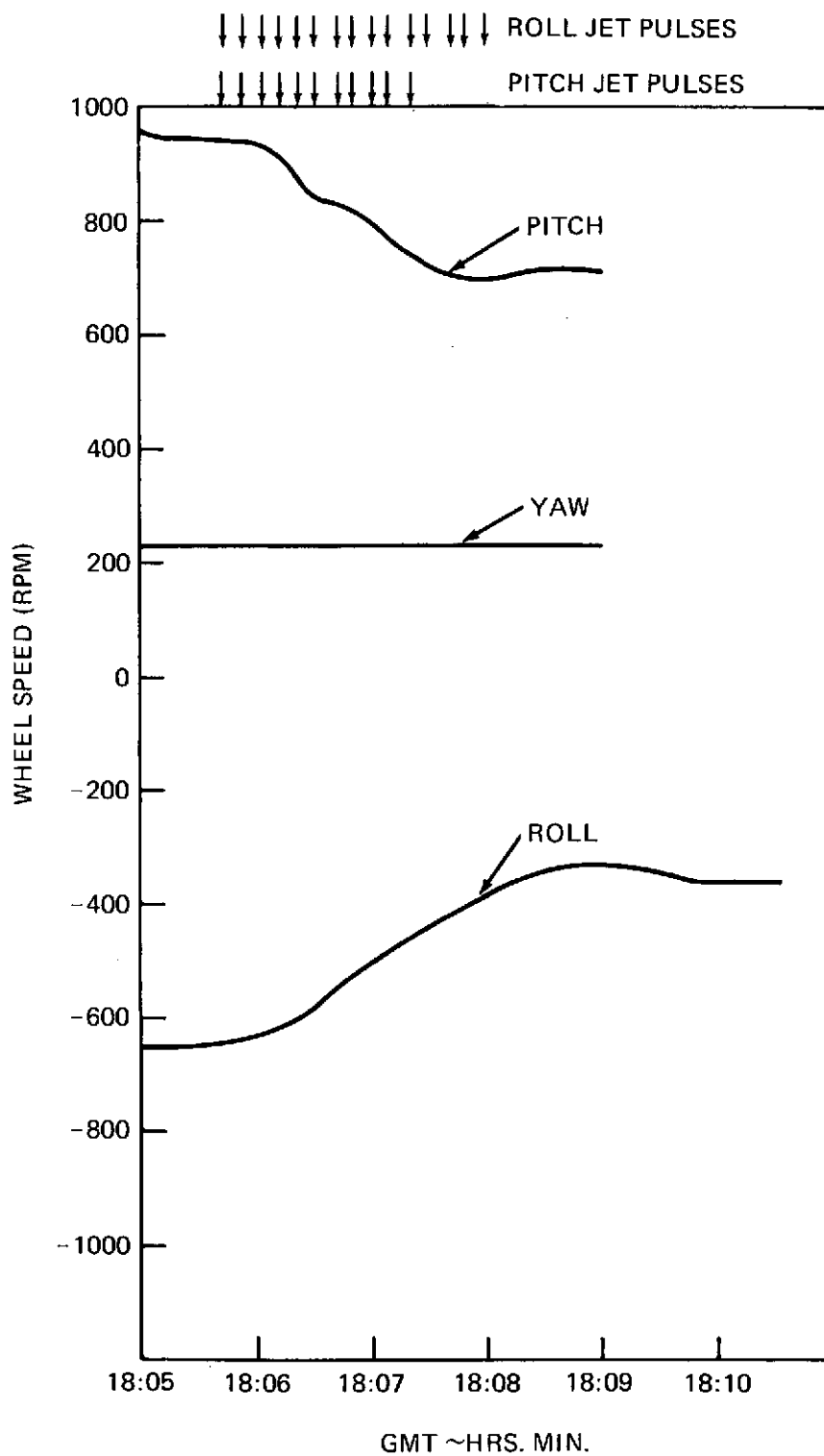


Figure 9-45. First Wheel Unload (Day 151)

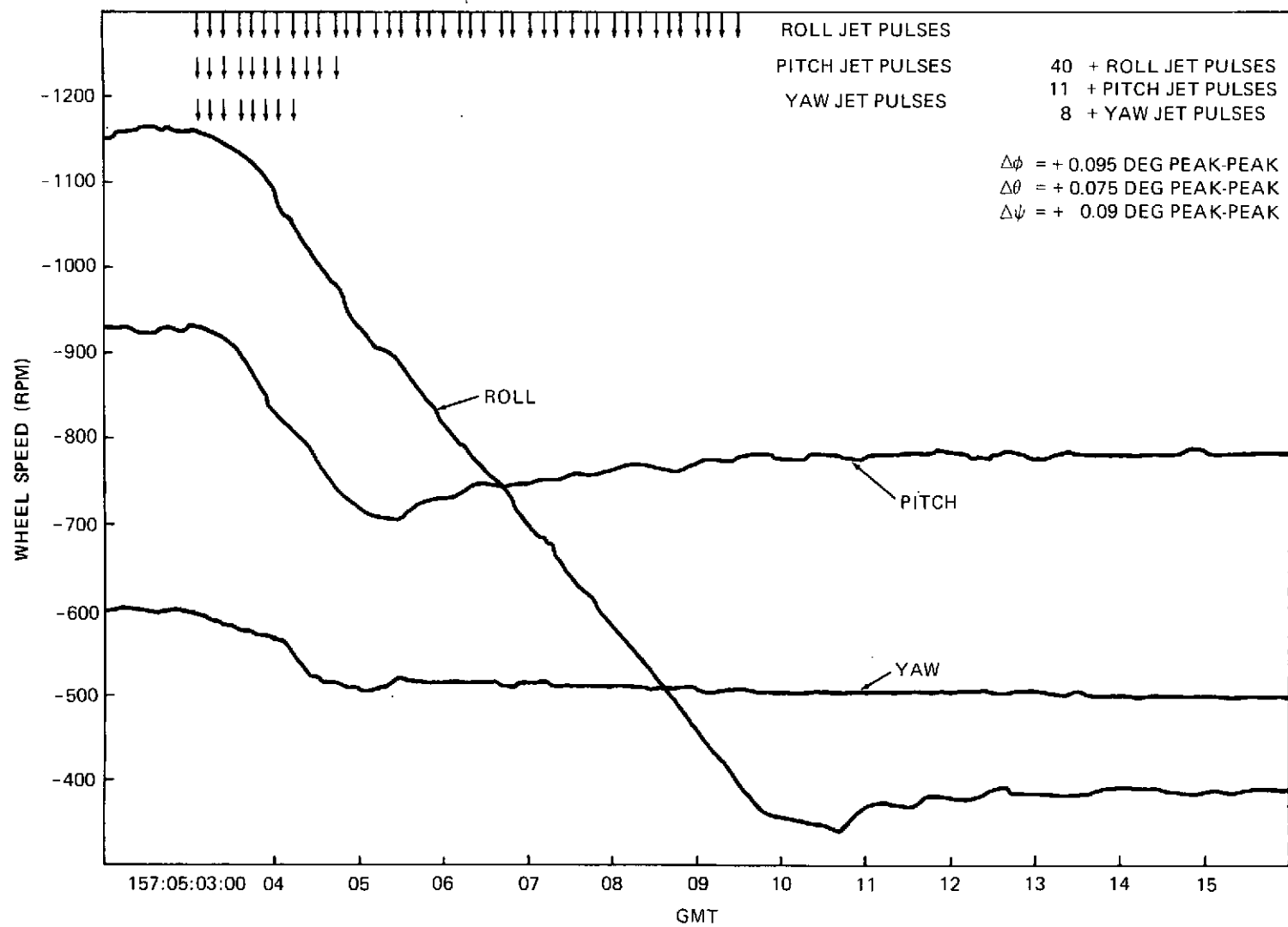


Figure 9-46. Second Wheel Unload (Day 157)

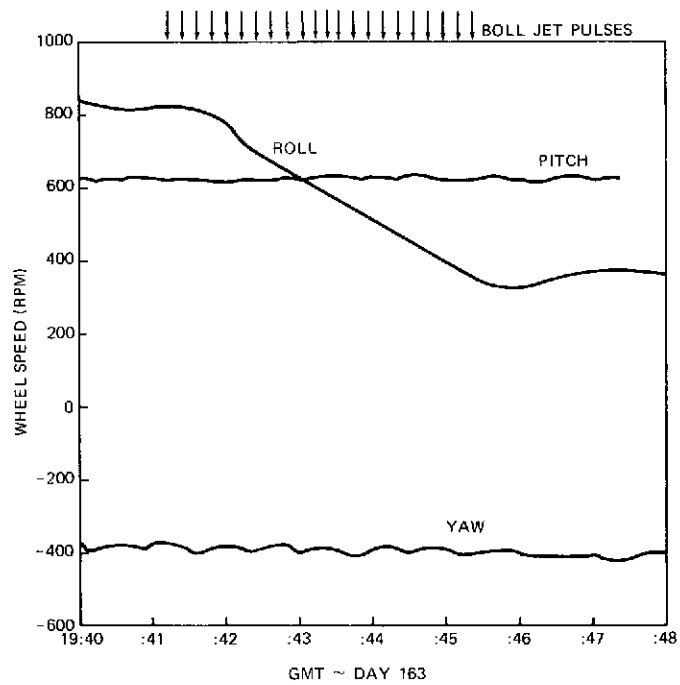


Figure 9-47. Third Wheel Unload

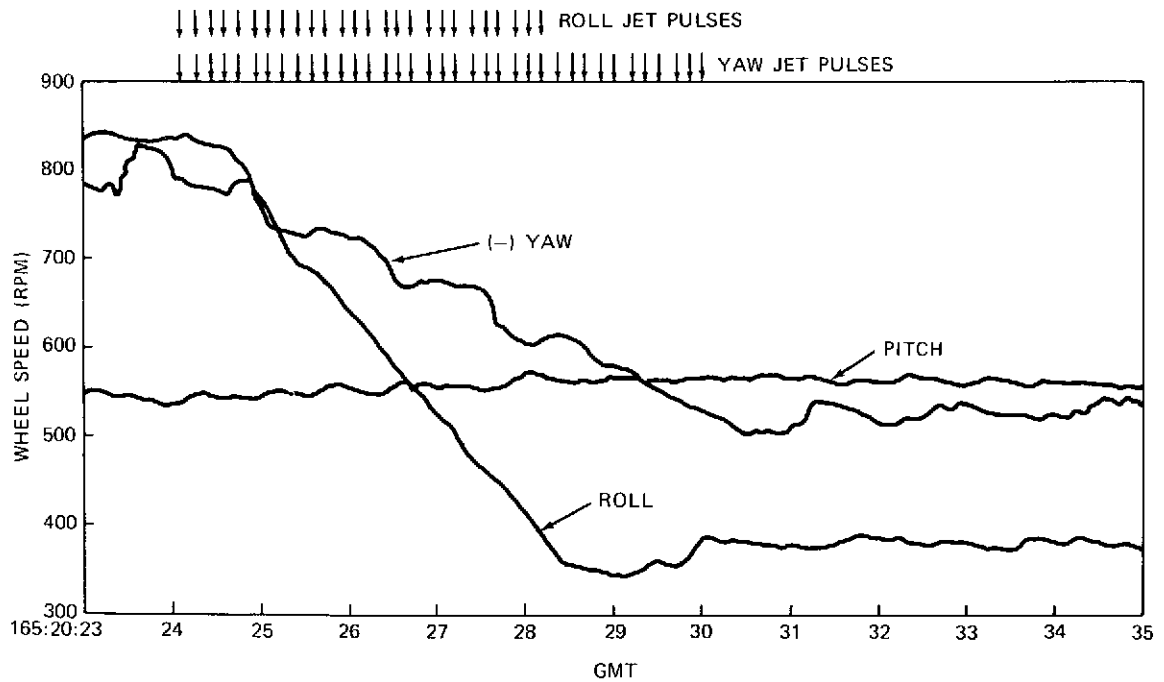


Figure 9-48. Fourth Wheel Unload (Day 165)

9-71

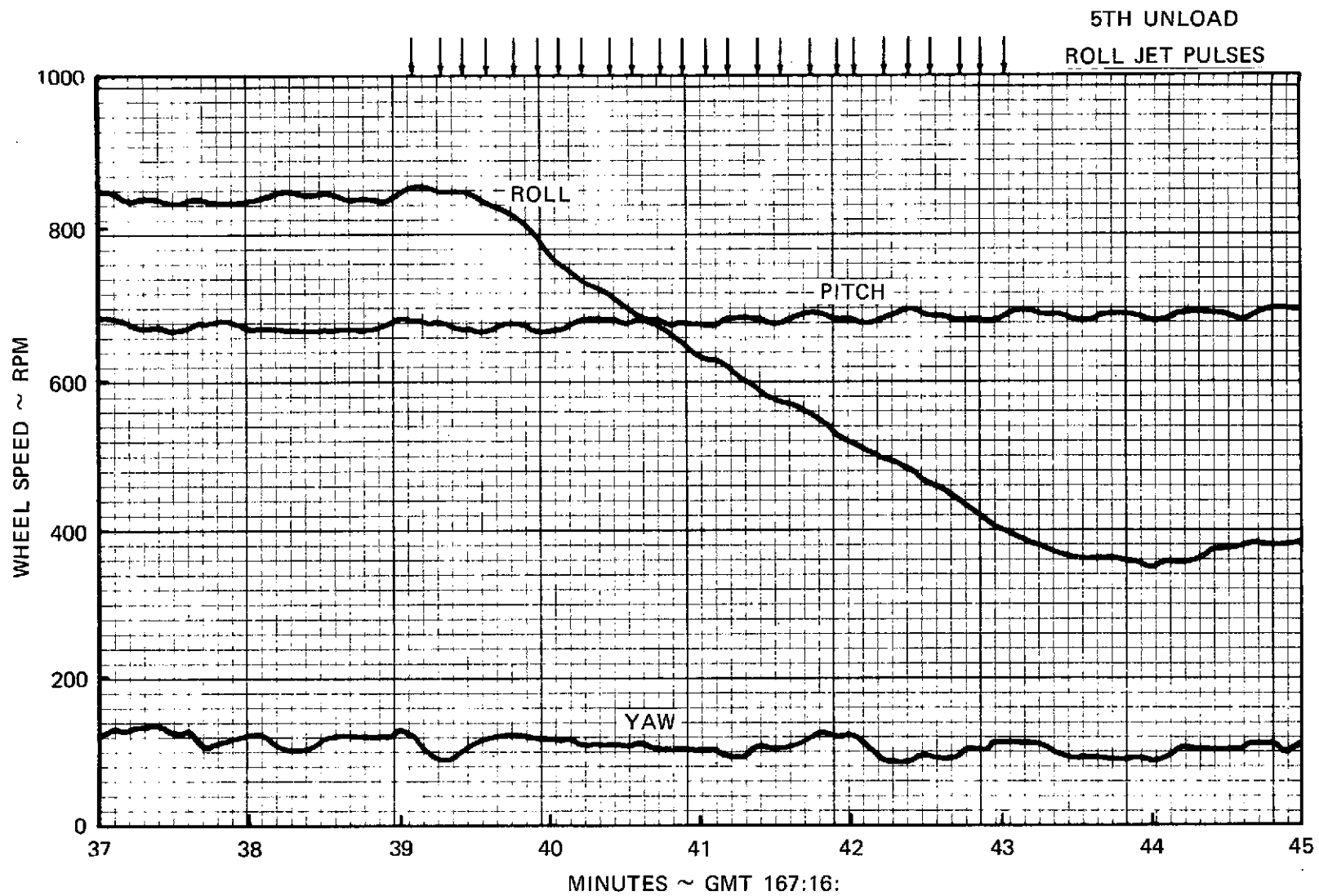


Figure 9-49. Fifth Wheel Unload

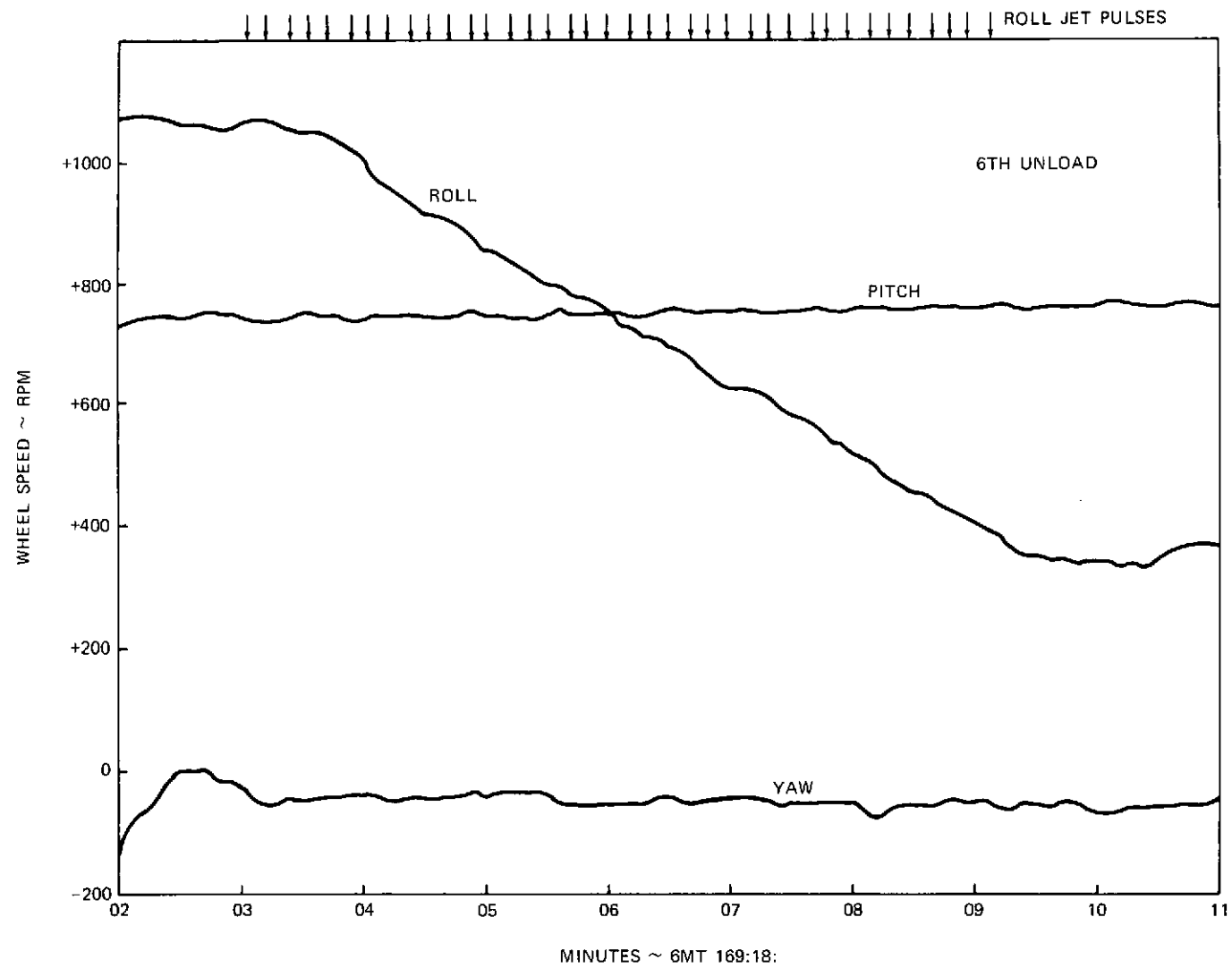


Figure 9-50. Sixth Wheel Unload

This is especially visible in the second unload in which the yaw axes wheel time history was significantly perturbed by the roll and pitch unload torques coupling with the existing pitch and roll momentum.

Table 9-12 summarizes the effective unload torques for the first six wheel unload activities. Variations in the torque values is attributable to the aforementioned crosscoupling effects which will be treated in detail in a subsequent report. However, the results do indicate that the unload jet performance is within expected limits.

9.5.4 Estimated Unload Fuel Requirements

Evaluation of the jet unloading performance on an impulse per pulse basis results in values which are in good agreement with the expected value of 0.02 lb-sec/pulse. This data is summarized in Table 9-13.

To date, the only SPS #1 thruster not used for momentum unload is the -yaw jet. However, the momentum build-up experienced has only been in the roll-yaw plane and due to the smaller jet lever arm in the yaw axis, only the roll axis will be unloaded on a scheduled basis in the interest of fuel economy. Based on data accumulated for the first 6 unload cycles, it is estimated that approximately 20 roll jet pulses every two days will be required to prevent saturation of the roll/yaw wheels due to secular momentum build-up. Extrapolated to one-year this suggests an unload fuel requirement of less than 1 pound per year which may be compared to a budgeted allotment of approximately 1.4 pounds. The 1 pound per year is conservative since the predictions are based on solar disturbances which are maximum near the winter and summer solstice periods. Momentum accumulations due to gravity gradient are small and, for the data accumulated to date, are not separable from the relatively large solar torques.

9.6 ANOMALIES

9.6.1 RGA #1 Earth Acquisition Anomaly

This section analyzes the problem encountered during the initial earth acquisition attempt by ATS-6. The problem was a lack of controlled motion to zero attitude error in roll after the earth was acquired by the ESA. The roll angles

Table 9-12
Effective Unload Jet Torques

Unload Number	Unload Torque (oz-in)			Number of Firing		
	Roll	Pitch	Yaw	Roll	Pitch	Yaw
1	-2.66	-2.88	---	-15	-11	---
2	2.66	2.86	1.25	-40	+11	+8
3	-2.54	---	---	-25	---	---
4	-2.45	---	1.08	-26	---	+37
5	-2.47	---	---	-25	---	---
6	-2.49	---	---	-38	---	---

Normalized Averages: Roll = 2.55, Pitch = 2.85,
Yaw = 1.17 oz-in

Table 9-13
Effective Jet Unload Impulses

Unload Number	Initial Wheel Speeds RPM			Final Wheel Speed RPM			No. of Pulses			Jet Impulse #Sec/Pulse		
	R	P	Y	R	P	Y	R	P	Y	R	P	Y
1	640	940	-	360	720	-	-15	-11	-	0.020	0.0219	-
2	-1160	-926	-600	-380	-730	-520	+40	+11	+8	0.021	0.0192	-
3	820	-	-	360	-	-	-25	-	-	0.0198	-	-
4	835	-	-790	380	-	-930	-26	-	+37	0.0188	-	0.0190
5	840	-	-	380	-	-	-25	-	-	0.0198	-	-
6	1060	-	-	360	-	-	-38	-	-	0.0198	-	-

*This value may be affected by Cross Coupling. Average normalized value (3 axes combined) is 0.0199

held, with some oscillation at about 8 to 9°. Normal attitude control to zero error was achieved when RGA #2 was substituted for RGA #1 in the control loop.

9.6.1.1 Data Review

Figure 9-51 shows the time history of on-line plotted RGA roll telemetry during boom deployment.

Figure 9-52 shows the time history of on-line plotted RGA roll telemetry during sun acquisition.

Figure 9-53 shows the time history of on-line plotted RGA roll telemetry attitudes, and jet action during early acquisition, including the acquisition anomaly.

Figure 9-54 shows the time history of ESA roll output during the start of earth acquisition mode.

Table 9-14 contains a compilation of RGA roll telemetry at discrete times. Also tabulated are independent measurements of vehicle rates and inferred vehicle rates based on other considerations.

9.6.1.2 Interpretation

Both RGA's were on before lift-off. Roll RGA telemetry indicated 0.02 deg/sec. (A single signal indicates the combination signal at the RGA output.) The low indicated rate was well within expectation.

The boom drop was normal and took about two minutes to complete. RGA telemetry indicated roll rates of $-0.28^\circ/\text{sec}$ before deployment and $-0.19^\circ/\text{sec}$ after. The short time between beginning and end and the indicated low pitch and yaw rates (0 and $0.4^\circ/\text{sec}$) suggest that the RGA roll readings were about a fixed inertial axis. The expected ratio of roll inertias from before to after deployment was 1:2.1. Actual vehicle rates can be inferred from this data by noting that the vehicle rates should vary inversely with the inertia ratio. The inferred vehicle rates are $-0.18^\circ/\text{sec}$ before, and $-0.09^\circ/\text{sec}$ after deployment with a bias of $-0.1^\circ/\text{sec}$, i.e., the RGA 1 and 2 gyros indicated $0.1^\circ/\text{sec}$ less than true rate.

About 50 minutes later the roll RGA indicated the same rate ($-0.19^\circ/\text{sec}$) and RGA 2 was turned off. RGA telemetry then jumped to $-0.27^\circ/\text{sec}$. Assuming

Figure 9-51. Boom Deployment - Roll Axis

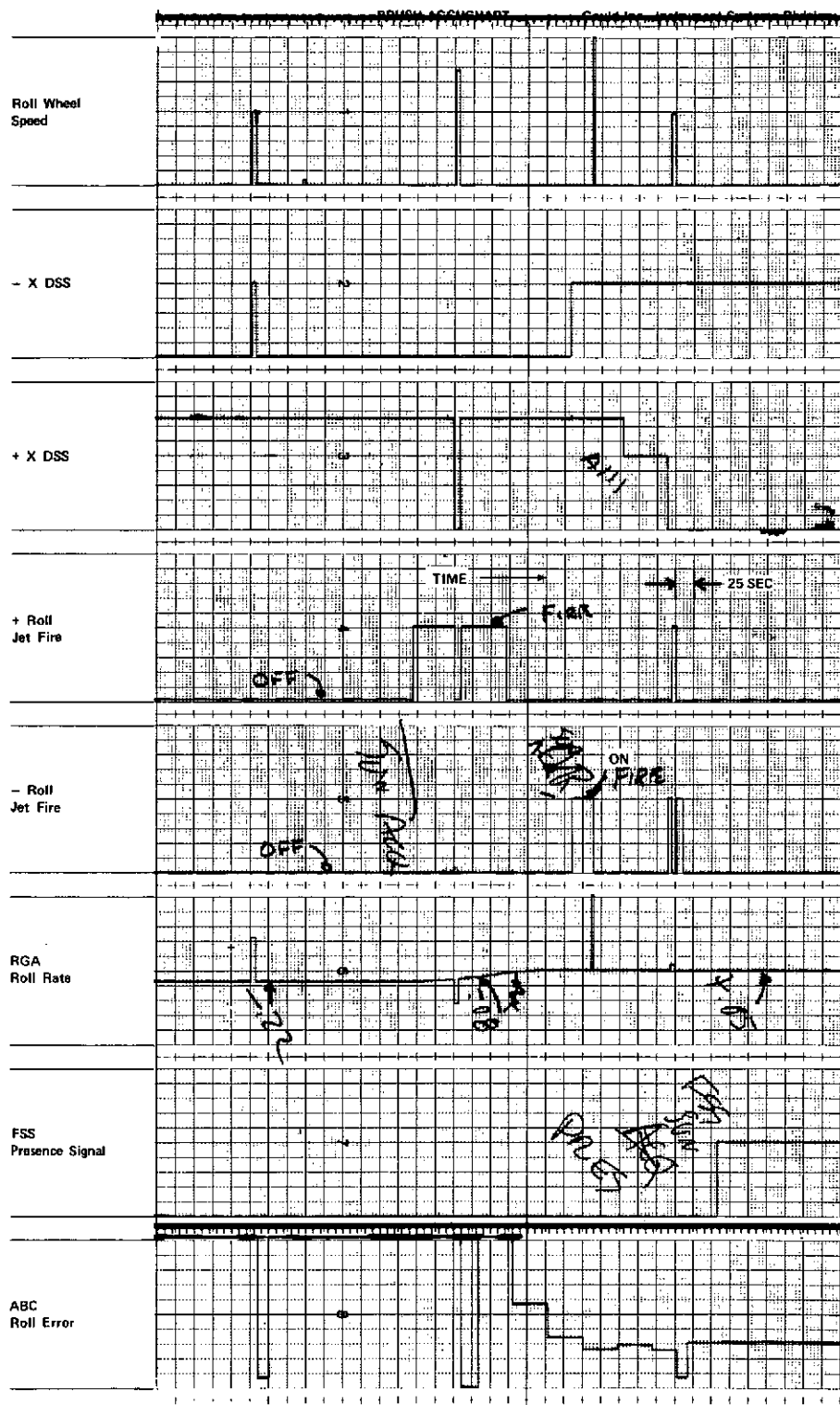


Figure 9-52. Sun Acquisition - Roll Axis



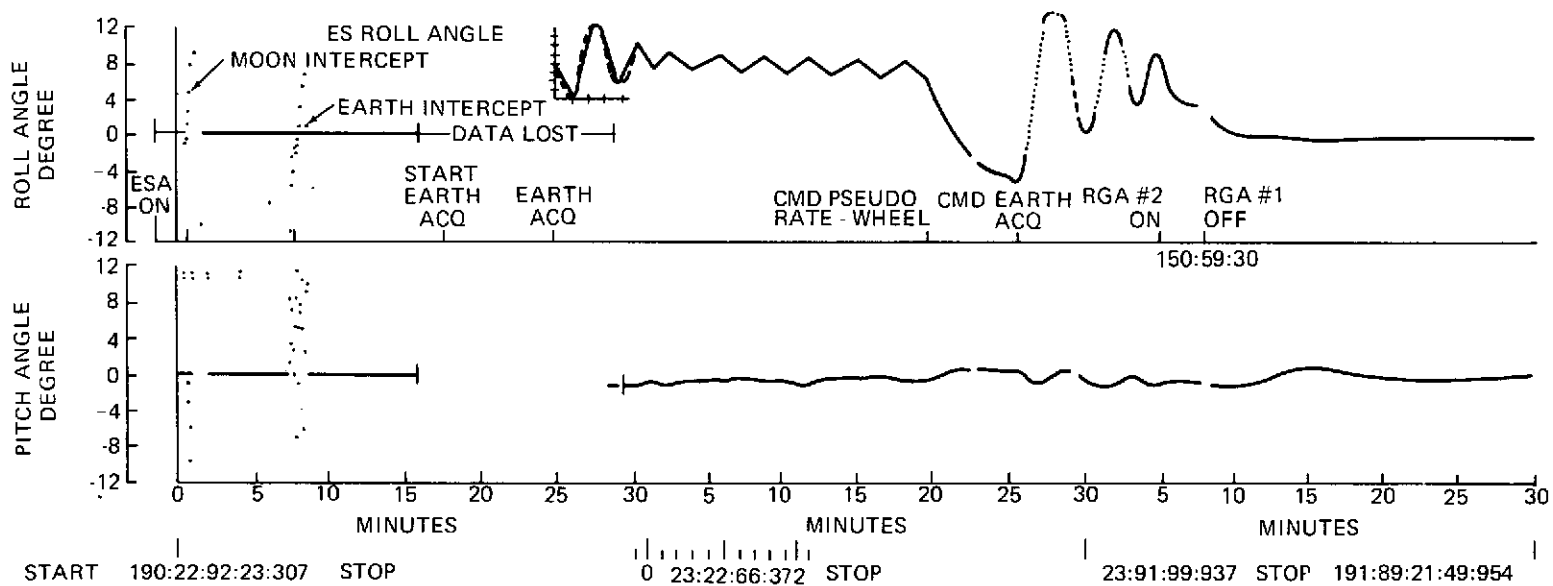


Figure 9-54. Earth Acquisition - ESA Pitch & Roll

Table 9-14

RGA Roll Telemetry

	Time	RGA 1 & 2 T/M ^o /sec	RGA 1 T/M (deg/sec)	"True" Rate (deg/sec)	Inferred "True" Rates (deg/sec)
Before Lift-off	150-18	-0.02		0	
Boom Drop					
Before	19-38-47	-0.279			-0.179
After	19-42-50	-0.186			-0.086
RGA 2 Off	150-20-34		-0.266		-0.086
During Pseudo Rate	22-52		+0.033	0.24 (Interferometer) 0.25 (wheel mo- mentum)	
EA Compd.	23-10		-0.305		
	-R jet off				
	Before 23-16-50		-0.385		-0.32
Earth Acquisition	At 23-18-4		-0.305	-0.24 (Interferometer)	
	During Oscillation 23-30		-0.185		~0
Later Check 151		-0.093		0 (DOC hold)	
RGA 2 Off			-0.153	0 (DOC hold)	
15 Minutes Later			-0.053	0 (DOC hold)	
14 Minutes Later			-0.126	0 (DOC hold)	
25 Minutes Later			-0.139	0 (DOC hold)	

no change in vehicle roll rate, the RGA 1 telemetry bias is given by the difference between true and telemetry rates. If the inferred rate computed above is used as "true", then the RGA 1 roll telemetry bias is $-0.18^{\circ}/\text{sec}$ ($= -0.27 + 0.09$). It should be noted that RGA circuitry tends to average RGA 1 and RGA 2 outputs when both are on. The approximate doubling in estimated telemetry bias from $-0.1^{\circ}/\text{sec}$ with both RGA's on to $-0.18^{\circ}/\text{sec}$ with RGA 1 only on is consistent with RGA 2 having zero bias and RGA 1 having $-0.18^{\circ}/\text{sec}$ bias at this time.

After sun acquisition at 150:21:10 Z RGA roll telemetry indicated near zero rate ($\sim 0.05^{\circ}/\text{sec}$) and "pseudo-rate wheels" was commanded. Indicated roll RGA telemetry remained essentially constant. Two independent means were now available for measuring roll rate:

1. The angular momentum stored in the pitch and yaw wheels was interchanged as the vehicle rolled while holding on the sun line. Using the characteristic period of the wheel drive signals the roll rate can be estimated at $+0.25^{\circ}/\text{sec}$. (See Figure 9-8).
2. The Interferometer was turned on before earth acquisition. Ground transmitters excited the Interferometer at about 150:22:59.

Indicated roll rate from Interferometer count changes was $+0.24^\circ/\text{sec}$ and the RGA 1 roll telemetry bias was therefore $-0.19^\circ/\text{sec}$ ($= +0.05 - 0.24$) at this time.

When Earth acquisition was commanded at 150:23:10, the negative roll jet fired in response to the $-0.25^\circ/\text{sec}$ command by the control system. Firing continued until RGA roll telemetry reached $-0.30^\circ/\text{sec}$ which is only $-0.05^\circ/\text{sec}$ less than the nominal ACS requirement to shut off the jet. It therefore appears as if the ACS was working correctly in response to the sensor output.

In Figure 9-53, the roll rate is seen to lag the jet action with a large out-of-specification lag (0.5 sec in nominal). The same phenomenon was observable during sun acquisition (Figure 9-52).

As the lagging RGA output decreased to below $-0.25^\circ/\text{sec}$ the control system correctly caused the positive roll jets to fire to control the rate. Roll RGA telemetry rate indicated as low as $-0.39^\circ/\text{sec}$ (150:23:16:15) before the rate increased to $-0.24^\circ/\text{sec}$ as measured by the Interferometer. At that time, the roll RGA indicated $-0.31^\circ/\text{sec}$.

The essential agreement between the RGA rate ($-0.31^\circ/\text{sec}$) and the Interferometer measurement ($-0.24^\circ/\text{sec}$) indicates that there is little or no bias in the RGA telemetry as such but there is an offset in the RGA output affecting both telemetry and output to the controller.

An estimate of the RGA offset can be made by considering the ACS control response during the attitude oscillation following earth acquisition. A rate signal from the RGA equivalent to about $-0.19^\circ/\text{sec}$ is required to null the ESA roll output of about 9.3 deg. The RGA telemetry at this time was $-0.19^\circ/\text{sec}$ which agrees with the result noted above that the gyro had a true offset of $-0.19^\circ/\text{sec}$ and essentially no telemetry bias.

Figure 9-54 which shows the vehicle roll history at earth acquisition indicates that the RGA offset was going toward zero slowly because the average ESA roll angle required for ACS "equilibrium" control was decreasing.

A re-check of RGA 1 and 2 on together followed by a RGA 2 turn-off was performed on day 151. The data indicated a roll RGA 1 value of $-0.151^\circ/\text{sec}$ after RGA 2 turn-off, which is consistent with the above. Changes with time are noted. These changes occurred without concurrent vehicle rates and therefore suggest that the RGA electronics associated with the measurement and conversion of RGA gimbal pick-off voltages to RGA output voltages are the source of the anomalous behavior.

9.6.1.3 Conclusions

1. During and after boom deployment, the RGA 1 roll output had an offset $-0.19^\circ/\text{sec}$ seen both at its telemetry and its output terminal. RGA 2 roll gyro had negligible offsets in both outputs.
2. Because the RGA telemetry indicated no essential error before launch, it may be concluded that the degradation in RGA 1 output occurred during launch and/or separation. The degradation is probably in the RGA electronics.

9.6.2 PSA Tracking Anomalies

On day 153, the PSA was activated and successfully acquired and tracked Polaris. However, the unit appeared to be tracking particles assumed to be products of outgassing. The PSA was then powered down and reactivated on day 155. Polaris acquisition and track was again successful, but similar tracking anomalies were again observed. Figures 9-55 through 9-58, are plots of the PSA2 yaw angle error signal, the Polaris acquired discrete, yaw wheel speed and the star intensity signal. In the plots the star intensity update rate is 48 seconds, while the other parameters are updated at 3 second intervals. The traces indicate several different types of tracking anomalies and suggest theories for their causes. These include a) solar reflections from the solar array or reflecting particles in the field of view causing false target tracking. b) solar reflections into the sun detector causing improper actuation of the PSA sun shutter.

Examination of the star intensity signal and PSA 2 Angle traces during the first 12 minutes of Figure 9-55, shows intensity variations associated with "small" PSA 2 hits ($-0.4^\circ + 1.0^\circ$). As indicated by the wheel speed, the ACS was responding to these high and low frequency PSA 2 yaw angle outputs. The false targets caused incremental negative polarity outputs for about the first 5 minutes of the plot. At 7 minutes, the unit rapidly tracked an object that was located about $+1.0$ degrees from Polaris for approximately 6 seconds. At 12 minutes, PSA 2 then acquired an object that appeared to originate at the Polaris location (-0.78 degrees) and tracked it to about $+2.9$ degrees. Although the 48-second Star Intensity signal does not indicate loss-of-target, the tracker switched to the flyback-and-sweep mode which is automatically initiated when the unit loses acquisition of the target being tracked. The loss-of-target-acquisition is however shown by the 3-second TLM sample rate Star Acquired signal. The ACS phasing is such that a positive rotation about the positive yaw axis causes a positive polarity change in the PSA 2 yaw angle signal. In response to this condition, the control loop issues wheel or jet drive signals to command negative yaw axis acceleration in order to null the positive polarity PSA 2 yaw angle signal. Therefore, the 5.3 degree per minute positive polarity target rate

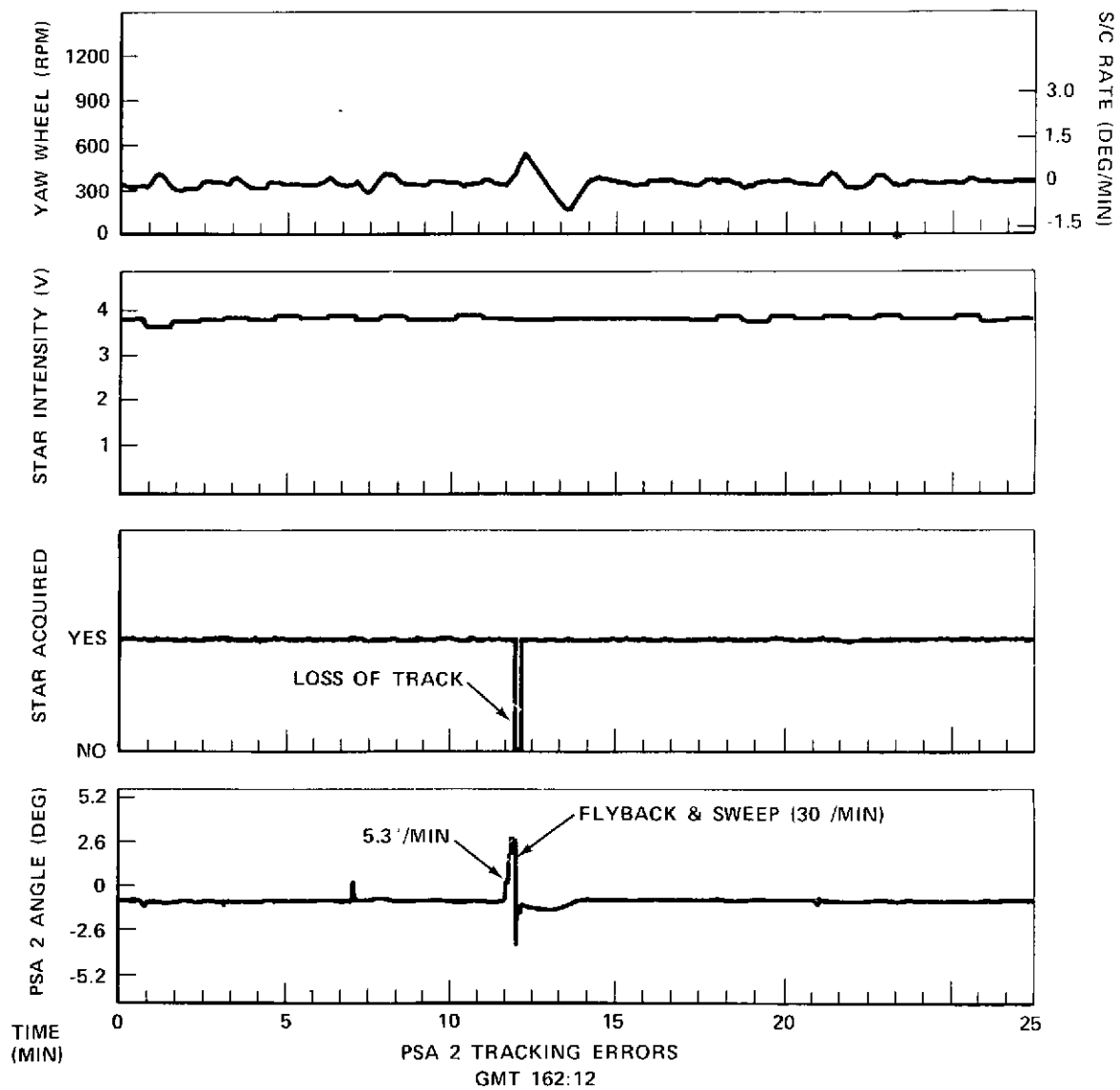


Figure 9-55

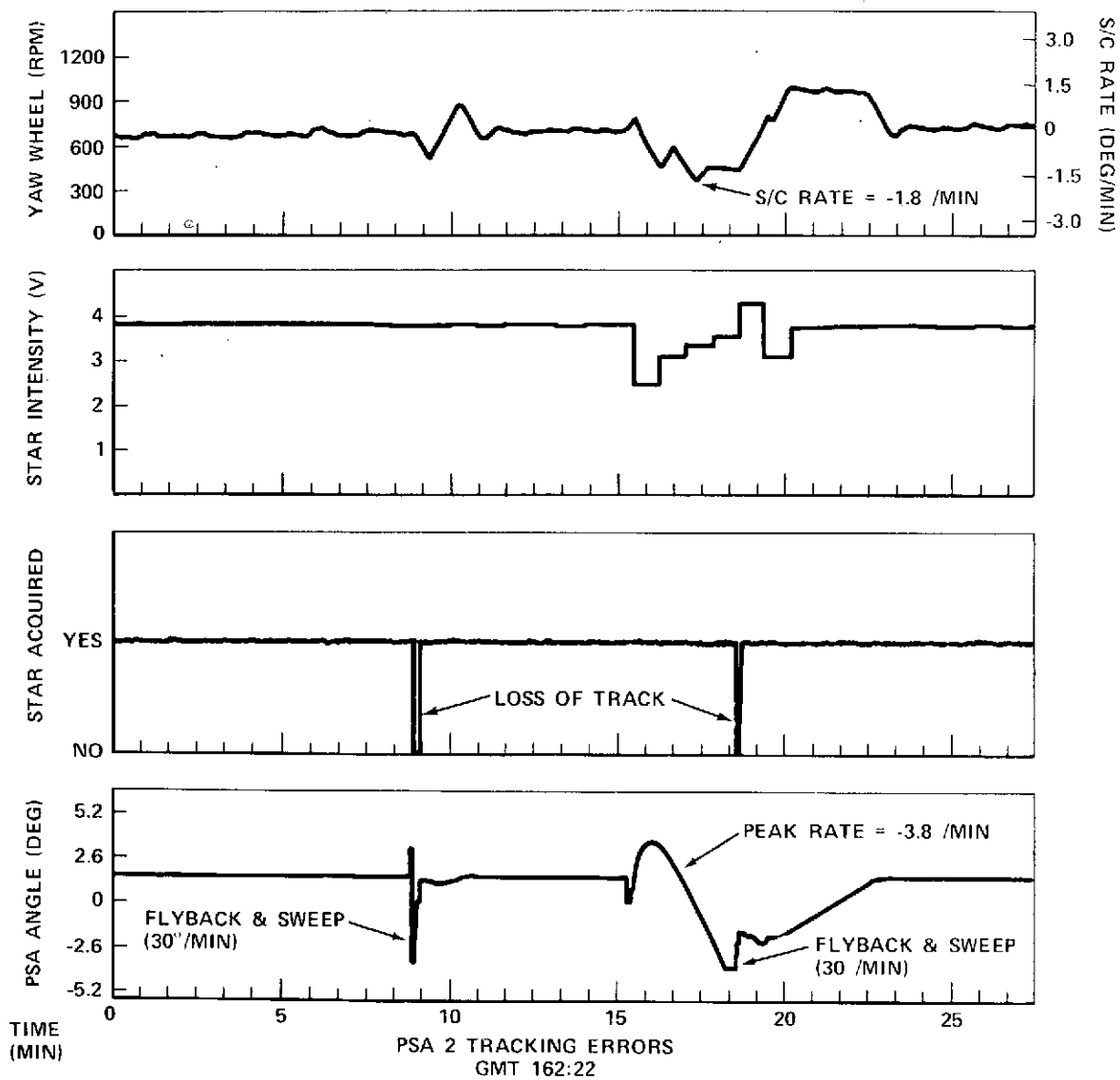


Figure 9-56

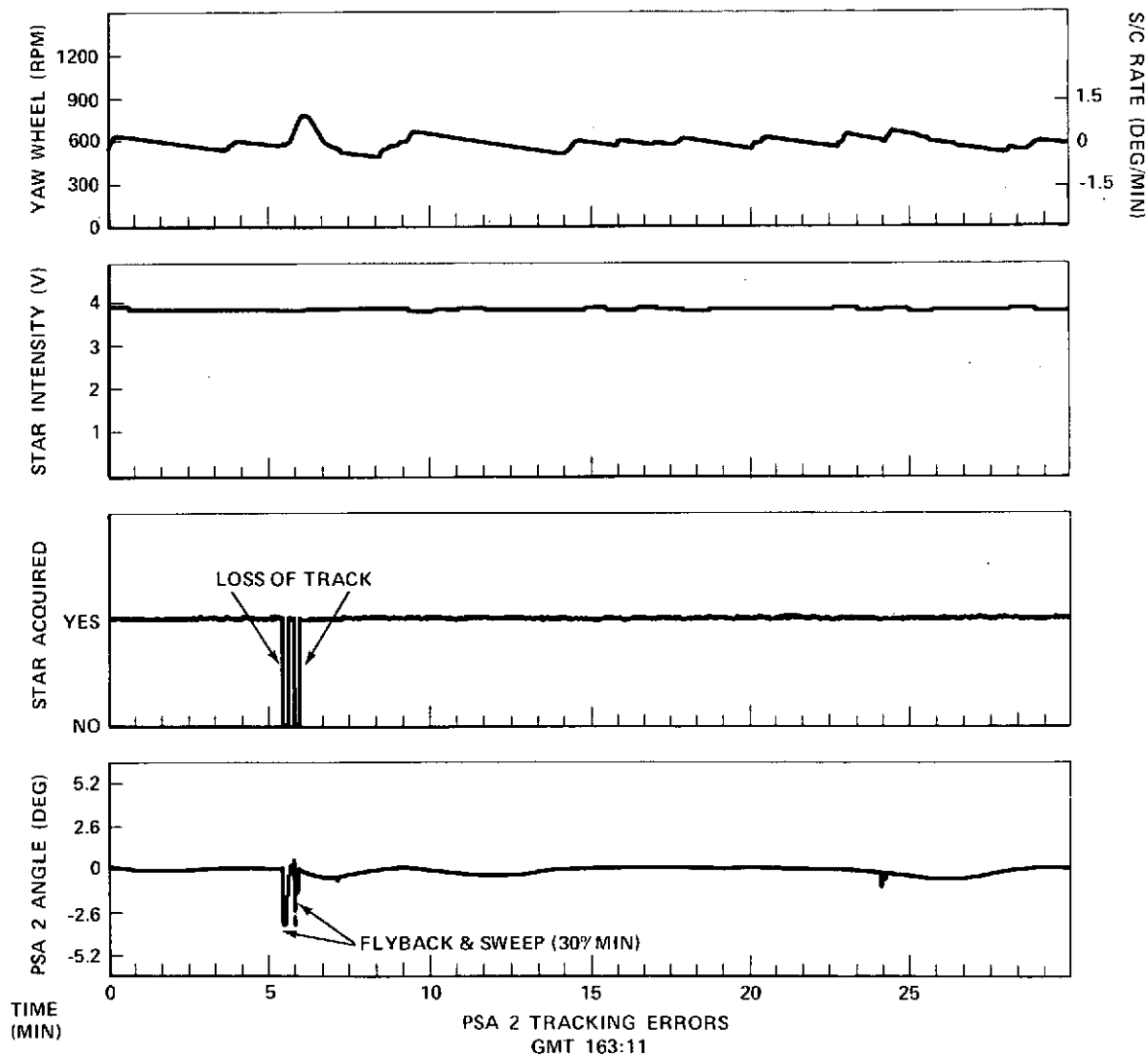


Figure 9-57

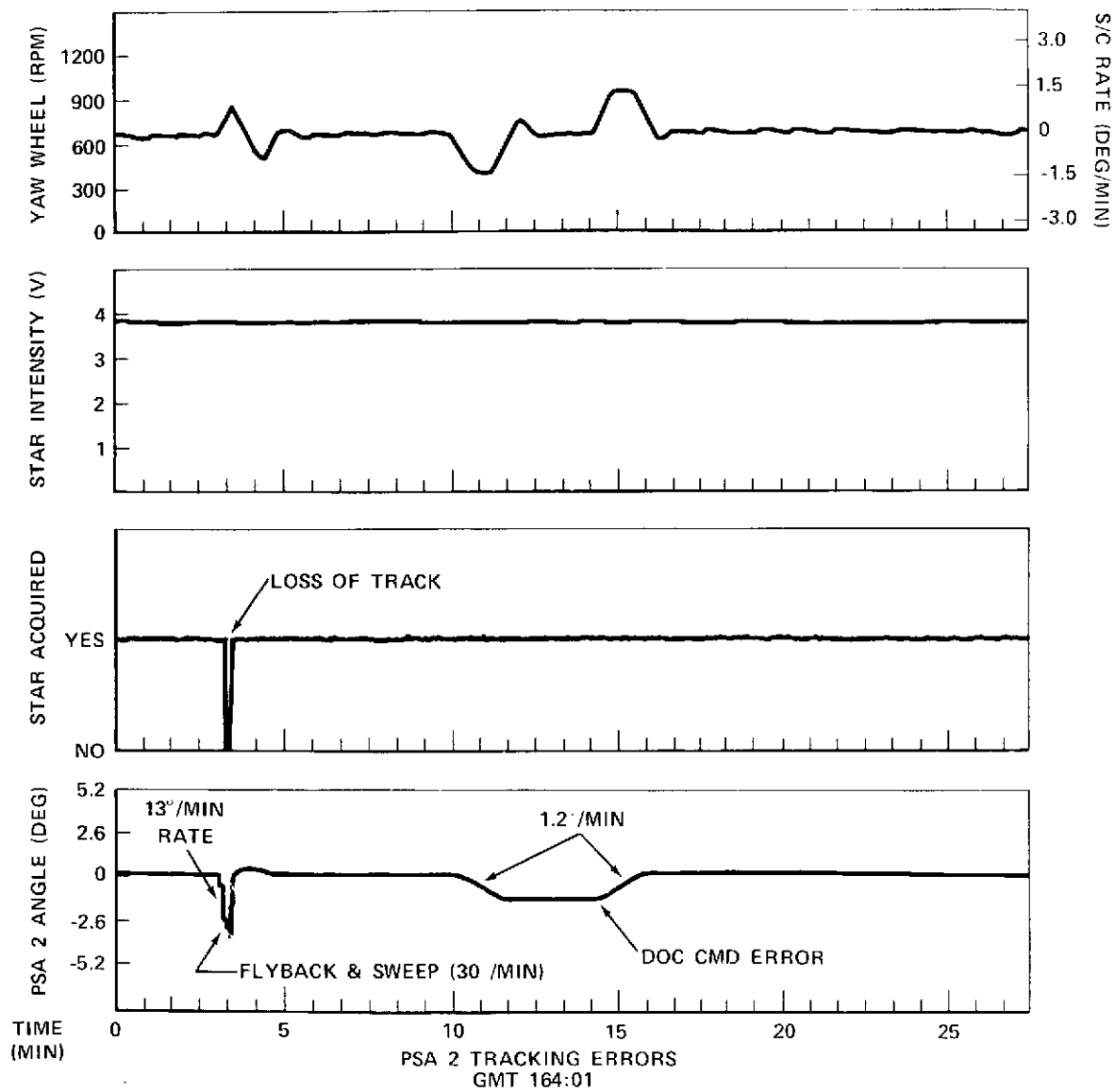


Figure 9-58

shown in Figure 9-55 caused the ACS to issue wheel commands to accelerate the spacecraft in a negative sense (negative yaw rate) in an attempt to reduce the magnitude of the PSA 2 yaw signal. Due to ACS response characteristics, the spacecraft had only corrected for about 0.3 degrees of the total +2.9 degree by the time the flyback-and-sweep occurred. It can be seen that Polaris was successfully acquired at about -0.3 degrees from the point at which the "bogey" target track was initiated. The PSA 2 yaw signal continued to increase in a negative sense due to the negative rate (-1.0 deg/min) the spacecraft had achieved in trying to track the false target. This error peaked at about -0.6 degrees.

Referring to Figure 9-56: at an elapsed time of 9 minutes, the tracker acquired a false target about +1.6 degrees from Polaris within a time span of less than one telemetry update (3 secs). Although not verifiable by the star intensity signal, either the brightness of the false target or actuation of the sun shutter caused a loss of target track thus initiating a flyback-and-sweep. Polaris was acquired and the resulting spacecraft error motion was about -0.5 degrees. At an elapsed time of 15 minutes on this recording, the unit acquired and tracked a false target that had a positive yaw rate motion as indicated by the PSA 2 yaw signal. This target traversed from 0 deg. to +3.6 deg. in about 40 seconds at which time it apparently changed direction and moved across the tracker field-of-view with a negative rate. The unit tracked the target to its saturated output level of about -3.6 degrees. The PSA output remained at about -3.6 degrees for about 150 seconds. Although the tracker yaw angle signal saturates at this level, its field-of-view extends about 2 degrees beyond this region. The false target was apparently tracked to the limits of the field-of-view but its yaw motion was too rapid for the spacecraft to follow and, as indicated by the loss of acquisition signal, it passed out of the field-of-view and the resulting automatic flyback-and-sweep reacquired Polaris. The spacecraft had moved approximately -3 degrees at the time Polaris was reacquired. Because of the negative yaw rate incurred in trying to track the false target, the PSA yaw signal showed an overshoot characteristic. In addition to this, there was about a -0.5 deg. "glitch" about 30 seconds after Polaris was reacquired. This object was tracked for about 20 seconds after which Polaris was reacquired and tracked. The tracking anomalies shown in this recording (Figure 9-56) are not typical especially in terms of the large variations observed in the star intensity signal. The aforementioned "glitch" was associated with an unusually high increase in star intensity (decrease in voltage).

Figure 9-57 depicts a "double hit" anomaly which is usually associated with gradual variations in the PSA 2 yaw angle signal. The small variations in star intensity in this recording are typical of this type of anomaly.

Figure 9-58 shows a "double hit" phenomenon which was associated with a DOC yaw command attitude software deficiency. At approximately 164:01:15 and 164:13:15, the DOC would issue erroneous pitch and yaw command attitude signals. The response shown in Figure 9-58 is typical of the yaw response to the DOC command error. Both DOC 1 and DOC 2 have been successfully reprogrammed and the pitch and yaw attitude anomalies no longer occur.

The tracking anomalies appear to be a function of time of day. Figure 9-59 is a plot of frequency of occurrence of tracking errors as a function of spacecraft local time.

Local 6 AM is equivalent to GMT 12 h 16 min. At this time, the +X axis is in its closest alignment to the sunline. Twelve hours later, the -X axis has an equivalent relationship to the sunline. The curve was generated by compiling the data obtained between days 158 and 178. The total number of tracking errors observed in half-hour intervals over the 24 hour orbit period for these days was averaged. The plot is indicative of the probability of observing a tracking error during any specific half-hour interval over the orbit. The largest number of anomalies appear to be centered around 4:30 AM and 8:30 AM local time. The smallest number occurs between 11 and 12 PM at which time the solar panels and reflector are not between the sun and the tracker field-of-view.

Figure 9-60 shows the frequency of occurrence of anomalies each day for days 158 - 178. This figure was prepared in order to assess whether or not the frequency was diminishing as a function of time. The data is inconclusive and studies of this phenomenon are continuing.

Although PSA 2 performance periodically results in loss of Polaris track, the DOC is operated in a mode which automatically switches the YIRU into the control loop when PSA 2 has lost acquisition. Subsequent automatic reacquisition of Polaris results in the DOC reselecting the PSA 2 reference and thus ground control intervention is not required.

At times, after a PSA 2 anomaly, the vehicle had a yaw attitude so large that reacquisition of Polaris could not automatically be accomplished. At these times yaw backup control using DSS was commanded. In this mode this DSS, with one-half degree resolution, is used as yaw sensor and the DOC, utilizing stored data, computes the required DSS output to maintain the same yaw attitude as would be achieved if the PSA 2 were operating. Polaris acquisition was then obtained by flyback and sweep, after stable DSS operation was achieved. Yaw attitude errors up to 0.5 degree have been observed, e.g. at 151:14:09. However, the errors can be much less since the attitude tends to hover about the transition angle towards which the vehicle is driven by the external torques.

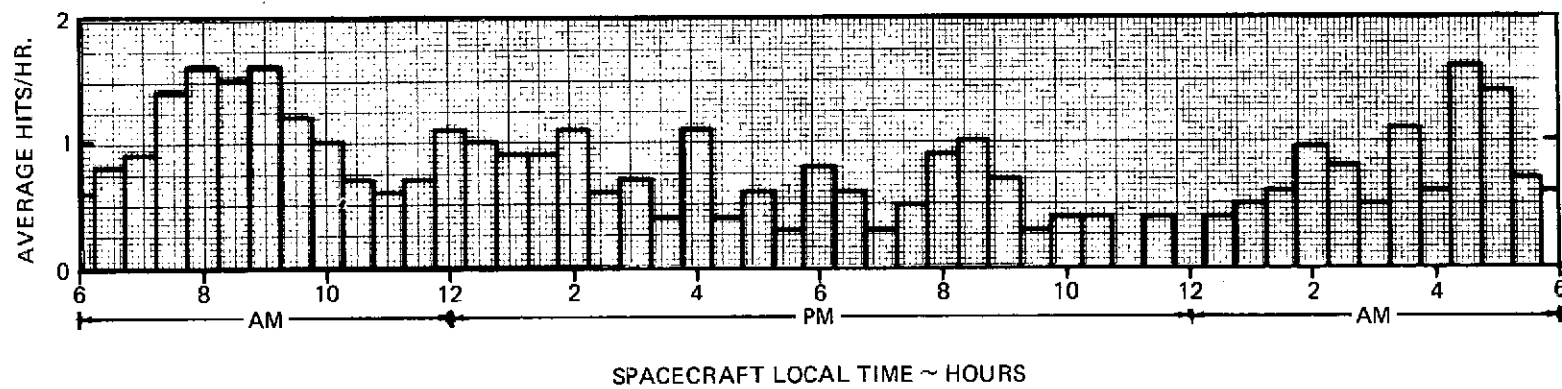


Figure 9-59. Average PSA 2 Tracking Anomalies ~GMT Day 158 - 178

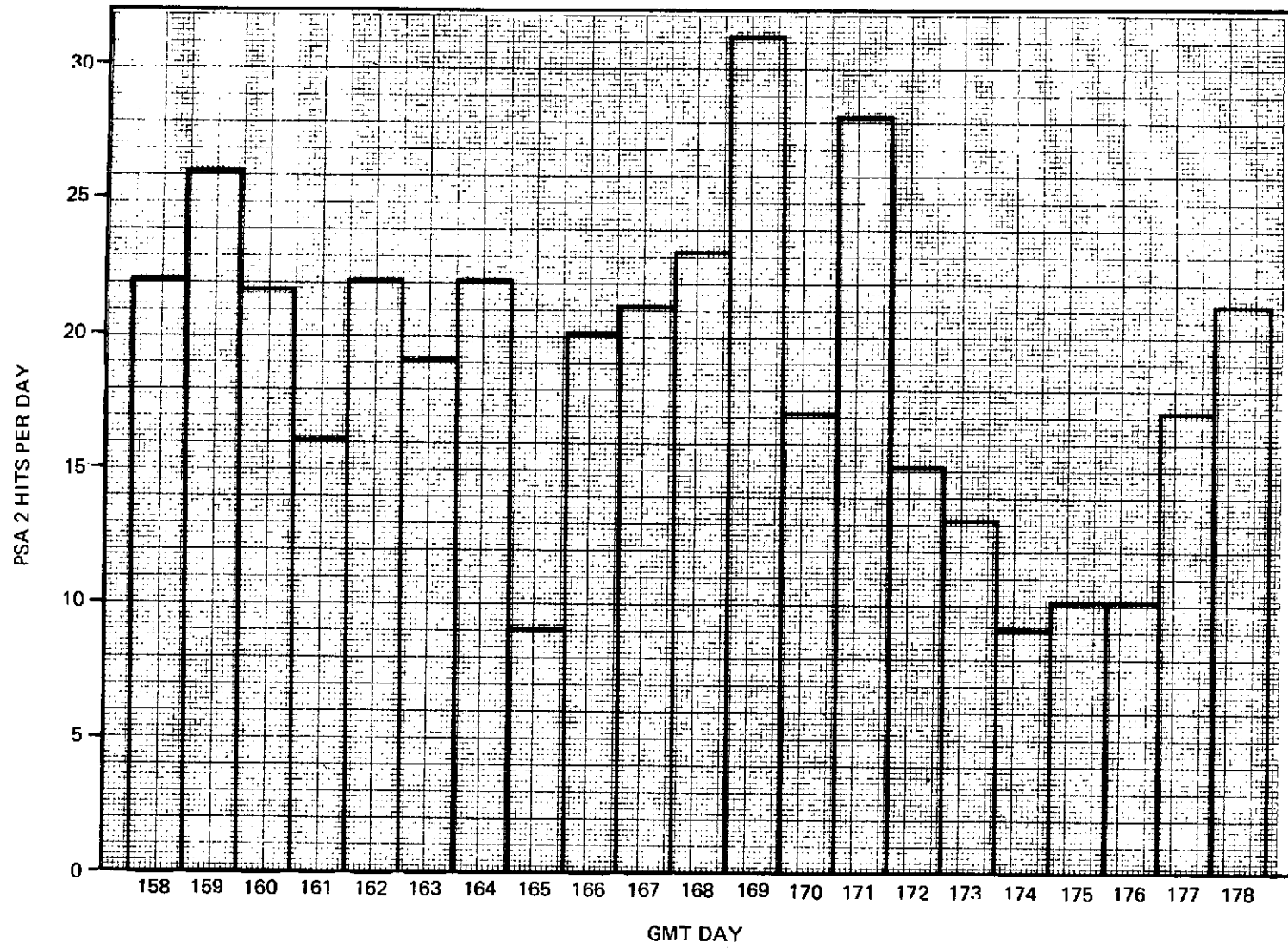


Figure 9-60. Histogram of PSA 2 Anomalies

9.6.3 YIRU Bias Anomaly

The YIRU drift characteristic is shown in Figure 9-61. The data was obtained while PSA 2 was in yaw axis control in Local Vertical Orbit Plane East Mode. In this mode the DOC is utilized to maintain the +Z axis along the local vertical and the +X axis in the orbital plane. When PSA 2 is used the DOC computes and commands the necessary yaw outputs so as to compensate for the diurnal motion of Polaris. The plot indicates a maximum YIRU drift term of 0.0622 deg/hr using the PSA as a reference. The YIRU electronics design provides for drift compensation over a ± 1.5 deg/hr range. This large rate bias range was provided so that during offset pointing operations, components of the orbital rate due to roll axis offsets up to ± 5.75 deg could be compensated (Rosman requires approximately ± 5.5 deg roll offset).

Compensation of the roll axis offset induced rates has been attempted several times. On occasion the results have indicated that the rate bias compensation drops out after about 15 minutes. At other times, the compensation remains for extended periods.

The residual drift causes the YIRU to move into its mechanical stops which are located ± 4 degrees about its null reference. The rate of drift is a function of the roll offset angle (target latitude) which is about 1.4 deg/hr for Rosman. The cause of loss of the YIRU bias compensation is not fully understood at this time and is the subject of further evaluation and test.

9.6.4 DOC Command Angle Anomaly

Pitch attitude and yaw attitude command angle anomalies were observed in both DOCs twice each day. The phenomenon was observed only during normal ACS operations in the Offset Point Ground Coordinates mode at approximately 13:20 and 12 hours later at 01:10. At these times the pitch command attitudes would change polarity and the yaw command attitudes would change in magnitude by ± 0.75 deg. The command errors were transient in nature and were such that the incorrect commands were issued by the DOCs for approximately $3 \frac{3}{4}$ minutes. After this interval, the correct command angles would be issued until the next occurrence 12 hours later.

The spacecraft response to the incorrect command angles is shown in Figures 9-62 and 9-63 which illustrate spacecraft attitude response to the transient commands in terms of the ESA roll and pitch angles and PSA 2 yaw angle. For completeness, the roll, pitch, and yaw wheel speeds are also presented. At 159:13, DOC 1 was controlling in the Offset Point-Ground Coordinates mode with the vehicle Z axis pointing at the equator at 94 deg West longitude. At 159:13:19,

9-92

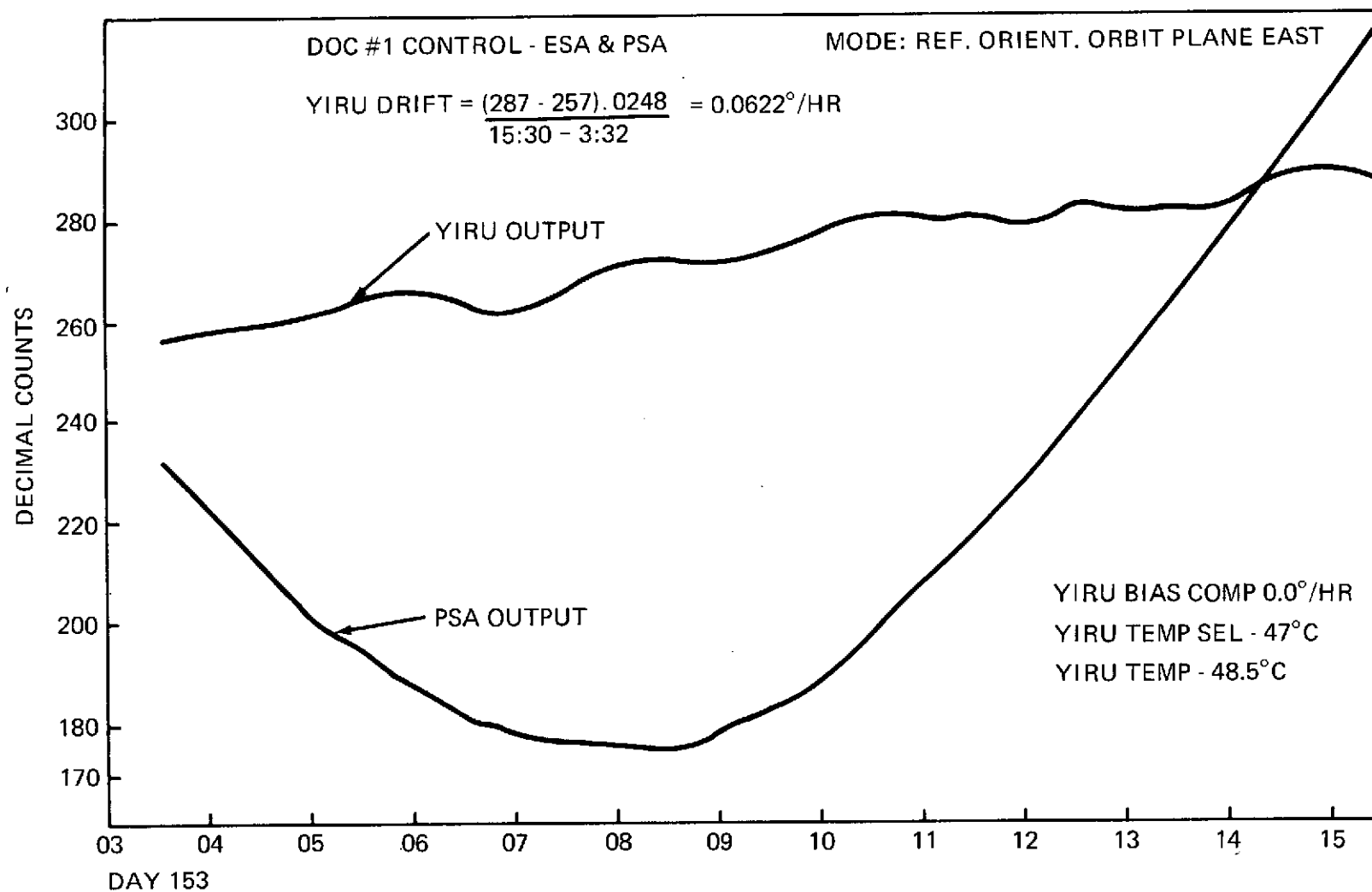
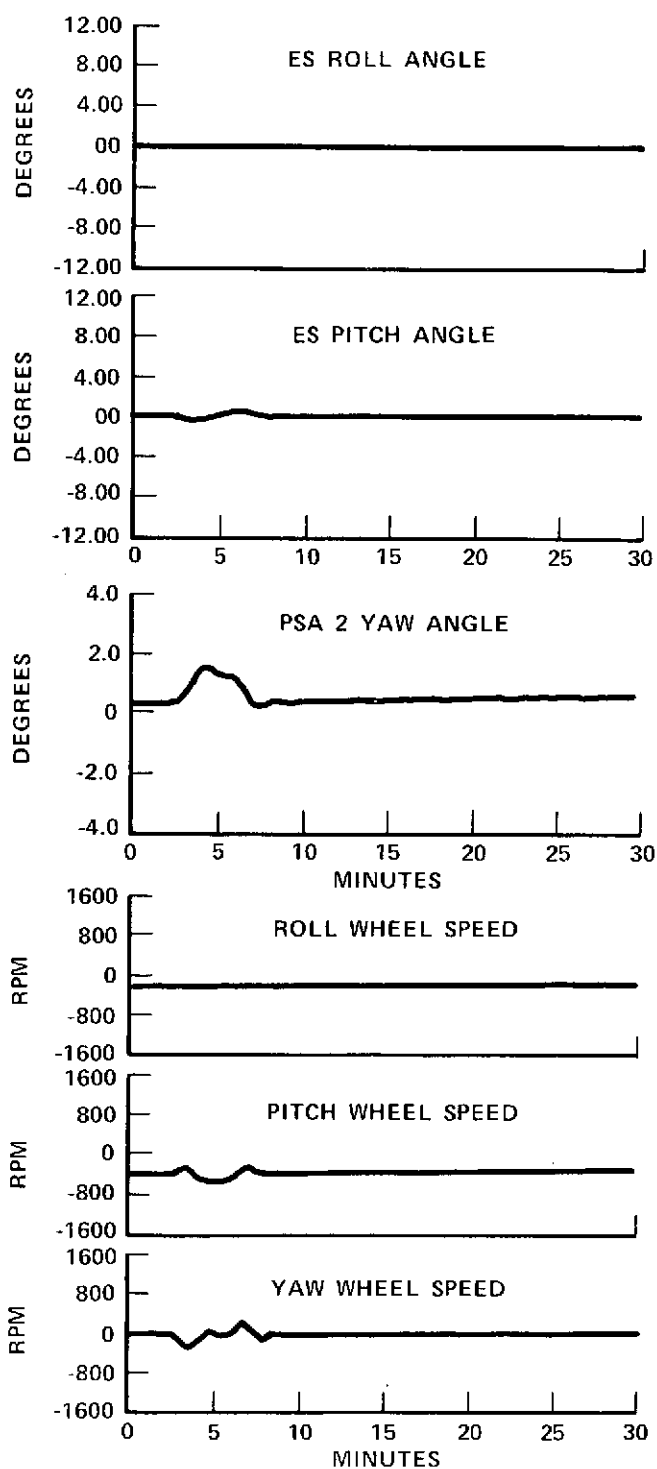


Figure 9-61. YIRU Drift Characteristic



START 159:13:17.18T

STOP 159:13:46:97.904

Figure 9-62. DOC Command Anomaly (A.M.)

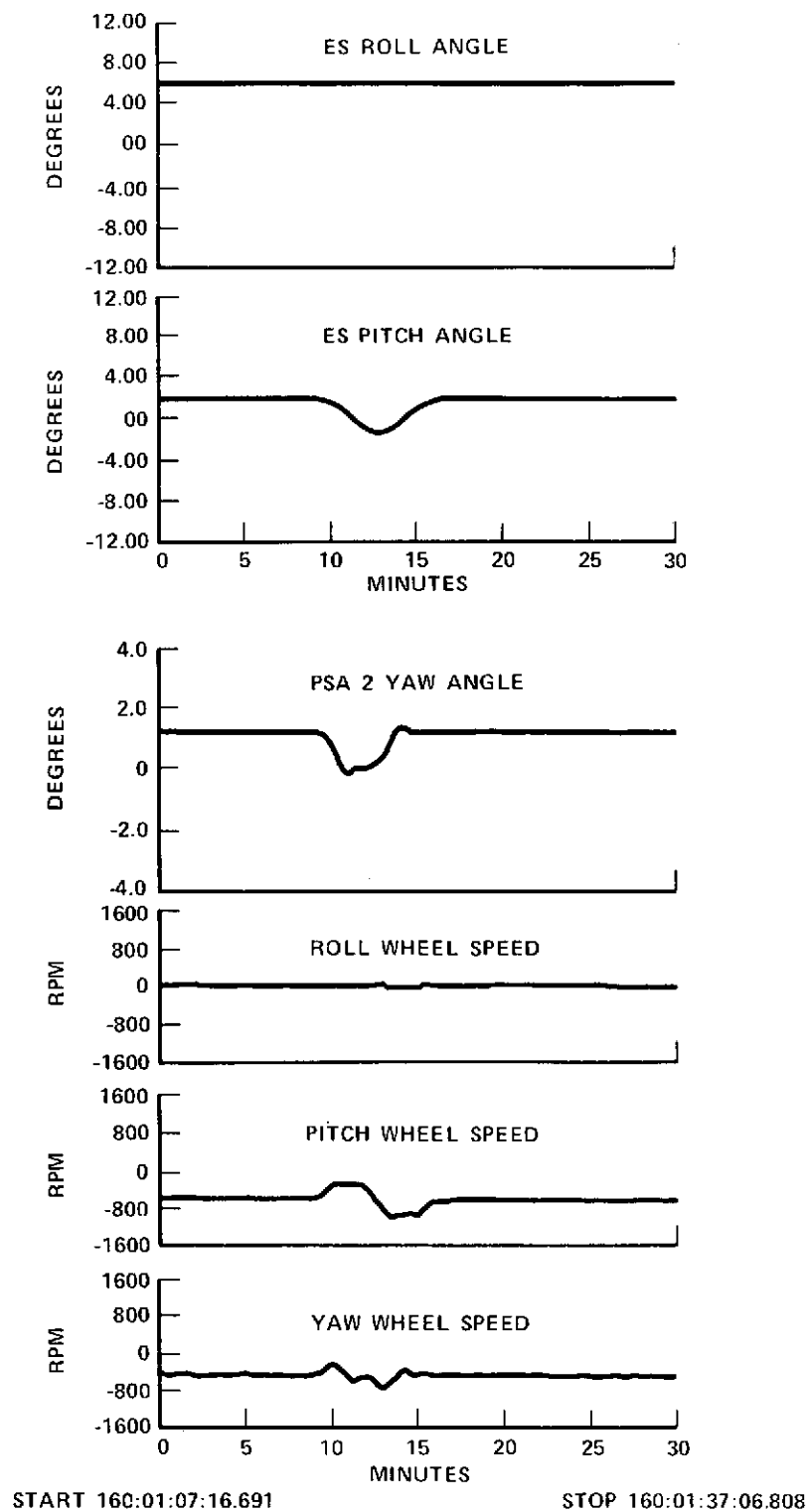


Figure 9-63. DOC Command Anomaly (P.M.)

the pitch command angle anomaly caused a pitch attitude transient of $-.32$ degrees and a yaw transient of about -1.0 degree. The total time from the initiation of the incorrect command angles to settling after correct command angle issuance was approximately $6\frac{1}{2}$ minutes.

The corresponding transient some 12 hours later started at 160:01:15. Then the ACS was in Offset Point-Ground Coordinates mode with the Z axis pointing at Rosman. The DOC pitch command caused a pitch attitude transient from $+1.84$ to -1.5 degree and back to $+1.84$ deg. The corresponding yaw angle transient covered about -1.2 deg. The incorrect command angles were generated for about 3 minutes and the overall transient lasted 6 minutes.

The command angle discrepancies were isolated by Honeywell analysts to an overflow in the register for one of the elements of the inertial-to-local-vertical transformation matrix. On Day 163, DOC 2 memory locations pertinent to the parameters in the command attitude algorithm were reprogrammed via the DOC Uplink Program. This was performed while DOC 1 was in control. Subsequent passes at approximately 163:13:15 and 164:01:15 were monitored for DOC 2 pitch and yaw command attitude errors. It was verified that the preliminary software modification was satisfactory and DOC 2 was then placed in control. On Day 179 DOC 1 was successfully reprogrammed in the same manner and is currently being used for control with no further anomalies.

9.6.5 Interferometer AGC IF #2 Anomaly

The Interferometer subsystem, after being off between days 2 and 5, was commanded ON again to perform spacecraft axis calibration. Interferometer AGC #2 failed to respond. After 45 minutes of operation AGC #2 responded correctly and continued to perform properly.

While this anomaly has occurred several times it does not preclude satisfactory operation of the Interferometer on frequency 1 and it in no way compromises spacecraft performance. This may be understood in view of the fact that the F 2 channel is a redundant angle sensor for single station F 1 operation. For two station F 1 and F 2 operation, frequency F 1 may be switched, alternately, between station 1 (Rosman) and station 1 (Mojave) - as an example, and yaw data may be computed.

Nominally the telemetered AGC voltage varies from 3.0 volts to 0.8 volt for variations of R-F signal inputs to the Receiver/Converter from -95 dBm to -55 dBm. The AGC voltage is also utilized within the I. F. Amplifier to control I. F. gain over its dynamic range. The anomaly observed indicates that the AGC amplifier output went to zero volts for no R-F input to the

Receiver/Converter. This level of AGC voltage (zero volts) cuts off or reduces the gain of the I. F. Amplifier, when in fact the amplifier should be at full gain.

Based on this behavior, a preliminary failure analysis was performed at IBM. Through this analysis it was determined that if any of three (3) components associated with the AGC amplifier initially malfunctioned in an open-circuited state, the AGC amplifier output would go to zero volts, and hence cut off the I. F. amplifier. Further investigation is being pursued to determine the malfunction mechanism associated with the AGC amplifier. This is being accomplished by simulating component failures in the engineering model I. F. amplifier located at IBM.

SECTION 10
SPACECRAFT PROPULSION SUBSYSTEM (SPS)

SECTION 10

SPACECRAFT PROPULSION SUBSYSTEM (SPS)

10.1 SUBSYSTEM PERFORMANCE

The SPS operated as expected during launch and has performed well during the first 30 days in orbit:

- 1) All commanded functions have responded as designed.
- 2) All telemetry channels are normal. During ground testing, an RFI problem with erroneous SPS 2 catalyst bed temperatures was observed. This appeared initially to have corrected itself. However, when the prime focus feed was utilized, errors returned. A special "calibration" test to quantify the effect is recommended below.
- 3) The line evacuation of SPS 1 using ACS sun acquisition mode errors to activate jets was not completely "automatic" because of small yaw errors, and an orbit-control jet (OCJ) was manually commanded open for five minutes to evacuate the OCJ manifold. Propellant bleed-in was then done by commanding the latch valves open.

SPS 2 was evacuated manually, putting it in a near-ready condition for jet actuation. Because no propellant has been bled in, it is safer from a thermal standpoint.

- 4) The SPS 1 jets were used successfully during the initial acquisition, one reacquisition, two orbit correction maneuvers and eleven wheel unloads.

Performance during the steady state orbit correction firings was very close to predicted and resulted in very small errors in the predicted changes in drift rate and other orbital parameters. Because of the highly accurate Titan III-C launch and Transtage orbit insertion, approximately 18 lbs. of the fuel allocated for reference attitude/orbit acquisition was not expended.

Jet operation during the acquisition maneuvers was satisfactory although the initial maneuver was inefficient in fuel consumption due to rate sensor errors and bias. During the reacquisition many -yaw short pulses were observed. This condition will be investigated further.

The .2 sec. on/10 sec. off jet duty cycle during wheel unload is giving consistent values of impulse and based on known wheel momentum changes, the delivered impulse appears to be as predicted. Additional studies will be required to more accurately determine jet performance in the short pulse mode.

- 5) Tank pressure blowdown correlates well with calculated propellant consumption and will improve as the pressure moves down from the steep part of the curve. However, because of variations in the telemetered pressure-temperature data, one or two daily cycles must be known before a pressure value can be selected for use with the blown-down curve. These variations may be due to the fact that tank temperature is measured in liquid, while the pressure is dependent on the gas temperature, which varies more widely.
- 6) Initial inorbit temperature cycle data indicated that the truss mounted (OCJ) thruster valves were warmer than predicted, and it was decided to turn off the catalyst bed heaters until just before jet firings.

Tank temperature cycling is somewhat greater than expected, but catalyst bed temperatures and the thermostatically controlled line temperatures are cycling as predicted.

Catalyst bed temperature gives a good indication of jet operation and the valve temperature rise due to heat soak-back following jet firing is not excessive.

No functional failures or anomalies have occurred, jet performance is good and while some component temperature cycles are not as predicted, all temperatures are well within acceptable limits.

10.2 PRELAUNCH/LAUNCH

Launch configuration of the SPS is illustrated in Table 10-1.

The tank pressures at launch were 371 and 377 psia nitrogen gas at 20°C. Temperature telemetry was checked periodically from the time the tanks were loaded with hydrazine on May 18 (55.6 lb. Tank 1 and 55.0 lb. Tank 2) until launch. Table 10-2 lists the catalyst bed temperatures from one week before launch through initial acquisition. The prelaunch data includes the anomalous telemetry values for the SPS 2 OCJ beds. These anomalies were first observed during ground RFI tests and remained after RFI shielding had been added to the SPS ACE connectors. The all-up RFC test then indicated that the use of the omni antenna would essentially eliminate these errors, and that they would be significantly reduced when using the prime focus feed. Instability had also been observed in this telemetry during the spacecraft vibration test.

Similar effects were seen during the initial phases of the launch when the SPS 2 OCJ temperatures oscillated as much as 30°C. Table 10-2 shows that the temperature errors disappeared after the shroud was jettisoned, but then reappeared in a few cases. In evaluating OCJ temperatures care must be exercised because of the differential heating effect of the shifting sun angle on OCJ thrusters. A special test, turning off the prime focus feed elements and switching to the omni antenna, will be required to sort out the relative effects of prime focus RF power on the cat-bed temperatures.

Table 10-1
Launch Configuration

	SPS 1 On & In Control	SPS 2 On
EVM LV's	Close	Close
OCJ LV's	Close	Close
Cross LV	Close	
Tank LV's	Open	Open
Valve Heaters	Prime On	Prime On
Line Heaters*	Low Auto	Low Auto
Bed Heaters	Off	Off
Ground Control Jets	Enable	

*Prime and backup

Table 10-2
SPS Cat Bed Temperatures/RFI

		5-24-74 SC PWR On	5-30-74 4:05 AM SC PWR On	SHROUD 5:01 AM Pre- Launch (LC40)	T-4 MIN Pre- Launch	NO SHROUD (OMNI) T+45 Shroud Off, Pre- Shadow Cool	T+1:30 Post Shadow Warm	T+6:14 Trans- Orbit	DEPLOYED T+8:03 SPS 1 On, Sun On SPS 2	T+9:32 SPS 1 On, Sun On SPS 1	T+15:29 1:70 Post Yaw, Sun On SPS 2
SPS 1	1 -R	23	23	23	23	27	19	23	100	140	145
	2 +R	15	15	19	19	19	19	27	104	136	132
	3 -P	23	23	19	19	19	15	27	83	156	128
	4 +P	23	23	27	27	15	15	27	120	144	160
SPS 1	5 +Y	27	23	31	27	31	11	27	85	144	140
	6 -Y	15	11	19	19	23	11	23	87	132	104
	7 WP	19	15	19	19	27	11	23	79	144	112
	8 WB	15	11	15	15	23	11	19	83	160	128
SPS 2	9 -R	27	23	19	19	23	15	19	15	7	31
	10 +R	23	27	19	15	19	19	23	15	7	7
	11 -P	19	19	15	15	19	15	27	3	55	11
	12 +P	11	11	11	11	11	11	19	39	11	47
SPS 2	13 -Y	31	27	27	31	27	11	23	23	-5	47
	14 +Y	95	71	51	43	23	15	23	27	-9	23
	15 EP	35	35	43	43	15	7	19	43	-9	55
	16 EB	79	59	67	58	23	11	27	39	-5	63

NOTE: During early 1st stage burning SPS 2 OCJ temps were unstable (± 30 C) while shroud was on.

The predicted warming trend of the SPS propellant lines and thruster valves due to atmospheric pressure decrease was observed during the ascent phase. All line heaters were on at launch; the SPS 1 and 2 backup heaters went off at T+2:30 and T+2:45 hours and the prime heaters went off at T+2:46 and T+3:32 hours. The prime heaters came back on within a half hour and stayed on for one hour. This cycle was repeated before separation. Once in-orbit operations began, the primary heater on and off times increased to 12 HRS ON/12 HRS OFF for SPS 1 and 16 HRS ON/8 HRS OFF for SPS 2, while the backup heaters had a much shorter duty cycle. The different on-times were probably due to the different daily sun-shadow patterns on the two systems.

Tank pressure remained steady throughout the ascent while cat-bed temperatures varied as a function of sun angle and earth shadow.

10.3 LINE EVACUATION/PROPELLANT BLEED IN

In preparing the SPS 1 for jet operation, the 10 psig nitrogen in the EVM and OCJ manifolds down-stream of the EVM and Truss latching valves was evacuated (150:20:34 to 150:21:00). The method was to be "automatic" by commanding the ACS to Sun Acquisition Mode using jets, before the latch valves had admitted hydrazine to the jet manifold lines, thereby allowing attitude errors to open roll, pitch and yaw jets. However, only roll and pitch errors were large enough to activate the appropriate thruster valves, so that only the manifolds within the EVM were evacuated. It was necessary to command open the #7 jet (Prime Westward) for five minutes to accomplish evacuation of the OCJ manifold.

The SPS 1 EVM and Truss latch valves were then opened (150:21:06) bleeding propellant into the manifolds. The initial Tank 1 pressure drop seemed excessive at latch valve opening but a closer estimate of the internal manifold volumes (12.6 cubic inches, equivalent to .47 lb. N_2H_4) accounts for the 6 psi pressure drop from 371 to 365 psia.

The evacuation and bleed in of SPS 2 was delayed for one day to assess in-orbit temperature cycling before filling hydrazine into the back-up system. The evacuation was then accomplished by ground command to roll, pitch and the eastward prime thruster (151:20:40 to 21:20). As a further thermal safety measure, SPS 2 propellant bleed-in was not done and will not be until the back-up system is actually needed.

10.4 JET USAGE/PERFORMANCE

10.4.1 Spacecraft Acquisition Maneuvers

The detailed assessment of spacecraft performance from an attitude control viewpoint is located in Section 9. Only specific areas of SPS interest will be discussed here.

Table 10-3 lists the total jet ON times for the three axes for each maneuver during the initial acquisition during days 150-151 and the reacquisition maneuvers on day 161. The length of individual jet firings is distributed as follows:

Number of Jet Actuations

<u>Jet On Time, sec</u>	<u>Initial Acquisition</u>	<u>Reacquisition</u>
200	1	0
100-200	3	0
75-100	9	0
50-74	5	4
25-49	7	5
10-24	14	1
4-9	34	20
0-3	13	29

The on times are fairly long with most firings over 10 seconds. Because of this, an average specific impulse of 210 seconds was used in calculating the quantities of propellant used. The reacquisition did not require a Polaris (yaw) maneuver, but even were fuel to be added to account for it, the amount of fuel used was significantly less (by a factor of 4) than during the initial acquisition. The discussion of RGA rate and bias errors in the ACS section details the maneuvers that used the extra fuel during the first acquisition. Subsequent acquisitions should require only 0.4 to 0.5 lbs. of fuel.

A maneuver-by-maneuver analysis of spacecraft motion to determine jet performance has not been made, partly because of the complexity of separating jet firings during simultaneous motion in several axes. However, the relative order and magnitude of jet on-times is as expected for the three axes in arresting or generating rotation rates. The calculated jet on-times for initiating a .25°/sec rate in roll, pitch and yaw are 62.5, 47.5 and 101 seconds respectively.

Table 10-3
Acquisition Jet Usage

Initial Acquisition:	<u>Roll</u>		<u>Pitch</u>		<u>Yaw</u>		<u>Total On Time, sec.</u>	<u>Wt* Propellant, lb.</u>
	+R	-R	+P	-P	+Y	-Y		
Sun	131 sec.	50	166	94	220	35	696	.40
(GMT)	(150:21:10 to 16:00)		(21:10 to 21:19)		(21:10: to 21:21)			
Earth	737	759	81	105	0	0	1682	.96
	(150:23:10 to 24:02)		(23:18 to 23:20)		—			
Yaw	0	0	0	0	75	45	120	.07
	—		—		(151:01:46 to 02:20)			1.43 lb.
Reacquisition:								
Sun	9 sec.	0	51	69	108	186	423	.24
(GMT)			(161:11:48 to 12:01)					
Earth	39	87	0	6	0	24	156	.09
			(161:12:01 to 13:11)					.33 lb.

*Jet thrust = .120 lbf; Specific Impulse = 210 sec.

10.4.2 Initial Orbit Correction

The highly accurate orbit attained by the Titan IIIC-Transtage required only small corrections by the SPS. In general, the spacecraft was West of the desired 94°W station with a small westward drift. Two correction firings of jet #7 were initiated in days 157 and 158. The first was an 8 minute calibration firing followed the next day by a 31.5 minute run.

Table 10-4 shows the pertinent data. The deviations between the calculated correction and the actual orbit change were very small:

	Measured Deviations	
	1st Burn	2nd Burn
Drift Rate, deg/day	0	0.0011
Semi Maj. Axis, km	0.196	0.30
Eccentricity	0.0001	0.000044
Inclination, deg	0.004	0.0002
RA Node, deg	0.06	0.06
V, ft/sec	0.001	0.024

The #7 orbit control jet thrust vector is canted in the -Y direction above the spacecraft center of mass causing #3 (minus) pitch jet firings for attitude control. The -P jet contributes about 2.4% of the total orbit correction impulse (approximately equal to duty cycle); 1st Burn = 2.1%, 2nd Burn = 2.4% (see Table 10-4). The theoretical duty cycle calculated from the ratio of #7 and #3 (-P) jet moment arms about the spacecraft center of mass is 1.7%. Uncertainties in location and cant angles of the jets, center-of-mass location and jet impulse all contribute to the difference.

The total fuel used for the orbit correction was 1.28 lb., while 1.43 lb. were used for reference attitude acquisition. A total of 21.22 lb. had been allocated for these maneuvers which provides an extra reserve of 18.5 lb.

10.4.3 Wheel Unloading

Eleven wheel unloads have been performed as of June 28, (day 179). A detailed analysis of all unloads is found in the Section 9. During initial spacecraft maneuvering, the pattern of wheel speed cycling and momentum exchange was not clear and the initial unloads were inefficient in jet fuel. Figure 10-1 illustrates the current Roll-Yaw wheel momentum exchange through the orbit day when the spacecraft is undisturbed by slew or other maneuvers. Wheel speeds were allowed to increase as they accumulated and exchanged momentum. Unloading was done in roll because of the larger jet moment arm (6.3') compared to

Table 10-4
Initial Orbit Correction

	#1		#2	
	Start	Stop	Start	Stop
EDT	74-06-06 15:47:27		74-06-06 15:49:07	
Orbit Data:				
Semi Maj Axis, km	42186.4	42181.2	42180.9	42160.7
Eccentricity	.0007	.0006	.000624	.000156
Inclination, deg	1.749	1.748	1.748	1.748
RA Node, deg	266.12	266.06	266.06	265.97
Drift Rate, deg/day	.271 W	.203 W	.205 W	.0536 E
Sub Sat Long, deg	96.45	96.44	96.52	96.53
Spacecraft Wt, lb.	2971.0	2970.7	2970.7	2969.7
Jet #7 Duration, sec.		480		1888.4
V, ft/sec		.63		2.42
Wp, lb.		.27		1.01
Thrust, lbf. (ave)		.122		.122
Tank 1 Press, psia	359.4	355.4	357.4	345.4
Tank 1 Temp, °C	26	25	26	25
Remaining Fuel, lb. *	54.2	54.1	54.1	53.1
AC Jet .1 sec Pulses				
-Pitch (I, lb sec)	103	(1.22)	460	(5.42)
+Yaw	2		43	
-Roll	0		15	

*As determined by Maneuver Program

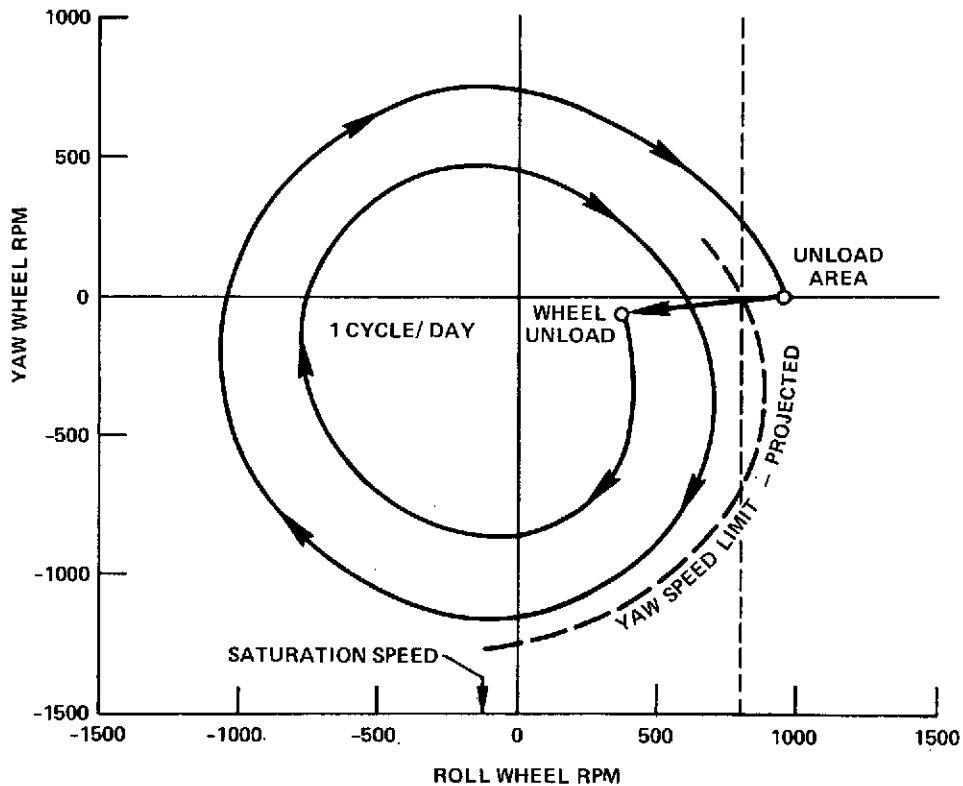


Figure 10-1. Current Pattern of Wheel Unload
When Pointed to Rosman

yaw (2.5'). This was accomplished when the roll wheel speed is maximum and the yaw wheel speed approaches zero, about 8 hours before the time the yaw wheel would exceed its saturation speed. Two days were required to reach this condition and about twenty .2 sec ON/10 sec OFF pulses unload the roll wheel an equivalent 410 RPM.

The first unload in both Roll and Pitch gave the following data:

AXIS	RPM	Wheel Impulse lbf sec	.2/10 Jet Pulses	Jet Impulse lbf sec
Roll	286	.308	15	.330
Pitch	261	.280	11	.242

Uncertainties of 5 to 10% in wheel speed, impulse bit and on-time contribute to the +6.7 and -13.5% differences between the wheel and jet impulse. Refined analysis may sort out the contributions of the various errors.

Figure 10-2 illustrates the -R jet performance for the wheel unload duty cycle. Note that both the jet bit impulse and specific impulse increase as the .2/10 pulses accumulate.

Current wheel unload fuel consumption is as follows using $I_{bit} = .022$ lbf-sec average and $I_s = 140$ sec average:

.0031 lb/20 pulse unload
.052 lb to date (11 unloads)
.573 lb/year (20 pulses/2 days)
(6.22 lb was allocated for 54 mo. of unload
= 1.38 lb/year)

10.5 TANK BLOWDOWN/PROPELLANT CONSUMPTION

Figures 10-3 and 10-4 are the blowdown curves for Tanks #1 and #2. All propellant has been drawn from Tank #1.

The total propellant drawn from Tank #1 was calculated as 3.56 lb* with 52.04 lb. remaining.

*Includes 0.47 lb of propellant used during bleed-in of propellant lines.

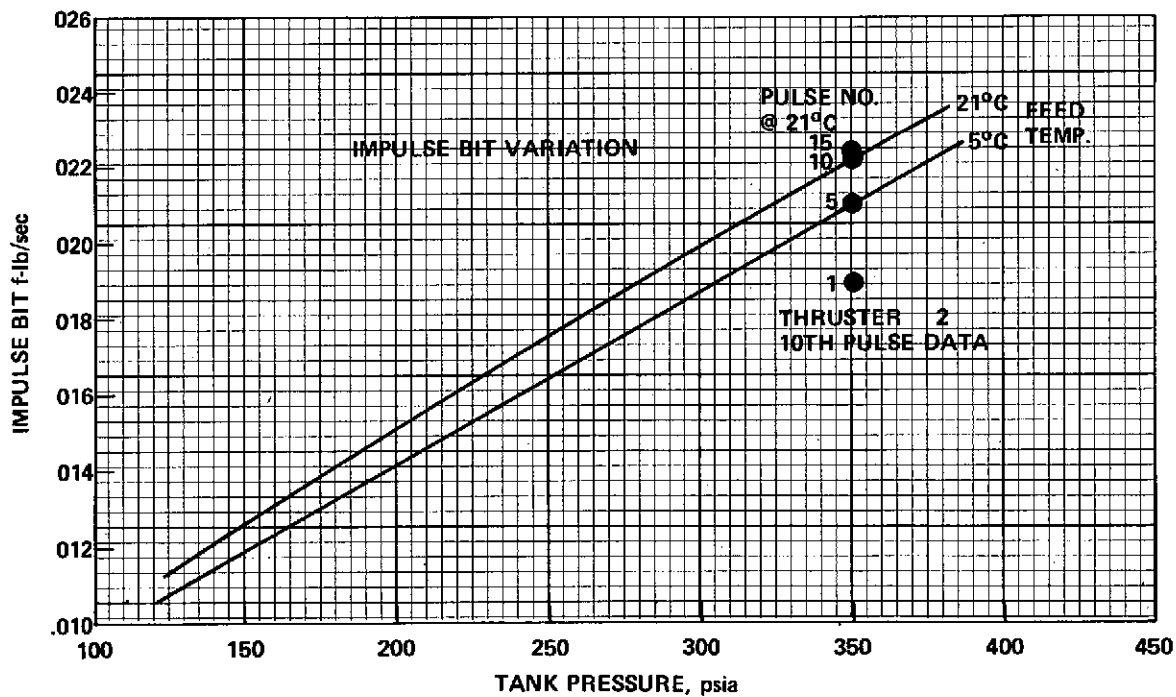
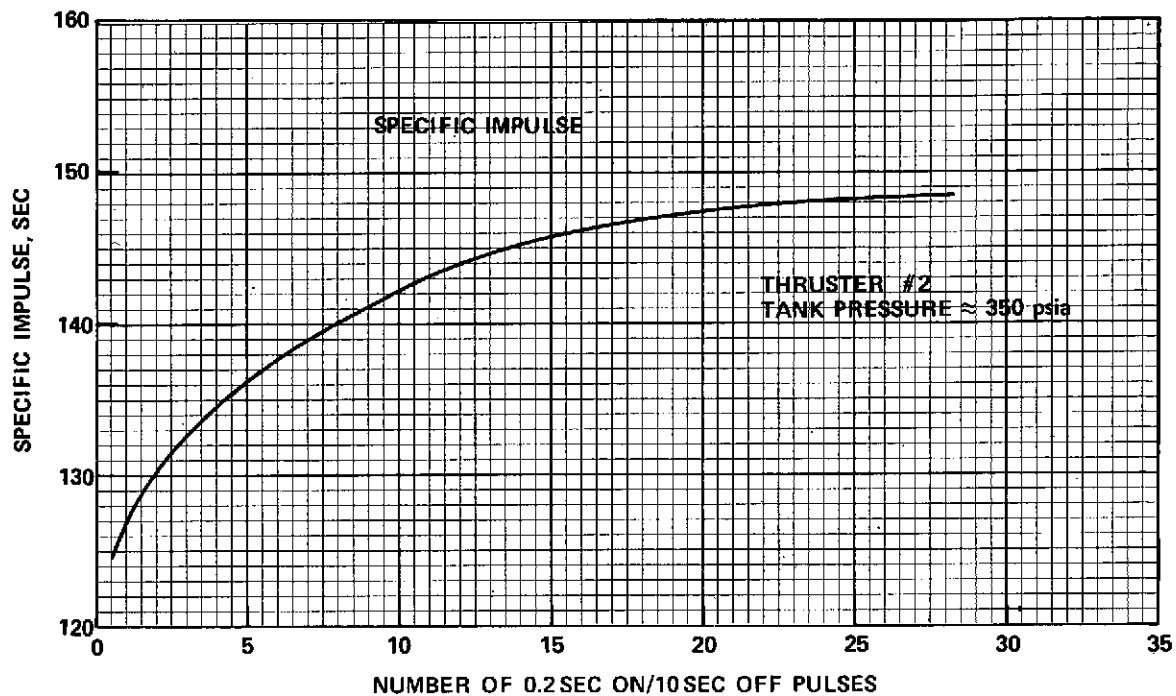


Figure 10-2. Wheel Unload Duty Cycle (-R Jet Performance)

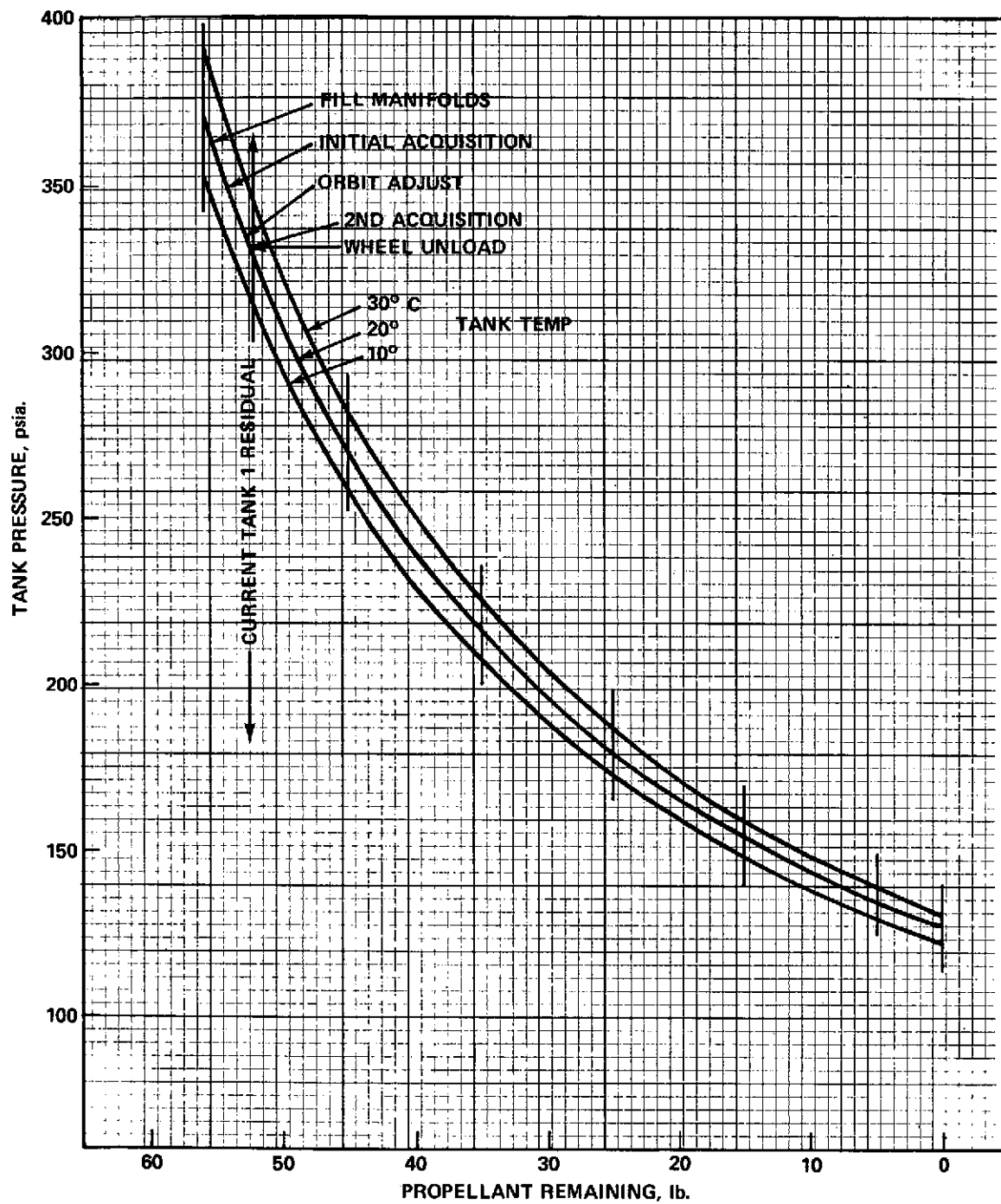


Figure 10-3. Blowdown Curve SPS Tank #1

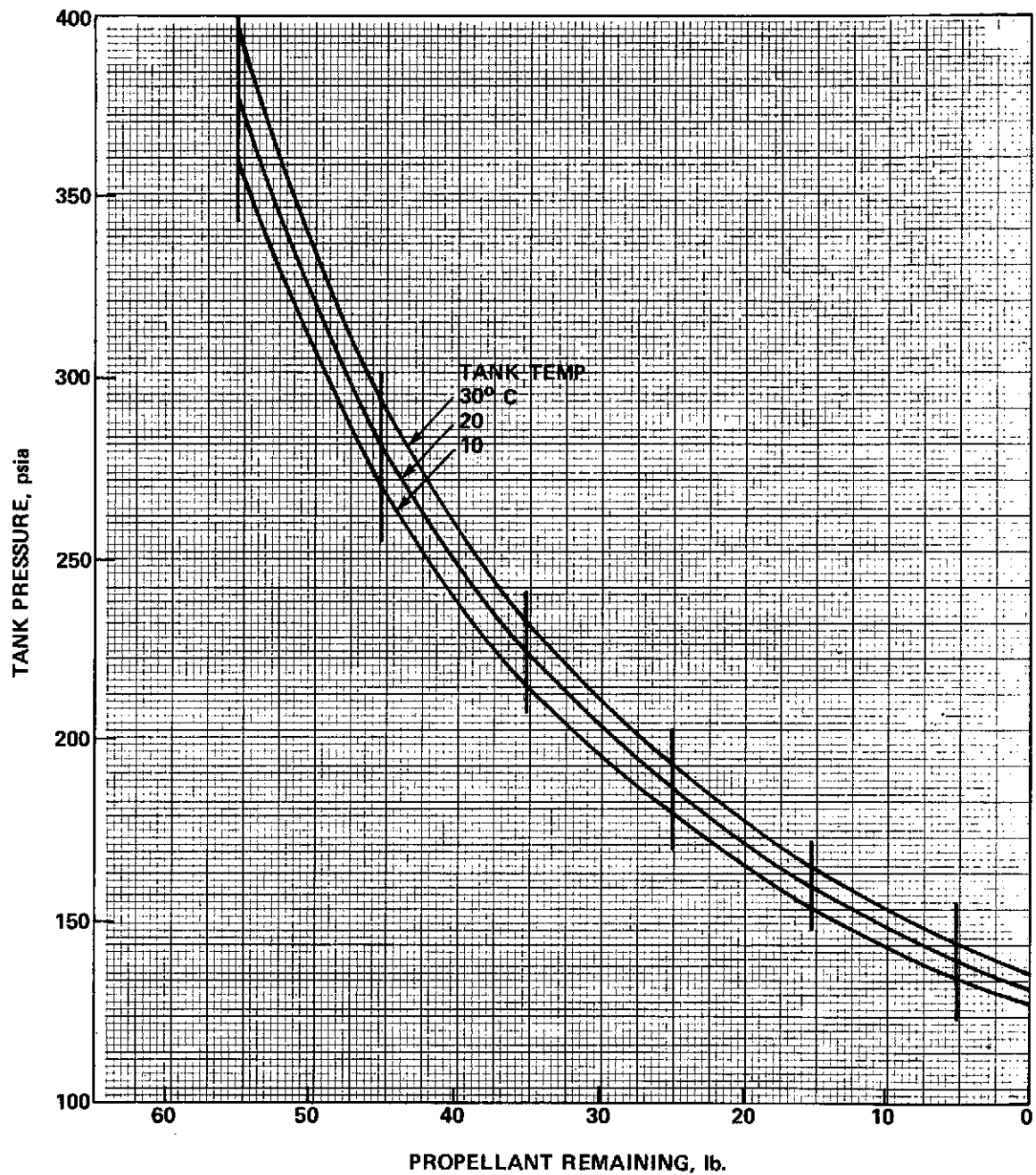


Figure 10-4. Blowdown Curve SPS Tank #2

C-4

0.47 lb	SPS 1 Manifold Fill (bleed-in)
1.43	Initial Acquisition
1.28	Initial Orbit Correction (2 burns)
0.33	1st Reacquisition
0.052	11 Wheel Unloads
3.56 lb	

This calculation is compared to the values shown on the blow-down curve, indicating 52.04 lb. remaining in Tank #1 at a pressure of 330 psia (20° C). The total weight of fuel remaining in the spacecraft is 106.57 lbs. (55.0 + 55.6 - 3.56 - 0.47 (SPS 2 Manifold fill).)

The variation of tank gas pressure with temperature is theoretically linear with a positive slope of 1.9 psi/° C. The telemetry resolution of tank pressure and temperature is 1 psi and .5° C, but because only 8 bits of this data are processed and the CRT temperature values have been rounded, the readout resolution is 2 psi and 1° C.

The tank pressure variation with temperature is not linear but displays considerable variation (see Figure 10-5). The pattern has a generally positive slope over its 24 hour cycle time but does not follow the same path cycle to cycle. The cause is uneven heat exchange and unequal thermal inertia in the tank. The temperature sensor is located in the liquid although the pressure is determined by the temperature of the pressurizing gas. The liquid and gas temperatures are out of phase and when combined with the 2 psi and 1° C readout resolution result in an erratic hysteresis cycle. The uncertainty in tank pressure as it relates to propellant quantity is not currently interfering with subsystem evaluation. However, an investigation into the possibility of retrieving the 9th tank pressure telemetry bit to double the sensitivity should be made.

10.6 COMPONENT TEMPERATURES

Figures 10-6 through 10-9 are typical 24 hour cycles of the thruster valve, propellant line, catalyst bed and tank temperatures. The data was taken while SPS 1 and 2 prime valve heaters were on, the prime and backup line heaters were in the Lo-Auto Mode and catalyst bed heaters were off.

Predictions had indicated a daily temperature range for the valves of from 5 to 75° C. The actual initial cycle was from 25 to 96° C with the prime cat-bed heaters on. This was considered somewhat high and the bed heaters were turned off. The valve temperatures have since cycled between approximately 12 and 88° C depending on sun angle.

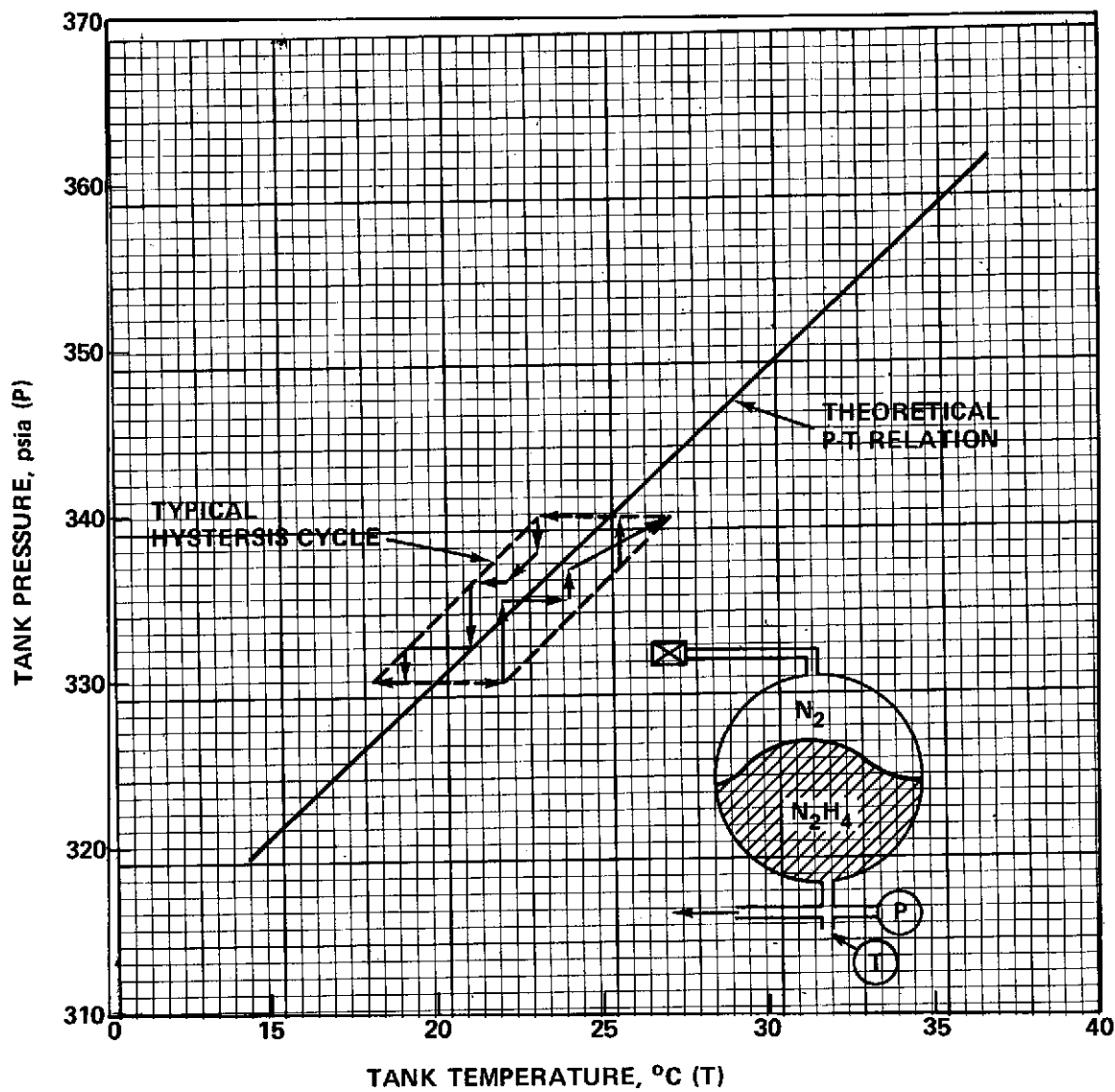


Figure 10-5. Propellant Tank Pressure vs. Temperature Hysteresis

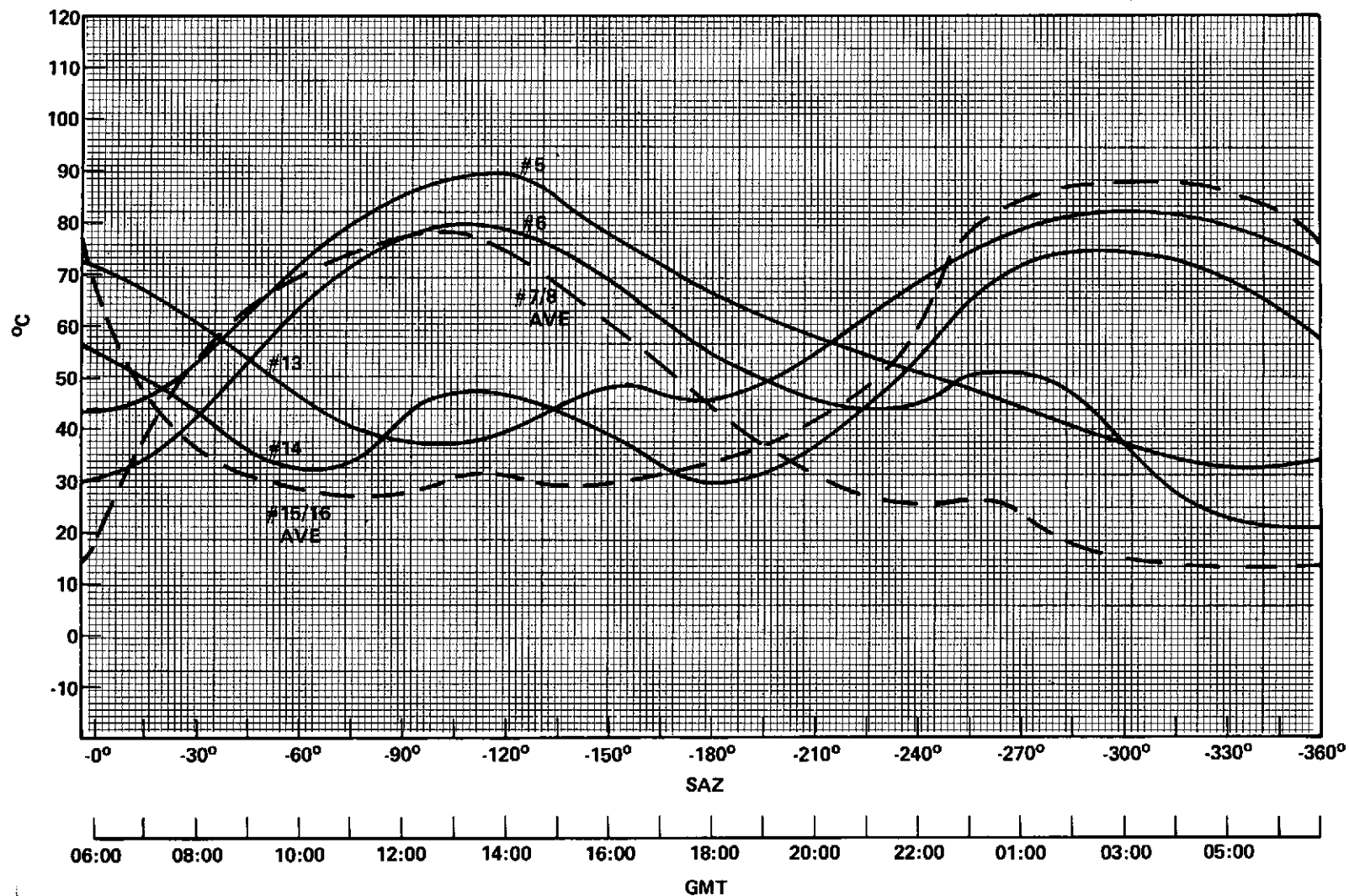


Figure 10-6. Thruster Valve Temperatures (24-Hour Cycle)

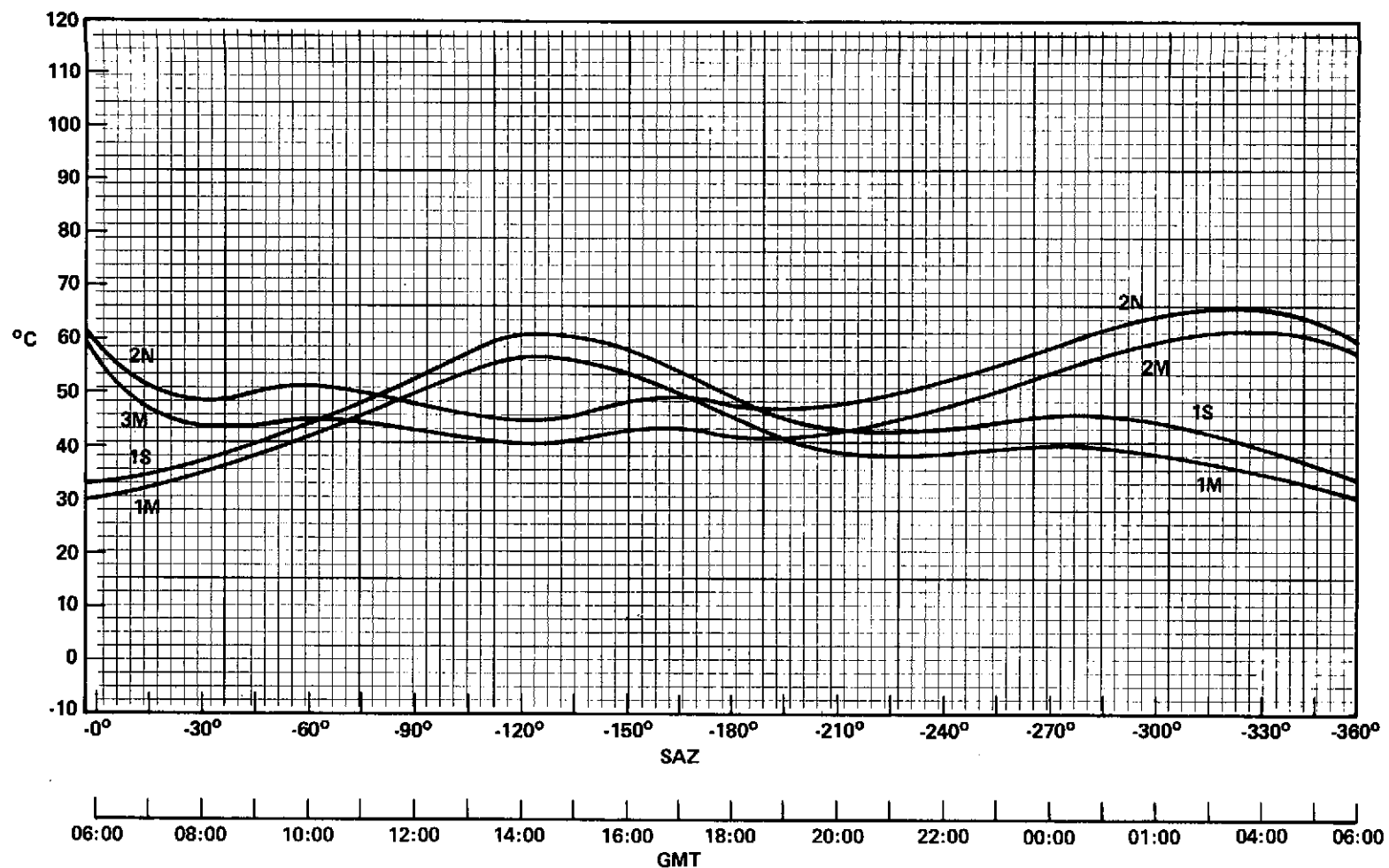


Figure 10-7. Propellant Line Temperatures (24-Hour Cycle)

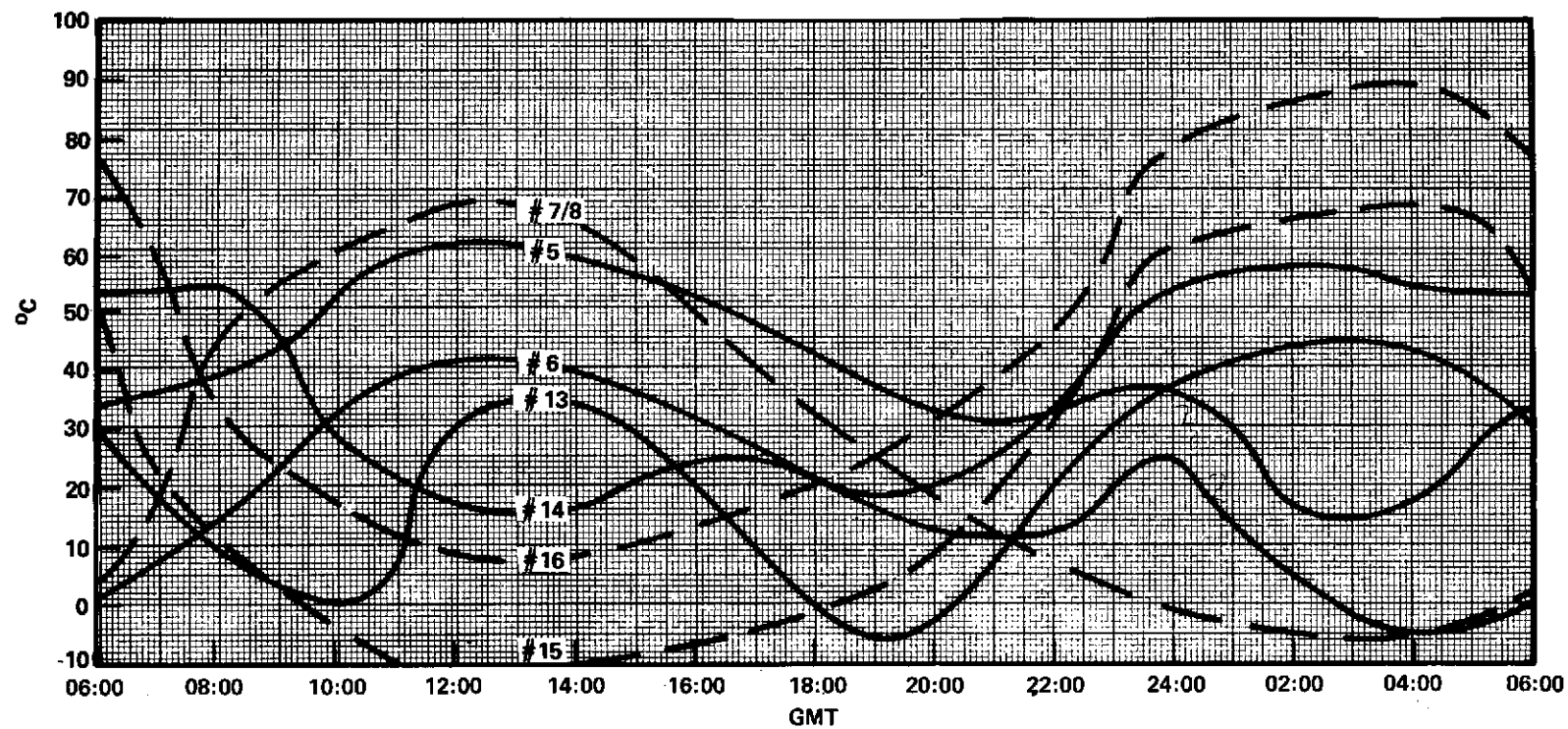


Figure 10-8. Catalyst Bed Temperatures (24-Hour Cycle)

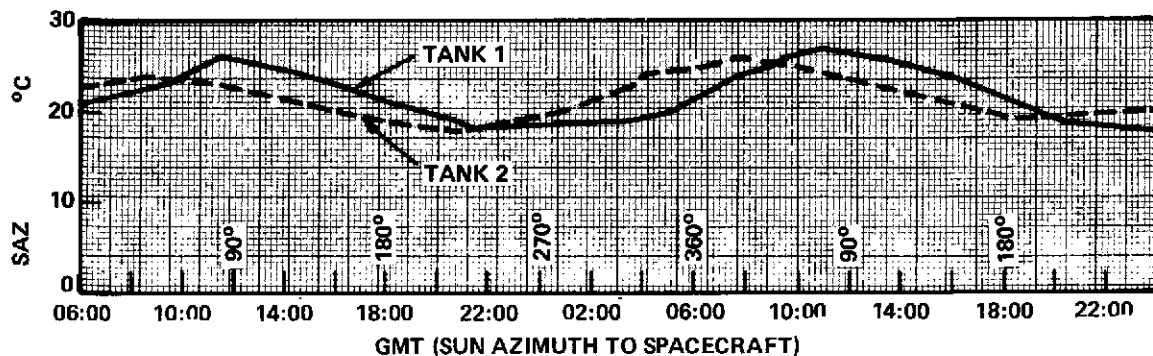


Figure 10-9. Tank Temperatures (24-Hour Cycle)

The difference in shape of the SPS 1 and 2 component cycles is due partly to the daily sequence of exposure to sunlight and shadow as the spacecraft sun angle changes. The line temperatures are under thermostatic control and consequently exhibit a much narrower cycle. The pronounced difference in temperature between the two SPS 2 orbit control thrusters that is reflected in their valve temperatures will be checked during the special RFC test. The minimum catalyst bed temperature of about -15°C should not be a problem since low temperature cycle tests at GSFC and Fairchild were run to -50°C without damage.

The temperature rise of the #7 catalyst bed during steady state jet firing was as predicted, reaching a steady state value of 640 to 650°C in 90 seconds. The -pitch thruster (2.4% duty cycle) reached 450°C during the 8 minute burn and 505°C during the 31 minute burn. Minor pulsing of attitude jets is clearly evident from the bed temperature telemetry. The #7 thruster valve cooled down from an initial temperature of 66°C to 46°C during the long steady state burn and after jet cutoff increased to a maximum value of 78°C .

10.7 RECOMMENDATIONS

Two areas require additional test and analysis. A special request is being prepared for the RFI test to determine the effect of PFF operation on catalyst bed temperatures. Additional statistical analyses should be applied to jet pulse performance to improve accuracy of performance estimates.

SECTION 11
COMMUNICATION SUBSYSTEM

SECTION 11

COMMUNICATION SUBSYSTEM

11.1 COMMUNICATION SUBSYSTEM

The Communication Subsystem (C/S) consists of an integrated, multifrequency transponder, the 30 foot reflector and associated prime focus feed antenna configuration designed to accommodate the individual requirements of the following ATS-6 experiments and modes:

1. HET (Health Education Telecommunications) Experiment
2. TDRE (Tracking and Data Relay Experiment)
3. SITE (Satellite Instructional Television Experiment)
4. PLACE (Position Location and Aircraft Communication Experiment)
5. Monopulse Tracking
6. MMW (Millimeter Wave) Experiment
7. COMSAT Propagation Experiment
8. RFI (Radio Frequency Interference) Experiment
9. VHRR (Very High Resolution Radiometer) Experiment
10. VHF High Gain RF Link
11. Range and Range Rate (S/C Orbit Determination)
12. On-Board Television Camera
13. RBE (Radio Beacon Experiment)

The four basic functional elements of the C/S are: antennas, receivers, IF amplifiers, and transmitters. A simplified block diagram of the C/S consisting of these basic functional elements along with supporting functional elements are shown in Figure 11-1. The performance requirements for the Communication Subsystem are established in the ATS-6 Spacecraft Specification 862-0001D.

The C/S performance during the first 30 days of operation have shown that the ATS-6 mission requirements for the C/S have been met. A summary of performance is tabulated in Table 11-1. The table shows that the in-orbit performance has met or exceeded requirements.

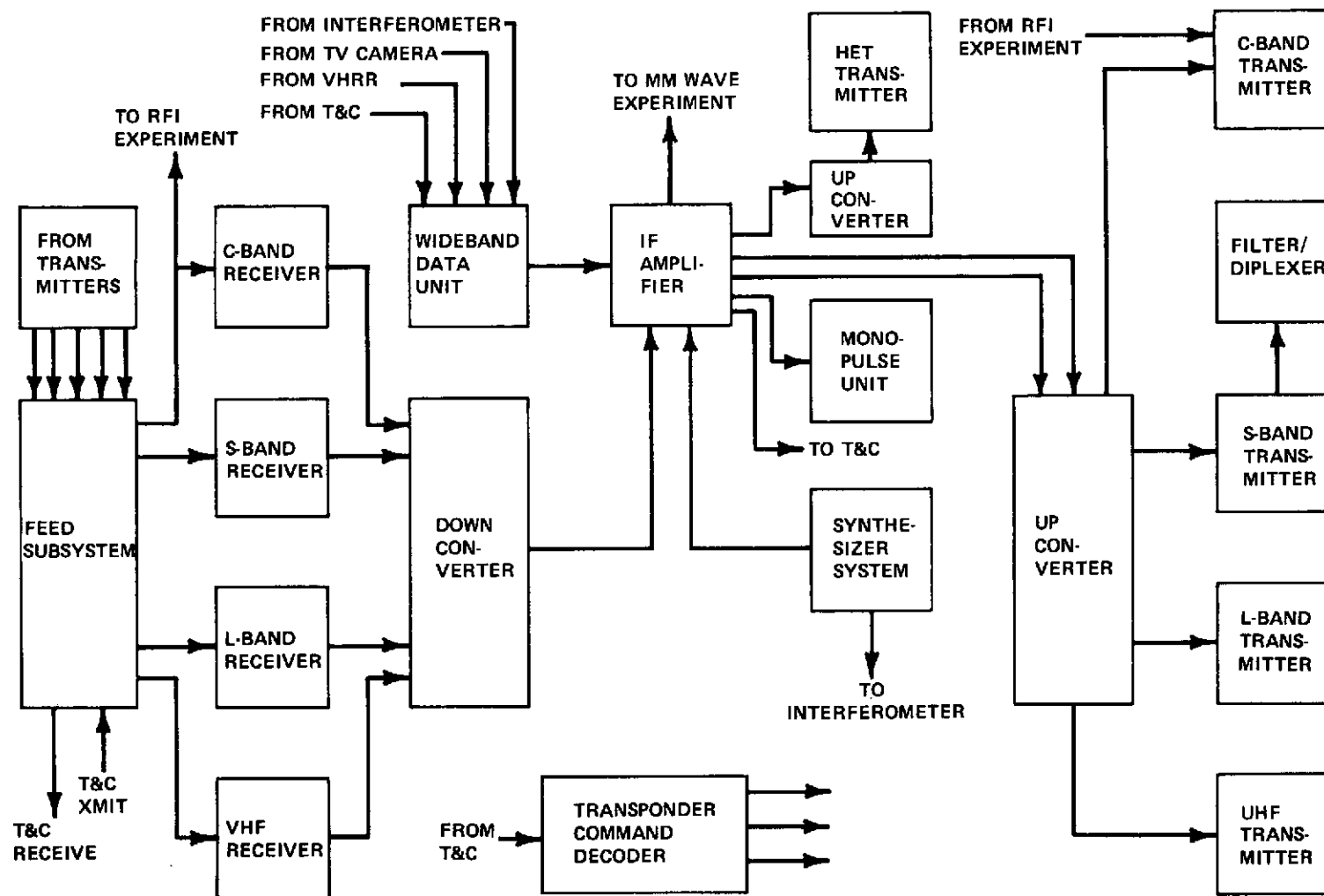


Figure 11-1. Simplified Communication Subsystem Diagram

Table 11-1

Communication Subsystem Performance Comparison

Frequency (MHz)	Antenna	Required G/T (dB/°K)		In-Orbit* G/T (dB/°K) Approx. Peak
		Peak	FOV	
6350	ECH	-17.0	-20.0	-14.0
6350	PFF	13.5	10.5	TBD**
2250	On-Axis	9.5	—	10.4
1650	Fan	-2.0	-5.0	-2.6
		EIRP (dBw)		(dBw)
3950	ECH	26.0	24.1	25.7
3950	PFF	48.2	43.5	48.3
2670	S-2	52.3	48.9	TBD**
2570	S-1	52.3	48.7	TBD**
2075	On-Axis	51	—	52.5
1550	Fan	45	42	42.1
860	PFF	51	48	52.6

*Calculated values based on in-orbit measurements.

**Requires refinement of ground station/spacecraft test set-up.

The only anomaly noted during this period was the appearance of periodic power drops ("glitches") on the C-band received signal at ROSMAN and Mojave on the ground receiver AGC. This problem has not affected data quality in any way. This anomaly is described in detail in section 11.5.

11.2 OPERATIONAL MODES

Summaries of the performance of the operational modes previously tested are presented in the following paragraphs.

11.2.1 TDRE

The objective of the Tracking and Data Relay Experiment is to demonstrate the capability of providing continuous communication between a low earth orbiting spacecraft (during the visible portion of its orbital pass below ATS-6) and a single ground station control center. The low-earth satellites to be used for this purpose are NIMBUS and Geos. A related, recent additional requirement is to relay television pictures of the planned Apollo-Soyuz rendezvous mission in mid 1975. Since there was no NIMBUS spacecraft in low earth orbit capable of communication with ATS-6, a NIMBUS simulator at ROSMAN was successfully used to confirm experiment performance. During this operation ROSMAN commanded and sent data to the NIMBUS simulator via ATS-6. NIMBUS telemetry was similarly sent to ROSMAN via ATS-6. The ROSMAN/ATS-6 link was at C-band; the NIMBUS/ATS-6 link was at S-band. This test demonstrated the first successful coherent operation of the synthesizer which was locked to the C-band carrier on the uplink, resulting in a phase coherent S-band transmission from the spacecraft. The ATS-6 boresight tracking of a simulated NIMBUS low orbit spacecraft was successfully demonstrated to an accuracy of ± 0.2 degrees, compared to a specification requirement of 0.5 degree. Details can be found in section 9 of this report. The capability of steerable S-band beams was demonstrated during the S-band Cross Antenna Pattern. The pattern plot is given in section 11.3.

11.2.2 SITE

The objective of the Instructional Television is to demonstrate capability of broadcasting via satellite to small receiving stations located throughout a large geographical area. Although this experiment is to be used in India, the experiment was checked out during this reporting period. A 25 MHz bandwidth FM-TV signal was transmitted from ROSMAN at C-band and successfully received simultaneously at ROSMAN and GSFC at 860 MHz using 10-foot ground antennas. Television reception was excellent as indicated by a picture quality of 5 by 5 and sound quality of 3 by 3.

11.2.3 PLACE

The objective of the Position Location and Aircraft Communication Experiment is to demonstrate a communication link between ground stations and a large number of aircraft and to define the location of these aircraft. Since there were no aircraft capable of communicating with ATS-6, during the first month of flight, PLACE simulators were used at ROSMAN and Kings Point, Long Island. Communication was successfully demonstrated via ATS-6. The ROSMAN/ATS-6 link was at C-band; the PLACE simulator/ATS-6 link was at L-band. All communication checkout with the PLACE simulator has been done on the L-band fan

beam. An antenna pattern of both the L-band fan beam and L-band pencil beam were taken (see section 11.3).

11.2.4 Monopulse Tracking

The ATS-6 Communication Subsystem contains three monopulse sensing receivers capable of operating with received signals in the C-, S-band and VHF frequency regions. The S-band and VHF monopulse receivers are operated at center frequencies of 2250 MHz and 150 MHz respectively in the wideband mode (bandwidth of 40 MHz) and 2253 MHz and 153 MHz respectively in the narrow-band mode (bandwidth of 120 kHz). The C-band monopulse receiver can operate at center frequencies of 5950 MHz, 6150 MHz and 6350 MHz in the wideband mode and at 5953 MHz, 6153 MHz and 6350 MHz in the narrow-band mode.

The three monopulse receivers were checked out as open loop and closed loop sensors for the spacecraft X and Y axes. All three receivers produced the correct attitude error signal polarities in the correct axes and were capable of being used by the ACS to actively control the spacecraft attitude about the X and Y axes.

Monopulse error curves were obtained for C- and S-band in the wideband mode (C-band at 6150 MHz only) and VHF in the narrowband mode about the spacecraft roll (X) and pitch (Y) axes with the earth sensor (ESA) in control of the spacecraft attitude. These error curves are shown in Figures 11-2, 11-3, and 11-4, along with "ideal" error curves.

Table 11-2 lists the error curve characteristics along with design goals. At C-band and S-band the error curve slopes are relatively close the design goal values. The C-band roll slope is about 16 percent low while its pitch slope is about 4 percent high. The C-, and S-band error slopes are quite acceptable as determined by their closed-loop operation with the Attitude Control Subsystem. The C- and S-band acquisition regions are also close to the design goals as indicated in Table 11-2. It is significant that the C- and S-band monopulse null axes were measured to be coaxial within ± 0.004 degrees. Tests were also made wherein the C- and S-band monopulse sensors were alternately switched into control of the ACS. It was noted that the spacecraft 3-axis pointing does change (drift) during the transition period, and so spacecraft commanding should be accomplished in the minimum amount of time once the monopulse signal is removed (monopulse detector input signal disconnected).

The VHF error curves are somewhat disappointing. The VHF slopes are about 70 to 80 percent low and never reach their saturated error voltages. A number of checks were made to determine the cause of the low VHF slopes but no cause was determined. Both RCP and LCP ground radiation polarizations were

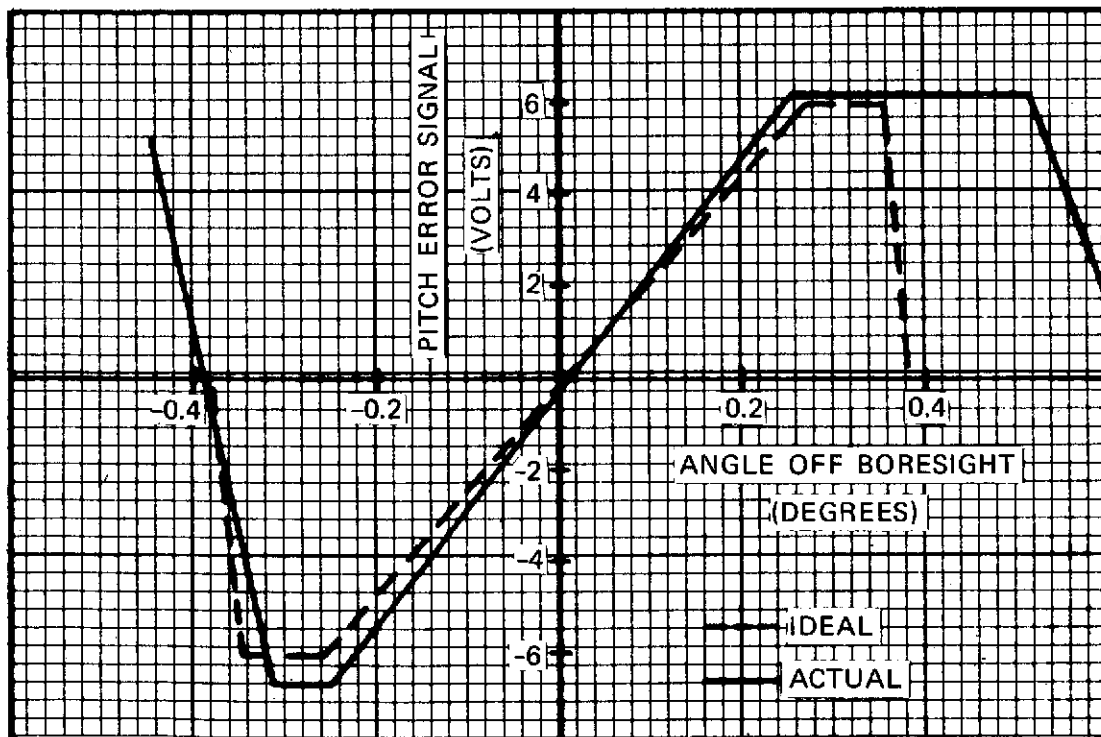
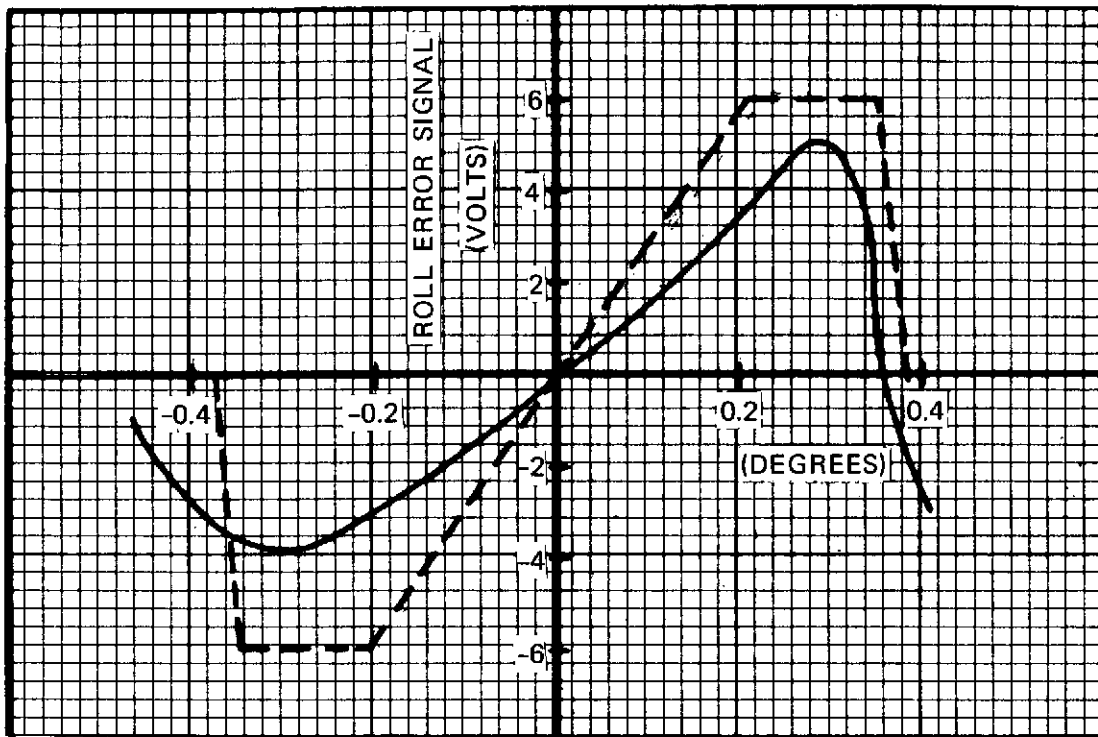


Figure 11-2. C-Band Monopulse

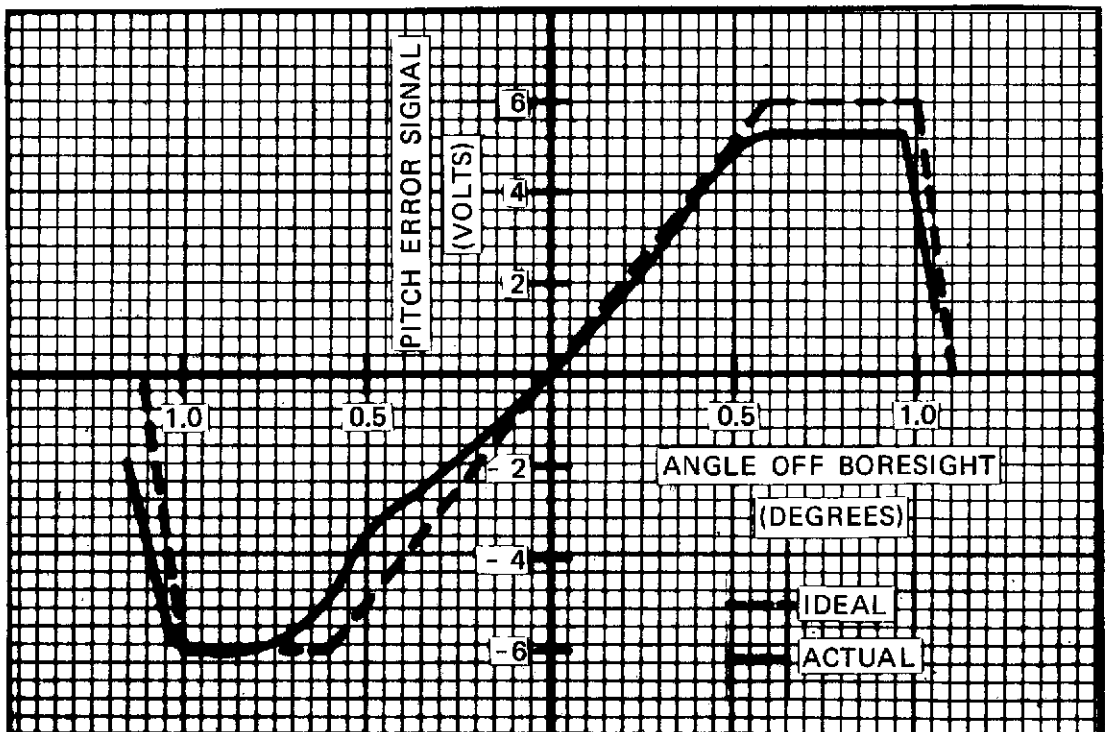
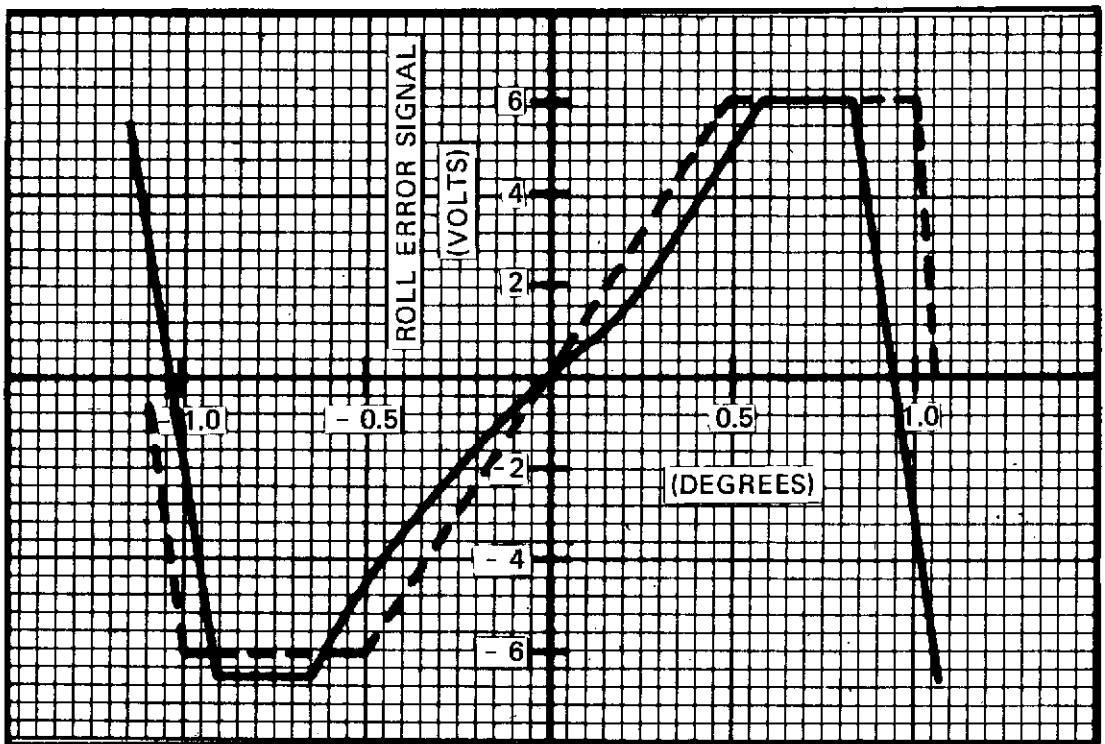


Figure 11-3. S-Band Monopulse

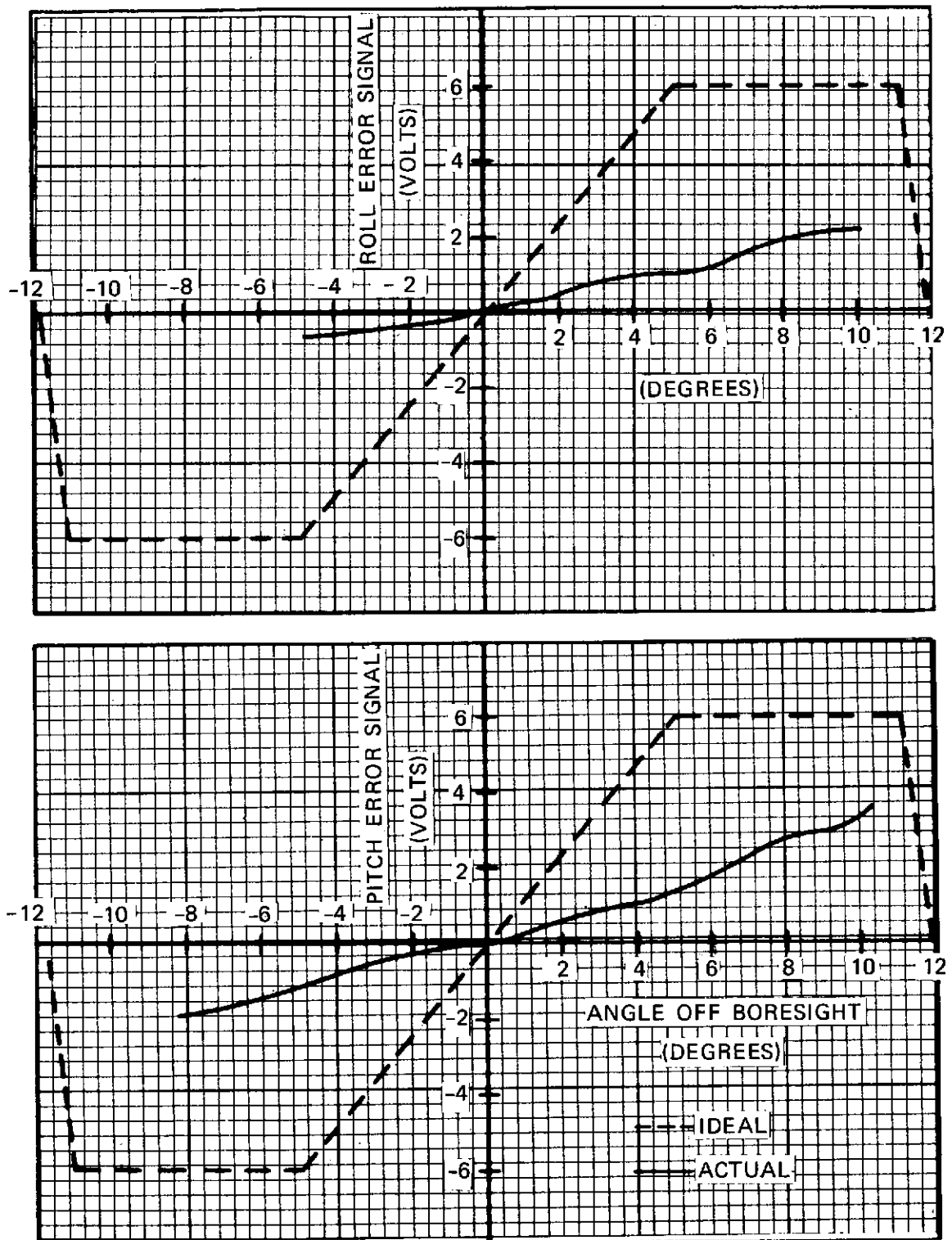


Figure 11-4. VHF Monopulse

Table 11-2
Monopulse Error Signal Characteristics

Monopulse Band/Axis	Slopes (Volts/Degree)		Acquisition Range (Degrees)		Null(1) Offset (Degrees)
	Actual	Goal	Actual	Goal	
C, Roll	20	24	+0.3 -0.3	±0.35	—
C, Pitch	25	24	+0.5 -0.35	±0.35	—
S, Roll	7	8	+0.8 -0.9	±1.0	0.004S
S, Pitch	7	8	+0.95 -1.00	±1.0	0.004E
VHF, Roll	0.2	1	>+10 <-5	±11.0	0.5N
VHF, Pitch	0.3	1	>+10 <-8	±11.0	2.0E

(1) The null offset is relative to the C-band Monopulse axis for S-band, but relative to the ESA for VHF.

attempted and it was determined that RCP produced the better received signal level. With RCP radiation the spacecraft VHF antenna gain was determined to be about 14 dB as expected. At this point it appears that a problem could exist in the VHF monopulse receiver error channels at a point common to both the roll and pitch channels. The problem appears to be an excess insertion loss of about 10 to 14 dB. In spite of the low error slopes, the VHF monopulse was capable of serving as a sensor to control the spacecraft roll and pitch axis. While used in the ACS control loops, the VHF null pointing was 0.5 degrees North and 2.0 degrees East of the ground station (Rosman) as determined by the earth sensor angles. It is suspected that these large errors are in part due to the low loop gain due to the low monopulse error gains, and that they could be reduced by increasing the VHF gains in the DOC.

Monopulse testing also showed that the redundancy provisions are functioning correctly. During the in-flight evaluation period, the following was also accomplished with favorable results:

- a. Each of the three IF amplifiers was used in both wide-band and narrow-band monopulse modes.
- b. Both monopulse detectors were operated.
- c. The detector C-band gain setting was tried while receiving a VHF signal.

In conclusion, C- and S-band monopulse sensors worked very well and the VHF sensor was acceptable. Further monopulse testing with VHF should include:

- a. Testing with linear ground polarization, using linear East-West, linear North-South and Northeast to Southwest.
- b. Reprogramming the DOC to increase the VHF monopulse gains by a factor of about 4 and then re-determining the VHF acquisition and pointing capabilities.

11.2.5 MMW Experiment

The objective of the MMW experiment is to obtain data related to the propagation characteristics of the space/earth transmission medium at Ka and Ku bands. TV pictures were successfully transmitted to ATS-6 from ROSMAN at C-band and cross-strapped at both 20 GHz and 30 GHz to a MMW terminal located at ROSMAN using an 18 inch parabolic antenna on ATS-6.

11.2.6 COMSAT Propagation Experiment

The objective of the COMSAT Propagation Experiment is to obtain data related to the propagation characteristics of the space/earth transmission medium at 12 and 18 GHz. The propagation experiment has been operated almost continuously since its initial turn-on. The experiment has been receiving signals from many ground stations at both 12 and 18 GHz, and transponding the signals back to Andover, Maine at C-band using the spacecraft earth coverage horn (ECH). The COMSAT Propagation Experiment uses a polarization on the ECH orthogonal to that used by the communication subsystem.

11.2.7 RFI

The objective of the Radio Frequency Interference Experiment is to provide data on the mutual interference between satellite and terrestrial telecommunications

systems over a 500 MHz band at C-band. The spacecraft attitude control subsystem has been able to point the 30 foot dish to within ± 0.1 degree of ROSMAN. (With bias calibration of the C-band monopulse, and the ACS roll (pitch sensor, pointing accuracy could be improved to less than 0.05 degree.) Uplink signals have been received via the 30 foot antenna, successfully transponded in the C/S RFI equipment, and transmitted back to the RFI terminal at C-band over the ECH.

11.2.8 VHRR

The objective of the Very High Resolution Radiometer is to photograph the earth's disc from synchronous attitude. The Wideband Data Unit with the C/S successfully modulated high quality video signals both for the IR (infra-red) and visible spectrums on to the C-band downlink carrier. The addition of multiplexing the Interferometer High Speed Data Link (IHSDL) did not degrade the quality of the Radiometer pictures. Evaluation of the IHSDL has not been completed. Preliminary examinations indicate that the IHSDL quality should be quite good.

11.2.9 VHF High Gain RF Link

During the first day in orbit prior to conducting the yaw flip maneuver, the T&C subsystem was reconfigured from the launch mode into the normal mode. In the normal mode, one command and one telemetry link was switched from one of the T&C omni antennas to the Prime Focus Feed (PFF). The command link margin improved by 11.5 dB and the telemetry link margin improved by 1.1 dB. The 30 foot antenna gain was measured at 13.6 dB over the omni antenna gain.

11.2.10 Range and Range Rate

C-band Ranging (ATSR) was accomplished during the 4th day in orbit to determine the orbit of the S/C and to permit correction of the initial orbit to a final station keeping location above $94^{\circ} \pm 0.1^{\circ}$ W longitude. Ranging for purposes of refining the exact orbit parameters for DOC updating is regularly scheduled once every two weeks.

11.2.11 HET (Health, Education Telecommunications) Experiment

The objective of HET is to demonstrate the capability of simultaneous broadcasting of up to two different TV programs via satellite to two different geographical locations. Although there were some initial problems with the 10 foot S-band ground antenna feed polarization, subsequent HET tests were successful. Normal program transmission included transmitting an FM TV signal at C-band and transponding two S-band downlink frequencies simultaneously (one frequency per antenna beam). TV reception on the C-band monitor over the ECH was also

well received. During the checkout period just prior to the Appalachian Regional Commission (ARC) and Veteran Administration (VA) becoming operational, the HET S-band receive terminals were reporting excellent quality TV program reception. Picture and sound quality were reported as 5 by 5 and 3 by 3 respectively.

11.2.12 TV Camera

The objective of the TV Camera experiment was to televise a picture of the solar array booms and the 30-foot parabolic reflector as deployed in orbit. During the fourth day in orbit, the TV Camera was turned on. Figures 11-5 and 11-6 taken at different times, show the successful deployment of the 30-foot reflector and the solar array booms. The TV signal was transmitted using the C/S Wide-band Data Unit to modulate the C-band transmitter over the ECH.

11.2.13 Radio Beacon Experiment

The objective of the Radio Beacon Experiment (RBE) was to provide spacecraft-to-ground radio link at 40 MHz, 140 MHz, and 360 MHz for investigating particles which effect radio propagation beyond the atmosphere.

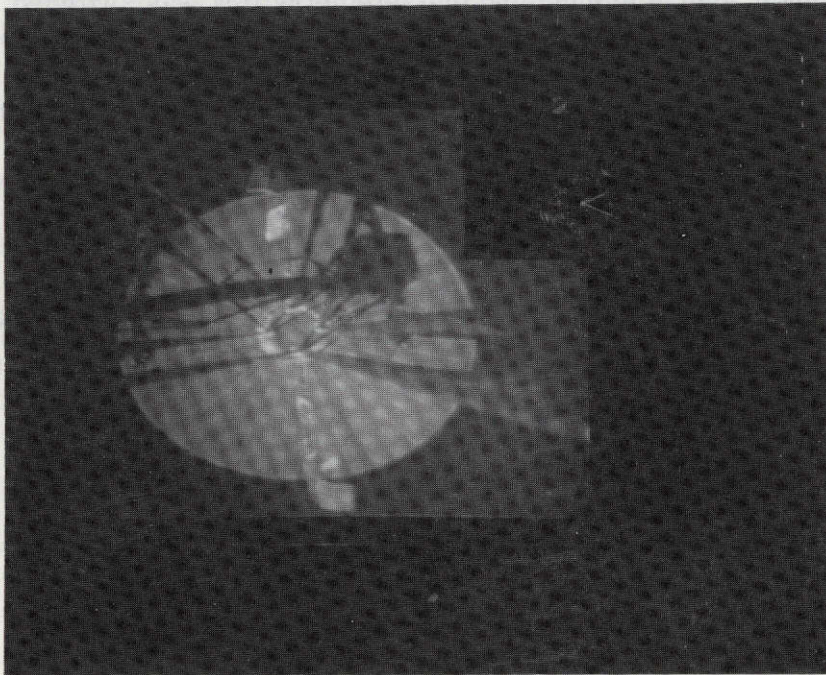


Figure 11-5. Television Camera Transmission

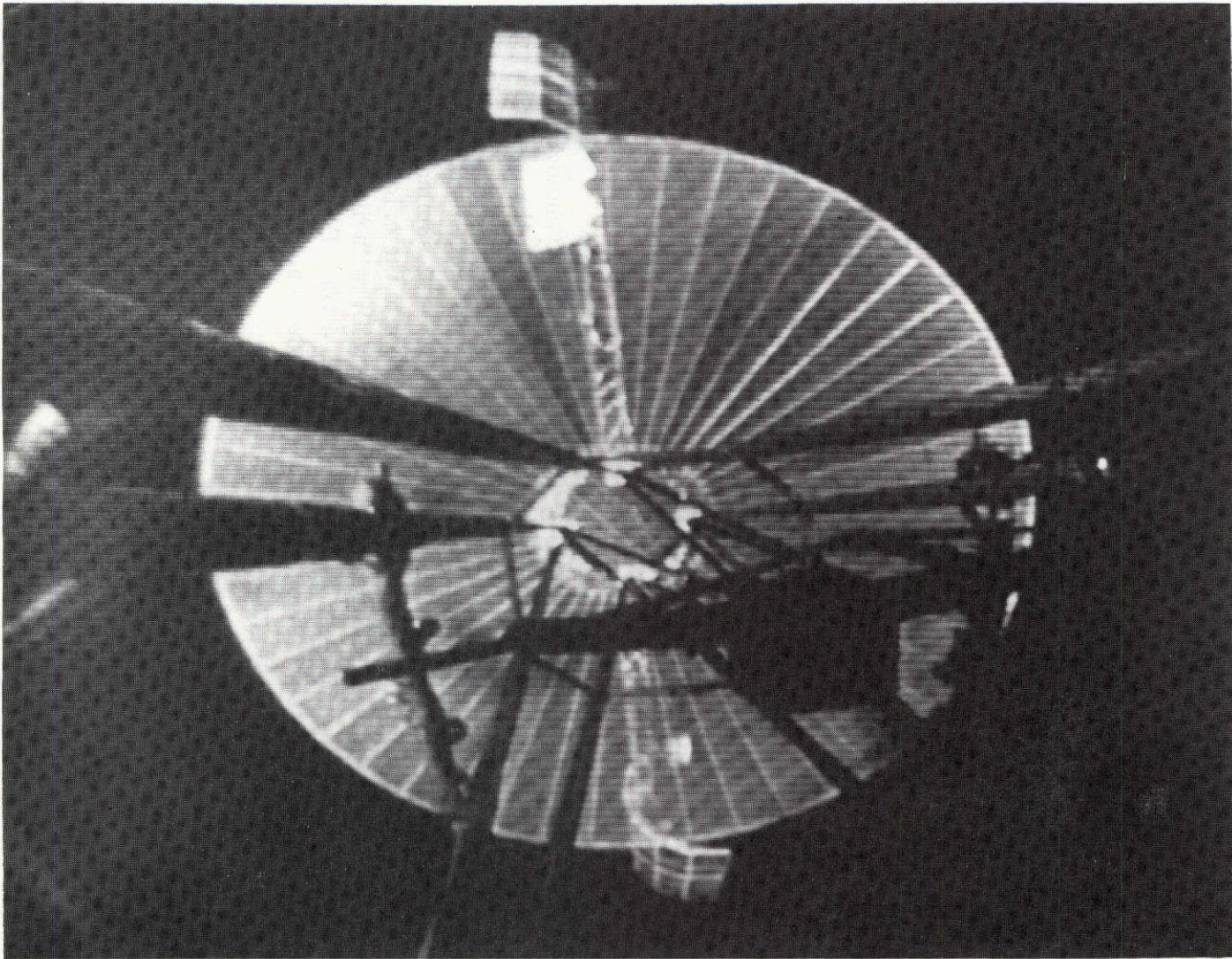


Figure 11-6. Television Camera Transmission

During the initial in-flight evaluation period, all RBE command functions were checked out successfully. In addition, special commanding tests were performed to determine if the RBE 140 MHz radiated signal desensitized the spacecraft VHF command receivers. These tests included reducing the ground EIRP so that the command receivers operated near their thresholds with no RBE interference.

One RBE anomaly observed was that the Automatic Level Control (ALC) telemetry indicated 0.00 volts. This was also observed during RFC tests at Fairchild. Since the ALC function worked well even though the telemetry sensor was faulty, a decision was made by GSFC/FI to launch with this condition.

The output power levels of the three RBE transmitters were measured via telemetry. The range of these levels are:

Frequency (MHz)	Level (Watts)
40	1.14 - 1.39
140	1.30 - 1.35
360	1.51 - 1.55

11.3 TRANSPONDER SIGNAL CHARACTERISTICS

During the period from June 2 to June 11, spectrum analyzer photographs were taken at the ROSMAN ground station. This section describes the spectrum photos for the various down-links given in Figures 11-7 through 11-12. In addition to the spectrum photos, these figures give data used to generate link calculations for up-link and down-link performance. Table 11-3 summarizes the AGC up-link and down-link signals and compares them to the calculated values. The calculated results and AGC readings correlate well, with discrepancies within tolerances of ground terminal parameters (± 1.5 dB). Differences can be attributed to the fact that no serious attempt was made to achieve a true bore-sight condition with maximum gain.

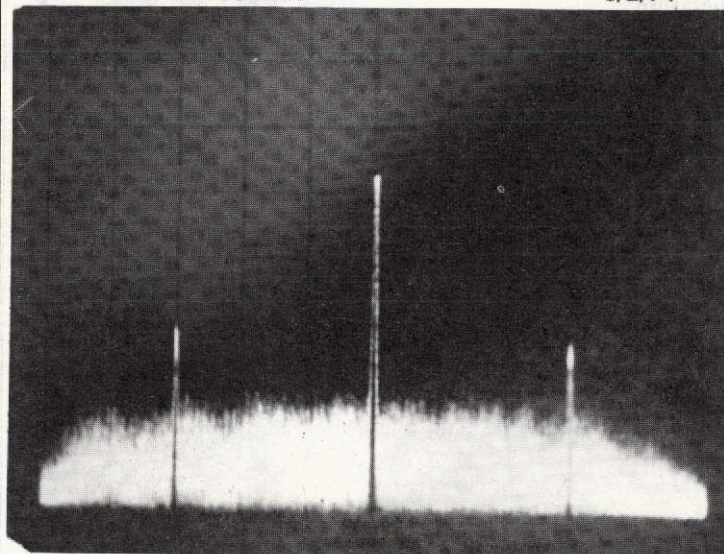
Figure 11-7 depicts a transponded C-band carrier signal with two sideband signals produced by the desired C-band beacon signal whose frequency is shifted 30 MHz from the carrier. Figures 11-8 and 11-9 show a C-band up-link carrier transponded at S-band and L-band respectively. The only spurs noted during the entire series of tests can be seen in Figures 11-10 and 11-11, which are for

COMM. SUBSYSTEM QUICK LOOK DATA SHEET (FOR LINK CALCULATIONS)

1. Spectrum Analyzer Picture (Downlink)

FROM ROSMAN

6/2/74



153:18:07

GMT Start 153:17:20
Place Rosman
Date 6-2-74
Band C

Spectrum Analyzer Controls

Bandwidth 300 kHz
Scan Width 10 MHz/div
Scan Time 2 m Sec/div
Log. Ref. Level 0 dBm
Vertical Display 10 dB/div
Video Filter Off

2. Satellite AGC reading (TLM # COMM-001)	<u>-63</u>	dBm
3. Uplink Frequency (f1)	<u>6350.000000</u>	MHz
4. Downlink Frequency (f2)	<u>3950.001317</u>	MHz
5. Corrected Frequency (f3)	<u>3950.001317</u>	MHz
6. <u>Uplink</u>		
1. Transmitter Power (PT)	<u>60</u>	dBm
2. Antenna Gain (G_T)	<u>59.9</u>	dB
3. Effective Radiated Power (ERP)	<u>119.9</u>	dBm
4. Atmospheric Losses	<u>200.0</u>	dB
5. Antenna Gain (G_R)	<u>17.2</u>	dB
6. Calculate Power at Satellite	<u>-62.9</u>	dBm
7. Satellite Location (Longitude)	<u> </u>	°
8. Slant Range (to ROSMAN)	<u>22300 St. miles</u>	°
9. <u>Downlink</u>		
1. Transmitter Power (TLM-COMM-001)	<u>38.4</u>	dBm
2. Antenna Gain (G_T)	<u>18.2</u>	dB
3. Effective Radiated Power (ERP)	<u>56.6</u>	dBm
4. Atmospheric Losses	<u>195.8</u>	dB
5. Antenna Gain (G_R)	<u>58.3</u>	dB
6. Calculate Power received at earth stations	<u>-80.9</u>	dBm

Figure 11-7. C-Band Downlink with Beacon

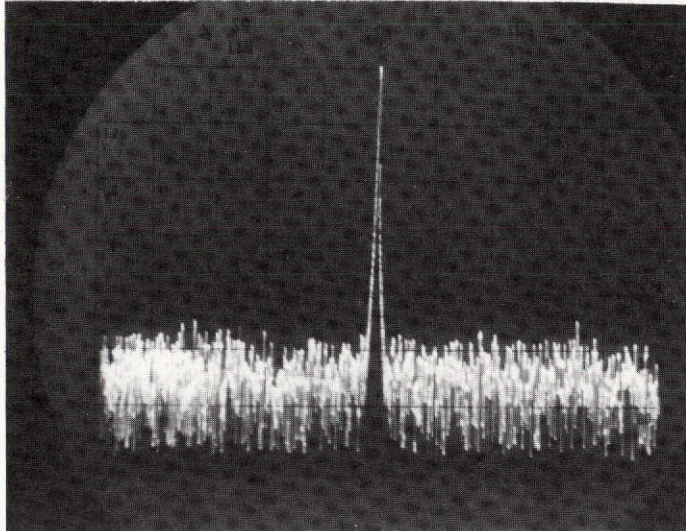
10. <u>Earth stations</u>	1. AGC reading	<u>-82</u>	<u>dBm</u>
	2. Antenna Gain (GR)	<u>58.3</u>	<u>dB</u>
	3. System Noise Temperature	<u>67</u>	<u>°K</u>
	4. Receive Figure of Merit (G/T)	<u>40.0</u>	
11. Total Path Lose (db) (includes path, atmospheric, and slant range)			<u>dB</u>
12. Satellite Configuration (PRINT-COMBAT/COMM-001. as part of this data) Page Number		<u>2</u>	<u>.</u>
13. Operations Mode (TDRE, ITV, etc.)		<u>C-Band Ranging</u>	
14. Notes:			
C-Band Beacon ON			
70001.317 kHz (After down conv.)			
Polarization 6 76.9°			

Figure 11-7. (Continued)

COMM. SUBSYSTEM QUICK LOOK DATA SHEET (FOR LINK CALCULATIONS)

1. Spectrum Analyzer Picture (Downlink)

ROSMAN S-BAND 6/10/74



70 MHz

GMT Start 161:19:58
Place Rosman
Date 6-10-74
Band S-Band

Spectrum Analyzer Controls

Bandwidth 10 kHz
Scan Width 1 MHz/div
Scan Time 3 m Sec/div
Log. Ref. Level dBm
Vertical Display 10 dB/div
Video Filter None
HP 8551B & 852A

2. Satellite AGC reading (TLM #COMM-001)

Computer not available dBm

3. Uplink Frequency (f1)

6150.000000 MHz

4. Downlink Frequency (f2)

2075.003040 MHz

5. Corrected Frequency (f3)

 MHz

6. Uplink

1. Transmitter Power (PT)

53 dBm

2. Antenna Gain (G_T)

59.7 dB

3. Effective Radiated Power (ERP)

112.7 dBm

4. Atmospheric Losses

199.6 dB

5. Antenna Gain (G_R)

17.4 dB

6. Calculate Power at Satellite

-69.5 dBm

7. Satellite Location (Longitude)

 °

8. Slant Range (to ROSMAN)

 °

9. Downlink 1. Transmitter Power (TLM-COMM-001)

42.5 dBm

2. Antenna Gain (G_T)

40.1 dB

3. Effective Radiated Power (ERP)

82.6 dBm

4. Atmospheric Losses

190.2 dB

5. Antenna Gain (G_R)

34.1 dB

6. Calculate Power received at earth stations

-73.5 dBm

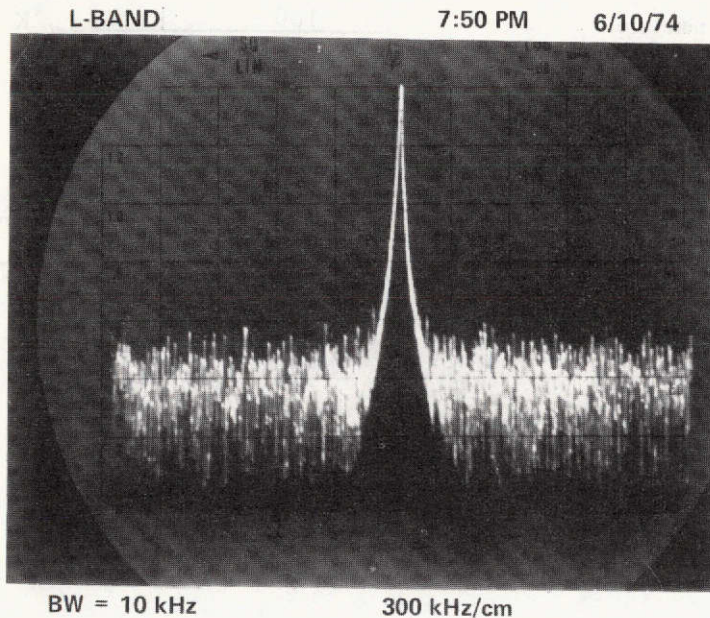
Figure 11-8. S-Band Downlink Signal

10. <u>Earth stations</u>	1. AGC reading	<u> -71 </u>	dBm
	2. Antenna Gain (GR)	<u> 34.1 </u>	dB
	3. System Noise Temperature	<u> 230 </u>	°K
	4. Receive Figure of Merit (G/T)	<u> </u>	
11. Total Path Lose (db) (includes path, atmospheric, and slant range)		<u> </u>	dB
12. Satellite Configuration (PRINT-COMBAT/COMM-001. as part of this data) Page Number		<u> 2 </u>	
13. Operations Mode (TDRE, ITV, etc.)		<u> </u>	
14. Notes:			

Figure 11-8. (Continued)

COMM. SUBSYSTEM QUICK LOOK DATA SHEET (FOR LINK CALCULATIONS)

1. Spectrum Analyzer Picture (Downlink)



GMT Start 161:23:38
Place _____
Date 6-10-74
Band L

Spectrum Analyzer Controls

Bandwidth 10 kHz
Scan Width 300 MHz/div
Scan Time 3 m Sec/div
Log. Ref. Level _____ dBm
Vertical Display 10 dB/div
Video Filter None

2. Satellite AGC reading (TLM #COMM-001)

Computer not available dBm

3. Uplink Frequency (f1)

6150.000000 MHz

4. Downlink Frequency (f2)

1550.003860 MHz

5. Corrected Frequency (f3)

_____ MHz

6. Uplink

1. Transmitter Power (PT)

63 dBm

2. Antenna Gain (G_T)

59.7 dB

3. Effective Radiated Power (ERP)

122.7 dBm

4. Atmospheric Losses

199.6 dB

5. Antenna Gain (G_R)

17.4 dB

6. Calculate Power at Satellite

_____ dBm

7. Satellite Location (Longitude)

_____ °

8. Slant Range (to ROSMAN)

_____ °

9. Downlink

1. Transmitter Power (TLM-COMM-001)

45.5 dBm

2. Antenna Gain (G_T)

31.8 dB

3. Effective Radiated Power (ERP)

79.3 dBm

4. Atmospheric Losses

187.6 dB

5. Antenna Gain (G_R)

34.2 dB

6. Calculate Power received at earth stations

-76.1 dBm

Figure 11-9. L-Band Downlink Signal

10. <u>Earth stations</u>	1. AGC reading	<u>-76.2</u>	dBm
	2. Antenna Gain (GR)	<u>34.2</u>	dB
	3. System Noise Temperature	<u>150</u>	°K
	4. Receive Figure of Merit (G/T)	<u> </u>	
11. Total Path Lose (db) (includes path, atmospheric, and slant range)		<u> </u>	dB
12. Satellite Configuration (PRINT-COMBAT/COMM-001. as part of this data) Page Number		<u> 2 </u>	
13. Operations Mode (TDRE, ITV, etc.)		<u> </u>	
14. Notes:			

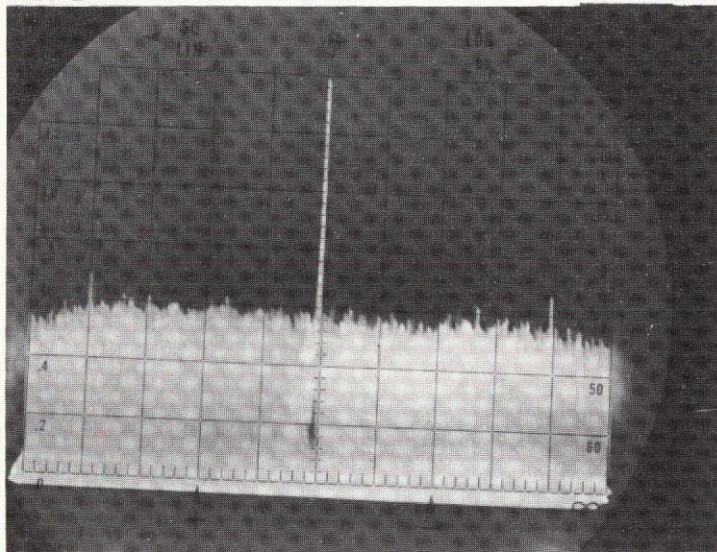
Figure 11-9. (Continued)

COMM. SUBSYSTEM QUICK LOOK DATA SHEET (FOR LINK CALCULATIONS)

1. Spectrum Analyzer Picture (Downlink)

HET 2

6/11/74



GMT Start 162:20:12

Place

Date 6-11-74

Band HET 2

Spectrum Analyzer Controls

Bandwidth 3 kHz

Scan Width -3 MHz/div

Scan Time 30 m Sec/div

Log. Ref. Level dBm

Vertical Display 10 dB/div

Video Filter None

2. Satellite AGC reading (TLM #COMM-001)	<u>-68</u>	dBm
3. Uplink Frequency (f1)	<u>6150</u>	MHz
4. Downlink Frequency (f2)	<u>Het 2 2670</u>	MHz
5. Corrected Frequency (f3)	<u></u>	MHz
6. <u>Uplink</u>		
1. Transmitter Power (PT)	<u>60</u>	dBm
2. Antenna Gain (G_T)	<u>59.7</u>	dB
3. Effective Radiated Power (ERP)	<u>119.7</u>	dBm
4. Atmospheric Losses	<u>199.6</u>	dB
5. Antenna Gain (G_R)	<u>13.5</u>	dB
6. Calculate Power at Satellite	<u>-66.4</u>	dBm
7. Satellite Location (Longitude)	<u></u>	°
8. Slant Range (to ROSMAN)	<u></u>	°
9. <u>Downlink</u>		
1. Transmitter Power (TLM-COMM-001)	<u>41.4</u>	dBm
2. Antenna Gain (G_T)	<u>40.7</u>	dB
3. Effective Radiated Power (ERP)	<u>82.1</u>	dBm
4. Atmospheric Losses	<u>192.4</u>	dB
5. Antenna Gain (G_R)	<u>50.9</u>	dB
6. Calculate Power received at earth stations	<u>-59.4</u>	dBm

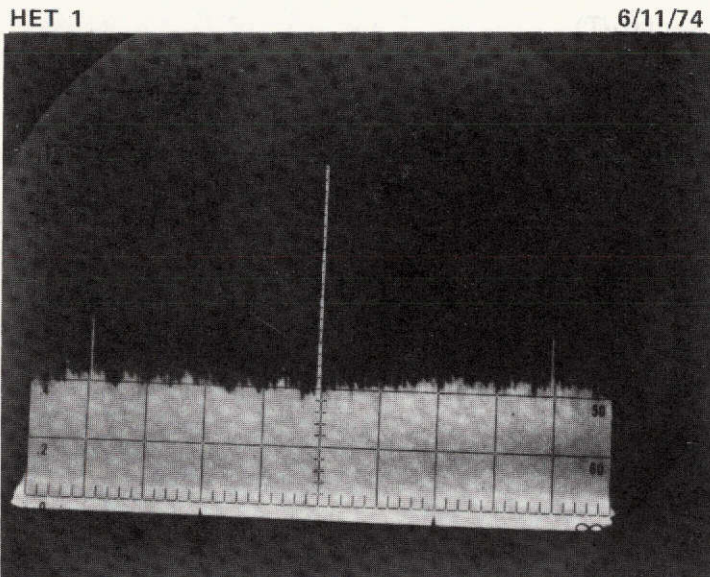
Figure 11-10. HET 2 Downlink Signal

10. <u>Earth stations</u>	1. AGC reading	<u>Not calibrated</u>	<u>dBm</u>
	2. Antenna Gain (GR)	<u>50.9</u>	<u>dB</u>
	3. System Noise Temperature	<u></u>	<u>°K</u>
	4. Receive Figure of Merit (G/T)	<u></u>	
11. Total Path Lose (db) (includes path, atmospheric, and slant range)		<u></u>	<u>dB</u>
12. Satellite Configuration (PRINT-COMBAT/COMM-001. as part of this data) Page Number		<u>2</u>	<u>.</u>
13. Operations Mode (TDRE, ITV, etc.)		<u></u>	
14. Notes:			

Figure 11-10. (Continued)

COMM. SUBSYSTEM QUICK LOOK DATA SHEET (FOR LINK CALCULATIONS)

1. Spectrum Analyzer Picture (Downlink)



GMT Start 162:21:26

Place _____

Date _____

Band HET 1

Spectrum Analyzer Controls

Bandwidth 3 kHz

Scan Width 3 MHz/div

Scan Time 30 m Sec/div

Log. Ref. Level _____ dBm

Vertical Display 10 dB/div

Video Filter None

2. Satellite AGC reading (TLM #COMM-001)	<u>-69</u>	dBm
3. Uplink Frequency (f1)	<u>6150</u>	MHz
4. Downlink Frequency (f2)	<u>Het 1 2569</u>	MHz
5. Corrected Frequency (f3)	_____	MHz
6. <u>Uplink</u>		
1. Transmitter Power (PT)	<u>60</u>	dBm
2. Antenna Gain (G_T)	<u>59.7</u>	dB
3. Effective Radiated Power (ERP)	<u>119.7</u>	dBm
4. Atmospheric Losses	<u>199.6</u>	dB
5. Antenna Gain (G_R)	<u>13.5</u>	dB
6. Calculate Power at Satellite	<u>-66.4</u>	dBm
7. Satellite Location (Longitude)	_____	°
8. Slant Range (to ROSMAN)	_____	°
9. <u>Downlink</u>		
1. Transmitter Power (TLM-COMM-001)	<u>42.0</u>	dBm
2. Antenna Gain (G_T)	<u>41.2</u>	dB
3. Effective Radiated Power (ERP)	<u>83.2</u>	dBm
4. Atmospheric Losses	<u>192.1</u>	dB
5. Antenna Gain (G_R)	<u>50.9</u>	dB
6. Calculate Power received at earth stations	<u>-58</u>	dBm

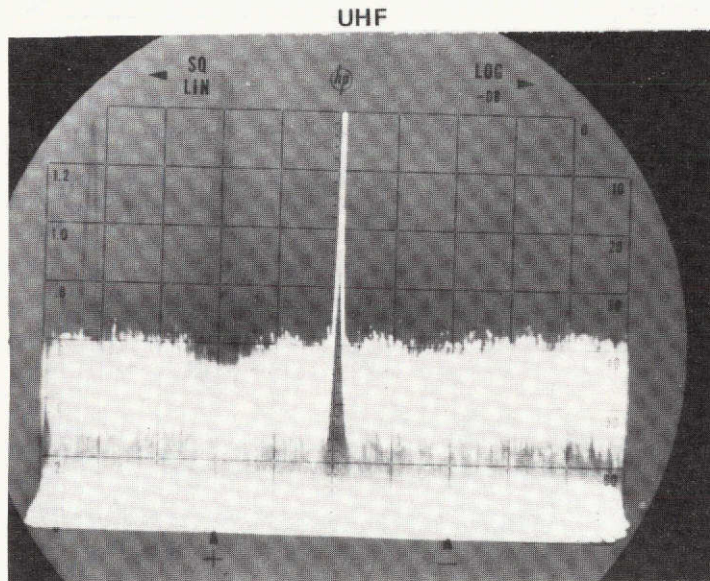
Figure 11-11. HET 1 Downlink Signal

10. <u>Earth stations</u>	1. AGC reading	<u>Not calculated</u>	dBm
	2. Antenna Gain (GR)	<u>50.9</u>	dB
	3. System Noise Temperature	<u> </u>	°K
	4. Receive Figure of Merit (G/T)	<u> </u>	
11. Total Path Lose (db) (includes path, atmospheric, and slant range)		<u> </u>	dB
12. Satellite Configuration (PRINT-COMBAT/COMM-001. as part of this data) Page Number		<u> 2 </u>	
13. Operations Mode (TDRE, ITV, etc.)		<u> </u>	
14. Notes:			

Figure 11-11. (Continued)

COMM. SUBSYSTEM QUICK LOOK DATA SHEET (FOR LINK CALCULATIONS)

1. Spectrum Analyzer Picture (Downlink)



GMT Start 164:07:32

Place _____

Date _____

Band UHF

Spectrum Analyzer Controls

Bandwidth 10 kHz

Scan Width 1 MHz/div

Scan Time 3 m Sec/div

Log. Ref. Level _____ dBm

Vertical Display 10 dB/div

Video Filter None

2. Satellite AGC reading (TLM #COMM-001)

-56 dBm

3. Uplink Frequency (f1)

6350.000000 MHz

4. Downlink Frequency (f2)

860.010700 MHz

5. Corrected Frequency (f3)

_____ MHz

6. Uplink

1. Transmitter Power (PT)

63 dBm

2. Antenna Gain (G_T)

59.9 dB

3. Effective Radiated Power (ERP)

122.9 dBm

4. Atmospheric Losses

200.0 dB

5. Antenna Gain (G_R)

17.2 dB

6. Calculate Power at Satellite

-59.9 dBm

7. Satellite Location (Longitude)

_____ °

8. Slant Range (to ROSMAN)

_____ °

9. Downlink

1. Transmitter Power (TLM-COMM-001)

49.3 dBm

2. Antenna Gain (G_T)

33.5 dB

3. Effective Radiated Power (ERP)

82.8 dBm

4. Atmospheric Losses

182.6 dB

5. Antenna Gain (G_R)

28.3 dB

6. Calculate Power received at earth stations

-72.5 dBm

Figure 11-12. UHF Downlink Signal

10. <u>Earth stations</u>	1. AGC reading	<u>Not calibrated</u>	dBm
	2. Antenna Gain (GR)	<u>28.3</u>	dB
	3. System Noise Temperature	<u></u>	°K
	4. Receive Figure of Merit (G/T)	<u></u>	
11. Total Path Loss (db) (includes path, atmospheric, and slant range)		<u></u>	dB
12. Satellite Configuration (PRINT-COMBAT/COMM-001. as part of this data) Page Number		<u>2</u>	
13. Operations Mode (TDRE, ITV, etc.)		<u></u>	
14. Notes:			

Figure 11-12. (Continued)

Table 11-3
Received Signal Strength (dBm)

Spacecraft				Ground	
Uplink	Measured AGC (dBm)	Calculated (dBm)	Downlink	Measured AGC (dBm)	Calculated (dBm)
C1	-63	-62.9	C2	-82	-80.9
C2	NA	-69.5	S1	-71	-73.5
C2	NA	-59.5	L1	-76.2	-76.1
C2	-68	-66.4	HET 2	NA	-59.4
C2	-69	-66.4	HET 1	NA	-58
C1	-56*	-59.9	UHF 1	NA	-72.5

*Ground antenna was peaked on S/C.

the two HET down-link transmissions. Some ground interference had been noted during this period. These spurs have not been seen in any subsequent HET tests which included other IF configurations. Actual HET operation has taken place with excellent picture transmission. Figure 11-12 shows an up-link C-band signal transponded at UHF (860 MHz). In general, the transponded signals looked clean.

Figure 11-13 provides photographs of up-link and down-link baseband video for the ITV signal. Fidelity is excellent with only Gaussian noise affecting the down link signal.

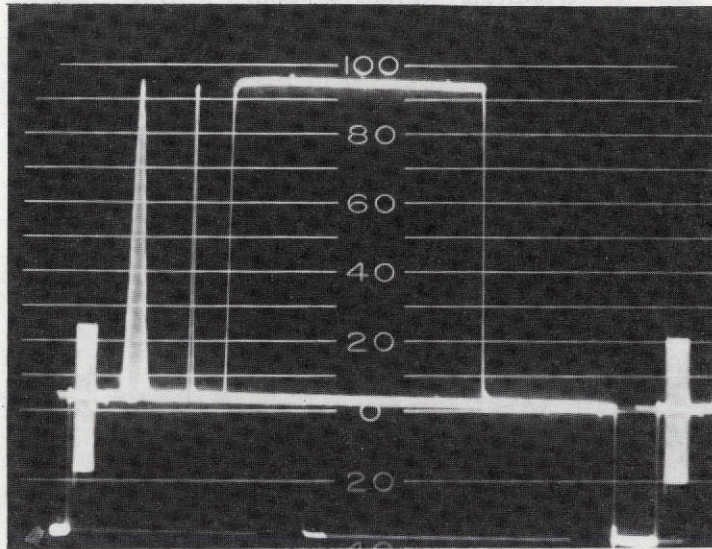
Figure 11-14 shows the TV camera video modulating the Wide Band Data Unit (WBDU). Extraneous signals were well below threshold and presented no interference as shown by the excellent picture transmission given in Figure 11-5 and 11-6.

Figure 11-15 was obtained during the COMSAT propagation experiment with the ground receiver receiving a 4150 MHz from the Earth Coverage Horn (ECH). Figure 11-16 shows spectrum photos obtained during the C-band ECH Receive Antenna pattern testing. Two carriers were used: one from Rosman and one from Mojave.

164:10:08

860 UPLINK

6/13/74

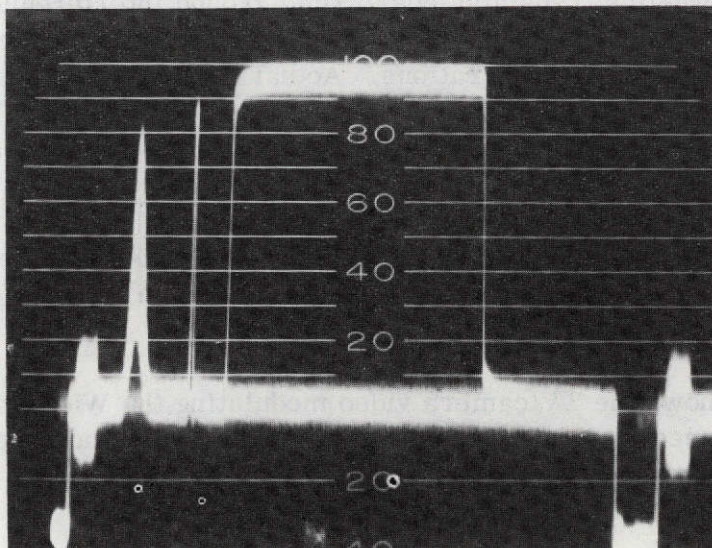


Uplink

164:10:07

860 DOWNLINK

6/13/74



860 DOWNLINK

Downlink

Figure 11-13. SITE TV Signal

TV CAMERA 154:02:30 6/2/74 10:30 PM

TIME — 154:02:30
DATE — 6/2/74

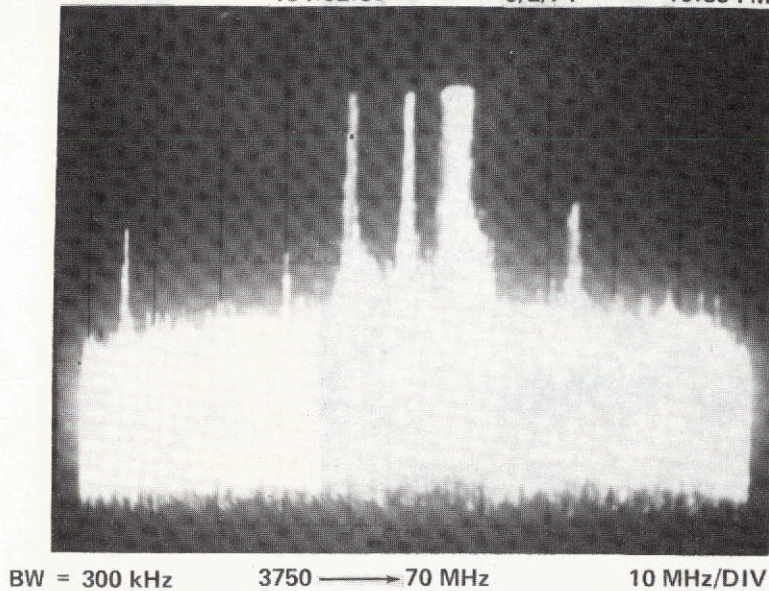
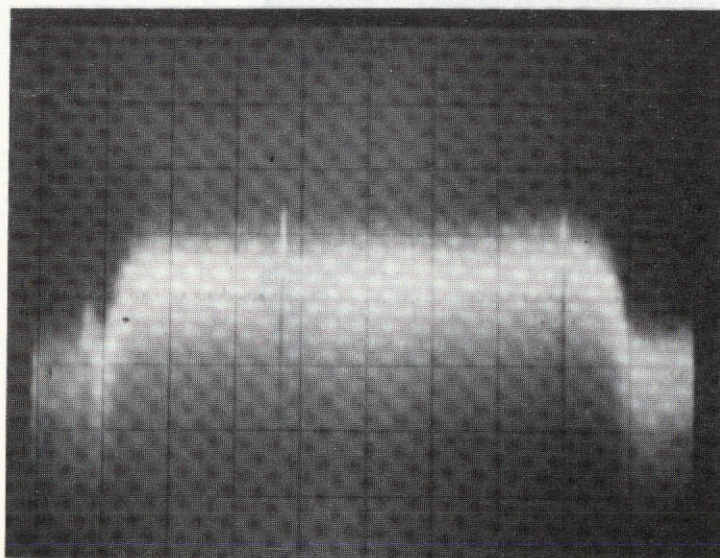
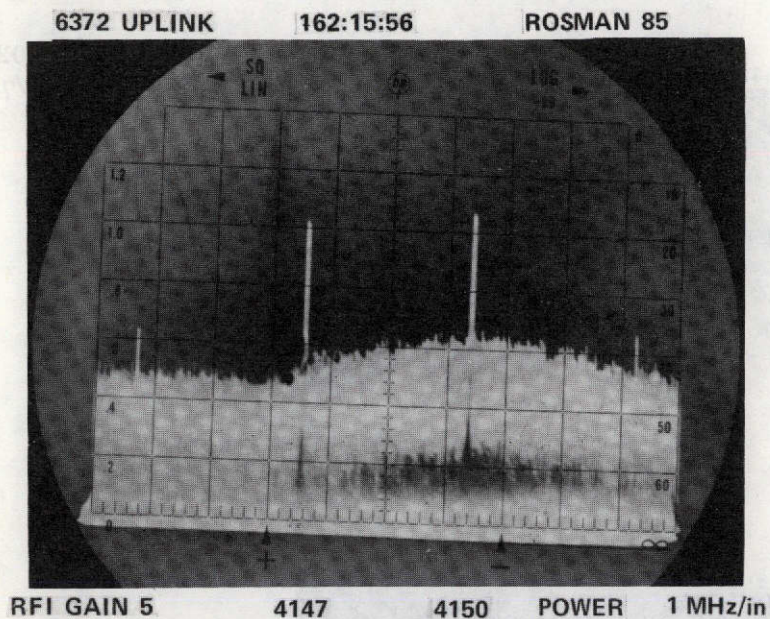


Figure 11-14. TV Camera



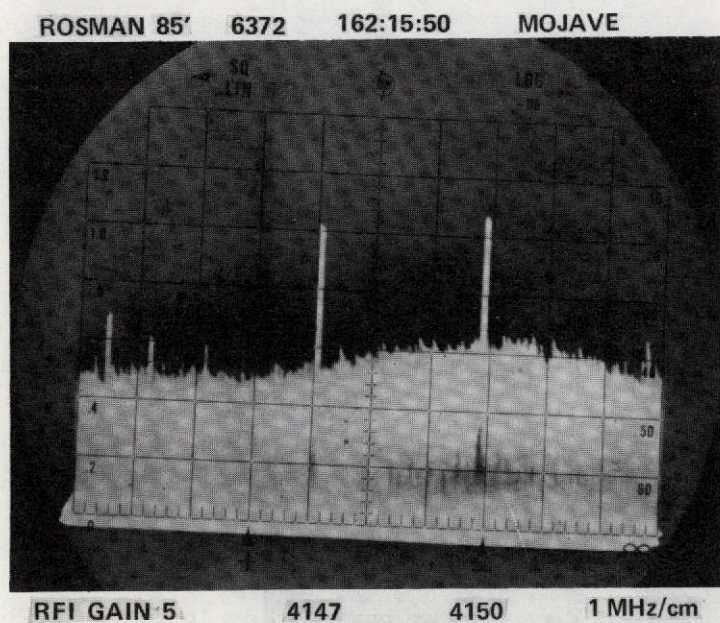
RCVR TUNED TO 4150 MHz

Figure 11-15. COMSAT Propagation Signal Spectra



TIME — 162:15:50
DATE —

(a) From ROSMAN



TIME — 162:15:56
DATE —

(b) From Mojave

Figure 11-16. RF Spectra used to evaluate ECH
Receive Antenna Patterns

The C-band power drop photos (Figure 11-17) were taken during a trouble-shooting period. These so called "glitches" or limited power drops are discussed in section 11.5. Figure 11-17a shows the momentary change of amplitude on the carrier. Figure 11-17b shows the close-in spectra using the WBDU with low level interfering signals. Figure 11-17c, taken with zero scan width and storage, shows the actual power drop similar to that seen on the strip chart recorders.

Figure 11-18 shows the multiple modulated carriers used in C-band (ATS-R) ranging from the Rosman and Santiago earth stations, while Figure 11-19 shows the C-band carrier and IF beacon from Mojave and Denver.

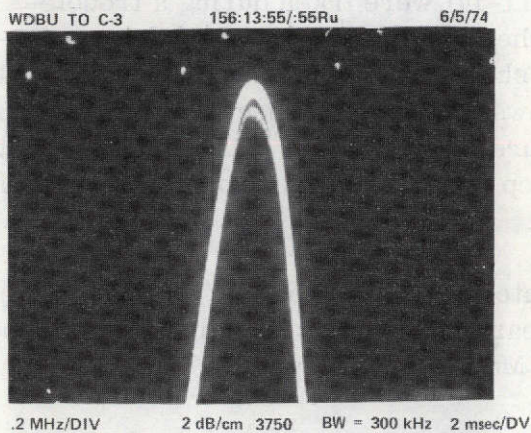
11.4 ANTENNA PATTERNS

During the first month of spacecraft operation, antenna patterns were measured of the ATS-6 reflector/feed at various frequencies and of the C-band earth coverage horn (ECH). Table 11-4 summarizes the status of the antenna patterns. A preliminary analysis of the printouts has been made for some antenna patterns where computer-generated antenna patterns were not available.

Antenna patterns were measured by first positioning the spacecraft Z-axis in an attempt to point the center of the applicable antenna beam at ROSMAN. The spacecraft Z-axis was then slewed in a predetermined pattern about ROSMAN while the RF signal received at ROSMAN was recorded. The data were later correlated with angle information and conventional antenna pattern plots were produced. The angle information (spacecraft attitude) was generated in real time by the on-line attitude determination program ONATT at ATSOCC and sent to ROSMAN for recording with the signals received from the spacecraft.

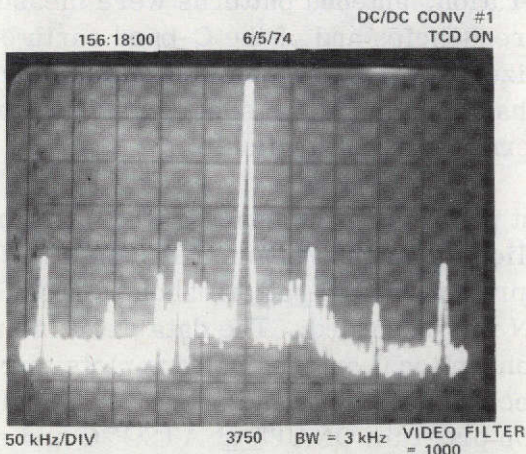
The spacecraft maneuvers for the UHF (860 MHz) patterns are shown in the polar plot of Figure 11-20. The radial excursions extend out to about $\pm 5^\circ$ from bore-sight at ROSMAN. This angle range covers the first side lobe. Of the four antenna pattern cuts taken (two principal and two oblique), two patterns are shown in Figure 11-21 and 11-22. The North-South cut shows good symmetry and deep first nulls thereby indicating that focusing is excellent. A comparison of the measured in-orbit pattern and that obtained on the 30 foot hard dish at Philco-Ford is shown in Figure 11-23.

A comparison of the S-band on-axis receive antenna pattern is shown in Figure 11-24. The "X" in the figure represents measured in-orbit data; the "dash line" represents the test data taken on the 30 foot hard dish at Philco-Ford. The figure shows a close correlation between N-S cut antenna pattern measured in-orbit and the test data.



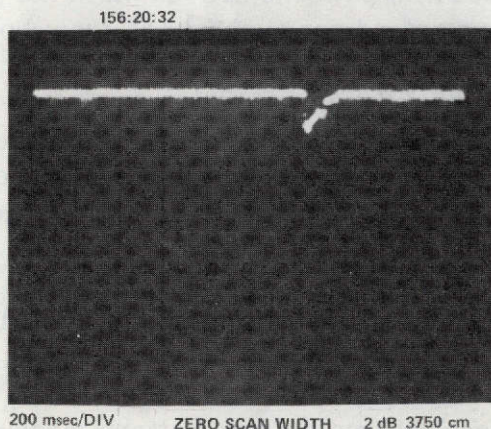
TIME — 156:13:55/:55PM
DATE — 6/5/74

(a)



TIME — 156:18:00
DATE — 6/5/74

(b)



TIME — 156:20:32
DATE —

(c)

Figure 11-17. C-Band Power Drops

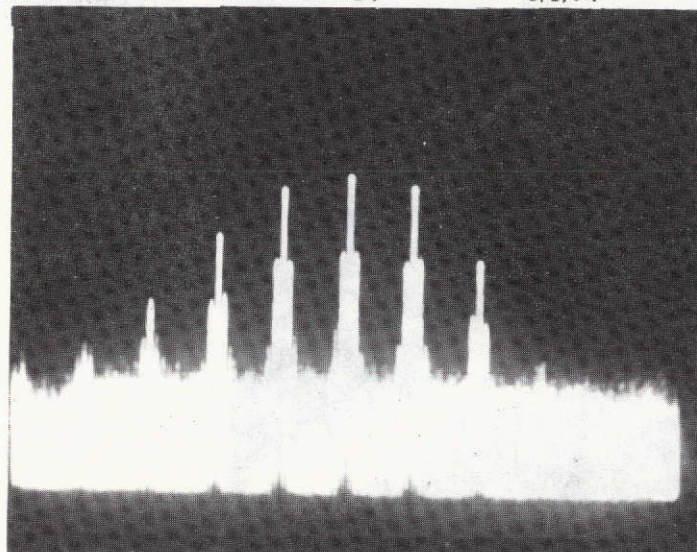
RANGING

ROSMAN 154

6/3/74

TIME — 154:

DATE — 6/3/74



BW = 100 kHz

5 MHz/DIV

(a) From ROSMAN

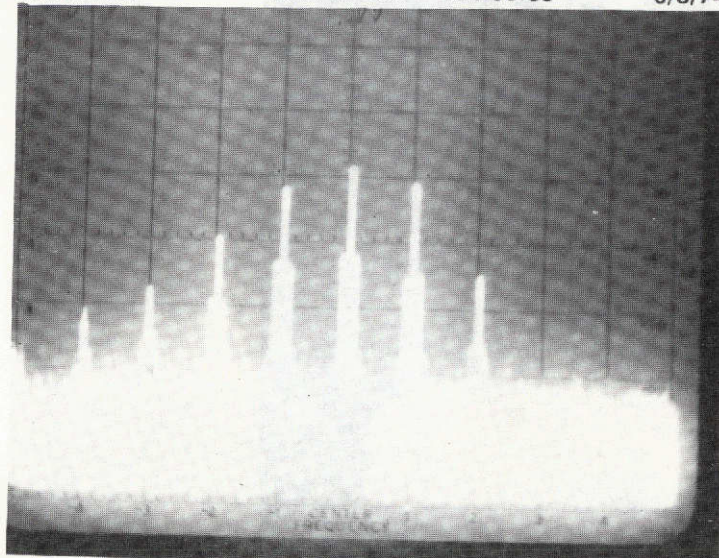
RANGING

SANTIGGO 154:05:38

6/3/74

TIME — 154:05:38

DATE — 6/3/74



1:38 AM

BW = 100 kHz

5 MHz/DIV

(b) From Santiago

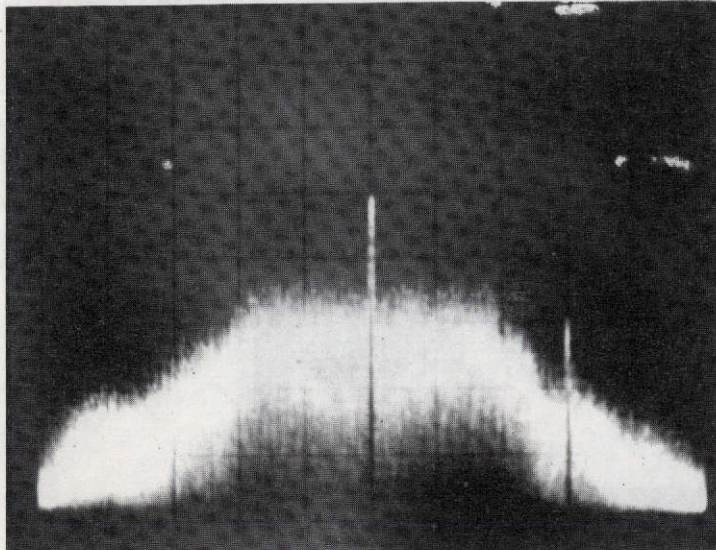
Figure 11-18. ATS-R C-Band Ranging Signal Spectra

FROM MOJAVE

6/2/74

TIME — 156:17:56

DATE — 6/2/74



153:17:56

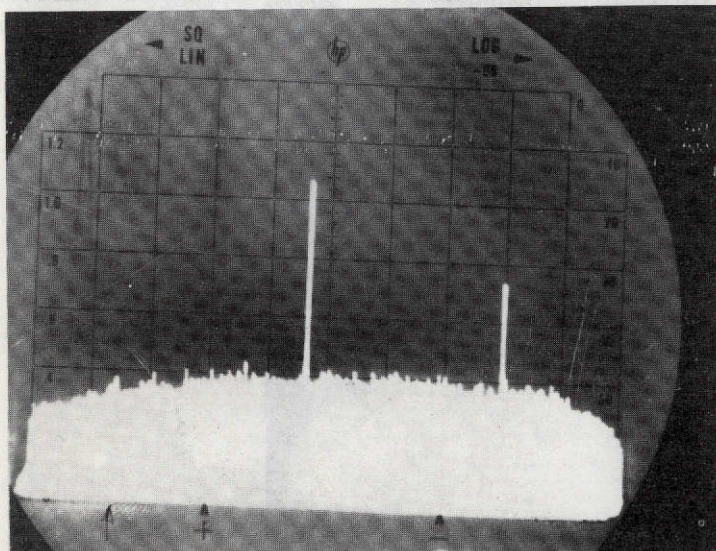
(a) From Mojave

DN CONV. OUT

10 MHz/DIV

TIME — 164:19:00:10

DATE —



164:19:00:10 GMT

DENVER

(b) From Denver

Figure 11-19. C-Band Carrier & IF Beacon to Rosman From Mojave & Denver

Max. Attitude Errors
Deg.

Leg #	R	P	Y
1	.031	.039	.016
2	.039	.070	.437*
3	.078	.039	.039
4	.039	.070	.070
5	.039	.070	.048
6	.100	.039	.055
7	.039	.039	.039
8	.070	.048	.039
9	.048	.031	.031

*PSA 2 Lost Acquisition

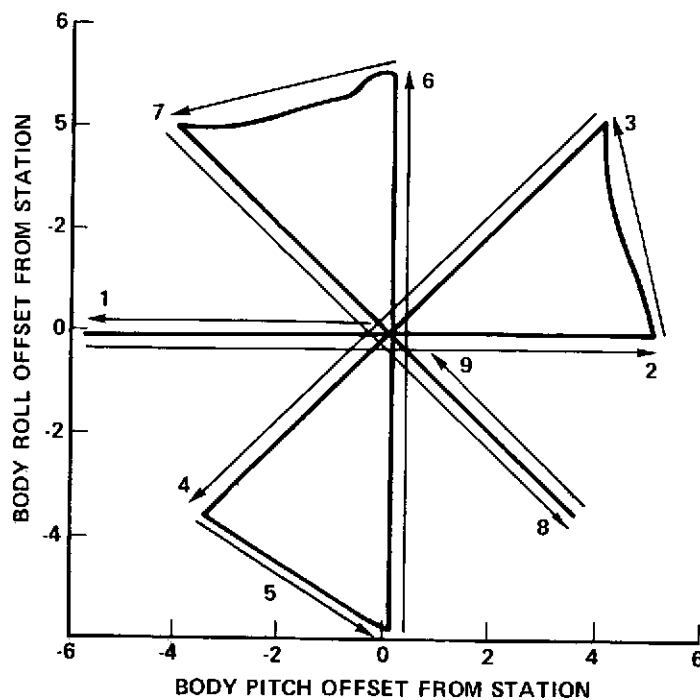


Figure 11-20. Antenna Pattern Maneuver (5 Degree)

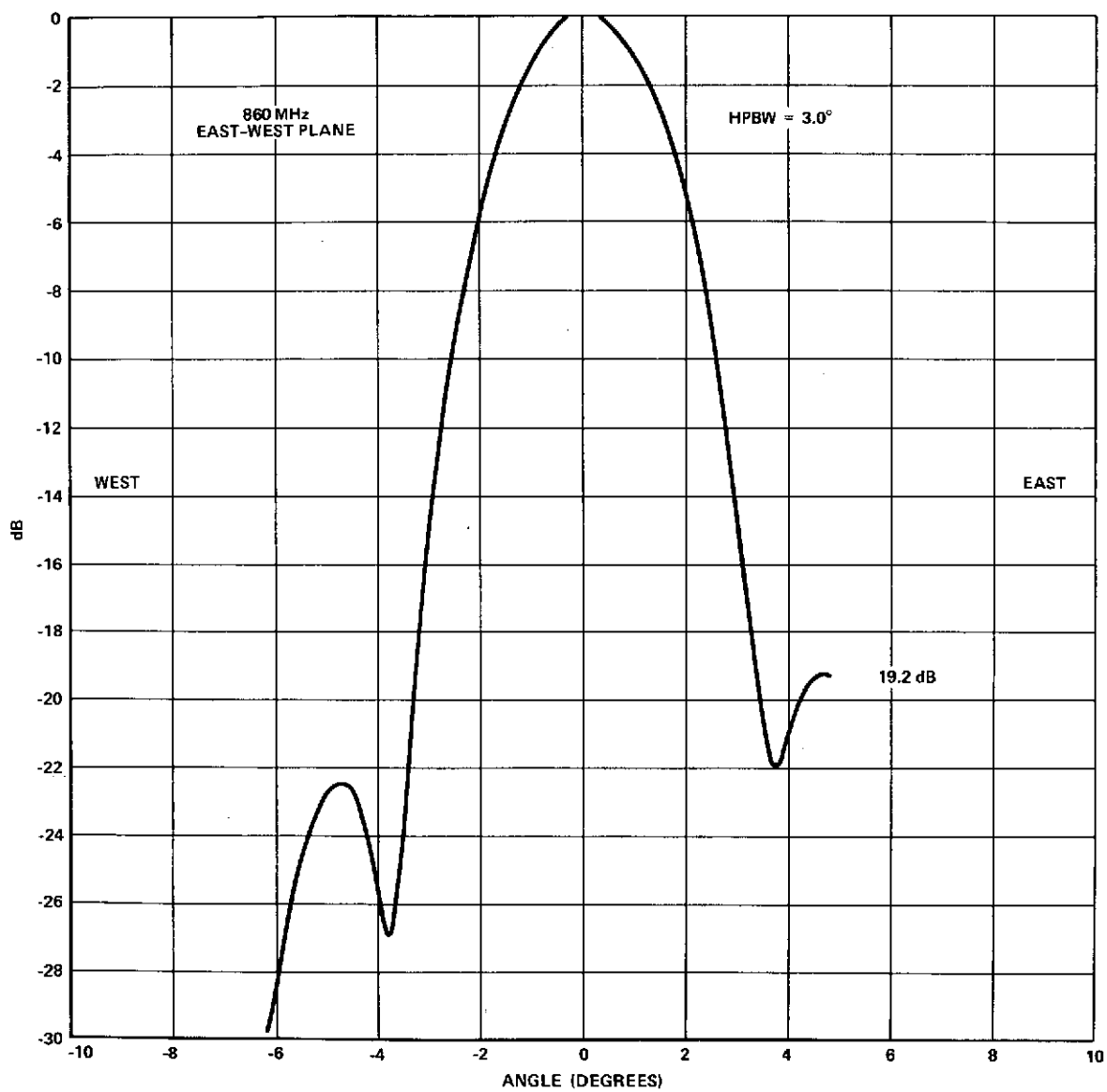


Figure 11-21. ATS-6 In-Orbit Pattern Data

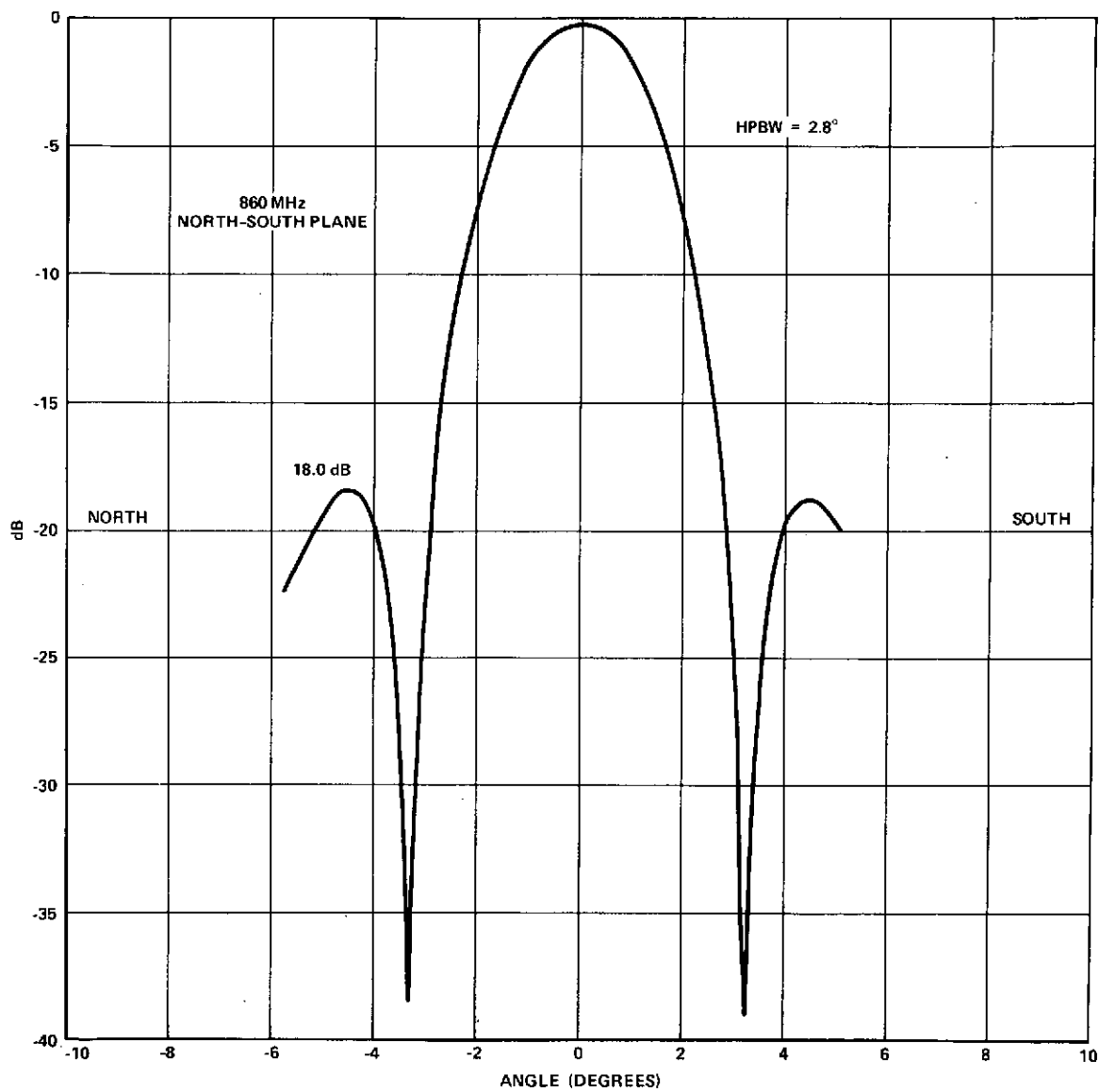


Figure 11-22. ATS-6 In-Orbit Pattern Data

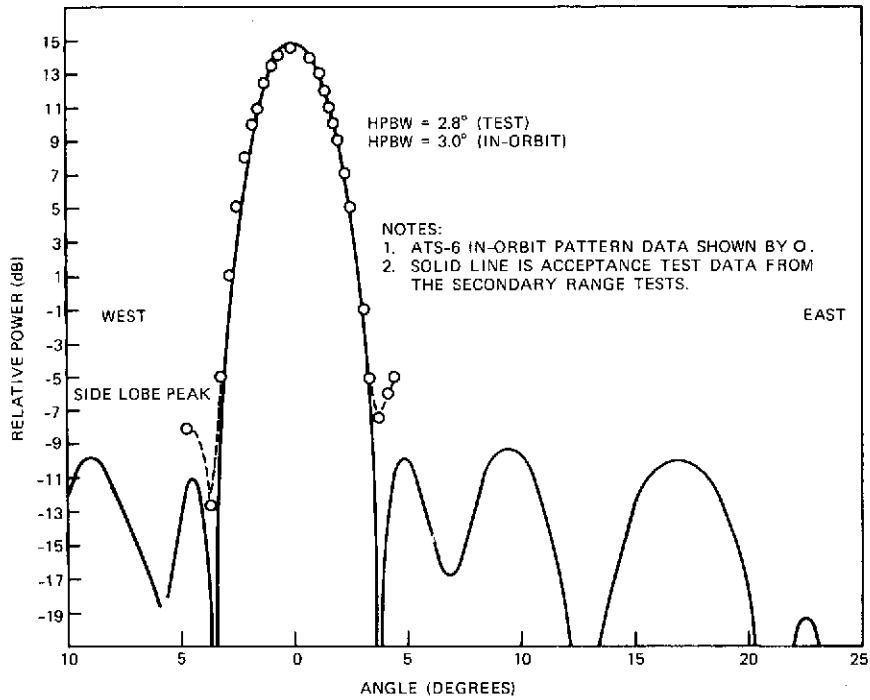


Figure 11-23. UHF (ITV) Pattern Data

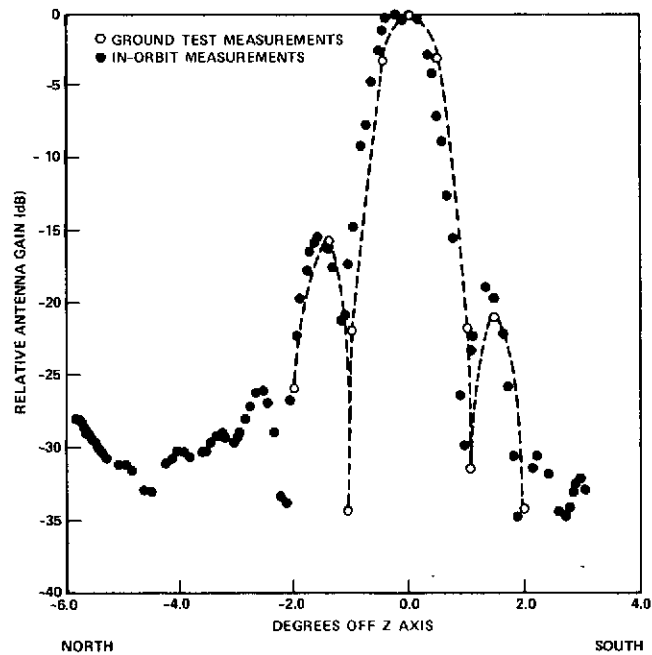


Figure 11-24. S-Band On-Axis Receive at Spacecraft

Table 11-4
Antenna Pattern Status

Type of Pattern	Computer Plotted	Hand Plotted	Tabular Data
C-Band ECH Receive			
C-Band ECH Transmit			
C-Band PFF Receive			
S-Band On-Axis Receive	X		
S-Band On-Axis Transmit			X
S-Band N5 Beam Transmit			X
HET S1 Transmit			X
HET S2 Transmit			X
S-Band Cross		X	X
L-Band Fan Transmit	X		
L-Band Pencil			X
UHF Transmit	X		X

The generation of the antenna pattern for the S-band Cross was unique. As the spacecraft was slewed, the S-band elements were selected by ground command at the approximate crossover of adjacent beams. The results are shown in a series of four graphs (Figures 11-25 through 11-28). For comparative purposes, the acceptance test data is shown above the in-orbit results. The difference in level between the two sets of data is arbitrary and does not represent the difference in absolute gain.

The L-band fan transmit antenna pattern is shown in Figure 11-29. The dip in antenna gain on-axis was predicted from pre-launch test data taken at the Philco-Ford range.

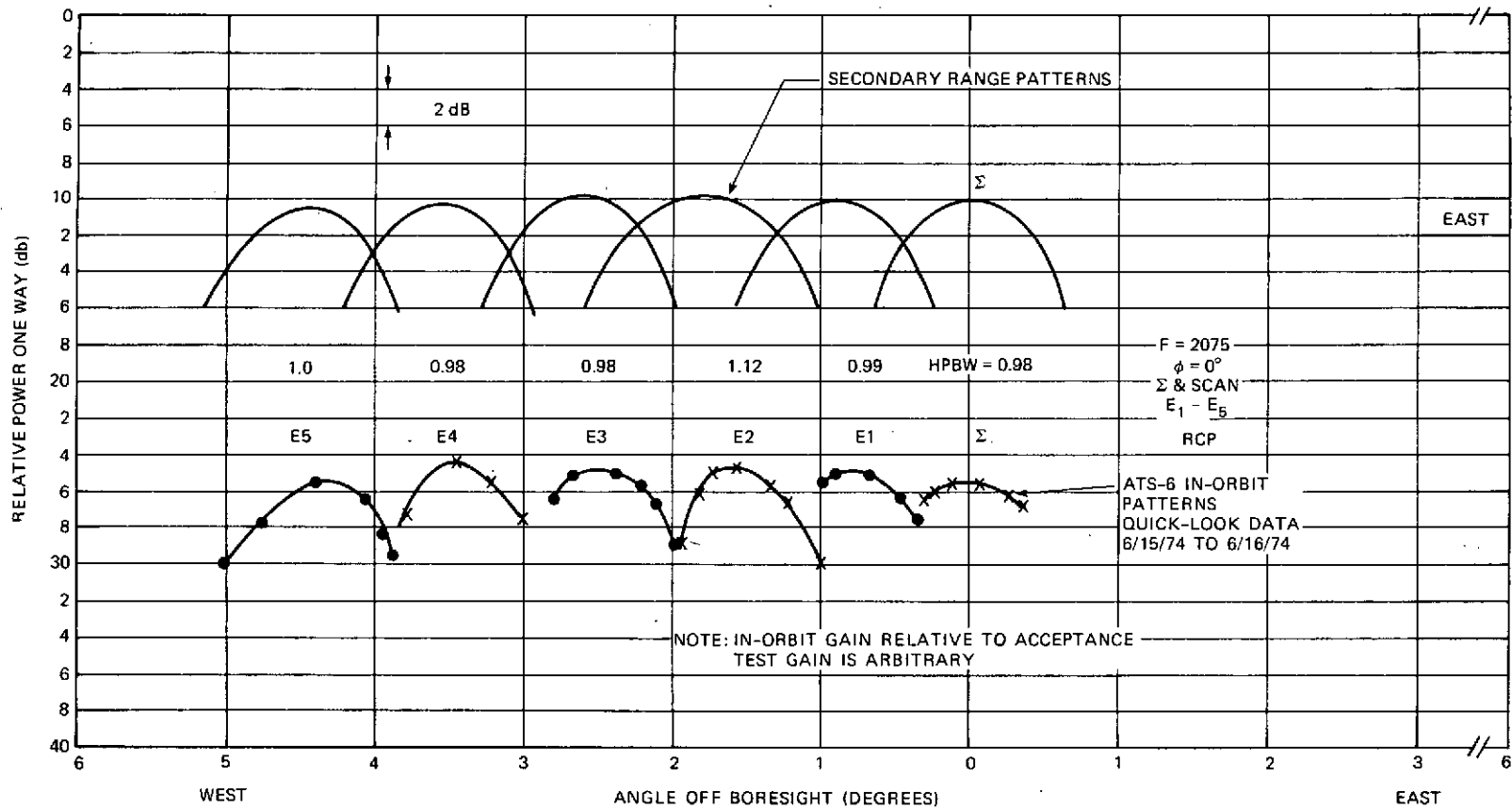


Figure 11-25. S-Band Cross Patterns (East Arm)

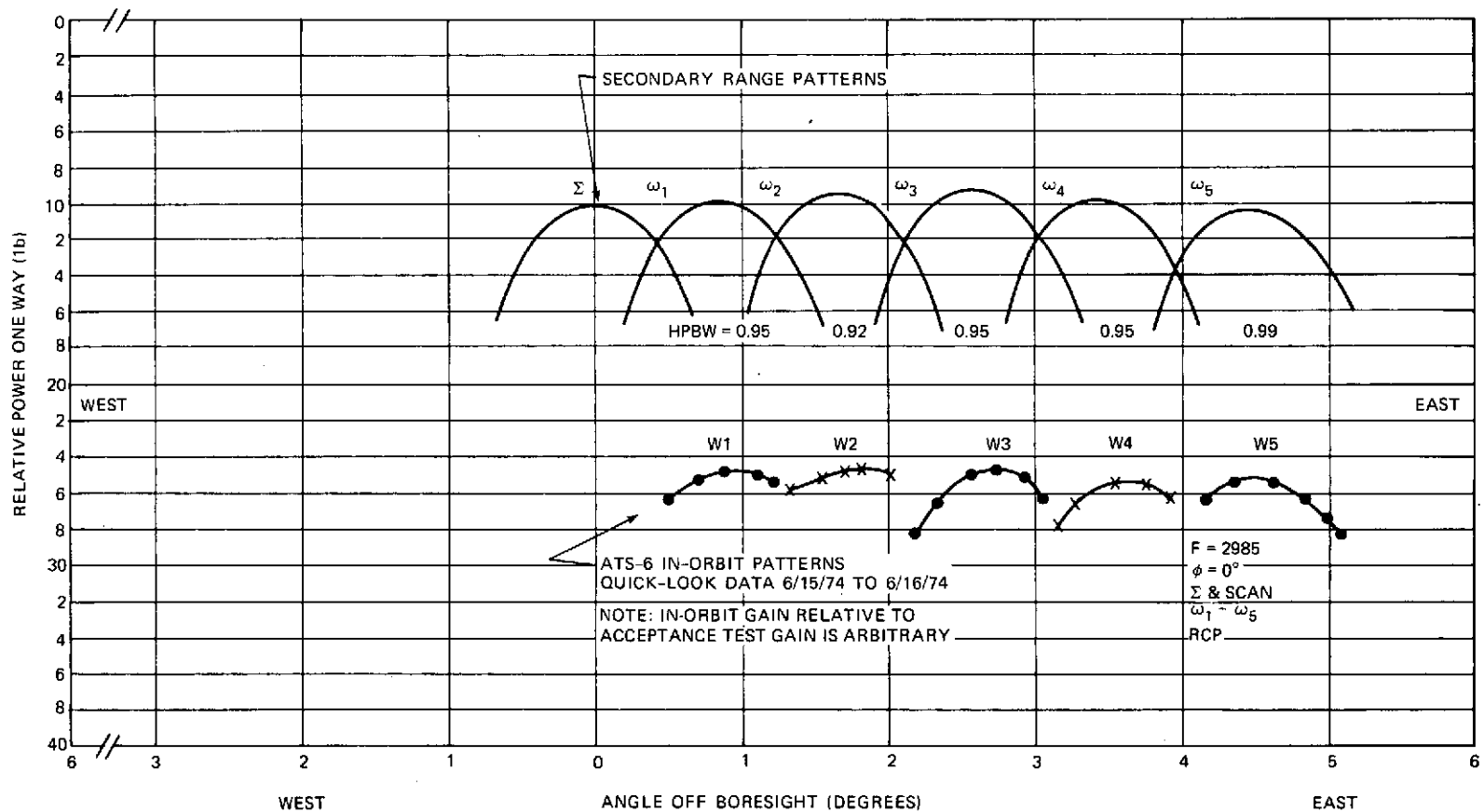


Figure 11-26. S-Band Cross Patterns (West Arm)

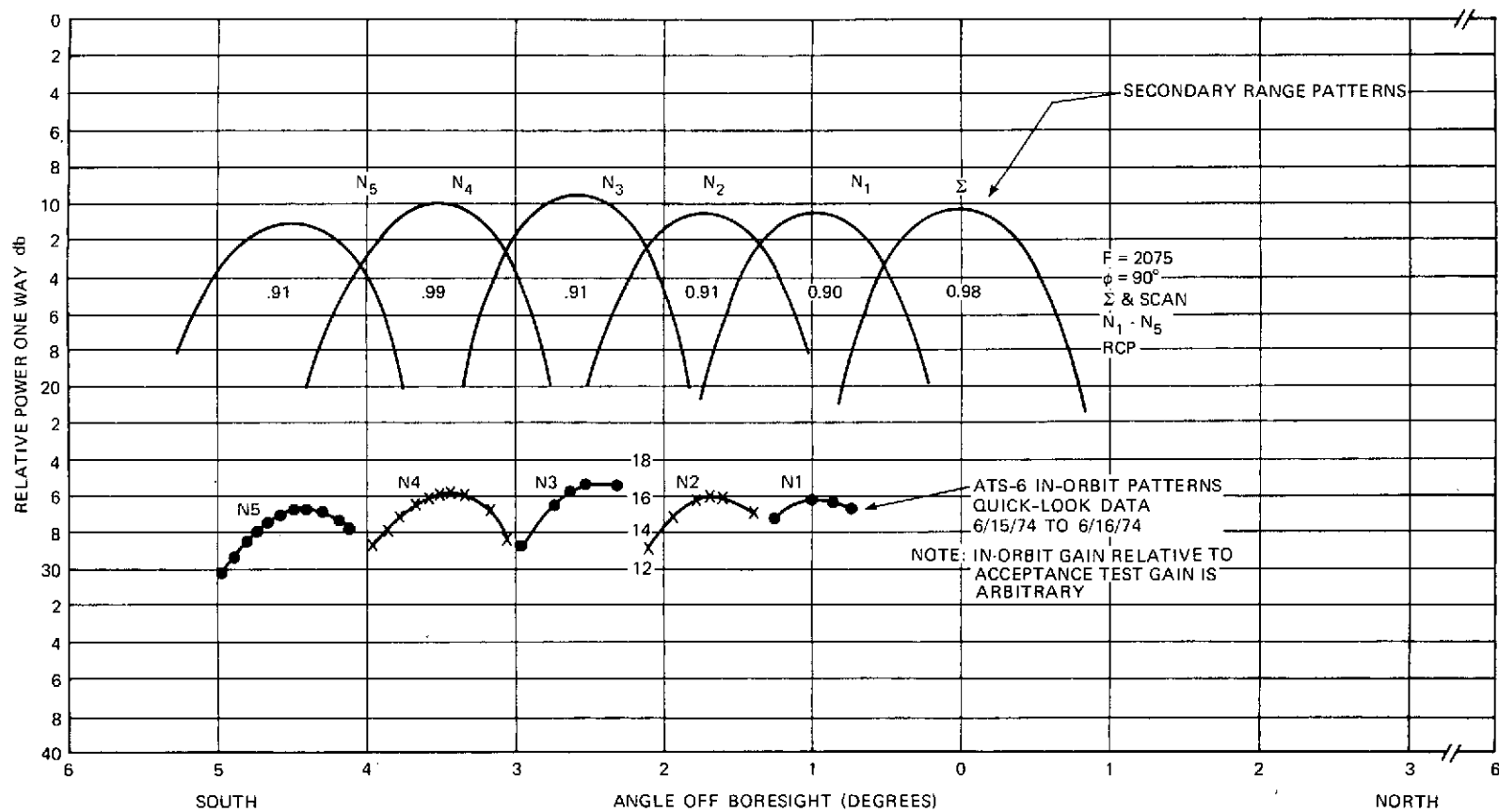


Figure 11-27. S-Band Cross Patterns (North Arm)

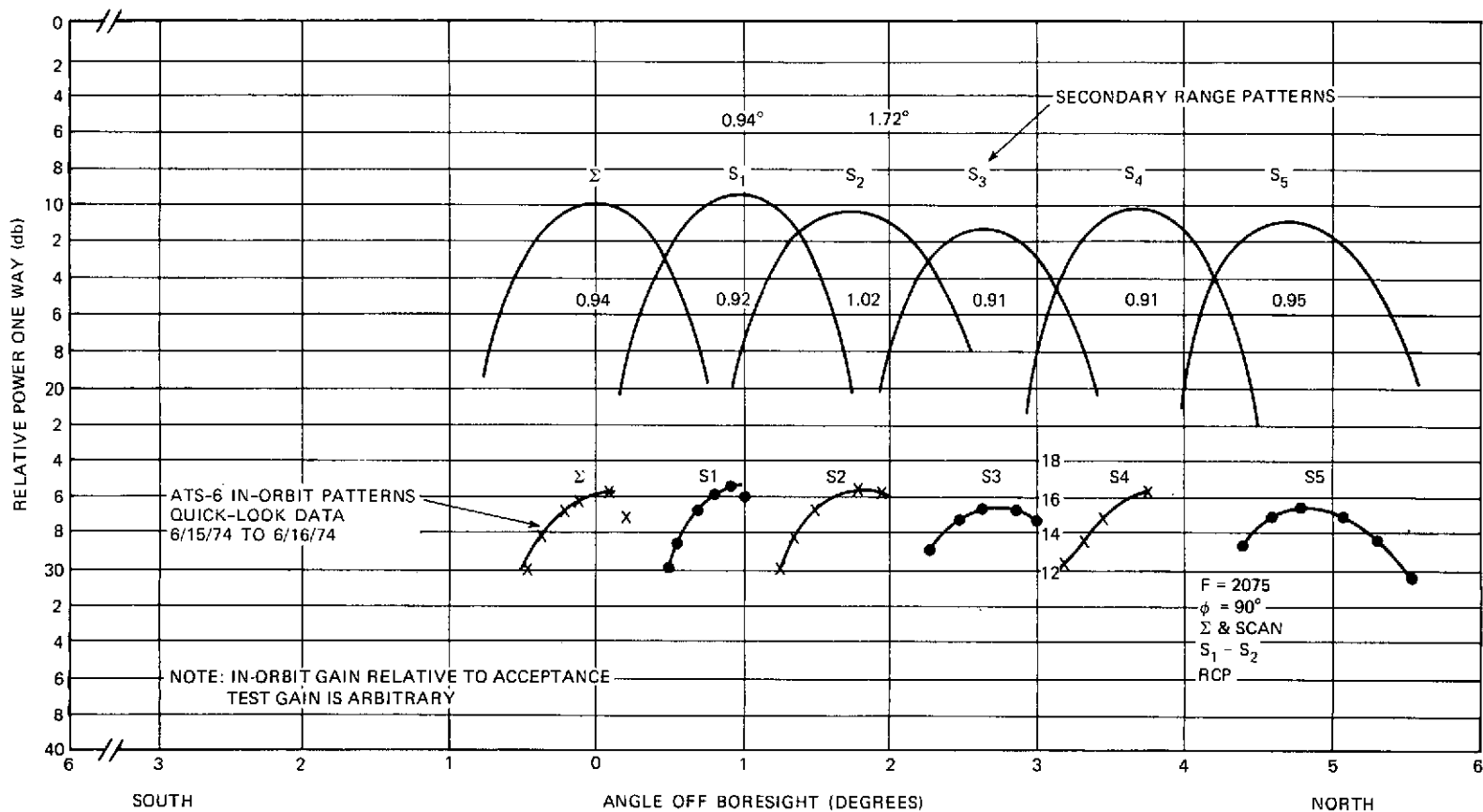


Figure 11-28. S-Band Cross Patterns (South Arm)

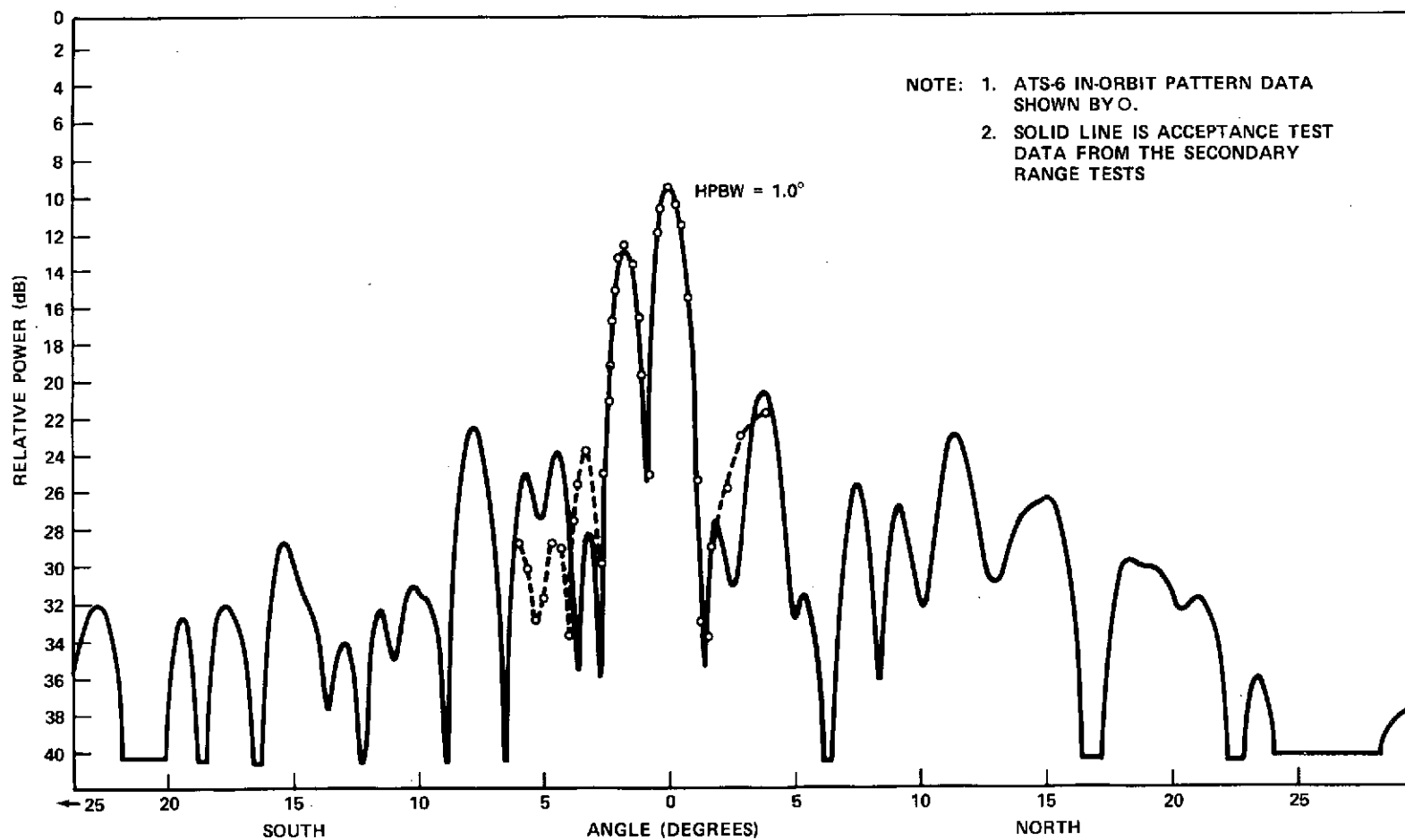


Figure 11-29. L-Band Fan Antenna Pattern

A comparative tabulation of in-orbit data and pre-launch data is given in Table 11-5. Data in parenthesis was taken on hard dish at Philco-Ford. No significant differences exist.

11.5 ANOMALOUS PERFORMANCE

Recurring power drops ("glitches") ranging from 0.2 to 2.0 dB in C-band down-link transmissions were observed on strip-chart recordings of ROSMAN ground receiver AGC. Initial periodicity ranged between 20 and 120 seconds with pulse width approximately 200 milliseconds. Various causes were hypothesized including premature TWT turn-on with sufficient time for outgassing, corona, multi-pacting and external radio interference. A series of trouble-shooting sequences were run introducing configuration changes involving IF amplifiers, synthesizer, TCD and WBDU, but without effect. The use of the on-board WBDU eliminates any contributions introduced by the uplink. Operation at reduced power levels substantially alleviated the problem. Pending the results of a ground simulation test, it was decided to continue operations at reduced power.

Table 11-5
ATS-6 Antenna Pattern Summary Data

Pattern	Half Power Beam Width (HPBW) In Degrees Side Lobe Gain (SL) in dB											
	West-to-East			NE-to-SW			South-to-North			NW-to-SE		
	SL	HPBW	SL	SL	HPBW	SL	SL	HPBW	SL	SL	HPBW	SL
S-Band, Xmit, On-Ax. 6/15/74, Run 6	15.7 (13.4)	.93 .98	12.6 13.8	12.9	1.01	18.1	17.3 (14.9)	.98 .97	13.3 15.4)	13.8	1.07	17.0
S-Band Cross 6/15/74 to 6/16/74	See Figures 11-25 through 11-28											
S-Band, Xmit, N-5 Element. Run 7. 6/15/74	8.1	-	9.0	7.5	-	9.2	20.5	1.1 (.97)	6.6	6.5	-	20.1
HET Xmit, S-1 Element. Run 9. 6/16/74	19.4	.64	20.5	12.7	-	16.7	19.0	*	12.2	7.9	-	16.2
S-2 Element. Run 10 6/16/74	17.5	-	29.2	9.8	-	25.0	19.0	*	14.4	9.5	-	22.1
L-Band Xmit, Pencil Run 11, 6/16/74	11.6 (13.0)	- 1.3	14.1 16.7	11.5	-	30.7	18.8 (19.0)	1.3 1.3	10.4 11.8)	11.5	-	22.4
L-Band Xmit, Fan Run 12, 6/16/74	1.4 dB DIP (4.0 dB DIP)						11.6 (11.1)	1.0 1.0	2.8 3.4)			
UHF, Part 1, Run 4 Part 2, Run 5 6/15/74	22.5 (24.2)	3.03 2.8	19.2 (25.8)	15.4	2.82 2.7	15.4 (15.2)	21.7 (19.6)	2.73 2.7	18.0 (27.4)	14.4 (17.2)	2.87 2.8	15.4 (14.7)

*HPBW not available from in-orbit data. For comparison, acceptance test data (hard dish) shown in parenthesis.
shown in parenthesis.

A 10 dB IF pad was switched in along with a 6 dB pad at the output of the triplexer-combiner. With the WBDU, only the 6 dB pad could be used. Statistical observations have led to characterizing the probability density distribution. The results appear in Figures 11-30 through 11-33. Observations were made with both the ECH and PFF switched in. Curve fitting has shown the form of a Cauchy distribution, which is typical of high-voltage breakdown.

A ground simulation/test effort was initiated at the Philco-Ford facility in California, using a qualification model TWTA and F-prime C-band output components in a thermal-vacuum chamber. Similar power drops were observed, and attempts to isolate the problem have identified an apparent power handling problem in the C-Band transmitter output filter. Preliminary results indicate the phenomenon is a low energy gas discharge caused by residual epoxy contaminants inside the filter. The impact of the problem on ATS-6 C-Band transmitter mission life is under continuing investigation.

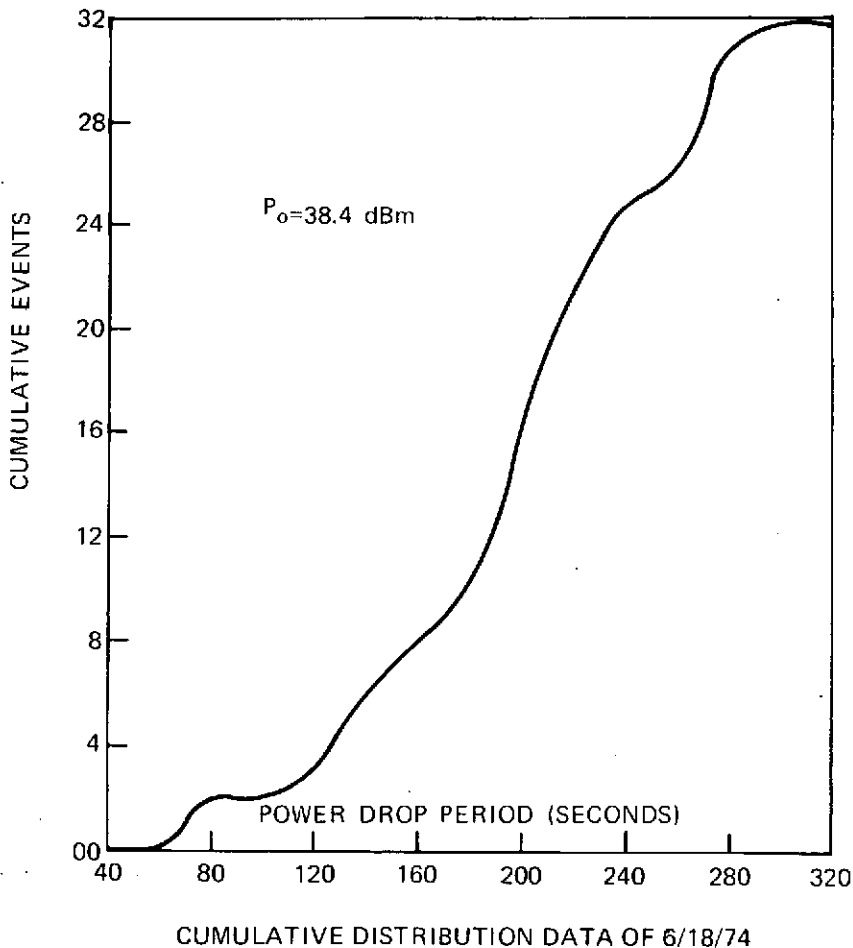


Figure 11-30. Cumulative Distribution Data of 6/18/74

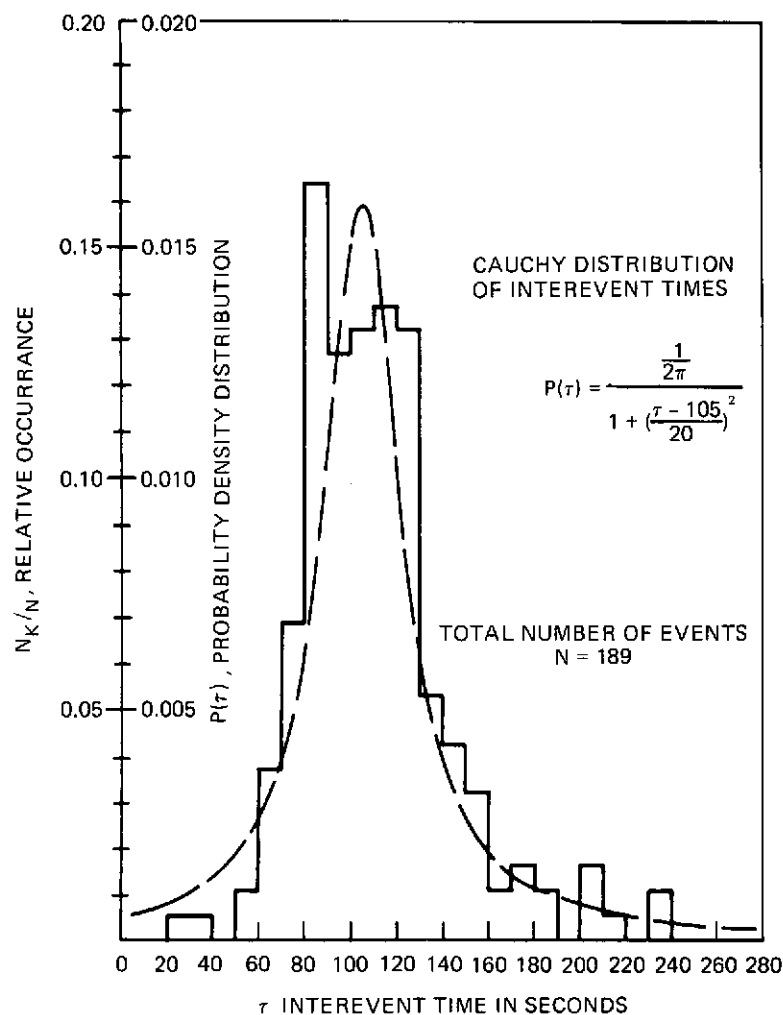


Figure 11-31. Cumulative Distribution Data of 6/5/74

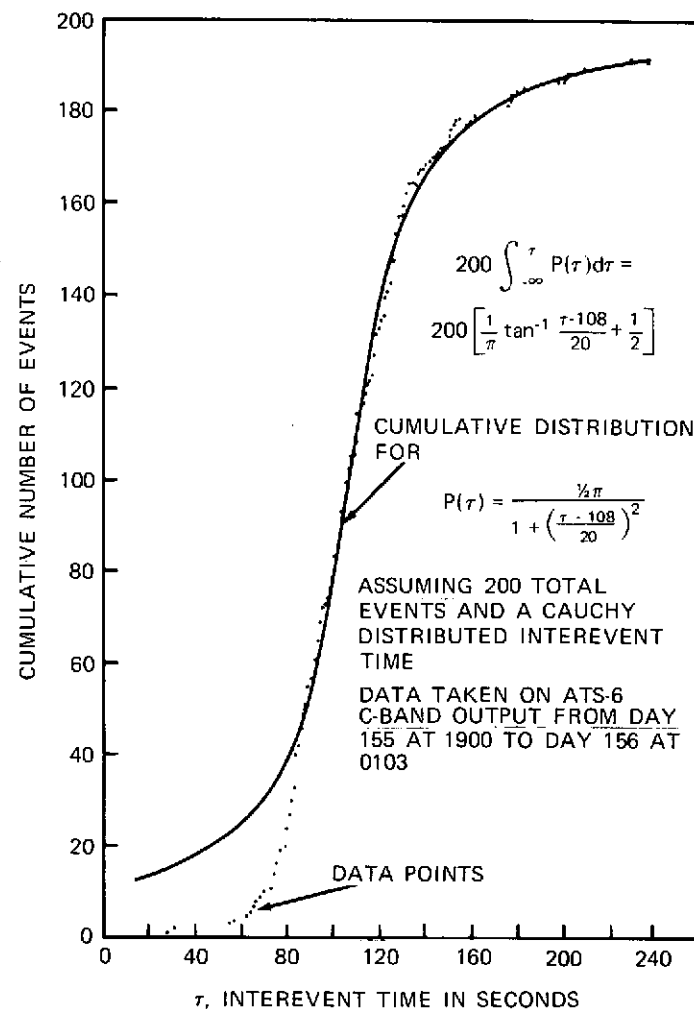


Figure 11-32. Cumulative Distribution Data of 6/5/74

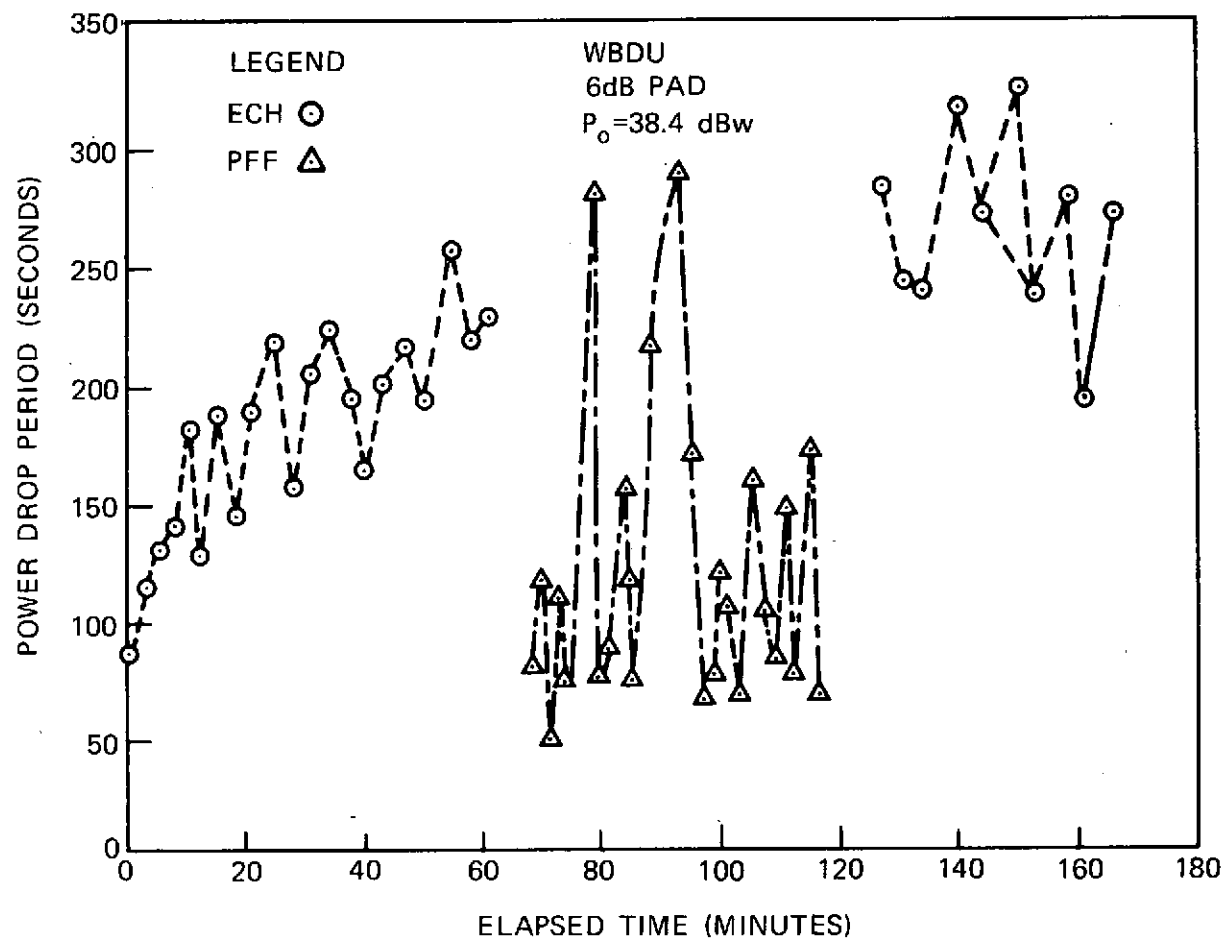


Figure 11-33. Cumulative Distribution Data of 6/18/74

SECTION 12

EXPERIMENT SUBSYSTEM (GFE)

SECTION 12

EXPERIMENT SUBSYSTEM (GFE)

12.1 SUBSYSTEM PERFORMANCE

During spacecraft checkout all the GFE Experiments except for the Ion Engines were activated in functional configuration. The Ion Engine LIC's and Master Converters were turned on to provide thermal dissipation in support of other spacecraft activities, but normal system operation was not scheduled.

The functional GFE Experiments were configured to all operational modes, as listed in Table 12-1 and performance was satisfactory, with the few exceptions noted.

Table 12-1
Checkout of Experiment Modes

EXP	MODE	EXP	MODE
PROPAGATION	"A" UNITS "B" UNITS	EME	UCLA
MMW	20 GHz HORN		HAC
	30 GHz HORN		GSFC
	20 GHz PARABOLA		ASC
	30 GHz PARABOLA		UMINN
ATFE	FEED-BACK CONTROL		UNH
QCM	DACU 1		UCSD
	DACU 2		MDAC
	DEGAS		
VHRR	VISIBLE		
	IR		
	VISIBLE CALIBRATION		
	ROSMAN		
	SUB-SAT		
	SINGLE FRAME		
	SECTOR SCAN		

The Experiment support systems have been monitored closely and, with one exception, have been found to be well within specified limits. That exception is yaw jitter amplitude which has not yet been measured with sufficient accuracy and has been presented conservatively. It is anticipated that the yaw jitter amplitude performance will be adequate to properly support Experiments, and that future data analysis will demonstrate this parameter to be within specification.

The support given to Experiments by the spacecraft Electrical Power, Telemetry and Command, Thermal Control, Communications, and Attitude Control Sub-systems has been excellent.

12.2 EXPERIMENT DESCRIPTION

12.2.1 Millimeter Wave Experiment

The Millimeter Wave experiment equipment consists of two transmitters, one radiating at 20 GHz and the other at 30 GHz. For two of the three operating modes, all of the elements comprising the transmitters have redundant elements which may be switched in by command. For the third mode (communications) no redundancy is provided for some of the system elements. The equipment is divided into four major units: the RF multiplier, the 20/30 GHz modulator/power amplifier, the 20/30 GHz horn antenna assembly, and the 20/30 GHz parabolic antenna, all of which are located in the earth viewing module of the spacecraft. The equipment requires approximately 70 watts of power from the spacecraft bus.

12.2.2 Propagation Experiment

Figure 12-1 is a block diagram of the propagation experiment transponder. The transponder is a single-frequency conversion repeater with separate inputs at 13.19 to 13.20 GHz and 17.79 to 17.80 GHz; its combined outputs are amplified and retransmitted at 4.150 GHz. Full redundancy is provided for each trans-lation and for the combined output amplifiers.

12.2.3 Environmental Measurements Experiment

The environmental measurements experiment (EME) is a scientific satellite experiment package consisting of eight experiments, a PCM encoder, real time clock, command interface control, power supply, solar aspect sensor, and an active thermal control system.

The EME package is located on a structure at the base of the 30-foot parabolic reflector on the outboard side of the reflector hub. The purpose of the EME is

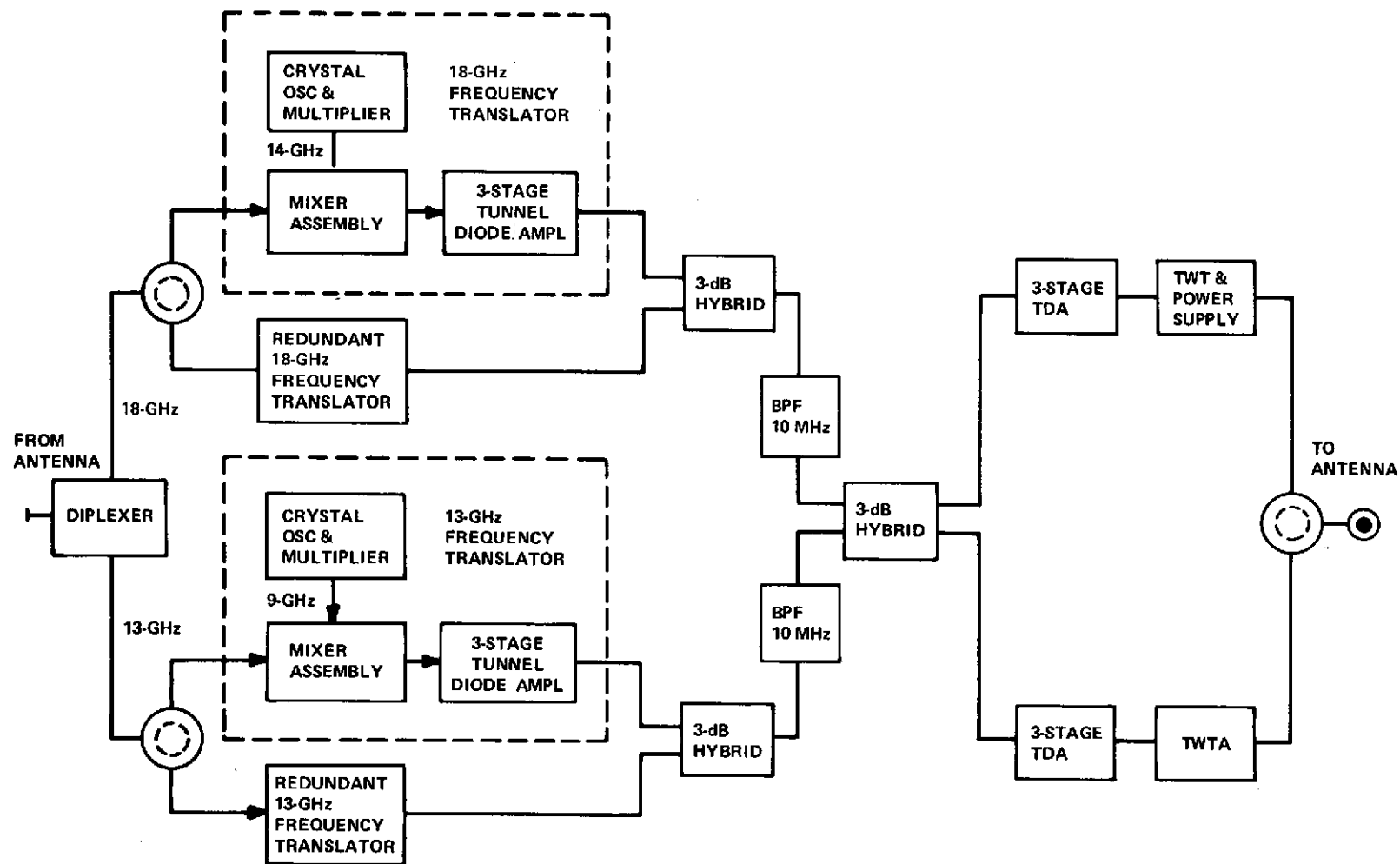


Figure 12-1. Block Diagram of the Propagation Experiment Transponder

to gain additional scientific knowledge of a synchronous orbit earth environment. Table 12-2 summarizes EME objectives.

12.2.4 Quartz Crystal Microbalance (QCM) Contamination Monitor

The primary objective of this experiment is to provide data regarding the presence of contaminants on the spacecraft. This is done by the use of a quartz

Table 12-2
ATS-6/EME Experiments

Experiment	Experiment Characterization	Purpose
McDonnell Douglas	Solar Cosmic Ray	Study solar cosmic rays, entry and propagation within magnetosphere, make detailed measurements of trapped electrons.
University of New Hampshire	Low Energy Proton-Electron	Make swept and pitched angle measurements of low energy electrons and protons in the magnetosphere.
GSFC/NOAA	Low Energy Proton	Study low energy protons.
University of Minnesota	Electron-Proton Spectrometer	Investigate the origin of the Van Allen trapped radiation.
UCSD	Auroral Particles	Study the distribution of low energy electrons and protons.
UCLA	Magnetometer	Study the magnetic field at synchronous distances.
Hughes	Solar Cell Radiation Damage	Measure life characteristics and performance degradation of solar cells in space.
Aerospace	Omnidirectional Spectrometer	Measure omnidirectional fluxes and spectra of electrons and protons.

crystal microbalance (QCM) which measures extremely small mass accretions. Sources of contamination on the spacecraft, in addition to general outgassing, include material ejected from the spacecraft propulsion subsystems and the Ion Engine experiment.

The experiment flight hardware consists of two parts: a sensor assembly mounted externally on the North face of the Earth Viewing Module, and the electronic unit mounted internally on the same face. The sensor assembly contains the sensing and reference oscillating quartz crystals, heaters, and the electronic driving circuitry for the crystals. The electronics unit contains the signal processing, sensor temperature control, and command and telemetry circuitry.

12.2.5 Advanced Thermal Control Flight Experiment

The ATFE consists of a solar absorber, a thermal diode heat pipe, a simulated equipment package that contains phase-change material, a feedback-controlled variable conductance heat pipe, and a space radiator. Items of supporting hardware are a solid-state electronics module, temperature sensors, foil heaters, support structure, and thermal insulation.

The ATFE is mounted in the East wall of the Earth Viewing Module with only the outboard surfaces of the solar absorber and radiator exposed to the external environment.

12.2.6 Ion Engine Experiments

There are two Ion Engine systems, one on the North and the other on the South wall. Each consists of the Thruster subsystem and the Control Logic and Power Conditioning subsystem. The two subsystems are packaged separately and are connected by a three foot cable.

The Cesium bombardment ion thruster utilizes the magnetoelectrostatic plasma containment concept. A two-grid extraction system is employed to generate a high velocity ion beam and neutralizing electrons are produced by a plasma bridge neutralizer. Thrust vectoring is provided by the accelerator displacement method. Propellant is supplied by three capillary type reservoirs operating at different potentials.

12.2.7 Very High Resolution Radiometer Experiment (VHRR)

The VHRR is a two-axis scanning radiometer that gives both day and night cloud coverage information for the determination of cloud motions, tropical storm life cycles, extratropical storm life cycles, mesoscale phenomena, and cloud climatology studies. It operates in two different frequency ranges, one in the

infrared between 10.5 micron and 12.5 micron and one in the visible spectrum between 0.55 micron and 0.75 micron. Operating through an 8-inch Cassegrainian telescope, the instrument generates a picture in 20 minutes with a resolution of 10 km at the subsatellite point.

The VHRR is mounted on the North wall of the Experiment Module. The optical viewing port is located in the earth-viewing surface and the infrared detector cooler cone projects through the North wall.

12.3 OPERATIONAL MILESTONES

The following is a chronological listing of events in the experiment subsystem checkout.

<u>Day / Time</u>	<u>Event</u>	<u>Remarks</u>
Pre-Launch	QCM Experiment on (DACU 1) VHRR a. Chopper motor on b. Cone door closed c. Sun Shutter power on	All other experiments off
150:12:59	Launch	
150:22:11	EME a. LIC on b. UCLA on	Enable survival heaters
150:22:18	ATFE experiment on	
151:02:27	EME data being received on FDM	UCLA confirmed on
151:02:35	EME HAC on	Baseline test
151:10:00	Ion Engine 1 and 2 LIC on	Check operation of 6-Hour Timer automatic turnoff
151:16	VHRR EXP Power on	
151:19:30	VHRR Patch HTR on	Bakeout cooler
151:23:42	VHRR Cone HTR on	

<u>Day / Time</u>	<u>Event</u>	<u>Remarks</u>
154:21:10	Ion Engine 1 and 2 LIC and Master Converter on	Communications Module warmup (C-Band "Glitch")
156:00:11	EME HAC turned on and off automatically	Initiated by sun aspect automatically each day
156:08:45	Ion Engine 1 and 2 off	Ion Engine 2 Neutralizer Probe voltage dropped
157:09:06	ATFE Controller and PCM Box Auxiliary Heater on	To degas OSR's
157:11:45	ATFE PCM Box Aux Heater on	Overheating of Thermal Diode and Electronics Module
157:20:03	QCM Degas Heater on	Degas OSR's for 24 hours
157:21:36	Ion Engine 2 LIC and Master Converter on	To check previous anomaly; performance verified
157:23:01	Ion Engine 2 LIC off	
158:13:30	VHRR configured for Visible Scan data acquisition	
158:21:06	QCM Degas Heater off	
158:21:32/ 39/49	VHRR does not respond to Scan Start commands	Cold-start problem (see Section 12.5.4)
160:18:55	Propagation "A" units on	
160:19:59	Propagation "B" units on	
161:18:13	EME GSFC Experiment on	
164:21:06	MMW 20 and 30 GHz Horn Transmitter turn-on	20 GHz Horn transmitter trips out (see Section 12.5.5)
164:21:24	MMW 20 GHz Horn Transmitter on	Try again, no success

<u>Day / Time</u>	<u>Event</u>	<u>Remarks</u>
164:23:45	MMW 20 and 30 GHz Dish Transmitters On	Operation OK
165:01:01	Slew Spacecraft to check MMW dish antenna boresight/pattern	Pattern OK
165:03:54	Try MMW 20 GHz Horn Transmitter again	No success
165:03:59	Change Propagation Experiment To "A" Units	
165:04:06	Shut Down MMW	
165:11:25	Following EME Experiments Turned On: ASC MDAC UMINN	
165:13:27	VHRR Cone Heater Off, Cone Door Open	For IR Detector cool-down
165:15:54/ 19:57	VHRR/IHSDL WBDU Tests	Performance OK
166:17:42	EME, UCSD turned on	UCSD experiment overheating due to solar input
168:04:54	MMW 30 GHz Horn Transmitter on for antenna boresight/pattern	Pattern OK
168:16:12	First VHRR IR pictures	
169:16:59	EME UNH on	Anomaly in EME clock and telemetry (see Section 12.5.6)

12.4 INTERFACE DESCRIPTION

For purposes of interface analysis, the GFE Experiments may be treated as a group of individual subsystems, each of which has specific interfaces with supporting spacecraft subsystems.

Each experiment has interfaces with the Electrical Power Subsystem, and the Telemetry and Command Subsystem. With the exception of EME, which is mounted on the hub and thermally isolated from the spacecraft, each experiment has interfaces with the Thermal Control Subsystem.

A brief description of these interfaces follows.

12.4.1 Electrical Power Subsystem

Electrical power is supplied to each experiment through a Load Interface Circuit (LIC). A LIC is a voltage regulator which supplies 28 ± 0.6 volts to its experiment input. The LIC design incorporates an automatic tripout or disconnect circuit, which protects against loading the spacecraft power bus in the event of a short circuit or sustained abnormally high load in the Experiment. The LIC may be commanded ON or OFF at any time.

12.4.2 Telemetry and Command Subsystem

All experiment functions are controlled by commands received at the Command Decoder Distributor (CDD) and then routed to the proper experiment command address. The design of each experiment command driver circuit has been specified to be compatible with the CDD output, and each experiment has undergone extensive ground test to verify functional compatibility and reliability of the command interface performance.

Experiment telemetry data is routed from experiment output data conditioning circuits to the spacecraft Data Acquisition and Control Unit (DACU), where it is processed for transmission to the ground. Again, the interface circuit design between Experiment and DACU has undergone ground test for functional compatibility, reliability, and accuracy of data transmission.

In addition to the normal telemetry transmission circuits, which use the DACU, there is a special telemetry interface for the 1800 bps EME data stream. By proper configuration of the Data Switching Unit, the EME data stream is frequency-division-multiplexed with normal telemetry and is transmitted via VHF/PFF down-link.

12.4.3 Thermal Control Subsystem

The spacecraft thermal control system provides for conductive and radiative heat transfer necessary to maintain Experiment components within specified operating temperature limits. The GFE Experiments were designed to operate with an interface temperature of 5 to 35 degrees C, except for the Ion Engine Thruster which can tolerate an extended range of -10 to +75 degrees C.

With the exception of EME, every GFE Experiment has significant thermal interfaces with the spacecraft. Some Experiment components are thermally isolated from the spacecraft. Examples of thermally-isolated components are: VHRR Telescope, QCM Sensor, ATFE, except Electronics Module, MMW and Propagation Antennas.

12.4.4 Special Interfaces

12.4.4.1 MMW/COMM Cross-Strap—The MMW Communications Mode configuration provides a frequency translation from a 6 GHz uplink and allows a direct ground comparison of 20 GHz, 30 GHz, and 4 GHz signals simultaneously transmitted at C-band. The 6 GHz receiver is part of the spacecraft Communications Subsystem, and its output is cross-strapped to the MMW Experiment at IF (150 MHz).

12.4.4.2 VHRR/COMM—The VHRR video data is normally generated in the Experiment as a 72 kbps digital stream, and can be transmitted to ground station receivers by way of the Communications Subsystem Wideband Data Unit (WBDU). For economy of information bandwidth, the VHRR video is multiplexed with the Interferometer High Speed Data Link signal in one channel of the WBDU. Appropriate band cutoff filters are incorporated to prevent crosstalk between the two signals.

12.4.4.3 VHRR/ACS—In order to maintain VHRR image quality within the required distortion and registration tolerances, it is necessary that the spacecraft low-jitter mode provide highly stabilized 3-axis positions and rates. The jitter amplitude must be held within $\pm 0.01^\circ/24$ min (design goal), and the jitter rate within $\pm 0.001^\circ/\text{sec}$ in each axis.

12.4.5 Interface Performance

12.4.5.1 Electrical Power Subsystem—During the spacecraft checkout period, all of the GFE Experiments and their LIC's were operated. The LIC voltage regulation was well within specification limits during this period.

Table 12-3 summarizes the Experiment LIC output voltages and variations through the entire period.

12.4.5.2 Telemetry and Command Subsystem—All experiment commands during the spacecraft checkout period were properly executed. An anomaly experienced during turn-on of the 20 GHz Horn transmitter was subsequently attributed to a malfunction in the MMW hardware (see Section 12.5.5).

Telemetry data from Experiments was received without malfunction.

EME data was successfully received via the Telemetry Transmitter and the Prime-Focus Feed. This data normally is multiplexed with other data in the FDM.

12.4.5.3 Thermal Control Subsystem—Performance of the Thermal Subsystem was well within specification limits (5° to 35°C) for all Experiment interfaces that have local spacecraft instrumentation. For those interfaces that are not instrumented, internal Experiment temperatures were considered as an indication of interface thermal performance; nominal performance was observed in these cases.

An anomaly was noted in the QCM Sensor crystal temperature, which was above the expected nominal level. This anomaly is not interface related, since the QCM Sensor is thermally isolated from the spacecraft.

The Ion Engine Experiment was operated from 154:21:12 z to 156:08:42 z, at approximately 50 percent of maximum conducted heat load. The thruster

Table 12-3

Experiment LIC Output Voltages

Experiment	LIC Voltage
PROPAGATION	28.07 ± 0.01
QCM/ATFE	27.93 ± 0.01
MMW LIC 1	27.93 ± 0.01
MMW LIC 2	27.93 ± 0.01
Ion Eng 1	28.13 ± 0.01
Ion Eng 2	28.07 ± 0.01
VHRR	28.07 ± 0.01
EME	28.10 ± 0.01

interface temperature rose during this period to 32°C, and therefore could be expected to exceed 35°C at full dissipation. However, the allowable interface temperature range for the Ion Engine thrusters is specified as -10 to +75°C, due to their high dissipation and small mounting surface. Further observation of Ion Engine interface temperatures will be desirable when the Experiment is fully operational.

Table 12-4 summarizes interface temperature extremes observed during a typical operational day. Since the MMW Dish and Horn Assy are thermally isolated, they have no specific interface temperature requirements and the data is supplied for information purposes.

The MMW Modulator Amplifier did not operate for a sufficiently long period of time to reach thermal equilibrium. The following data is from 3 hours and 45 minutes of operation on day 165.

<u>Parameter</u>	<u>Final Temperature</u>
TWTA Deck Temp	22.0°C
EM, Near Mod Amp	22.5°C

Table 12-4

Interface Temperatures

TLM Channel	Parameter	Allowable Range (°C)	Observed	
			Minimum (°C)	Maximum (°C)
121, 08, 19	Ion Eng 1 (N. Wall)	-10 to 75	20.7	22.5
121, 10, 19	Ion Eng 2 (S. Wall)	-10 to 75	18.1	20.3
121, 11, 19	Ion Eng 2 (CLPC)	5 to 35	27.5	30.0
121, 04, 19	VHRR (N. Wall)	5 to 35	17.7	25.5
120, 04, 19	MMW Horns (EVP)	*	8.4	29.2
120, 02, 19	MMW Dish (EVP)	*	9.5	37.8
120, 05, 19	Propagation (EM Beam)	5 to 35	16.6	27.5
122, 09, 19	QCM Crystal High Temp	*	-30	-6.7

*Thermally isolated—spec. not applicable.

12.4.5.4 MMW/COMM Cross-Strap—The MMW/COMM cross-strap has not yet been fully evaluated with the MMW experiment in the COMM mode. The ground station receiver pre-amplifier was not operating properly, which prevented comprehensive tests being performed.

There has been no evidence of any experiment or spacecraft malfunction at this interface.

12.4.5.5 VHRR/COMM (WBDU)—On day 158, the VHRR was operated with visible detector scan, and data was received at the ground station. Subsequent scans with both visible and infrared detectors were successfully received without any evidence of WBDU interference problems.

On day 165 a VHRR/IHSDL compatibility test was completed with satisfactory results.

Preliminary data reviewed by the Experimenters revealed no crosstalk or mutual interference between the VHRR and Interferometer multiplexed signals.

12.4.5.6 VHRR/ACS (Low Jitter)—The VHRR was operated several times with the Attitude Control System in low jitter mode. Data for different operating periods was analyzed and is reported in Section 9 (ACS).

From the practical aspect, VHRR picture quality has been considered excellent, and no evidence of picture degradation due to ACS performance has been noted.

12.5 EXPERIMENT PERFORMANCE EVALUATION

The following evaluation is directed toward hardware performance rather than achievement of scientific objectives. The latter subject will be addressed at a later date by the individual Principal Investigator.

12.5.1 Propagation Experiment

Operation appeared to be nominal in all modes with no evidence of malfunction.

12.5.2 QCM Experiment

Electrical operation appeared to be nominal. Sensing crystal temperature was higher than anticipated by the Experimenter, but this will not significantly effect performance.

12.5.3 ATFE

Electrical operation appeared to be nominal. The Thermal Diode temperature was higher than anticipated by the experimenter. However, experiment objectives are not expected to be effected significantly.

12.5.4 VHRR Experiment

Successful operation in all modes has been achieved, and quick-look visible and infrared pictures have been received.

A "cold-start" problem was observed at 158:21:32, and thereafter. This anomaly had previously appeared during thermal-vacuum chamber testing. This may be overcome by starting the VHRR when the housing is warm and this procedure will be followed unless constrained by spacecraft operating considerations.

12.5.5 MMW Experiment

A malfunction occurred during the first turn-on of the 20 GHz Horn TWTA. It has been attributed to an overload which causes the transmitter power supply to trip off. Some difficulty had been experienced with this malfunction during ground testing. TWTA turn-on will be attempted again after allowing additional time for more complete outgassing.

A second 20 GHz transmitter, although connected to the parabolic antenna, will provide some measure of redundancy in the event that the horn transmitter cannot be activated.

All other modes of Experiment operation were nominal.

12.5.6 EME

After the activation of the University of New Hampshire Experiment, an anomaly in the EME telemetry encoder was observed. Investigation has not precisely disclosed the nature or the cause of the problem. As a precautionary measure the UNH Experiment has not been reactivated pending resolution of the anomaly.

From preliminary Experimenter's data it appears that the University of California at San Diego Experiment senses interference in the North (-Y) direction at approximately -11° elevation. Further investigation will be made of UCSD performance to identify the source of interference.

All other Experiment operational modes appear nominal.

12.5.7 Ion Engines

The Ion Engines have been operated only to the extent of activating the LIC's and Master Converters, to provide heat for bake-out of the EVM. Nominal operation was observed during the on-time.

Since full activation of the Experiment is not scheduled until a later time, no further evaluation can be made at present.

APPENDIX A
SAPPSAC EXPERIMENT

APPENDIX A

SAPPSAC EXPERIMENT

A.1 PERFORMANCE SUMMARY

SAPPSAC Experiment personnel supported the first 30 days of ATS-6 in-orbit operations in the areas of attitude determination and preliminary sensor evaluation. This support team included the services of three contractors who are presently involved with the SAPPSAC Experiment. Computer programming and operations support included on-line operations support during the first five days of in-orbit operations, where SAPPSAC was utilized in a Rosman PDP-11 computer for attitude determination. Off-line programming and analysis support involved implementation of SAPPSAC algorithms for off-line computation on an XDS-9300 computer at GSFC, which was used to evaluate telemetry data during periods when SAPPSAC was not on-line. A preliminary assessment of the interferometer as an attitude and orbit sensor was provided under a SAPPSAC support contract.

Table A-1 presents a summary of the on-line operation periods for SAPPSAC at the Rosman Tracking Station. The ATS-6 spacecraft was maintained in local vertical hold during the overall span of this data. Table A-2 presents subsequent data obtained in normal telemetry and processed for additional off-line analysis. The composite of this information constitutes the SAPPSAC operations support contained in the following discussion.

TABLE A-1

SAPPSAC On-line Attitude Determination

ATS-6 Mission Sequence	Start GMT	Stop GMT
Yaw Reference Maneuver	150 : 23 : 31 : 59	151 : 02 : 45 : 00
Interferometer Checkout	151 : 15 : 37 : 13	151 : 19 : 47 : 12
Polaris Acquisition	153 : 12 : 29 : 52	153 : 18 : 24 : 27
Interferometer Calibration	154 : 21 : 01 : 59	155 : 01 : 46 : 52

Table A-2

SAPPSAC Off-line Attitude Determination

ATS-6 Mission Sequence	Start GMT	Stop GMT
Rosman Pointing (ESA, PSA, F1)	161 : 14 : 23 : 18	161 : 14 : 25 : 24

A.2 RESULTS

A.2.1 Yaw Reference Maneuver

At 150:23:31:59 GMT the Rosman SAPPSAC computer went on-line in support of the ATS-6 Yaw Reference Maneuver. Predicted spacecraft ephemerides were used for position and velocity components. Initial attitude determinations were based upon normal telemetry from the YIRU and ESA. This data indicated the Earth Sensor to be acquired and that a stable yaw angle was being maintained.

At 151:00:29:53 SAPPSAC began to receive interferometer data at 6150 MHz utilizing the Rosman C-Band illuminator. This data was quite stable and produced a "projected" yaw angle of approximately 203.5 degrees (i.e. yaw angle projected into the North-East plane). Pitch and roll derived from the ESA indicated that the $+Z_b$ axis of the spacecraft was directed to within ± 0.5 degrees of the local vertical. Interferometer calibration was attempted for about 30 minutes, at which time (01:08:00) normal telemetry into the SAPPSAC Computer was temporarily lost. For the next 30 minutes several unsuccessful attempts were made to re-establish valid normal telemetry into the computer. At 01:38:35 telemetry input was re-established. It was decided to make no further attempts at interferometer flight calibration at this time and to proceed into the maneuver using pre-flight biases. Attitude measurements were obtained using the interferometer and ESA, indicating a positive projected yaw angle of 201.5 degrees with pitch and roll angles within ± 0.35 degrees of local vertical.

At approximately 01:44:53 telemetry indications of caged readings for the YIRU began with the spacecraft oriented relative to the sun as shown in Figure A-1. The Rosman "projected" yaw angle was computed using the spacecraft orbit predicted for this time. Projected sun angle was determined from the GMT. Using the interferometer/ESA for attitude determination, it was found that the $+X_b$ spacecraft axis lay 0.2 degrees from the projected sun line. Using DSS data this angle was computed to be 1.6 degrees. This produces a difference of 1.4 degrees in projected yaw angle between the two sets of measurements.

At 01:45:10 interferometer readings indicated the presence of a small negative yaw rate, which subsequently experienced several increases before reaching a rate in excess of -5 degrees per minute. These increments were attributed to multiple firings of the negative yaw jet. Telemetry data also indicated occasional firing of the positive yaw jet, which was attributed to the rate limiting control logic.

At 01:47:09 the interferometer X-component went through zero, indicating that Rosman lay in the spacecraft $Y_b - Z_b$ plane (see Figure A-2). In the interval between 01:58:00 through 02:00:00 noisy sensor readings were obtained in normal telemetry (e.g a 6° ESA Roll angle in the midst of 0.6° Roll data and anomaly Interferometer readings at 01:58:44). Despite these few noisy readings, telemetry was considered generally satisfactory.

At 02:01:45 the interferometer Y-component went through zero, indicating that Rosman lay in the spacecraft $X_b - Z_b$ plane (see Figure A-3). The average yaw rate between 01:47:09 and 02:01:45 was -6.16 degrees per minute. This rate is within the specified spacecraft ACS specs tolerance of 0.1 ± 0.005 degrees per second. With a linearly polarized signal, one would expect Interferometer data to be very noisy or to disappear at about this orientation. However, telemetry indicated stable, low noise performance. This was attributed to the following two factors:

(a) The 85 ft Rosman II antenna provided sufficient received power margin to minimize the noise except near the zero-signal region.

(b) Rosman station personnel performed a rotation of the polarized signal during the yaw maneuver to eliminate a zero-signal region.

At 02:13:09 the interferometer X-component went through zero, indicating that once again Rosman lay in the $Y_b - Z_b$ plane of the spacecraft (see Figure A-4). The average yaw rate between 02:01:45 and 02:13:09 was -7.89 degrees per minute. This rate is within the maximum value specified in the Yaw Maneuver procedures. It is estimated that the spacecraft passed through zero yaw at about 02:15:00. During this portion of the Yaw Reference Maneuver pitch and roll angles fluctuated by as much as 1.5 degrees.

At approximately 02:15:00 telemetry indicated that the YIRU had been uncaged. This was evidenced by a jump in the telemetry readings from -.01 degrees to -.23 degrees. Subsequent YIRU telemetry indicated a yaw overshoot to -0.78 degrees which then reversed direction and attained a maximum value of + 0.24 degrees. After this point, telemetry indicated negative yaw with small excursions about -0.2587 degrees.

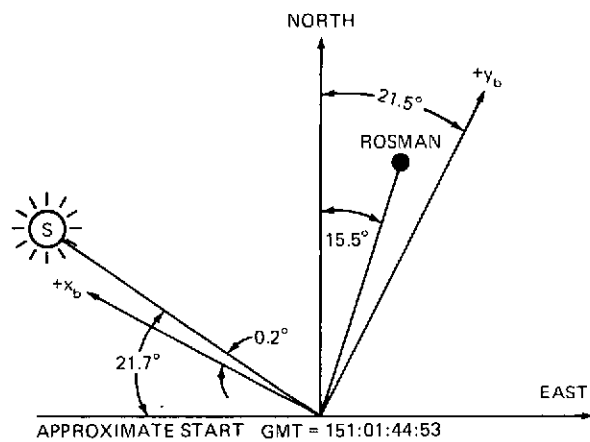


Figure A-1.

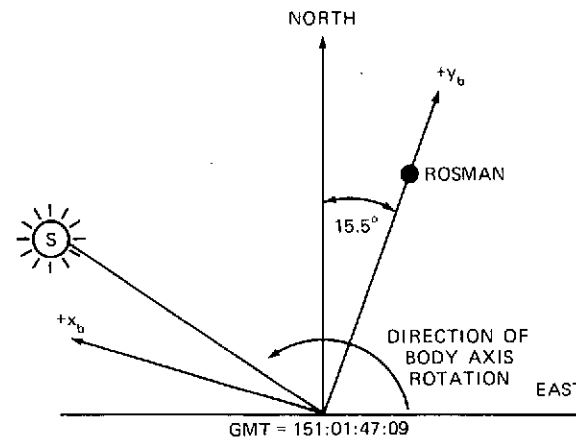


Figure A-2.

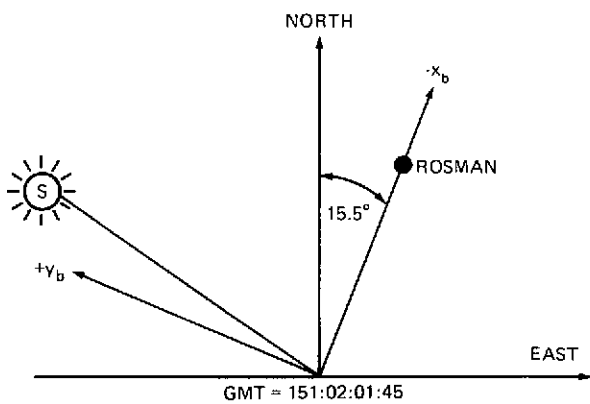


Figure A-3.

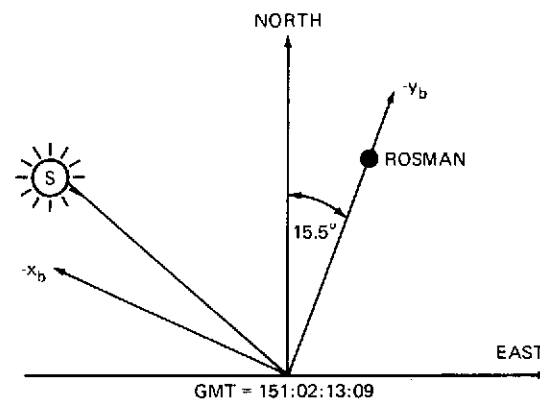


Figure A-4.

Figures A-1 through A-4. Yaw Reference Maneuver Performance

Interferometer telemetry indicated a yaw angle of approximately $+2.5^\circ$ near the time YIRU uncaged readings appeared. Subsequent interferometer readings showed a minimum yaw angle of about $+0.7^\circ$ at 02:17:01, followed by oscillatory readings which stabilized to a value of about $+1.7^\circ$ at 2:26:33. After 02:26:50, interferometer telemetry readings remained constant indicating that the interferometer had been powered OFF while ground illuminators were in operation. At 02:26:33 the YIRU indicated a plus yaw angle of 0.16° (converted telemetry input value). Assuming YIRU to be referenced North at null reading, one finds a discrepancy of approximately 1.5° in yaw angle as derived from YIRU and terminal interferometer measurements. There are a number of factors which could readily explain this difference. First, referencing the YIRU with the sun sensor can contribute in excess of 0.5° in yaw error. Secondly, variations in actual versus predicted orbit inclination can influence the null reading. Thirdly, interferometer calculations were performed using pre-flight biases. Yaw determination for the ESA/interferometer combination is quite sensitive to bias errors in pitch and roll readings (e.g. an error of one vernier count which in pitch or roll would produce an attitude error of about 0.014° will produce a yaw error of 0.014°). This means that a calibration bias correction of 107 vernier counts could produce the entire discrepancy. Subsequent interferometer bias determinations indicate that the predominant error lies in referencing of the YIRU relative to celestial north. Interferometer bias determinations are discussed under Section A.2.3. SAPPsAC on-line support for the Yaw Reference Maneuver was terminated on the Rosman computer at GMT 151:02:45:00.

A.2.2 Interferometer Checkout

At 151:15:37:13 GMT the Rosman SAPPsAC computer was again placed on-line during interferometer checkout operations. The spacecraft was in local vertical hold mode using the ESA/YIRU for attitude control inputs to DOC. Between 151:15:15:32 and 151:15:16:20 GMT the interferometer was powered ON in normal mode. This was followed by stable telemetry verification of DLO lock. In the following ten minute interval Rosman station was in a search mode using the 85 foot dish at 6150 MHz, attempting to lock-up on the ATS-6 spacecraft. At 151:15:25:46 telemetry indicated a sudden change in the Interferometer Frequency 1 AGC level from -113 dbm to -86 dbm, which verified that the 85 foot dish had achieved signal lock on the spacecraft. At this point the Mojave station was still in the process of locking up their 40 foot dish antenna at 6155 MHz. It was not until 151:18:10:08 that telemetry indicated a sudden change in Interferometer Frequency 2 AGC level from -93 dbm to approximately -78 dbm at which time the F1 AGC had further improved to -73 dbm. During the interval between 151:15:25:46 and 151:18:42:46 the interferometer was commanded through the coarse, vernier, pitch, roll, F1, F2, CAL ON, and CAL OFF modes as a preliminary check of hardware performance.

At 151:18:42:49 the interferometer was commanded into the following mode: Vernier/Coarse, Pitch/Roll, F1/F2, DOC Interface On, and CAL OFF. It remained in this mode until SAPPSAC support of operations was terminated at 151:19:47:12. Throughout this interval the Polaris 2 sensor was powered OFF, and the ESA was powered ON and acquired. On-line SAPPSAC attitude computations utilized the ATS-6 pre-launch orbit predicted ephemerides and pre-flight sensor biases. For the ESA, zero bias terms were assumed in both pitch and roll channels. For the interferometer, array and post-switch biases were taken from IBM ground test data, while receiver/converter biases were based upon the final tests at Fairchild Industries using the Interferometer High Data Rate Acquisition System (IHDRAS). Table A-3 summarizes these bias terms.

Table A-3
SAPPSAC Preflight Interferometer Biases

Function	Counts
Course Array Pitch — XNCA(1)	2044.0
Course Array Roll — XNCA(2)	1989.5
Vernier Array Pitch — XNVA(1)	764.5
Vernier Array Roll — XNVA(2)	112.0
Rec./Conv. Freq. 1 — XNF(1)	1049.0
Rec./Conv. Freq. 2 — XNF(2)	1040.0
Post-Switch Freq. 1 — XNS(1)	0
Post-Switch Freq. 2 — XNS(2)	8

The first four terms in this table constitute the array coarse and vernier biases, followed by receiver/converter biases, and then the two post-switch biases. During on-line operations of SAPPSAC attitude determinations were performed by sequencing through combinations of ESA/YIRU, ESA/F1 Interferometer, ESA/F2 interferometer, and F1/F2 interferometer. This data, taken over a ten minute interval beginning 151:18:42:49, indicates close agreement between the different sensor combinations without any flight calibration. The Euler rotation sequence used by SAPPSAC is pitch, roll, and yaw, taken with respect to the orbit plane. During this period of on-line operation, roll angle ranged between values of -0.016° and $+0.062^{\circ}$, pitch angle ranged between values of -0.014° and $+0.199^{\circ}$, and yaw ranged between values of -0.622° and -1.22° . Agreement between the attitude determinations was better than 0.02° in roll, 0.06° in pitch, and 0.6° in yaw.

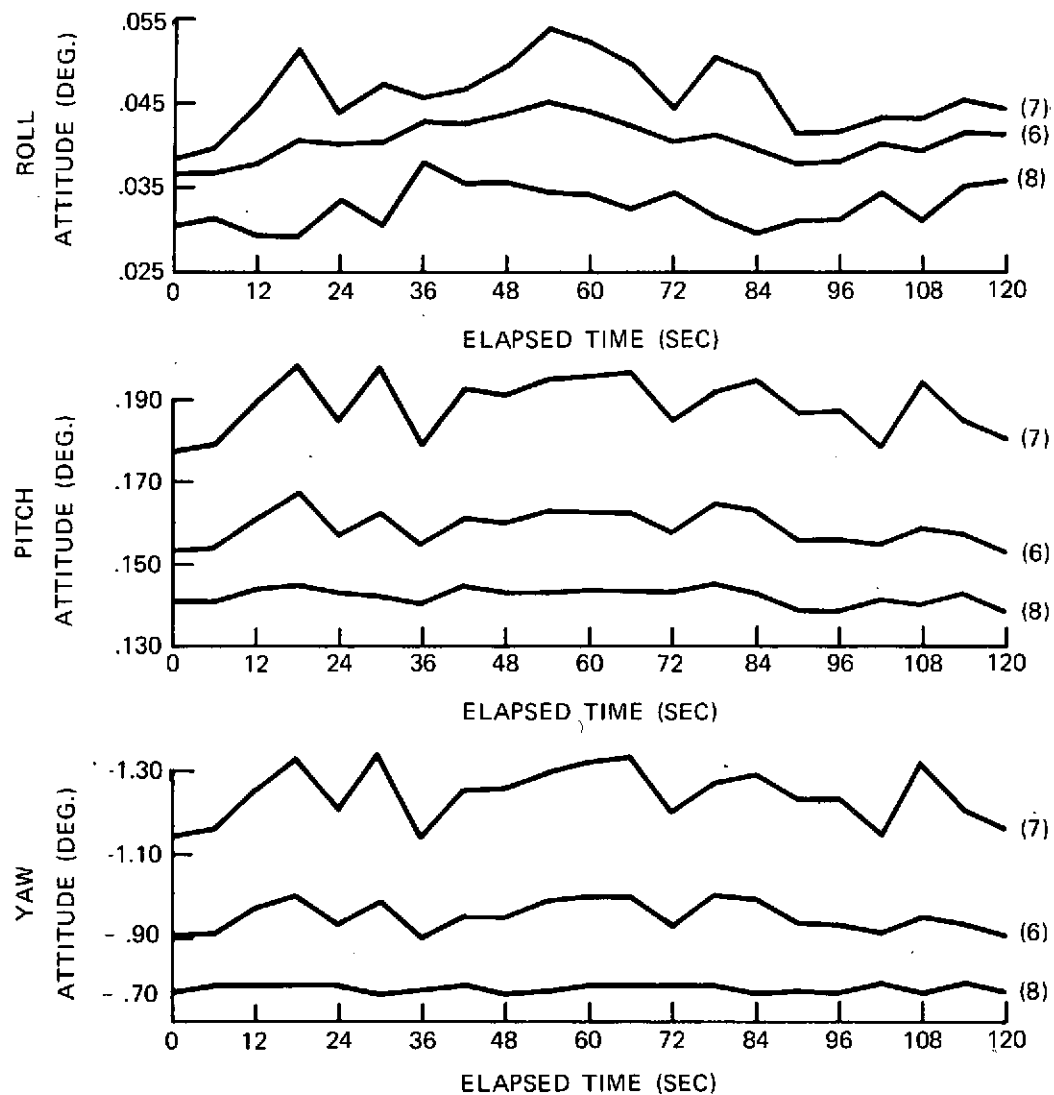
Prior to separation of the Titan Transtage from the ATS-6 spacecraft a brief period of ranging was performed, which was used to generate orbit ephemerides at 151:18:30:49 GMT. These ephemerides were then used in the off-line analysis to recompute spacecraft attitude over the same time span. These results are shown in Figure A-5. The ranged ephemerides had little effect on the relative magnitudes of Euler angles, since the achieved orbit was very close to the predict orbit. The scale selected in Figure A-5 illustrates the quantization effect for both the ESA and interferometer signals. This is particularly evident in the case of yaw attitude, where the minimum values were generated by the two interferometer signals. Over the two minute interval yaw variations were maintained to within 0.04° , while using the ESA and interferometer yaw quantization effects were pronounced.

Since SAPPSSAC utilizes the ESA and two interferometer signals to compute on-line orbit for ATS-6, further analysis was performed to determine bias adjustments for the interferometer that would maximize orbit determination relative to ranging near epoch. The preliminary study assumed zero pitch and roll biases for the ESA. Figure A-6 shows the results of propagating sensor readings and orbit elements through a two minute interval beginning 151:18:42:49, where interferometer biases had been adjusted to the values shown in Table A-4.

Table A-4
Interferometer Biases Adjusted
for Orbit Determination

Function	Counts
XNCA(1)	2044.0
XNCA(2)	1989.5
XNVA(1)	735.6
XNVA(2)	148.6
XNF(1)	1051.2
XNF(2)	1040.0
XNS(1)	0
XNS(2)	8.0

Since only 21 points were used in this analysis, calculation of the mean has a confidence level of 0.22 times the standard deviation. From Figure A-6 we see that the calibration yields a confidence of about 8.7 KM in latitude and longitude components and 1.9 KM radially. The mean values shown are the result of adjusting interferometer biases to match the ranged orbit propagated over this



NOTES:

- (1) ATTITUDE SENSORS-
ESA
ROSMAN INTERFEROMETER (F1)
MOIAVE INTERFEROMETER (F2)
- (2) PRE-FLIGHT SENSOR BIASES
- (3) START = 151:18:42:49
- (4) LOCAL VERTICAL HOLD
- (5) PSA SENSOR OFF
- (6) MEAN VALUE OF ESA/F1,
ESA/F2, AND F1/F2
- (7) MAX VALUE OF ESA/F1,
ESA/F2, AND F1/F2
- (8) MIN VALUE OF ESA/F1,
ESA/F2, AND F1/F2

Figure A-5. ATS-6 Attitude Determination Starting 151:18:42:49

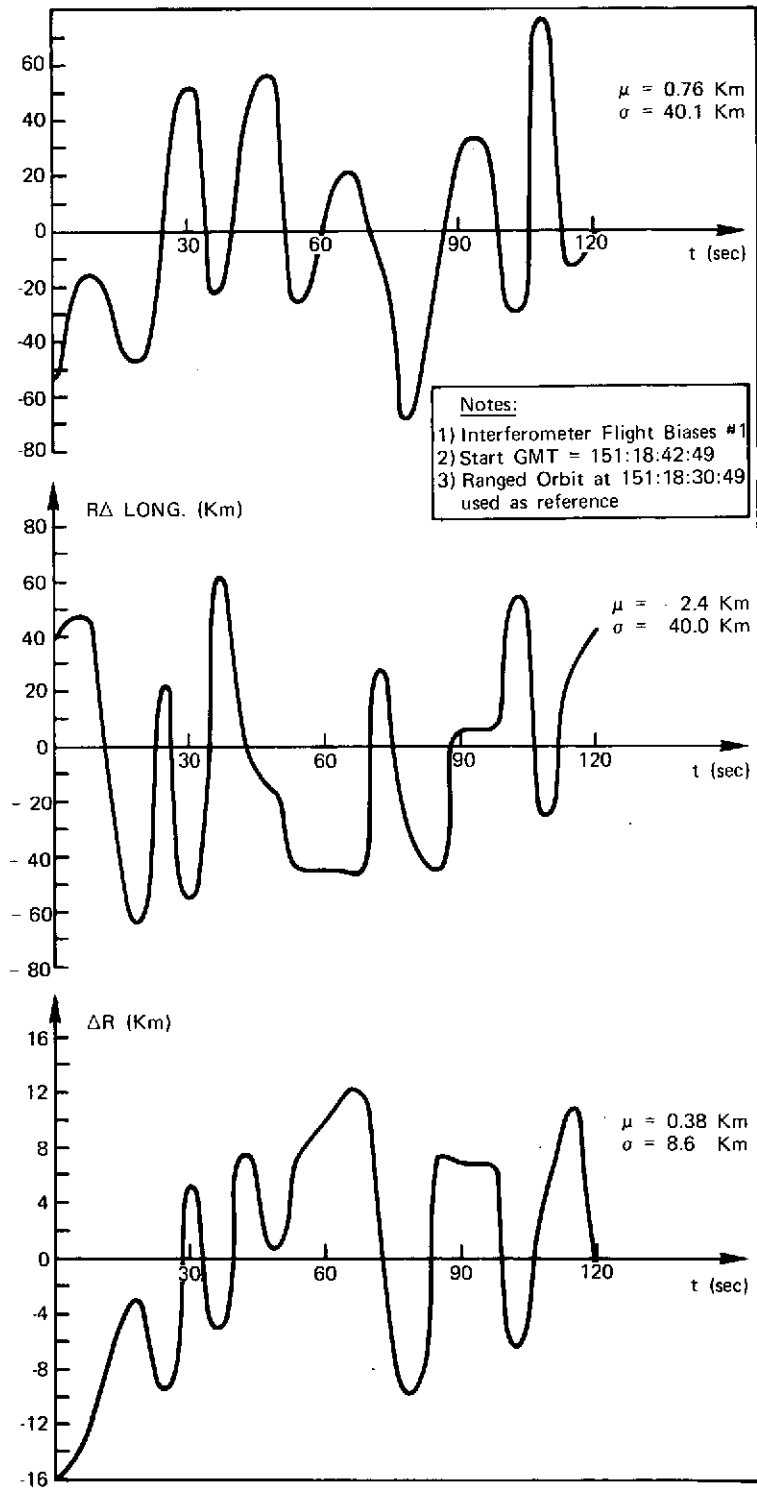


Figure A-6. ATS-6 Orbit Estimation Using Spacecraft Interferometer/Earth Sensor Telemetry

time interval. In order to assess properly this method of orbit determination, it will be necessary to process sensor data segments of from 1 to 5 hours duration over time intervals where ranged orbit data is also available. Since there may be diurnal as well as long term aging of biases, the periods of data acquisition must be carefully scheduled. If such data indicates the sensor biases to be either stable or predictable, one can expect to obtain orbit estimates using ESA and two IF channels having residuals of better than 10 KM in latitude and longitude components and better than 1 KM radially.

The interferometer biases given in Table A-4 were then used to recompute attitude over the same time span. These results are shown in Figure A-7. The mean values of the computed Euler angles have changed slightly, however, the adjusted biases produced better than a factor of two decrease in the spread of data in all axes. This establishes that bias adjustment using orbit consistency is a viable means of calibrating the interferometer as an attitude sensor. Due to the extensive computation requirements, no attempt was made to further refine interferometer biases using this technique.

One further refinement in interferometer receiver/converter biases was made utilizing SAPPSAC test data taken during 155:00:27 through 155:00:34. This data produced the following biases:

$$\text{XNF}(1) = 1049.75 \text{ Counts}$$

$$\text{XNF}(2) = 1037.5 \text{ Counts}$$

The revised biases were used to recompute attitude for a 2 minute period beginning 151:18:42:49. This is shown in Figure A-8. This provided some slight additional decrease in the spread of data over that shown in Figure A-7.

Figure A-9 shows a five minute span of attitude determination using the IF1/IF2 interferometer combination. This data confirms the quantization of 0.014° in pitch and roll axes and 0.014° in yaw. The influence of spacecraft orbit position on attitude angles can also be seen from this figure, where for brief segments of constant sensor T/M readings, small changes in roll, pitch, and yaw occur. There is also a striking difference in dynamic behavior between roll and pitch axes during this span, which cannot be accounted for by inertia properties alone.

A.2.3 Polaris Acquisition

At 153:12:29:52 GMT the Rosman SAPPSAC computer was again placed on-line in support of the Polaris Acquisition Maneuver. The active sensors during this interval were YIRU, ESA, and PSA. The two interferometer stations were powered OFF. At 153:14:25:28 GMT noisy Polaris 2 sensor telemetry was received by SAPPSAC with no corresponding verification in telemetry of Polaris

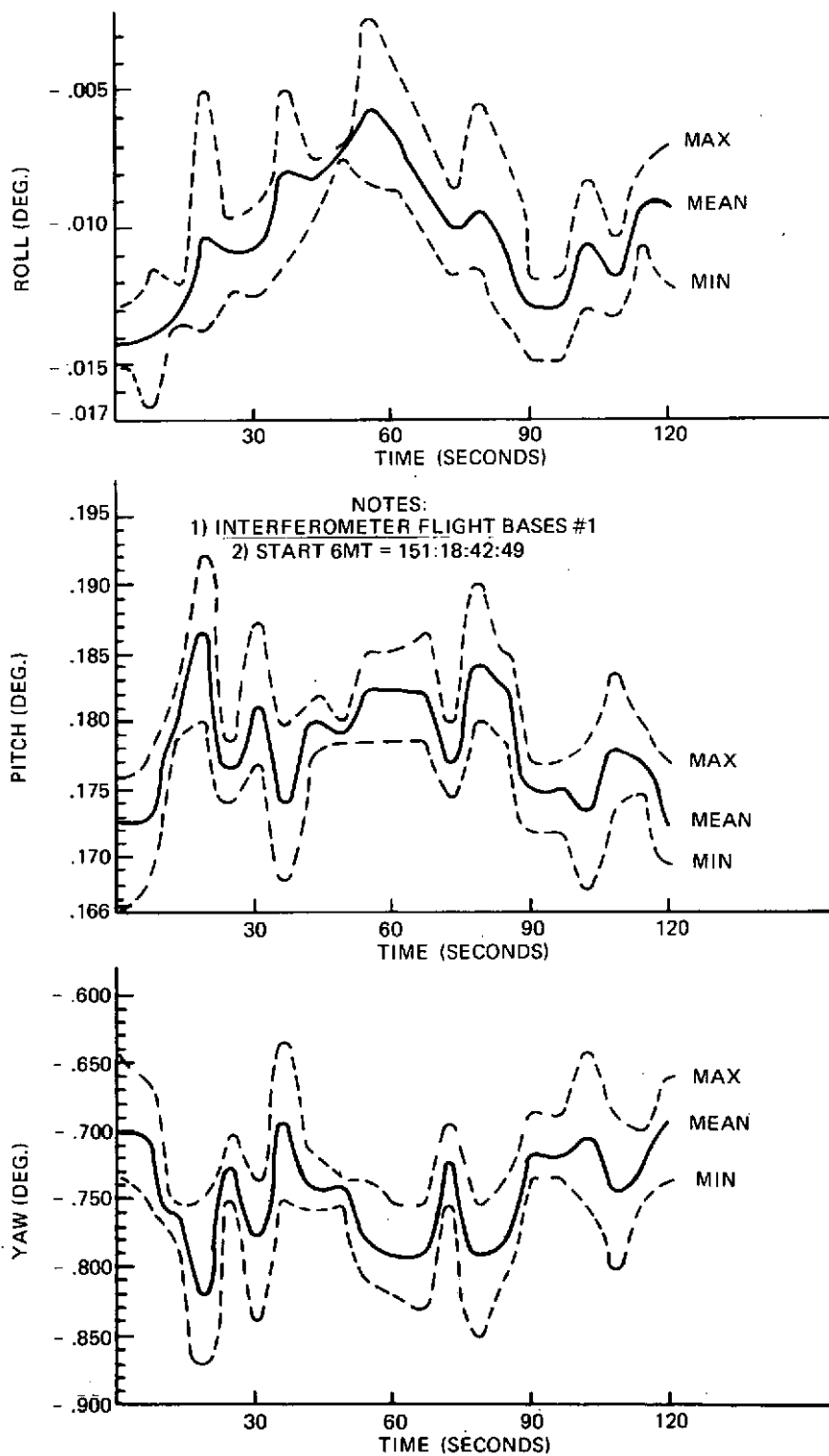


Figure A-7. ATS-6 Attitude Determination Starting 151:18:42:49

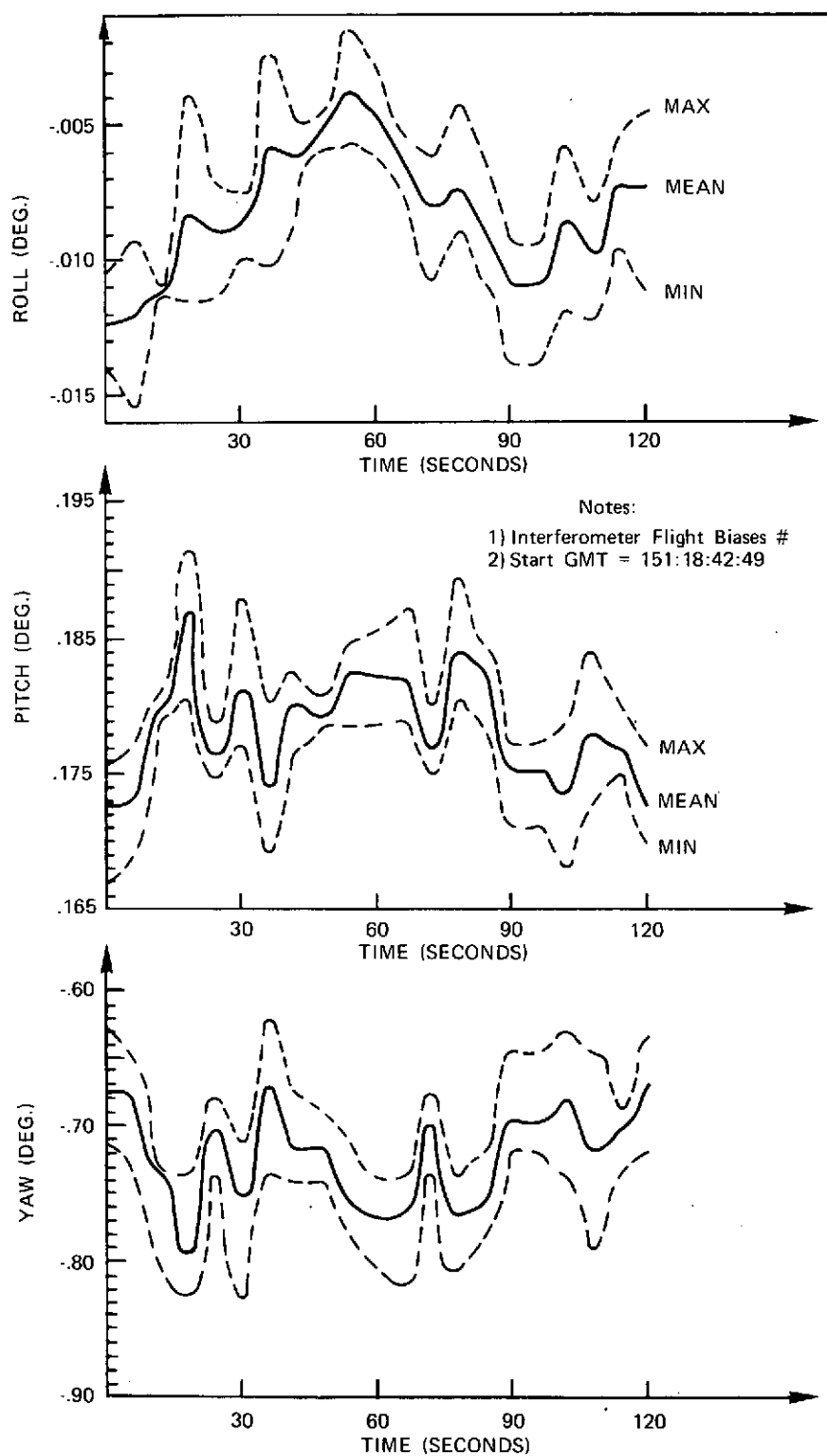
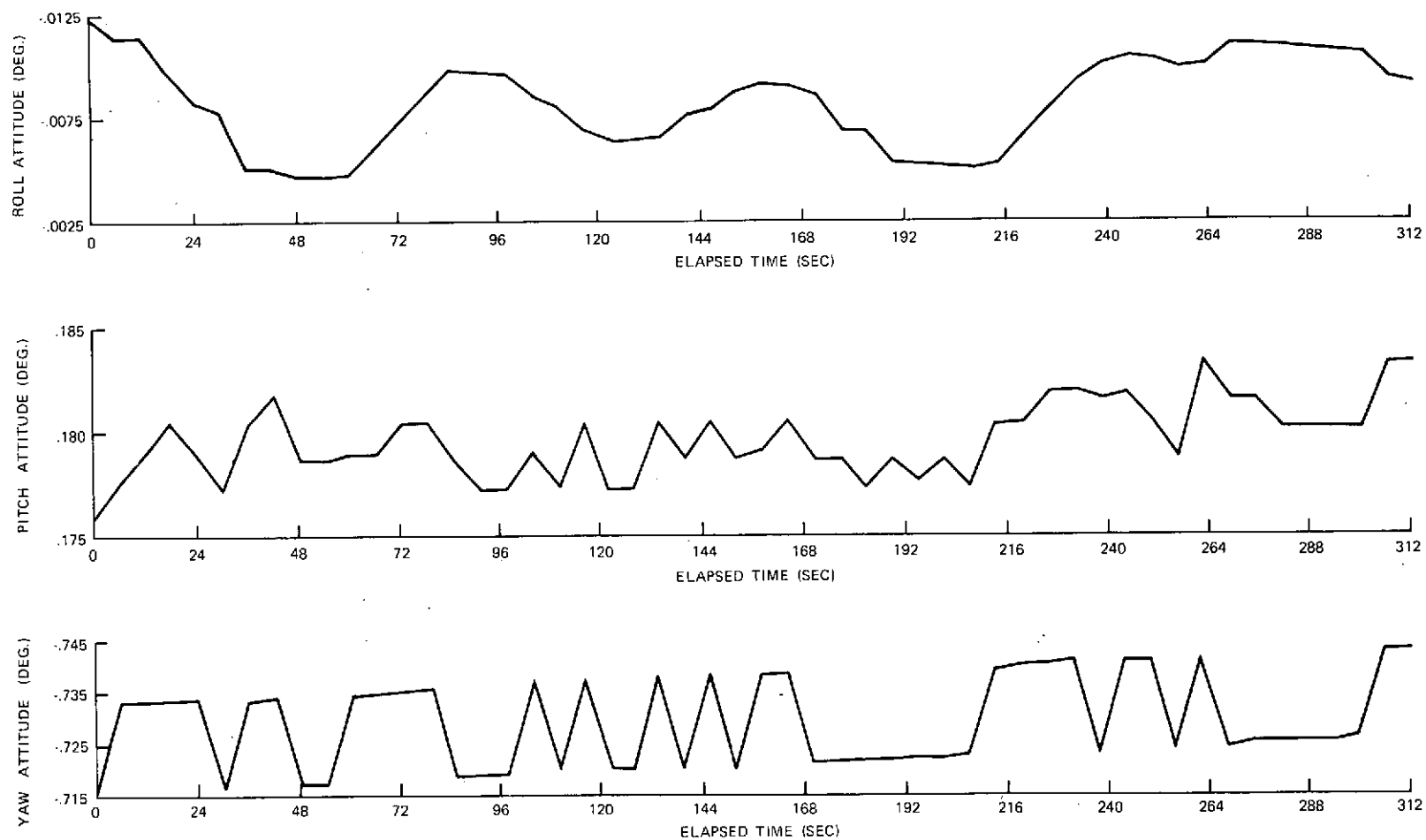


Figure A-8. ATS-6 Attitude Determination Starting 151:18:42:49

A-13



Notes:

- (1) Interferometer Flight Biases #2
- (2) Start GMT 151:18:42:49
- (3) Local Vertical Hold

Figure A-9. ATS-6 Attitude Determination Using 2 Interferometer Stations

acquire. There were several subsequent brief periods where Polaris indicated acquire and then lost acquire. At 153:14:31:16 telemetry readings began continuous verification of acquire with relatively constant Polaris data, up until 14:35:21 whereupon erratic behavior was encountered. At 15:00:57 the Polaris readings settled to the point that meaningful attitude determinations could be initiated. Figure A-10 presents a two minute span of this data beginning 153:15:24:48 GMT. The data indicated that the spacecraft was being held in near-local vertical mode with pitch angles ranging between 0.112° and 0.136° , roll angle between -0.22° and -0.28° , and yaw angle between 0.05° and 0.15° . Attitude rates appear to be extremely small during this interval. Figure A-11 presents a similar plot for the pierce point coordinates in terms of latitude and longitude intercept with the $+Z_b$ spacecraft axis and bearing from north. Examination of the data spread reveals the magnification which occurs between space angles and ground track angles. For the case of local vertical pointing, this factor is approximately six. Since bearing and yaw angles are referenced to the spacecraft, the magnification factor is one.

A.2.4 Interferometer Calibration

At 154:21:01:59 GMT the Rosman SAPPSAC computer was placed on-line in support of the Interferometer Calibration activity. The active sensors during this interval were ESA, IF1 and IF2 Interferometers. The PSA was powered OFF during these tests. Considerable difficulty was experienced in obtaining lockup on the F2 channel from either Rosman or Mojave beacons. At 155:00:08:19 telemetry began indication that both AGC channels on F1 and F2 were operating in a lockup manner. At 155:00:27:44 a CAL ON command was verified in telemetry. Later at 155:00:33:41 a CAL OFF command was verified in telemetry.

Figure A-12 presents a two minute span of data taken during this test beginning at 155:00:33:32. This data shows the pitch, roll, and yaw angles for each of the three combinations ESA/F1, ESA/F2, and F1/F2, where the measured receiver/converter biases were employed. Once again, quantization inherent in the ESA and Interferometer signals can readily be detected. The data spread in pitch and roll is less than 0.035° , and in yaw is less than 0.4° . SAPPSAC on-line support was terminated at 155:01:46:52.

A.2.5 Rosman Pointing (ESA, PSA, F1)

Since all previous data were taken in the local vertical hold mode, a further off-line analysis was performed to compare the PSA, ESA, and F1 Interferometer in an offset pointing mode near Rosman. Figure A-13 presents a two minute span of data beginning 161:14:23:18. This data shows the bearing angle and pierce point latitude and longitude for each of the three combinations ESA/F1, ESA/PSA,

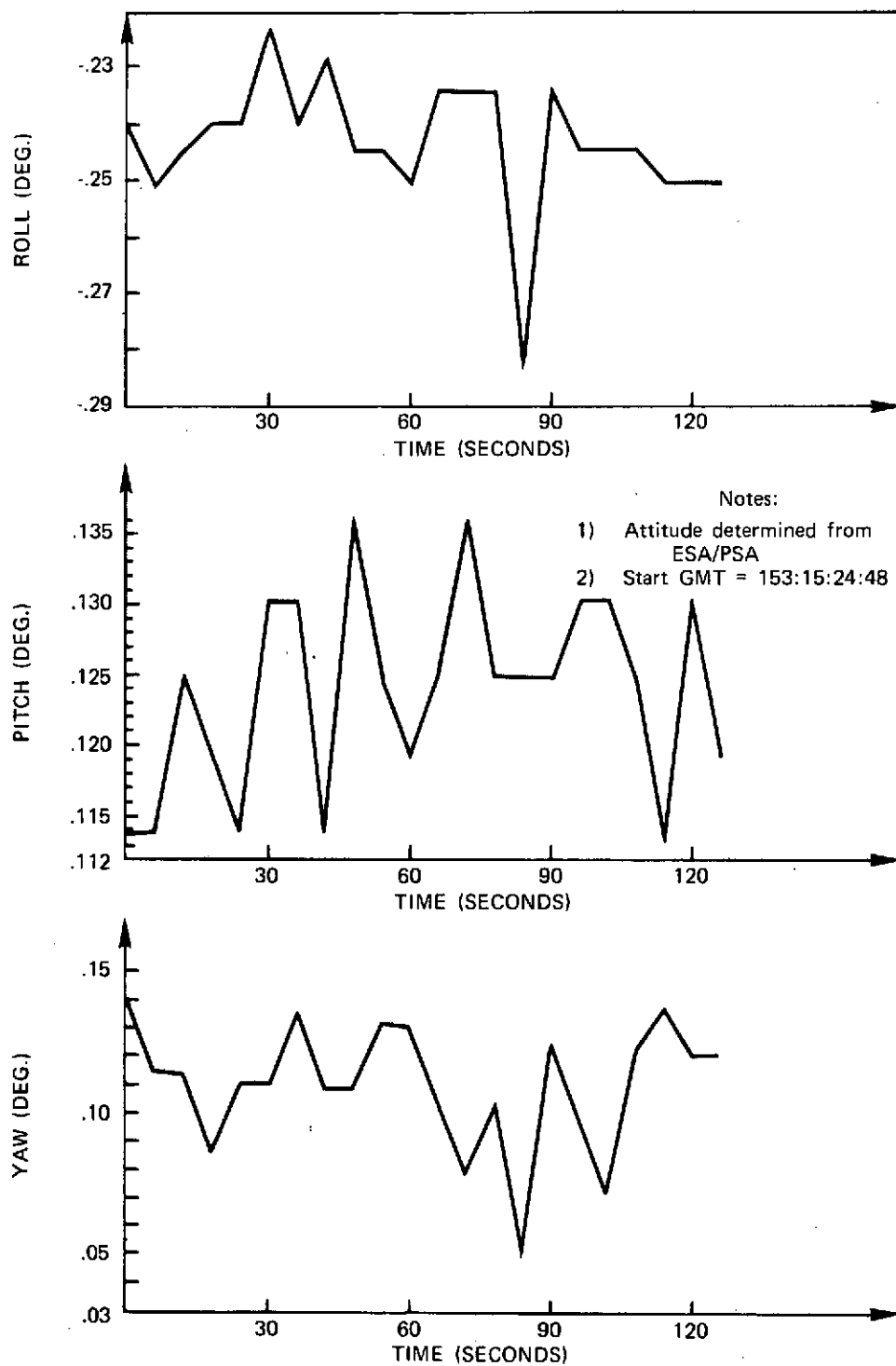


Figure A-10. ATS-6 Attitude Determination Starting 153:15:24:48

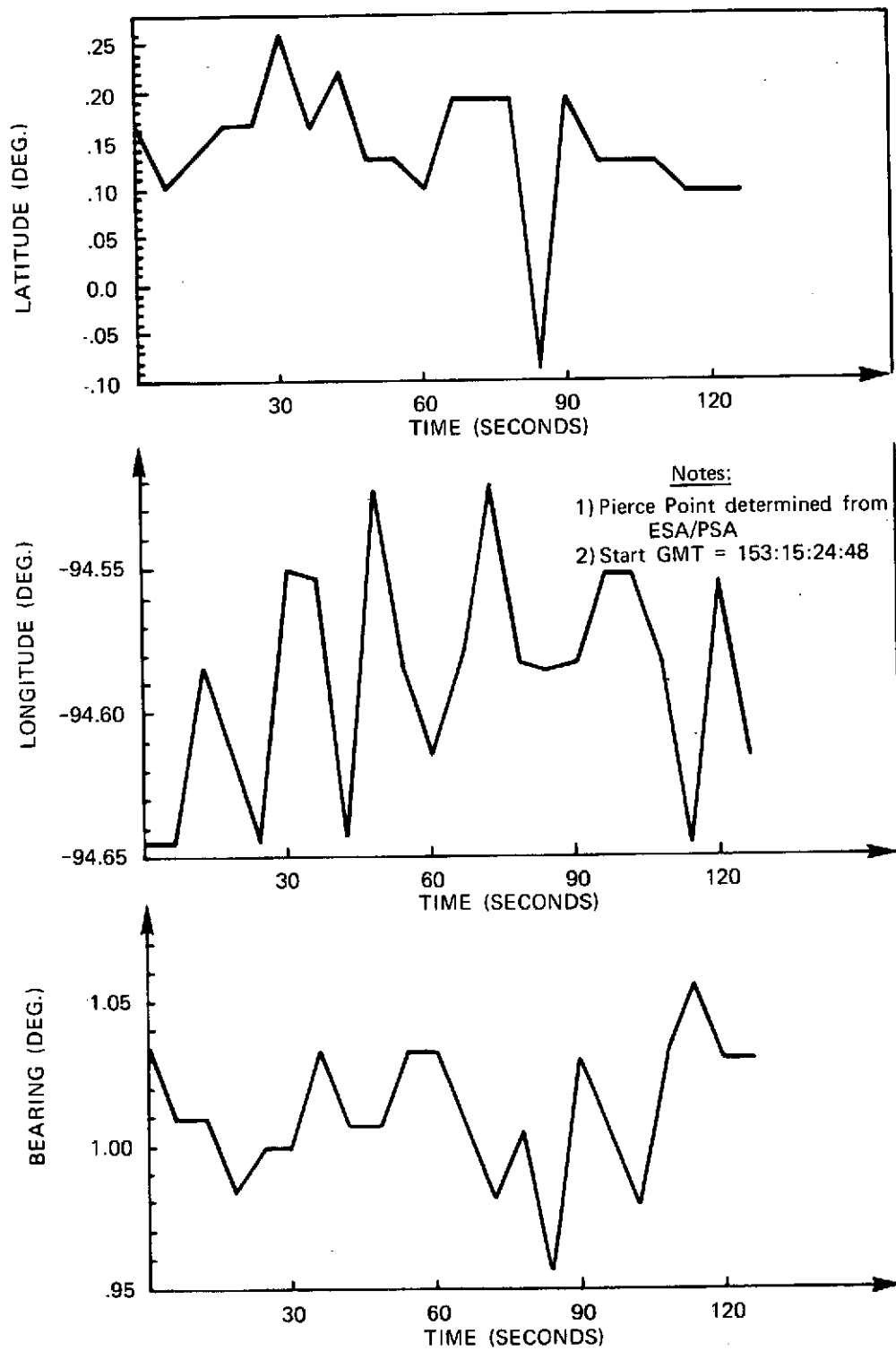


Figure A-11. ATS-6 Pierce Point Coordinates Starting 153:15:24:48

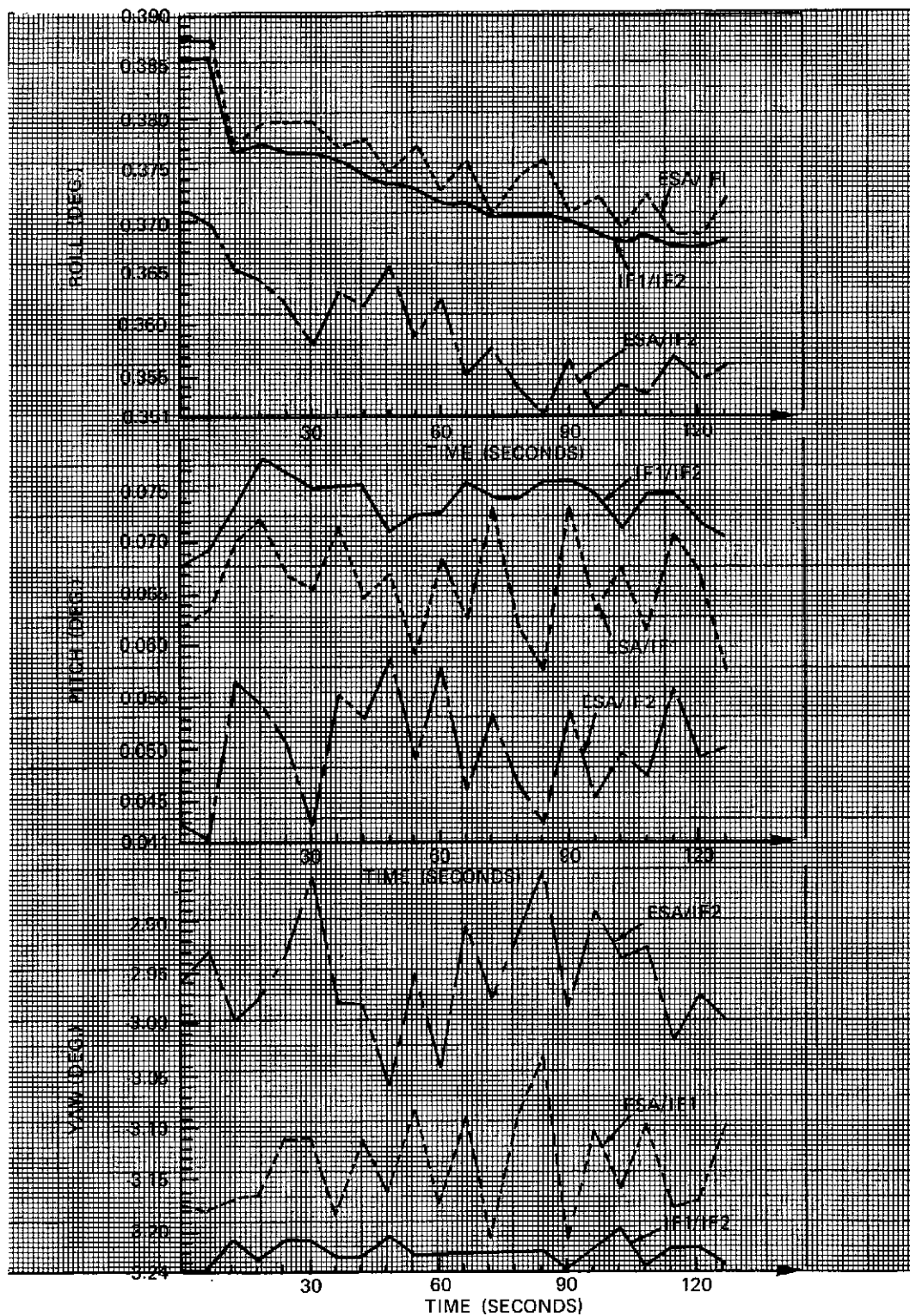


Figure A-12. ATS-6 Attitude Determination Starting 155:00:33:32

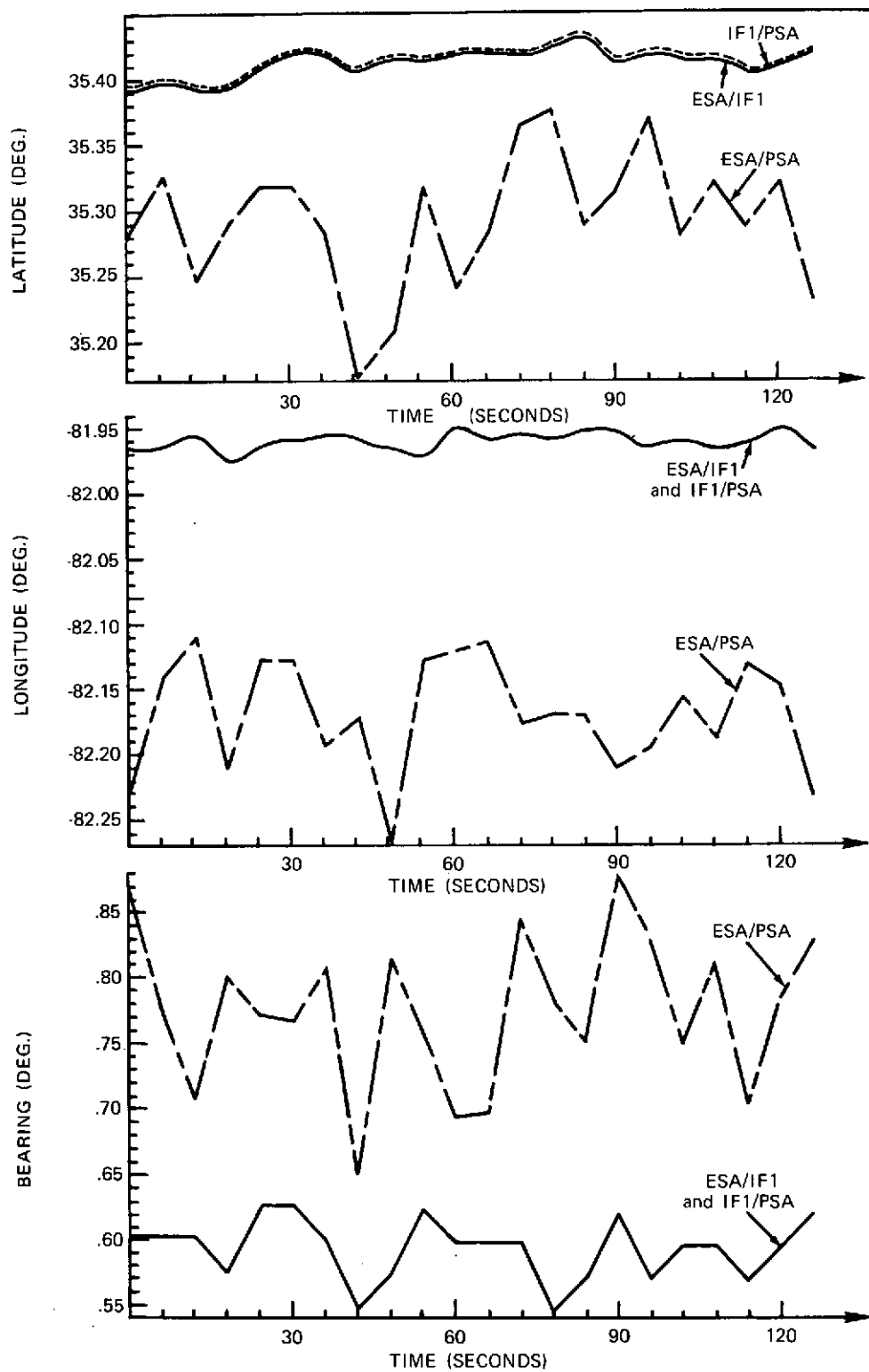


Figure A-13. ATS-6 Pierce Point Coordinates Starting 161:14:23:18

and F1/PSA. The data spread is less than 0.3° in latitude, longitude, and bearing. It should be noted that ESA/F1 and F1/PSA agree closely in all three components. The ESA/PSA combination appears to have an approximate 0.2° bias relative to the other two combinations.

APPENDIX B
ABBREVIATIONS

Appendix B
Abbreviations and Acronyms

A-H	AMPERE HOUR
A/D	ANALOG TO DIGITAL
A/E	ABSORBTIVITY TO EMISSIVITY
ABC	ANALOG BACKUP CENTRCLL
AC	ALTERNATING CURRENT
AC	ATTITUDE CONTROL
ACE	ACTUATOR CONTROL ELECTRONICS
ACS	ATTITUDE CONTROL SUBSYSTEM
ADPE	AUTOMATIC DATA PROCESSING EQUIPMENT
AF	AUDIO FREQUENCY
AFC	AUTOMATIC FREQUENCY CONTROL
AFMTC	AIR FORCE MISSILE TEST CENTER
AGC	AUTOMATIC GAIN CONTROL
AGE	AEROSPACE GROUND EQUIPMENT
AGREE	ADVISORY GROUP ON RELIABILITY ELECTRONIC EQUIPMENT
AI	APPLIED INFORMATION INDUSTRIES
AM	AMPLITUDE MODULATED
AMB	APOGEE MOTOR BOOST
AMP	AMPLIFIER
ANC	AUTOMATIC NUTATION CONTROL SYSTEM
AOS	ACQUISITION OF SATELLITE
APL	APPLIED PHYSICS LABORATORY
APS	AUXILIARY PROPULSION SUBSYSTEM
APT	AUTOMATIC PICTURE TRANSMISSION
ARC	APPALACHIAN REGIONAL COMMISSION
ART	ADVANCED RESEARCH AND TECHNOLOGY
ASC	AEROSPACE CORPORATION
ASSY	ASSEMBLY
AST	ATLANTIC STANDARD TIME
ATC	AIR TRAFFIC CONTROL
ATC	ACTIVE THERMAL CONTROL
ATCS	AIR TRAFFIC CONTROL SATELLITE
ATDM	ASYNCHRONOUS TIME DIVISION MULTIPLEXING
ATFE	ADVANCED THERMAL CONTROL FLIGHT EXPERIMENT
ATHC	ACTIVE THERMAL CONTROL
ATS	APPLICATIONS TECHNOLOGY SATELLITE
ATS-F	APPLICATIONS TECHNOLOGY SATELLITE F
ATS-G	APPLICATIONS TECHNOLOGY SATELLITE G
ATS-R	APPLICATIONS TECHNOLOGY SATELLITE-RANGING
ATSOCC	ATS OPERATIONS CONTROL CENTER
BB	BASEBAND
BCD	BINARY CODED DECIMAL

Appendix B
Abbreviations and Acronyms (Continued)

BCU	BENCH CHECKOUT UNIT
BECO	BOOSTER ENGINE CUTOFF
BER	BIT ERROR RATE
BPI	BITS PER INCH
BPS	BITS PER SECOND
BSA	BIT SYNCHRONIZATION ACQUISITION
BTC	BINARY TIME CODE
BTE	BENCH TEST EQUIPMENT
BTU	BRITISH THERMAL UNIT
BW	BANDWIDTH
C.G.	CENTER OF GRAVITY
CAI	COMPUTER ASSISTED INSTRUCTION
CATV	COMMUNITY ANTENNA TELEVISION
CBW	CONSTANT BANDWIDTH
CC	CONTROL CENTER
CCIR	INTERNATIONAL RADIO CONSULTATIVE COMMITTEE
CCITT	INTERNATIONAL TEL AND TEL CONSULTATIVE COMMITTEE
CCL	CLOSED CONFERENCE LOOP
CCTV	CLOSED CIRCUIT TELEVISION
CDA	COMMAND AND DATA ACQUISITION
CDD	COMMAND/DECODER DISTRIBUTOR
CDP	CENTRAL DATA PROCESSOR
CDU	COMPUTER DISPLAY UNIT
CE-ION	CESIUM ION
CEI	CONTRACT END ITEM
CETEC	COMMUNICATION EXPERIMENT TEST AND EVALUATION CONSOLE
CFE	CONTRACTOR FURNISHED EQUIPMENT
CHARS	CHARACTERS
CHRT	CHANNEL REFERENCE TIME
CIC	COMMAND INTERFACE CONTROL
CITE	CONTROL ITEM TEST EQUIPMENT
CJ	CLOCK JITTER
CL	CLOCK
CLB	CONTROL LOGIC BLOCK
CLC	CHANNEL LEVEL CONTROL
CM	COMMAND MEMORY
CMD	COMMAND
CMS	COMPOSITE MULTIPLEX SIGNAL
CNR	CARRIER TO NOISE RATIO
CNTRLF	ORBITAL MANEUVER CONTROL PROGRAM
COM	COMMUNICATIONS
COMPUT	COMPUTING CENTER (GSFC)
COMSAT	COMMUNICATION SATELLITE
CPB	CORPORATION FOR PUBLIC BROADCASTING

Appendix B
Abbreviations and Acronyms (Continued)

CPT	COMMON PILOT TONE
CR	CONTROL ROOM
CRB	CHANGE REVIEW BOARD
CRT	CATHODE RAY TUBE
CRT	CHANNEL REFERENCE TONE
CSS	COARSE SUN SENSOR
CTC	COMPREHENSIVE TERMINAL C-BAND
CTEC	COMMUNICATION TEST EQUIPMENT CONSOLE
CTS	COMPREHENSIVE TERMINAL S-BAND
CW	CARRIER WAVE
D/A	DIGITAL TO ANALOG
DAC	DIGITAL TO ANALOG CONVERTERS
DACU	DATA ACQUISITION AND CONTROL UNIT
DACU	DATA ACQUISITION AND CONTROL UNIT
DAF	DATA ACQUISITION FACILITY
DD	DIGITAL DATA
DDHS	DIGITAL DATA HANDLING SYSTEM
DDP	DIGITAL DATA PROCESSOR
DEC.	DECLINATION
DHE	DATA HANDLING EQUIPMENT
DISC	DISCRIMINATOR
DLO	DOUBLE LOCAL OSCILLATOR
DMA	DIRECT MEMORY ACCESS
DOC	DIGITAL OPERATIONAL CONTROLLER
DOD	DEPARTMENT OF DEFENSE
DOO/BATT	DEPTH OF DISCHARGE OF BATTERY
DODS	DEFINITIVE ORBIT DETERMINATION SYSTEM
DP	DIGITAL PROCESSOR
DPS	DATA PROCESSING SYSTEM
DPT	DIGITAL PICTURE TERMINAL
DR&A	DATA REDUCTION AND ANALYSIS
DRSS	DATA RELAY SATELLITE SYSTEM
DSS	DIGITAL SUN SENSOR
DSU	DATA SWITCHING UNIT
DTC	DIGITAL TIME CODE
DTL	DIODE-TRANSISTOR LOGIC
OTS	DATA TRANSMISSION SYSTEM
DUT	DENVER UPLINK TERMINAL
EBR	ELECTRON BEAM RECORDER
ECH	EARTH COVERAGE HORN
ED	EXPERIMENTER DATA
EDT	EASTERN DAYLIGHT TIME
EIRP	EFFECTIVE ISOTROPIC RADIATED POWER

Appendix B
Abbreviations and Acronyms (Continued)

EMC	ELECTROMAGNETIC COMPATIBILITY
EME	ENVIRONMENTAL MEASUREMENTS EXPERIMENT
EMI	ELECTROMAGNETIC INTERFERENCE
EOT	END OF TAPE
EPS	ENERGETIC PARTICLE SENSOR
ERL	ENVIRONMENTAL RESEARCH LABORATORIES
ERP	EFFECTIVE RADIATED POWER
ES	EARTH SENSOR
ESSA	ENVIRONMENTAL SCIENCE SERVICES ADMINISTRATION
EST	EASTERN STANDARD TIME
ETP	ENGINEERING TEST PROCEDURE
ETR	EASTERN TEST RANGE
ETV	EDUCATIONAL TELEVISION
EVM	EARTH VIEWING MODULE
EXATO	ATS-F EXPERIMENTERS ATTITUDE AND ORBIT TAPE PROGRAM
FAA	FEDERAL AVIATION ADMINISTRATION
FACTBL	ATS-F ACQUISITION PROGRAM
FC	FREQUENCY CARRIER
FCHP	FEEDBACK-CONTROLLED HEAT PIPE
FD	FREQUENCY DIVERSITY
FDM	FREQUENCY DIVISION MULTIPLEX
FDX	FULL DUPLEX
FET	FIELD EFFECT TRANSISTOR
FHC	FAIRCHILD-HILLER CORPORATION
FI	FAIRCHILD INDUSTRIES
FM	FREQUENCY MODULATED
FMECA	FAILURE MODE EFFECTS AND CRITICALITY ANALYSIS
FOB	FIELD OPTICAL BENCH
FOV	FIELD OF VIEW
FRT	FLIGHT READINESS TEST
FSK	FREQUENCY SHIFT KEYING
FSS	FINE SUN SENSOR
FT	FREQUENCY TRANSLATION
FTP	FLIED TEST PROCEDURES
GAC	GROUND ATTITUDE CONTROL
GEOS	GEODETTIC EARTH ORBITING SATELLITE
GFE	GOVERNMENT FURNISHED EQUIPMENT
GFRP	GRAPHITE FIBER REINFORCED PLASTIC
GHZ	GIGAHERTZ
GIE	GROUND INSTRUMENTATION EQUIPMENT
GMI	GENERAL MANAGEMENT INSTRUCTION
GMT	GREENWICH MEAN TIME
GND	GROUND

Appendix B
Abbreviations and Acronyms (Continued)

GPE	GROUND PROCESSING EQUIPMENT
GR&RR	GODDARD RANGE AND RANGE RATE
GSE	GROUND SUPPORT EQUIPMENT
GSFC	GODDARD SPACE FLIGHT CENTER
GST	GROUND SYSTEM TEST
HAC	HUGHES AIRCRAFT COMPANY
HDX	HALF DUPLEX
HEPAT	HIGH ENERGY PROTON ALPHA DETECTOR
HET	HEALTH, EDUCATION, TELECOMMUNICATIONS
HEW	DEPARTMENT OF HEALTH, EDUCATION AND WELFARE
HF	HIGH FREQUENCY (3 TO 30 MHZ)
HIS	HEALTH INFORMATION SERVICE
HR	HIGH RESOLUTION
HS	HIGH SPEED
HSE	HIGH SPEED EXECUTE
HZ	HERTZ
I/O	INPUT/OUTPUT
ICD	INTERFACE CONTROL DOCUMENTATION (FHC)
IDB	INPUT DATA BLOCK
IDCS	IMAGE DISSECTOR CAMERA SYSTEM
IF	INTERMEDIATE FREQUENCY
IFOV	INSTANTANEOUS FIELD OF VIEW
IGFOV	INSTANTANEOUS GEOMETRIC FIELD OF VIEW
IGS	INERTIAL GUIDANCE SYSTEM
IHDRAS	INTERFEROMETER HIGH DATA RATE ACQUISITION SYSTEM
IHS	INDIAN HEALTH SERVICE
IHSDL	INTERFEROMETER HIGH SPEED DATA LINK
IMU	INERTIAL MEASUREMENT UNIT
INT	INTERFEROMETER
INTELSAT	INTERNATIONAL TELECOMMUNICATIONS SATELLITE
IP	IONOSPHERIC PROPAGATION
IPD	INFORMATION PROCESSING DIVISION
IPS	INCHES PER SECOND
IR	INFRA RED
IRA	INERTIAL REFERENCE ASSEMBLY
IRU	INERTIAL REFERENCE UNIT
IT	INTENSIVE TERMINAL
ITFS	INSTRUCTIONAL TELEVISION FIXED SERVICE
ITL	INTEGRATE-TRANSFER-LAUNCH
ITU	INTERNATIONAL TELECOMMUNICATIONS UNION
ITV	INSTRUCTIONAL TELEVISION
JOBURG	JOHANNESBURG
JPL	JET PROPULSION LABORATORIES
KASATS	KASHIMA (JAPAN) ATS

Appendix B
Abbreviations and Acronyms (Continued)

KEV	KILO ELECTRON VOLTS
KHZ	KILCHERTZ
KPPS	THOUSAND PULSES PER SECOND
KSC	KENNEDY SPACE CENTER
KW	KILCWATTS
L/V	LAUNCH VEHICLE
LASER	LIGHT AMPLIFIC BY STIMULATED EMISSION OF RADIATION
LASS	LATERAL ACCELERATION SENSING SYSTEM
LAST	LOW ALTITUDE SATELLITE POINTING
LAT	LOCAL APPARENT TIME
LBR	LASER BEAM RECORDER
LC	LAUNCH COMPLEX
LCC	LAUNCH CONTROL CENTER
LCE	LASER COMMUNICATIONS EXPERIMENT
LCP	LEFT(HAND) CIRCULAR POLARIZED
LCS	LARGE CORE STORAGE
LEDs	LIGHT EMITTING DIODES
LEPAT	LOW ENERGY PROTON ALPHA DETECTOR
LHA	LOCAL HOUR ANGLE
LHC	LEFT HAND CIRCULAR
LIC	LOAD INTERFACE CIRCLIT
LL	LONG LINES
LMST	LOCAL MEAN SUN TIME
LO	LOCAL OSCILLATOR
LOC	LAUNCH OPERATIONS CENTER
LOP	LAUNCH OPERATIONS PLAN
LOP	LINE OF POSITION
LOS	LINE OF SIGHT
LSB	LEAST SIGNIFICANT BIT
MA	MULTIPLE ACCESS
MARAD	MARITIME ADMINISTRATION
MDAC	MCDONNELL-DOUGLAS AIRCRAFT CORPORATION
MEV	MILLION ELECTRON VOLTS
MGC	MISSILE GUIDANCE COMPUTER
MHZ	MEGAHERTZ
MI	MODULATION INDEX
MICS	MANAGEMENT INFORMATION AND CONTROL SYSTEM
MIL	MILITARY (SPEC OR STD)
MMW	MILLIMETER WAVE (EXPERIMENT)
MOD	MODULATOR
MOI	MOMENT OF INERTIA
MOJATS	MOJAVE ATS
MOP	MISSION OPERATIONS PLAN
MR	MILLIRADIANS

Appendix B
Abbreviations and Acronyms (Continued)

MS	MILLISECOND
MSB	MOST SIGNIFICANT BIT
MSC	MANNED SPACECRAFT CENTER (HOUSTON)
MSC&AD	MISSION SUPPORT COMPUTING AND ANALYSIS DIVISION
MSE	MOBILE SUPPORT EQUIPMENT
MSFN	MANNED SPACE FLIGHT NETWORK
MSL	MEAN SEA LEVEL
MST	MOUNTAIN STANDARD TIME
MT	MULTITONE
MTBF	MEAN TIME BETWEEN FAILURES
MTTF	MEAN TIME TO FAILURE
MUX	MULTIPLEX
NASA	NATIONAL AERONAUTICS AND SPACE ADMINISTRATION
NASCOM	NASA COMMUNICATIONS NETWORK
NASCOP	NASA COMMUNICATIONS OPERATIONS PROCEDURES
NASCOP	NASA COMMUNICATIONS OPERATING PROCEDURES
NCC	NETWORK COORDINATION CENTER
NDPF	NASA DATA PROCESSING FACILITY
NEDT	NOISE-EQUIVALENT TEMPERATURE DIFFERENCE
NHB	NASA HANDBOOK
NI-CD	NICKEL-CADMIUM
NM	NAUTICAL MILE
NOAA	NATIONAL OCEANIC AND ATMOSPHERIC ADMINISTRATION
NOP-JPL	NASA PASADENA OFFICE, JET PROPULSION LABORATORY
NPC	NASA PUBLICATIONS CONTROL
NPR	NOISE POWER RATIO
NRZ	NON RETURN TO ZERO
NSP	NASA SUPPORT PLAN
NSSDC	NATIONAL SPACE SCIENCE DATA CENTER
O&I	OPERATIONS AND INSTRUMENTATION
OC	ORBIT CONTROL
OCC	OPERATION CONTROL COMPLEX
OFFATT	ATS-F OFF-LINE ATTITUDE DETERMINATION PROGRAM
OMNI	OMNIDIRECTIONAL
OPSCON	OPERATION CONTROL CENTER <FOR LAUNCH>
OSC	OSCILLATOR
OSR	OPTICAL SOLAR REFLECTOR
OSSA	OFFICE OF SPACE SCIENCE AND APPLICATIONS
OV	ORBITING VEHICLE
PA	POWER AMPLIFIER
PAFB	PATRICK AIR FORCE BASE
PAM	PHASE AMPLITUDE MODULATION
PBS	PUBLIC BROADCAST SERVICE
PCE	PROPULSION CONTROL ELECTRONICS

Appendix B
Abbreviations and Acronyms (Continued)

PCM	PHASE-CHANGE MATERIAL
PCM	PULSE CODE MODULATION
PCM-DHE	PCM TELEMETRY DATA HANDLING EQUIPMENT
PCU	POWER CONTROL UNIT
PDT	PACIFIC DAYLIGHT TIME
PEP	PEAK ENVELOPE POWER
PFF	PRIME FOCUS FEED
PFM	PULSE FREQUENCY MODULATION
PL	PROGRAM LANGUAGE
PLACE	POSITION LOCATION AND AIRCRAFT COMMUNIC EXPERIMENT
PLF	PAYLOAD FAIRING
PLL	PHASE LOCK LOOP
PM	PHASE MODULATED
PMT	PHOTOMULTIPLIER TUBE
PN	PSEUDO NOISE
POP	PROJECT OPERATIONAL PLAN
PP	PROJECT PLAN
PPL	PREFERRED PARTS LIST
PPS	PULSES PER SECOND
PRO	PROGRAM REQUIREMENTS DOCUMENT
PRS	PARABOLIC REFLECTOR SUBSYSTEM
PRU	POWER REGULATION UNIT
PS	POWER SUPPLY
PS	POLARIS SENSOR
PSD	POWER SPECTRAL DENSITY (G2/H3)
PSI	POUNDS PER SQUARE INCH
PSIA	POUNDS PER SQUARE INCH ABSOLUTE
PSK	PHASE-SHIFT KEYING
PSP	PROGRAM SUPPORT PLAN
PST	PACIFIC STANDARD TIME
PTZF	PAN, TILT, ZOOM AND FOCUS
PU	PLUG-IN UNIT
QCM	QUARTZ CRYSTAL MICROBALANCE
QNATT	ATS-F ON-LINE ATTITUDE DETERMINATION PROGRAM
QPL	QUALIFIED PRODUCTS LIST
R	ROLL
R&D	RESEARCH AND DEVELOPMENT
REQAP	RELIABILITY AND QUALITY ASSURANCE PROCEDURES
RERR	RANGE AND RANGE RATE
R/P	ROLL TO PITCH RATIO
RAPP	RELIABILITY ASSURANCE PROGRAM PLAN
RCP	RIGHT(HAND) CIRCULAR POLARIZED
RCV	RECEIVE
RCV-ECH	RECEIVE-EARTH COVERAGE HORN

Appendix B
Abbreviations and Acronyms (Continued)

RCVR	RECEIVER
REM	ROCKET ENGINE MODULES
RF	RADIO FREQUENCY
RFI	RADIO FREQUENCY INTERFERENCE
RFSW	RF SWITCH
RGA	RATE GYRO ASSEMBLY
RME	ROCKY MOUNTAINS EAST
RMS	ROOT MEAN SQUARE
RMU	REMOTE MULTIPLEX UNIT
RMW	ROCKY MOUNTAINS WEST
ROSATS	ROSMAN ATS
ROT	RECEIVE ONLY TERMINAL
RPM	REVOLUTIONS PER MINUTE
RSO	RANGE SUPPORT OFFICE
RSR	RANGE-SAFETY REPORT
RT	REAL TIME
RTJP	REAL-TIME JET PULSE
S/C	SPACECRAFT
S/C	SPACECRAFT
S/N	SIGNAL TO NOISE RATIO
S/P	SPLIT PHASE
SAGS	SMALL APERTURE GROUND STATION
SAMOC	SPACECRAFT ATTITUDE MANEUVERING OPTIMAL CONTROL
SAMSO	SPACE AND MISSILE SYSTEMS ORGANIZATION
SAPPSAC	SELF-ADAPTIVE PRECISION POINTING SPACECRAFT ATTITUDE CONTROL
SAS	SOLAR ASPECT SENSOR
SATAN	SATELLITE AUTOMATIC TRACKING ANTENNA NETWORK
SATCOM	SATELLITE COMMUNICATIONS
SATS	SMALL APPLICATIONS TECHNOLOGY SATELLITE
SC	SIGNAL CONDITIONER
SC	SPACECRAFT CLOCK
SCAMA	SWITCHING, CONFERENCING AND MONITORING ARRANGEMENT
SCAMP	SMALL COMMAND ANTENNA MEDIUM POWER
SCE	SPACECRAFT COMMAND ENCODER
SCL	SPACECRAFT CLOCK
SCO	SUBCARRIER OSCILLATOR
SCU	SIGNAL CONDITIONING UNIT
SD	SYSTEM DESIGN (FHC)
SDL	SPECIAL DATA LINK
SEC	SECOND
SEC	SYNCHRONOUS EQUATORIAL CIRCULAR (ORBIT)
SECO	SUSTAINER ENGINE CUTOFF
SEMS	SPACE ENVIRONMENT MONITOR SYSTEM
SHF	SUPER HIGH FREQUENCY

Appendix B

Abbreviations and Acronyms (Continued)

SIRD	SUPPORT INSTRUMENTATION REQUIREMENTS DOCUMENT
SITE	SATELLITE INSTRUCTIONAL TELEVISION EXPERIMENT
SLC	SPACECRAFT LAUNCH COMPLEX
SLV	STANDARD LAUNCH VEHICLE
SMAB	SOLID MOTOR ASSEMBLY BUILDING
SMR	SWITCHING MODE REGULATOR
SNR	SIGNAL-TO-NOISE RATIO
SPDT	SINGLE POLE DOUBLE THROW
SPM	SOLAR PROTON MONITOR
SPS	SPACECRAFT PROPULSION SUBSYSTEM
SRM	SOLID ROCKET MOTOR
SRT	SAPPSAC REMOTE TERMINAL
SSB	SINGLE SIDEBAND
SSC	SPIN-SCAN CLOUD CAMERA
SST	SUPERSONIC TRANSPORT
STA	STATION
STADAN	SPACE TRACKING AND DATA ACQUISITION NETWORK
STATS	SYSTEM TEST FOR A.T..S.
STC	SYSTEM TEST COMPLEX
STV	SOLAR THERMAL VACUUM
SYNC	SYNCHRONOUS
SYNCOM	SYNCHRONOUS COMMUNICATION
T&C	TELEMETRY AND COMMAND
T&CS	TELEMETRY AND COMMAND SUBSYSTEM
T&CS	TELEMETRY AND COMMAND SUBSYSTEM
T&ORE	TRACKING AND DATA RELAY EXPERIMENT
T&DRSS	TRACKING AND DATA RELAY SATELLITE SYSTEM
T&DS	TRACKING AND DATA SYSTEM DIRECTORATE
T&E	TEST AND EVALUATION
T&FD	TIME AND FREQUENCY DISPERSION
TACO	TEXAS ANTENNA COMPANY
TBD	TO BE DECIDED
TGG	TIME CODE GENERATOR
TCU	TEMPERATURE CONTROL UNIT
TDA	TUNNEL DIODE AMPLIFIER
TDC	TRANSPONDER COMMAND DISTRIBUTION
TDM	TIME DIVISION MULTIPLEX
TDU	TELETYPE DATA UNIT
TE	TEST EQUIPMENT
TGS	TRANSPORTABLE GROUND STATION
TH	THERMAL
TIROS	TELEVISION AND INFRA RED OBSERVATION SATELLITE
TLN	TELEMETRY
TM	TELEMETRY
TM	TELEMETER
TP	TEST PROCEDURE

Appendix B
Abbreviations and Acronyms (Continued)

TR	TRACKING RANGE
TRUST	TELEVISION RELAY USING SMALL TERMINALS
TSM	THERMAL STRUCTURAL MODEL
TT&C	TELEMETRY, TRACKING, AND COMMAND
TTY	TELETYPE
TV	TELEVISION
TV	THERMAL VACUUM
TVC	THRUST VECTOR CONTROL
TVI	TELEVISION INTERFERENCE
TWT	TRAVELING WAVE TUBE
TWTA	TRAVELING WAVE TUBE AMPLIFIER
TWX	TELETYPE
UCLA	UNIVERSITY OF CALIFORNIA AT LOS ANGELES
UCSD	UNIVERSITY OF CALIFORNIA AT SAN DIEGO
UDMH	UNSYMMETRICAL DIMETHYLHYDRAZINE
UES	UNIVERSAL ENVIRONMENTAL SHELTER
UHF	ULTRA HIGH FREQUENCY
ULO	UNMANNED LAUNCH OPERATIONS
UNH	UNIVERSITY OF NEW HAMPSHIRE
USS	UNITED STATES SHIP
UT	UNIVERSAL TIME
UTC	UNIVERSAL TIME CODE
VA	VETERANS ADMINISTRATION
VCO	VOLTAGE CONTROLLED OSCILLATOR
VCOXO	VOLTAGE CONTROLLED CRYSTAL OSCILLATOR
VDL	VOICE DIRECT LINES
VECO	VERNIER ENGINE CUTOFF
VHF	VERY HIGH FREQUENCY
VHR	VERY HIGH RESOLUTION
VHRR	VERY HIGH RESOLUTION RADIOMETER
VHRE	VERY HIGH RESOLUTION RADIOMETER EXPERIMENT
VIB	VERTICAL INTEGRATION BUILDING
VISSR	VISIBLE INFRARED SPIN-SCAN RADIOMETER
VLf	VERY LOW FREQUENCY
VSWR	VOLTAGE STANDING WAVE RATIO
VTR	VIDEO TAPE RECORDER
VTVM	VACUUM TUBE VOLTMETER
WAMI	WASHINGTON, ALASKA, MONTANA, IDAHO
WB	WIDEBAND
WBVCO	WIDEBAND VOLTAGE-CONTROLLED OSCILLATOR
WD	WIDEBAND DATA
WEFAX	WEATHER FACSIMILE
XMT-ECH	TRANSMIT-EARTH COVERAGE HORN
XMTR	TRANSMITTER
Z	GREENWICH MEAN TIME
ZCD	ZERO CROSSING DETECTOR